



Proceedings of the SilviLaser Conference 2021

Vienna, Austria, 28–30 September 2021

Editors: Markus Hollaus, Norbert Pfeifer

ORGANISERS



umwelt  data

STAR SPONSOR



SPONSORS



Published by Technische Universität Wien (TU Wien), Department of Geodesy and Geoinformation, Vienna, Austria, as issue 104 of the series *Geowissenschaftliche Mitteilungen* (ISSN 1811-8380).

Date of publication: 1 December 2021

© Front matter: Technische Universität Wien

© Papers: paper authors

DOI: 10.34726/wim.1861

PREFACE

SilviLaser 2021 was the 17th conference in a series focused on the applications of LiDAR and related technologies for assessing and managing forest ecosystems. The main aim of the conference was to bring together research scientists, data providers, device manufacturers, and practitioners from around the world to share their experience in the development and application of LiDAR to improve our understanding of forest ecosystem functioning and facilitate their sustainable management through improved forest assessment and inventory. An additional aim of the conference was to discuss alternative methods for three-dimensional forest mapping in addition to the different LiDAR systems. Especially in the case of terrestrial and UAV-based methods, many new systems have been established in recent years, some of which are already suitable for practical use.

In order to emphasize the practical application of the different methods, we also organized an extensive field campaign where a wide range of institutions and equipment manufacturers demonstrated their systems live in the forest. Additionally, the company Rieggl supported this field campaign by providing an airborne laserscanning flight over the field sites. Finally, detailed reference data was collected by the company Umweltdata, BOKU and TU Wien. The recorded data will soon be freely accessible and thus available to the community for a wide variety of scientific work. These unique data sets will also form the basis for an international benchmark on the topic of parameter retrieval from different 3D recording methods.

The SilviLaser 2021 was organized by TU Wien in cooperation with the company Umweltdata GmbH and took place in Vienna from 28th to 30th of September 2021. Due to the Covid pandemic, the conference was held as hybrid conference. To take into account the different time zones of remote and onsite participants, all presentations were recorded and were available to all conference participants even after the end of the conference via the conference platform. This platform also allowed us to communicate with all conference participants and sponsors, whether they were present virtually or physically. In this way, we could guarantee the best possible interaction of on-site and virtual participants.

In total, 129 high quality extended abstracts were submitted to the SilviLaser conference and were reviewed by the scientific committee. After few withdrawals due to pandemic reasons (i.e. travel restrictions), 119 contributions, divided in 30 pico and 89 oral presentations, were presented during the conference. Additionally, eight excellent keynote presentations were given by Juha Hyyppä, Mike Wulder, Amy Neuenschwander, Xinlian Liang, Quinghua Guo, Gottfried Mandlbürger, Håkan Olsson, and Martin Pfennigbauer, Peter Rieger and Bernhard Groiss.

These proceedings contain the extended abstracts of all pico and oral presentations. Selected full papers based on these presentations will be published in the special issue “Advances of laser scanning in forest science and silviculture” in the *International Journal of Applied Earth Observation and Geoinformation* very soon.

Finally, we would like to thank all the conference participants for their participation and presentations and all the helpers and the local organising team for their tireless efforts.

Markus Hollaus
December 2021

SCIENTIFIC COMMITTEE

We would like to thank the members of the scientific committee for reviewing all submissions:

Last name	First name	Affiliation on file (potentially out of date)
Abegg	Meinrad	Swiss Federal Institute for Forest, Snow and Landscape Research WSL
Alonzo	Michael	American University
Andersen	Hans-Erik	USDA Forest Service
Armston	John	University of Maryland
Breidenbach	Johannes	NIBIO
Burt	Andrew	Sylvera
Calders	Kim	Ghent University
Campos	Mariana Batista	UNESP - São Paulo State University
Chasmer	Laura	University of Lethbridge
Coops	Nicholas	The University of British Columbia
Côté	Jean-François	Canadian Wood Fibre Centre, Natural Resources Canada
Culvenor	Darius	Environmental Sensing Systems
Dalla Corte	Ana	Federal University of Paraná
Danson	Mark	University of Salford
Disney	Mathias	UCL Geography
Duncanson	Laura	University of Maryland, College Park
Durrieu	Sylvie	INRAE - UMR TETIS
Glenn	Nancy	Boise State University
Gobakken	Terje	Norwegian University of Life Sciences, Department of Ecology and Natural Resource Management
Gorgens	Eric	Universidade Federal dos Vales do Jequitinhonha e Mucuri
Hill	Ross	Bournemouth University
Hirata	Yasumasa	Forestry and Forest Products Research Institute
Hollaus	Markus	TU Wien
Holler	Wilson	Embrapa Forestry
Hopkinson	Chris	University of Lethbridge
Huang	Huaguo	Beijing Forestry University
Hudak	Andy	USDA Forest Service Rocky Mountain Research Station
Kato	Akira	Chiba University
Kükenbrink	Daniel	Swiss Federal Institute for Forest, Snow and Landscape Research WSL
Li	Zengyuan	Institute of Forest Resource Information Techniques
Liang	Xinlian	Wuhan University
Liesenber	Veraldo	Santa Catarina State University (UDESC)

Last name	First name	Affiliation on file (potentially out of date)
Lim	Kevin	Lim Geomatics Inc.
Lines	Emily	Department of Geography, University of Cambridge
Maas	Hans-Gerd	TU Dresden
Maltamo	Matti	University of Eastern Finland
Mandlbürger	Gottfried	TU Wien
Mikolka-Flöry	Sebastian	TU Wien
Monnet	Jean-Matthieu	Irstea
Moorthy Parvathi	Sruthi Krishna	University of Maryland College Park
Morsdorf	Felix	University of Zürich
Olsson	Håkan	SLU
Packalen	Petteri	University of Eastern Finland, School of Forest Sciences
Pang	Yong	Chinese Academy of Forestry
Persson	Henrik	Swedish University of Agricultural Sciences
Pfeifer	Norbert	TU Wien
Puliti	Stefano	Norwegian Institute of Bioeconomy Research (NIBIO)
Puttonen	Eetu	Finnish Geospatial Research Institute in the National Land Survey of Finland
Rehush	Nataliia	WSL
Renaud	Jean-Pierre	Office National des Forêts
Rüetschi	Marius	Swiss Federal Institute for Forest, Snow and Landscape Research WSL
Rutzinger	Martin	Universität Innsbruck
Schadauer	Klemens	BFW
Stereńczak	Krzysztof	Forest Research Institute
Treitz	Paul	Queen's University
van Aardt	Jan	Rochester Institute of Technology
Vega	Cédric	IGN
Vepakomma	Udaya	FPIInnovations
Vincent	Gregoire	IRD
Wang	Yunsheng	Finnish Geospatial Research Institute
White	Joanne	Canadian Forest Service
Wilkes	Phil	UCL
Wulder	Mike	Canadian Forest Service, Natural Resources Canada
Wynne	Randolph	Virginia Tech

LOCAL ORGANIZING COMMITTEE

Markus Hollaus, TU Wien, chair

Carina Brachner, TU Wien

Günther Bronner, Umweltdata

Gudrun Eppich, Umweltdata

Katharina Fehn, TU Wien

Felix Ortag, TU Wien

Norbert Pfeifer, TU Wien

Characterising understorey Plant Area Index with TLS

Phil Wilkes^{1,2}, Mathias Disney^{1,2}, Cecilia A. L. Dahlsjö³ and Yadvinder Malhi³

¹University College London, Department of Geography, Gower Street, London, WC1E 6BT, UK
Email: {p.wilkes, mathias.disney}@ucl.ac.uk

²NERC National Centre for Earth Observation (NCEO)

³Environmental Change Institute, School of Geography and Environment, University of Oxford, South Parks Road, Oxford OX1 3QY, UK
Email: {cecilia.dahlsjo; yadvinder.malhi}@ouce.ox.ac.uk

1. Introduction

Leaf Area Index (LAI), measured as one half of the total green leaf area per unit horizontal ground surface area, is a key metric for estimating biophysical structure and function; as such LAI is listed as an Essential Climate Variable. LAI can be difficult to quantify, particularly in forest environments, where e.g. saturation, leaf angle distribution, leaf clumping and the inability to separate leaf and wood confound accurate estimation. A number of methods have been developed to estimate LAI such as leaf litter traps, digital hemispherical photography and terrestrial laser scanning (TLS) (Woodgate *et al.* 2015).

The understorey vegetation layer in forests plays an important role in overall forest function, for example providing habitat for small mammals. The understorey layer is also dynamic and can respond rapidly to changes in light environment e.g. caused by tree fall or in response to defoliating pathogens. Quantifying understorey LAI can be difficult owing to measurement difficulty and for this reason is often overlooked.

Here we present methods (and preliminary results) that use TLS to estimate understorey Plant Area Index (PAI) - no distinction is made between wood and leaf material - that is applied across fifteen plots in Wytham Woods, UK. PAI estimates were computed by modifying the “hinge angle” method of Jupp *et al.* (2008); further, to increase the sampled area, the TLS instrument was mounted on a pneumatic mast.

2. Methods

A multi-year project has been established in Wytham Woods, UK, to monitor the woodland response to canopy decline as a result of ash dieback. Fifteen 40 m x 40 m plots were installed through the forest; 5 plots are ash dominant where the ash trees have been girdled to simulate a rapid decline in the tree canopy (winter 2020/21), 5 plots are ash dominant control and 5 plots are non-ash dominant control (predominantly *Acer pseudoplatanus* and *Fagus sylvatica*).

TLS has so far been conducted twice at the fifteen plots (summer and winter); further acquisitions are planned for 2023. Scanning was done with a RIEGL VZ-400 (Horn, Austria) where scans were performed with an angular resolution of 0.04 degrees in an upright position. Scan positions were located along the 4 edges of the plot (to avoid disturbing understorey vegetation and other experimental equipment) and in the centre (Figure 1). The scanner was mounted on a pneumatic mast and pumped to heights of 2 m, 3 m, 4 m and additionally at 6 m in the plot centre (Figure 1); this was done to capture different portions of the plot as well as to reduce operator bias i.e. locating the scanner in an open area. Considering only the 120° - 125° zenith ring (see below), and scanning as in Figure 1, resulted in ~15% of the total plot area being captured. If only a 2 m tripod had been used <2% of the plot would have been captured.

To compute estimates of PAI, the “hinge angle” method of Jupp *et al.* (2008) was modified. First vertically resolved angular dependent gap probability P_{gap} was derived:

$$P_{gap}(\Theta, z) = 1 - \frac{\sum w_i(w_i < z, \Theta)}{N(\Theta)} \quad (1)$$

where z is height below the scanner, Θ is the zenith ring interval, w is a weighting dependent upon the number of targets intercepted by each outgoing pulse and N is the total number of outgoing pulses. PAI as a function of height can then be derived as:

$$PAI(z) \approx -1.1 \log(P_{gap}(\theta))(2)$$

To approximate the hinge angle of 57.5° Jupp *et al.* (2008) analysed $\Theta = [55^\circ, 60^\circ]$. Here, to estimate PAI below the scanner, the polar opposite zenith ring where $\Theta = [120^\circ, 125^\circ]$ was extracted. To not conflate vegetation and the ground surface in undulating terrain, a digital elevation model (DEM) with a resolution of 0.5 m was created from all data (i.e. not limited to a zenith ring) from all scan heights at a single scan position. This also allows for a more accurate estimate of vegetation height to be computed.

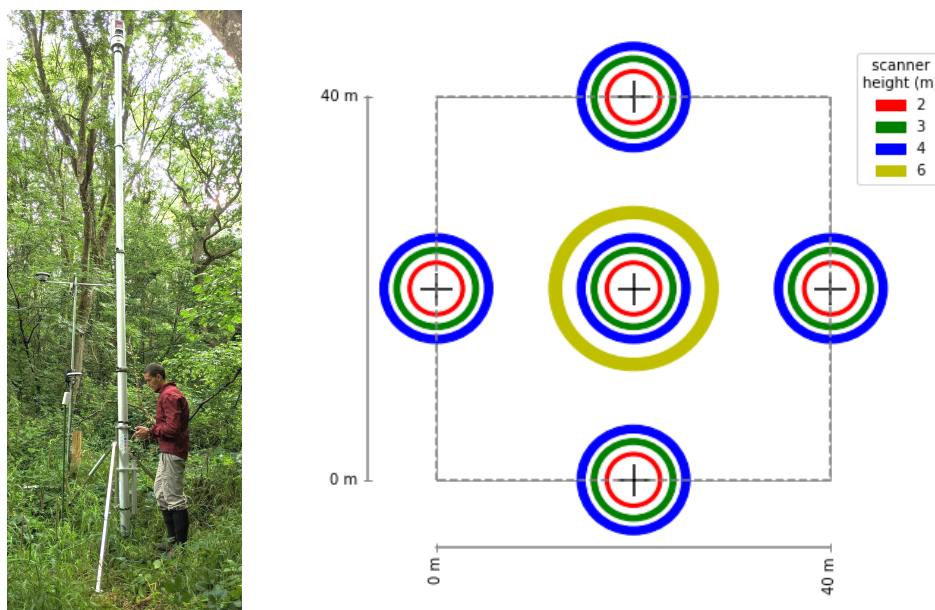


Figure 1. Pneumatic mast extended to 6 m with RIEGL VZ-400 mounted on top (left) and location of scan positions in a plot with area scanned by zenith ring $[120^\circ, 125^\circ]$ at different heights.

3. Results and Discussions

Vertically resolved PAI are presented in Figure 2 where profiles have been truncated between 0.1 - 2 m above ground. Maximum plot-level understorey PAI was 2.02 recorded at Plot 1B in summer, a minimum value of 0.09 was recorded in winter for Plot 1C. There is a clear distinction between ash dominant and non-ash plots where the former has a dense understorey. It is suggested that this is a result of ash canopies being less dense (evident in full canopy PAI curves), therefore allowing more light to penetrate to the understorey below that result in abundant bramble thickets. PAI was on average ~50% of summer PAI in winter and the understorey layer was noticeably lower in height, particularly in the bramble dominated ash plots (e.g. ash (control) plot 3 in Figure 2).

The benefits of using the mast is an open question. Preliminary results would suggest that PAI values do not differ between scans captured at different heights owing to the homogeneity of the plots. The additional time and expense of mast hire and deployment therefore may not be worthwhile; however, if only scanning from 2 m, care must be taken to not bias the sample by scanning in a clear area and ensure scanning is conducted on, or inside, the plot boundary.

Other methods for measuring understorey PAI have not been trialed so far in this experiment. Leaf litter traps are also installed but are at a height of 1 m above ground level; installing litter traps at ground level could be problematic e.g. damage due to animal activity. PAR sensors are installed at heights of 0.3 m and 3 m on weather stations at the plot centres and could be used as a reference data set; larger samples (at different heights) could be gathered using an LAI sensor such as LiCOR LAI-2200. However, TLS is not dependent on light conditions and has been shown to be more precise than other methods in forest environments (Calders *et al.* 2018).

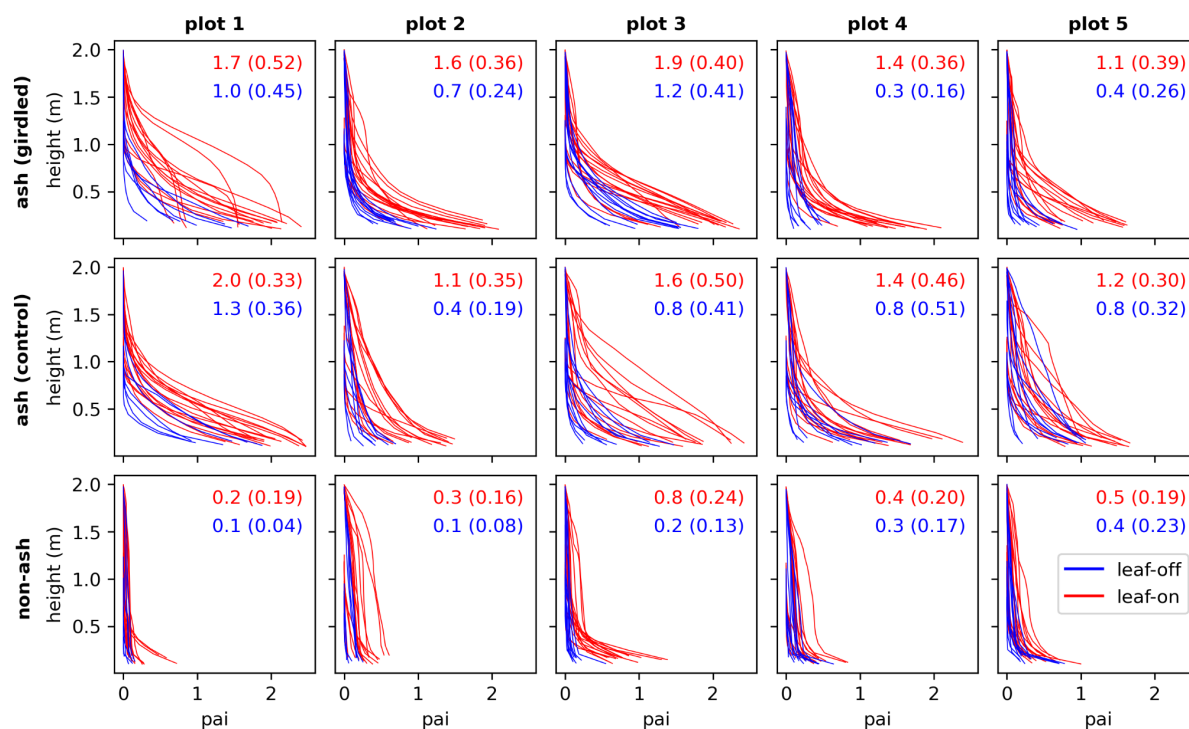


Figure 2. Vertically resolved PAI curves for each scan captured. Profiles have been truncated between 0.1 - 2 m and normalised so that PAI is 0 at 2 m. Values in red and blue are mean (standard deviation) PAI for summer and winter respectively.

Conclusions

This paper presents results from TLS scanning of forest understorey conducted in Wytham Woods, UK. A modified version of the “hinge angle” approach of Jupp *et al.* (2008) appears to be successful for characterising vertically resolved understorey PAI. Further scanning of the plots will allow an analysis of the impacts of changing light conditions on understorey vegetation following ash dieback.

Acknowledgements

This work is funded by NERC (NE/T007648/1). PW and MD also acknowledge funding from NERC National Centre for Earth Observation (NCEO). YM acknowledges funding from the Jackson Foundation. The authors would also like to thank the foresters of Wytham Woods, particularly for rescuing us from the mud!

References

- Calders, K., Armston, J. D., Newnham, G. J., Herold, M., & Goodwin, N. R. (2014). Implications of sensor configuration and topography on vertical plant profiles derived from terrestrial LiDAR. *Agricultural and Forest Meteorology*, 194(August), 104–117. <https://doi.org/10.1016/j.agrformet.2014.03.022>
- Calders, K., Origo, N., Disney, M., Nightingale, J., Woodgate, W., Armston, J., & Lewis, P. (2018). Variability and bias in active and passive ground-based measurements of effective plant, wood and leaf area index. *Agricultural and Forest Meteorology*, 252(September 2017), 231–240. <https://doi.org/10.1016/j.agrformet.2018.01.029>
- Jupp, D. L., Culvenor, D. S., Lovell, J. L., Newnham, G. J., Strahler, A. H., & Woodcock, C. E. (2008). Estimating forest LAI profiles and structural parameters using a ground-based laser called “Echidna”. *Tree Physiology*, 29(2), 171–181. <https://doi.org/10.1093/treephys/tpn022>
- Woodgate, W., Jones, S.D., Suarez, L., Hill, M.J., Armston, J.D., Wilkes, P., Soto-Berelev, M., Haywood, A., Mellor, A., 2015. Understanding the variability in ground-based methods for retrieving canopy openness, gap fraction, and leaf area index in diverse forest systems. *Agric. For. Meteorol.* 205, 83–95.

Predicting bilberry yields using ALS and other auxiliary data combined with NFI field plots

I. Bohlin¹, M. Maltamo², H. Hedenås¹, T. Lämås¹, J. Dahlgren¹, L. Mehtätalo³

¹Swedish University of Agricultural Sciences, Department of Forest Resource Management, SE-901 83 Umeå, Sweden
Email: {inka.bohlin; henrik.hedenas; tomas.lamas; jonas.dahlgren}@slu.se

²University of Eastern Finland, School of forest Sciences, P.O. Box 111, Joensuu, Finland
Email: matti.maltamo@euf.fi

³Natural Resources Institute Finland, Yliopistokatu 6, 80100 Joensuu, Finland
Email: lauri.mehtatalo@luke.fi

1. Introduction

Wild berries are the most utilized non-wood forest products by Nordic people (e.g. Kardell 1980, Turtiainen 2015) and essential nutriment of many animal species. Predicting and mapping non-wood forest products has been challenging because of the characteristics of non-wood products like small size, seasonality, rarity, difficult location, etc. In addition collecting field data for modelling is laborious and expensive. In the earlier studies field measurements of bilberries and accurate description of tree stock and site type have been used to model berry yields (Miina et al. 2009, Turtiainen 2015). However the general drawback of field measurements based approaches is that accurate field data is typically not available for the applications of the elaborated models.

Since 2003 worldwide unique berry yield data has been collected annually in the Swedish National forest inventory (NFI) (Fridman et al. 2014). The number of bilberries and cowberries are counted in small vegetation plots, inside the NFI plots and the annual berry yields of ripen berries kg ha⁻¹ are estimated to national and to county level. This unique time series of bilberry and cowberry data also offers high possibilities for spatial and temporal studies of berry yields in Sweden. That data combined with wall-to-wall remote sensing data (e.g. McRoberts et al. 2010), such as airborne laser scanning (ALS) data describing the forest structure and terrain variables and satellite and aerial images describing the forest types and tree species, offers possibilities to improve the forecasting of berry yields and maps in landscape level, of high interest to many users.

In this study we combined bilberry data from Swedish NFI with nationwide ALS data to predict bilberry yields. The specific aims were 1) to develop general prediction model for bilberry yield based on ALS data and other existing wall-to-wall data and 2) to identify laser based structural features of forest that can be linked to locations of the highest yield, highly interesting by the berry pickers. This information can be used for multi-objective forest planning, developing the next generation berry yield forecasting applications and mapping berry yields in forest landscape.

2. Data and methods

We used bilberry yield data from the Swedish NFI from 2007 to 2016 covering whole Sweden. Detailed berry inventory was done in two 0.25m² circular berry plots inside the NFI plot and the sum of flowers and berries of two berry plots was calculated. The final number of plots used for modelling was 13 715 and varied between years and geographical locations of laser scanning.

The number of flowers and berries is depended on the inventory day of the growing season. The time difference between middle of July (bilberries expected to be ready for picking) and Julian day of field data collection was used as one predictor variables in the models. This variable indicated the change in berry amount (% per day) over the season.

We used ALS data from Swedish National Land Survey from 2009 to 2014. All ALS based and other wall-to-wall metrics calculated were extracted from the 7 m buffer around the center of the NFI field plots (corresponds the size of temporary NFI plots). ALS point cloud data were extracted from each NFI plot and point cloud metrics were calculated using the FUSION software (McGaughey 2021). Percentage of first echoes above height limit of 2 meter called “canopy cover”, Elev.P95 (height, where 95 % of the first echoes are accumulated) called “tree height” and “shrub cover” from first echo data

((percentage of echoes below 2 meter – percentage of echoes below 0.5 m)/(percentage of echoes below 2 meter), %), were selected to identify the critical structural differences in presence/absence data (high berry yield/no berries) to locate the highest bilberry yields. Other auxiliary data used on models included e.g. ALS based terrain variables, bioclimatic variables (worldclim.com), tree species variables from SLU forest map, Corine-land cover map, and soiltype and soildepth maps. The mean and standard deviation of raster cells (continues variables) or the maximum (categorical variables) were extracted from each plot to represent the predictor variables for the models.

Models were created for bilberry yields (number of berries) using generalized linear mixed effect models. Models for bilberry counts were expressed by the log-link function with Poisson response. The hierarchy and unbalanced structure of the data was taken account by random effects at different levels (county, laser-block, cluster). Mixed effect models were fitted using glmmPQL function of the R-software (<https://www.r-project.org/>) and bias-correction was applied in prediction for new dataset.

The structural differences of commonly used ALS based variables were demonstrated in histograms of presence/absence (high bilberry yield /no berries) data. Only bilberry plots with ripen berries were included. Five percent of the plots with the highest berry amount was selected to represent the high bilberry yield.

3. Results

The ALS based canopy cover was found to be important variable in bilberry model. Other significant variables were e.g. ALS based height variance, shrub cover, height above sea, slope, soil wetness and terrain ruggedness, satellite based species specific volume and percentage, seasonality of temperature and precipitation and annual precipitation, inventory year, soil type and land use class. The time difference between Julian day when berries were expected to be ripen and inventory day was also significant predictor variable and this variable showed 1,5 % decrease for bilberry per day during the season. R^2 was 0.4 for the full bilberry model and 0.08 for the fixed part and there was high variation between plots in the prediction accuracy. Model underestimated especially the higher berry yields.

Based on our study the highest bilberry yield was identified in forests with canopy cover of 50 % (Figure 1, left), the canopy height of 15 meter and the shrub cover close to zero. Even though our model could not give very accurate estimates for the berry yields, the model can be used as an effective tool for predicting the most potential locations for the berry yields in forest landscape. To demonstrate this we predicted the most potential locations of bilberry yields in small study area (Figure 1, right).

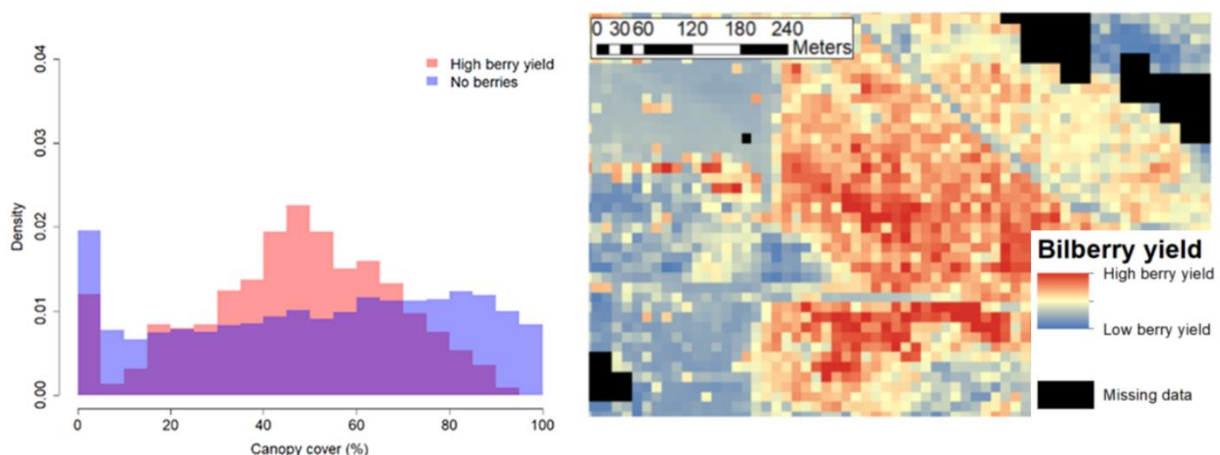


Figure 1: Density distribution of ALS based canopy cover in plots with high bilberry yield and no berries (left) and predicted potential locations of bilberry yields in forest landscape (right).

4. Discussion and conclusions

This is the first study where ALS and other wall-to-wall remote sensing variables were used to model bilberry yields and also first berry yield models done in Sweden. Here we also obtained valuable information about suitable remote sensing based variables for predicting bilberry yields and about the ALS based structural features which are reflecting the locations of the highest bilberry yield. Our maps

of potential berry yields are much needed as input for e.g. land-use planning at landscape level (e.g. European Commission 2016). For local berry pickers, the berry yield maps makes it easier to find the berries in the forest landscape.

Our results are supporting the earlier findings, which have showed that best bilberry yield can be found in mature stands with conifer dominance which are not too dense (e.g. Raatikainen et al. 1984, Miina et al. 2009, Turtiainen 2015). In addition more important than e.g. tree species is the light reaching bilberry stand. It has been found that the crown density of 10–50 % allows bilberry to flower and produce berries optimally (e.g. Raatikainen et al. 1984). This supports especially the usability of ALS based canopy cover in prediction of bilberry yields.

Our study also supports the earlier findings that accurate prediction of berry yields is difficult because of the complexity of berry yield production; variables used in the models can not catch the spatial and temporal variation of berry yields for accurate berry yield modelling. But models can be used as an effective tool for predicting the most potential locations for the berry yields.

More accurate wall-to-wall prediction of berry yields would demand more accurate information about tree species and especially site fertility, which has been critical variable in earlier berry yield models (e.g. Miina et al. 2009, Turtiainen 2015), but not accurately available in wall-to-wall data yet. To improve the yearly prognoses of berry yields more accurate temporal and spatial data, such as weather, pollination, site type and operational history data together with localized observations of berry yield developments could improve estimates.

Despite the difficulties of modelling bilberry yields, our model could be imported to the forest planning system, like Heureka in Sweden (Wikström et al. 2011) and then the stand level prognosis of bilberry yield development under different forest management alternatives could be produced (e.g. Turtiainen 2015). This would support the forest owners growing interest for integrating multiple aspects of forest in management planning. So far no berry yield models have been integrated in forest planning systems in Sweden.

Acknowledgements

This study is supported by FORMAS, project “Adding non-wood forest products as part of ecosystem services: Improving berry yield mapping prediction and mapping” (2016–20056) and Academy of Finland Flagship Programme “Human-Machine Interplay - Building Resilience, Redefining Value Networks and Enabling Meaningful Experiences (UNITE)” (decision number 337655), which are acknowledged.

References

- European Commission, 2016, Mapping and assessment of ecosystems and their services. *Mapping and assessing the condition of Europe's ecosystems: Progress and challenges. 3rd Report – Final, March 2016*, European Union, 178 p.
- Fridman J, Holm S, Nilsson M, Nilsson P, Ringvall AH and Ståhl G, 2014, Adapting National Forest Inventories to changing requirements – the case of the Swedish National Forest Inventory at the turn of the 20th century. *Silva Fennica* 48(3), article id 1095.
- Kardell L, 1980, Occurrence and production of bilberry, lingonberry and raspberry in Sweden's forests. *Forest Ecology and Management* 2: 285–298.
- McGaughey RJ, 2021, FUSION/LDV: Software for LIDAR data Analysis and Visualization, January 2021 – FUSION Version 4.20. *United States Department of Agriculture*, Washington DC, 212 p.
- McRoberts RE, Cohen WB, Næsset E, Stehman SV, Tomppo EO, 2010, Using Remote sensing data to construct and assess and forest attribute maps and related spatial products. *Scandinavian Journal of Forest Research* 25(4):340-367.
- Miina J, Hotanen J-P and Salo K, 2009, Modelling the abundance and temporal variation in the production of bilberry (*Vaccinium myrtillus* L.) in Finnish mineral soil forests. *Silva Fennica* 43(4): 577–593.
- Raatikainen M, Rossi E, Huovinen J, Koskela M-L, Niemelä M and Raatikainen T, 1984, The yields of the edible wild berries in central Finland. *Silva Fennica* 18, 199–219. (In Finnish with English summary).
- Turtiainen M, 2015, Modelling bilberry and cowberry yields in Finland: different approaches to develop models for forest planning calculations. *Dissertationes Forestales* 185, 56 p.
- Wikström P, Edenius L, Elfving B, Eriksson LO, Lämås T, Sonesson J, Öhman K, Wallerman J, Waller C and Klintebäck F, 2011, The Heureka forestry decision support system: An overview. *Mathematical and Computational Forestry & Natural-Resource Sciences* 3(2): 87–94.

Examining Structural Complexity of Scots Pine Trees – A Comparison between Terrestrial Laser Scanning and Photogrammetric Point Clouds

N. Tienaho¹, N Saarinen², T. Yrttimaa^{2,1}, V. Luoma¹, E. Honkavaara³, N. Viljanen³, S. Huuskonen⁴, J. Hynynen⁴

¹Department of Forest Sciences, University of Helsinki, P.O. Box 27, 00014 University of Helsinki, Finland
Email: noora.tienaho@helsinki.fi, ville.luoma@helsinki.fi

²School of Forest Sciences, University of Eastern Finland, P.O. Box 111, 80101 Joensuu, Finland
Email: ninni.saarinen@uef.fi, tuomas.yrttimaa@uef.fi

³Department of Remote Sensing and Photogrammetry, Finnish Geospatial Research Institute, National Land Survey of Finland, Geodeetinrinne 2, FI-02430 Masala, Finland
Email: eija.honkavaara@nls.fi, niko.viljanen@nls.fi

⁴Natural Resources Institute Finland, Latokartanonkaari 9, 00790 Helsinki, Finland
Email: saija.huuskonen@luke.fi, jari.hynynen@luke.fi

1. Introduction

Forest structural complexity is related to various ecological processes and ecosystem services (e.g. Pommerening 2002, Neill & Puettmann 2013, Hardiman et al. 2013). It can also improve the forests' ability to adapt to environmental changes. In order to implement the management for complexity and to estimate its functionality, the level of structural complexity must be defined.

Structural complexity can be described mathematically by fractal analysis (Mandelbrot 1977). Fractal dimension describes how complex a self-similar object is (Camarretta et al. 2020), and a box dimension is a method for estimating the fractal dimension of an object that is not exactly self-similar but fractal-like (Feldman 2012, Seidel 2018). In forestry applications, the box dimension has been used to measure the complexity of individual trees (e.g. Seidel et al. 2019a, b, Saarinen et al. 2021). The box dimension reflects simultaneously a number of different structural attributes (Seidel et al. 2019b) and has been associated, for example, with tree species, availability of light (Seidel 2018), type and strength of competition (Seidel 2018, Dorji et al. 2019), and tree growth (Seidel et al. 2019a, Saarinen et al. 2021).

This study compares the structural complexity of Scots pine (*Pinus sylvestris*, L.) trees measured by two remote sensing techniques, namely, terrestrial laser scanning (TLS) and aerial imagery acquired with unmanned aerial vehicle (UAV). The premise is that TLS provides the best available information on structural complexity as the point density in TLS point clouds is larger than in UAV, and as TLS is able to penetrate vegetation. Research question are: 1) do TLS and UAV measured structural complexity differ significantly from each other, 2) what explains the possible divergence between the structural complexity, and 3) does the forest structure affect the divergence between TLS and UAV measured structural complexity of individual Scots pine trees?

2. Data and Methods

The Scots pine tree dominated study area is located in southern Finland, site biome is southern boreal forest zone, and the fertility is mesic heath (Saarinen et al. 2021). During the 2000s, the study area was exposed to six different thinning treatments plus one control group with no treatment. Thinning treatments included two levels of thinning intensity (moderate, intensive) and three thinning types (from below, from above, systematic from above).

The study area was field measured during 2018–2019 (Saarinen et al. 2021). Both TLS and UAV measurements were implemented in the fall of 2018. TLS point clouds were acquired using Trimble TX5 3D phase-shift laser scanner, and UAV imagery was acquired using Gryphon Dynamics quadcopter equipped with two Sony A7R II digital cameras. TLS produced point clouds directly whereas aerial imagery was converted into point clouds with structure from motion (SfM) technology.

Box dimension (D_b) values for each Scots pine tree ($n=2065$) were calculated from TLS and UAV measured 3D point clouds. D_b -values were calculated with the natural logarithms of boxes needed (N) and the edge length of each box divided by the initial box size (r). The slope of the trend line determined the D_b -value. Welch's t-test was used to compare the means of TLS and UAV measured D_b -values. The dispersions of D_b -values, tree heights and point clouds were examined with standard deviations, and the distribution of TLS and UAV measured points was examined by dividing trees longitudinally into two equal parts and calculating the proportion of points below and above. The differences between the ranges of TLS and UAV measured x-, y- and z-axes were examined by subtracting UAV ranges from TLS ranges. Simple linear regression was used to examine whether the number of TLS and UAV measured points explained the variation in D_b -values and whether the number of the smallest boxes explained the variation in D_b -values. Linear mixed-effect model was used to examine whether different thinning treatments affected TLS and UAV measured D_b -values. Tukey's honest significant test was used to scrutinise between which thinning treatments there was a statistically significant difference in D_b -values. The correlations between different variables were tested with Pearson correlation test.

3. Results

TLS and UAV measured D_b -values differed significantly from each other (p -value <0.001) and did not provide comparable information on the structural complexity of the individual Scots pine trees. On average, UAV measured D_b -values were 5% larger than TLS measured values. The divergence between the TLS and UAV measured D_b -values was explained by the differences in the number and distribution of the points in the point clouds and by the differences in the estimated tree heights and number of boxes in the box dimension method.

TLS measured 15 times more points than UAV. On average, 65% of TLS measured points were placed below and 35% above the midpoint of the tree height. With UAV, the percentages were 22% below and 78% above. The standard deviations of the points with respect to all axes were bigger in UAV measurements compared to TLS. High correlation occurred between TLS and UAV measured D_b -values (75%) and between the number of UAV measured points and D_b -values (71%). The enhancement in the amount of UAV measured points did not erase the divergence between TLS and UAV. Compared to field measurements, UAV underestimated the tree heights more than TLS, and the number of the smallest boxes was on average 64% bigger in UAV than in TLS. The number of the smallest boxes affected the variation in TLS and UAV measured D_b -values ($R^2= 0.79, 0.68$, respectively).

Forest structure significantly affected the variation of both TLS and UAV measured D_b -values (p -values <0.001), but the divergence between TLS and UAV measured D_b -values remained in all the treatments. Plots with no treatment differed from all other thinning treatments except from the moderate systematic thinning. D_b -values were the largest with intensive thinning treatments and the smallest on plots with no treatment. The largest point densities were found on plots with intensive thinning from below and the lowest on control plots. In terms of the individual tree detection, the number of obtained points in the point cloud, and the distribution of these points, UAV measurements were better in sparse compared to dense forest structure.

4. Discussion

The standard deviations of the points were larger in UAV measurements compared to TLS since TLS measured points were more closely clustered near the stem, whereas with UAV, the outer edges of the crown affected more. With UAV, more points were obtained from the upper part of the tree but at the same time, the ground vegetation was not properly excluded, which increased the standard deviation of the points. The smaller ranges UAV measured points is explained by the fact that UAV method was not able to observe the extreme points as well as TLS and was averaging the treetops and sides. In general, the more the tree height is underestimated, the smaller the initial box size in D_b -calculations is, and the smaller the boxes, the more of them are needed to cover trees. Because a larger number of scattered boxes yields a higher D_b -value, the UAV measured D_b -values were higher than TLS measured.

The competitive pressure has been confirmed to reduce D_b -values (Juchheim et al. 2017, Dorji et al. 2019, Seidel et al. 2019a, Saarinen et al. 2021). In this study, the thinning intensity was observed to affect more than the thinning type. Largest D_b -values were reached on the plots with intensive thinnings (less competition and more space to grow). On the control plots, the D_b -values were smaller and also the standard deviations of the points were smaller. That is, the trees were structurally less complex and more similar to each other when compared to trees on the other plots.

5. Conclusions

Photogrammetric point clouds generated from UAV imagery did not result in comparable structural complexity information to TLS. UAV measurements were better in forests with intensive thinning indicating the method's better suitability in sparse forest conditions. Future research should study whether TLS and UAV can be used as complementary techniques to provide more accurate and holistic view of the structural complexity in the perspective of both tree- and stand-level. UAV-LiDAR data should be studied also as it may better characterize crown and stem.

Acknowledgements

The study was funded by the Academy of Finland (project numbers 315079 and 327861).

References

- Dorji, Y, Annighöfer, P, Ammer, C and Seidel, D, 2019, Response of Beech (*Fagus sylvatica* L.) trees to competition. New insights from using fractal analysis. *Remote Sensing*, 11: 2656.
- Feldman, DP, 2012, *Chaos and fractals. An elementary introduction*. Oxford University Press, Oxford, UK.
- Hardiman, BS, Gough, CM, Halperin, A, Hofmeister, K., Nave, LE, Bohrer, G and Curtis, PS, 2013, Maintaining high rates of carbon storage in old forests. A mechanism linking canopy structure to forest function. *Forest Ecology and Management*, 298: 111–119.
- Juchheim, J, Annighöfer, P, Ammer, C, Calders, K, Raunonen, P and Seidel, D, 2017, How management intensity and neighborhood composition affect the structure of beech (*Fagus sylvatica* L.) trees. *Trees* 31:1723–1735.
- Mandelbrot, BB, 1977, *The fractal geometry of nature*. W.H. Freeman company, New York, USA.
- Neill, AR and Puettmann, KJ, 2013, Managing for adaptive capacity. Thinning improves food availability for wildlife and insect pollinators under climate change conditions. *Canadian Journal of Forest Research* 43(5): 428–440.
- Pommerening, A, 2002, Approaches to quantifying forest structures. *Forestry* 75: 305–324.
- Saarinen, N, Calders, K, Kankare, V, Yrttimaa, T, Luoma, V, Junttila, S, Huuskonen, S, Hynynen, J and Verbeeck, H, 2021, Understanding 3D structural complexity of individual Scots pine trees with different management history. *Ecology and Evolution* 11: 2561–2572.
- Seidel, D, 2018, A holistic approach to determine tree structural complexity based on laser scanning data and fractal analysis. *Ecology and Evolution* 8: 128–134.
- Seidel, D, Annighöfer, P, Stiers, M, Zemp, CD, Burkardt, K, Ehbrecht, M, Willim, K, Kreft, H, Hölscher, D and Ammer, C, 2019a, How a measure of tree structural complexity relates to architectural benefit-to-cost ratio, light availability, and growth of trees. *Ecology and Evolution* 9: 7134–7142.
- Seidel, D, Ehbrecht, M, Dorji, Y, Jambay, J, Ammer, C and Annighöfer, P, 2019b, Identifying architectural characteristics that determine tree structural complexity. *Trees* 33: 911–919.

Quantifying forest dynamics in a free-air CO₂ enrichment experiment using terrestrial laser scanning

Kim Calders¹, Glenn Newnham², Matthias Boer³, Mathias Disney^{4,5}, David Ellsworth³, Martin Herold⁶, Belinda Medlyn³, Stuart Phinn⁷, Pasi Raunonen⁸, Peter Scarth⁷, Dan Wu⁷, John Hickson⁹, Hans Verbeeck¹

¹CAVElab - Computational & Applied Vegetation Ecology, Faculty of Bioscience Engineering, Ghent University, Belgium; ²CSIRO, Private Bag 10, Clayton South, VIC 3169, Australia; ³Hawkesbury Institute for the Environment, Western Sydney University, Locked Bag 1797, Penrith, NSW, 2751 Australia; ⁴UCL Department of Geography, Gower Street, London WC1E 6BT, UK; ⁵NERC National Centre for Earth Observation (NCEO), UK; ⁶Laboratory of Geo-Information Science and Remote Sensing, Wageningen University & Research, Droevendaalsesteeg 3, 6708 PB Wageningen, The Netherlands; ⁷Remote Sensing Research Centre, School of Earth and Environmental Sciences, University of Queensland, Brisbane 4072, Australia; ⁸Computing Sciences, Tampere University, Korkeakoulunkatu 7, 33720 Tampere, Finland; ⁹School of Geography, University of Nottingham, Nottingham, UK.

1. Introduction

Deforestation and forest degradation account for about 12% of global anthropogenic carbon emissions, which is second only to fossil fuel combustion (Le Quéré et al., 2009). This estimate is highly uncertain due to inadequate estimates of forest carbon stocks and is expected to range from 6 to 17% (van der Werf et al., 2009). Carbon emissions are partly compensated for by carbon uptake from the regrowth of secondary forests and the rebuilding of soil carbon pools following afforestation. However, the global distribution of terrestrial carbon sinks and sources is highly uncertain. Constraining the inaccuracy of these carbon estimates is essential to quantify benefits of avoided deforestation, return on investment in forest management and to support effective future climate mitigation actions (Pan et al., 2011). The debate concerning a possible Amazon forest die-back, i.e. catastrophic losses of forest cover and biomass, illustrates the growing concern that terrestrial ecosystems (and tropical forests in particular) might not be able to maintain uptake of anthropogenic emissions at the current rate (Huntingford et al., 2013). A better understanding of forest growth dynamics will improve our understanding of the carbon cycle and mechanisms responsible for terrestrial sources and sinks of carbon, reducing their uncertainties of magnitude and distribution (Pan et al., 2011).

Our current knowledge about forest growth is limited, mainly due to challenges in accurately measuring tree structure, e.g. tree height and aboveground biomass (AGB), repeatedly and objectively. Diameter at breast height (DBH) is often used to indirectly estimate height or AGB through empirical relationships (i.e. allometric models), or to quantify forest growth (Ellsworth et al., 2017) as it is relatively easy to measure. However, due to the difficulty and high cost of destructively sampling trees, the measurements that underpin those allometric models are based on a limited sample size, which is also heavily biased towards smaller trees.



Figure 1: Illustrations of the free-air CO₂ enrichment experiment EucFACE.

Novel techniques using 3D terrestrial LiDAR (also referred to as terrestrial laser scanning, TLS) can provide us with a more accurate way to estimate the structure of trees (Calders et al., 2015a). TLS can objectively measure the canopy structure in 3D with high detail and accuracy, and recent work on characterising forest structure using TLS showed (a) a much better agreement with destructively harvested reference measurements compared to traditional techniques (Calders et al., 2015a); and (b) superiority and stability of TLS measurements in the context of repeatable measurements (Calders et al., 2015b).

2. Measuring forest growth in a free-air CO₂ enrichment experiment

EucFACE is a free-air CO₂ enrichment experiment that consists of six circular 25 m rings in a mature broadleaved evergreen forest (Figure 1). The main species is *Eucalyptus tereticornis*, which has a distribution through sub-tropical and temperate zones in Australia. Three rings have been exposed to a CO₂ increment of +150 parts per million (i.e. the projected global atmospheric CO₂ concentration for 2050) compared to ambient concentrations since 2012, with the other three rings serving as control plots. TLS data has been collected at EucFACE rings in 2012, 2015, 2018 and 2020 using a RIEGL VZ-400. Figure 2 shows a cross section through the TLS data of one of the rings in 2012. The objective of this work is to test the hypothesis that “*elevated CO₂ concentration levels have an effect on forest growth?*”. Here, we will show results from estimating tree growth explicitly through 3D TLS data over an eight-year period, taking into account the full structure of the tree, and link this to elevated CO₂ concentration levels. We will show results from both (a) gap fraction analysis and (b) the extraction of tree point clouds from within each EucFACE ring. We will then show the time progression of stand structural dynamics of plant area index, as well as individual tree parameter dynamics including DBH, tree height and crown area.

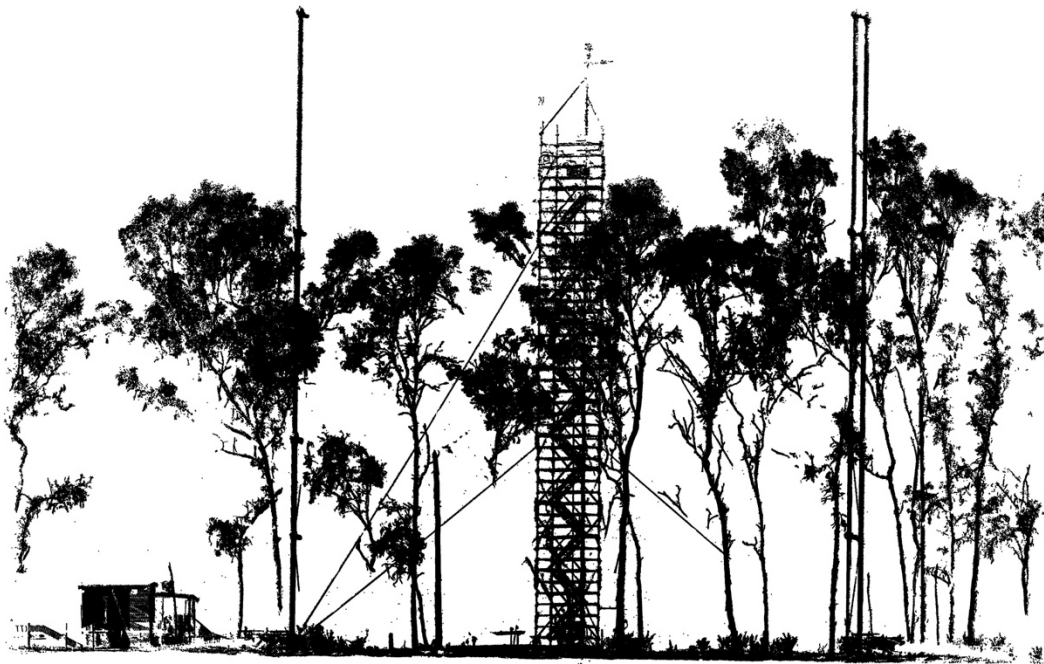


Figure 2: Terrestrial laser scanning 2012 data cross section of ring 1 of the EucFACE experiment.

Acknowledgements

KC was funded by the European Union’s Horizon 2020 research and innovation programme under the Marie Skłodowska-Curie grant agreement No 835398.

References

- Calders, K. et al. (2015a) Nondestructive estimates of above-ground biomass using terrestrial laser scanning. *Methods Ecol. Evol.* 6, 198-208.
- Calders, K. et al. (2015b) Monitoring spring phenology with high temporal resolution terrestrial LiDAR measurements. *Agric. For. Meteorol.* 203, 158-168.
- Ellsworth, D. et al. (2017) Elevated CO₂ does not increase eucalypt forest productivity on a low-phosphorus soil. *Nat. Clim. Change* 7, 279–282.
- Huntingford, C. et al. (2013) Simulated resilience of tropical rainforests to CO₂-induced climate change. *Nat. Geosci.* 6, 268-273.
- Le Quéré, C. et al. (2009) Trends in the sources and sinks of carbon dioxide. *Nat. Geosci.* 2, 831-836.
- Pan, Y. et al. (2011) A Large and Persistent Carbon Sink in the World's Forests. *Science* 333, 988-993
- van der Werf, G. R. et al. (2009) CO₂ emissions from forest loss. *Nat. Geosci.* 2, 737–738

Quantifying Structural Response in a Through-fall Drought Experiment Using Terrestrial Laser Scanning

Louise Terryn¹, Kim Calders¹, Patrick Meir^{2,3}, Hans Verbeeck¹

¹CAVELab - Computational & Applied Vegetation Ecology, Faculty of Bioscience Engineering, Ghent University, Belgium
Email: {Kim.Calders; Louise.Terryn; Hans.Verbeeck}@UGent.be

²School of GeoSciences, University of Edinburgh, Edinburgh, UK

³Research School of Biology, Australian National University, Canberra, ACT, Australia
Email: patrick.meir@anu.edu.au

1. Introduction

Terrestrial ecosystems provide a very wide range of essential ecosystem services, but these services are under increased levels of stress due to climate change. An increase in global temperature is leading to more extreme events, such as forest fires and droughts. Drought is one of the most important potential threats to tropical forests, and can result in forest die-back, i.e. catastrophic losses of forest cover and biomass. This illustrates the growing concern that terrestrial ecosystems (and tropical forests in particular) might not be able to maintain uptake of anthropogenic emissions at the current rate (Huntingford et al., 2013; Verbesselt et al., 2016).

Ecosystem structure and climate are closely-linked: changes in climate lead directly to physical changes in ecosystem structure and vice versa (Grimm et al., 2013). Different global change factors, such as fire, nutrient deposition and drought, could have an impact on forest structure. Feedbacks between canopy structure and seasonal droughts, for example, suggests that tree phenological and hydrological strategies are linked in tropical forests, which could determine which tree species will survive under shifting precipitation regimes (Smith et al., 2019). To improve our understanding of these mechanisms and ecosystem resilience, we require information of the fine-scale structural heterogeneity between individual trees, as well as forest structural differences at larger spatial scales. This will be key for effective forest management and to support climate mitigation actions appropriately (Houghton et al., 2009; Pan et al., 2011).

Drought experiments simulate drought conditions by excluding rainfall from a given zone, and local consequences on soil, tree or ecosystem functioning are monitored. These drought experiments bring highly valuable information on the mechanisms involved in the response of ecosystems to drought (Bonal et al., 2016). Inducing plot-level droughts is logistically and financially difficult, but it is important to operate at a relatively large scale because many adult trees have laterally extensive root systems (Laurance 2015).

Novel techniques using 3D laser scanning (LiDAR – Light Detection and Ranging) can provide us with a new way to estimate the structure of individual trees (Calders et al., 2015; Raunonen et al., 2013; Hackenberg et al., 2015). Terrestrial laser scanning (TLS) can measure the canopy structure in 3D with high detail, and several algorithms have recently been developed to produce full 3D models of trees down to fine (cm) scale. Terryn et al. (2020) calculated 17 different structural tree metrics in the context of tree species identification.

Within this study we explore the same structural metrics to determine if induced drought affects tropical tree structure on a time-span of 3 years using TLS.

2. Data and Methods

2.1 Study site

The Daintree drought experiment is a through-fall drought experiment which has been maintained continuously since 2015 in a lowland rainforest at the Daintree Rainforest Observatory near Cape Tribulation, in north Queensland, Australia (detailed in Laurance, 2015, Tng et al., 2018). The experiment comprises one 0.6 ha control plot with no drought infrastructure and a 0.4 ha drought plot. The site is characterised by a mean annual rainfall of 5143 mm/year and a mean temperature of 24.4°C.

2.2 Laser scanning data collection

TLS data were collected in August 2018 (during the dry season) from the Daintree drought experiment plot (Figure 1). TLS was collected using a RIEGL VZ-400 terrestrial laser scanner (RIEGL LaserMeasurement Systems, Horn, Austria), which provides multiple returns for a single outgoing laser pulse. The control part of the plot was scanned in a 10 m by 10 m regular grid and at each scan location an additional scan was acquired with the instrument tilted at 90° from the vertical to sample a full hemisphere. The drought experiment part of the plot was scanned under the drought panels as well as a few scans in the gutters between the panels (Figure 1). Reflective targets were used to co-register all the scan locations to a single point cloud using RIEGL's RiSCAN PRO software package. The co-registration of the scan positions was further optimized with the Multi-Station Adjustment (MSA) algorithm, within the RiSCAN PRO software package. The MSA algorithm modifies the orientation and position of each scan in several iterations to calculate the best overall fit.



Figure 1 Illustration of the drought experiment and the RIEGL VZ-400 terrestrial laser scanner.

2.3 Expected tree structure quantification

Individual trees from the control as well as the experiment will be automatically extracted from TLS using a novel individual tree segmentation routine based on shortest-path calculations (Raumonen et al., 2021). Next, tree structure will be modelled through Quantitative Structural Models (QSM) built with *TreeQSM* (Raumonen et al., 2013). From these QSMs different structural tree metrics relating to branching structure and, crown and tree dimensions will be obtained (Terry et al., 2020). The process from TLS point cloud to individual tree structural features is illustrated in Figure 2.

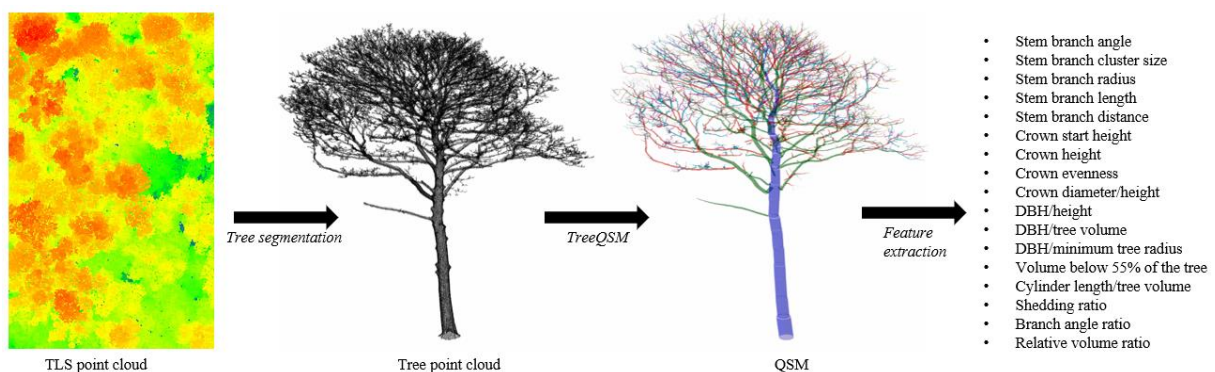


Figure 2 Illustration of the feature extraction process.

3. Expected outcomes

Tng et al. (2018) showed that species-specific systematic variation in hydraulic-related wood anatomy and leaf traits was a response to 24 months of drought stress in the Daintree drought experiment. They showed that relative to controls, drought-affected individuals variously exhibited trait measures consistent with increasing hydraulic safety (e.g. narrower or less vessels, reduced vessel groupings,

lower theoretical water conductivities, less water storage tissue and more abundant fiber in their wood, and more occluded vessels) (Tng et al., 2018). These responses could in their turn result in changes in the 3D structure of the drought-affected trees. We expect that some structural traits might take longer to respond to stress, and some others (e.g. leaf and branching angles) to show responses.

Acknowledgements

The fieldwork was funded by BELSPO (Belgian Science Policy Office) in the frame of the STEREO III programme - project 3D-FOREST (SR/02/355). We thank the Daintree Research Observatory for their assistance with fieldwork.

References

- Bonal, D., Burban, B., Stahl, C., Wagner, F. and Hérault, B., 2016. The response of tropical rainforests to drought—lessons from recent research and future prospects. *Annals of forest science*, 73(1), pp.27-44.
- Grimm, N.B., Chapin III, F.S., Bierwagen, B., Gonzalez, P., Groffman, P.M., Luo, Y., Melton, F., Nadelhoffer, K., Pairs, A., Raymond, P.A. and Schimel, J., 2013. The impacts of climate change on ecosystem structure and function. *Frontiers in Ecology and the Environment*, 11(9), pp.474-482.
- Hackenberg, J., Spiecker, H., Calders, K., Disney, M. and Raunonen, P., 2015. SimpleTree—an efficient open source tool to build tree models from TLS clouds. *Forests*, 6(11), pp.4245-4294.
- Houghton, R.A., Hall, F. and Goetz, S.J., 2009. Importance of biomass in the global carbon cycle. *Journal of Geophysical Research: Biogeosciences*, 114(G2).
- Huntingford, C., Zelazowski, P., Galbraith, D., Mercado, L.M., Sitch, S., Fisher, R., Lomas, M., Walker, A.P., Jones, C.D., Booth, B.B. and Malhi, Y., 2013. Simulated resilience of tropical rainforests to CO₂-induced climate change. *Nature Geoscience*, 6(4), pp.268-273.
- Laurance, S., 2015. A raincoat for a rainforest. *Australasian Science*, 36(9), pp.20-22.
- Pan, Y., Birdsey, R.A., Fang, J., Houghton, R., Kauppi, P.E., Kurz, W.A., Phillips, O.L., Shvidenko, A., Lewis, S.L., Canadell, J.G. and Ciais, P., 2011. A large and persistent carbon sink in the world's forests. *Science*, 333(6045), pp.988-993. [13] Calders, K., Newnham, G., Burt, A., Murphy, S., Raunonen, P., Herold, M., ... & Kaasalainen, M. (2015). Nondestructive estimates of above-ground biomass using terrestrial laser scanning. *Methods in Ecology and Evolution*, 6(2), 198-208.
- Raunonen, P., Brede, B., Lau, A., Bartholomeus, H., 2021. A Shortest path based tree isolation method for UAV Lidar data, in: *IGARSS 2021 International Geoscience and Remote Sensing Symposium*, July 12-16, Brussels. Brussels.
- Raunonen, P., Kaasalainen, M., Åkerblom, M., Kaasalainen, S., Kaartinen, H., Vastaranta, M., Holopainen, M., Disney, M. and Lewis, P., 2013. Fast automatic precision tree models from terrestrial laser scanner data. *Remote Sensing*, 5(2), pp.491-520.
- Smith, M.N., Stark, S.C., Taylor, T.C., Ferreira, M.L., de Oliveira, E., Restrepo-Coupe, N., Chen, S., Woodcock, T., Dos Santos, D.B., Alves, L.F. and Figueira, M., 2019. Seasonal and drought-related changes in leaf area profiles depend on height and light environment in an Amazon forest. *New Phytologist*, 222(3), pp.1284-1297.
- Terryn, L., Calders, K., Disney, M., Origo, N., Malhi, Y., Newnham, G., Raunonen, P. and Verbeeck, H., 2020. Tree species classification using structural features derived from terrestrial laser scanning. *ISPRS Journal of Photogrammetry and Remote Sensing*, 168, pp.170-181.
- Tng, D.Y., Apgaua, D.M., Ishida, Y.F., Mencuccini, M., Lloyd, J., Laurance, W.F. and Laurance, S.G., 2018. Rainforest trees respond to drought by modifying their hydraulic architecture. *Ecology and evolution*, 8(24), pp.12479-12491.
- Verbesselt, J., Umlauf, N., Hirota, M., Holmgren, M., Van Nes, E.H., Herold, M., Zeileis, A. and Scheffer, M., 2016. Remotely sensed resilience of tropical forests. *Nature Climate Change*, 6(11), pp.1028-1031.

Vegetation fuel type dynamics and classification using multitemporal LiDAR

Alba García-Cimarras¹, José Antonio Manzanera¹, Rubén Valbuena²

¹ Research Group SILVANET, Universidad Politécnica de Madrid (UPM), ETSI Montes, Forestal y del Medio Natural, 28040 Madrid, Spain.
Email: alba.gcimarras;joseantonio.manzanera@upm.es

²Thoday Building, School of Natural Sciences, Bangor University, Bangor LL57 2UW, UK
Email: r.valbuena@bangor.ac.uk

1. Introduction

Traditionally, the studies on vegetation dynamics have used spectral sensors, but they have some limitations such as the inability to penetrate forest canopies (Keane et al 2001). LiDAR technology has proven to be a reliable tool to measure forest structure parameters (Botallico et al 2017) and it is able to overcome that drawback. In this study, forest vertical structure has been associated to the seven different fuel types of the Prometheus classification system (Prometheus S.V 1999).

The purpose of this study is to present a cost-effective methodology to provide a fuel type classification and dynamics of the vegetation based on conditional rules and according to the Prometheus classification system.

2. Data and Methods

2.1 Study area

The study area was located in La Rioja (Spain) and it was a tile with a side of two Km with south-west corner coordinates in UTM: 504,000; 4,660,000 (Figure 1).



Figure 1. Location of the study area (García-Cimarras et al 2021)

2.2 LiDAR data

The discrete LiDAR data used in this study was open-access and provided by the Spanish Geographic Institute (IGN). Two different datasets were used in order to compare the vegetation structure: the 2010 dataset, with a scan density of $0.5 \text{ pulses} \cdot \text{m}^{-2}$ and the 2016 dataset, that had a scan density of $2 \text{ pulses} \cdot \text{m}^{-2}$. The LiDAR data was processed, and the metrics were extracted for a $20 \times 20 \text{ m}$ spatial resolution grid, using FUSION software v.4.10 and RStudio v.1.3.1093.

2.3 Fuel type Classification

In order to assign a fuel type (FT) to each cell, the rules shown in Table 1 were followed:

Table 1. Fuel type classification system used for the LiDAR data. Mode: the stratum with the highest number of returns, 2nd Mode is the second height interval with more returns. 3rd Mode: the third height interval with more returns. Max.Elev: maximum elevation (García-Cimarras et al 2021)

Ground (%)	Cover (%)	Mode (m)	2 nd Mode (m)	3 rd Mode (m)	Max.Elev (m)	Description	Fuel Type		
>60		0.0-0.3				Pastures	FT1		
		0.3-0.6				Pastures	FT1		
		0.6-2.0				Low shrubs	FT2		
		2.0-4.0				Medium shrubs	FT3		
	<50			0.0-0.3			High shrubs	FT4	
				0.3-0.6			Pastures	FT1	
				0.6-2.0			Low shrubs	FT2	
				2.0-4.0			Medium shrubs	FT3	
		>4.0			0.6-2.0			High shrubs	FT4
					2.0-4.0			Forest without understory	FT5
	≤60			0.0-0.3			Forest with shrub layer	FT6	
				0.3-0.6			Forest with shrub layer	FT6	
				0.6-2.0		>12.0	Forest with shrub layer	FT6	
				2.0-4.0		≤12.0	Forest with vertical continuity	FT7	
≥50				0.0-0.3		>12.0	Forest with shrub layer	FT6	
				0.3-0.6		≤12.0	Forest with vertical continuity	FT7	
				0.6-2.0		>12.0	Forest without understory	FT5	
		>4.0			0.3-0.6		>12.0	Forest with shrub layer	FT6
					0.6-2.0		≤12.0	Forest with vertical continuity	FT7
					2.0-4.0		0.0-0.3	Forest without understory	FT5
			0.3-0.6			Forest with shrub layer	FT6		
			0.6-2.0			Forest with vertical continuity	FT7		

2.4 Data validation

For the data validation, 15 cells (when available) per fuel type and dataset were randomly selected. Then, a fuel type was assigned to each validation cell by observing the point cloud displayed in FUSION LDV and contrasted with the conditional classification showed in Table 1. The accuracy assessment was performed with a confusion matrix and summarized using overall accuracy and user's accuracy, weighted producer's accuracy (Olofsson 2013, Stehman 1996), and Kappa coefficient.

3. Results and Discussion

The overall accuracy was nearly identical for the 2010 and 2016 datasets (80.72% and 81.26%, respectively). User's and producer's accuracies were generally high (from 0.60), but most of the error was found in forest with vertical continuity (FT7; 0.18 in the 2010 dataset), forest with shrubs (FT6; 0.19 in the 2016 dataset) and low shrubs (FT2; 0.09 in the 2010 dataset). The Kappa coefficient was 0.73 for both datasets. Figure 2 shows the classification results for both datasets.

It can be seen that in 2016, low shrubs (FT2) had an even lower presence compared to 2010 dataset. Also, the area that was classified as forest with shrubs (FT6) in 2016 in the north-east of Figure 1 a), was classified in 2016 as forest without shrubs (FT5). Some potentially hazardous transitions from fuel

types without forest (FT5) or forest with shrubs (FT6) to forest with vertical continuity (FT7) were detected, especially in the south-west area.

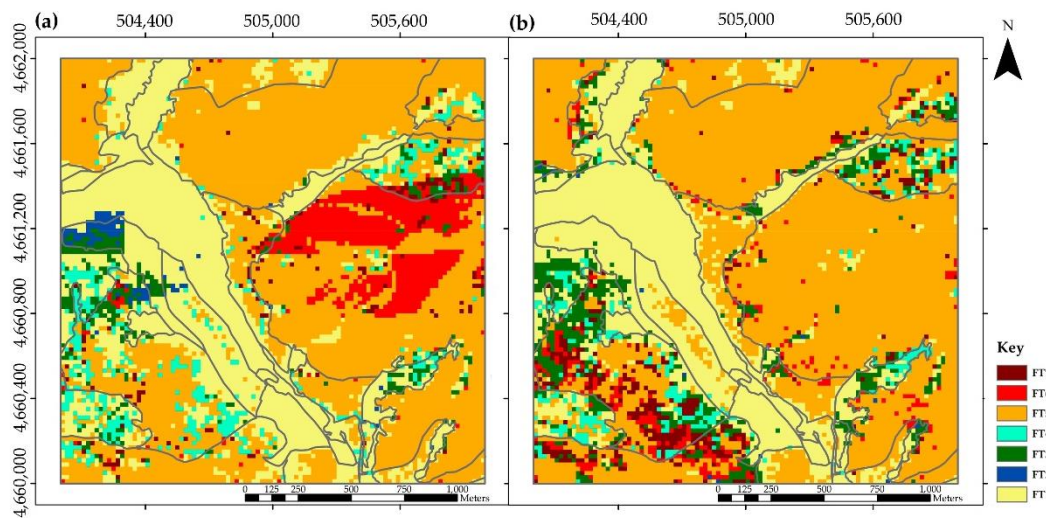


Figure 2. Classification results for the 2010 (a) and 2016 (b) LiDAR datasets. Borders of vegetation cover types (grey lines) from the Spanish National Forest Map are shown for reference (García-Cimarras et al 2021)

4. Conclusions

We present an inexpensive, simple, and accurate methodology to detect areas where of vegetation changes and growth, especially the understory layer, which can lead to an increase in fire hazard. It can save resources, especially where the difficult access makes impossible or too expensive the collection of field data. Additionally, it can be helpful to improve the management and the decision-making process. LiDAR data has proven to be able to provide vital information with an adequate accuracy of the fuel type transitions that occurred.

Acknowledgements

This research was funded by the Spanish Ministry of Education, grant number FPU17/00423.

References

- Bottalico F, Chirici G, Giannini R, Mele S, Mura M, Puxeddu M, McRoberts R.E, Valbuena R, Travaglini D, 2017, Modeling Mediterranean forest structure using airborne laser scanning data. *Int. J. Appl. Earth Obs. Geoinf.*, 57: 145–153.
- García-Cimarras A, Manzanera J.A, Valbuena R, 2021, Analysis of Mediterranean Vegetation Fuel Type Changes Using Multitemporal LiDAR. *Forests*, 12: 335.
- Instituto Geografico Nacional IGN. Available online: <http://centrodedescargas.cnig.es/CentroDescargas/index.jsp> (accessed on 30 May 2020).
- Keane R.E, Burgan R, van Wagendonk J, 2001, Mapping wildland fuels for fire management across multiple scales: Integrating remote sensing, GIS, and biophysical modeling. *Int. J. Wildl. Fire*, 10(4): 310-319.
- McGaughey R.J, 2018, FUSION/LDV: Software for LIDAR Data Analysis and Visualization.
- Olofsson P, Foody G.M, Stehman S.V, Woodcock C.E, 2013, Making better use of accuracy data in land change studies: Estimating accuracy and area and quantifying uncertainty using stratified estimation. *Remote Sens. Environ.*, 129: 122–131.
- Prometheus S.V. Project., 1999, Management Techniques for Optimisation of Suppression and Minimization of Wildfire Effect. Eur. Comm. Contract Number ENV4-CT98-0716. Available online: <https://cordis.europa.eu/project/id/ENV4980716> (accessed on 11 March 2021).
- R Core Development Team, 2018, R: A Language and Environment for Statistical. 2018. 2. Available online: <https://rstudio.com/products/rstudio/download/> (accessed on 11 March 2021).
- Stehman S.V, 1996, Estimating the kappa coefficient and its variance under stratified random sampling. *Photogramm. Eng. Remote Sens.*, 62: 401–407.

Tree crown segmentation from LiDAR data based on a symmetrical structure detection algorithm (SSD)

L. Huo¹, E. Lindberg¹, J. Holmgren¹

¹ Swedish University of Agriculture Sciences, SE-901 83 Umeå, Sweden
Email: langning.huo@slu.se, eva.lindberg@slu.se, johan.holmgren@slu.se

1. Introduction

During the past two decades, the potential of Light Detection and Ranging (LiDAR) in forest applications has been revealed by both scientific research and commercial products. One major application of LiDAR is estimation of forest parameters at a single-tree level, e.g. individual tree height, diameter at breast height (DBH), crown diameter, stem, and crown volume. Accurate estimates of these forest parameters can be achieved using different scanning platforms, including airborne laser scanning (ALS), terrestrial laser scanning (TLS), and mobile terrestrial laser scanning (MLS). Attention has been focused on the dominant and subdominant trees; fewer algorithms have focused on low vegetation (Ferraz et al., 2012; Harikumar et al., 2019; Paris et al., 2016), especially the small trees below the top canopy. In this study, we propose an individual tree segmentation (ITS) method, based on the symmetrical structure of trees (SSD). The SSD algorithm aims at segmenting point clouds of dominant trees and low vegetation accurately, which would be crucial for identifying low vegetation in the future.

2. Data and Methods

2.1 Data

The study area, Krycklan (64°14'N, 19°50'E), is located in the north of Sweden, within boreal forest. The common tree species are Scots pine (*Pinus sylvestris*), Norway spruce (*Picea abies*), and birch (*Betula pendula* and *Betula pubescens*). A field inventory of 80 m square plots was conducted in 2016. Each 80 m × 80 m plot was divided into 16 subplots of 20 m. For each tree, the positions and DBH were measured and the tree height was calculated from allometric relationships between height and DBH from sampling trees. In total, 251 subplots from 23 plots were used in the study, with exclusion of the subplots with selective cuts during the period from the field inventory to the laser scanning. Subsequently, “plot” refers to the 20 × 20 m subplots. Plot data are presented according to density level (Table 1).

Table 1. Attributes of the study plots.

Category	Density class	Threshold [stems]	Number of plots	Stem density [stems/ha]		DBH [cm]		Tree height [m]	
				Mean	Std	Mean	Std	Mean	Std
D-1	Low	≤700	71	637	241	20.2	3.4	16.0	1.5
D-2	Medium	700–1100	28	704	306	23.4	5.4	17.5	3.2
D-3	High	>1100	18	1383	732	14.7	3.1	12.0	1.9

Multispectral ALS data were acquired on June 28, 2019, with a RIEGL VQ-1560i-DW. This resulted in a scan width of 582 m and a measurement density of 24 pulses per m² and channel in each flight strip. TLS data were collected in 2016 using a Trimble TX8 from 4 × 4 scanning stations. The TLS point clouds were co-registered to ALS using the Iterative Closest Point (ICP) algorithm implemented in MATLAB. Then ALS and TLS point cloud for each plot was merged.

2.2 Methods

For this algorithm, the detection and segmentation of dominant trees were based on the symmetrical structure of individual trees. Pine and spruce, the most common tree species in Sweden, usually have

symmetrical tree shapes: conical tree crowns and cylinder stems. In this study, points of dominant trees (P_{dominant}) were identified by creating cylinder spaces for individual dominant trees. The upper cylinder A was designed for tree crowns, with the CR identified as the radius of the cylinder. The lower cylinder B was designed for stems, with the detected CBH as the height of the cylinder. To obtain a proper space for P_{dominant} , the key parameters were CR and CBH.

Step 1 Definition of target point clouds for individual trees. We generated seed points from local maximum heights (LMH) detected from the nDSM smoothed by Gaussian filtering. We defined the target point clouds for individual trees as the points within 3 m horizontal distance to the seed points.

Step 2 Plotting the symmetry curve. The coordinates of the target point cloud were transformed from (x, y, z) to (h, r, q) using the method proposed by Huo and Zhang (2019), where h is the voxel height, r is the horizontal voxel distance to the origin, and q is the horizontal angle. Let $V = \{v_c\}_{c=1}^C$ be the set of voxels with coordinates $h = H_i$ and $r = R_j$, with H_i being the height of the voxels and R_j the distance to the centre of the voxels. If more than $\frac{3}{4}$ voxels in Set V were occupied by laser returns, we determined that a symmetrical structure existed at (R_j, H_i) . The curve was plotted for (R_j, H_i) , as in Figure 1 (a-1, b-1).

Step 4. Determination of true/false treetops. We determined a seed as true treetops if (1) there was less than 50% R among the upper 1/3 tree height are zero (designed for pines); or (2) there was less than 50% R among the lower 1/2 tree height are zero (designed for spruces).

Step 5 Detection of CR and CBH from symmetry curves. The symmetry curves were first smoothed, and from the curves, CR was determined as the point (R_u, H_u) , and CBH as (R_l, H_l) (Figure 1 a-2, b-2). The value of (R_u, H_u) was set to the first point from the top when R no longer increased more than 0.25 m from H_i to H_{i+1} . R_u represented the radius of the symmetrical crown. Point (R_l, H_l) was at the lower part of the curve, indicating the lower edge of a tree crown with a height of H_l and a radius of R_l . Detection continues from H_u to a lower H , until the first local minimum R emerges, with the value (R_l, H_l) .

Step 1.6 Creation of the clipping space. For each treetop, a clipping curve (Figure 1 a-e, b-e) was created to include the space for the individual tree according to the (R_u, H_u) and (R_l, H_l) values. Laser points inside the clipped space were classified as P_{dominant} (Figure 1).

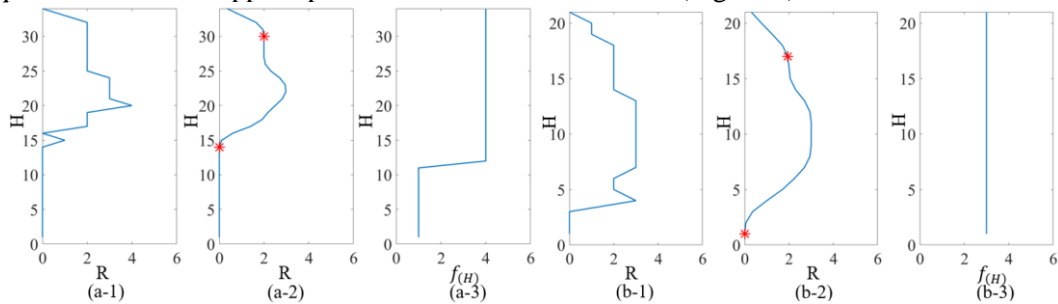


Figure 1. Two examples of the symmetry curve. (a-1, b-1) An unsmoothed symmetry curve, and (a-2, b-2) a smoothed symmetry curve, with (R_u, H_u) (upper red stars) and (R_l, H_l) (lower red stars). (a) An example of a pine with a funnel space. (b) An example of a spruce with a cylindrical space.

Detection results were validated by matching with the field data. The detection rate (DR), recall (R), precision (P), and F-scores (F) were calculated.

3. Results and Discussion

When averaging all the plots, the SSD algorithm achieved a value of 0.86 for DR (Table 2). Similar to other ITC segmentation algorithms, the detection rates decreased for plots with higher densities. Figure 2 shows two examples of the SSD segmentation.

By testing the symmetrical structure of trees, the SSD algorithm segments point clouds of the dominant trees and low vegetation. The next potential use of the SSD algorithm could be the identification and analysis of low vegetation, by removing the point clouds of dominant trees from a plot and keeping the point clouds of low vegetation.

Table 2. Detection accuracy of SSD algorithm

Attribute	Category*	DR	R	P	F
Density	D-1	0.93	0.93	0.83	0.88
	D-2	0.87	0.88	0.89	0.89
	D-3	0.78	0.80	0.93	0.86
All plots		0.86	0.87	0.83	0.84

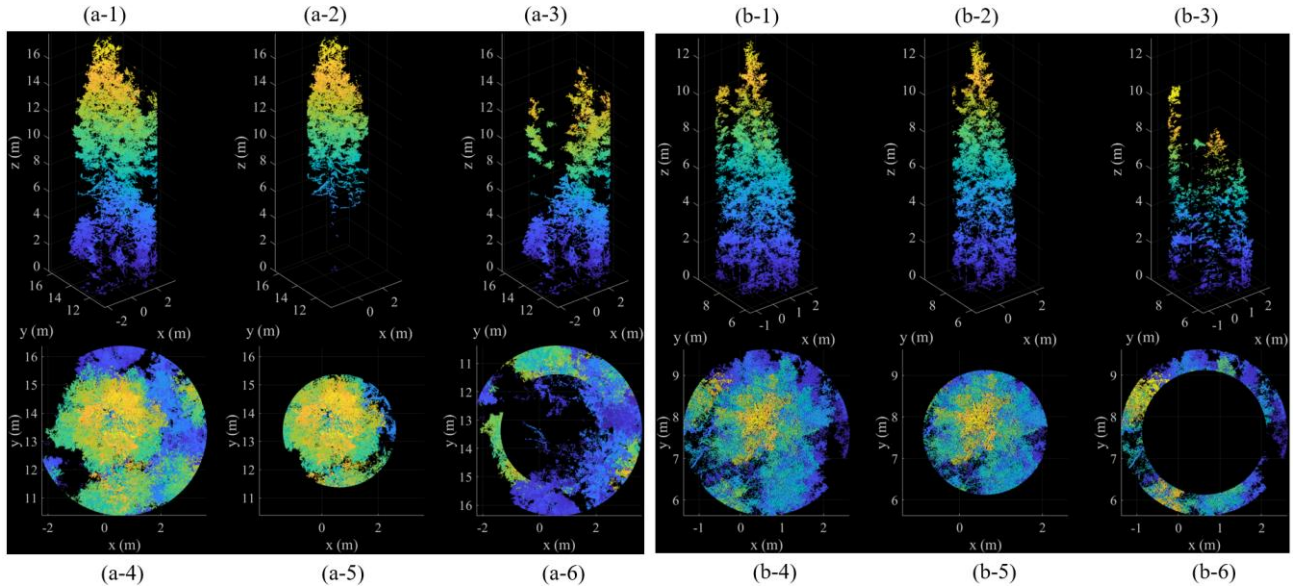


Figure 2. Two examples of classifying P_{dominant} . (a) Point clouds of a pine. (b) Point clouds of a spruce. (1 – 3) Side view of the P_{target} , P_{dominant} and the rest of the points, respectively. (4 – 6) Top view of the P_{target} , P_{dominant} and the rest of the points, respectively.

4. Conclusions

In this study, we proposed an algorithm of ITS by testing the symmetrical structure of individual trees. The crown radius and crown base height were estimated from a vertical symmetry curve of a tree. By creating cylinder spaces of the dominant trees, laser points were segmented into dominant trees and low vegetation. The SSD algorithm achieved 0.87 detection rate and 0.84 F-scale when matching the detected trees with the field records. Segmenting point clouds of dominant trees and low vegetation accurately could potentially contribute to the identification of low vegetation.

Acknowledgements

This research was financed by the Kempe Foundations, as part of the Finnish and Swedish bilateral research program Tandem Forest Value, and the Swedish Foundation for Strategic Environmental Research with the research program Mistra Digital Forest.

References

- Ferraz, A., Bretar, F., Jacquemoud, S., Gonçalves, G., Pereira, L., Tomé, M., & Soares, P. (2012). 3-D mapping of a multi-layered Mediterranean forest using ALS data. *Remote Sensing of Environment*, *121*, 210–223.
- Harikumar, A., Bovolo, F., & Bruzzone, L. (2019). A Local Projection-Based Approach to Individual Tree Detection and 3-D Crown Delineation in Multistoried Coniferous Forests Using High-Density Airborne LiDAR Data. *IEEE Transactions on Geoscience and Remote Sensing*, *57*, 1168–1182.
- Huo, L., & Zhang, X. (2019). A new method of equiangular sectorial voxelization of single-scan terrestrial laser scanning data and its applications in forest defoliation estimation. *ISPRS Journal of Photogrammetry and Remote Sensing*, *151*, 302–312.
- Paris, C., Valduga, D., & Bruzzone, L. (2016). A Hierarchical Approach to Three-Dimensional Segmentation of LiDAR Data at Single-Tree Level in a Multilayered Forest. *IEEE Transactions on Geoscience and Remote Sensing*, *54*, 4190–4203.

Comparing the vertical structure of tropical forests as seen by space- and airborne lidar and P-band SAR tomography

X. Liu¹, C. S. Neigh², M. Forkel¹

¹TU Dresden, Institute for Photogrammetry and Remote Sensing, 01062 Dresden, Germany

²NASA Goddard Space Flight Center, Mail Code 618, Greenbelt, MD 20771, USA

Email: xiao.liu@mailbox.tu-dresden.de

1. Introduction

Forests cover 31% of the global land area, and monitoring forest resources are therefore critical for understanding earth's ecosystems. The NASA's Global Ecosystem Dynamics Investigation (GEDI) mission uses a full-waveform lidar system to measure forest structure from space (Dubayah, R., et al., 2020). However, lidar observations are impacted by cloud cover and haze in tropical forests. Synthetic Aperture Radar (SAR) can penetrate clouds. In addition, the long-wavelength SAR system such as P-band can record backscattered signal under the canopy. As the first P-band SAR satellite in the world, ESA's BIOMASS satellite is planned to launch in 2022 (Le Toan, T., et al., 2011). During its SAR tomography (TomoSAR) phase, multi-pass SAR images with different elevation angles will be processed to retrieve the reflectivity profiles of forests. TomoSAR profiles show some similarities with lidar waveforms because they are continuous indicators of the vertical structure of forests. Therefore, the difference in wavelength, imaging geometry and operating spatial coverage between GEDI on the International Space Station and BIOMASS in a polar orbit create the potential for forests measuring and monitoring at a global scale in temperate and tropical ecosystems. Here, we compare full-waveform lidar observations from GEDI and airborne systems with TomoSAR images in P-band as acquired by the AfriSAR2016 campaign over Lopé, Gabon.

2. Data and Methods

2.1 Data

Our research area is located in Lopé National Park (Figure 1), where is mainly covered by savanna (0 to 15 m in height) and forests (30 to 50 m), with tree canopy cover ranging from 0 to 0.99. The maximum terrain slope can reach 20°. In order to exclude the influence from background solar illumination, we only use GEDI data acquired at night. The GEDI L1B Version 1 product (Dubayah, R., et al., 2020) and GEDI L2A Version 1 product (Dubayah, R., et al., 2020) are filtered according to quality and degrade flags. GEDI and LVIS can achieve 1 m vertical accuracy, determined by the 15 ns and 11 ns bandwidth. The airborne lidar data and airborne P-band SAR data were acquired by NASA's Land, Vegetation and Ice Sensor (LVIS) team (Blair, J. B., et al., 2018) and by DLR's F-SAR system, during AfriSAR2016 campaign (Hajnsek, I., et al., 2011). Some key parameters of the data are listed in Table 1.

Table 1. Key parameters of the data.

Sensor	Platform	Wavelength	Acquisition time	Resolution	Reference ellipsoid	Geolocation accuracy
GEDI	Spaceborne	1064 nm	14.08.2019	25 m	WGS-84	10-20 m
LVIS	Airborne	1064 nm	02.03.2016	18 m	WGS-84	1 m
FSAR	Airborne	69 cm	10.02.2016	2 × 3.84 m	WGS-84	0.15 m

2.2 SAR Tomography

SAR Tomography (TomoSAR) assumes the recorded complex value in each azimuth-range cell is the integration of backscattered signal along cross range direction. The multitrack SAR images acquired at different positions can then be used to estimate reflectivity profile, which indicates the volumetric information of imaging objects. For our forests scenario, a 20 m × 20 m multilook window was used to generate covariance matrix from 10 Single Look Complex (SLC) images at HV polarization.

We applied the popular Capon method (Lombardini, F., et al., 2003) and then transform retrieved profiles from SAR geometry to a geographic coordinate system (Pardini, M., et al., 2018). The vertical Rayleigh resolution of TomoSAR changes from 8 m (near range) to 40 m (far range) along slant range direction, which is determined by the imaging geometry and wavelength. However, Capon can achieve better vertical resolution (Cazcarra-Bes, V., et al., 2019). Considering the similarity with lidar waveform, we use the term “waveform” to describe these derived profiles as well. Based on the local maxima above 0.1 in normalized TomoSAR waveform, we estimated the relative height (RH) metrics.

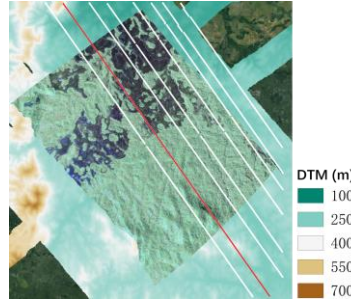


Figure 1: Lopé. From Google basemap to top: LVIS DTM, P-band Pauli SLC and GEDI footprints.

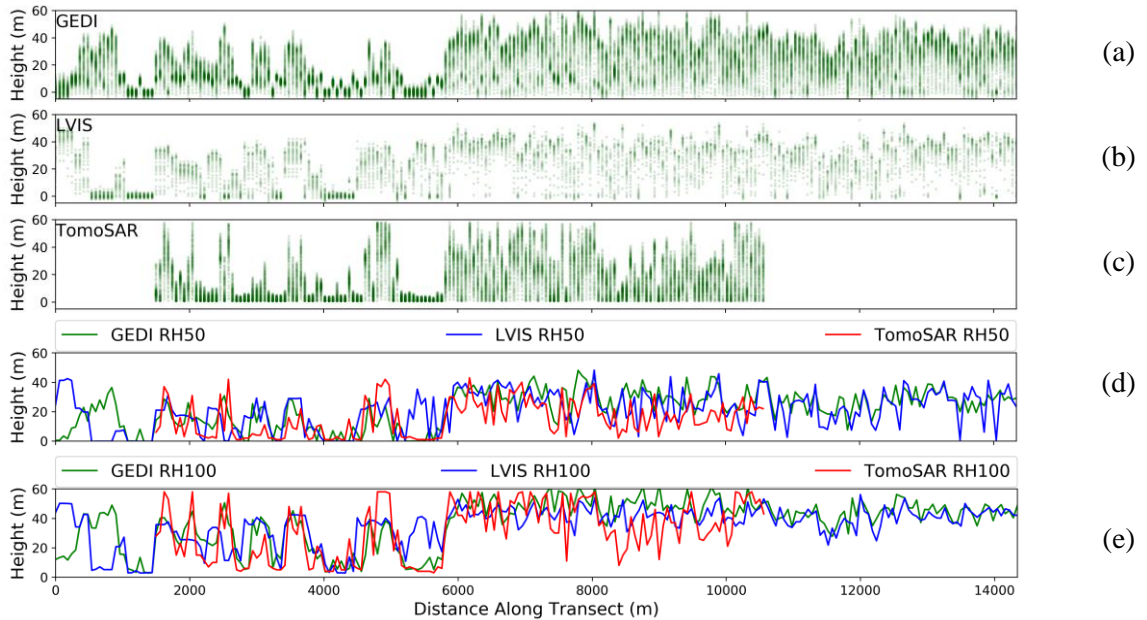


Figure 2: (a)-(c): Slice of RH0 to RH100. (d)-(e): Slice of RH50 and RH100.

3. Results and Discussion

In Figure 2 (a)-(c), we plot the RH0-100 along a full power beam BEAM1000 (i.e., red points in Figure 1). The coverage beam and full power beam are two beam patterns of GEDI, and full power beam has a design specification to detect the ground through 98% canopy cover. Note RH0-100 from GEDI L2A Version 1 product and TomoSAR are sampled with 1% while only RH in step of 5% is available for LVIS. In the overlapped area (1500~10500m), these three sensors present similar forest top height. The distribution of GEDI RH metrics is more consistent with LVIS than TomoSAR, especially in the hilly area from 8000 m to 10000 m (see Figure 1). As we can see from Figure 2 (d)-(e), TomoSAR RH50 and RH100 both generally matches well with lidar. It means, besides forest top height, there is also similarity in the vertical distribution of waveforms as well as corresponding forest structure.

We also analysed the RH50 and RH100 from LVIS and TomoSAR with all GEDI data processed using two different algorithms, i.e., a1 (default) and a5, to figure out the influence of ground detection algorithms in dense forests. The main difference between a1 and a5 is the threshold and smoothing settings used to interpret the received waveform. LVIS metrics are highly related with TomoSAR for both RH50 and RH100 (Figure 3). However, the GEDI metrics derived with a5 and selected with minimum sensitivity of 0.96 show significantly improved relation with LVIS and TomoSAR.

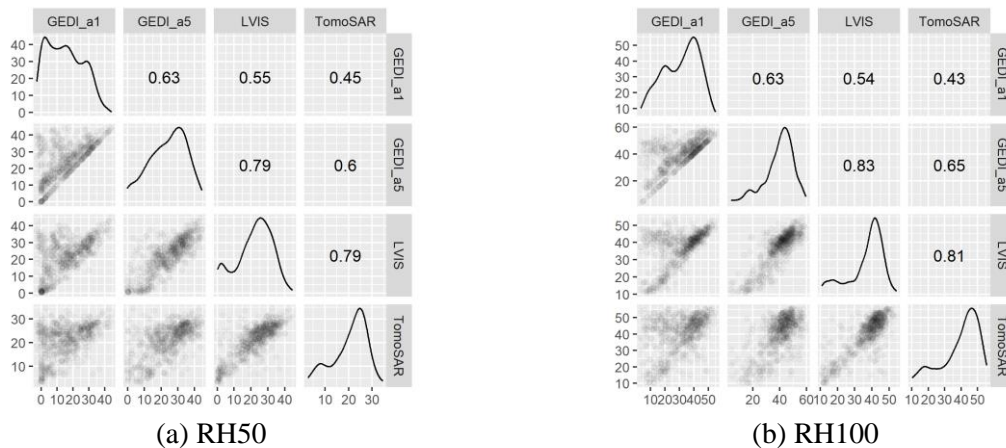


Figure 3: (a): RH50 with GEDI_a1 and a5. (b): RH100 with GEDI_a1 and a5. (upper triangle) Pearson correlation, (diagonal) variable distribution, and (lower triangle) scatterplots of each pair are showed.

4. Conclusions

In this abstract, we compared the relative height (RH) metrics from GEDI, LVIS and airborne P-band TomoSAR. Both GEDI and TomoSAR show some consistency with LVIS data. The agreement between GEDI and the BIOMASS TomoSAR RH metrics may be affected by coarser resolution and the three-year time lag between both observations. Nevertheless, the continuous spatial and temporal coverage of SAR data provides us an opportunity to measure and monitor forest vertical structure at a larger scale than lidar. The retrieved vertical profiles can then be converted to biomass profiles (Caicoya, A., et al.). Thus, the use of GEDI products as reference points in forests without airborne lidar or in-situ plots is likely to be a fruitful avenue for the development of 3-dimensional forest biomass products from future BIOMASS TomoSAR observations.

Acknowledgements

The authors would like to thank ESA, LVIS team and GEDI team for providing SAR, LVIS and GEDI data. This work was supported by China Scholarship Council (CSC).

References

- Dubayah, Ralph, et al. "The Global Ecosystem Dynamics Investigation: High-resolution laser ranging of the Earth's forests and topography." *Science of remote sensing* 1 (2020): 100002.
- Le Toan, Thuy, et al. "The BIOMASS mission: Mapping global forest biomass to better understand the terrestrial carbon cycle." *Remote sensing of environment* 115.11 (2011): 2850-2860.
- Dubayah, R., et al. (2020). GEDI L1B Geolocated Waveform Data Global Footprint Level V001 [Data set]. NASA EOSDIS Land Processes DAAC. Accessed 2021-04-16 from https://doi.org/10.5067/GEDI/GEDI01_B.001.
- Dubayah, R., Hofton, M., Blair, J. B., Armston, J., Tang, H., Luthcke, S. (2020). GEDI L2A Elevation and Height Metrics Data Global Footprint Level V001 [Data set]. NASA EOSDIS Land Processes DAAC. Accessed 2021-04-16 from https://doi.org/10.5067/GEDI/GEDI02_A.001.
- Hajnsek, I., et al., "Technical assistance for the development of airborne SAR and geophysical measurements during the AfriSAR campaign," Eur. Space Agency, Paris, France, Final Tech. Rep. 4000114293/15/NL/CT, 2011. [Online]. Available: <https://earth.esa.int/documents/10174/134665/AfriSAR-Final-Report>.
- Blair, J. B. and Hofton, M. 2018. AfriSAR LVIS L1B Geolocated Return Energy Waveforms, Version 1. [Indicate subset used]. Boulder, Colorado USA. NASA National Snow and Ice Data Center Distributed Active Archive Center. doi: <https://doi.org/10.5067/ED5IYGVTB50Z>. [Date Accessed].
- Lombardini, Fabrizio, and Andreas Reigber. "Adaptive spectral estimation for multibaseline SAR tomography with airborne L-band data." *IGARSS 2003. 2003 IEEE International Geoscience and Remote Sensing Symposium. Proceedings (IEEE Cat. No. 03CH37477)*. Vol. 3. IEEE, 2003.
- Pardini, M., et al. "L- and P-band 3-D SAR reflectivity profiles versus lidar waveforms: The AfriSAR case." *IEEE Journal of Selected Topics in Applied Earth Observations and Remote Sensing* 11.10 (2018): 3386-3401.
- Cazcarra-Bes, Victor, et al. "Comparison of tomographic SAR reflectivity reconstruction algorithms for forest applications at L-band." *IEEE Transactions on Geoscience and Remote Sensing* 58.1 (2019): 147-164.
- Caicoya, Astor Toraño, et al. "Forest above-ground biomass estimation from vertical reflectivity profiles at L-band." *IEEE Geoscience and Remote Sensing Letters* 12.12 (2015): 2379-2383.

Estimating Timber Volume using Harvester Data and Airborne Laser Scanner Data from Multiple Acquisitions

L. Noordermeer, E. Næsset, T. Gobakken

Faculty of Environmental Sciences and Natural Resource Management, Norwegian University of Life Sciences, NMBU, P.O. Box 5003,
NO-1432 Ås, Norway
Email: {lennart.noordermeer; erik.naesset; terjje.gobakken}@nmbu.no

1. Introduction

Airborne laser scanning (ALS) data have played a central role in the field of forest inventory over the last decades (White et al. 2016). Forest attributes are commonly estimated from ALS data by linking field reference data to ALS metrics in statistical models (Næsset 2002). Herein, accurately georeferenced field data are essential, and remain a main cost component in operational forest inventories (Gobakken and Næsset 2008).

In the context of cost saving, data recorded by forest harvesters are emerging as a potential supplement to, or replacement for, traditional field measurements in operational forest inventories (Lindroos et al. 2015). Cut-to-length harvesters measure and store large amounts of data on the dimensions and characteristics of harvested logs. In addition, harvesters are commonly equipped with Global Navigation Satellite System (GNSS) receivers which provide a spatial reference and time stamp for each harvested tree (Olivera 2016).

Newly developed harvester positioning systems enable georeferencing of individual trees with submeter accuracy (Hauglin et al. 2017; Noordermeer et al. 2021). Previous studies have shown that accurately georeferenced harvester data can be linked to ALS data to estimate timber volume (Hauglin et al. 2018) and stem diameter distributions (Maltamo et al. 2019). The mentioned studies used ALS data from a single acquisition, and experimentally installed sensors to monitor the position of the harvester head relative to the machine. Recently developed technology in cut-to-length harvesters of several manufacturers allows for measuring and recording coordinates of harvested trees automatically with standardized sensor hardware (Westerberg 2014; Bhuiyan et al. 2016; La Hera and Morales 2019), enabling extensive and automatic georeferenced tree-level data collection. These data may prove beneficial to a range of inventory applications that fall outside the scope of periodic forest inventories, such as short-term planning of timber harvesting within a region in which a harvester operates. It is therefore important to assess the suitability of data collected by harvesters equipped with industry standard positioning systems for volume estimation, using ALS datasets acquired with different scanners and over multiple years.

The aim of this study was to assess the accuracy of timber volume estimated from harvester data obtained using industry standardized crane sensor systems and differential GNSS positioning, and ALS data acquired over multiple years.

2. Data and Methods

2.1 Harvester data

Harvester data were collected from 33 logging operations between March 2019 and June 2021 using a single-grip Komatsu 931XC harvester. The operations were located in Innlandet county in southeastern Norway. As optional equipment supplied by the manufacturer, a sensor was mounted on the crane which measured the angle between the inner and outer boom (Bhuiyan et al. 2016), enabling improved crane tip positioning. In addition, we replaced the harvester's standard GNSS with a real-time kinematic Septentrio AsteRx-U GNSS receiver, with which tree positions were georeferenced with submeter accuracy (Noordermeer et al. 2021). Harvester production report (HPR) files were exported in StanFord 2010 format (Arlinger et al. 2012) which, among other things, included log volumes and coordinates of crane tip positions during fellings. We summed log volumes for each harvested stem and linked the volumes to the corresponding crane tip positions.

2.2 ALS Data

ALS data were acquired in the years 2013, 2016, 2017, 2019 and 2020 (Table 1) covering different areas which in some cases overlapped. Therefore, the delay between ALS and harvester data acquisition varied from one to eight years. For each logging site, we clipped the most recently acquired ALS data from within the spatial extent of the site, and classified the laser echoes as ground or non-ground. We then normalized the ALS data, i.e., the height above ground was calculated for all echoes classified as non-ground.

Table 1. Airborne laser scanning acquisition parameters.

Year	Instrument	Time period	Pulserate (kHz)	Scan rate (Hz)	Flying altitude (m)	Echo density (m ⁻²)
2013	TopEye S/N 444	May-July	200	92	1500	7.7
2016	Riegl LMS Q-1560	September	400	100	2900	3.2
2017	Riegl VQ-1560 I	July	700	240	2300	6.8
2019	Leica ALS70-HP	August	495	69	1150	5.9
2020	Riegl VQ-1560 II	June	749	158	1100	10.4

2.3 Enhanced area approach

We generated hexagonal grids by tessellating the logging sites into 200 m² cells, and segmented individual trees within the logging sites from the ALS data using the *itcSegment* package in R (Dalponte 2016). We used the obtained crown segments to adjust grid cell borders as proposed by Packalen et al. (2015) to improve correspondence between harvester and ALS data (Figure 1). In contrast to the mentioned study, however, we labelled trees as “in” or “out” based on the proportion of tree crown area overlapping the sampling area, and not the position of the detected tree apex falling in- or outside the sampling area boundary. We then extracted harvester stem volume data from within the adjusted grid cells, and calculated cell-level volumes as the sum of timber volumes recorded by the harvester, scaled to a per ha unit. From the laser echoes that fell within the spatial extent of the adjusted grid cells, we computed canopy metrics from echoes of all categories (first, intermediate and last) with a height > 2 m above the ground. The canopy metrics included the heights at the 10th, 20th, ... and 90th percentile of echo height distributions, and the mean height, standard deviation, skewness and coefficient of variation of echo heights. We also computed canopy density metrics by dividing the height range between 2 m and the 95th percentile into 10 fractions of equal height, and computing the proportion of echoes between the lower limit of each fraction to the total number of echoes.

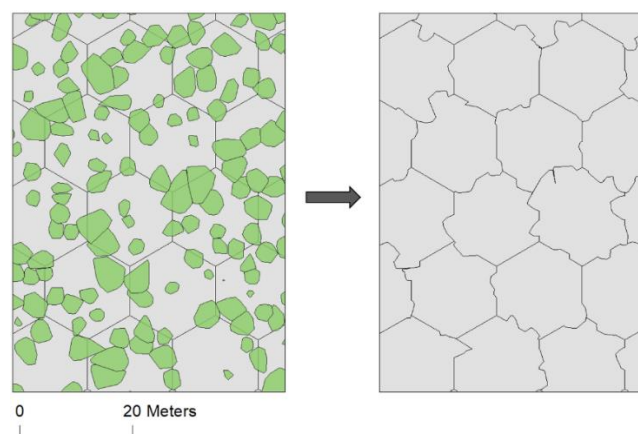


Figure 1. The enhanced area based approach used in this study. A hexagonal sampling grid overlaid with tree crowns segmented from the ALS data (left) and grid cells adjusted for segmented trees crowns (right).

2.4 Timber Volume Estimation

We estimated the mean timber volume per ha for the 33 logging operations in a leave-one-operation-out fashion. We removed one operation from the dataset, and fitted a random forest model with data from the remaining operations. We used the model to predict timber volume for grid cells within the testing operation, and repeated the procedure until all grid cells obtained predictions. We estimated the mean timber volume per ha for each operation as the mean of volume predictions, and compared these values to the mean timber per ha recorded by the harvester. To assess the accuracy of timber volume estimates, we computed the root mean square error between harvester and ALS estimates relative to the mean recorded by the harvester (RMSE%). Finally, we tested whether the year of ALS data acquisition had a statistically significant effect on the prediction errors using an analysis of variance (ANOVA) test.

3. Results and Discussion

Figure 2 shows mean timber volumes recorded by the harvester plotted against corresponding values estimated from the ALS data for the 33 logging operations. The leave-one-operation-out cross validation procedure revealed a RMSE% of 11.4. This level of accuracy was comparable to the results obtained by Packalén and Maltamo (2007), who estimated timber volume at stand level by using manually measured field plots and ALS data from a single acquisition, and obtained a RMSE% of 10.4. We obtained better accuracies than Saukkola et al. (2019) who estimated timber volume at stand level by using harvester data georeferenced with an autonomous GNSS, i.e., without differential GNSS positioning, and ALS data from a single acquisition, and obtained a RMSE% of 25.9.

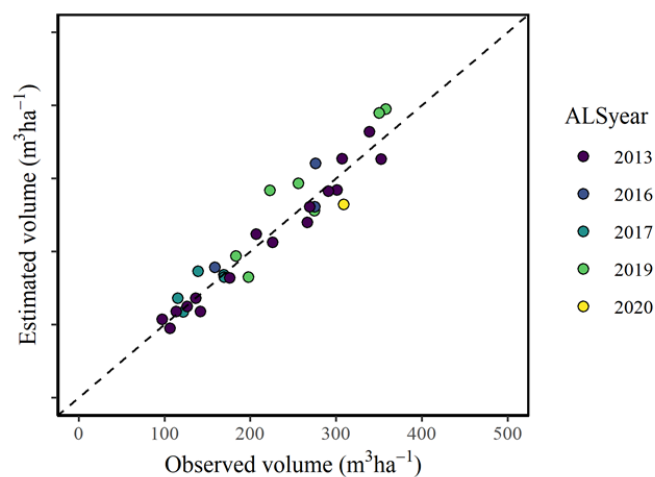


Figure 2: Timber volume recorded by the harvester plotted against timber volume estimated from airborne laser scanner data for the 33 logging operations.

Even though data from five different ALS acquisitions were used, and the number of years between ALS acquisition and harvesting varied considerably from one to eight years, the ANOVA test showed that the year of ALS acquisition did not have a statistically significant effect on prediction errors obtained for grid cells ($p = 0.37$). Thus, a single random forest model fitted with data from all years provided a practical solution for predicting and subsequently estimating timber volume.

The proposed approach can be used for updating operational forest inventories in situations where field data are not available, and timely data is needed for short-term operational planning. Harvester and ALS data may prove particularly useful for operational planning, where volume estimates are typically needed within a short time frame, for example for the selection of stands for harvesting in the near future. Such decisions typically require data with greater spatial and temporal resolution than those provided by periodic forest management inventories, which are commonly only carried out every 10-15 years.

Acknowledgements

This research was funded by the Research Council of Norway (Project No. 309671). The harvester data were provided by Valdres Skog AS and the ALS data were provided by the Norwegian mapping authority Kartverket.

References

- Arlinger J, Nordström M, Möller JJ. 2012. StanForD 2010: modern communication with forest machines. Arbetsrapport från Skogforsk.(785).
- Bhuiyan N, Möller J, Hannrup B, Arlinger J. 2016. Automatisk gallringsuppföljning–Arealberäkning samt registrering av kranvinkel för identifiering av stickvägsträd och beräkning av gallringskvot. Arbetsrapport från Skogforsk.(899).
- Dalponte M. 2016. R Package 'itcSegment': User Manual. cran.r-project.org/web/packages/itcSegment/https://egment/itcSegment.pdf.
- Gobakken T, Næsset E. 2008. Assessing effects of laser point density, ground sampling intensity, and field sample plot size on biophysical stand properties derived from airborne laser scanner data. *Can J For Res.* 38(5):1095-1109.
- Hauglin M, Hansen E, Sørngård E, Næsset E, Gobakken T. 2018. Utilizing accurately positioned harvester data: modelling forest volume with airborne laser scanning. *Can J For Res.* 48(8):913-922.
- Hauglin M, Hansen EH, Næsset E, Busterud BE, Gjevestad JGO, Gobakken T. 2017. Accurate single-tree positions from a harvester: A test of two global satellite-based positioning systems. *Scand J For Res.* 32(8):774-781.
- La Hera P, Morales DO. 2019. What Do We Observe When We Equip a Forestry Crane with Motion Sensors? *Croat J For Eng.* 40(2):259-280.
- Lindroos O, Ringdahl O, La Hera P, Hohnloser P, Hellström TH. 2015. Estimating the position of the harvester head—a key step towards the precision forestry of the future? *Croat J For Eng.* 36(2):147-164.
- Maltamo M, Hauglin M, Næsset E, Gobakken T. 2019. Estimating stand level stem diameter distribution utilizing harvester data and airborne laser scanning. *Silva Fenn.* 53(3):1-19.
- Næsset E. 2002. Predicting forest stand characteristics with airborne scanning laser using a practical two-stage procedure and field data. *Remote Sens Environ.* 80(1):88-99.
- Noordermeer L, Sørngård E, Astrup R, Næsset E, Gobakken T. 2021. Coupling a differential global navigation satellite system to a cut-to-length harvester operating system enables precise positioning of harvested trees. *Int J For Eng.* 1-9.
- Olivera A. 2016. Exploring opportunities for the integration of GNSS with forest harvester data to improve forest management. Doctoral thesis. University of Canterbury, Christchurch, New Zealand.
- Packalén P, Maltamo M. 2007. The k-MSN method for the prediction of species-specific stand attributes using airborne laser scanning and aerial photographs. *Remote Sens Environ.* 109(3):328-341.
- Packalén P, Strunk JL, Pitkänen JA, Temesgen H, Maltamo M. 2015. Edge-tree correction for predicting forest inventory attributes using area-based approach with airborne laser scanning. *IEEE Journal of Selected Topics in Applied Earth Observations and Remote Sensing.* 8(3):1274-1280.
- Saukkola A, Melkas T, Riekkö K, Sirparanta S, Peuhkurinen J, Holopainen M, Hyyppä J, Vastaranta M. 2019. Predicting forest inventory attributes using airborne laser scanning, aerial imagery, and harvester data. *Remote Sens.* 11(7):797.
- Westerberg S. 2014. Semi-automating forestry machines: motion planning, system integration, and human-machine interaction. Doctoral thesis. Sweden: Umeå Universitet.
- White JC, Coops NC, Wulder MA, Vastaranta M, Hilker T, Tompalski P. 2016. Remote sensing technologies for enhancing forest inventories: A review. *Canadian Journal of Remote Sensing.* 42(5):619-641.

Airborne LiDAR System Optimisation for Foliage Penetration

Dr. Uwe Bacher¹, Ronald Roth²

¹Hexagon Geosystems, Leica Geosystems Technologies GmbH, Friedrichstrasse 100, 73430 Aalen, DE
Email: uwe.bacher@hexagon.com

²Hexagon Geosystems, Geospatial Content Solutions, 4600 Forbes Boulevard, Lanham, Maryland, US 20706
Email: ron.roth@hexagon.com

1. Introduction

There is a significant history of using LiDAR point cloud data for determining various forest parameters. Although there are some general rules-of-thumb for parameters such as off-nadir angle and laser footprint size when trying to maximize penetration through tree cover, there are more variables that can contribute to effective foliage penetration. This study will evaluate the use of several flight and system parameters that can now be varied with the introduction of newer megahertz-pulse-rate LiDAR systems.

As a precursor to developing conclusions from the tests, several metrics for analyzing foliage penetration are compared, and one metric chosen for the remaining analysis.

The operation variables that can be manipulated in the system allow trade-offs between such things as pulse energy and pulse rate in an effort to maximize the number of “hits” on the forest floor and thus obtain more detailed DEMs from which to evaluate forest parameters such as tree height. Results based on recent testing by PASCO using Leica TerrainMapper will be compared to results from earlier-generation systems to reveal if the “conventional wisdom” still applies, or whether operational parameters should indeed be adjusted to further maximize foliage penetration.

Although the study is performed on a specific type of LiDAR system, the results can be applied to other system types in the current generation of high-pulse-rate linear-mode LiDAR systems. Furthermore, a discussion of the parallels to, and implications for further development of, single-photon LiDAR systems will be made.

2. Data and Methods

Airborne data were collected from two sites. A comparison of the two sites is given in Table 1 below:

Table 1. Test Flight comparison.

Parameter	Flight 1	Flight 2
Area		10 km ²
Terrain Relief		100 m
Dates	Mid October 2018	Late January 2019
Variables tested	Pulse energy (low, med, high) Off-nadir angle (10, 20 degrees)	Pulse energy (low, med, high) Scan pattern (planar sine, circle) Detector threshold (two steps below default)

The initial flight seeks to verify the conclusions from the 2004 study by Roth and Marsh, in particular the relationship between off-nadir angle and relative penetration.

The second flight seeks to expand on the test to include a comparison of planar scanning (similar to that used in the 2004 test) and the circular scan pattern normally used in the test system. It should be noted that the planar scanning tests performed in 2004 were performed at maximum off-nadir angles of 27.5 degrees, where the more recent tests were limited to a maximum 40-degree FOV. One difference

between planar and circular scan patterns is that the circular pattern results in a constant off-nadir angle, whereas off-nadir angle varies across the planar-canned FOV.

In addition to varying the scan pattern, the second flight provided variations in both pulse energy and detector threshold.

3. Results and Discussion

As expected, increasing laser pulse energy (and thus SNR), increases the probability that any given laser pulse will result in one or more valid returns. While multiple returns are beneficial, many types of classification algorithms used to derive tree height depend on a significantly dense bare earth DEM.

Three metrics were compared for evaluation of the propensity of the laser pulse to result in valid returns below the top of the canopy:

- (1) Forest Penetration Factor (FPF) = total returns/total laser shots
- (2) Ground Return Factor (GRF) = total ground returns/total laser shots
- (3) Ground Fill Factor (GFF) = total cells with at least one ground return/total cell in AOI

The first two metrics provide some indication of the ability to characterize the quality of forest capture, and the portion of laser shots resulting in successful ground detection. However, GFF provides a better picture of the “completeness” of the forest floor capture and was therefore used for to judge the effect of varying different acquisition parameters. In addition to getting additional returns from the edges of larger (i.e., already detected) canopy openings, an increase in GFF indicates that returns are also received from smaller canopy opening is different locations that were not previously detected. For the purposes of the study, a 1m grid size was used.

In the first flight, increases in SNR were beneficial, providing a roughly 10% increase in GFF when measured with a 1m grid size. Reducing the FOV from 40 to 20 degrees provided an average 8% increase in GFF. Changing both variable together produced a compounding effect.

In addition to varying SNR, variations in the second flight allowed measurement of the effect of scan pattern (sine versus circular) as well as detection threshold. This second flight confirmed the trends of the first flight, with a roughly 10% increase in GFF over the range of SNRs tested.

Data from sine and circular scan patterns at the same FOV of 40 degrees showed that GFF was approximately 5% better for the particular cypress forest sample plot. This may not be entirely conclusive and may vary by vegetation type.

The effect of reducing detection threshold predictably produced some benefit, with approximately 7% increase in GFF by lowering the detection threshold slightly from the default setting. Further reductions, while likely producing additional forest floor measurements, predictably increased the occurrence of noise points (false returns). These noise points will require additional processing time both in the generation of the raw point cloud and in subsequent filtering steps. Therefore, users would be advised to take care when considering changing the detection threshold value, as there was no detectable increase in GFF between the two lower threshold settings.

A comparison between a typical linear-mode LiDAR design and that of a single-photon LiDAR system (Leica SPL100) shows some potential in this alternative technology. The very small laser divergence (<0.1 mr) of each “beamlet” in the SPL100 potentially provides a better concentration of laser energy through small canopy openings. Furthermore, the current SPL100 scanner design produces the same circular pattern that showed advantages on the linear-mode test system. Some study of foliage penetration of single-photon LiDAR in comparison to linear-mode has been undertaken previously by Sinclair, but the results are based on GRF as opposed to GFF. Therefore, further study is needed.

4. Conclusions

Evaluation of sample data from the linear-mode LiDAR system shows that, of the three metrics proposed as a measure of foliage penetration, Ground Fill Factor is the most informative.

Conventional wisdom of limiting the maximum off-nadir angle to approximately 20 degrees (i.e., 40 degree FOV) appears to hold, as some increase in GFF has been seen in data even between 20- and 10-degree off-nadir angles.

From the flight data, it is clear that increasing SNR setting as a flight planning or design parameter has significant benefit. However, from a commercial standpoint, it is preferable that this increase in SNR not be at the expense of lower effective pulse rate, an effect which would be typical and expected. Therefore, other methods for increasing the amount of laser energy making it through upper levels of the canopy are required.

From the tests performed using linear-mode LiDAR, the implication is that minimizing laser output divergence is one key to obtaining higher SNR, given limited size “holes” in the forest canopy. This has the greatest benefit in “closed canopy” situations, where the openings in the canopy are limited both in number and in size. In more open canopy situations (e.g., lodgepole pine forest in the western US), the benefit would not be so pronounced.

Another possibility for increasing SNR lies in a reduction in laser pulse width. Provided adequate detector response times, reducing laser pulse width (within the limits of the particular laser type used) proportionally increases the peak power in each laser pulse. It should be noted that the optoelectronic design of the receiver is critical in this respect, as excessive reduction of laser pulse width can result in a reduction in the effective response of the detector. When optimized, a reduced pulse width presents a good balance between increased peak pulse power and detector/electronic roll-off. This can allow both increases in GFF as well as increased detail in forest canopy.

An additional benefit to shorter pulse widths is the potential for reductions in minimum pulse separation. As with reduced divergence, reducing minimum pulse separation can allow return reflections to be differentiated in vertical layers of canopy that are closer together. In addition to hardware design, this minimum return separation is also affected by the processing software, particularly that used for separation of random noise from legitimate target returns.

While providing some benefit, reducing detection threshold should not be taken to an extreme, as the result will be additional noise points being processed and then having to be filtered out.

Single-photon LiDAR holds the promise of an enabling technology, with high efficiency at any given point density, and can potentially make nation-wide forest inventory at individual tree levels practical. Current single-photon systems have the low beam divergence mentioned above, giving great potential for forest applications as well as the preferred circular scan pattern. The main areas of further development of the single-photon technique lie more on the software side with improvements to reduce the aggressiveness of noise filters so that legitimate points are not removed.

Acknowledgements

The Authors wish to acknowledge the contributions of Naohiro Miaysaku, Director – Sensing Division, PASCO Corporation, Tokyo, Japan. The PASCO team was instrumental in acquiring both airborne linear-mode LiDAR data and ground truth data that was the main source for this study.

The authors also acknowledge the data samples and feedback provided by Ian Sinclair, Ontario (CA) Ministry of Natural Resources and Forestry in the use of single-photon airborne LiDAR data collected as part of the OMNR Forest Inventory project.

References

- Roth R and Marsh D, Optimizing LIDAR system settings for maximum forest canopy penetration. *2004 International LIDAR Mapping Forum*, Denver (US)
- Sinclair I, 2020, Case Study: Evaluating the potential of Single-Photon LiDAR for Ontario’s eFRI. *2020 Geospatial Content Solutions User Group Meeting*, Seville (ES).

How to consider the effects of time of day, beam strength, and snow cover in ICESat-2 based estimation of boreal forest biomass?

L. Korhonen¹, A. Bruguère¹, P. Varvia¹, J. Toivonen¹, P. Packalen¹, M. Maltamo¹, S. Saarela^{2,3}, S.C. Popescu⁴

¹University of Eastern Finland, School of Forest Sciences, Joensuu, Finland
Email: {lauri.korhonen; andre.bruguere; petri.varvia; janne.toivonen; petteri.packalen; matti.maltamo}@uef.fi

²Swedish University of Agricultural Sciences, Faculty of Forest Sciences, Umeå, Sweden
Email: svetlana.saarela@slu.se

³Norwegian University of Life Sciences, Faculty of Environmental Sciences and Natural Resource Management, Ås, Norway
Email: svetlana.saarela@nmbu.no

⁴Texas A&M University, Department of Ecology and Conservation Biology, College Station, United States
Email: s-popescu@tamu.edu

1. Introduction

The launching of two novel spaceborne lidar sensors back in 2018 provided scientists with new data sources for global monitoring of forest above-ground biomass (AGB). The GEDI (Global Ecosystem Dynamic Investigation) sensor was mounted on the international space station and does not acquire data from the boreal forest zone above 52°N (Dubayah et al. 2020). However, the ICESat-2 (Ice, Cloud and land Elevation Satellite 2) is in polar orbit and thus provides plenty of data from boreal forests (Markus et al. 2017). The ICESat-2 ATLAS (Advanced Topographic Laser Altimeter System) is a profiling lidar sensor that provides strip samples of terrain height measurements using multiple beams. Despite being primarily designed for snow and ice monitoring, ICESat-2 can also provide relatively accurate canopy height observations (Neuenschwander et al. 2020) that can be used to predict forest biomass (Narine et al. 2020).

Construction of ICESat-2 based AGB models for boreal forests requires consideration of several effects that may influence the observed accuracy. The ATLAS is a photon-counting lidar that operates at 532 nm wavelength and is therefore subject to solar noise photons that must be omitted by filtering (Popescu et al. 2018). Data collected in sunlit conditions inherently has more noise photons than night data, which could hamper their simultaneous use. The ATLAS has three strong and three weak lidar beams, and the weak beams may have a considerably poorer capability to observe canopy heights than the strong beams (Neuenschwander et al. 2020). In addition, boreal forests have snow cover during the winter. Snow on the forest floor and trees increases the reflectance at the 532 nm wavelength compared to summer conditions. If there is plenty of snow, the allometries between AGB and observed canopy heights could also be different, if the ground elevation is estimated from the ATLAS data.

Our objective is to investigate how the effects of time of day, beam strength and snow cover should be considered when constructing models for boreal forest AGB estimation using ICESat-2 data.

2. Data and methods

Our study site is a 60 × 50 km forest area located in Eastern Finland. The dominant tree species are Scots pine (*Pinus sylvestris*), Norway spruce (*Picea abies*), and birches (*Betula* spp.). The snowy season typically lasts from late November to late April.

We used airborne laser scanning (ALS) data and field plots acquired for an operational forest inventory in 2019. A total of 797 field plots with AGB ≥ 5 t ha⁻¹ were measured and used as training data. The ground AGBs were predicted by tree level allometric models that used diameter and height as inputs (Repola 2008, Repola 2009). The ALS data were collected 7 June – 9 July 2019 using a Leica ALS 80HP scanner at 1700 m above ground level, which resulted in a nominal pulse density of 5 m⁻². The publicly distributed data was however resampled to 0.5 pulses m⁻², which was still sufficient for AGB modelling using the area-based approach. The public ALS data were used to compute a set of

canopy height distribution variables for the field plots. We also extracted a set of spectral variables from an atmospherically corrected Sentinel-2 satellite image obtained 14 June 2019. These data were used to construct a model that was applied to predict reference AGBs for the ICESat-2 tracks in the study area. The model was constructed using regression analysis, and its predictors were selected using optimization by simulated annealing (Packalen et al. 2012). The final model included four predictor variables (two ALS, two Sentinel-2) and its relative root mean square error (RMSE) was 20.2%.

We used a total of five ICESat-2 passes from 2019 (2 and 22 February, 22 June, 18 and 22 August) to obtain a set of predictor variables representing day and night conditions with and without snow. We used ATL03 geolocated photon product (version 3), but the noise photons were removed based on the ATL08 land and vegetation product. A set of 15 x 90 m segments were placed at the ICESat-2 ground tracks. Each segment consisted of four 15 x 15 m cells, for which the reference AGBs were predicted using the ALS and Sentinel-2 data. The predicted AGBs were aggregated for the segments, and the segment AGBs were further used as reference values in ICESat-2 based AGB modelling.

The noise-filtered ATL03 photons located within the segments were used to compute a set of canopy height distribution variables based on normalized photon heights. The processing chain was similar to the ALS data. The variables included average height (avg), average square height (qav), standard deviation of height (std.), canopy height percentiles (p1, p5, ..., p99), and canopy density percentiles (d1, d5, ..., d99). Based on these variables, we constructed separate regression models for each of the eight ATL03 subsets (day/night, weak/strong beam, snow/no-snow), as well as a combined model where the time of day (night), beam strength (strong) and snow cover (snow) were included as dummies. In addition to the canopy height distribution variables listed above, sun elevation (sunelev), snow depth (snowdepth) and photon count (count) within the segment were used as additional predictors.

3. Results and discussion

In terms of RMSE (Table 1), winter models (RMSE 27–35%) showed smaller errors than summer models (34–61%). In winter conditions also the weak beam data were useful in AGB estimation, as the respective RMSEs were only 1–2 percent points larger than the strong beam RMSEs. With winter data, the day models also showed smaller RMSEs (27–28%) than night models (33–36%). However, the current winter results only represent the snow and weather conditions during the two ICESat-2 passes in February 2019. Weather could explain the observed differences, as the winter night data set had 20% of the photons removed as noise, which was above average for night conditions.

Table 1. The AGB models constructed for the different subsets based on the ATL03 data in the order of increasing RMSE.

Season	Time of day	Beam	n	Model	R ²	RMSE
Winter	Day	Strong	1150	$\sqrt{\text{AGB}} = 6.27 - 3.69\text{E-}3 \sqrt{\text{count}} + 0.13 \text{p99} + 2.62 \sqrt{\text{avg}}$	0.79	27%
Winter	Day	Weak	198	$\sqrt{\text{AGB}} = 23.99 + 0.14 \text{p99} - 1.31 \sqrt{\text{count}}$	0.73	28%
Winter	Night	Strong	901	$\sqrt{\text{AGB}} = 40.65 - 0.22 \sqrt{\text{count}} + 4.10 \sqrt{\text{avg}} - 4.60 \sqrt{\text{snowdepth}}$	0.82	33%
Summer	Night	Strong	2728	$\sqrt{\text{AGB}} = 0.76 + 4.21 \sqrt{\text{avg}} - 0.22 \sqrt{\text{qav}}$	0.77	34%
Winter	Night	Weak	874	$\sqrt{\text{AGB}} = -110.26 - 3.04 \text{sunelev} - 0.34 \text{p60} - 0.57 \sqrt{\text{count}} + 3.93 \sqrt{\text{avg}}$	0.75	35%
All	All	All	7158	$\sqrt{\text{AGB}} = 2.62 - 1.42 \text{night} - 0.67 \text{strong} + 2.08 \text{snow} + 3.54 \sqrt{\text{avg}}$	0.68	41%
Summer	Day	Strong	312	$\sqrt{\text{AGB}} = -21.65 + 3.78 \text{sunelev} + 0.84 \text{std} + 0.26 \text{p90} + 0.16 \sqrt{\text{count}}$	0.77	50%
Summer	Night	Weak	433	$\sqrt{\text{AGB}} = 1.69 + 3.02 \sqrt{\text{avg}}$	0.61	56%
Summer	Day	Weak	177	$\sqrt{\text{AGB}} = -55.50 + 10.73 \text{sunelev} + 0.026 \text{p99} + 0.61 \text{b95} - 5.88 \sqrt{\text{b80}}$	0.39	61%

Without snow, only the strong beam night data provided an RMSE that was comparable to winter models (34%). Strong beam day data also performed well if measured by R² (0.77), but its RMSE was

large (50%) as the sampled forest area had a small average AGB. Weak beam summer models had the poorest relative RMSEs (56–61%). The model that combined all data sets had larger RMSE than most of the individual models (41%) despite having time of day, snow cover and beam strength as statistically significant dummy variables.

4. Conclusions

The effects of snow cover and beam strength should be considered when constructing ICESat-2 based models for boreal forest AGB. It is better to construct separate models for different beams and snow conditions instead of merging everything into a single model. ATL03 data from snowy forests is well suited for AGB modelling, probably because of the increased reflectance at 532 nm, which makes weak beam data also usable. Time of day only had a clear effect on weak beam data without snow, where the night data provided a considerably smaller RMSE. In other cases, it could be possible to utilize both day and night data in a single model without compromising accuracy, at least if time of day is included as a predictor variable. The noise photon classification contained in the ATL08 product seemed sufficient for AGB modelling, although alternative noise filtering algorithms should also be tested in the future.

Acknowledgements

This study was funded by the Academy of Finland (grant number 332707).

References

- Dubayah R, Blair JB, Goetz S, Fatoyinbo L, Hansen M, Healey S, Hofton M, Hurtt G, Kellner J, Luthcke S, Armston J, Tang H, Duncanson L, Hancock S, Jantz P, Marselis S, Patterson PL and Silva C, 2020, The global ecosystem dynamics investigation: High-resolution laser ranging of the Earth's forests and topography. *Science of Remote Sensing*, 1: 100002.
- Markus T, Neumann T, Martino A, Abdalati W, Brunt K, Csatho B, Farrell S, Fricker H, Gardner A, Harding D, Jasinski M, Kwok R, Magruder L, Lubin D, Luthcke S, Morison J, Nelson R, Neuenschwander A, Palm S, Popescu S, Shum CK, Schutz BE, Smith B, Yang Y and Zwally J, 2017, The Ice, Cloud, and land Elevation Satellite-2 (ICESat-2): Science requirements, concept, and implementation. *Remote Sensing of Environment*, 190: 260-273.
- Narine LL, Popescu SC and Malambo L, 2020, Using ICESat-2 to estimate and map forest aboveground biomass: A first example. *Remote Sensing*, 12(11): 1824.
- Neuenschwander A, Guenther E, White JC, Duncanson L and Montesano P, 2020, Validation of ICESat-2 terrain and canopy heights in boreal forests. *Remote Sensing of Environment*, 251: 112110.
- Packalen P, Temesgen H and Maltamo M, 2012, Variable selection strategies for nearest neighbor imputation methods used in remote sensing based forest inventory. *Canadian Journal of Remote Sensing*, 38(5): 557-569.
- Popescu SC, Zhou T, Nelson R, Neuenschwander A, Sheridan R, Narine L and Walsh KM, 2018, Photon counting LiDAR: An adaptive ground and canopy height retrieval algorithm for ICESat-2 data. *Remote Sensing of Environment*, 208: 154-170.
- Repola J, 2008, Biomass Equations for Birch in Finland. *Silva Fennica*, 42(4): 605-624.
- Repola J, 2009, Biomass Equations for Scots Pine and Norway Spruce in Finland. *Silva Fennica*, 43(4): 625-647.

Vegetation Stratum Occupancy Prediction from Airborne LiDAR 3D Point Clouds

E. Kalinicheva^{1,2}, L. Landrieu¹, C. Mallet¹, N. Chehata^{1,3}

¹Université Gustave Eiffel, IGN-ENSG, LASTIG, F-94160 Saint-Mandé, France
Email: {ekaterina.kalinicheva, loic.landrieu, clement.mallet}@ign.fr

²INRAE, UMR 1202 BIOGECO, Université de Bordeaux, France

³EA G&E Bordeaux INP, Université Bordeaux Montaigne, France
Email: nesrine.chehata@bordeaux-inp.fr

1. Introduction

Estimating the structure of vegetation is a crucial first step for many environmental and ecological applications (Daubenmire 1956). In particular, pasture land management requires estimating the occupancy of the different vegetation strata within agricultural parcels. This is a time-consuming undertaking, often performed with *in situ* ocular approximate measurements. Nowadays, airborne platforms allow public and private actors to gather high accuracy geometric and radiometric data over large areas (Chen 2007). Bolstered by the compelling improvements (Guo et al., 2020) and increased accessibility of deep learning for 3D point clouds, we propose a 3D deep learning method to estimate the occupancy of different vegetation strata from airborne LiDAR and camera sensors.

Our method predicts raster occupancy maps for three vegetation strata (lower, medium, and higher) from 3D point clouds. Our training scheme allows our network to only be supervised with aggregated occupancy values at the plot level, which are easier to produce than point or pixel-level annotations. We also propose to use priors on the stratum elevation and the occupancy maps to improve the legibility and interpretability of the resulting maps.

2. Data and Methods

We present a new open-access dataset allowing for training and evaluating stratum occupancy regression methods from 3D LiDAR data. We then propose our network architecture along a training scheme for inferring raster occupancy maps while only training with aggregated values.

2.1 Dataset Composition

Our proposed dataset comprises 199 cylindrical plots of 10 m radius corresponding to typical pasture land parcels in South-Eastern France. Each plot contains between 3000 and 17000 3D points, and each point is attributed with a total of 9 features: (i) absolute 3D coordinates, (ii) RGB and Near-Infrared reflectance obtained with aerial cameras, (iii) uncalibrated laser intensity and return number provided by the aerial LiDAR.

Data normalization. The z -value of each point is normalized by subtracting the z -value of the lowest point in a 0.5 m-cylindrical neighborhood. Moreover, all values are normalized between 0 and 1 over the entire dataset.

Annotations. Each plot has been annotated by a human expert *in situ* providing the lower, medium, and higher stratum occupancy ratio, $(\hat{o}_L, \hat{o}_M, \hat{o}_H) \in [0,1]^3$ respectively (Figure 1). The occupancy value \hat{o}_L characterizes the proportion of the ground surface occupied by grass or low vegetation, as opposed to rocks, soil, or sand. \hat{o}_M characterizes the proportion of the surface of the plot occupied by the footprint of medium vegetation located between 0.5 and 1.5 m. This type of vegetation, typically bush-like, is the most accessible by pasture animals. Finally, the higher stratum occupancy \hat{o}_H is defined as the ratio of the plot surface occupied by the footprint of the canopy of trees over 1.5 m. Note

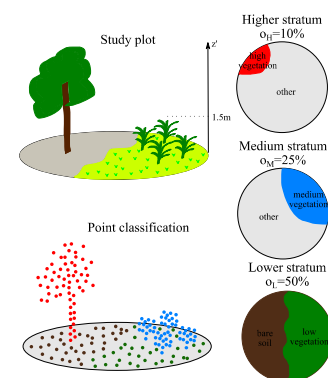


Figure 1: **Objective.** Our method aims to predict the vegetation occupancy of three strata from a point cloud.

that the trunks of trees over 1.5 m do not contribute to the medium occupancy. We argue that regressing the occupancy maps is intrinsically a semantic-constrained endeavor, and we thus opt for a neural network-based machine learning method.

2.2 Methodology

Given the attributed 3D point cloud corresponding to a study plot (see Figure 1), we aim to produce the vegetation occupancy maps for each vegetation stratum (lower, medium and higher level). We first compute a soft prediction for each point among four different classes: bare soil, low vegetation, medium vegetation, and high vegetation. We then project the resulting probabilistic point prediction onto the rasterized disks corresponding to the three target strata. The occupancy ratio at plot level is then obtained by averaging the prediction in each stratum. We propose a weakly-supervised scheme which allows the network to predict a class for each 3D point as well as vegetation occupancy rasters while only using aggregated occupancies, corresponding to 3 values for each plot.

Pointwise prediction. Given the relative geometric simplicity of single plots, we use an architecture inspired by the PointNet network of Charles et al. (2017) to compute the pointwise predictions. We denote the predicted probabilities for a point $i \in [1, 2, \dots, N]$ as follows: $(p_{i,S})$ for bare soil, $(p_{i,L})$ for lower, $(p_{i,M})$ for medium and $(p_{i,H})$ for high vegetation respectively (Figure 2).

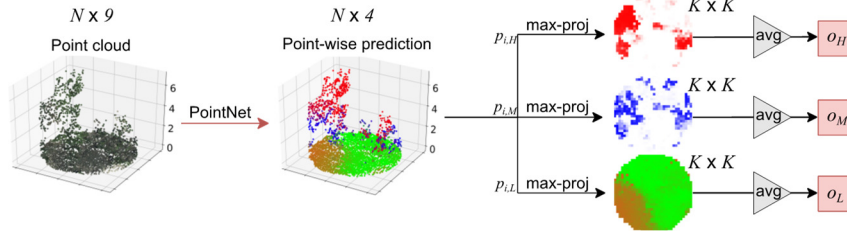


Figure 2: **Neural Architecture.** Our network performs the semantic segmentation of a 3D point cloud within four different classes. The resulting probabilities are projected onto rasters corresponding to different strata. Finally, the occupancies map are aggregated into the stratum vegetation ratio.

Point projection. The pointwise predictions are used to compute occupancy maps for each stratum, as shown in Figure 2. We consider three rasters of $K \times K$ pixels aligned with the projection of the cylindrical plot on the horizontal axes, and corresponding to the lower, medium, and higher vegetation strata. We associate the pixel j of stratum $s \in \{L, M, H\}$ with the set of 3D points Π_j whose vertical projection falls in the pixel's extent. We define the pixel occupancy o_s^j as the maximum for all points of Π_j of the probability of belonging to the vegetation stratum s :

$$o_s^j = \max_{i \in \Pi_j} p_{i,s} . \quad (1)$$

Finally, the stratum occupancy ratios o_L, o_M, o_H are defined as the average of the pixels' occupancies in the corresponding stratum:

$$o_s = \frac{1}{K^2} \sum_{j \in K \times K} o_s^j . \quad (2)$$

Elevation modeling. The model described above does not explicitly model the distribution of elevations within each stratum. In theory, points that are several meters above the ground can contribute to the lower stratum as long as the stratum-wise aggregated values are in agreement with the ground truth. We propose to explicitly model the elevation of points within each stratum in an automated way with the goal of making the occupancy maps more interpretable, and increasing generalizability.

We model the normalized elevation of all points of all clouds with a mixture of two Gamma distributions corresponding to the lower stratum, and to the medium and higher strata respectively. The distribution parameters can be efficiently estimated with the expectation–conditional–maximization algorithm, as detailed by Young et al. (2019). Using the Bayes theorem, this allows us to compute the likelihood of the elevation of each point given its stratum prediction.

Loss functions. The model is trained using three loss functions: (i) the mean absolute error between the predicted and ground truth plot occupancy, (ii) the average entropy of each pixel occupancy value, (iii) the average negative log-likelihood of points' elevation conditioned by their pointwise predictions:

$$l = l_{data} + \alpha l_{entropy} + \lambda l_{likelihood} \quad (3)$$

with α and λ regularization strengths, set to 0.2 and 1 respectively during all experiments. We chose to regularize with the entropy of pixel occupancy to implement the prior that most pixels should be either empty (no vegetation) or full (completely covered).

Our network is implemented in PyTorch and trained with ADAM optimizer and a batch size of 20 and with raster size $K = 32$. Our code, the data, as well as the precise configuration of all layers can be accessed at the following URL: https://github.com/ekalinicheva/plot_vegetation_coverage.

3. Results

To assess the performance of our model, we implemented a handcrafted approach and a simple deep learning baseline. The handcrafted approach classifies points among the different strata with a decision tree algorithm based on colors and elevation, while the rest of our pipeline is unchanged. The deep learning baseline directly predicts the stratum occupancy: o_L, o_M, o_H from the raw 3D point cloud with a simple PointNet network.

The qualitative results of our method and concurrent approaches are presented in Table 1. Our method outperforms the baselines, at the cost of added computation time compared to the simple deep baseline. Moreover, as seen in Figure 3, our method also allows visualizing the stratum occupancies.

Table 1. **Quantitative Results.** We report the accuracy of the predicted aggregated plot occupancy, along with the inference speed.

Method	Absolute error, %					Inference time, plots/s
	stratum	lower	medium	higher	average	
Handcrafted		21.9	20.7	10.3	17.6	20
PointNet Baseline		17.4	13.5	7.7	12.8	400
Ours		15.5	13.6	7.5	12.2	125

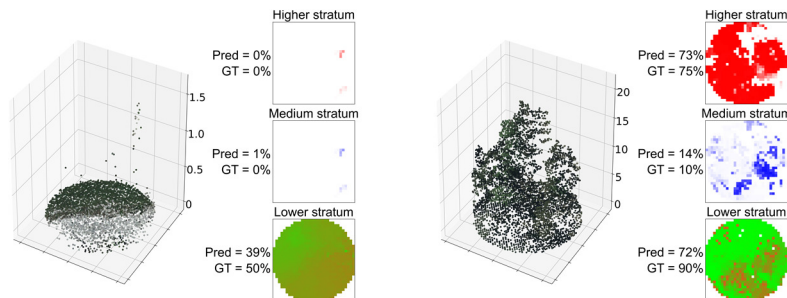


Figure 3: **Qualitative Results.** Our method predicts aggregated stratum occupancy along with the corresponding rasterized occupancy maps. Here, the pixels are colored according to the value of the predicted occupancy: shades of green, blue, and red indicate pixels with high-predicted vegetation coverage for the lower, medium, and higher strata respectively, while brown corresponds to bare soil.

4. Conclusion

In this paper, we presented a 3D deep learning method for predicting occupancy across vegetation strata. Using only three aggregated values per example plot, our model is able to perform a pointwise classification and to produce vegetation occupancy rasters with a high precision and a small computational cost. We also release the first deep learning-dataset to train and evaluate such methods.

References

- R. Q. Charles, H. Su, M. Kaichun and L. J. Guibas, *PointNet: Deep Learning on Point Sets for 3D Classification and Segmentation*. In CVPR, 2017.
- D. S. Young, Xi Chen, D. C. Hewage, and R. Nilo-Poyanco, *Finite mixture-of-gamma distributions: estimation, inference, and model-based clustering*. Advances in Data Analysis and Classification, 2019.
- R. Daubenmire, *A canopy-coverage method of vegetation analysis*. Northwest Sci, 1959.
- Q. Chen, *Airborne LiDAR data processing and information extraction*. PE&RS, 2007.
- Y. Guo, H. Wang, Q. Hu, H. Liu, L. Liu, and M. Bennamoun. *Deep learning for 3D point clouds: A survey*. IEEE transactions on pattern analysis and machine intelligence, 2020.

Shading effects of trees revealed using TLS and QSMs

Rafael Bohn Reckziegel¹, Jonathan P Sheppard¹, Christopher Morhart¹, Hans-Peter Kahle¹

¹ Chair of Forest Growth and Dendroecology - University of Freiburg, Tennenbacher Str. 4, 79106 Freiburg im Breisgau, Germany
Email: rafael.bohn.reckziegel@iww.uni-freiburg.de

1. Introduction

Terrestrial laser scanning (TLS) is a consistent technique for the 3D digitization of landscapes, which is enabling the quantification of landscape components with unprecedented level of details and accuracy. This effective, precise and non-invasive technology is ideal for assessing tree form and stand structure, as well as monitoring temporal dynamics of forests and agroforestry systems.

An established methodology is to scan trees from multiple positions, followed by the extraction of individual tree point clouds, and the reconstruction of tree structures with cylinder-fitting algorithms (e.g. *TreeQSM*, Raunonen et al. 2013). The retrieved tree structures are often called quantitative structure models (QSMs). These contain essential topological, geometrical and volumetric information related to functional properties of the scanned tree. The QSMs present the opportunity to measure and manipulate tree structures in order to study manifold ecological issues, e.g. the light availability at ground level under. Initial work by Roskopf et al. (2017), and Bohn Reckziegel et al. (2021), has demonstrated the potential of combining QSMs with the inclusion of virtual leaves to assess the shading effects of trees. Furthermore, the selection of targeted branches is possible by retrieving QSM-cylinders matching specific database queries.

In this study, we aim to quantify the changes in insolation reduction caused by tree structures reshaped by pruning treatments. We use field-tested pruning approaches as guidance for our computer-based pruning simulations to the QSMs. The application of analogous tree structures for creating multiple pruning and shading scenarios is innovative. Finally, virtual pruning of tree structures can support the design and selection of adequate tending operations to control light distribution in agroforestry systems.

2. Data and Methods

We selected four wild cherry trees (*Prunus avium* L.) belonging to a widely spaced tree plantation located in the proximity of Breisach, southwest Germany (48°4'24''N; 7°35'26''E, 182 m a.s.l.). Trees were digitized from a minimum of four scan positions with a terrestrial laser scanner Z+F IMAGER® 5010 (Zoller+Fröhlich GmbH, Wangen, Germany), under leaf-off conditions. The 3D structures of the four trees were retrieved with the MATLAB implementation of *TreeQSM* version 2.3 using the segmented tree point clouds.

We defined pruning treatments according to Springmann et al. (2011) including low and high intensity variants: removal of complete whorls as a conventional approach (p5w and p3w), and; removal of branches according to branch collar diameter and/or angle in relation to the stem, as a selective approach (p3d and p2d). The pruning treatments were implemented as algorithms written as independent functions in the open source language R version 3.5.3 (R Core Team 2019), to retrieve QSM-cylinders matching the specific database queries.

The resulting 20 tree structures were fed into a shadow model (Bohn Reckziegel et al. 2021) with fine spatiotemporal resolution to simulate the shade cast over a twelve months period (October 2013 until September 2014), and to estimate the insolation reduction on the ground. Shade projections were simulated for a quarter of a hectare with a grid-cell size of 10 cm x 10 cm, and time steps of 10 min, while factual solar radiance data from a nearby weather station were added to the model.

3. Results

The four trees differed in terms of total wood volume and crown characteristics, hence the simulated pruning interventions removed from 32% up to 59% of the tree's total volume. Low intensity pruning regimes varied for each tree both in relative and absolute terms, with an absolute difference ranging from 1.2 litres to a maximum difference of 5.5 litres. In between the high intensity approaches, selective pruning was less invasive than the conventional pruning. Total leaf area of the retrieved tree structures stayed below 50% of unpruned trees.

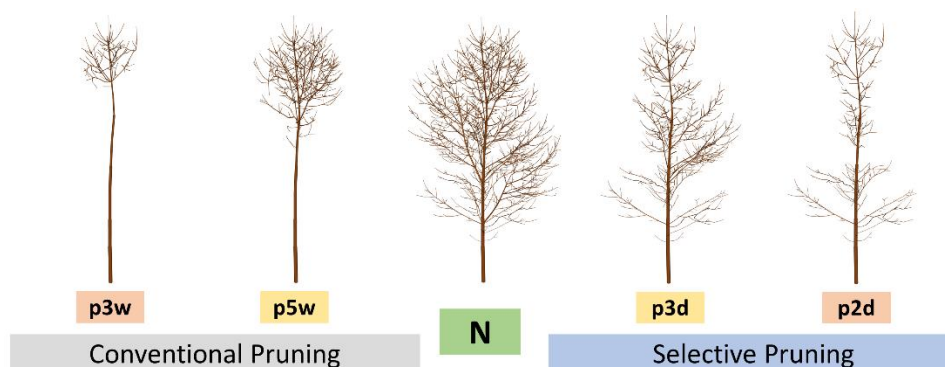


Figure 1 – Example of unpruned (N) and pruned variants of the same tree: left, conventional pruning; right, selective pruning; in yellow, low intensity pruning variants (p5w, p3d); in orange, high intensity pruning variants (p3w, p2d).

The control trees had the greatest shading effects; these were greater in area and in insolation reduction than any of the pruned variants (Table 1). Although shaded area varied throughout trees and treatments, selectively pruned trees had greater insolation reduction than conventional pruning.

Table 1 - Shading effects of unpruned and pruned structures of tree T1 for the simulation period of October 2013 to September 2014.

Tree	Shaded Area	Total Insolation Reduction	Mean Insolation Reduction	Mean Daily Insolation	Mean Daily Insolation Reduction
	m ²	MJ	MJ m ²	MJ m ² day ⁻¹	MJ m ² day ⁻¹
T1N	333.5	54,346	162.9	11.67	0.45
T1p3d	262.4	37,864	144.3	11.72	0.40
T1p2d	227.6	30,125	132.4	11.75	0.36
T1p5w	220.7	23,499	106.5	11.82	0.29
T1p3w	136.8	13,148	96.1	11.85	0.26

* Yearly insolation under "full light conditions" of 4,422 MJ m⁻² yearly and 12.11 MJ m⁻² day⁻¹ for the simulated period.

The spatial distribution of the annual shading effects of the unpruned and pruned T1 are shown in Figure 2. We found similar arrangement and trends for the shading effects of the trees. Overall, we noticed a smooth reduction in insolation spreading more than 20 m largely to the north of the sample tree. In a zoomed viewpoint, the grid-cells with more intensive insolation reduction can be seen. The control treatment showed a highly shaded centre, with a centralized higher insolation reduction four to eight meters from the tree position towards the north. Selectively pruned trees displayed similar patterns than the control treatment, although with reduced shaded area and less intense shading at the core. Conventional pruning softened the shading effects of all trees, with exception of a condensed semicircle arc spreading approximately four meters away from tree trunk, which is a clear manifestation of the resultant crown shape.

4. Discussion

High intensity pruning simulations suggested a removal of up to 60% of total tree volume, which could make these treatments too severe to be applied in reality. The low intensity treatments had a more appropriate removal of woody biomass ($\approx 40\%$ of tree volume). A change in the parameterisation of the pruning functions could be required for applying these same treatments to other tree species. The assessment of the annual insolation reduction showed that selective pruning is an option to attenuate the shading effect of tree structures, while conventional pruning radically minimizes shading. In areas where shading is relevant for crop production, or for the attenuation of climatic extremes, pre-designed selective pruning interventions are to be prioritized.

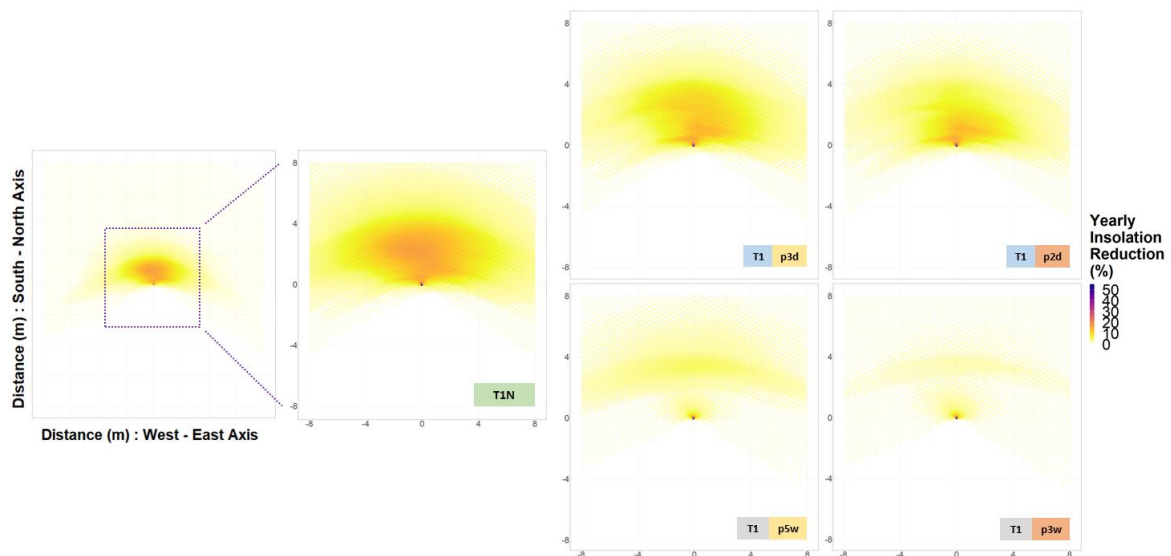


Figure 2 – Shading effects of tree T1 and from its analogous pruned tree structures for the twelve months period.

5. Conclusions

Pruning is a silvicultural intervention capable of influencing the light regime at ground level. Thus, the combined approach presented in this study is a way to facilitate management of the light resource at an individual tree level. It supports decisions about and demystifies the presence of trees in agricultural systems. Besides, virtual pruning of QSMs has the potential to become a tool for investigating, assessing and planning, alternatives to woody biomass production, management of ladder fuels, provision of ecosystem services, and the aesthetic view of landscapes.

Acknowledgements

This research was supported by the German Federal Ministry of Food and Agriculture (BMEL) within the projects Agro-Wertholz (support code 22031112) and SidaTim (support code 2815ERA04C) and by the German Federal Ministry of Education and Research (BMBF) within the ASAP project (grant number 01LL1803A).

References

- Bohn Reckziegel, Rafael; Larysch, Elena; Sheppard, Jonathan P.; Kahle, Hans-Peter; Morhart, Christopher. 2021. "Modelling and Comparing Shading Effects of 3D Tree Structures with Virtual Leaves" *Remote Sens.* 13, no. 3: 532. <https://doi.org/10.3390/rs13030532>
- Raumonen, P., M. Kaasalainen, M. Akerblom, S. Kaasalainen, H. Kaartinen, M. Vastaranta, M. Holopainen, and P. Lewis. "Comprehensive quantitative tree models from terrestrial laser scanner data." *Remote Sens.* 5, no. 2 (2013): 491-520.
- Springmann, Simeon, Robert Rogers, and Heinrich Spiecker. "Impact of artificial pruning on growth and secondary shoot development of wild cherry (*Prunus avium* L.)." *Forest Ecology and Management* 261, no. 3 (2011): 764-769.
- Roskopf, Elena; Morhart, Christopher; Nahm, Michael. 2017. "Modelling Shadow Using 3D Tree Models in High Spatial and Temporal Resolution" *Remote Sens.* 9, no. 7: 719. <https://doi.org/10.3390/rs9070719>

Towards Tree Green Crown Volume: A Methodological Approach using Terrestrial Laser Scanning

Zihui Zhu, Christoph Kleinn, Nils Nölke

Forest Inventory and Remote Sensing, Faculty of Forest Sciences and Forest Ecology, University of Göttingen, Büsingenweg 5, 37077 Göttingen, Germany

Email: {zzhu; ckleinn}@gwdg.de; nils.noelke@forst.uni-goettingen.de

1. Introduction

Tree crown variables are relevant in a number of contexts: they are not only “engines” of tree growth (Li et al 2017, Pretzsch et al 2015), but contribute – amongst others - filtering pollutants from the air, increasing storm resistance, shadowing of lower layers (and of houses in case of urban trees), offering habitat for various taxa, etc. Crown projection area has been long used as a major variable to describe crowns and their extension. One may ask whether the crown projection area alone does for all purposes sufficiently exhaustively characterize tree crowns, as, for example, for one and the same crown projection area, tree crowns may have very different 3D crown shapes, volumes and densities.

In this study, we introduce a new 3D crown variable named tree green crown volume (*TGCvol*). We use TLS-based (Terrestrial Laser Scanning-based) *k*-means clustering as a proxy for the assessment of this complex variable: *TGCvol* is one of those crown variables that are difficult to define and difficult to assess; and research needs to resort to proxies to make empirical studies feasible. To the best knowledge of the authors, *TGCvol* has so far not been introduced nor assessment approaches presented. The goal of this study is to introduce this concept, to develop and evaluate a TLS-based approach to assess the *TGCvol*, to describe its scale dependency and to discuss challenges regarding definitions, measurements and analyses.

2. Material and Methods

2.1 Definition

While the basic idea behind *TGCVol* is easily described as “the sum of spaces in the crown filled with leaves” – it turns out to be difficult to come up with an unambiguous definition that may form the basis for a likewise unambiguous measurement protocol. Many crown variables bring the same challenge with respect to direct measurement: their observation is, therefore, based on the assessment of meaningful proxies. For example, leaf area density (LAD) is often proxied by TLS scans with 3D voxelization (Béland et al 2014). Following the basic idea, *TGCVol* is proxied in this study by *k*-means convex hull clustering: we use the green TLS hits identified by the RGB information to recognize “leaf clusters”. *TGCVol* is then defined as the sum of all the volumes of envelopes of “leaf clusters”.

2.2 Data collection

We selected 26 sample trees within the city of Göttingen, Germany. Per tree, field measurements as dbh, crown base height and tree height were taken and the tree was scanned from 6 positions to guarantee a detailed 3D representation of outer and inner parts of the crowns.

2.3 Determining tree green crown volume

Our approach to assess *TGCvol* went in three steps: (1) woody elements removal, (2) *k*-means clustering, and (3) convex hull wrapping. The woody elements (stem and branches) were removed from the point

cloud of the single tree; the remaining points were considered as leaf hits. The k -means clustering approach (MacQueen 1967) was then applied to cluster groups of nearby leaf hits. k is the initial parameter that represents the total number of clusters to be produced. We started always with $k = 1$. The convex hull of this one single cluster is wrapping the total crown volume $CVol$ (see Figure 1a). We increased k so that more and smaller clusters were generated separating more and more the green and empty spaces within the crown (Figure 1). Around each cluster of hits, a convex hull was wrapped. The value for $TGCvol$ is calculated by summing up all the volumes of all these convex hulls. We increased k stepwise up to the value of $k=1400$. For each value of k , the sum of the wrapped clusters constitutes the $TGCvol$ at this particular spatial resolution. A suitable or even optimal value of k will depend on the specific subject-matter objective of a study and was not a focus of this research.

To make the values comparable between trees of different sizes, we developed the tree green crown volume index $TGCVI$ which is the percentage of tree green crown volume $TGCvol$ within the total crown volume $CVol$ ($k=1$): $TGCVI=TGCvol/ CVol$. $TGCVI$ tends towards a value of 1 when leaves occur uniformly all over the crown at a minimum density.

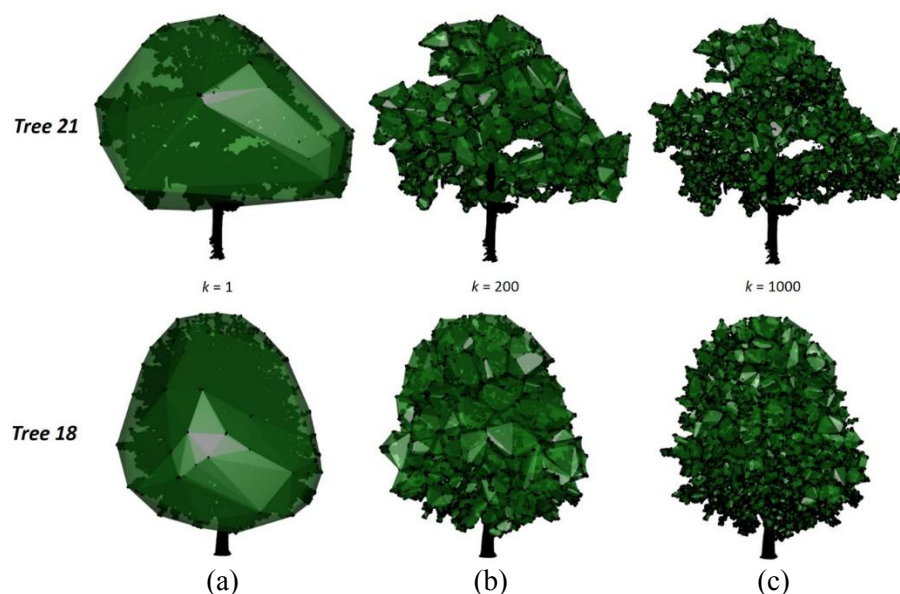


Figure 1. Illustration of the k -means clustering approach to generate hulls of green volume within the crown (sample trees 21 and 18): convex hulls were wrapped around: (a) $k=1$ cluster (wrapping the total crown volume); (b) $k=200$ clusters; and (c) $k=1000$. “Leaf clusters” can be seen more evenly distributed in the crown of Tree18 than of Tree21.

3. Results and Discussion

When refining the separation of green and empty spaces by increasing the number of clusters k , the green crown volume decreases. This describes the scale dependency of determining $TGCvol$. For our sample trees, $TGCvol$ decreased rapidly and then levelled out for values of k beyond 200-300 (see also Figure 2).

$TGCvol$ is not evenly distributed within the crown but comes in a clustered pattern: it is obvious that determining $TGCvol$ is scale-dependent. This is clearly illustrated in Figure 2 when plotting $TGCvol$ over the number of clusters: the finer the separation between green and empty spaces, the smaller the overall $TGCvol$. The scale is here derived from the number of clusters, which implicitly defines how fine the clustering is.

Our study is a pilot study to further develop measurement and analysis approaches towards a better description of tree green crown volume. The limited number of 26 sample trees in one single environment (urban trees) and without considering many different crown shapes does not allow further inferences about factors that determine amount and pattern of $TGCvol$; rather, our study was to

introduce the concept of *TGCvol* to better describe the foliage distribution in tree crowns and present a first case study for its assessment, identifying remaining methodological challenges.

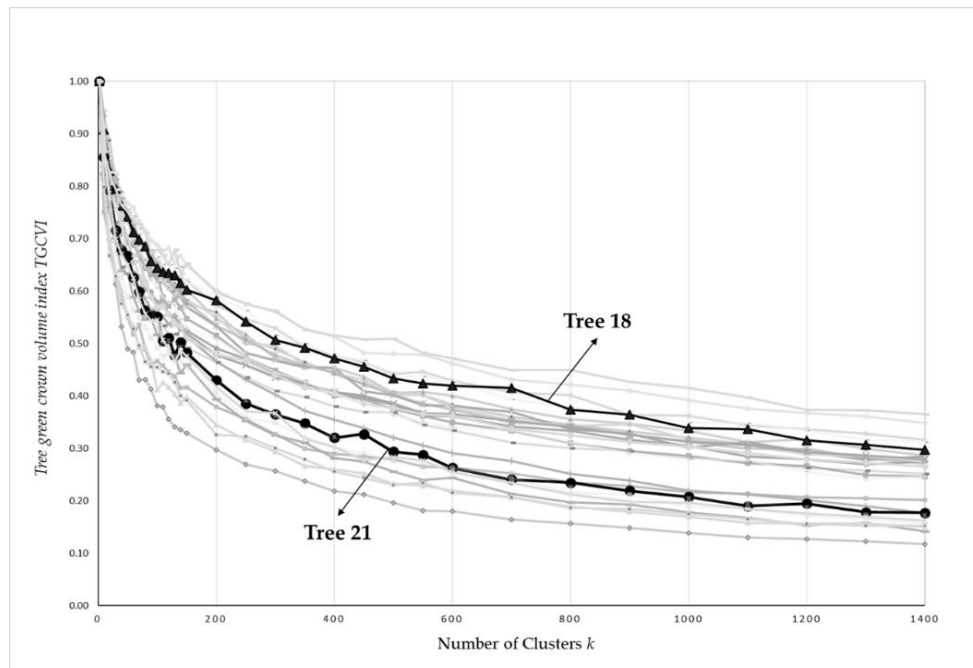


Figure 2. *TGCVI* over number of clusters k . As to be expected: the more clusters are formed, the finer is the separation of green and empty spaces within the crown which leads to decreasing values of *TGCVI*. The axis y is the normalized *TGCVI*. Tree 21 and tree 18 are highlighted by the bold line with markers.

4. Conclusions

We see various useful applications of *TGCvol* in particular in the context of trees outside the forest, for example in modelling of urban trees for habitat suitability and heat mitigation: a lower green volume will probably result in a lower heat mitigation and also influence the habitat quality for different taxa; but we also acknowledge (and addressed it in this paper) that there are numerous methodological challenges that wait to be resolved.

Acknowledgments

The initial motivation for this research originated from urban tree research within the DFG (German Science Council) funded research group FOR2423. We gratefully acknowledge the DFG project funding. We would like to thank the Chinese Scholarship Council CSC that supports the first author with a PhD scholarship.

References

- Li Y, Kröber W, Bruelheide H, et al., 2017, Crown and leaf traits as predictors of subtropical tree sapling growth rates[J]. *Journal of Plant Ecology*, 10(1): 136-145.
- Pretzsch H, Biber P, Uhl E, et al., 2015, Crown size and growing space requirement of common tree species in urban centres, parks, and forests[J]. *Urban Forestry & Urban Greening*, 14(3): 466-479.
- MacQueen J, 1967, Some methods for classification and analysis of multivariate observations[C]. *Proceedings of the fifth Berkeley symposium on mathematical statistics and probability*, 1(14): 281-297.
- Béland M, Baldocchi D D, Widłowski J L, et al., 2014, On seeing the wood from the leaves and the role of voxel size in determining leaf area distribution of forests with terrestrial LiDAR[J]. *Agricultural and Forest Meteorology*, 184: 82-97.

A method to estimate silhouette to total area ratio (STAR) from TLS point clouds

Daniel Schraik¹, Aarne Hovi¹, Miina Rautiainen^{1,2}

¹Aalto University, School of Engineering, Department of Built Environment, PO Box 14100, 00076 Aalto, Finland
Email: daniel.schraik@aalto.fi

²Aalto University, School of Electrical Engineering, Department of Electronics and Nanoengineering, Finland

1. Introduction

Correcting for clumping of needles into shoots has become a standard procedure in radiative transfer analyses of conifer forests. Clumping needs to be corrected due to the near-ubiquitous assumption of the Poisson canopy, i.e. the random distribution of plant elements throughout the canopy. While there are many ways to quantify clumping, the silhouette to total area ratio (STAR) has become the standard procedure for correction the clumping of conifer needles into shoots. STAR is the ratio of the orthogonal projection area of a body, averaged over all directions of the sphere, to its total surface area. A simple, convex body always has a STAR of $\frac{1}{4}$, whereas a composite body, such as a conifer shoot, has a STAR less than $\frac{1}{4}$. The concept of STAR originates from one of Augustin-Louis Cauchy's theorems, which was adapted for use in radiative transfer modeling of plant stands by Lang (1991).

STAR as a clumping quantifier was proven essential in accurately modeling reflectance of conifer stands (Rautiainen and Stenberg 2005). Within the concept of photon recollision probability (Knyazikhin et al. 1998, Stenberg et al. 2016), STAR can be used to quantify the photon recollision probability in a hierarchy of canopy elements, such as shoots, crowns, and stands (da Silva 2008). However, the hierarchical STAR remained a theoretical concept applicable only to simulation data due to a lack of measurement methods.

With the increasingly wide-spread use of terrestrial laser scanning (TLS) and the development of preprocessing and estimation routines for forest ecology, we have the necessary tools to develop a measurement method for STAR at the crown and stand level.

In this presentation, we present a method that is capable to estimate STAR from point cloud at any hierarchical level. We empirically validated our method with data from destructive leaf area measurements, and photogrammetric silhouette area measurements in small spruce trees.

2. Data and Methods

2.1 Estimating STAR from point cloud data

We scanned 14 spruce trees (*Picea abies* (L.) H. Karst.) from Southern Finland with a Leica P40 scanner at resolutions of 0.15 and 0.32 mrad in 2018. The scans were performed from six positions, 10 m from the tree and spread evenly across azimuth directions. We used five 4.5" Leica B&W co-registration targets for the co-registration of the point clouds. The point clouds were preprocessed in Leica Cyclone, and the point clouds were exported with the individual scan positions retained in the data to allow conversion into rays.

The point cloud data was then used to estimate the attenuation coefficient in a voxel grid covering the crowns' volumes. We used the unbiased estimator developed by Pimont et al. (2018), which is based on the modified contact frequency and accounts for biases introduced by the finite number of beams entering a voxel, and the finite size of the plant elements. The one-sided leaf area density within a voxel can then be estimated through dividing the attenuation coefficient by G , the average projection area of unit leaf area. Multiplication by the voxel volume, summing over all voxels, and doubling then yields the total (two-sided) leaf area of the tree.

The second part of STAR is the silhouette area, which we estimated from the attenuation coefficient by ray tracing, using the Beer-Lambert law to calculate attenuation as the rays traveled through each voxel. The set of all rays formed a synthetic image, where each pixel corresponded to the fraction of

transmitted radiation in an orthogonal projection. The sum over the synthetic image, multiplied by the squared beam spacing (i.e. the pixel area) yields the silhouette area. The silhouette area was averaged over 72 directions to approximate a spherical integral.

Both above steps, estimating of attenuation coefficient (and leaf area density) and silhouette area, were carried out with voxel sizes between 5 cm and 90 cm. The measurements are described in more detail in Schraik et al. 2019.

2.2 Reference data

The total leaf area of each tree was determined destructively. We measured the trees' biomass of needles and branches up to a diameter of 2 cm. For a sample of 20 shoots per tree, we determined the leaf area, the leaf weight, and the twig weight. The fraction of leaves of the tree biomass, multiplied by the leaf area per leaf mass, yielded the total leaf area.

The directional silhouette area was determined at six directions coincident with the TLS scan locations. We used a Sony A7R camera with a 28mm lens to take photos of the trees. The photographs were taken with a white background, and were converted into binary images. Given the pixel size of the camera sensor, and the average distance between the camera and the tree crown (estimated from the point clouds), we calculated the silhouette area as the sum of the image covered by the tree.

3. Results and Discussion

Estimates for crown-level STAR were highly dependent on voxel size, and ranged from about 0.075 to 0.25. Generally, STAR estimates increased with increasing voxel size. At 90 cm voxel size, STAR was about 0.25, which can be explained simply by most trees being covered in 1 to 4 voxels, at which point the crown clumping is incorporated already into the leaf area estimates, and the resulting voxel structure can be seen as a turbid medium approximation. There seemed to be an optimal voxel size that depends on the spatial structure of the tree crown. It should be fine enough to resolve the empty space between branches, but also large enough to ensure a high number of beams inside each voxel. In our data, this voxel size seemed to be around 10 to 20 cm.

The dependence of voxel size was similar in leaf area estimates, but the trend was negative. The 90 cm voxel size resulted in estimates closest to the destructive measurements (less than 2% overestimation), whereas the 10 cm voxels overestimated leaf area by about 67%. The silhouette area estimates were less sensitive to voxel size, but exhibited a positive trend with increasing voxel size. In 10 cm voxels, silhouette area was overestimated by about 22%, while in 90 cm voxels the bias increased to about 28%.

However, it is premature to conclude that larger voxel sizes work better in leaf area estimation, because there are a number of factors at play. Soma et al. (2018) found a similar bias for small voxel sizes, but a significantly larger error in large voxels already at 70 cm in oak and pine branches. We suspect that the modified contact frequency may have a tendency to overestimate leaf area, particularly in conifer trees because the TLS footprint is too large to resolve the fine shoot structure, therefore potentially introducing a bias into estimates that is independent of the voxel size. In addition, since plant elements inside a voxel are assumed to be randomly distributed, clumping at scales smaller than the voxel size may cause a negative bias on leaf area estimates that depends on the voxel size. Together, these two biases may cancel each other out at certain voxel sizes, as we suspect was the case at 90 cm voxel size in our validation experiment.

4. Conclusions

We presented a method to quantify the silhouette to total area ratio from TLS point clouds. Our method relies on voxel-based estimates of leaf area density, which are orthogonally projected to obtain their silhouette area. As such, our method relies on the accuracy of leaf area density estimates, which is a subject of ongoing research. We validated our method using small spruce trees, which showed that the voxel size plays a crucial role in quantifying STAR as well as leaf area density. Based on our findings,

we suspect that using voxel sizes between 10 and 20 cm appear to provide a reasonable trade-off between fine-scale detail and computational feasibility.

Acknowledgements

The authors received funding from the European Research Council (ERC) under the European Union's Horizon 2020 research and innovation programme (grant agreement No 771049). The article reflects only the authors' view and the Agency is not responsible for any use that may be made of the information it contains.

References

- Da Silva, D., Boudon, F., Godin, C., Sinoquet, H., 2008. Multiscale framework for modeling and analyzing light interception by trees. *Multiscale Modeling & Simulation* 7 (2), 910–933. <https://doi.org/10.1137/08071394x>.
- Knyazikhin, Y., Martonchik, J.V., Myneni, R.B., Diner, D.J., Running, S.W., 1998. Synergistic algorithm for estimating vegetation canopy leaf area index and fraction of absorbed photosynthetically active radiation from MODIS and MISR data. *Journal of Geophysical Research: Atmospheres* 103 (D24), 32257–32275. <https://doi.org/10.1029/98jd02462>.
- Lang, A., 1991, Application of some of cauchy's theorems to estimation of surface areas of leaves, needles and branches of plants, and light transmittance. *Agric For Meteorol* 55 (3–4), 191–212. [https://doi.org/10.1016/0168-1923\(91\)90062-u](https://doi.org/10.1016/0168-1923(91)90062-u).
- Pimont, F., Allard, D., Soma, M., Dupuy, J.-L., 2018. Estimators and confidence intervals for plant area density at voxel scale with t-Lidar. *Remote Sens Environ* 215, 343–370. <https://doi.org/10.1016/j.rse.2018.06.024>.
- Rautiainen, M., Stenberg, P., 2005. Application of photon recollision probability in coniferous canopy reflectance simulations. *Remote Sens Environ* 96 (1), 98–107. <https://doi.org/10.1016/j.rse.2005.02.009>.
- Schraik, D., Hovi, A., Rautiainen, M., 2021. Crown level clumping in Norway spruce from terrestrial laser scanning measurements. *Agric. For. Meteorol.* 296, 108238. <https://doi.org/10.1016/j.agrformet.2020.108238>.
- Soma, M., Pimont, F., Durrieu, S., Dupuy, J.-L., 2018. Enhanced measurements of leaf area density with t-LiDAR: evaluating and calibrating the effects of vegetation heterogeneity and scanner properties. *Remote Sens* 10 (10), 1580. <https://doi.org/10.3390/rs10101580>.
- Stenberg, P., Möttus, M., Rautiainen, M., 2016. Photon recollision probability in modelling the radiation regime of canopies—a review. *Remote Sens. Environ.* 183, 98–108. <https://doi.org/10.1016/j.rse.2016.05.013>.

Modelling the Detection Rate of Terrestrial Laser Scanning in Multi Scan Mode

T. Ritter¹, C. Gollob¹, A. Nothdurft¹

¹University of Natural Resources and Life Sciences, Vienna, (BOKU), Institute of Forest Growth, Peter-Jordan-Str- 82, Vienna 1190, AUSTRIA

Email: {tim.ritter ; christoph.gollob ; arne.nothdurft}@boku.ac.at

1. Introduction

Terrestrial laser scanning (TLS) has been successfully applied in the context of manifold forestry applications and enables a fast and automatic acquisition of the forest structure (Fardusi et al. 2017). A major challenge of TLS applications in forestry is occlusion (Abegg et al. 2017), because the laser is often obstructed by other trees or understory vegetation. In order to obtain a complete point cloud, the multi scan mode is preferably used in most studies (Ritter et al. 2020). However, systematic studies regarding efficiency of different scanner position layouts and size or shape of sample plots are still rare. Recently, Ritter et al. (2020) developed a methodology to model the detection probability of multi-scan TLS, by extending the traditional distance sampling framework (Buckland et al. 2001) to account for multiple scan positions. Data from single scans was sufficient to parameterize the underlying detection model, making the model easily adoptable to different forest types and sighting conditions. By comparing the model results to real world data of circular sample plots with different radii and scanner position layouts (Gollob et al. 2019), it was shown that beside a minor discretization bias associated with small sample sizes, the model was able to accurately predict the detection probability of TLS on these plots (Ritter et al. 2020).

In this research, the methodology proposed by Ritter et al. (2020) is used to model the detection probability of TLS for rectangular sample plots of different size and aspect ratio and for different scanner position layouts. In total, 54 Variants are compared regarding their detection rate and sampling effort.

2. Data and Methods

The distance sampling framework (Buckland et al. 2001) is based on the assumption that the detectability of objects typically decreases with increasing distance r between the observer (i.e. the laser scanner in our application) and the object of interest (i.e. a tree) and can be modelled by a distance-depending detection function $g(r)$. For single scan applications, the mean detection probability (detection rate) within a circular sample plot of area a and radius ω can be estimated by

$$\hat{P}_a = \frac{2}{\omega^2} \int_0^{\omega} r \times g(r) dr \quad (1)$$

(Astrup et al. 2014).

Ritter et al. (2020) extended the framework to multi scan applications with I scanner positions, assuming that the probability of detecting an arbitrary tree located at position j in a distance of r_{ij} from the scanner position i is independent from the probability to detect the same tree from any other scanner position $i' \neq i$ for $i', i \in \{1, \dots, I\}$. This probability can then be estimated by $g(r_{ij})$, so that the probability to detect a tree located at location j becomes

$$P_j = 1 - \prod_{i=1}^I (1 - g(r_{ij})) \quad (2)$$

An arbitrary sized and shaped sample plot can be described by a set of J raster cells. For every raster cell centroid, Eq. 2 can be applied to predict the probability to detect a tree located within the cell. Thus, the mean detection probability (detection rate) P_a per sample plot can be estimated as the arithmetic mean of all raster cell estimates P_j within the plot (Eq. 3)

$$\hat{P}_a = \frac{1}{J} \sum_{j=1}^J \left(1 - \prod_{i=1}^I (1 - g(r_{ij})) \right) \quad (3)$$

(r_{ij}) can be parameterized from single scan reference data (Ritter et al. 2020).

In the following, we use the extended hazard rate type detection function (Ritter et al. 2020) with parameter estimates obtained by fitting the function to freely available single scan data from Lower Austria (Gollob et al. 2020). The detection probability of trees having a diameter at breast height (dbh) of 20cm or more, was modeled for the algorithms of (Gollob et al. 2019) on rectangular sample plots with different size and aspect ratio (Table 1) and with different scanner position layouts (Figure 1).

3. Results and Discussion

The modelled detection probabilities P_j for the cells of a $0.1\text{m} \times 0.1\text{m}$ raster obtained with the different multi scan layouts are depicted in Fig. 1. The detection rate \hat{P}_a for different rectangular sample plots, centered at the origin of the local coordinate system are presented in Table 1.

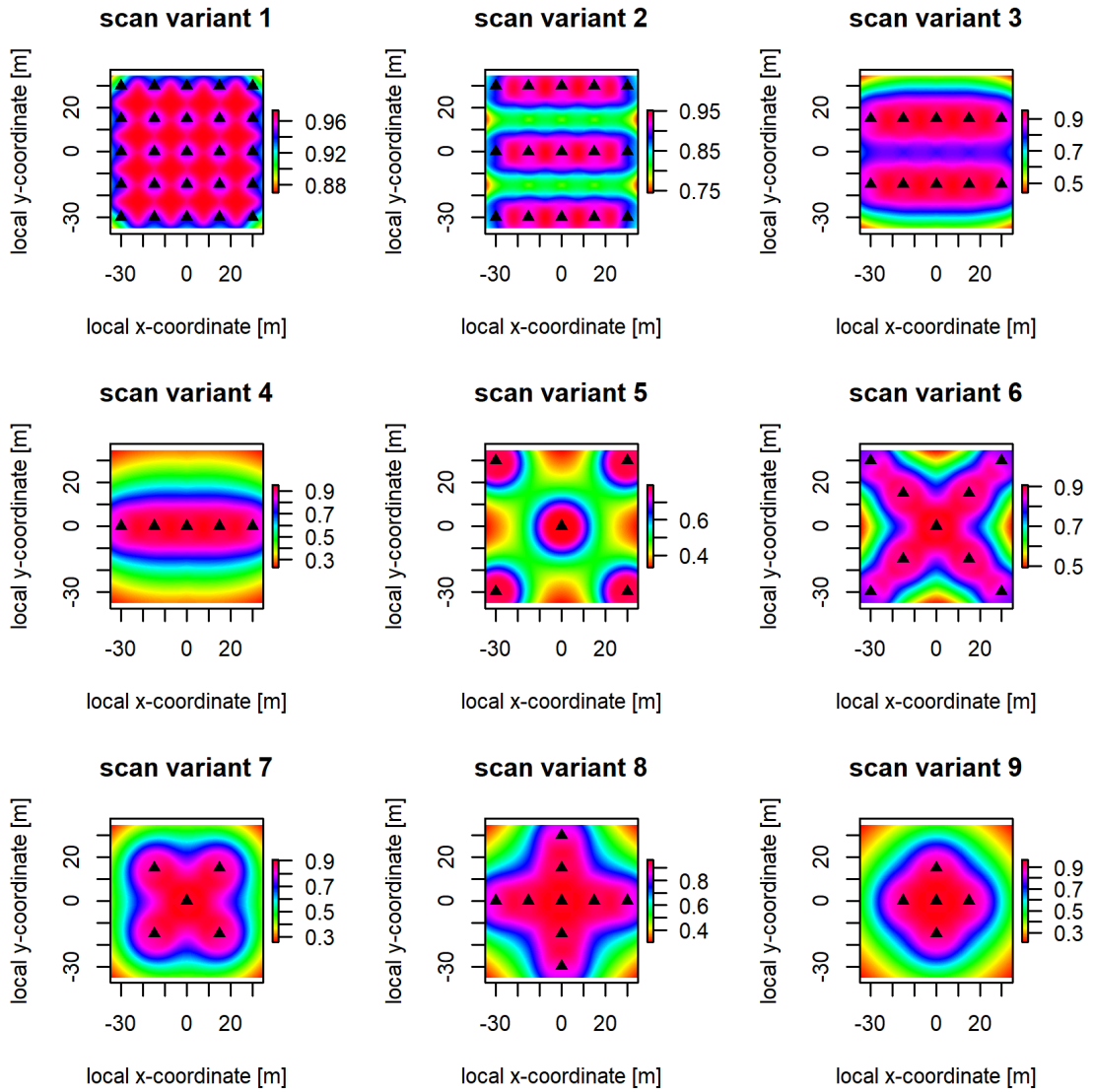


Figure 1. Modelled detection probability P_j for different scan variants. The black triangles symbolize scanner positions.

The scanner position layout strongly influences the detection rate. As an example, scan variant 5 on a 30m×30m sample plot yields a detection rate of 65.22% with a total of 5 scans, while scan variant 9 yields a detection rate of 93.06% with the same sampling effort (Table 1). The aspect ratio of the sample plot is another crucial factor, having two 900m² sample plots, one being 60m×15m, the other one being 30m×30m, detection rates obtained by the same scan variant differ remarkably, e.g., 86.85% vs. 93.06% for scan variant 9.

Table 1. Detection rate estimates for different scanner position layouts and sample plot sizes

Scan variant	Sample plot size					
	60m×60m (=3600m ²)	60m×30m (=1800m ²)	60m×15m (=900m ²)	30m×30m (=900m ²)	30m×15m (=450m ²)	15m×15m (=225m ²)
1 (25 scan positions)	96.49%	96.50%	96.50%	96.51%	96.51%	96.51%
2 (15 scan positions)	88.56%	88.56%	92.25%	88.82%	92.65%	92.65%
3 (10 scan positions)	87.08%	88.56%	84.86%	88.82%	84.99%	94.99%
4 (5 scan positions)	67.51%	85.54%	91.75%	86.55%	92.48%	92.48%
5 (5 scan positions)	54.81%	55.17%	57.37%	65.22%	71.17%	78.27%
6 (9 scan positions)	81.88%	82.76%	81.02%	88.26%	88.63%	90.12%
7 (5 scan positions)	75.19%	80.83%	79.73%	88.16%	88.62%	90.12%
8 (9 scan positions)	81.90%	90.27%	93.64%	93.78%	95.28%	96.04%
9 (5 scan positions)	72.02%	83.28%	86.85%	93.06%	94.96%	96.04%

The modelled detection rates for the scanner position layouts and sample plot shapes presented in this research were not compared to real world data. However, the methodology used for modelling was already intensively tested with several other sample plot shapes and scanner position layouts and proved to yield accurate results (Ritter et al. 2020). Thus, we are confident that the provided estimates are reliable.

The detection function was fitted to single scan reference data from lower Austria, making the results valid only for stands with comparable structure and sighting conditions. However, fitting the detection function to different reference data is straightforward and associated with a comparatively low effort (Ritter et al. 2020).

4. Conclusion

The methodology by Ritter et al. (2020) allows a model-based comparison of the detection rates with different scanning position layouts, sample plot-sizes and -shapes. The benefits from a well-planned multi-scan layout justify the necessary extra effort, especially in larger sampling campaigns

References

- Abegg, M., Kükenbrink, D., Zell, J., Schaepman, M., Morsdorf, F., Abegg, M., Kükenbrink, D., Zell, J., Schaepman, M.E., and Morsdorf, F. 2017. Terrestrial Laser Scanning for Forest Inventories—Tree Diameter Distribution and Scanner Location Impact on Occlusion. *Forests* **8**(6): 184. doi:10.3390/f8060184.
- Astrup, R., Ducey, M.J., Granhus, A., Ritter, T., and von Lüpke, N. 2014. Approaches for estimating stand-level volume using terrestrial laser scanning in a single-scan mode. *Can. J. For. Res.* **44**(6): 666–676. doi:10.1139/cjfr-2013-0535.
- Buckland, S.T., Anderson, D.R., Burnham, K.P., Laake, J.L., Borchers, D.L., and Thomas, L. 2001. Introduction to distance sampling: Estimating abundance of biological populations. Oxford Univ. Press.
- Fardusi, M.J., Fardusi, M.J., Chianucci, F., and Barbati, A. 2017. Concept to Practice of Geospatial-Information Tools to Assist Forest Management and Planning under Precision Forestry Framework: a review. *Ann. Silv. Res.* **41**(1): 3–14. doi:10.12899/asr-1354.
- Gollob, C., Ritter, T., and Nothdurft, A. 2020. Comparison of 3D point clouds obtained by terrestrial laser scanning and personal laser scanning on forest inventory sample plots. *Data* **5**(4): 1–13. doi:10.3390/data5040103.
- Gollob, C., Ritter, T., Wassermann, C., and Nothdurft, A. 2019. Influence of Scanner Position and Plot Size on the Accuracy of Tree Detection and Diameter Estimation Using Terrestrial Laser Scanning on Forest Inventory Plots. *Remote Sens.* **11**(13): 1602. doi:10.3390/RS11131602.
- Ritter, T., Gollob, C., and Nothdurft, A. 2020. Towards an optimization of sample plot size and scanner position layout for terrestrial laser scanning in multi-scan mode. *Forests* **11**(10): 1–23. doi:10.3390/f11101099.

Correcting TLS Estimation for Shading by Other Trees Using a Horvitz-Thompson-like Estimator

K. Kansanen², P. Packalen², M. Maltamo² and L. Mehtätalo¹

¹Natural Resources Institute Finland (Luke), Yliopistokatu 6, 80100 Joensuu, Finland
Email: lauri.mehtatalo@luke.fi

² University of Eastern Finland, P.O. Box 111, 80101 Joensuu, Finland
Email: kasperkansanen@gmail.com, petteri.packalen@uef.fi, matti.maltamo@uef.fi.

1. Introduction

In circular plot sampling, a sample plot is defined by the plot location, and trees within a given distance (called plot radius) from that point constitute a sample. However, not all trees may be visible to the center point of the plot because they are hidden by the other tree stems or other obstacles (such as rocks) that may be present on the sample plot. In traditional field inventories, this is not a problem because the field crew can temporarily move from the plot center to see all trees. However, that is not the case if a terrestrial laser scanner is used for data collection using single scan from the plot center. For example, Seidel and Ammer (2014) reported that approximately 2.5-7.5% of the plot area may be not sampled due to this shadowing effect. Therefore, there is a need for methods to adjust the estimators of populations totals from TLS sampling for this non-detection.

We are not the first authors to tackle this problem. Lovell et al. (2011) outlined a method based on a gap probability in a Poisson forest. Duncanson et al (2014) and Astrup et al (2014) have proposed methods based on classical distance sampling. Seidel and Ammer (2014) determined a correction factor based on the shadowed area. Olofsson and Olsson (2018) proposed an estimator that is based on using the area visible to the scanner as a sampling window. Their method was further extended by Kuronen et al (2019) to allow different correction factors for different detection conditions for the observed trees. That is, the estimator can take into account how big proportion of a tree stem should be visible to make the tree observable to the laser scanner. In the method of Kuronen et al. (2019), the plot edge is partially at the applied maximum radius of the plot or at edges of the observed tree stems. Therefore, the estimator is biased because the realized tree locations determine the plot size, and there are lot of trees that are located on the plot border, in similar ways as in the point-to-object sampling (see e.g. Ducey 2018).

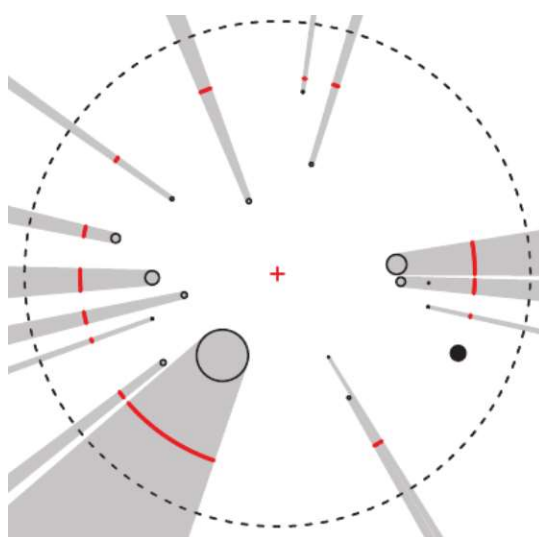


Figure 1. Illustration of the proposed estimation approach when the condition for detectability is visibility of the center point of the tree to the scanner for tree number 17 on a plot delineated by the dashed line (Kansanen et al 2020).

In this paper, we discuss a new estimator (Kansanen et al 2020) that is based on the ordering of the trees according to their distance from the plot center. The estimator is unbiased under the assumption of complete spatial randomness (CSR) of tree locations in the hidden part of the plot. The estimation is based on CSR, but it is conditioned on the observed tree locations. In practice, it means that the model assumptions affect the estimation only in the hidden parts of the sample plot. An estimator for the variance of the estimator is also presented and used for constructing 95% confidence intervals for estimated stand density.

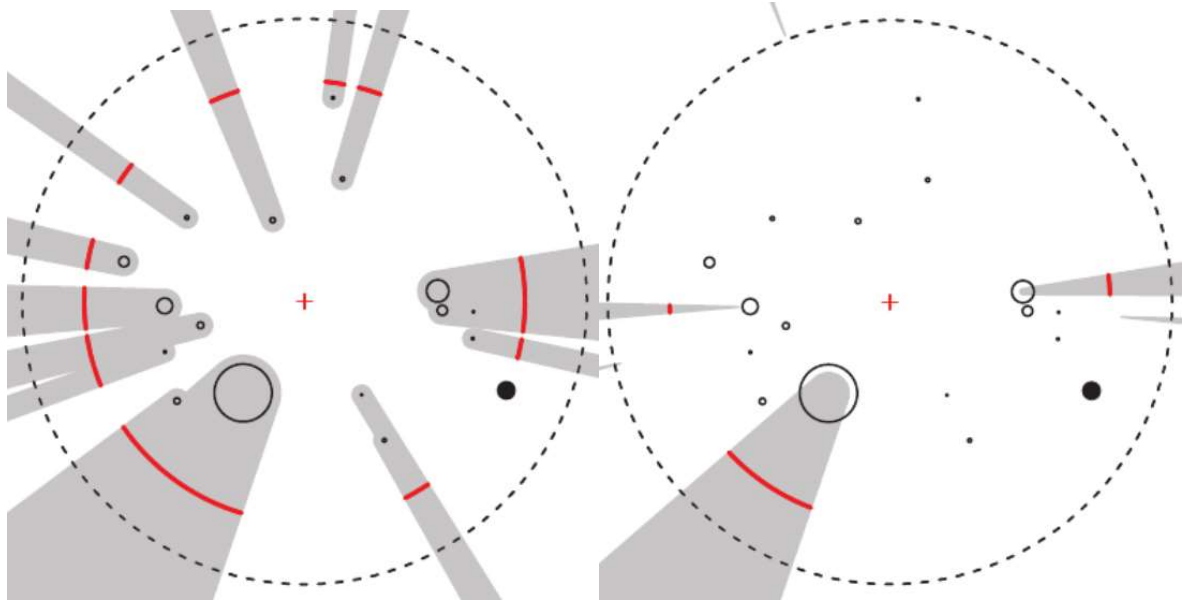


Figure 2. Illustration of the proposed estimation approach when the condition for detectability is full visibility (left) and visibility of any part of the tree the tree (right) to the scanner for tree number 17 on a plot delineated by the dashed line (Kansanen et al 2020).

2. Data and methods

Consider trees observed by a TLS device on a fixed plot and order them according to their distance from the plot center. We refer closer trees here as “earlier” in such an ordered sequence. The first tree of the sequence is observed for sure, because there are no trees behind which to hide. Let us then consider the second tree, and condition on its distance r_2 from the plot center. Assuming that a tree remains unobserved if its center point is hidden behind the earlier trees, the second tree would have been unobserved if it were located on such part of the perimeter of a r_2 -radius disc that is hidden behind the earlier trees. This provides an estimated detection probability for the tree as a ratio of the visible part and the total perimeter length of the r_2 -radius circle centered at the origin. In the same way, we can compute the detection probabilities for the other trees as well. For example, the red line in Figure 1 illustrates those sections of perimeter of a r_{17} -radius circle where the 17th tree of a would be hidden. In Figure 1, a tree is assumed to be detectable when the center point of the stem is visible to the scanner (detection condition “center”). Figure 2 illustrates the two other detection conditions, called “any” and “full”.

After the detection probabilities have been estimated, tree characteristics can then be estimated using a Horvitz-Thompson-like estimator

$$\hat{T} = \sum \frac{t_i}{\hat{\pi}_i}$$

where \hat{T} is the estimator of the population total T , t_i is the total of observed tree i , and $\hat{\pi}_i$ is the detection probability of tree i . The estimator is called Horvitz-Thompson-like estimator because the detectability is an estimate of the inclusion probability of sampling unit i , not a known true inclusion probability. When stand density (trees per plot) is estimated, $t_i=1$ for all trees i . Therefore, the estimator essentially includes for each observed tree a number $n_i = \frac{1}{\hat{\pi}_i} > 1$, which gives the estimated number of trees similar

to the observed tree i . The later the tree is in the ordered sequence, the larger is n_i . An R-implementation of the estimator is available in function `HTest_cps` of R-package `lmfor` (Mehtätalo 2019).

The proposed estimator is evaluated using simulated forests where the spatial pattern varies from strong regularity to strong clustering. In addition, a data set of 111 square 30 by 30 meter mapped forest plots from Eastern Finland are used to evaluate the estimator, by simulating circular, 10-meter radius TLS plots on them. The spatial pattern of tree locations on these plots is slightly regular.

3. Results and discussion

We show that the estimator is unbiased if the tree locations follow the assumption of complete spatial randomness and present an estimator for its variance. The performance of the estimator is illustrated in plots of simulated forests of different spatial patterns as well as on real mapped forests. The empirical results showed better or similar performance than the estimator of Kuronen et al (2019) and Olofsson and Olsson (2019). In the field plots, the relative RMSE of our estimator on 10-meter plots was 4.6, 6.2 and 8% for the number of stems under the “any”, “center” and “full” detection conditions, respectively, and the mean errors were 0.4, 2.1 and 4.1%. The constructed confidence intervals under the nominal 95% level of confidence covered the true number of trees in 96.5-97.5% of the cases, which indicates that the variance estimator is slightly biased but the bias happens to a safe, conservative direction under regular pattern of tree locations. Under simulated plots with complete spatial randomness, the observed coverage probabilities were very close to the nominal ones.

We also discuss, from a statistical point of view, the question of using single scans from multiple plots or multiple scans from a smaller number of plots in practical inventories. Application of similar ideas in individual tree detection based on aerial inventories are also discussed.

Acknowledgements

The work has been funded by Academy of Finland (grant 310073).

References

- Ducey, M. J. (2018). Design-unbiased point-to-object sampling on lines, with applications to areal sampling. *European Journal of Forest Research*, 137(3), 367-383. doi:10.1007/s10342-018-1109-0
- Duncanson, L., Cook, B., Hurtt, G. and Dubayah, R. 2014. An efficient, multi-layered crown delineation algorithm for mapping individual tree structure across multiple ecosystems. *Remote Sensing of Environment* 154: 378-386.
- Kuronen, M., Henttonen, H.M. and Myllymäki, M. 2019. Correcting for non-detection in estimating forest characteristics from single-scan terrestrial laser measurements. *Canadian Journal of Forest Research* 49:96-103.
- Kansanen, K., Packalen, P., Maltamo, M. and Mehtätalo, L. 2020. Horvitz-Thompson-like estimation with distance-based detection probabilities for circular plot sampling of forests. *Biometrics* (early view). <https://www.doi.org/10.1111/biom.13312>
- Lovell, J., Jupp, D., Newnham, G. and Culvenor, D. 2011. Measuring tree stem diameters using intensity profiles from ground-based scanning lidar from a fixed viewpoint. *ISPRS Journal of Photogrammetry and Remote Sensing* 66:46-55.
- Mehtätalo, L. 2019. `lmfor`: Functions for Forest Biometrics. URL: <https://CRAN.R-project.org/package=lmfor>
- Olofsson, K. and Olsson, H. 2018. Estimating tree stem density and diameter distribution in single-scan terrestrial laser measurements of field plots: a simulation study. *Scandinavian Journal of Forest Research* 33:365-377.
- Seidel, D. and Ammer, C. 2014. Efficient measurements of basal area in short rotation forests based on terrestrial laser scanning under special consideration of shadowing. *iForest - Biogeosciences and Forestry* 7: 227-232.

Ecologically informed bird habitat characterization with airborne laser scanning

R. Kuzmich¹, R.A. Hill², P. Treitz¹, P. Bellamy³, S. A. Hinsley⁴

¹Queen's University, Mackintosh-Corry Hall, Room E208 Kingston, Ontario, Canada K7L 3N6
Email: 17rjw2@queensu.ca; paul.treitz@queensu.ca

²Bournemouth University, Talbot Campus, Fern Barrow, Poole, BH12 5BB, United Kingdom
Email: rhill@bournemouth.ac.uk

³Royal Society for the Protection of Birds, Centre for Conservation Science, Potton Rd, Sandy SG19 2DL
Email: paul.bellamy@rspb.org.uk

⁴UK Centre for Ecology and Hydrology, Wallingford, Crowmarsh Gifford, Wallingford, Oxfordshire, UK
Email: sahi@ceh.ac.uk

1. Introduction

As forests undergo succession there is a directional change in tree species composition and three-dimensional structure over time (Packham and Harding 1982). Across the landscape of Cambridgeshire, United Kingdom (UK) are many small woods undergoing succession embedded in a broader agricultural context. Within this dynamic environment occur bird species with variable habitat needs. Blue Tit (*Cyanistes caeruleus*) and Chaffinch (*Fringilla coelebs*) are habitat generalists, though preferences for woodland (Redhead et al. 2013) and hedgerow (Fuller et al. 1997) habitats have been noted, respectively. Chiffchaff (*Phylloscopus collybita*) and Willow Warbler (*Phylloscopus trochilus*) are habitat specialists, respectively favouring mature (Hinsley et al. 1996) and early successional (Bellamy et al. 2009) forests. The aim of this study is to characterize the habitat used by these species within a successional context using airborne laser scanning (ALS) data. ALS is suitable for describing forest structure (Lim et al. 2003), including successional contexts (van Ewijk et al. 2011), and is appropriate for characterizing bird habitat as birds use structural cues to select habitat (MacArthur et al. 1962).

2. Data

This study uses ALS data acquired in 2000, 2005, 2012 and 2015, and bird survey data from those same and two subsequent years. ALS were acquired during the leaf-on period and the characteristics are included in Table 1. Bird data were collected along transects across multiple revisits during spring and early summer mornings using a spot mapping method based on the Common Birds Census of the British Trust for Ornithology (Marchant 1983). Woods used in this study include Gamsey (4.9 ha), Lady's (8.4 ha), Raveley (7.2 ha), Ridley (9.4 ha), and two areas adjacent to Monks Wood National Nature Reserve previously used as farmland which were abandoned in 1996 (New Wilderness: 2.1 ha) and 1961 (Old Wilderness: 3.9 ha). These woods are populated by Common Ash (*Fraxinus excelsior*), English Oak (*Quercus robur*), Field Maple (*Acer campestre*) and Elm (*Ulmus spp.*), and shrub species including Common Hazel (*Corylus avellana*), Hawthorn (*Crataegus spp.*) and Blackthorn (*Prunus spinosa*).

Table 1. ALS acquisitions characteristics for all years.

ALS year	Scanner	Flight date	Returns per pulse	Returns per square metre
2000	Optech ALTM 1210	2000-06-10	2	0.27
2005	Optech ALTM 3033	2005-06-26	2	0.45
2012	Leica ALS50-II	2012-09-15	4	10.54
2015	Leica ALS50-II	2015-06-22	4	2.1

3. Methods

Terrain-normalized ALS structural variables describing the full vertical profile (e.g., ground level to top of canopy) and three strata (hereby S1, S2 and S3) were extracted from a circular plot with a 15 m radius

at locations where the target bird species were present. The three strata correspond to actual levels of vegetation within the canopy (i.e., S1: shrub, <2 m; S2: understorey, 2-8 m; and S3: overstorey: >8 m). Structural variables describing the full profile and for each stratum include skewness, kurtosis, standard deviation, mean, and maximum height. Canopy closure and foliage height diversity metrics were also extracted. Global habitat models for each species were developed using random forest, a machine learning algorithm that generates a collection of decision trees to perform a classification (Breiman 2001), with data across all six woods and all studied years. Random forest output includes variable importance and a measure of out-of-bag (OOB) error (Breiman 2001). The area under the receiver operating characteristic curve (AUROC) was also calculated as a measure of the predictive performance (Fielding and Bell 1997).

4. Results

All four bird species were well modelled and the results are summarized in Table 2, which also includes the range of values characterizing the habitat occupied by each species. Willow Warbler had the lowest OOB error, followed by Blue Tit, Chaffinch, and Chiffchaff. Error associated with presence/absence differed in their magnitude for each species. For Blue Tit, error was relatively even for presence (17.1 %) and absence (16.7 %). Error associated with absence was lower for Chaffinch (16.6 %, versus 19.3 %) and Willow Warbler (7.8 %, versus 12.4 %). For Chiffchaff, error was lower for presence (24.2 %) than absence (33.8 %). AUROC values followed a similar pattern to OOB error, from highest to lowest: Willow Warbler, Blue Tit, Chaffinch and Chiffchaff. Maximum height of the full profile was important to all bird species. Chiffchaff was also associated with structural variables in S3 (maximum height and standard deviation). Willow warbler was associated with S1 (standard deviation and kurtosis). For Blue tit, foliage height diversity and S3 standard deviation were important. The most important variables for Chaffinch were canopy closure and the mean height of the full profile.

Table 2. Top three variables for each species identified by random forest, with model accuracy.

Species	Variable 1 & range	Variable 2 & range	Variable 3 & range	OOB Error	AUROC
Chiffchaff	Maximum height <i>12.5-18.6 m</i>	S3 maximum height <i>12.8-18.8 m</i>	S3 standard deviation <i>1.1-2.4 m</i>	29.0 %	0.79
Willow Warbler	S1 standard deviation <i>0.5-0.7 m</i>	S1 kurtosis <i>1.7-3.2</i>	Maximum height <i>4.6-9.6 m</i>	10.1 %	0.95
Blue Tit	Foliage height diversity <i>0.8-0.9</i>	Maximum height <i>11.3-17.6 m</i>	S3 standard deviation <i>1.1-2.3 m</i>	16.9 %	0.90
Chaffinch	Canopy closure <i>4-38 %</i>	Mean height <i>3.5-9.5 m</i>	Maximum height <i>10.1-16.7 m</i>	18.0 %	0.90

5. Discussion

The ability of ALS-derived variables to describe three-dimensional habitat structure has been shown in previous studies (Bakx et al. 2019; Bradbury et al. 2005; Goetz et al. 2007; Zellweger et al. 2013). Our study demonstrates that there are structural components to the habitat used by Chiffchaff, Willow Warbler, Blue Tit, and Chaffinch that can be quantified with ALS. Our results support ecological descriptors of habitat preferences. For instance, characteristics of the overstorey strata were significant to Chiffchaff whereas it is the shrub strata that is important to Willow Warbler, which is aligned with mature and early successional forest structures. In contrast, we found that Blue Tit and Chaffinch, considered habitat generalists, are not using space equally across the full vertical profile but are discriminating within specific height intervals. Our results also show that species are more specific in the structural components that they are either using (i.e., Chiffchaff) or not using (i.e., Chaffinch and Willow Warbler), suggesting that structural components can act as a deterrent or as an attractor. ALS data provides valuable information regarding the structure of bird habitat and ALS data availability is

increasing. Using ecological knowledge of the habitat structure (i.e., distinct strata), forest succession (i.e., changes over time), and bird species (i.e., habitat preference) to derive meaningful variables aids in result interpretability, and is useful for management and conservation applications.

6. Conclusions

This study uses ecologically informed ALS-derived structural variables to quantify Chiffchaff, Willow Warbler, Blue Tit, and Chaffinch habitat across six woods in Cambridgeshire, UK. All species were accurately modelled and their habitat could be characterized with random forest. Our results support ecological studies examining structural aspects of the habitat used by these bird species (e.g., Fuller et al. 2001), and remote sensing studies using ALS (e.g., Bellamy et al., 2009). A future study will build on these results to identify and quantify habitat across space and over time for each species.

Acknowledgements

We thank Ailidh Barnes for 2017 bird transects, Markus Melin and Peter Davies for digitising bird maps. ALS data were provided by the UK Natural Environment Research Council (NERC) Airborne Research and Survey Facility (ARSF), and by the Environment Agency of England and Wales. This work was funded by the Natural Sciences and Engineering Research Council (NSERC) Discovery Grant to P. Treitz and Alexander Graham Bell Canada Graduate Scholarship to R. Kuzmich.

References

- Bakx T R M, Koma Z, Seijmonsbergen A C and Kissling W D, 2019, Use and categorization of Light Detection and Ranging vegetation metrics in avian diversity and species distribution research. *Diversity and Distributions*, 25(7): 1045-1059.
- Bellamy P E, Hill R A, Rothery P, Hinsley S A, Fuller R J and Broughton R K, 2009, Willow Warbler *Phylloscopus trochilus* habitat in woods with different structure and management in southern England. *Bird Study*, 56:338-348.
- Bradbury R B, Hill R A, Mason D C, Hinsley S A, Wilson J D, Balzter H, Anderson G Q A, Whittingham M J, Davenport I J and Bellamy P E, 2005, Modelling relationships between birds and vegetation structure using airborne LiDAR data: a review with case studies from agricultural and woodland environments. *Ibis*, 147: 443-452.
- Breiman L, 2001, Random forests. *Machine Learning*, 45: 5-31.
- Fielding A H and Bell J F, 1997, A review of methods for the assessment of prediction errors in conservation presence/absence models. *Environmental Conservation*, 24(1): 38-49.
- Fuller R. J, Trevelyan R J and Hudson R W, 1997, Landscape composition models for breeding bird populations in lowland English farmland over a 20 year period. *Ecography*, 20: 295-307.
- Fuller R J, Chamberlain D E, Burton N H K and Gough S J, 2001, Distributions of birds in lowland agricultural landscapes of England and Wales: How distinctive are bird communities of hedgerows and woodland? *Agriculture, Ecosystems and Environment*, 84: 79-92.
- Goetz S, Steinberg D, Dubayah R and Blair B, 2007, Laser remote sensing of canopy habitat heterogeneity as a predictor of bird species richness in an eastern temperate forest, USA. *Remote Sensing of Environment*, 108: 254-263.
- Hinsley S A, Bellamy P E, Newton I and Sparks T H, 1996, Influences of population size and woodland area on bird species distributions in small woods. *Oecologia*, 105: 100-106.
- Lim K, Treitz P, Wulder M, St-Onge B and Flood M, 2003, LiDAR remote sensing of forest structure. *Progress in Physical Geography*, 27(1): 88-106.
- MacArthur R H, MacArthur J W and Preer J, 1962, On bird species diversity, II. Prediction of bird census from habitat measurements. *The American Naturalist*, 96: 167-174.
- Marchant J H, 1983, *BTO common bird census instructions*. British Ornithology Trust, Tring, UK.
- Packham J R and Harding D J L, 1982, *Ecology of Woodland Processes*. Arnold, London, UK.
- Redhead J W, Pywell, R F, Bellamy P E, Broughton R K, Hill R A, and Hinsley S A, 2013, Great tits *Parus major* and blue tits *Cyanistes caeruleus* as indicators of agri-environmental habitat quality. *Agriculture, Ecosystems and Environment*, 178: 31-38.
- van Ewijk K Y, Treitz, P M and Scott N A, 2011, Characterizing forest succession in central Ontario using lidar-derived indices. *Photogrammetric Engineering & Remote Sensing*, 77(3): 261-269.
- Zellweger F, Braunisch V, Baltensweiler A and Bollmann K, 2013, Remotely sensed forest structural complexity predicts multi species occurrence at the landscape scale. *Forest Ecology and Management*, 307: 303-312.

Terrestrial LiDAR Derived Allometric Models for Guyana and Suriname

Alvaro Lau¹, Hansrajie Sukhdeo², Verginia Wortel³, Harm Bartholomeus¹, Artie Sewdien³, Vera Bekkers¹, Martin Herold¹

¹Wageningen University & Research, Laboratory of Geo-Information Science and Remote Sensing, Droevendaalsesteeg 3, 6708 PB Wageningen, The Netherlands

Email: {alvaro.lausarmiento; vera.bekkers; harm.bartholomeus; martin.herold}@wur.nl

²Guyana Forestry Commission, Water Street 1, Georgetown, Guyana

Email: hans.sukhdeo@gmail.com

³Centre for Agricultural Research in Suriname, Prof. Dr.Ir.J.Ruinardlaan 1, Paramaribo, Suriname

Email: {wortelv; artiesewdien}@gmail.com

1. Introduction

Tropical forests play a role in climate mitigation and ecosystem services. For that, international funding has been set up to support forest monitoring, specifically in developing countries through Reducing emissions from deforestation and forest degradation (REDD+) (Nesha et al. 2021). Countries (like in this study Guyana and Suriname) who are establishing a REDD+ program, need to design and implement a national Measurement, Reporting and Verification (MRV) system as part of their REDD+ program. Within the MRV systems, aboveground biomass (AGB) estimations are mostly calculated using allometric models, which are largely dependent on the data used, producing uncertainties and systematic errors of tree AGB estimations when applied to other species, size, structure, or geographical conditions (Lau et al. 2019).

Terrestrial Light Detection and Ranging (LiDAR) along with quantitative structure models (Raumonen et al. 2013) have been proven to be a valuable tool to assess the woody structure of trees (Brede et al. 2017) and to estimate tree AGB (Burt et al. 2021) regardless of the tree species, size, structure, or geographical conditions. Lau et al. (2019) proved the feasibility to develop country-specific TLS-derived allometric models and it is of interest now to explore the inclusion of more validation trees; for that, the aim of this study is to develop allometric models from TLS-derived parameters which estimates AGB of trees in Guyana and Suriname in a reliable and accurate way.

2. Data and Methods

2.1 Study area

Four forest types were used in this study which aimed to increase the representativity of trees in Guyana and Suriname. One study area was located in Guyana, with a mixture of white sand plateau and mixed forest, with a dominance of evergreen trees (Guyana Lands and Surveys Commission 2013). The other three areas were located in Suriname; a moist ever green forest, a high and low swamp forest and a periodic swamp forest (Atmopawiro 2016).

2.2 TLS-derived attributes and QSM-derived aboveground biomass

Terrestrial LiDAR datasets were collected with a RIEGL VZ-400 3D terrestrial laser scanner (RIEGL Laser Measurement Systems GmbH, Horn, Austria). We scanned a total of 155 tropical trees (Guyana $n = 72$ and Suriname $n = 83$) following TLS data acquisition and plot design described in Lau et al. (2019). Trees were identified and manually isolated from the pointcloud. These trees were field inventoried and diameter at breast height (D), total tree height (H), and crown diameter (CD) were estimated directly on the standing tree. Tree species specific wood density (WD) was matched using the recorded WD from the fieldwork and the Global Wood Density Database – GWDD (Zanne et al. 2009).

Likewise, D, H, CD were estimated directly on the individual pointcloud. Finally, aboveground biomass was estimated from volume using quantitative structure model *TreeQSM* (Raumonen et al. 2013) and their respective wood density from GWDD.

2.3 Tree Inventory and fresh mass sampling

A total of fifty-one trees (Guyana $n = 23$ and Suriname $n = 28$) were chosen as validation data. Those trees were destructively sampled and weighed. Fresh mass was measured directly in the field while the larger branches and parts were measured through volume estimation. Moreover, we collected wood samples to estimate water content and were weighed in the field.

2.4 TLS-derived and pantropical allometric models

We developed two model forms based on the work in Lau et al. (2019). For that, we used TLS-derived attributes (D, H and CD) and WD to evaluate the accuracy of AGB estimation by only using TLS-derived parameters. The first model uses diameter at breast height, tree height, wood density, and crown diameter (hence, D.WD.H.CD), while for the second one, we removed tree height (D.WD.CD). The allometric models were based on data transformed to the natural logarithm and built using least-squares linear regression. In addition, we estimated AGB using pantropical allometric models from Chave et al. (2005) as seen in Table 1.

Table 1. Pantropical models from Chave et al. (2005), including diameter at breast height (D), species specific wood density values according to the GWDD (WD), and total tree height (H) to estimate aboveground biomass (AGB).

Model	Form AGB =
Ch05.II.3	$WD \cdot e^{(-1499 + 2.1481 \cdot \ln(D) + 0.207 \cdot \ln(D)^2 - 0.0281 \cdot \ln(D)^3)}$
Ch05.I.5	$0.0509 \cdot WD \cdot D^2 \cdot H$

2.5 Model assessment

Finally, we assessed how well the TLS-derived allometric models predict AGB using R-square (R^2), root means square error (RMSE), and concordance correlation coefficient (CCC). For comparing with the allometric models in Table 1, our assessment included the estimation of the model error (in Mg, 1) and the standard deviation (SD) of error.

$$AGB_{error} (Mg) = AGB_{est} - AGB_{ref} \quad (1)$$

3. Results and Discussion

TLS-derived allometric models D.WD.H.CD and D.WD.CD were able to estimate AGB with high accuracy ($R^2 = 0.94$, RMSE = 1.39 Mg, CCC=0.96 and $R^2 = 0.95$, RMSE = 1.25 Mg, CCC=0.97, respectively, see Figure 1a and Figure 1b). On the other hand, pantropical model Ch05.II.3 and Ch05.I.5 also performed with high accuracy ($R^2 = 0.92$, RMSE = 1.54 Mg, CCC=0.96 and $R^2 = 0.88$, RMSE = 1.88 Mg, CCC=0.94, respectively, see Figure 1c and Figure 1d); although slightly lower than the TLS-derived allometric models.

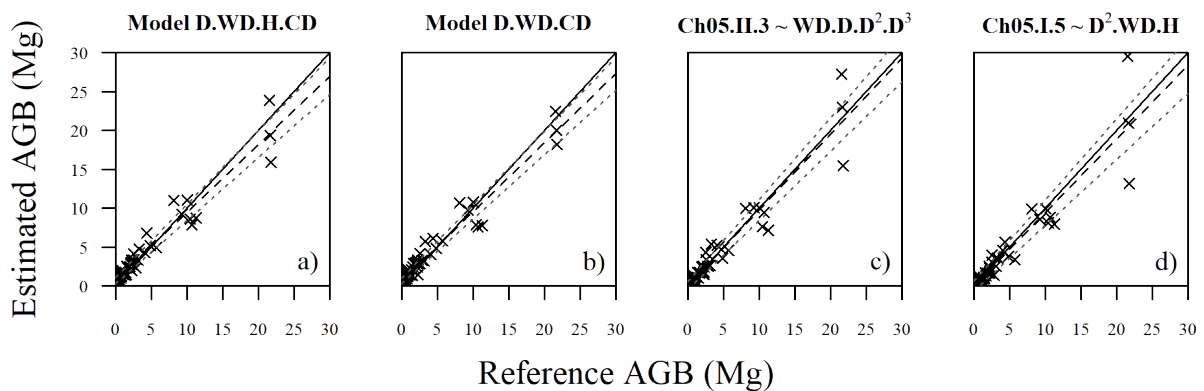


Figure 1: Relationships between AGB from harvested trees (X-axis) and AGB from allometric models (Y-axis). TLS-derived models with D, WD, H and CD (a), and without H (b), pantropical model Ch05.II.3 (c), and Ch05.I.5 (d). Black solid line is 1:1 relationship; dashed lines depict linear fit; and dotted lines indicate 95% confidence interval for the linear fit.

TLS-derived allometric models have a mean model error of -0.22 Mg (slight underestimation), while pantropical model Ch05.II.3 and Ch05.I.5 have a mean model error of -0.05 Mg and -0.24 Mg (slight underestimation), respectively. Regarding SD of error, TLS-derived allometric model D.WD.H.CD and D.WD.CD showed an SD of error of 1.38 Mg and 1.24 Mg, respectively, and pantropical model Ch05.II.3 and Ch05.I.5 showed and SD of error of 1.56 Mg and 1.88 Mg, respectively.

The slightly underestimation of the TLS-derived allometric models in this study might be due to the limited number of samples used ($n = 155$) as opposed as the hundreds (or even thousands) of samples used to calibrate these pantropical models. With the advances on tree segmentation and semi-automatization of tree modelling, a larger sample size can be used to update and calibrate TLS-derived allometric models. TLS helps to increase the sample size of without increase the destructive sampling of tropical trees.

4. Conclusions

TLS-derived allometric models were developed for Guyana and Suriname which estimate aboveground biomass of trees in a reliable and accurate way. As mentioned in Lau et al. (2019), pantropical model Ch05.II.3 provides a good AGB estimate using only WD and D. With the advances of tree segmentation and semi-automatization of tree modelling, we can increase our sample size without the need of destructive sampling. Finally, more research needs to be done to provide robust local TLS-derived allometric models which allow the reduction of uncertainties and increase efficiency of MRV system in REDD+ countries.

Acknowledgements

Our field data was collected through research collaborations between Wageningen University and Guyana Forestry Commission and Centre for Agricultural Research in Suriname, respectively. A special thanks to the forestry team in the Guyana Forestry Commission and Centre for Agricultural Research in Suriname for all the assistance before, during, and after the fieldworks.

References

- Atmopawiro, V. 2016. "Proposed Structure of Forest Typology for Suriname. Unpublished Manuscript." Paramaribo, Suriname.
- Brede, Benjamin, Alvaro Lau, Harm M. Bartholomeus, and Lammert Kooistra. 2017. "Comparing RIEGL RiCOPTER UAV LiDAR Derived Canopy Height and DBH with Terrestrial LiDAR." *Sensors* 17 (10): 2371. <https://doi.org/10.3390/s17102371>.
- Burt, Andrew, Matheus Boni Vicari, Antonio C. L. da Costa, Ingrid Coughlin, Patrick Meir, Lucy Rowland, and Mathias Disney. 2021. "New Insights into Large Tropical Tree Mass and Structure from Direct Harvest and Terrestrial Lidar." *Royal Society Open Science* 8 (2): rsos.201458. <https://doi.org/10.1098/rsos.201458>.
- Chave, Jérôme, C. Andalo, Sandra Brown, M. A. Cairns, Jeffrey Q. Chambers, D. Eamus, H. Fölster, et al. 2005. "Tree Allometry and Improved Estimation of Carbon Stocks and Balance in Tropical Forests." *Oecologia* 145 (1): 87–99. <https://doi.org/10.1007/s00442-005-0100-x>.
- Guyana Lands and Surveys Commission. 2013. *Guyana National Land Use Plan*. Edited by Guyana Lands and Surveys Commission. Georgetown: Guyana Lands and Surveys Commission.
- Lau, Alvaro, Kim Calders, Harm Bartholomeus, Christopher Martius, Pasi Raunonen, Martin Herold, Matheus Vicari, Hansrajie Sukhdeo, Jeremy Singh, and Rosa Goodman. 2019. "Tree Biomass Equations from Terrestrial LiDAR: A Case Study in Guyana." *Forests* 10 (6): 527. <https://doi.org/10.3390/f10060527>.
- Nesha, Mst Karimon, Martin Herold, Veronique De Sy, Amy E. Duchelle, Christopher Martius, Anne Branthomme, Monica Garzuglia, Orjan Jonsson, and Anssi Pekkarinen. 2021. "An Assessment of Data Sources, Data Quality and Changes in National Forest Monitoring Capacities in the Global Forest Resources Assessment 2005–2020." *Environmental Research Letters* 16 (5): 054029. <https://doi.org/10.1088/1748-9326/abd81b>.
- Raunonen, Pasi, Mikko Kaasalainen, Markku Åkerblom, Sanna Kaasalainen, Harri Kaartinen, Mikko Vastaranta, Markus Holopainen, Mathias I. Disney, and Philip Lewis. 2013. "Fast Automatic Precision Tree Models from Terrestrial Laser Scanner Data." *Remote Sensing* 5 (2): 491–520. <https://doi.org/10.3390/rs5020491>.
- Zanne, Amy E., G. Lopez-Gonzalez, David a. Coomes, J. Ilic, S. Jansen, Simon L S.L. Lewis, R.B. B Miller, N.G. G Swenson, M.C. C Wiemann, and Jérôme Jerome Jérôme Chave. 2009. "Data from: Towards a Worldwide Wood Economics Spectrum." *Ecology Letters*. Dryad Digital Repository. <https://doi.org/10.5061/dryad.234>.

Quantifying Tree Crown Plasticity with TLS Data for Improved Individual-tree Growth Models

T. P. Pitkänen¹, S. Bianchi¹, A. Kangas²

¹Natural Resources Institute Finland (Luke), Latokartanonkaari 9, FI-00790 Helsinki, Finland
Email: {timo.p.pitkanen; simone.bianchi}@luke.fi

²Natural Resources Institute Finland (Luke), Yliopistokatu 6, FI-80130 Joensuu, Finland
Email: Annika.kangas@luke.fi

1. Introduction

Given certain site conditions, growth of individual trees and consequent spatiotemporal dynamics of forest stands depend principally on inter-tree competition for light as well as other potentially limiting resources (Caplat et al. 2008, Kolobov and Frisman 2016). Various models have been developed to predict tree growth, but most of them are relatively simplistic: trees are conceptualized as vertically oriented and stationary objects defined primarily by their stem diameter, and competition between them is determined as a result of tree sizes and stand-level characteristics. These models are applicable for providing reasonably accurate estimates of tree growth over various conditions, but too naïve to cover the whole range of actual variation.

To narrow down the gap between the model outputs and the underlying complex determinants of tree growth, both spatial and structural parameters have been added to the models. Spatially explicit models have been developed to improve competition assessment by using the locations of single trees, which conventionally are measured as x,y coordinates of the breast height or the tree base. While the spatially explicit dependencies and related causalities can improve our understanding of forest structure, the use of actual tree locations instead of distance-independent approaches had seemed to add little additional value when predicting tree growth and mortality, even in structurally complex forests (Kuehne et al. 2019). In terms of structural characteristics, the primary focus has been on the crown, given that aboveground interactions between trees are mediated by the size, shape, and relative position of their crown elements (Davies and Pommerening 2008). Inclusion of crown dimensions has been mostly limited to simple and easily measurable parameters such as height of the crown base or living crown ratio, which can be considered as indicators of the past competition experienced by the tree (e.g. Hasenauer et al. 2006).

The approaches described so far are however not taking full advantage of all the crown-related structural parameters. Crown radius, area or volume are important characteristics in terms of the photosynthetic capacity of a tree, to either substitute or complement the crown length. Furthermore, tree crowns are characterized by a high degree of plasticity which is affected by microscale competition on the available resources (Davies and Pommerening 2008), and trees have potential to lean towards less contested spaces as a result of phototropism (Strigul et al. 2008). These dynamics may be a partial reason for the low performance of spatially explicit models, which base only on stem coordinates (García 2014a). Lee & Garcia (2016), for example, found that accounting for tree plasticity reduced the importance of the stand spatial structure in a tree growth model for mixed-species stands.

The practical complication with crown-related structural parameters has been the inability to extract them by conventional field measurement tools, but modern technologies such as terrestrial laser scanning (TLS) enable capturing this information from standing trees in their natural environment (Seidel et al. 2011, Krůček et al. 2019). In our study, we take advantage of TLS data collected from various locations in Finland, reflecting a range of site conditions in boreal forests. We focus on Scots pines (*Pinus sylvestris* L.) and Norway Spruces (*Picea abies* (L.) Karst.) in pure and mixed stands by measuring various advanced crown-related parameters. We link this information to the location and characteristics of the neighbouring trees, intending to quantify the effects of inter-individual competition and consequent plasticity of the tree crowns in 3D space. Finally, we aim at estimating models to predict the extracted crown parameters with subsequent potential to improve individual tree growth models.

2. Data and Methods

TLS data applied in this study was acquired in 2017–18 as a part of large plot-wise data collection plan. Of altogether over 250 plots with manual tree measurements ($r = 9.00$ m), 12 pine-dominated and 12 spruce-dominated stands were selected for this study (Figure 1). These plots represented mature forests with different site characteristics and tree densities, located in southern and middle Finland where competition on light was expected to be limiting tree growth, and were visually assessed as feasible for the extraction of individual tree clouds. The selected 24 plots had 255 manually measured tally trees, which had been determined using a relascope-based sampling strategy. The tally trees included 128 Scots pines, 103 Norway spruces and 24 trees of other species, which had diameters at breast height (DBH) between 73 and 425 mm and tree heights between 5.7 and 29.1 m, respectively.

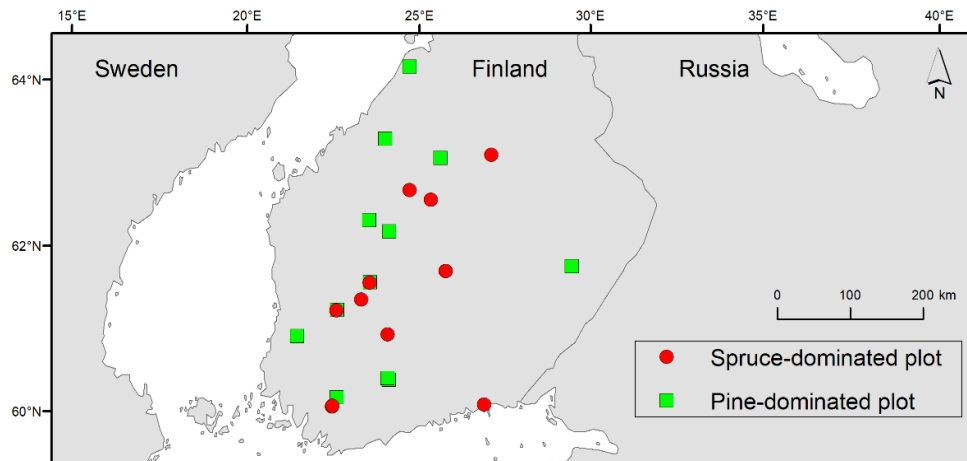


Figure 1: Location of the study plots. Some of the plots are closely located, and therefore overlapping on the applied map scale. Background map: © EuroGeographics for the administrative boundaries.

Each plot was scanned using Leica P40 terrestrial laser scanner from 4-5 stations. Distinct scans were then co-registered and processed through automated analyses to locate the trees. First, a digital terrain model was created to indicate the ground level, and thereafter the trees were detected based on point concentrations organized as near-vertical planes. Breast height coordinates and diameters were predicted using a further developed version of slice-based circle fitting method as presented by Pitkänen et al. (2019), and stem directions were estimated using the lowest part of the stem. TLS points of all the tally trees were semi-automatically extracted from the plot-wise clouds by first assigning connected point clusters in the vicinity of the tree to the candidate single-tree cloud, and then manually cleaning the remaining parts of the neighbouring trees. All the plots also included a number of other trees without field measurements. They were not extracted as individual TLS point clouds due to the high workload of data processing but recognized as competitor trees in the analyses based on their location and DBH.

All the crown parts of the tally trees were then extracted, and their extents were modelled using 3-D convex hulls. They were then calculated crown base height (from the tree base), crown height, width, volume, and surface area. Various indices regarding to the crown shape and symmetry were calculated as well, and coordinates of the crown centroid and treetop (i.e. the highest TLS point) were extracted to measure their potential shift from the breast height coordinates. Further, competition between the trees was assessed using size ratios of the various earlier calculated features, weighted by subject-to-competitor distances (Pommerening and Maleki 2014). Then, all the crown-related parameters were correlated to tree, stand and competition characteristics with a generalized linear mixed modelling (GLMM) framework to identify the dependencies and potential drivers of these features.

Further, we considered the crown extent as the tree assimilation zone as defined in Garcia (2014a, 2014b), and assumed similar dynamics to also occur underground for the root system. Using the package *siplab* (Garcia, 2014b) of R Statistical software (R Core Team, 2021), species-specific functions for predicting the centroid of the assimilation zone (i.e. of the crown) were fitted. A default uniform resource spatial distribution was used, and then the parameters of the influence function, allotment and resource efficiency were fitted to the observed data.

3. Results and Discussion

The GLMM models will reveal the significance of the stand characteristics, spatial arrangement of the trees and competition between the individuals for the observed crown characteristics and their plasticity. Further, the assimilation zone, predicted using the *siplab* framework, will provide a starting point for enhancing individual tree growth models. Part of the associated outcomes, however, will be further elaborated in the forthcoming studies.

4. Conclusions

TLS technology can provide important eco-physiological information on trees and forests, which is based on non-destructive point cloud measurements at a millimetre level accuracy. This study applies TLS-derived information to identify species-specific drivers and dynamics related to resource competition, which is reflected by the morphological plasticity of trees. Further, preliminary simulation of assimilation zones is expected to have linkages with growth modelling of individual trees, therefore providing potential for further research according to the key findings.

Acknowledgements

We are grateful for the Academy of Finland Flagship Programme for financial support: Forest-Human-Machine Interplay - Building Resilience, Redefining Value Networks and Enabling Meaningful Experiences (UNITE); decision number 337655.

References

- Caplat P, Anand M and Bauch C, 2008, Symmetric competition causes population oscillations in an individual-based model of forest dynamics. *Ecological Modelling*, 211(3–4):491–500.
- Davies O and Pommerening A, 2008, The contribution of structural indices to the modelling of Sitka spruce (*Picea sitchensis*) and birch (*Betula* spp.) crowns. *Forest Ecology and Management* 256:68–77.
- García O, 2014a, Can plasticity make spatial structure irrelevant in individual-tree models? *Forest Ecosystems*, 1(16):1–13.
- García O, 2014b, Siplab, a spatial individual-based plant modelling system. *Computational Ecology and Software*, 4(4):215–222.
- Hasenauer H, Kindermann G and Steinmetz P, 2006, The tree growth model MOSES 3.0. In: Hasenauer H (ed), *Sustainable Forest Management – Growth Models for Europe*. Springer, Berlin, Heidelberg.
- Kolobov AN and Frisman EY, 2016, Individual-based model of spatio-temporal dynamics of mixed forest stands. *Ecological Complexity*, 27:29–39.
- Krůček M, Trochta J, Cibulka M and Král K, 2019, Beyond the cones: How crown shape plasticity alters aboveground competition for space and light – Evidence from terrestrial laser scanning. *Agricultural and Forest Meteorology* 264(15):188–199.
- Kuehne C, Weiskittel AR and Waskiewicz J, 2019, Comparing performance of contrasting distance-independent and distance-dependent competition metrics in predicting individual tree diameter increment and survival within structurally-heterogeneous, mixed-species forests of Northeastern United States. *Forest Ecology and Management*, 433:205–216.
- Lee MJ and García O, 2016, Plasticity and Extrapolation in Modeling Mixed-Species Stands, *Forest Science*, 62(1):1–8.
- Pitkänen TP, Raunonen P and Kangas A, 2019, Measuring stem diameters with TLS in boreal forests by complementary fitting procedure. *ISPRS Journal of Photogrammetry and Remote Sensing* 147:294–306.
- Pommerening A and Maleki K, 2014, Differences between competition kernels and traditional size-ratio based competition indices used in forest ecology. *Forest Ecology and Management* 331:135–143.
- R core team, 2021, R: A language and environment for statistical computing. R Foundation for Statistical Computing, Vienna, Austria. URL: <https://www.R-project.org/>
- Seidel D, Leuschner C, Müller A and Krause B, 2011, Crown plasticity in mixed forests – Quantifying asymmetry as a measure of competition using terrestrial laser scanning. *Forest Ecology and Management* 261(11): 2123–2132
- Strigul N, Pristinski D, Purves D, Dushoff J and Pacala S, 2008, Scaling from trees to forests: tractable macroscopic equations of forest dynamics. *Ecological Monographs* 78(4):523–545.

UAV-Laser Scanning based Metrics for Individual Tree Volume Estimation across Forest Types

B. Brede¹, N. Barbier², H. Bartholomeus¹, R. Bartolo³, K. Calders⁴, G. Derroire⁵, A. Lau¹, S. Levick⁶, S. M. Krishna Moorthy^{4,7}, P. Raunonen⁸, L. Terry⁴, H. Verbeeck⁴, T. Whiteside³, M. Herold¹

¹Wageningen University & Research, Laboratory of Geo-Information Science and Remote Sensing, Wageningen, The Netherlands
Email: {benjamin.brede;harm.bartholomeus;alvaro.lausarmiento;martin.herold}@wur.nl

²UMR AMAP, Univ. Montpellier, IRD, CNRS, CIRAD, INRAE, Montpellier, France
Email: nicolas.barbier@ird.fr

³Department of Agriculture, Water and the Environment, Supervising Scientist Branch, Canberra 2601, Australia
Email: {Renee.Bartolo; Tim.Whiteside}@awe.gov.au

⁴CAVELab - Computational & Applied Vegetation Ecology, Department of Environment, Ghent University, Belgium
Email: {Kim.Calders; Louise.Terry; Hans.Verbeeck}@UGent.be

⁵CIRAD, UMR EcoFoG (Agroparistech, CNRS, Inrae, Université des Antilles, Université de la Guyane), Kourou, French Guiana, France
Email: geraldine.derroire@cirad.fr

⁶CSIRO Land and Water, PMB 44, Winnellie, NT 0822, Australia
Email: Shaun.Levick@csiro.au

⁷Department of Geographical Sciences, University of Maryland, College Park, USA
Email: sruthikp@umd.edu

⁸Mathematics, Tampere University, Korkeakoulunkatu 1, 33720 Tampere, Finland
Email: pasi.raunonen@tuni.fi

1. Introduction

Upcoming satellite missions targeting the estimation of forest Above-Ground Biomass (AGB) require an expansion of calibration and validation capabilities (Duncanson et al., 2019). In this context, forest inventories in combination with Allometric Scaling Model (ASM) represent a traditional and well-understood tool. However, ASMs are often based on a small number of harvested trees only, which are typically easier to harvest small trees, resulting in biases in the ASMs (Duncanson et al., 2019).

Terrestrial Laser Scanning (TLS) has been demonstrated to be an unbiased estimation tool for single tree wood volume and AGB, especially in large trees (Calders et al., 2015). However, TLS field data acquisition is labour-intensive and time consuming with a typical productivity of 3-7 days per ha for structurally complex forests (Wilkes et al., 2017). In recent years, Unoccupied Aerial Vehicle Laser Scanning (UAV-LS) has evolved into a mature technique for the collection of point clouds on hectare scales. Pilot studies have already shown the use of UAV-LS for estimation of individual tree metrics (Wallace et al., 2014). A recurring challenge is the accurate automatic segmentation, which is required to allow UAV-LS to be used across large scales. Additionally, structurally complex evergreen tropical forests have not been extensively targeted yet.

In this context, the aim of this study was to explore the potential of individual tree metrics derived from automatically segmented UAV-LS point clouds to estimate tree wood volume across a range of forest sites with varying structural complexity.

2. Data and Methods

2.1 Study Sites

In total, four sites were selected in this study that represent a structural complexity gradient. Speulderbos (The Netherlands) is a temperate mixed forest site containing European beech and oak, as well as Norway spruce, Giant fir and Douglas fir. The Paracou site (French Guiana) is a lowland wet, old-growth tropical forest with more than 750 woody species. Robson Creek (Australia) is a simple notophyll vine forest in the wet tropical NE Queensland. Litchfield (Australia) is a savanna site with a sparse canopy and affected by wild fires.

2.2 TLS and QSM-based Wood Volume Reference

At all sites, TLS data were collected in regular grid patterns with RIEGL VZ-400 scanners, and 10 to 20 m spacing and linking positions with retro-reflective targets following good practice guidelines for

TLS forest plot surveys (Wilkes et al., 2017). Subsequently, the single scan positions were registered to form a co-registered point cloud per site. In total 200, 204, 200 and 489 individual trees were manually segmented from these point clouds for Speulderbos, Paracou, Robson Creek and Litchfield, respectively. Finally, Quantitative Structural Models (QSM) were built with *TreeQSM* (Raumonen et al., 2013) and tree wood volume was estimated based on the QSM cylinder volumes.

2.3 UAV-LS Segmentation and Metrics

UAV-LS data were collected with a RIEGL RICOPTRER with VUX-1UAV. After processing the data into point clouds for each site following recommended procedures (Brede et al., 2017), the point clouds were automatically segmented using a novel individual tree segmentation routine based on shortest-path calculations and adapted to high density UAV-LS data (Raumonen et al., 2021). For each TLS reference tree, the best overlapping UAV-LS tree was identified as the one with the highest Jaccard index or Intersection-over-Union metric based on the voxelised individual tree point clouds. Finally, individual tree metrics were derived from the UAV-LS point clouds: tree heights (H100/H95/H50: difference between highest point/95%/50% percentiles and DTM), crown dimensions (CA: crown area in, CD: crown diameter, CP: crown perimeter), volume based on alpha-hull (V), graph based metrics based on graph-representation of the tree as a side product of the segmentation (GN: number of nodes in the graph, GEL: total edge length in the graph), and compound variables (HCD: H100 times CD, GELCD: GEL times CD).

3. Results and Discussion

UAV-LS metrics displayed different capabilities for explaining the variation in wood volume at each site (Figure 1, Table 1). In particular, H100 and CD behaved asymptotically across sites, effectively limiting capabilities to predict large tree volume with a single structural parameter. On the other hand, CA, V, and GEL were linearly related with wood volume across sites.

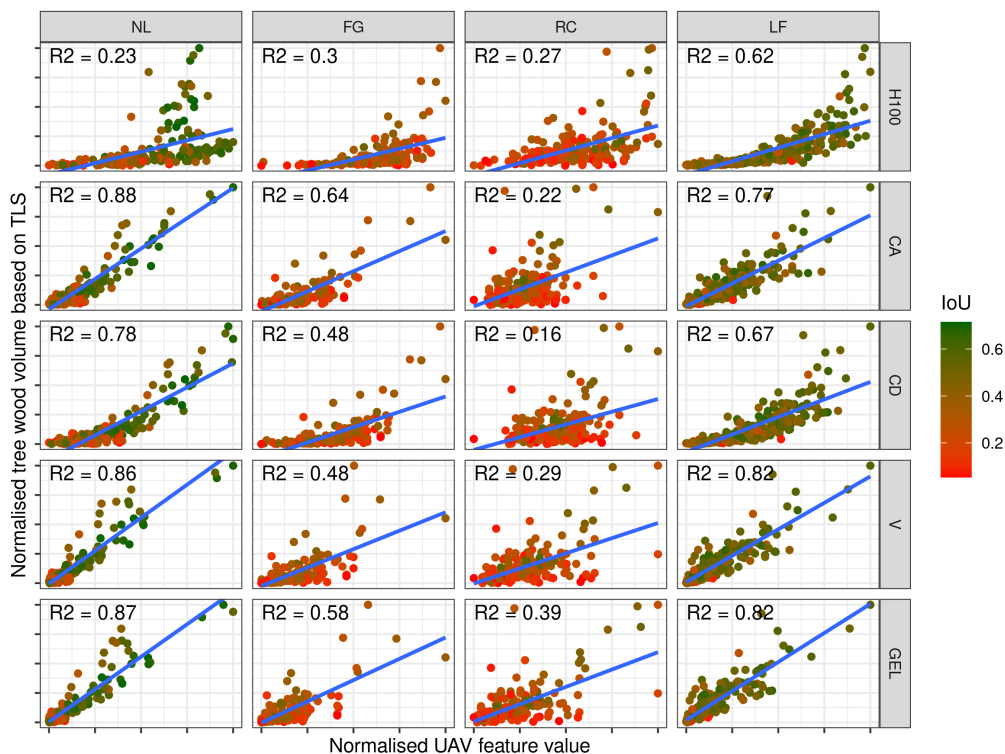


Figure 1: UAV metrics correlation with TLS QSM derived individual tree wood volume. UAV metrics and QSM volumes were normalised to facilitate comparison between sites. Sites: NL = Speulderbos (NL), FG = Paracou (F), RC = Robson Creek (AUS), LF = Litchfield (AUS). UAV metrics were normalised. Metrics: H100 = tree heights, CA = crown area, CD = crown diameter, V = volume based on alpha-hull, and GEL = total edge length. Blue lines indicate linear trends. IoU refers to Intersection-over-Union of UAV automatic segmented tree compared to TLS reference tree.

Table 1: Explained variation (R^2) of UAV metric for TLS reference tree volumes.

Group	Metric	NL	FG	RC	LF
Height	H100	0.23	0.30	0.27	0.62
	H95	0.23	0.34	0.19	0.58
	H50	0.25	0.38	0.22	0.53
Crown	CA	0.88	0.64	0.22	0.77
	CD	0.78	0.48	0.16	0.67
	CP	0.78	0.48	0.17	0.69
Volume	V	0.86	0.48	0.29	0.82
Graph	GN	0.87	0.50	0.31	0.81
	GEL	0.87	0.58	0.39	0.82
Compound	HCD	0.73	0.53	0.29	0.76
	GELCD	0.84	0.63	0.40	0.76

4. Conclusions

This study explored a range of UAV-LS derived metrics for individual tree wood volume estimation, both well used metrics as well as newly derived metrics possible with the high density UAV-LS. In particular, CA and a graph-based metric showed linear relationships with wood volume, making them suitable to build prediction models and scale estimation across UAV-LS covered areas.

Acknowledgements

This work was carried out as part of the IDEAS-QA4EO and ForestScan contracts funded by ESA-ESRIN. K.C. was funded by the European Union's Horizon 2020 research and innovation programme under the Marie Skłodowska-Curie grant agreement No 835398. The Australian fieldwork was funded by BELSPO (Belgian Science Policy Office) in the frame of the STEREO III programme - project 3D-Forest (SR/02/355).

References

- Brede, B., Lau, A., Bartholomeus, H.M., Kooistra, L., 2017. Comparing RIEGL RiCOPTER UAV LiDAR Derived Canopy Height and DBH with Terrestrial LiDAR. *Sensors* 17, 2371. <https://doi.org/10.3390/s17102371>
- Calders, K., Newnham, G., Burt, A., Murphy, S., Raunonen, P., Herold, M., Culvenor, D., Avitabile, V., Disney, M., Armston, J., Kaasalainen, M., 2015. Nondestructive estimates of above-ground biomass using terrestrial laser scanning. *Methods Ecol. Evol.* 6, 198–208. <https://doi.org/10.1111/2041-210X.12301>
- Duncanson, L., Armston, J., Disney, M., Avitabile, V., Barbier, N., Calders, K., Carter, S., Chave, J., Herold, M., Crowther, T.W., Falkowski, M., Kellner, J.R., Labrière, N., Lucas, R., MacBean, N., McRoberts, R.E., Meyer, V., Næsset, E., Nickeson, J.E., Paul, K.I., Phillips, O.L., Réjou-Méchain, M., Román, M., Roxburgh, S., Saatchi, S., Schepaschenko, D., Scipal, K., Siqueira, P.R., Whitehurst, A., Williams, M., 2019. The Importance of Consistent Global Forest Aboveground Biomass Product Validation. *Surv. Geophys.* <https://doi.org/10.1007/s10712-019-09538-8>
- Raunonen, P., Brede, B., Lau, A., Bartholomeus, H., 2021. A Shortest path based tree isolation method for UAV Lidar data, in: IGARSS 2021 International Geoscience and Remote Sensing Symposium, July 12-16, Brussels. Brussels.
- Raunonen, P., Kaasalainen, M., Åkerblom, M., Kaasalainen, S., Kaartinen, H., Vastaranta, M., Holopainen, M., Disney, M., Lewis, P., 2013. Fast Automatic Precision Tree Models from Terrestrial Laser Scanner Data. *Remote Sens.* 5, 491–520. <https://doi.org/10.3390/rs5020491>
- Wallace, L., Lucieer, A., Watson, C.S., 2014. Evaluating tree detection and segmentation routines on very high resolution UAV LiDAR data. *IEEE Trans. Geosci. Remote Sens.* 52, 7619–7628. <https://doi.org/10.1109/TGRS.2014.2315649>
- Wilkes, P., Lau, A., Disney, M.I., Calders, K., Burt, A., Gonzalez de Tanago, J., Bartholomeus, H., Brede, B., Herold, M., 2017. Data Acquisition Considerations for Terrestrial Laser Scanning of Forest Plots. *Remote Sens. Environ.* 196, 140–153. <https://doi.org/10.1016/j.rse.2017.04.030>

Convex hull: Another Perspective about Model Predictions and Map Derivatives from Remote Sensing Data

J.P. Renaud^{1,2}, A. Sagar^{2,3}, P. Barbillon⁴, O. Bouriaud², C. Deleuze¹, C. Vega²

¹Office National des Forêts, Département RDI,

8 allée de Longchamp, F-54600 Villers lès Nancy, France

Email: {jean-pierre.renaud-02; christine.deleuze}@onf.fr

²Institut National de l'Information Géographique et Forestière (IGN), Laboratoire d'Inventaire Forestier (LIF),
14 rue Girardet, 54000 Nancy, France

Email: {cedric.vega; ankit.sagar}@ign.fr

³UMR Silva, Université de Lorraine, faculté des Sciences et Technologies

Campus Aiguillettes, 54506 Vandoeuvre Les Nancy

⁴UMR MIA-Paris, Université Paris-Saclay, AgroParisTech, INRAE 16 rue Claude Bernard, 75 231 Paris Cedex 05

Email: pierre.barbillon@agroparistech.fr

1. Introduction

In forest inventories as well as in the process of building models, obtaining an efficient sample is a central goal to reach precise estimates of forest attributes (Hawbaker et al. 2009, Frazer et al. 2011, Grafström et al. 2014, Saarela et al. 2015, Bouvier et al. 2019). In a model-based approach, a plots sample must cover adequately the variability of the considered forest attributes in order to minimise prediction error. Different strategies have been proposed to efficiently distribute the field sampling units in the auxiliary space of the remote sensing data (e.g. Hawbaker et al. 2009, Grafström et al. 2014). Some authors have proposed to stratify Airborne Laser Scanning data (ALS) to optimize sampling (Hawbaker et al. 2009, Frazer et al. 2011), and Maltamo et al. (2011) compared different field plot selection strategies in order to optimise models precision.

Interestingly, White et al. (2013) applied convex hull approach to show uncovered forest structures by the field calibration sampling units, since large prediction errors could be associated with model extrapolations, resulting in potentially biased map derivatives. In this research, we use convex hull to identify the proportion of extrapolated pixels, computed their distance to the calibration domain and estimated bias associated to the linear model predictions on an ALS case study.

2. Data and Methods

The study area is based on an ALS flight performed in February 2019 in Northeastern France, which covers a forested area of 18,646 ha, with a pulse emission density of 16 points per m². Within this area, a set of 487 systematic field plots were carried out in the Mouterhouse forest (5,324 ha) during the winter of 2019-2020 (Figure 1). The Mouterhouse forest consisted of broadleaved, mixed and coniferous stands (respectively 43%, 23% and 34% on an area basis) and is representative of the whole ALS area. The main species are Scots pine, sessile oak, beech, Douglas fir and Norway spruce. Diameter and tree species were measured in these calibration plots of 15-meter radius spaced at every ~300 meters. An independent set of 56 plots, located in the same forest area was used for validation.

In order to evaluate the effect of different sampling efforts, the systematic plots grid was thinned by half successively to obtain coarser grids, up to a remaining minimum of 8 plots. The resulting grid sizes obtained were then respectively of 487, 247, 115, 56, 25, 11 and 8 plots.



Figure 1: The ALS flight area in orange, with the Mouterhouse forest in green (left) and for illustration, its initial systematic grid (487 plots in black) (middle) and thinned once (247 plots in red) (right).

For 71% of the ALS acquisition area (in orange in Figure 1), no plots were available, giving the opportunity to examine the impact of model application out of its calibration area. Standard area-based metrics were computed from the ALS tiles using the R package lidR (Roussel and Auty 2021). A simple linear model was built to estimate basal area (G), quadratic mean diameter (Dg) and plot density (N). It

included 3 independent variables: mean and standard deviation of all pulse heights and the average slope of the pixels (or of the field plots), computed from the digital terrain model (DTM) (Bouvier et al. 2015).

From these independent variables, convex hulls were computed for all calibration configurations using the geometry package (Habel et al. 2019). It yielded points of the convex hulls and a function allowing to know if a pixel to be predicted belong to the inside or outside space of the hull. The proportion of extrapolated pixels and their distance to the proximal point inside the hull were computed for all pixels of the Mouterhouse forest, as well as for the extended ALS area. Using the validation dataset, it was then possible to compute prediction bias and their distance to the most proximal calibration plot.

3. Results and Discussion

The conventional way to evaluate precision gain associated with sampling efforts is to examine validation RMSEs. In Figure 2, this indicator appears to reach a plateau around 50 calibration plots. With this number of plots however, the proportion of extrapolated pixels in our area of interest (AOI) has not reach a plateau and remains relatively high (ca. 40%). The extrapolation plateau seems rather to occur in the range of 200-300 plots (14-22% extrapolation). Figure 2 also shows a minor difference in the proportion of extrapolated pixels between the two AOI examined. Extrapolation tends to be slightly higher (by ~3%) within the extended AOI, where no calibration plots were present. With a lower amount of calibration plots, the extrapolation distance also tends to increase (Figure 2).

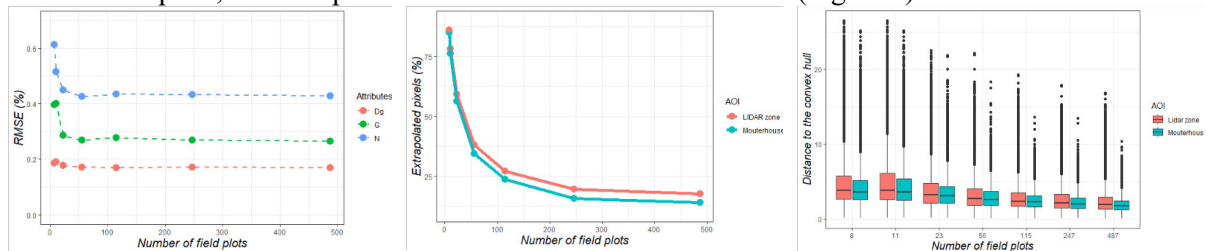


Figure 2: Impact of sampling effort on root means squared errors (RMSE) of validation plots for the different forest attributes examined (left) and on the proportion of pixels located outside the convex hull according to the area of interest (whole ALS or only Mouterhouse) (middle). Boxplots of the distances to the hull are also presented (right).

As large prediction errors might be associated with model extrapolation, Figure 3 presents for each forest attributes examined, the bias obtained with the validation datasets as a function of their distance to to the most proximal calibration plot. Large positive and negative bias were observed (from -303% to +161%). However, a negative trend appears to occur as a function of distance (a distant position being associated with an overestimation of the model). This trend appears to be low for Dg, but high for G and N. This result indicates that it is not only possible to identify pixels that are extrapolated, but also suggest the possibility to correct this result based on the relationship between bias and extrapolation distance.

In this study, we used a simple model, but a preliminary work also showed that more complex models are generating larger proportion of extrapolated pixels. This is certainly associated to the curse of dimensionality. Therefore, the approach used in this study could be considered as an interesting tool to compare competing ALS models.

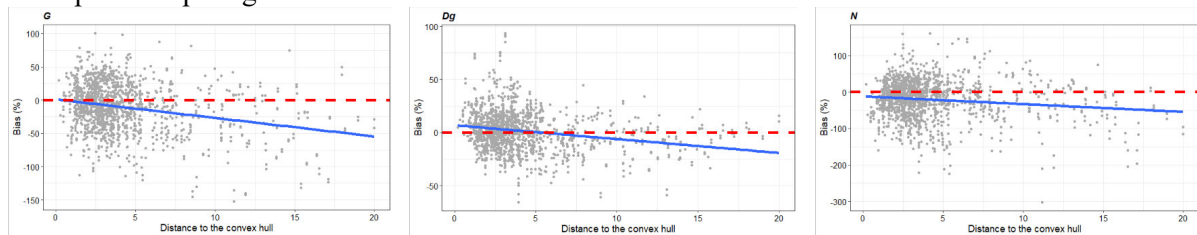


Figure 3: Relative bias for the different forest attributes examined associated to the extrapolated validation plots as function of their distance to to the most proximal calibration plot. (Attributes are basal area (left), quadratic mean diameter (middle), and plot density (right).)

Extrapolated pixels are easily identified using this approach and can then be mapped. Therefore, the spatial distribution of these extrapolated pixels (mapped) could provide additional information that require further attention. This information could reveal important aspects for forest managers, indicating areas where model predictions are out of the calibration domain.

Finally, as Knn is frequently used with ALS, the use of convex hull could also be considered as an interesting tool for further investigations, since this modelling method is also known to be sensitive to extrapolation.

4. Conclusions

The study showed the possibility to identify (and afterward map) pixels that are extrapolated using a convex hull approach. It also showed that prediction bias tends to increase with distance to the calibration domain and that low amount of calibration plots tend to increase these distances. Convex hull is certainly an interesting tool to evaluate model “representativeness” over an AOI and could then serve to compare models in a phase of model selection. It could also serve at the stage of sampling effort determination. Further studies are nevertheless required to evaluate this tool to correct extrapolation bias.

Acknowledgements

We acknowledge the Laboratoire Interdisciplinaire des Environnements Continentaux (*CNRS et l'Université de Lorraine*) for supplying the ALS data and the Agence Territoriale de Mulhouse (*ONF*) for the field data. We thank Steen Magnussen for enlightening discussions, as well as Brad Barber and David Sterratt for their help with the geometry package. We thank Alain Munoz, Flavien Lamiche, and Vincet Pérez (*ONF*) for their help in preparing and supplyina data. *ONF* Département RDI is supported by the French National Research Agency (*ANR*) as part of the “Investissements d’Avenir” program (*ANR-11-LABX-0002-01*, Lab of Excellence *ARBRE*). Ankit Sagar received the financial support of the French PIA project “Lorraine Université d’Excellence”, reference *ANR-15-IDEX-04-LUE*, through the project *Impact DeepSurf*.

References

- Bouvier M, Durrieu S, Fournier RA, Renaud JP. 2015. Generalizing predictive models of forest inventory attributes using an area-based approach with airborne LiDAR data. *Remote Sens Environ* 156: 322–334.
- Bouvier M, Durrieu S, Fournier RA, Saint-Geours N, Guyon D, Grau E and Boissieu F. 2019. Influence of Sampling Design Parameters on Biomass Predictions Derived from Airborne LiDAR Data. *Can J Remote Sens* 45: 650–672. <https://doi.org/10.1080/07038992.2019.1669013>
- Frazer GW, Magnussen S, Wulder MA, Niemann KO. 2011. Simulated impact of sample plot size and co-registration error on the accuracy and uncertainty of LiDAR-derived estimates of forest stand biomass. *Remote Sens Environ* 115: 636–649. <https://doi.org/10.1016/j.rse.2010.10.008>
- Grafström A, Saarela S, Ene LT. 2014. Efficient sampling strategies for forest inventories by spreading the sample in auxiliary space. *Can J For Res* 44: 1156–1164. <https://doi.org/10.1139/cjfr-2014-0202>
- Habel K, Grasman, R, Gramacy RB, Mozharovskyi P and Sterratt DC. 2019. geometry: Mesh Generation and Surface Tessellation. R package version 0.4.5. <https://CRAN.R-project.org/package=geometry>.
- Hawbaker TJ, Keuler NS, Lesak AA, Gobakken T, Contrucci K, and Radeloff VC. 2009. Improved estimates of forest vegetation structure and biomass with a LiDAR-optimized sampling design. *J Geophys Res G Biogeosciences* 114: 11 p. <https://doi.org/10.1029/2008JG000870>
- Maltamo, M, Bollandas, OM, Næsset, E, Gobakken, T, and Packalen, P. 2011. Different plot selection strategies for field training data in ALS-assisted forest inventory. *Forestry*, Vol. 84 (1): 23–31. [doi:10.1093/forestry/cpq039](https://doi.org/10.1093/forestry/cpq039)
- Roussel JR and Auty D. 2021. Airborne LiDAR Data Manipulation and Visualization for Forestry Applications. R package version 3.1.1. <https://cran.r-project.org/package=lidR>
- Saarela, S, Schnell, S, Grafstrom, A, Tuominen, S, Hyyppa, J, Nordkvist, K, Kangas, A, and Stahl, G. 2015. Effects of sample size and model form on the accuracy of model-based estimators of growing stock volume. *Can. J. For. Res.* 45(11): 1524–1534. [doi:10.1139/cjfr-2015-0077](https://doi.org/10.1139/cjfr-2015-0077)
- White JC, Wulder MA, Varhola A, Vastaranta M, Coops NC, Cook BD, Pitt D, Woods M. 2013. A best practices guide for generating forest inventory attributes from airborne laser scanning data using an area-based approach. *Canadian Forest Service*, 50 p.

Assessing Approaches to 3D Tree Reconstruction from Terrestrial Laser Scanning Data

W. Yang¹, M. Disney¹, P. Wilkes¹, M. B. Vicari¹

¹Department of Geography, University College London, Gower Street, UK, WC1E 6BT
Email: {w.yang.17; mathias.disney; p.wilkes; matheus.vicari.15} @ucl.ac.uk

1. Introduction

3D reconstruction of tree models is useful for a wide range of fields and a number of methods have been proposed using terrestrial laser scanning (TLS) data to generate visually realistic results, but the results vary among different methods and parameters settings.

To quantitatively validate the reconstructed models, one way is to use synthetic point clouds simulated from tree models with known architecture, but the reference models are not real trees which cannot represent evaluation in real nature environments. Another common approach is to compare model estimations with manually measured data obtained from harvested trees or segmented branches. Destructive sampling is a reliable way to provide real ground-truth reference, but the process of manual measurements is time-consuming and laborious, resulting in small size of datasets with simple structure in existing literatures.

When it comes to specific assessment metrics, a number of global indices are summarized to evaluate geometry reconstruction, for example, average distance between the input points and the generated model (Du et al., 2019), absolute and relative error of tree parameters such as branch length, diameter and volume (Lau et al., 2018). Although these indices provide a general assessment of geometry quality, there is a possibility of getting the right answer in a wrong way. On the other hand, topology reconstruction is more difficult to validate. To assess the accuracy of branch order, Lau et al. (2018) visually paired each manually measured branch to the model counterpart, and used a confusion matrix to reveal the accuracy, but they only considered branches that could find a pair in modelled results, so the overall accuracy was high up to 99%. Boudon et al. (2014) proposed an evaluation framework that detects similarity of topological structure between two skeleton models, but it only applies to skeleton-based reconstruction methods and needs experienced researchers to manually define tree skeletons for reference. Therefore, a universal and comparative method to validate 3D tree models is still lacking, especially regarding topology, while the correct topological connection is the prerequisite for retrieving accurate tree structure parameters.

This work validates two widely used reconstruction methods, TreeQSM (Raumonen et al., 2013) and SimpleTree (Hackenberg et al., 2015), using simulated point clouds based on TLS-measured forest structure. The evaluation demonstrates that the simulation approach based on TLS-measured tree structure can be an alternative way to assess QSM reconstructions, but further studies are needed for both geometry and topology assessment.

2. Data and Methods

2.1 Simulated TLS Point Clouds

A Monte-Carlo ray tracing library, librat (Disney et al., 2006), was used to simulate 1 ha plot of tree models from leaf-off Wytham Woods 3D models (Calders et al., 2018). Scans were simulated with the same parameter settings as the real TLS scanning described in Calderys et al. (2018). Then the simulated point clouds were downsampled and individual trees were extracted (Figure 1). We selected five trees with a range of sizes from three species for further tree reconstruction and validation.



Figure 1 Simulated point clouds of 3D trees measured in Wytham Woods (coloured by individual tree). Left: top view. Right: Front view.

Table 1 Characteristics of five tree models used in simulation. (X and Y coordinates denote the trees' location in the simulated plot.)

Tree ID	X (m)	Y (m)	Height (m)	DBH (cm)	Species (Common name)
ww_60	42.1	170.8	21.5	66.1	Acer pseudoplatanus (Sycamore)
ww_81	133.1	162.3	22.5	99.7	Quercus robur (Oak)
ww_446	86.7	110.9	30.5	146	Acer pseudoplatanus (Sycamore)
ww_827	103.2	136.8	24.5	28.9	Acer pseudoplatanus (Sycamore)
ww_1361	126.9	120.4	23.4	21.8	Fraxinus excelsior (Ash)

2.2 Reconstruction and Validation of 3D Tree Models

The reconstruction methods compared here are TreeQSM and SimpleTree. As TreeQSM has been constantly updated over the years but many research had been conducted using version 2.0.0, so we compared both the old version (v2.0.0) and a newer one (v2.3.1). For each tree point cloud, the candidates of input parameter sets were selected by an open-source software optqsm (Burt, 2019), and hundreds of quantitative structure models (QSMs) were generated from all combinations of input candidates. The optimal QSM is selected based on the metric of 'all_mean_dis', i.e., minimizing the mean of point to cylinder distance from all cylinders. In SimpleTree software, we used the plug-in 'QSM sphererfollowing method – advanced for plot' which does not require input parameters from users.

To evaluate the model results, common tree parameters that can be obtained from both methods are compared with the reference values from original tree models.

3. Results and Discussion

The comparison results of three tree parameters are presented in Figure 2. Both methods showed the capability to retrieve highly accurate tree height (bias less than 1%), whereas for DBH estimates, SimpleTree models had 10% underestimation on average, and the possible reason for this is the under-fitting phenomenon in the main trunk of the large trees in this test (Figure 3). In terms of volume, models reconstructed from SimpleTree tended to overestimate the crown and resulted in an overall 38% overestimation in total volume among these five trees. On the contrary, both versions of TreeQSM mis- or under-fitted twigs, so the total volume estimates are slightly lower than the reference values. Compared between two versions, the newer one had less underestimation in total volume, which is mainly attributed to reconstructing more small branches that the older version did not fit. Further quantitative comparison using more trees and more metrics in both geometry and topology will be conducted. Preliminary results would suggest that for applications focusing on volume aspect, e.g., non-destructive estimation in above-ground biomass through TLS-QSM method, TreeQSM v2.3.1 is a better choice, but for applications beyond volume, we recommend examining other metrics as well.

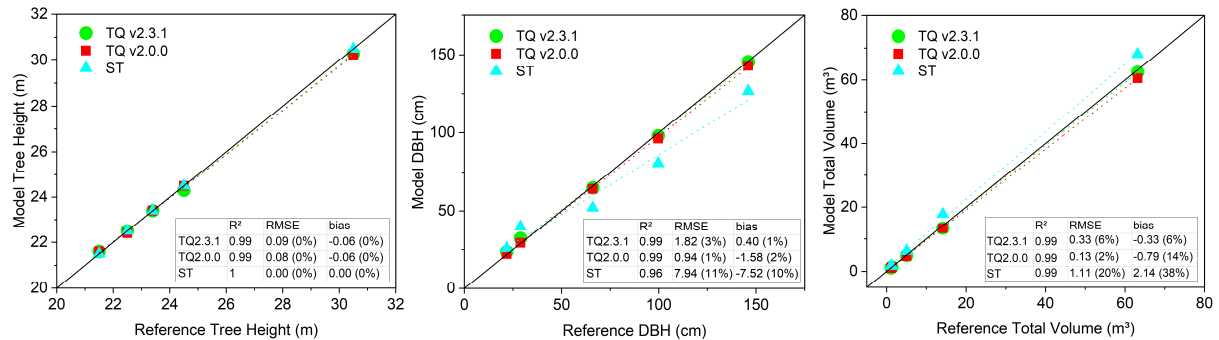


Figure 2 Comparison between reference values and model estimations from two versions of TreeQSM (TQ v2.3.1 and TQ v2.0.0) and SimpleTree (ST).

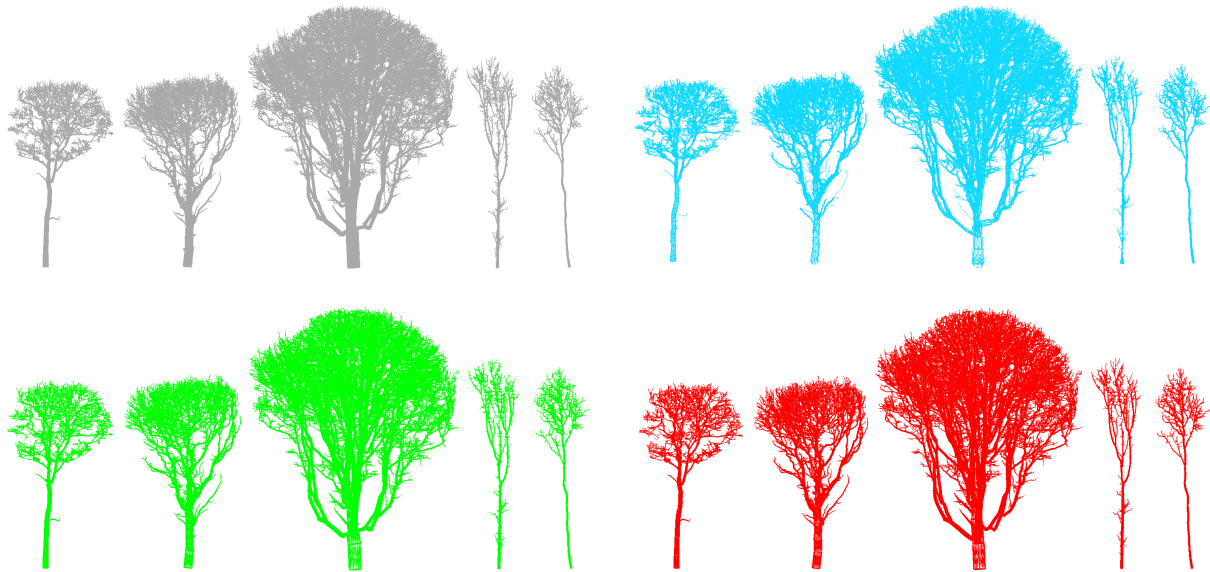


Figure 3 Simulated point clouds (grey) of five tested trees and their corresponding reconstructed QSMs from SimpleTree (blue), TreeQSM v2.3.1 (green) and TreeQSM v2.0.0 (red). The Trees ID from left to right are ww_60, ww_81, ww_446, ww_827 and ww_1361, respectively.

4. Conclusions

A universal and comparative method to validate 3D tree reconstruction methods is still lacking, especially regarding topology. One of the challenges is to obtain a good benchmark dataset of point clouds with comprehensive manual measurements of the reference trees. We evaluated two versions of TreeQSM and SimpleTree models with simulated data based on TLS-measured forest structure, and the results show that the newer version of TreeQSM retrieved better results in volume aspect. Further studies are needed for both geometry and topology assessment, which will benefit optimal model selection and promote the development of methods to reconstruct more complete and authentic tree models that can advance understanding of tree structure and function.

References

- Boudon F, Preuksakarn C, Ferraro P, Diener J, Nacry P, Nikinmaa E & Godin C, 2014, Quantitative assessment of automatic reconstructions of branching systems obtained from laser scanning. *Annals of Botany*, 114(4): 853-62.
- Burt A, 2019, *optqsm* [Online]. GitHub. Available: <https://github.com/apburt/optqsm> [Accessed 2020].
- Calders K, Origo N, Burt A, Disney M, Nightingale J, Raunonen P, Åkerblom M, Malhi Y & Lewis P, 2018, Realistic Forest Stand Reconstruction from Terrestrial LiDAR for Radiative Transfer Modelling. *Remote Sensing*, 10(6): 933.
- Disney M, Lewis P & Saich P, 2006, 3D modelling of forest canopy structure for remote sensing simulations in the optical and microwave domains. *Remote Sensing of Environment*, 100(1): 114-132.
- Du S, Lindenbergh R, Ledoux H, Stoter J & Nan L, 2019, AdTree: Accurate, Detailed, and Automatic Modelling of Laser-Scanned Trees. *Remote Sensing*, 11(18): 2074.
- Hackenberg J, Spiecker H, Calderys K, Disney M & Raunonen P, 2015, SimpleTree —An Efficient Open Source Tool to Build Tree Models from TLS Clouds. *Forests*, 6(12): 4245-4294.
- Lau A, Bentley L P, Martius C, Shenkin A, Bartholomeus H, Raunonen P, Malhi Y, Jackson T & Herold M, 2018, Quantifying branch architecture of tropical trees using terrestrial LiDAR and 3D modelling. *Trees*, 32(5): 1219-1231.
- Raunonen P, Kaasalainen M, Åkerblom M, Kaasalainen S, Kaartinen H, Vastaranta M, Holopainen M, Disney M & Lewis P, 2013, Fast Automatic Precision Tree Models from Terrestrial Laser Scanner Data. *Remote Sensing*, 5(2): 491-520.

Exploring the effect of leaves on tree woody surface area estimation with quantitative structural models

David W. MacFarlane^{1*}, Georgios Arseniou¹, Andrew Burt², Vicari, M. B.², Mathias Disney^{2,3}, Kim Calders⁴

¹Department of Forestry, Michigan State University, East Lansing, Michigan, USA. ²UCL Geography, North West Wing, Gower Street, London WC1E 6BT. ³NERC National Centre for Earth Observation, Leicester, UK. ⁴Computational & Applied Vegetation Ecology Laboratory, Department of Environment, Faculty of Bioscience Engineering, Ghent, University, Belgium *corresponding author: macfar24@msu.edu

1. Introduction

Advances in terrestrial laser-scanning technology (TLS) and associated data processing algorithms now allow for comprehensive measurements of the structural complexity of trees. Point cloud data generated by TLS can be processed by Quantitative Structural Models (QSMs) to allow for estimation of total surface areas and volumes of trees, by creating a network of connected cylinders approximating the stem and branch network of the trees (Raumonen et al. 2013). One of the challenges for computing the woody surface area of trees is the presence of leaves, because leaves occlude woody parts from being seen by the laser and QSMs may interpret leaves as woody structures (Burt et al. 2021). Another issue is that foliage cannot be represented by cylinders (Stovall et al. 2017). It is not always possible to scan trees during the leaf-off period and evergreen trees are never in a leaf-off condition, unless dead. So, investigators sometimes use QSMs on trees in the leaf-on condition, assuming that, underestimation of woody surface area and volume from occlusion and overestimation from counting leaves as woody parts, cancel out. Here, we tested that assumption for broadleaved, deciduous trees, using needleleaf evergreens as a control. We also used the leaf-removal algorithm of Vicari et al. (2019) to see how artificial leaf removal might pre-process a leaf-on point cloud before estimating wood surface area with a QSM to simulate estimation in a leaf-off condition.

2. Data and Methods

Thirteen trees of two broadleaf, deciduous species (8 *Quercus rubra* and 5 *A. rubrum*) and ten needleleaf evergreens of two species (5 *Tsuga canadensis* and 5 *Pinus strobus*) were scanned during the early spring (April) of 2017, when the deciduous trees were in the leaf-off condition, and then again in the summer (July), in the deciduous leaf-on condition, with a RIEGL® VZ-400, at Harvard Forest (Petersham, MA, USA), to produce point clouds of each tree in both periods. Additionally, leaves of the deciduous species were virtually removed from the summer-scanned point clouds with the *tlseparation* algorithm of Vicari et al. (2019), to examine how similar a leaf-removed condition is to leaf-off. QSMs were produced from the three types of point-clouds, using the TreeQSM algorithm (Raumonen et al 2013), generating cylinders outlining all woody parts of the stem and branches; the sum of all of these was the total surface area of woody parts (woody surface area, WSA, m²) of each tree. After scanning, trees were felled and measured in detail, including total-tree one-sided leaf area (LA, m²)- leaves were collected and weighed from throughout the crowns of the felled trees and sub-samples were weighed and had their surface area scanned on a flatbed scanner. Leaf area per unit leaf mass was then extrapolated to the tree's total estimated leaf mass. this enabled estimation of the total LA of each tree. The trees ranged in size from 8 to 50 cm, stem diameter at breast height, and 8 to 25 m in height. Data were error-checked and imported into the R statistical software environment and analysed with custom code to determine the influence of leaves on tree surface area estimation.

3. Results

The results showed a strong, positive correlation between woody surface area with leaves on (WSA_{on}) and off (WSA_{off}) for broad-leaved deciduous trees, but with a positive bias, such that WSA_{on} was significantly higher than WSA_{off} (Fig. 1). There was also a strong, positive correlation between WSA_{spring} and WSA_{summer} for needleleaf evergreens, but the relationship was more variable and showed

a slightly negative bias (Fig. 1). The leaf removal algorithm removed a significant amount of woody material from the point cloud when trying to separate leaves from the leaf-on point clouds of the deciduous trees (Fig. 2A), resulting in a positive difference between $WSA_{\text{off}} - WSA_{\text{removed}}$, which increased as the total leaf area of the tree increased (Fig. 2B).

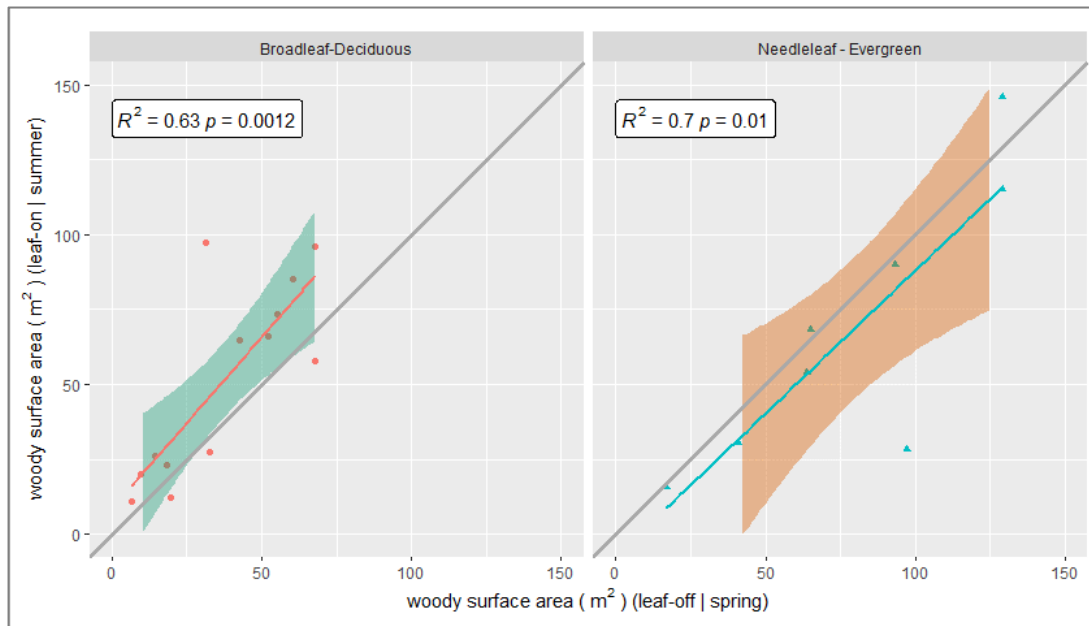


Figure 1. Total woody surface area of trees computed from a QSM with leaves on and leaves off for deciduous trees and summer versus spring scans for the evergreen species.

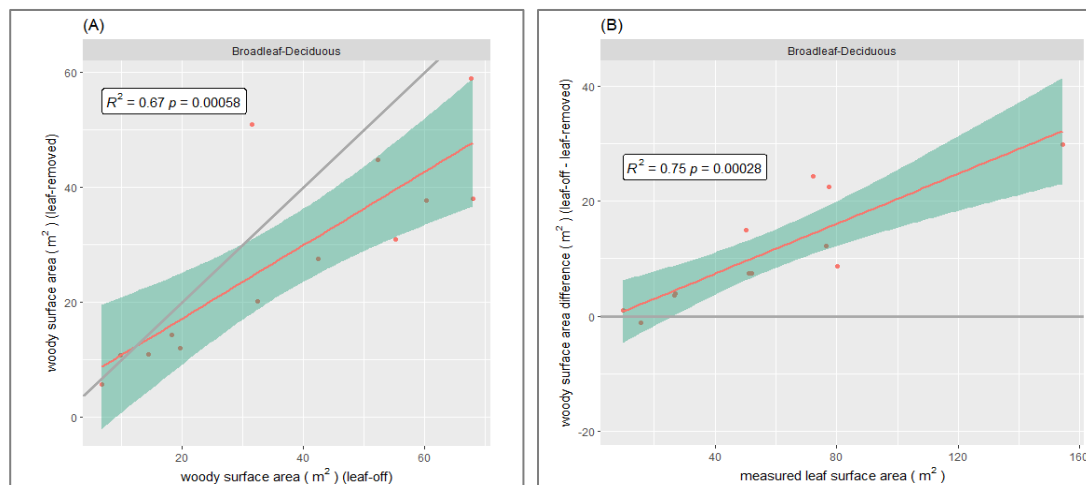


Figure 2: (A) Total woody surface area of deciduous trees with leaves removed from leaf-on scans with an algorithm, prior to processing with a QSM, plotted against the same trees with woody surface area computed from a QSM from leaf-off scans. (B) The difference between woody surface area computed with leaves off versus woody surface area with artificial leaf removal from leaf-on scans, plotted against the measured total tree leaf area from destructive sampling.

4. Discussion

The results of this study show that possible overestimation and underestimation biases in estimates of tree woody surface area, when applying a QSM to a tree in the leaf-on condition, do not strictly cancel each other out, in agreement with the findings of Calders et al. (2018). The net result was an overestimation bias for deciduous trees, that apparently comes from adding leaves to the surface area of smaller branches at the periphery of the crown. When needle-leaved evergreens, scanned in a leaf-on condition at two different times of year (spring and summer) were used as a control, there were differences in the estimated woody surface area, with a slight trend toward lower woody surface area

estimated in the summertime. This may be due to greater occlusion of the stem by more full fascicles of needles during the summer. Evergreens regularly shed older needles, though they retain multiple cohorts, thus always maintaining leaves, with their maximum leaf area in summer. The whorled branching architecture and the way that needles directly attach to shoots may also make it more difficult to see woody parts in summer, but follow-up studies are needed, perhaps with deciduous conifers.

When the leaf-separation algorithm was applied to the point clouds of deciduous trees with their leaves-on, the algorithm turned a bias of overestimation of woody surface area into a negative bias, which suggests that smaller branches in the periphery of the crowns were miss-classified as leaves. So, the algorithm overcompensated for the positive bias mentioned above. The fact that the bias increased as the actual surface area of the leaves of the trees increased, indicates that the algorithm would be most effective when trees have relatively low leaf areas. Larger trees with larger leaf areas likely have more complex point clouds, resulting in greater confusion of leaves and branches, which should affect the performance of the leaf-separation algorithm (Vicari et al. 2019, Wang et al. 2019). Significant total tree volume underestimation has been previously found after artificial leaf-removal (Wang et al. 2019), however, Burt et al. (2021) showed that the leaf-removal significantly reduced bias in total tree above-ground biomass from TLS data compared to biomass estimates based on leaf-on point-clouds. In general, leaf-separation algorithms may be necessary for estimating woody surfaces areas of evergreen trees or trees in the leaf-on condition, but the algorithms will need improvement to produce reliable estimates.

5. Conclusion

Applying a QSM to broadleaf, deciduous trees in the leaf-on condition resulted in an overestimation bias for estimates of the woody surface area underneath the leaves. Scanning evergreens both in spring and in summer showed the possibility for seasonal differences, and here, lower woody surface area in summer, possibly due to occlusion of, or confusion with, woody parts and dense fascicles of needle-leaves. Leaf removal algorithms should be applied with caution, as they may simply reverse the direction of bias in estimation of woody surface area.

Acknowledgements

The authors thank the staff at Harvard forest for making this experiment possible, particularly David Orwig and Audrey Barker Plotkin. We acknowledge the contribution of numerous research technicians from Michigan State University, Virginia Technological University and University of Maine for help with exhaustive sampling of tree leaves, and specifically thank Sam Clark, Garret Dettmann, Jereme Frank, Phil Radtke and David Walker for their efforts to get accurate leaf area measurements. We also thank the UNAVCO for their assistance with leaf-off TLS fieldwork.

References

- Burt, A., Vicari, M.B., da Costa, A.C.L., Coughlin, I., Meir, P., Rowland, L. and Disney, M., 2021. New insights into large tropical tree mass and structure from direct harvest and terrestrial lidar. *Royal Society Open Science* 8: 201458. <https://doi.org/10.1098/rsos.201458>
- Calders, K., Origo, N., Disney, M., Nightingale, J., Woodgate, W., Armston, J. and Lewis, P., 2018. Variability and bias in active and passive ground-based measurements of effective plant, wood and leaf area index. *Agricultural and Forest Meteorology*, 252, pp.231-240.
- Raunonen, P., Kaasalainen, M., Åkerblom, M., Kaasalainen, S., Kaartinen, H., Vastaranta, M., Holopainen, M., Disney, M.I., Lewis, P.E., 2013. Fast automatic precision tree models from terrestrial laser scanner data. *Remote Sens. Vol.5* (2013), p.491–520.
- Stovall, A.E.L., Vorster, A.G., Anderson, R.S., Evangelista, P.H. & Shugart, H.H., 2017. Non-destructive aboveground biomass estimation of coniferous trees using terrestrial LiDAR. *Remote Sensing of Environment Vol.200* (2017),p. 31–42.
- Vicari, M.B., Disney, M., Wilkes, P., Burt, A., Calderys, K. and Woodgate, W., 2019. Leaf and wood classification framework for terrestrial LiDAR point clouds. *Methods in Ecology and Evolution*, 10(5), pp.680-694.
- Wang, D., Takoudjou, S.M., Casella, E., 2019. LeWoS: A universal leaf-wood classification method to facilitate the 3D modelling of large tropical trees using terrestrial LiDAR. *Methods in Ecology and Evolution Vol. 11* (2019), p. 376-389.

Spatial Prediction of Forest Inventory Results from Portable Laser Scanning using Airborne Laser Scanning Data and Spatial Hierarchical Bayes Models

A. Nothdurft¹, C. Gollob¹, R. Kraßnitzer¹, G. Erber², T. Ritter¹, K. Stampfer², A.O. Finley³

¹University of Natural Resources and Life Sciences, Vienna, (BOKU), Institute of Forest Growth, Peter-Jordan-Str- 82, Vienna 1190, AUSTRIA

Email: {arne.nothdurft ; christoph.gollob ; ralf.krassnitzer ; tim.ritter}@boku.ac.at

²University of Natural Resources and Life Sciences, Vienna, (BOKU), Institute of Forest Engineering, Peter-Jordan-Str- 82, Vienna 1190, AUSTRIA

Email: {gernot.erber ; karl.stampfer}@boku.ac.at

³Department of Forestry, Michigan State University, East Lansing, MI 48824-1222, USA

Email: {finleya@msu.edu}

1. Introduction

A novel approach was developed to reduce labor costs associated with traditional measurements in forest inventory and to predict the growing stock timber volume for smaller spatial entities. Forest inventory field work was completely conducted with a portable laser scanning system (PLS). The approach was tested in a case study to predict the storm-felled growing stock in the upper Gailtal valley in Carinthia, Austria in consequence of the cyclone “Adrian” in October 2018.

2. Data and Methods

Field measurements on 62 randomly selected circular sample plots with 20 m radius were performed using a GeoSLAM ZEB HORIZON (GeoSLAM Ltd., Nottingham, UK) portable laser scanning system. Tree position finding and diameter at breast height (DBH) measurement were accomplished using fully automated routines described in Ritter et al. (2017) and in Gollob et al. (2019, 2020). For both the sample plots, and the windthrow target areas, a broad set of auxiliary variables was derived from fine-resolution pixelated canopy height data that stemmed from an airborne laser scanning (ALS) campaign.

A hierarchical Bayesian spatially varying coefficients model was constructed to model the relationship between the auxiliary variables from the sample plots and their counterparts that were computed for equally sized grid cells within the target units. Spatially structured errors on the model coefficients were represented by Matérn correlation functions for the continuously indexed geolocations of the grid cell and the sample plots centroids. Spatial predictions of the storm-felled timber volume were provided for different spatial scales (windthrow area, sub-region, complete study area) through MCMC composition sampling from the joint posterior predictive distribution using methodology implemented in the R-package spBayes (Finley et al., 2007, 2015).

3. Results

Leave-on-out (LOO) cross-validations showed that the coverage rate of 95% posterior predictive distribution credible intervals were close to the nominal level. For the 212 ha sum of the windthrow areas, the total prediction of the storm damages was 133,775 m³ and the 95% credible interval ranged from 122,935 m³ to 144,308 m³. The average coefficient of variation (CV) of the per-area predictions was 25%. Predictions for larger windthrow areas with relevant storm damages were more precise.

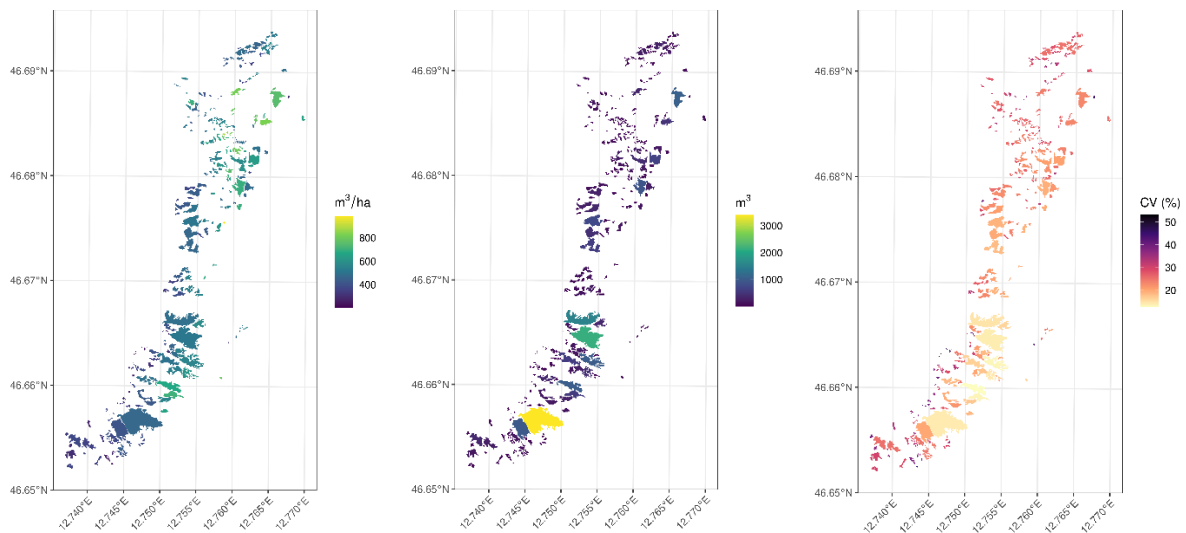


Figure 1: posterior predictive distribution mean, total, and coefficient of variation of the growing stock volume for the windthrow damages in the Frohn sub-region.

4. Discussion

A broad set of auxiliary variables from the ALS derived canopy height model was tested, but only the average canopy height was a meaningful regressor variable. Similar findings were made in Breidenbach & Astrup (2012) and in Magnussen et al. (2014).

Prior forest inventory data was not available for the study region. However, the terrestrial measurement with the portable laser scanning system was highly efficient. The work capacity was up to 25 plots per day, despite the alpine terrain.

Prior independent tests with data representing manifold forest structural conditions revealed that the automated routines in Ritter et al. (2017,) and in Gollob et al. (2019, 2020) achieved average detection rates of 99% for trees with dbh ≥ 10 cm and false positive rates of around 1%. By using these methods, the RMSE of the automated dbh measurement was below 3 cm, and the bias was below 0.5 cm. Hence, it was no longer considered as necessary to collect additional reference data on the study site sample plots using traditional measurement instruments, and the forest inventory was exclusively conducted with the portable laser scanner.

5. Conclusion

A cost-saving approach was elaborated for the inventory and the mapping of the growing stock timber resources in forest landscapes. The approach is highly automatized using portable laser scans from field plots and ALS data to support the hierarchical Bayesian spatial prediction methodology.

Acknowledgements

This study was conducted under umbrella of the project Digi4+ that was financed by the Austrian Federal Ministry of Agriculture, Regions and Tourism under project number 101470. The authors appreciate the support during the fieldwork that was given by the forest owners, Clemens Wassermann, Günter Kronawetter and the team of the Carinthian Forest Service.

References

Breidenbach, J., Astrup, R., 2012, Small area estimation of forest attributes in the Norwegian National Forest Inventory, European Journal of Forest Research, 131(4), 1255—1267.

- Gollob, C., Ritter, T., Nothdurft, A., 2020, Forest Inventory with Long Range and High-Speed Personal Laser Scanning (PLS) and Simultaneous Localization and Mapping (SLAM) Technology. *Remote Sensing*, 12(9), 1509.
- Gollob, C., Ritter, T., Wassermann, C., Nothdurft, A., 2019, Influence of Scanner Position and Plot Size on the Accuracy of Tree Detection and Diameter Estimation Using Terrestrial Laser Scanning on Forest Inventory Plots, *Remote Sensing*, 11(13), 1602.
- Finley, A.O., Banerjee, S., Carlin, B.P., 2007, spBayes: An R Package for Univariate and Multivariate Hierarchical Point-Referenced Spatial Models. *Journal of Statistical Software*, 19(4), 1-24.
- Finley, A.O., Banerjee, S., Gelfand, A.E., 2015, spBayes for Large Univariate and Multivariate Point-Referenced Spatio-Temporal Data Models. *Journal of Statistical Software*, 63(13), 1-28.
- Magnussen, S., Mandallaz, D., Breidenbach, J., Lanz, A., Ginzler, C., 2010, National forest inventories in the service of small area estimation of stem volume, *Canadian Journal of Forest Research*, 44(9), 700-712.
- Ritter, T., Schwarz, M., Tockner, A., Leisch, F., Nothdurft, A., 2017, Automatic Mapping of Forest Stands Based on Three-Dimensional Point Clouds Derived from Terrestrial Laser-Scanning. *Forests*, 8, 265.

Mapping Natural Regeneration in Canopy Gaps from Seedlings to Saplings in Uneven-Aged Deciduous Forests using ALS Data

Louise Leclère¹, Nicolas Latte¹, Corentin Bolyn¹, Philippe Lejeune¹

¹Forest is Life, ULiège – Gembloux Agro-Bio Tech, Passage des Déportés 2, 5030 Gembloux, Belgium
Email: {louise.leclere, nicolas.latte, cbolyn, p.lejeune}@uliege.be

1. Introduction

Assessing regeneration state is essential for forests sustainable management. However, field surveys to collect data on regeneration are time consuming and difficult to implement. Remote sensing could therefore be an effective way to characterize regeneration.

Only few studies focused on forest regeneration characterisation using ALS data: understory coverage estimation (Latifi et al. 2017, Venier et al. 2019), post-fire vegetation characterization (Martin-Alcon et al. 2015), regeneration stems density and height estimation (Debouk et al. 2013, Imangholiloo et al. 2020).

Regeneration dynamic depends on the characteristics of canopy gaps. They increase availability of understory light, which is beneficial for regeneration development, especially for less shade-tolerant species (Ligot et al. 2014). Moreover, the regeneration that develops within canopy gaps is not overtopped by dominant trees and is therefore favourable to the production of high value wood. Some studies focus on the identification of understory types in canopy gaps (Vehmas et al. 2011). Another method was developed to distinct non-regenerating gaps from regenerated ones (Sénécal et al. 2018). The height growth of regeneration saplings within canopy gaps was also estimated using ALS time series (Vepakomma et al. 2008).

Using ALS data, the study's objectives were (i) to detect and map canopy gaps, (ii) to characterize and delineate four regeneration development stages within these canopy gaps and (iii) to differentiate ligneous stems from herbaceous and soil for the first development stage (height < 1.5 m).

2. Data and Methods

2.1 Study area

The study area was a forest of 1,708 ha located in Wallonia (southern Belgium) (Figure 1A). The mean annual rainfall was 1170 mm year⁻¹. The mean annual temperature was 8.7 °C. The altitude ranged from 263 to 478 m. The mean terrain slope was 7.8°. Mixed uneven-aged deciduous stands corresponded to 51% of the study area. Oak (*Quercus robur* L. and *Quercus petraea* (Mattuschka) Liebl.) corresponded to 35% of the total basal area, and beech (*Fagus sylvatica* L.), to 55%. The regeneration (i.e. from seedlings to established saplings) was composed of 83% of beech, 10% of spruce (*Picea abies* (L.) Karst.), 2% of sycamore maple (*Acer pseudoplatanus* L.), and 2% of oak.

2.2 ALS data

ALS data were acquired using the Teledyne-Optech Titan dual-wavelength sensor between the 6th and 9th May 2018 (leaf-on). The sensor allows the acquisition of both topographic and bathymetric point clouds (wavelengths equal to 1064 nm and 532 nm, respectively). The mean flight altitude was 684 m above sea level. The resulting recorded topographic and bathymetric point clouds density were 56 pts/m² and 48 pts/m², respectively. The raw point cloud was classified into ground and above-ground hits. A CHM at a spatial resolution of 0.5 m was generated.

2.3 Mapping of canopy gaps

Canopy gaps were detected and mapped using a thresholding method (Bonnet et al. 2015). The canopy gaps mapping was implemented using the CHM for uneven-aged stands.

Coniferous plantations representing 42 % of the forest area were discarded. A canopy gap was defined as a forest area with a maximum vegetation height of 10 m, a minimum surface area of 50 m² and a minimum width of 4 m. A fourth criterion (slope, calculated on the CHM, lower than 80°) was also applied to discard areas corresponding to low branches of neighbouring trees around gaps. All the threshold values were defined based on the literature, forest management inventories or field observations.

2.4 Mapping of regeneration development stages

Four regeneration development stages were defined based on vegetation height using CHM within canopy gaps (Table 1). It was assumed, and verified in the field, that there were no non-ligneous elements higher than 1.5 m. The first stage (s1) included seedlings, young saplings, herbaceous vegetation, litter and soil. The other stages ($1.5 \leq \text{height} < 10$ m) corresponded to older established saplings but not recruited trees.

Table 1. Height thresholds of regeneration development stages.

Development stage	Definition
First stage (s1)	CHM < 1.50 m
Second stage (s2)	$1.5 \leq \text{CHM} < 3$
Third stage (s3)	$3 \leq \text{CHM} < 6$
Fourth stage (s4)	$6 \leq \text{CHM} < 10$ m

2.5 Modelling ligneous stems cover for the first development stage

The ligneous stems cover (%) within the first stage was modelled using random forest and ALS data. The data used was collected in the field: 103 circular plots with a 2 m radius were set up on transects. Each plot was positioned with a high precision using an Emlid Reach RS+ GPS and the ligneous stems cover (%) was estimated visually.

A series of 86 ALS metrics was calculated considering point height, topographic and bathymetric intensities within plots (Latifi et al. 2017, Imangholiloo et al. 2020). Using *VSURF* (Genuer et al. 2015), the 11 metrics with the highest explanatory power (e.g. the mean, standard deviation and kurtosis of ALS point height) were selected and a random forest model was trained using the whole field dataset. This global model was assessed considering R², RMSE and bias.

A simple cross-validation was also applied to evaluate the model's accuracy: 100 iterations with 80% of the field data plots for training and 20% for validating. For each iteration, R², RMSE and bias were calculated.

After validation, the global model was used to predict the ligneous stems cover for the first development stage class on the entire study area using a regular grid.

3. Results and Discussion

Canopy gaps were detected and mapped using the thresholding method, and development stages were characterized and delineated within canopy gaps (Figure 1B).

The R², RMSE, and bias of the ligneous stems cover model (random forest) were 0.92, 0.09 and 0.00, respectively. The R², RMSE and bias of the cross-validation were 0.49 (± 0.17), 0.21 (± 0.04) and 0.01 (± 0.05), respectively. The ligneous stems cover for the first development stage class was predicted on the entire study area (Figure 1C).

A straightforward method was developed to detect canopy gaps and map regeneration development stages located within these gaps using ALS data. The method was applied to the entire forest area excluding coniferous plantations. The random forest model satisfactorily predicted the ligneous stems cover within the first development stage. Accuracy values were comparable to those of other similar studies (Latifi et al. 2017, Venier et al. 2019).

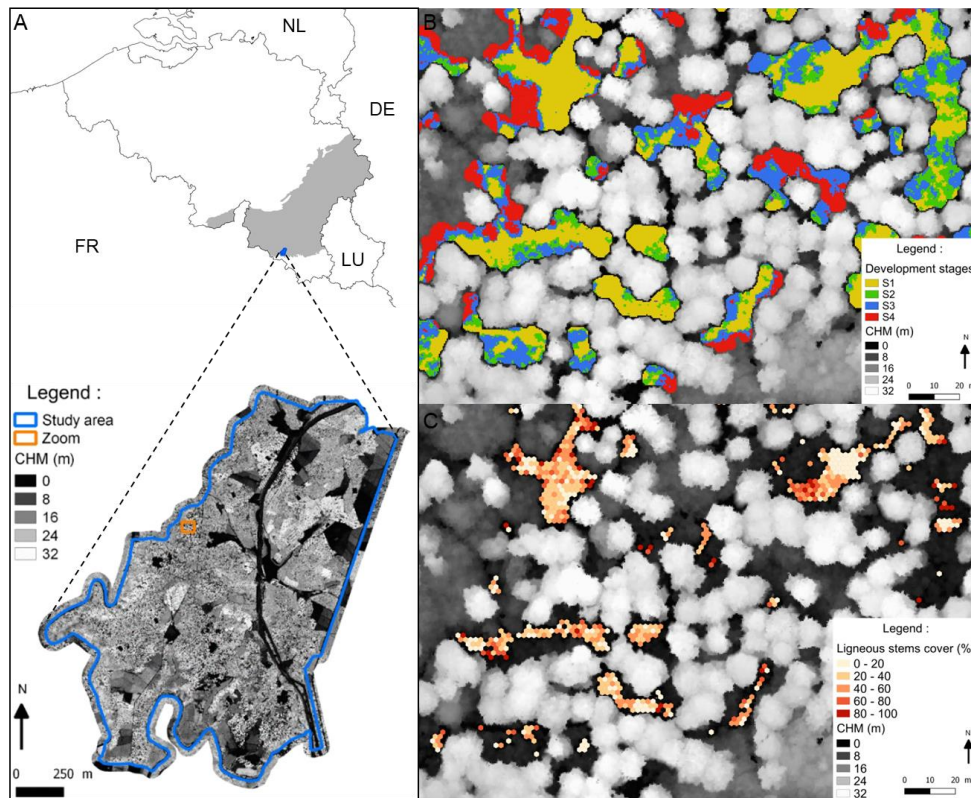


Figure 1. Study area location and maps. Panel A: Study area located in Belgium and study area's CHM. Panel B: Map of development stages within canopy gaps. Panel C: Map of ligneous stems cover for the first development stage.

5. Conclusion

The proposed method using ALS data is straightforward. It allowed to identify canopy gaps and map four regeneration development stages within these gaps at high spatial resolution (GSD = 0.5 m). The method also differentiates ligneous stems from herbaceous for the first development stage. This detailed regeneration mapping is really promising for forest management.

Acknowledgements

This research was supported by Interreg Grande Region - Regiowood II [019-2-03-032] and Walloon Region Forest Administration CARTOFOR project. The authors thank the Direction des Cours d'eau non navigables (Non-Navigable Waterways Directorate) – Service Public de Wallonie (SPW) (the public service in Wallonia) for the ALS acquisition and data sharing, as well as Borremans A., Delinte T., and Monseur A. for collecting data in the field.

References

- Bonnet S, Gaulton R, Lehaire F, Lejeune P, 2015, Canopy gap mapping from airborne laser scanning: An assessment of the positional and geometrical accuracy. *Remote Sensing*, 7(9) 11267–11294.
- Debouk H, Riera-Tatché R, Vega-García C, 2013, Assessing Post-Fire Regeneration in a Mediterranean Mixed Forest Using Lidar Data and Artificial Neural Networks. *Photogrammetric Engineering & Remote Sensing*, 79(12) 1121–1130.
- Genuer R, Poggi JM, Tuleau-Malot C, 2015, VSURF: An R Package for Variable Selection Using Random Forests. *The R Journal, R Foundation for Statistical Computing*, 7(2), 19–33.
- Imangholiloo M, Saarinen N, Holopainen M, Yu X, Hyypä J, Vastaranta M, 2020, Using leaf-off and leaf-on multispectral airborne laser scanning data to characterize seedling stands. *Remote Sensing*, 12(20) 1–20.
- Latifi H, Hill S, Schumann B, Heurich M, Dech S, 2017, Multi-model estimation of understorey shrub, herb and moss cover in temperate forest stands by laser scanner data. *Forestry: An International Journal of Forest Research*, 90(4) 496–514.

- Ligot G, Balandier P, Courbaud B, Jonard M, Kneeshaw D, Claessens H, 2014, Managing understory light to maintain a mixture of species with different shade tolerance. *Forest Ecology and Management*, 327 189–200.
- Martín-Alcón S, Coll L, De Cáceres M, Guitart L, Cabré M, Just A, González-Olabarría J R, 2015, Combining aerial LiDAR and multispectral imagery to assess postfire regeneration types in a Mediterranean forest. *Canadian Journal of Forest Research*, 45(7) 856–866.
- Senécal J F, Doyon F, St-Onge B, 2018, Discrimination of canopy gaps and non-regenerating openings in old-growth temperate deciduous forests using airborne LiDAR data. *Canadian Journal of Forest Research*, 48(7) 774–782.
- Vehmas M, Packalén P, Maltamo M, Eerikäinen K, 2011, Using airborne laser scanning data for detecting canopy gaps and their understory type in mature boreal forest. *Annals of Forest Science*, 68(4) 825–833.
- Venier L A, Swystun T, Mazerolle M J, Kreutzweiser D P, Wainio-Keizer K L, McIlwrick K A, Woods M E, Wang X, 2019, Modelling vegetation understory cover using LiDAR metrics. *PLoS One*, 14(11) 1–17.
- Vepakomma U, St-Onge B, Kneeshaw D, 2008, Height growth of regeneration in boreal forest canopy gaps - does the type of gap matter? An assessment with lidar time series. In: *SilviLaser 2008*. Edinburgh, UK, p. 9.

Forest Inventory with Apple iPad Pro and integrated LiDAR Technology

C. Gollob¹, T. Ritter¹, R. Kraßnitzer¹, A. Tockner¹, A. Nothdurft¹

¹ University of Natural Resources and Life Sciences, Vienna, (BOKU), Institute of Forest Growth, Peter-Jordan-Str- 82, Vienna 1190, AUSTRIA

Email: {christoph.gollob; tim.ritter; ralf.krassnitzer; andreas.tockner; arne.nothdurft}@boku.ac.at

1. Introduction

The estimation of stand- and individual tree information is one of the major goals of forest inventory. Conventionally, field data in forest inventory are collected at tree level on sample plots by means of manual measurements (e.g., caliper, tape). This is labor-intensive, time-consuming and prone to manifold measurement errors (Liang et al. 2016, 2018; Ritter et al. 2017). In recent years, modern laser-supported sensors and automatic routines for feature extraction were increasingly used instead of the traditional forest inventory methods. Nevertheless, most forest inventories still rely on manually collected tree information. The rationale is the sometimes time-consuming and incomplete data acquisition and the high purchase costs for terrestrial and personal laser scanners (TLS/PLS). In 2020, Apple (Apple Inc. Cupertino, California, USA) implemented a LiDAR (Light Detection and Ranging) sensor in the new 4th Generation of Apple iPad Pro. Consequently, LiDAR-generated 3D point clouds can nowadays be recorded with consumer-level devices for the first time.

The goal of the present study was to assess the accuracy of forest inventory variable estimates obtained by Apple iPad Pro under various stand and terrain conditions. The results of the iPad data were compared with PLS results on the same forest inventory plots, using the same algorithms for automatic tree detection and dbh modelling. Manual measurements on the sample plots served as reference data.

2. Data and Methods

A sample of 21 forest inventory plots was scanned in December 2020 using an iPad and a GeoSLAM ZEB Horizon (GeoSLAM Ltd. Nottingham, UK) PLS. The plots were selected in such a way that a broad variation in forest type (broadleaved, coniferous, and mixed), forest structure (one- or two-layered), and terrain property (flat to steep) was represented. On the iPad, multiple scanning apps were evaluated in a forest environment during a preliminary testing before settling on 3D Scanner App (<https://www.3dscannerapp.com/>) (Laan Labs, New York, US), Polycam (<https://poly.cam/>) (Polycam Inc., San Francisco, US) and SiteScape (<https://www.sitescape.ai/>) (SiteScape Inc., Waltham, US). Data acquisition with iPad and PLS started in the sample plot center. The sample plot radius was set to 7 m with a 0.5-1 m buffer zone for the scan survey. The recording of the entire sample plots consumed approximately 5–10 minutes for iPad and 3-7 minutes for PLS, depending on the possible walking speed. Using iPad, every individual tree was circled on the sample plot, while with PLS, only the whole sample plot was circumvented and crossed once. Screen shots from scanning with the iPad with all three apps can be found in Figure 1.

Following the field data collection, further point cloud processing and analysis was performed using statistical computing language R with the algorithms for tree detection and dbh estimation, presented in Gollob et al. (2020). The diameter modelling was carried out with five different approaches (2 GAMs, 2 circles, 1 ellipse), whereby these diameters were referred to as d_{gam} , d_{tegam} , d_{circ} , d_{circ2} and d_{ell} . The accuracy of tree detection was evaluated in terms of two measures: detection rate $d_r(\%)$ and commission error $c(\%)$. The accuracy and precision of dbh estimation were assessed by means of root mean square error (RMSE) and bias.

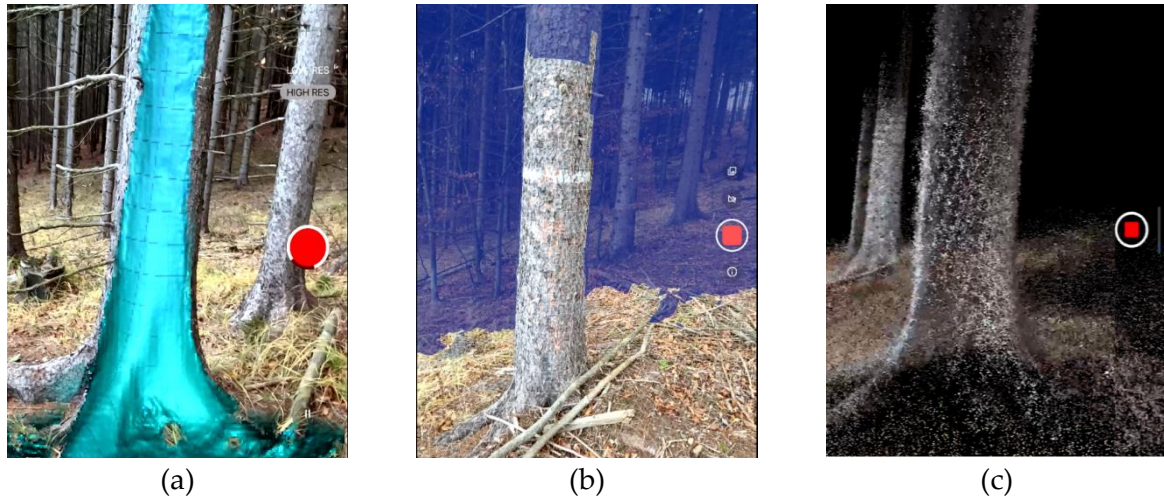


Figure 1: iPad data acquisition with (a) 3D Scanner App, (b) Polycam and (c) SiteScape.

3. Results and Discussion

The analysis of the 21 sample plots showed that the detection rate $d_r(\%)$ strongly depended on the lower dbh threshold (Table 1). Furthermore, iPad scans (3D Scanner App, Polycam and SiteScape) generally had lower detection rates than PLS scans. The average detection rates for 3D Scanner App, Polycam and SiteScape over all 21 sample plots and dbh thresholds ranged from 84.49% to 98.06%, from 76.67% to 94.68% and from 81.41% to 97.26%, respectively. The corresponding average detection rates for PLS ranged from 98.10% to 100%. The commission error $c(\%)$ increased slightly with increasing lower dbh threshold. In general, the average of the commission errors was smaller with all iPad apps than with PLS. Commission errors were below 4% across all technologies and thresholds.

Table 1. Detection rates and commission errors for PLS/iPad and lower dbh thresholds.

dbh	Detection Rate $d_r(\%)$				Commission Error $c(\%)$			
	PLS	3D			PLS	3D		
		Scanner App	Polycam	SiteScape		Scanner App	Polycam	SiteScape
≥ 5 cm	98.10	84.49	76.67	81.41	2.11	2.47	0.53	1.35
≥ 10 cm	99.52	97.33	90.65	95.06	2.58	2.55	0.60	1.40
≥ 15 cm	100.00	98.06	94.68	97.26	3.10	2.80	0.68	1.87

The performance of automatic dbh estimation for iPad and PLS is outlined in Table 2. The average RMSE for 3D Scanner App, Polycam and SiteScape over all 21 sample plots, dbh thresholds and fitting methods ranged from 3.10 cm to 3.40 cm, from 3.05 cm to 4.70 cm and from 3.18 cm to 3.48 cm, respectively. The corresponding average RMSE for PLS ranged from 1.50 cm to 1.92 cm. The average bias for 3D Scanner App, Polycam and SiteScape over all 21 sample plots, dbh thresholds and fitting methods ranged from -1.56 cm to -0.39 cm, from -0.92 cm to 0.58 cm and from -1.38 cm to -0.83 cm, respectively. The corresponding average bias for PLS ranged from -1.32 cm to -0.04 cm.

Table 2. RMSE and bias of dbh estimation for PLS/iPad and lower dbh thresholds.

dbh	method	RMSE (cm)				bias (cm)			
		PLS	3D Scanner App	Polycam	Site-Scape	PLS	3D Scanner App	Polycam	Site-Scape
≥5 cm	gam	1.85	3.12	4.08	3.20	-0.51	-1.01	0.39	-1.31
	tegam	1.78	3.10	4.70	3.18	-0.21	-1.06	0.58	-1.20
	circ	1.64	3.11	3.85	3.39	-0.73	-0.39	0.44	-0.90
	circ2	1.73	3.19	4.05	3.21	-0.54	-1.04	0.36	-1.17
	ell	1.92	3.11	4.20	3.20	-0.04	-1.03	0.28	-1.03
≥10 cm	gam	1.65	3.18	3.84	3.20	-1.05	-1.17	0.08	-1.28
	tegam	1.50	3.17	3.80	3.21	-0.73	-1.18	0.04	-1.17
	circ	1.65	3.18	3.55	3.41	-1.13	-0.52	0.12	-0.83
	circ2	1.64	3.24	3.80	3.22	-1.01	-1.20	0.05	-1.16
	ell	1.52	3.18	3.96	3.20	-0.66	-1.15	0.01	-1.03
≥15 cm	gam	1.78	3.38	3.09	3.26	-1.28	-1.52	-0.87	-1.38
	tegam	1.56	3.36	3.14	3.28	-1.00	-1.52	-0.83	-1.28
	circ	1.77	3.37	2.88	3.48	-1.32	-0.79	-0.80	-0.89
	circ2	1.77	3.40	3.05	3.28	-1.24	-1.56	-0.90	-1.26
	ell	1.60	3.36	3.29	3.21	-0.98	-1.46	-0.92	-1.08

One of the major advantages of applying mobile or personal laserscanning systems is rapid data acquisition on forest sample plots. Although the development of LiDAR devices is proceeding rapidly, it can be stated that the relatively high price of the devices often hinders a wider application at the level of forest practitioners. The PLS (GeoSLAM ZEB HORIZON) used in this study costs around € 50,000. Apple iPad pro costs around € 1,000 and thus easily provides access to LiDAR technology. While the used PLS with a maximum range of 100 m is well suited for capturing upper diameters, tree heights or canopy shapes, iPad measures the distance to surrounding objects only up to 5 meters. Thus, a disadvantage of the iPad method is that it is not capable of acquiring upper tree parameters. However, the technology of these consumer-level devices will also develop further quickly, which means that significantly higher ranges could then be achieved.

3. Conclusion

The LiDAR Sensor of the new iPad is capable for efficient data collection. A large proportion of the trees could be automatically detected, and dbh estimates showed sufficient accuracy, even with existing algorithms. With a further development of hardware and software, the iPad or similar consumer-level devices could provide a feasible, sufficiently accurate, and cost-effective solution for various measurements in near future. This would also mean another important step towards the practical use of digital forest inventory.

References

- Gollob, Christoph, Tim Ritter, and Arne Nothdurft. 2020. "Forest Inventory with Long Range and High-Speed Personal Laser Scanning (PLS) and Simultaneous Localization and Mapping (SLAM) Technology." *Remote Sensing* 2020, Vol. 12, Page 1509 12 (9): 1509. <https://doi.org/10.3390/RS12091509>.
- Liang, Xinlian, Juha Hyypä, Harri Kaartinen, Matti Lehtomäki, Jiri Pyörälä, Norbert Pfeifer, Markus Holopainen, et al. 2018. "International Benchmarking of Terrestrial Laser Scanning Approaches for Forest Inventories." *ISPRS Journal of Photogrammetry and Remote Sensing* 144 (October): 137–79. <https://doi.org/10.1016/J.ISPRSJPRS.2018.06.021>.
- Liang, Xinlian, Ville Kankare, Juha Hyypä, Yunsheng Wang, Antero Kukko, Henrik Haggrén, Xiaowei Yu, et al. 2016. "Terrestrial Laser Scanning in Forest Inventories." *ISPRS Journal of Photogrammetry and Remote Sensing* 115 (May): 63–77. <https://doi.org/10.1016/J.ISPRSJPRS.2016.01.006>.
- Ritter, Tim, Marcel Schwarz, Andreas Tockner, Friedrich Leisch, and Arne Nothdurft. 2017. "Automatic Mapping of Forest Stands Based on Three-Dimensional Point Clouds Derived from Terrestrial Laser Scanning." *Forests* 8 (8): 265. <https://doi.org/10.3390/f8080265>.

Investigating 3-D distribution of bio-chemical traits in tree canopy using UAS-based LiDAR and hyperspectral data

Xin Shen, Lin Cao*

Co-Innovation Center for Sustainable Forestry in Southern China, Nanjing Forestry University, 159 Longpan road, Nanjing, Jiangsu 210037, China
xinshen@njfu.edu.cn; lincao@njfu.edu.cn

Abstract

Quantifying three dimensional structure of individual tree canopy is proven to be critical for precision tree cultivation and sustainable forest management. Hyperspectral imagery has been used in species classification, biomass estimation, and bio-chemical traits measuring. However, due to the limitations of the hyperspectral instrument and the lack of fusion algorithm considering sensor imaging mechanism within vegetation community, combining the three dimensional structure and hyperspectral data to explore the spatially variations of bio-chemical traits in the tree canopy is sparse. Therefore, with the 3D distribution of bio-chemical traits to provide supports for physiological activity monitoring and nutrition diagnosis have attached little attention. In this study, high-density LiDAR point cloud and high-spatial resolution hyperspectral imagery from unmanned aerial system (UAS) platforms were used in combination, to quantify and analyze the three dimensional distribution of bio-chemical traits in individual tree canopy. A DSM based fusion method considering attenuation effect in radiative transfer process was developed to integrate the three dimensional LiDAR point cloud with hyperspectral imagery. A radiative transfer model was used to estimate the bio-chemical traits hierarchically. The horizontal and vertical distributions of bio-chemical traits in individual tree canopy were quantified using ANOVA analysis and Duncan's multiple comparison post hoc tests. Three dimensional distribution of bio-chemical traits in individual tree canopy were accessed and their correlation with accumulated solar radiation were analyzed. We found that the radiative transfer model had a strong ability to estimate bio-chemical traits, and most of the canopy structural had little effect on the accuracy of estimation. Horizontally, the portion of canopy that received solar radiation directly had a slightly lower bio-chemical traits, which means that the southern canopy portion has a lower bio-chemical traits for the individual tree located in the northern hemisphere. Vertically, the bio-chemical traits gradient was negatively correlated with the increase of tree height, because of being affected by shadows from the canopy of oneself and neighboring trees. This study explored the three dimensional bio-chemical traits distribution of individual tree canopy on the basis of mechanistic fusion of high-density LiDAR point cloud and high-spatial hyperspectral imagery. The methods and findings indicate a great potential of deep fused LiDAR point cloud and hyperspectral imagery in investigating solar-induced physiological activities, as well as nutrition diagnosis and productivity enhancement, which have wide application for precision forestry and ecology.

Keywords: LiDAR, hyperspectral data, bio-chemical traits. UAS, 3-D distribution

Tree Crown Segmentation and Morphological Modelling of Personal Laser Scanning Data

A. Tockner¹, T. Ritter¹, C. Gollob¹, A. Nothdurft¹

¹University of Natural Resources and Life Sciences (BOKU), Institute of Forest Growth, Peter-Jordan-Str- 82, Vienna 1190, AUSTRIA
Email: {andreas.tockner ; tim.ritter ; christoph.gollob ; arne.nothdurft}@boku.ac.at

1. Introduction

Key of LiDAR based forest inventory is the availability of suitable software to extract essential tree features (Calders et al 2020). Most relevant tasks of the computer algorithms are the automatic detection of stem positions, the segmentation of the complete 3D point cloud into single tree crowns, the precise measurement of tree height and stem diameter, and the reliable modelling of the crown morphology. These tasks can become challenging, especially in dense forest canopies with overlapping crowns. To overcome these issues, Gollob et al. (2020) proposed a tree detection algorithm based on density clustering applied to multiple horizontal layers that produces reliable results even in dense stands. Personal Laser Scanning (PLS) has several advantages compared to the stationary Terrestrial Laser Scanning (TLS) (Bienert et al. 2018). Most relevant is that the crowns are scanned from various angles, because the scan positions are not fixed with PLS. In this study, a novel algorithm is presented for the automatic segmentation of the single tree stems and crowns. Additionally, the accuracy of automatically derived crown features is evaluated by means of reference measurements collected in field and manual on-screen segmentations of the 3D point cloud.

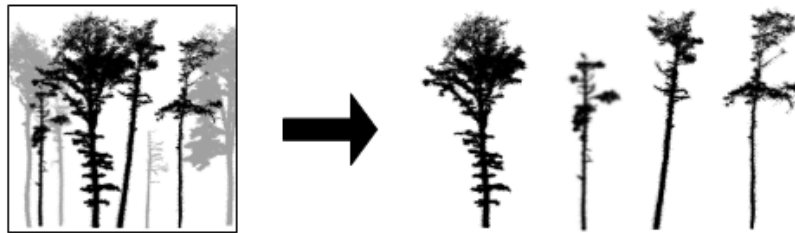


Figure 1: Segmenting the complete point cloud into single tree files to be measured subsequently.

2. Data and Methods

The ZEB HORIZON (GeoSLAM Ltd.) used for this research has an acquisition speed of 300.000 points/sec and a maximum beam range of 100 m, the average point density of the point clouds was 45k points per m². A single scan with the PLS system required one person approximately 30 minutes to fully capture one plot area of approximately 4.000 m² each. Sample plots were scanned around Maissau, Lower Austria (48° 34' 25"N and 15° 48' 45" E), the forests were single layered with medium density (average 870 trees per ha). The dominating tree species were Scots pine (*Pinus sylvestris* L.) and sessile oak (*Quercus petraea* (Matt.) Liebl.), which were complemented by admixture of Norway spruce (*Picea abies* (L.) H. Karst.), European larch (*Larix decidua* Mill.), black pine (*Pinus nigra* J. F. Arnold), European yew (*Taxus baccata* L.), douglas fir (*Pseudotsuga menziesii* (Mirbel) Franco) and wild cherry (*Prunus avium* L.). The field reference data for all trees on the sample plots were comprised of the relative stem location, tree species, DBH, tree height, and crown base height.

The routines to perform the individual tree detection, the automatic crown segmentation, and the parameter calculation were programmed in R software (R Foundation for Statistical Computing). The routines also used functionalities of existing R packages (mainly lidR, TreeLS and dbscan). Output tree files were stored in the "las" file-format (American Society for Photogrammetry and Remote

Sensing ASPRS). To assess the quality of the crown separation algorithm, 235 crowns were randomly selected throughout the stands for a manual on-screen segmentation using the CloudCompare program (Girardeau-Montaut 2017). The manually segmented point clouds were merged with the output files of the automatic crown segmentation to calculate performance measures in terms of the detection rate (number of correctly matched points divided by total number of manually segmented points), the commission error (number of surplus detected points divided by total automatically segmented points), and the overall accuracy (detection rate minus commission error).

3. Results and Discussion

By merging the manual and automatic derived crown files (as seen in Figure 2) the accuracy measures were calculated (average values and standard deviations crowns are given in Table 1). The average detection rate was 94 %, i.e. 6 % of the reference crown voxels (cubes of 2x2x2 cm) were not correctly assigned by the automatic segmentation. The average commission error was 14 %. The number of assigned surplus points was higher than the number of missed points, this can be explained by the inclusion of points in the upper crown section from neighbouring trees and of the understorey vegetation close to the stems that has been included in the automatic tree detection but was removed in the manually segmented trees.

Table 1. Congruence measures of the automatic segmented and manual reference crowns.

	<i>n</i> = 235	mean	<i>st.dev.</i>
detection rate		93.81 %	9.64 %
commission error		13.58 %	15.14 %
accuracy		80.23 %	16.89 %

When analysing single trees there is a considerable amount of commission in the upper crown regions that was mostly caused by shading effects in the point cloud due to interlocked crowns. Some of the misallocations were also caused by branches from distant trees that were found tangent to other tree stems.

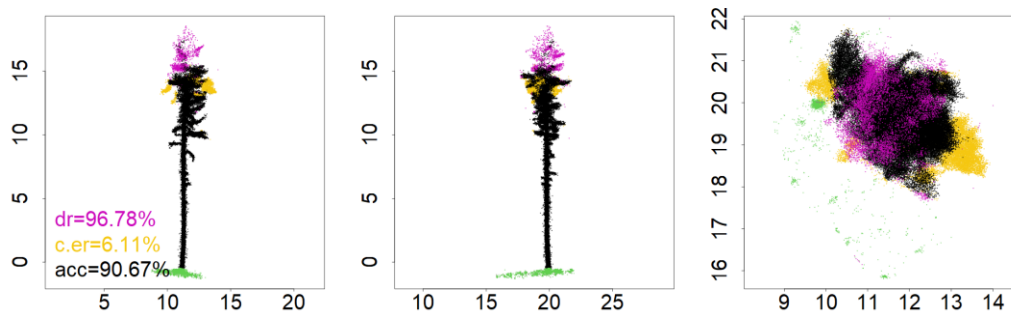


Figure 2: Matching manually clipped tree (pink) with automatic segmented crown (yellow), correctly assigned points black, (dr = detection rate, c.er = commission error, acc = accuracy).

Table 2 shows the differences between automatically measured individual tree parameters and field reference data. The automatically measured DBH and tree height showed only small deviations from the reference data. Please note that the exact definition of the DBH is often challenging in practice using traditional measurement instruments, especially for non-circular stem cross-sections. In fact, the manual DBH measurements can have large variation depending on the orientation of the calliper. In contrast, the automatic measurement is derived by fitting a natural cubic spline to the circumference of the local laser point cloud. Tree height was estimated with less precision than DBH, because the density of the point clouds was often reduced in the upper crown regions. The crown base height was underestimated on average 3.95 m. This bias mainly resulted from the automatic decision rule for the crown base height detection.

Further geometrical measures, such as the extent, the projection area, and the volume of the crown (see Figure 3) were measured with relative high accuracy and precision. The average crown extent (mean of x- and y-extent) and the projection area were only slightly overestimated and the average crown volume was slightly underestimated. Distant points, that might increase the volume, matter less

than missing parts within and especially in the upper crown sections. This phenomenon would suggest further improvements of the crown segmentation algorithm to mitigate a possible “overgrowing” into adjacent trees.

Table 2. Comparing the automatic measurements with field reference data.

$n=235$	mean.ref	RMSD	RMSD.pct	bias	bias.pct
DBH	26.8 cm	3.94	14.7%	-0.67	-2.5%
height	20.0 m	2.25	11.2%	-0.92	-4.6%
crown base	11.5 m	5.61	48.8%	-3.95	-34.3%
crown dimension ¹	4.6 m	0.65	14.1%	0.15	3.2%
crown projection area ¹	13.8 m ²	2.83	20.5%	0.19	1.4%
crown volume ¹	19.0 m ³	4.65	24.5%	-0.51	-2.7%

¹ comparing automatic segmentation with manually clipped reference crowns.

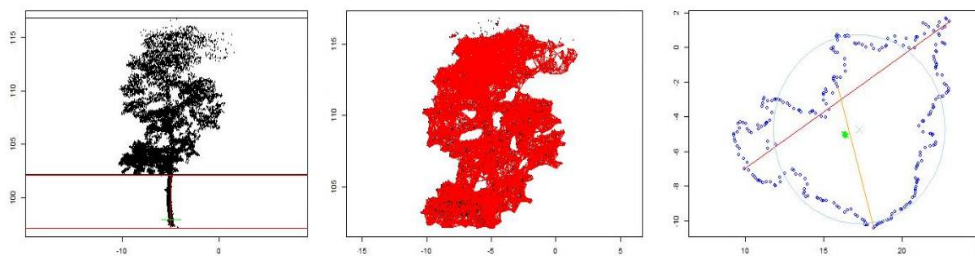


Figure 3: Automatic measurement of crown parameters for oak (left: crown base detection, middle: crown volume alpha hull, right: crown projection area and dimensions).

Precise crown segmentation is regarded as an essential functionality of automated 3D point cloud analysis to obtain geometrical crown features. The proposed automatic routine was successfully approved in comprehensive evaluations and showed only minor misallocations, mainly occurring in the upper crown sections. However, it was demonstrated that these few upper-crown discrepancies had only a negligibly small effect on the precision of the crown variable measurements, as the RMSD of the crown volume and crown projection area estimates were less than 5 %. Further research and software development is required to improve the automatic crown base detection and to find proper approximations of the crown volume using the manual field measurements, such that the latter could serve as reference data for further evaluations.

4. Conclusions

The proposed automatic crown segmentation algorithm provides accurate and precise crown measures of the single tree crown morphology. Hence, a detailed analysis of the spatial crown allocation patterns can be now performed in greater detail and on a larger scale than with traditional measurement techniques. These novel techniques will also facilitate a precise quantification of the inter-tree competition in the crown layer that will be useful for future analyses of individual tree growth patterns.

References

- Bienert, A., Georgi, L, Kunz, M, Maas, H-G and Von Oheimb, G, 2018, Comparison and Combination of Mobile and Terrestrial Laser Scanning for Natural Forest Inventories. *Forests*, 9(7), 395.
- Calders, K, Adams, J, Armston, J, Bartholomeus, H, Bauwens, S, Bentley, L, Chave, J, Danson, F, Demol, M, Disney, M, Gaulton, R, Krishna Moorthy, S, Levick, S, Saarinen, N, Schaaf, C, Stovall, A, Terry, L, Wilkes, P and Verbeeck, H, 2020, Terrestrial Laser Scanning in Forest Ecology: Expanding the Horizon. *Remote Sensing of Environment*, 251: 112102.
- Girardeau-Montaut, D.C 2017, 3D Point Cloud and Mesh Processing Software, Telecom ParisTechs: Palaiseau.
- Gollob, C, Ritter, T, Nothdurft, A, 2020, Forest Inventory with Long Range and High-Speed Personal Laser Scanning (PLS) and Simultaneous Localization and Mapping (SLAM) Technology. *Remote Sensing*, Basel, Switzerland, 12(9), 1509.

Assessing the ForeStereo sensor and the FORTLS R package for estimating stand variables in mature forests

Juan Alberto Molina-Valero¹, Isabel Aulló-Maestro², Ana Parras², César Pérez-Cruzado³, Fernando Montes²

¹Unidad de Gestión Ambiental y Forestal Sostenible (UXAFORES), Departamento de Ingeniería Agroforestal, Escuela Politécnica Superior de Ingeniería, Universidade de Santiago de Compostela, Benigno Ledo s/n, Campus Terra, 27002 Lugo, Spain.
Email: juanalberto.molina.valero@usc.es

²Centro de Investigación Forestal (INIA, CSIC), Ctra. De la Coruña km 7,5, 28040 Madrid.
Email: isabel.aullo@inia.es; parras@inia.es; fmontes@inia.es

³Proyectos y Planificación (PROEPLA), Departamento de Producción Vegetal y Proyectos de Ingeniería, Escuela Politécnica Superior de Ingeniería, Universidade de Santiago de Compostela, Benigno Ledo s/n, Campus Terra, 27002 Lugo, Spain.
Email: cesar.cruzado@usc.es

1. Introduction

Information about forest resources is essential for sustainable forest management and development of forest policies. Forest inventories, which are used as a means of estimating these resources, are continuously influenced by the technological development of remote sensing for data acquisition. Proximal sensing (PS) techniques, in which sensors capture information from short distances, have a strong potential to complement and enhance forest inventories (White et al., 2016). Moreover, the measurement approach of some of these techniques in fixed-point sampling makes them suitable for implementation in conventional forest inventories.

Although several PS devices are available, most are based on optical and LiDAR technologies. As an example of the former, ForeStereo is a passive optical sensor composed of two fish-eye cameras optimized for forestry use (Montes et al., 2019). The main advantages of optical sensors are their low weight and energy consumption, high efficiency in fieldwork and the option of using the image information to retrieve the species or health status of the trees. Terrestrial Laser Scanning (TLS) (LiDAR-based) devices have generated great interest in forest inventories in recent years (Liang et al., 2016). These devices have a well known capacity to generate high density 3-dimensional point clouds with millimetre spatial resolution, making them particularly valuable for enhancing forest inventories (White et al., 2016). In addition, free applications for processing and analysing TLS data have increasingly become available in recent years. For example, the recently developed R package FORTLS (Molina-Valero et al., 2021) is useful for extracting forest attributes at stand level based on a single-scan approach. Here, we assessed the performance of the ForeStereo sensor and the FORTLS package for estimating the following conventional forest inventory variables: density (N , trees ha⁻¹), basal area (G , m² ha⁻¹), mean diameter at breast height (\bar{d} , cm) and the diameter distribution.

2. Data and Methods

The data analysed correspond to 130 subjectively selected sample plots located in mature forest stands dominated (at least 90% of the G represented by the main tree species) by beech (*Fagus sylvatica* L.), maritime pine (*Pinus pinaster* ssp. *atlantica* Villar), Scots pine (*Pinus sylvestris* L.) and silver fir (*Abies alba* Mill.). These stands represent different European forest types: Nemoral and Mediterranean Scots pine forest (38 plots); Southwestern European mountainous beech forest, for both beech (38 plots) and beech-fir (11 plots) dominated communities; Atlantic Maritime pine forest (32 plots) and Mountainous Silver fir (11 plots) forest. These forest types cover a large area of the forest land in Spain. All plots were located in fully stocked stands with no evidence of recent disturbance or logging. Sampling was conducted between 2017 and 2019 and was implemented using a circular nested plot design, with 2 levels of nested plots. All live trees of diameter at breast height (dbh , measured at 1.3 m from the ground) greater than 7.5 cm in the first level (radius 5 m) and greater than 12.5 cm in the second level (radius 25 m) were measured with conventional inventory techniques. The plots were then also scanned from the plot centre with ForeStereo and TLS devices. Data were analysed with ForeStereo software and the

R package FORTLS (Molina-Valero et al., 2021) developed for ForeStereo and TLS devices, respectively. Analysis of stereo pairs of hemispherical images acquired by ForeStereo is based on image segmentation and region-based matching of stems, followed by fitting taper equations for dbh estimation. TLS point cloud analysis uses density-based cluster detection on the horizontal projection of points extracted from one or several slices at approximately 1.3 m height and dbh , and tree position is estimated by minimizing radius variance.

We assessed the performance of TLS and ForeStereo devices for estimating N , G , \bar{d} and diameter distribution. With this aim, we compared estimates based on field data with those obtained with ForeStereo and FORTLS for circular fixed area plots of 10 and 15 m radius. We also considered the occlusion correction methodology based on correcting the shadowing effect (Seidel and Ammer 2014), which is implemented in both ForeStereo and FORTLS. According to this correction, the effective reference sampling area is reduced by excluding the unsampled areas shadowed by trees. The performance of variable estimates was assessed by means of different statistics: relative RMSE (%), relative bias (%) and the Pearson correlation coefficient. Diameter distributions were assessed using the quadratic form distance: $d(H_{GroundTruth}, H_F) = \sqrt{(H_{GroundTruth} - H_F)^T A (H_{GroundTruth} - H_F)}$, where $H_{GroundTruth}$ is the matrix of histogram bin values as derived from calliper measurements and H_F is the matrix of histogram bin values derived from ForeStereo and TLS data. A is a similarity matrix, with $[a_{ij}]$ denoting the similarity between histogram bins i and j , calculated as $a_{ij} = 1 - |i - j| / \max(|i - j|)$. Lower values of the quadratic-form distance indicate greater similarity between histogram distributions.

3. Results and Discussion

In general, TLS data processed with FORTLS yielded lower RMSE and bias values and higher correlations than ForeStereo (Table 1). However, ForeStereo provided better estimates of N in *P. pinaster* stands of 10 m radius. This may be due to difficulties in distinguishing trees from shrub vegetation, which is especially dense in these stands. In these cases, FORTLS may have performed poorly because trees were detected at 1-1.6 m above ground level, in contrast to ForeStereo, which detected trees by matching the visible part of the stem. For almost all species and variables, FORTLS exhibited higher precision, accuracy and correlations for 15 m radius plots. Nevertheless, we did not observe any trends in the accuracy in estimates due to plot size with ForeStereo, even within the same species.

The estimates of N were most accurate with FORTLS for plots of 15 m radius ($\approx 4\%$ on relative bias) for all species except *P. pinaster*, for which ForeStereo yielded the lowest absolute value of relative bias with -5% . Although FORTLS tended to overestimate N for the 10 m radius plots, probably due to interception by branches or foliage, ForeStereo tended to underestimate N for 15 m radius plots as in a study case in mixed stands of *P. sylvestris* and *F. sylvatica* located in the Spanish Pyrenees (Montes et al., 2019), due to the increase in occlusions. The highest correlations corresponded to FORTLS estimates, with values of 0.89 for *P. sylvestris* and 0.85 for *F. sylvatica*. Estimates of G yielded the lowest relative bias with FORTLS for 10 m radius plots of *P. pinaster* and *P. sylvestris* (3 and -1%), and 15 m radius plots of *F. sylvatica* and *A. alba* (0 and 6 %), lower than the 8% reported by Seidel and Ammer (2014) for dense poplar SRF stands. In those cases, the occlusion correction methodology based on correcting the shadowing effect was also applied. Again, the highest correlations corresponded to FORTLS, with a particularly high value of 0.85 obtained for *P. sylvestris*, and the poorest correlations were attained with both PS techniques for mixed *A. alba-F. sylvatica* stands. The G estimates produced by ForeStereo for the mature stands analysed in this study showed greater bias and lower correlations than those reported by Montes et al. (2019) for young *P. sylvestris-F. sylvatica* stands, for which the best results were attained with 8 m radius plots. Regarding \bar{d} , lower values of relative bias were yielded by ForeStereo, i.e. -2% for *F. sylvatica* and -11% *P. pinaster* stands, and by FORTLS, i.e. 0% for *A. alba* and -8% for *P. sylvestris* stands. The values were always lower than the -16% reported by Seidel and Ammer (2014) for TLS data obtained in densely stocked poplar short rotation stands. As in previous studies (Seidel and Ammer 2014), \bar{d} was generally underestimated, probably due to systematic underestimation of dbh in small trees. The highest correlations were again yielded by FORTLS for *A. alba* (0.88) and *P. sylvestris* (0.89).

Quadratic-form distances (QFD) between diameter distributions retrieved from field data and PS techniques were lower considering plots of 15 m radius, especially when derived from ForeStereo, and they were always lower for TLS than for ForeStereo. The poorer performance of ForeStereo for 10 m radius plots may be due to the small sample of trees used for taper equation fitting. The best results were obtained for *P. sylvestris* with both PS techniques.

Table 2. Statistics calculated to assess accuracy in variable estimates.

		<i>N</i>			<i>G</i>			\bar{d}			QFD
		Bias	REMC	r	Bias	REMC	r	Bias	REMC	r	
Silver fir / beech-fir											
Fore-	10 m	-23	53	0.31	16	91	0.18	10	30	0.36	427
Stereo	15 m	-49	62	0.20	-9	69	0.32	20	36	0.53	245
FOR	10 m	16	37	0.64	27	54	0.22	0	13	0.75	202
TLS	15 m	5	23	0.77	6	32	0.40	-2	9	0.88	170
Beech											
Fore-	10 m	23	49	0.61	8	46	0.27	-11	27	0.31	297
Stereo	15 m	-15	37	0.49	-13	35	0.48	-2	22	0.22	180
FOR	10 m	11	26	0.83	6	29	0.59	-4	20	0.55	124
TLS	15 m	3	19	0.85	0	25	0.60	-4	13	0.61	122
Maritime pine											
Fore-	10 m	-5	42	0.37	-14	39	0.45	-13	20	0.51	379
Stereo	15 m	-32	50	0.11	-35	44	0.47	-11	19	0.48	207
FOR	10 m	33	77	0.38	3	32	0.67	-14	20	0.62	185
TLS	15 m	17	51	0.51	-5	25	0.73	-12	16	0.71	131
Scots pine											
Fore-	10 m	12	59	0.46	-10	42	0.58	-16	26	0.55	351
Stereo	15 m	-20	51	0.49	-33	47	0.57	-14	23	0.62	162
FOR	10 m	14	31	0.89	-1	23	0.80	-8	14	0.89	113
TLS	15 m	4	25	0.89	-8	20	0.85	-8	13	0.86	106

4. Conclusions

FORTLS produced better results than ForeStereo for estimating *G* in mixed *A. alba*-*F. sylvatica* stands and in pure *F. sylvatica*, *P. pinaster* and *P. sylvestris* stands and for estimating *N* and \bar{d} in mature mixed *F. sylvatica* and *P. sylvestris* stands, always yielding the highest correlations and lowest quadratic-form distances for 15 m radius plots. Nevertheless, ForeStereo performed better for estimating *N* and \bar{d} in *P. pinaster* stands, where dense understory intercepts LiDAR at 1.30 m height. The best results were achieved for 15 m radius plots in *P. sylvestris* stands. Nonetheless, differences between forest types or sites in plot radii that yielded improved estimates depended on forest structure and other factors influencing stand visibility. Future research should focus on exploiting the upper slices of the point cloud with TLS to prevent the understorey effect, increasing the range of detection with ForeStereo and combining both techniques to improve the precision provided by LiDAR and produce additional information for species classification or foliage health status monitoring from images.

References

- Liang X, Kankare V, Hyypä J, Wang Y, Kukko A, Haggrén H, and Vastaranta M, 2016. Terrestrial laser scanning in forest inventories. *ISPRS Journal of Photogrammetry and Remote Sensing*, 115:63-77.
- Molina-Valero, J.A., Ginzo Villamayor, M.J., Novo Pérez, A.M., Martínez-Calvo, A., Álvarez-González, J.G., Montes, F., Pérez-Cruzado, C. (2021). FORTLS: Automatic processing of TLS point cloud data for forestry purposes. R package version 1.0.2. <https://CRAN.Rproject.org/package=FORTLS>
- Montes F, Rubio-Cuadrado Á, Sánchez-González M de la O, et al (2019) Occlusion Probability in Operational Forest Inventory Field Sampling with ForeStereo. *Photogramm Eng Remote Sensing* 85:493–508.
- Seidel D, and Ammer, C, 2014, Efficient measurements of basal area in short rotation forests based on terrestrial laser scanning under special consideration of shadowing. *iForest-Biogeosciences and Forestry*, 7(4), 227.
- White JC, Coops NC, Wulder MA, Vastaranta M, Hilker T and Tompalski P, 2016. Remote sensing technologies for enhancing forest inventories: A review. *Canadian Journal of Remote Sensing*, 42(5):619-641.

Gaussian Process Regression for Airborne Laser Scanning Based Forest Inventory: Validation and Parameter Selection

P. Varvia¹, J. Rätty², L. Korhonen¹, P. Packalen¹

¹School of Forest Sciences, University of Eastern Finland, Joensuu, Finland
Email: {petri.varvia; lauri.korhonen; petteri.packalen}@uef.fi

²Division of Forest and Forest Resources, Norwegian Institute of Bioeconomy Research, Ås, Norway
Email: janne.raty@nibio.no

1. Introduction

Airborne laser scanning-based (ALS) forest inventories that utilize the so-called area based approach (ABA) are of great practical importance. While ABA can be considered a mature problem, with many well-established approaches to predict the forest attributes, there is still be room for improved prediction methods.

Gaussian process regression (GPR) (e.g. Rasmussen and Williams 2006) is a popular machine learning method related to kriging that is based on modelling the forest attributes and the ALS predictors jointly as a Gaussian process. The main advantages of GPR are the capability to accurately represent highly nonlinear relations with a modest number of tuneable parameters, ability to effectively use large number of predictors, and that it produces uncertainty estimates for the predictions.

GPR has shown promise in providing slightly better prediction accuracy than established methods (Varvia 2019). However, the previous results on GPR were limited by 1) using data from only one study area, 2) using cross-validation instead of a separate test set. The aim of this work is to rectify these limitations and additionally test automatic tuning of GPR parameters.

To benchmark the GPR performance, random forests (RF) were chosen as a reference method. RF was chosen because it has produced excellent results in ABA (Cosenza et al. 2021) and it can also handle large number of predictors.

2. Data and Methods

2.1 Materials

The data consist of field measurements from three sites in Finland, Nummi-Pusula, Kurikka-Seinäjoki, and Pokka and corresponding ALS data produced by Finnish Forest Center in 2019. The study sites represent forests from Southern, Western, and Northern Finland, respectively. ALS data are openly available on the download service of the National Land Survey of Finland.

The field data consist of 1125, 830, and 763 circular field plots with a radius of either 9 m or 12.62 m in Nummi-Pusula, Kurikka-Seinäjoki, and Pokka, respectively. To evaluate the performance of the two prediction methods rigorously, each data set was randomly split to separate training, validation, and test sets in a 40%/20%/40% fashion. Of these, the validation set was used to choose optimal model parameters and only the test set to evaluate final prediction performance.

The corresponding ALS data had a nominal pulse density of 0.8 m⁻². After height normalization using ground echoes, large number of predictors, including height quantiles, other height metrics and canopy densities were computed separately from first of many and only echoes, and last of many and only echoes. Intensity metrics were also calculated. Predictors that did not show appreciable variation between plots were removed. Final set contained 45 predictor variables, with same variables in every site. No further variable selection was done.

2.2 Methods

In this study, the total stem volume is predicted in the ABA framework. Gaussian process regression was implemented using an R package under development by the authors. In GPR, the choice of the so-called covariance function or kernel is one of the principal aspects that affects the predictions. As in our previous studies, isotropic Matérn 3/2 covariance function was used with Euclidean distance metric. This results in three tuneable parameters: length scale l , kernel variance σ_k^2 , and error variance σ_e^2 . The separate validation set was used to choose the optimal values for these parameters by minimizing the sum of squared prediction errors in the validation set. The optimization was done using simulated annealing with the R *optimization* package.

As a reference method, random forest (RF) was used. For RF, we used the popular implementation in the R *randomForest* package. While it is common practice to use the default values for RF parameters, such as the number of decision trees, to facilitate honest comparison, the number of predictor candidates per split (i.e. *mtry*) and the number of trees were optimized using the validation set as in GPR.

3. Results and Discussion

The RMSE and bias of the total volume predictions evaluated using the separate test set for the three study sites are presented in Table 1. In all three sites, GPR produced slightly more accurate predictions, with relative RMSE being consistently better by 0.3-0.9 percentage points. Both methods showed small negative bias in the predictions, with GPR being slightly less biased in Nummi-Pusula and Kurikka-Seinäjäjoki, while RF is slightly better in Pokka.

Table 1. Prediction performance in the test set. Units are in m^3/ha , relative metrics are shown inside parentheses.

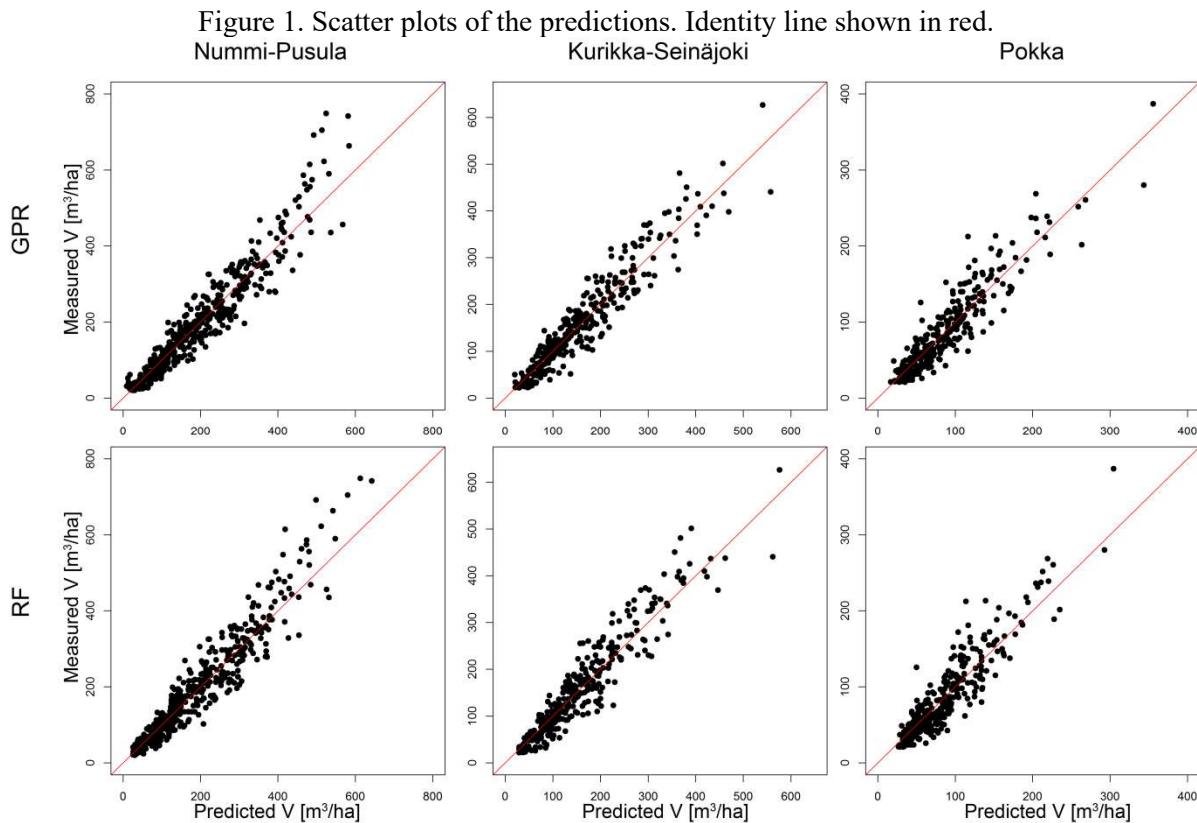
	RMSE (%)	Bias (%)
Nummi-Pusula	$n_{\text{test}}=450$	
GPR	42.3 (21.4%)	-2.4 (-1.2%)
RF	42.9 (21.7%)	-4.3 (-2.2%)
Kurikka-Seinäjäjoki	$n_{\text{test}}=332$	
GPR	33.1 (20.8%)	-1.0 (-0.6%)
RF	34.5 (21.7%)	-2.4 (-1.5%)
Pokka	$n_{\text{test}}=305$	
GPR	21.3 (24.2%)	-0.6 (-0.7%)
RF	22.1 (25.1%)	-0.4 (-0.5%)

Model parameters were optimized by simulated annealing using the validation set are shown in Table 2. Both the GPR and RF variables show large variability by study site. Parameter selection problems are generally difficult to optimize, due to usually having multiple local minima. Simulated annealing was chosen to mitigate this, but as a method it gives no guarantee that the converged solution is the global optimum. Given the small number of parameters, grid search would be still feasible and guarantee an optimal solution. In RF, the default parameters ($mtry=33\%$, $n=500$) are commonly used. The optimized values here were compared to the predictions using the default values and the difference in RMSE was negligible, supporting the common practice.

Table 2. Optimized parameter values by study area, σ_v^2 is the sample variance of total stem volume in the training set.

	GPR	RF
Nummi-Pusula	$l=25.6, \sigma_k^2=2.7\sigma_v^2, \sigma_e^2=0.51\sigma_v^2$	$mtry=42\%, n=494$
Kurikka-Seinäjäjoki	$l=29.6, \sigma_k^2=1.1\sigma_v^2, \sigma_e^2=0.03\sigma_v^2$	$mtry=17\%, n=487$
Pokka	$l=16.3, \sigma_k^2=2.3\sigma_v^2, \sigma_e^2=0.17\sigma_v^2$	$mtry=29\%, n=225$

GPR also produces prediction variances from which credible intervals can be computed. The 95% credible intervals (CI) covered 99.8% of the field measured volumes in Nummi-Pusula, 82.5% in Kurikka-Seinäjoki, and 99.0% in Pokka. The values imply that the variances were severely overestimated in Nummi-Pusula and Pokka, and underestimated in Kurikka-Seinäjoki. The variance estimation aspect could be potentially improved by incorporating CI coverage in the cost function used to find optimal parameter values.



4. Conclusions

In this work, Gaussian process regression was rigorously validated at three study sites representing boreal forest in Southern, Western, and Northern Finland. The prediction performance of GPR was compared with RF. The performance of the two methods was quite similar, although GPR produced consistently slightly lower RMSEs. Compared to RF, GPR has the additional capability to also simultaneously produce variance/interval estimates for the predictions. In conclusion, the results support the previous studies on the potential of GPR as a prediction method in the area-based approach.

Acknowledgements

This study was funded by the Academy of Finland (grant number 332707).

References

- Rasmussen C and Williams K, 2006, *Gaussian processes for machine learning*. MIT Press, Cambridge, MA, USA.
- Varvia P, Lähivaara T, Maltamo M, Packalen P, Seppänen A, 2019, Gaussian process regression for forest attribute estimation from airborne laser scanning data. *IEEE Trans. Geosci. Remote Sens.*, 57(6):3361–3369
- Cosenza D N, Korhonen L, Maltamo M, Packalen P, Strunk J L, Næsset E, Gobakken T, Soares P, Tomé M, 2021, Comparison of linear regression, k-nearest neighbour and random forest methods in airborne laser-scanning-based prediction of growing stock, *Forestry*, 94(2):311–323

Long Range High-Speed Personal Laser Scanner (PLS) applied to Simultaneous Localisation and Mapping (SLAM) Technology in Roundwood Measurement

F. de Miguel-Diez¹, S. Reder¹, E. Wallor¹, H. Bahr¹, J.-P. Mund¹, T. Cremer¹

¹University for Sustainable Development, Schicklerstr. 5 16225 Eberswalde (Germany)
Email: {felipe.diez; stefan.reder; evelyn.wallor; henrik.bahr; jan-peter.mund; tobias.cremer}@hnee.de

1. Introduction

The use of technologies such as Terrestrial Laser Scanning (TLS) has increased the efficiency and quality of forest inventories compared to traditional methods. Despite large innovations TLS is still considered labour-intensive and ineffective for large scale data acquisition. However, many of these shortcomings can be mitigated by applying a Personal Laser Scanner (PLS), a device applied to Simultaneous Localisation and Mapping (SLAM) technology. Gollob et al. (2020) examined this kind of device to estimate tree position and diameter and demonstrated its accuracy. However, to our knowledge the PLS has not yet been applied to the measurement of felled industrial roundwood. The log scaling process involves measuring the length of the logs and midpoint-diameters, the top-diameter or the diameters at both ends and then applying a determined formula (Edwards, 1998). This lengthy process does not ensure any reliable estimation of the log's volume, since the estimated volume is derived from empirical formulas based on analogue and manual measurements. The accumulated measured volume error when acquiring roundwood can lead to considerable economic losses for the roundwood purchaser since as stated by Fonseca (2005), approximately 60 - 85% of costs of producing wood products can lie in this initial purchase. Therefore, accuracy in the log scaling process is critically important. Likewise, process transparency and stakeholder trust in the roundwood supply chain can be keys to sustainable commercial success. This can be achieved since when using the PLS, the files containing the point clouds of the scanned roundwood are saved and can become accessible immediately allowing all stakeholders to access records of the roundwood purchased and recalculate its volume at any time. In this paper both methods, the PLS measurement of roundwood and its digitized procurement and transparent supply chain, are presented. The present study aims to examine the accuracy of the use of the PLS applied to SLAM technology in measuring log volume, to assess its reliability when measuring roundwood volume during the roundwood acquisition stage.

2. Data and Methods

In this study, fifty logs of Norway Spruce (*Picea abies* L.) were scanned and analysed. The logs were felled in the forestry district of Chorin (52° 53' 22'' N, 13° 52' 06'' E), located in Brandenburg, Germany. These logs belonged to the assortment industrial wood, with an average length of 2.53 m, ranging from 2.46 m to 2.65 m, and with an average midpoint diameter of 19.97 cm, ranging from 14.45 cm to 28.55 cm. Firstly, the logs were numbered with forest crayons then top, butt and midpoint diameters as well as the length of the log were measured manually, using the method explained by de Miguel-Diez et al. (2021). This step was carried out to recognise the logs later once the data were processed, and the logs were reproduced as point clouds. Afterwards, the volume of every log was measured using a xylometer and the resulting volumes were taken as reference values. Finally, each log was scanned digitally using a GeoSLAM ZEB HORIZON personal mobile laser scanner. The technical characteristics of this device are comprehensively presented by Gollob et al. (2020). After scanning, the files were converted into a point cloud with a *.LAZ format using the software GeoSLAM HUB 6.0.0.. These LAZ files were analysed using the software Cloud Compare (version 2.10.2., Cloud Compare, 2021). Here, the logs were segmented manually using the segmentation tool in Cloud Compare. The noise was removed using the low pass filter of Cloud Compare's "Filter noise" tool. In doing so, six neighbours around each point were extracted inputting a relative maximum error of 1.0 and removing all isolated points. Subsequently, the normals were computed using a plane local surface mode, as recommended for noisy samples by Girardeau-Montaut, in 2015 with a minimum spanning tree, considering twenty nearest neighbours to build the tree. Afterwards a mesh was generated using the

“Poisson” surface reconstruction method, which is suitable for surface reconstruction of noise affected samples (Kazhdan et al., 2006) and provided as plugin in Cloud Compare (see Figure 1). Twenty neighbouring sample points per node were considered for the log reconstruction with a centre point weight of 2. The Neumann constraint was chosen as boundary condition, as it is proven robust to missing data, e.g., on the bottom side of the logs (Kazhdan and Hoppe, 2013). Instead of using an octree depth, the target resolution was defined with 0.1 m. Once all the volumes were calculated, they were compared with each other by fitting a linear regression with the volumes measured using the xylometer and the volumes calculated in Cloud Compare from the PLS sample. In addition, paired t-tests were conducted in order to prove if the difference between the samples was statistically significant. The results were analysed using the programme RStudio (version 1.3.1093, RStudio Team, 2021). For the visualisation of the simulation results the R package *ggplot 2* was used (Wickham, 2009).

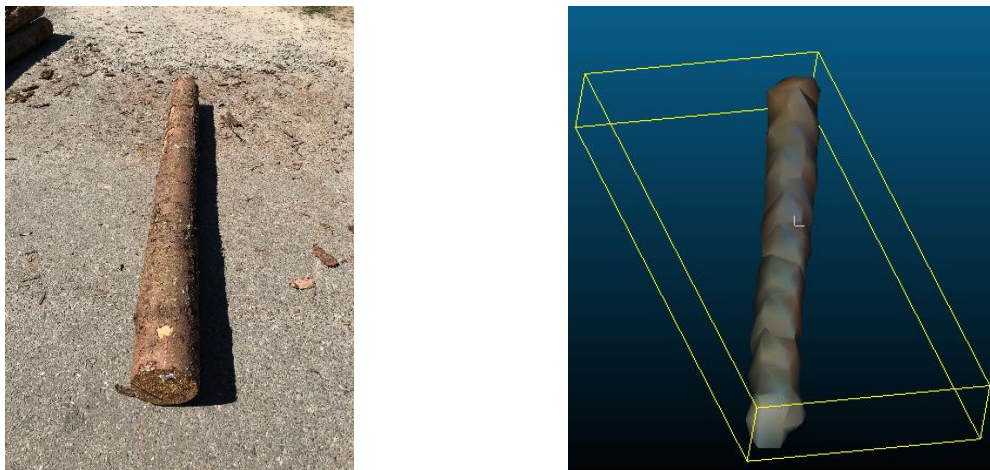


Figure 1: Real log (left) and mesh generated virtually from the PLS sample (right).

3. Results and discussion

The mean volume of all measured logs with xylometer was 81.4 dm^3 , ranging from 47.3 dm^3 to 167.3 dm^3 , and the mean volume calculated in Cloud Compare resulted in 81.5 dm^3 , ranging from 46.7 dm^3 to 166.2 dm^3 . When comparing the results using both methods, the adjusted R^2 obtained was very close to 1 (see figure 2). This can be interpreted as a marginal deviation from a linear relation.

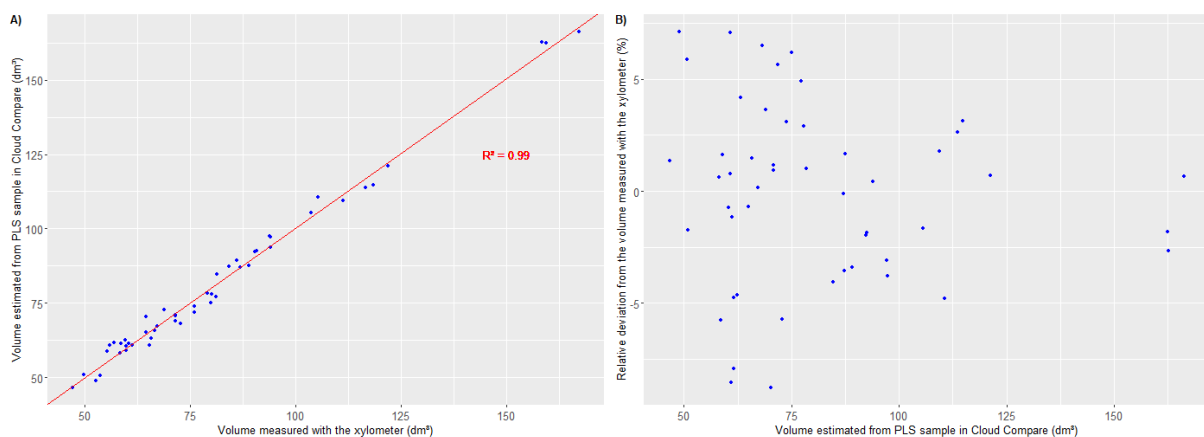


Figure 2: Linear regression concerning both measurement methods (A) and relative deviation of the volume estimated in Cloud Compare from the volume measured with the xylometer (%) (B).

The difference between all samples is normally distributed (Shapiro-Wilks, Sig = 0.134). The mean difference of the samples of 0.107 dm^3 (or 0.13%) (Std. Dev 2.913 dm^3 , 95%-Confidence Interval $[-0.720 \text{ dm}^3; 0.935 \text{ dm}^3]$) is not statistically significant (paired t-test; $t(49) = 0.260$,

Sig(2 - tailed) = 0.796). In addition, as depicted in Figure 2B the relative deviation (Dev%) becomes smaller when the log's volume increases which means that the estimation is more accurate for bigger logs (Dev% (Vol < 75 dm³) = ± 8%; Dev% (Vol > 150 dm³) ≤ 3%).

According to the device's product specifications the operational temperature ranges from 0 to 50 ° C (GeoSLAM Ltd., 2018). In addition, the product specifications indicates that the device's protection class is IP 54 (GeoSLAM Ltd., 2018). This implies that the use of this device is constrained by weather conditions, eg., heavy precipitations or freezing temperatures. Another important limitation of PLS in forest applications and timber-logging measurements is its susceptibility to airborne dust. In this study, the logs were scanned near to a sandy terrain in which the air was quite dusty, which was later observable in the point cloud. In particular, the dust in the air created salt-and-pepper noise which requires additional filtering prior to the digital measurement process. Under such conditions the samples result in unsharp surfaces of the scanned object which hinders object extraction, log modelling and any further analyses. Nevertheless, the Cloud Compare software provides several tools such as the "local surface model" or "number of samples per node" to solve this problem in most cases, allowing for log volume to be estimated accurately.

4. Conclusions

Concluding the analyses and results of this study, the use of PLS applied to SLAM technology provides accurate results when estimating the volume of the logs under realistic timber logging conditions. Errors in the point cloud, resulting from dusty air when taking the samples can be solved using filters and robust algorithms to reconstruct the log surfaces virtually.

Acknowledgements

This study was undertaken within the framework of the "HoBeOpt" project, which was financially supported via the Fachagentur Nachwachsende Rohstoffe (FNR), Germany, by the Federal Ministry of Food and Agriculture (BMEL) (Grant number: 22008518).

References

- Cloud Compare, 2021, Cloud Compare (version 2.10.2.) GPL software. Retrieved from <http://www.cloudcompare.org/>
- De Miguel-Díez F, Tolosana-Esteban E, Purfürst T, Cremer T, 2021, Analysis of the Influence That Parameters Crookedness and Taper Have on Stack Volume by Using a 3D-Simulation Model of Wood Stacks. *Forests*. 12(2):238. <https://doi.org/10.3390/f12020238>
- Edwards PN, 1998, Timber Measurement. A Field Guide. 4th ed., Forestry Commission Booklet 49, Edinburgh, UK.
- Fonseca MA, 2005, Measurement of Roundwood: Methodologies and Conversion Ratios. CABI Publishing, Oxfordshire, UK.
- GeoSLAM Ltd., 2018, ZEB HORIZON product specification. Retrieved from <https://geoslam.com/solutions/zeb-horizon/>.
- Girardeau-Montaut D, 2015, Cloud Compare version 2.6. 1 user manual. Available online at: Online at: [http://www.danielgm.net/cc/doc/qCC/CloudCompare% 20v2](http://www.danielgm.net/cc/doc/qCC/CloudCompare%20v2).
- Gollob C, Ritter T, Nothdurft A, 2020, Forest Inventory with Long Range and High-Speed Personal Laser Scanning (PLS) and Simultaneous Localization and Mapping (SLAM) Technology. *Remote Sensing*. 12(9):1509. <https://doi.org/10.3390/rs12091509>
- Kazhdan M and Hoppe H, 2013, Screened poisson surface reconstruction. *ACM Transactions on Graphics*. 32(3). Article 29. <https://doi.org/10.1145/2487228.2487237>
- Kazhdan M, Bolitho M, Hoppe H, 2006, Poisson Surface Reconstruction. SGP '06: Proceedings of the fourth Eurographics Symposium on Geometry Processing (2006). Pages 61-70.
- RStudio Team, 2020, RStudio: Integrated Development Environment for R. RStudio, PBC, Boston, USA. Available online: <http://www.rstudio.com/>. (accessed on 05 May 2021).
- Wickham H, 2009, ggplot2: Elegant Graphics for Data Analysis. Springer, New York, USA.

Structural Diversity in a Subtropical Forest: A Comparison of Individual Tree- and Pixel-based Approaches

Zhaoju Zheng¹, Yuan Zeng², Meredith Schuman¹, Bernhard Schmid¹,
Michael Schaepman¹, Felix Morsdorf¹

¹Remote Sensing Laboratories, Department of Geography, University of Zurich, Switzerland
Email: zhaoju.zheng@geo.uzh.ch

²State Key Laboratory of Remote Sensing Science, Aerospace Information Research Institute, Chinese Academy of Sciences

Abstract

Forest structural diversity is an important dimension of biodiversity, affecting light availability, tree survival and growth, ecosystem functioning and habitat for forest-dwelling organisms. With increasing forest biodiversity loss, it is important to monitor forest structure efficiently. Compared to traditional field sampling, airborne light detection and ranging (LiDAR) provides an effective and consistent way to monitor the three-dimensional structure of forests at different spatial units, typically in the form of pixels or individual tree crowns (ITCs). However, few studies have explored the differences between the ITC- and pixel-based approaches to mapping functional traits and diversity by remote sensing of forest vegetation. In this study, we used the two approaches to assess structural diversity in a subtropical forest. We firstly retrieved three morphological traits — 95th quantile height (H95), leaf area index (LAI) and foliage height diversity (FHD) from ITCs and pixels based on airborne LiDAR data. Then we compared trait distributions, trait–trait relationships and functional diversity patterns derived from ITCs and similarly-sized pixels. In addition, we investigated how much variability in morphological traits would be lost with increasing pixel size. We found that H95 derived from 3m pixels were highly correlated with the ITC-based H95 (Pearson $r = 0.95$), while the consistencies of ITC- and 3m pixel-based LAI and FHD were lower. The pixel-based retrieval tended to yield higher H95 and FHD and lower LAI values than ITC-based measures. These differences increased with pixel size, and the distributions tended to become more clustered. The between-unit variation in morphological traits at different pixel sizes indicated that less relative variability in traits could be explained by larger pixels. The spatial patterns of ITC- and pixel-based structural diversity were similar, but the scale-dependency analysis showed that ITC-based functional richness increased faster with area at small neighborhood scales, indicating that increased within-community diversity could be better captured by the ITC-based approach. It should be noticed that the choice of spatial unit and retrieval approach might change the semantics and interpretation of the derived morphological traits. These in-depth comparisons will help to increase our understanding of the scaling between local-ground, regional-airborne and global-spaceborne observations of forest structural diversity.

Perspectives on long-term TLS time-series to detect changes in tree crowns

M. B. Campos¹, S. Junttila², A. Shcherbacheva¹, Y. Wang¹, X. Liang¹, J. Hyypä¹, E. Puttonen¹

¹Department of Remote Sensing and Photogrammetry, Finnish Geospatial Research Institute (FGI), National Land Survey of Finland, Masala, Finland

Email: {mariana.campos; anna.shcherbacheva; yunsheng.wang; xinlian.liang; juha.hyypa; eetu.puttonen }@nls.fi

²School of Forest Sciences, University of Eastern Finland, Joensuu, Finland.

Email:samuli.junttila@uef.fi

1. Introduction

The 3D Terrestrial laser scanner (TLS) information play a key role in monitoring and understanding forest dynamics. The monitoring of structural changes in tree crowns can be used as a basis to understand their growth dynamics and overall canopy interactions in forests. Canopy structure and spatial distribution of leaves are major factors that affect the efficiency of energy and mass exchange processes of water vapor, photosynthetic activity and carbon assimilation between forest and the atmosphere (Hatfield and Dold 2019). Precise canopy change detection is a difficult task due to the non-static behavior and non-symmetric shape. At present, many questions about tree canopy dynamics remain unanswered, such as when and how tree canopy grows. Previous work has shown that TLS can overcome several of the methodological problems inherent to conventional canopy analysis with passive optical methods (Seidel et al. 2012), such as varying lighting conditions and occlusion. However, traditional TLS data acquisition surveys are laborious, which limits the number of works focusing in long term and high temporal resolution monitoring of tree canopy dynamics with TLS. To address this challenge, a permanent TLS measurement station with high spatial and temporal resolution was built in Hyytiälä forest research station, in southern Finland (Campos et al. 2021). The permanent TLS measurement station has been fully operational since April 2020 and it provides a TLS time-series with high spatial (0.006° angular resolution) and temporal resolution (1 scan per hour). Here, we present a data assessment of the measurement station point clouds with an aim to demonstrate the potential of long-term TLS time-series to provide new insights about structural changes in tree crowns over time. Our results show that long-term TLS time-series enable the accurate detection of the sprouting and growing of new leaves during the spring growth season of 2020 and in the beginning of 2021.

2. Long-term TLS time-series Dataset

The 13-month long TLS time-series data assessment was performed with the focus on detecting visual and quantitative crown changes (point cloud density and reflectance response) of a single deciduous Silver birch (*Betula pendula*). The Silver birch tree is located about 6 m away from the tower, with a 19m height and DBH of 173mm. The point cloud time-series of the Silver birch was collected with the permanent TLS measurement station over the entire growing season of 2020 till beginning of 2021-spring. More details about the TLS measurement station setting and output data can be found in Campos et al. (2021). 72 point clouds were selected and pre-processed to assess the potential of the measurement station data to detect changes in tree crowns. All selected scans were acquired in windless conditions during the night varying from 8 P.M to 2 A.M. The time-series used in the change assessment covered a time period from April 2020 to May 2021 with a temporal resolution of 5 days (~1 week). The data processing framework to detect changes in the Silver birch canopy from the time-series consisted of three main steps. These were i) tree segmentation from the full point cloud, ii) point cloud filtering, and iii) point cloud georeferencing in to ETRS89-TM35FIN frame (EPSG: 3067).

3. Results

Figure 1 presents the median reflectance response and the upper canopy height variation (90th percentile) of the birch tree crown over the observation period with the zero date set to 1 January 2020 (e.g. 2021 starts in day of the year 366). The reflectance response along the time-series can detect the first signal of the spring. In 2020, the reflectance values start to significantly increase after May 23 and decrease around September 22, which can be associated to the spring sprout of new green leaves and their falling in autumn. The dashed red and blue vertical lines in Figure 1 represent the time of solstices and equinoxes. In 2021, the reflectance values start to increase again around May 1st, manifesting the

beginning of a new growing season. The increase in the point cloud density can also confirm the leaf sprout and green biomass changes in the birch crown during this period. For instance, the point cloud density increased 13.4% in 2020, from 4.7 million points in April 16 to 5.3 million points in May 25 and 17% in 2021, from 5.2 million points in April 15 to 6.1 million points in May 25. Figure 1 illustrates a closely synchronized behaviour between changes in reflectance response and in the 90th height percentile variation. The 90th height percentile correspond to the height at which 90% of the points of the whole cloud are below it. This approach enables a reliable timing of change events in the crown. However, the height percentile information alone cannot quantify where in the crown growth happens. In this regard, changes in TLS reflectance response, point density and canopy area of the birch crown are further explored in Figure 2, Figure 3 and Table 1, respectively.

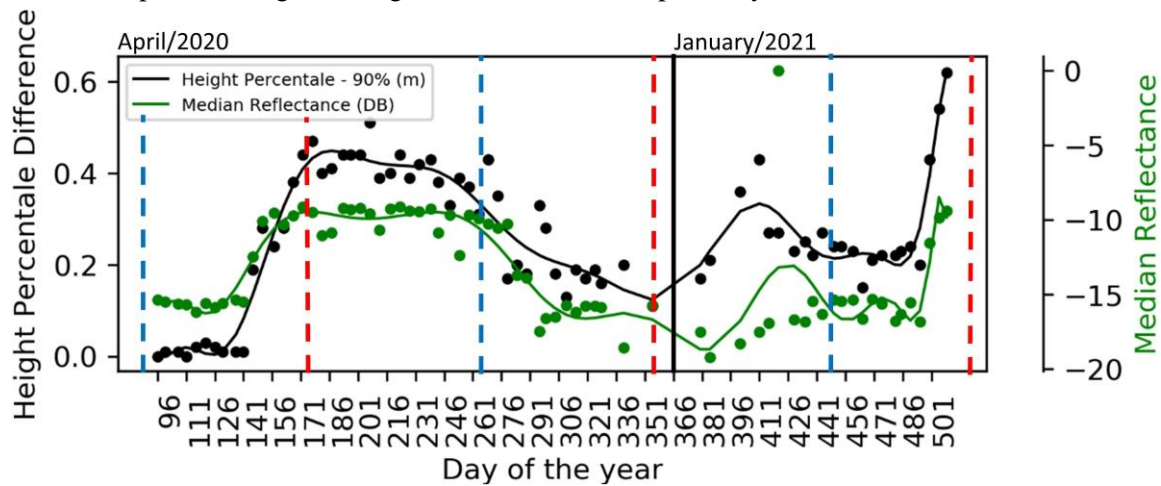


Figure 1: Polygonal fit of median reflectance response (green) and height percentile variation (black) of a Silver birch tree from April 2020 to May 2021. Red and blue dash lines are the solstices (summer, winter) and equinoxes (spring, autumn) days, respectively. Black line represents the begging of 2021.

To visualize the state and reflectance response of the Silver birch crown during the spring growing season, a top view of eight georeferenced point clouds from early-spring of 2020 (Day of the years - 107, 126, 137 and 146) and 2021 (Day of the years in Figure 1-470, 490, 500, 509) is presented in Figure 2. The point clouds coordinates (E, N) were converted to polar coordinates and presented according to the azimuth direction and distance from the tree stem centre position, ranging from 0 to 3m. The point clouds were colorized with respect to the reflectance parameter values, ranging from 0 to 2.

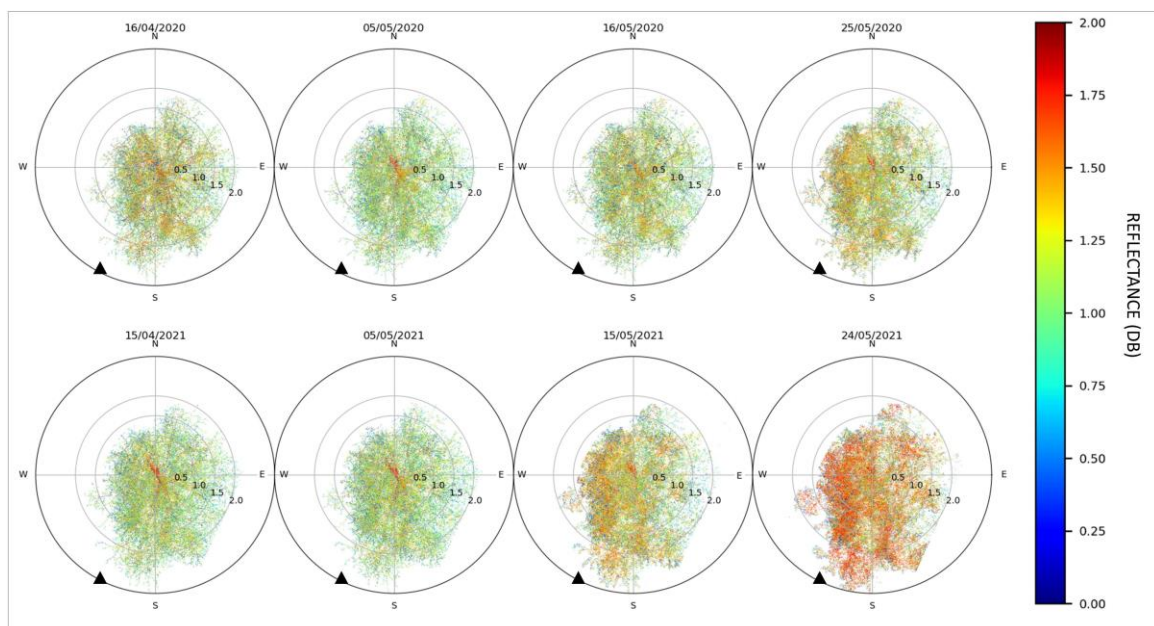


Figure 2: Seasonal variation in a Silver birch crown during the spring growth season of 2020 and 2021. The color scale presents individual laser point reflectance in logarithmic scale (0–2). The black triangle shows the direction to the permanent TLS measurement station.

For more accurate volumetric change assessment, point cloud density variation can be associated to volumetric dynamics on the tree crown using methods such as point cloud voxelization. A 2D point cloud voxelization is presented in Figure 3, in which a voxel size of 5×5 cm dimensions was used to detect the birch crown changes at 2021 (DoY- 470, 490, 500, 509). The tree crown changes can be observed comparing the point density in each voxel element at different times of the 2021 growing season. From mid-April to late-May, the density of points increase in the voxel of the centre of the crown. The number of point also increase in minor magnitude at tree edges, which can be associated to tree crown area growth. Table 1 present quantitative results of the tree crown change from the estimation of canopy area via alpha shape algorithm (Edelsbrunner and Mücke 1994). As show in Figure 3, the birch tree canopy area increases especially after Early-May. The estimated area increased 5% in 2020 and 12% in 2021 from mid-April to late-May. The response of the birch tree to the spring have started earlier in 2021 than 2020 (Figure 1), which can justify the difference in the percentage of increased area.

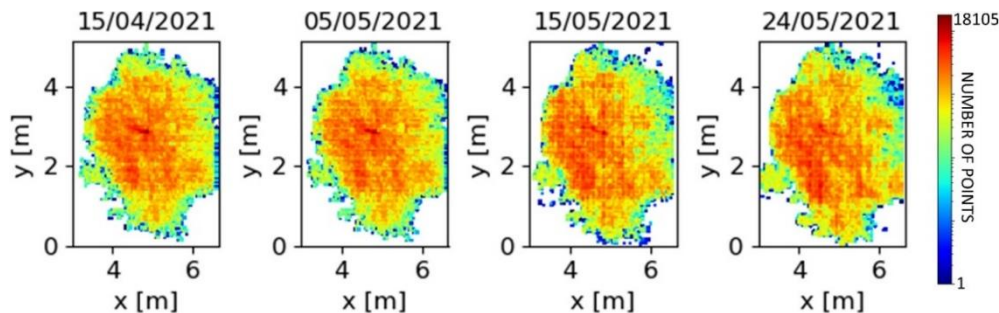


Figure 3: Seasonal variation in a Silver birch crown in the 2D voxel space between Mid-April and Late-May. The color scale presents the number of points per 2D voxel.

Table 1. Birch Tree canopy area in spring 2020 and 2021 computed with alpha shape.

Year	Mid/April	Early/May	Mid/May	Late/May
2020	10.01 m ²	9.93 m ²	10.01 m ²	10.44 m ²
2021	10.41 m ²	10.50 m ²	11.20 m ²	11.67 m ²

4. Conclusions

Our first results show that long-term TLS time-series can support the detection of structural changes in individual tree crowns. Reflectance detection enables the accurate timing of the sprouting and falling of leaves during the spring growth season of 2020 and in the beginning of season 2021. Correlation and regression analysis of reflectance, temperature, and other environmental factors relevant to tree life cycles will be performed in future to determine the exact sequence of events that drive tree sprouting and fall. High temporal resolution of the time-series allow canopy growth monitoring and quantification with several different methods, such as height percentile and voxel point densities. We demonstrate the potential of high-density TLS time-series as a plot scale measurement tool that captures accurate temporal snapshots of the actual state of the forest. These dense time-series information enable forest structure analyses on level that have not been achievable with earlier techniques. In future, our work will focus on expanding the present analysis to cover all high visibility trees in the monitoring area to quantify, time, and analyze their phenological events and the overall forest dynamics.

Acknowledgements

The authors would like to acknowledge the support from Academy of Finland, project numbers 330422, 316096/320075 - “Upscaling of carbon intake and water balance models of individual trees to wider areas with short interval laser scanning time series” and 334060 - “Monitoring and understanding forest ecosystem cycles using high temporal and spatial resolution terrestrial laser scanning time series”.

References

- Campos M B, Litkey P, Wang Y, Chen Y, Hyyti H, Hyypä J and Puttonen E, 2021, A Long-Term Terrestrial Laser Scanning Measurement Station to Continuously Monitor Structural and Phenological Dynamics of Boreal Forest Canopy. *Front. Plant Sci.* 11:606752. doi: 10.3389/fpls.2020.606752
- Edelsbrunner H., Mücke E. P, 1994, . Three-dimensional alpha shapes. *ACM Trans. Graph.*, 13(1):43–72.
- Hatfield J L, Dold C, 2019, Water-Use Efficiency: Advances and Challenges in a Changing Climate. *Front. Plant Sci.* 10:103. doi: 10.3389/fpls.2019.00103
- Seidel D, Fleck S, Leuschner, C, 2012, Analyzing forest canopies with ground-based laser scanning: A comparison with hemispherical photography. *Agricultural and Forest Meteorology*, 154:1-8.

Impact of sample size – empirical results from a hybrid inference two-phase inventory based on dense laser scanning

H. J. Persson¹, K. Olofsson¹, J. Holmgren¹

¹Swedish University of Agricultural Sciences, 901 83 Umeå, Sweden
Email: henrik.persson@slu.se

1. Introduction

Airborne laser scanning (ALS) from low flight altitudes will produce high-resolution data but is not efficient for large area mapping. ALS data can therefore be collected in strips to enable an accurate inventory of larger areas. High-resolution data from ALS can provide estimates of tree positions, tree height, and tree species, but reference data are commonly needed from field inventories for estimation of stem attributes. In this study, we apply ALS strip sampling as first phase in forest stands, and use sample trees from a second phase using terrestrial laser scanning (TLS). The TLS measures were used instead of manual field inventories to build regression functions, which were used to predict stem volume of all detected trees in the strips (first phase). The estimated volumes with respect to the number of strips in each forest stand was evaluated.

2. Material

2.1 Study area

The study area is located at 62.9°N 16.9°E in middle Sweden. A subset consisting of ten boreal forest stands covering 207 ha were used in this study. The forest was dominated by Norway spruce (*Picea abies* (L.) H. Karst.), Scots pine (*Pinus sylvestris* L.), and birch (*Betula* spp.), where pine (50%) and spruce (44%) constituted 94% of the growing stock and birch 6%. The stands had an average VOL of 235 m³/ha and the stand ages were between 98 and 150 years.

2.2 Harvester data

Two forest harvesters were used to harvest the ten forest stands in 2020, after ALS scanning. The harvester registered the tree species and measured the stem diameter along the trunk. We estimated the stem volume based on the DBH and height, using regional valid functions. The harvested areas were flown with a drone after harvest, carrying an optical camera. Ortho-photographs with 4 cm pixel resolution could be generated, which enabled us to delineate the harvested forest areas accurately.

2.3 Laser scanning data

The ALS system Riegl LMS-Q680i was acquiring data from a helicopter. The nominal flight speed 20 km/h, and the altitude 70 m above ground level. The nominal swath width was 90 m and the nominal point density ranged from 490 points/m² to 654 points/m², with an average of 593 points/m². The laser scanning of the 10 forest stands was performed 3 November 2019.

Terrestrial Laser Scanning (TLS) was conducted at the location of the field plot centers. The Trimble TX 8 instrument scanned in a hemispherical pattern with a point spacing of 11.3 mm at 30 m distance. The wavelength was 1.5 micrometer. The tree stem properties was estimated using the TLS data and an algorithm by Olofsson and Holmgren (2016).

3. Methods

3.1 Processing of ALS data

For automatic delineation of tree crowns, we used an algorithm based on density models of tree crown (Holmgren and Lindberg 2019). It first uses a canopy height model (CHM) to obtain an approximate height of potential tree height positions, at 0.25 m gridding. Template matching was then applied to

create a model similarity surface that was used as input in a watershed segmentation to generate an automatic delineation of all tree crowns.

3.2 Processing of TLS data

The algorithm used to estimate the stem profiles and VOL of the trees from a 3D point cloud was presented in Olofsson and Holmgren (2016). The volume of the stems were estimated as truncated cones connecting the centers of the modeled stem cylinders (Olofsson and Holmgren 2017). The top part of the tree (where the singletree detection algorithm was unable to detect the stem cylinder), was modeled as a complete cone reaching the highest registered laser point of the canopy.

3.3 Two-phase hybrid inference

The first phase consisted of ALS strips across the stands. These were selected to cover the systematically distributed TLS scan locations in phase two. Depending on the stand geometry, the number of strips varied between 3 and 5, but for some stands perpendicular flight lines of nearby stands made even more strips available. The strips (used in the results below) were randomly selected. All trees that were identified in both the TLS and ALS data within the strips were used to estimate model parameters with robust multiple linear regression, using the R-package MASS and the default Huber variance estimator (Huber 1981). The regression model was used to predict the VOL, \hat{y} , on all segmented trees, and the model had the form of:

$$\ln(\text{VOL}) = \alpha_0 + \alpha_1 X_1 + \dots + \alpha_p X_p \quad (1)$$

where the parameters $[\alpha_0, \alpha_p]$ for the p attributes X_i , $i \in [1, p]$ were the following statistical metrics computed from the ALS point clouds for the single tree segments: height percentile 10, 80, 95, and crown width. Since the dependent variable VOL was transformed using the natural logarithm, a correction for logarithmic bias was applied, by adding $s^2/2$ to (1) before taking the inverse transform of the prediction, s^2 being the residual variance from (1) (Finney 1941).

The population (stand) means ($\hat{\mu}_{Y_{VOL}}$) were estimated with a ratio-to-size estimator, as the size of the strips varied depending on the stand shape. The total volume T_k for each strip k was calculated by summing up the volumes \hat{y}_j predicted with the linear regression function for all trees M_k in the strip:

$$\hat{T}_k = \sum_{j=1}^{M_k} \hat{y}_j \quad (2)$$

Then, the mean ($\hat{\mu}_{Y_{VOL}}$) was estimated as

$$\hat{\mu}_{Y_{VOL}} = \frac{\sum_{k=1}^{M_c} \hat{T}_k}{\sum_{k=1}^{M_c} \hat{a}_k} \quad (3)$$

where \hat{a}_k denotes the total area of strip k , and M_c denotes the total number of strips in the stand.

An approximated variance (Ståhl et al. 2011) of the estimators in (3) and (5) is

$$\widehat{\text{Var}}(\hat{\mu}_{Y_{VOL}}) = s_{Y_{VOL}}^2 + \sum_{d=1}^p \sum_{e=1}^p \widehat{\text{Cov}}(\hat{\alpha}_d, \hat{\alpha}_e) \hat{T}'_d \hat{T}'_e \quad (4)$$

where the first term represents the variability due to the first-phase sampling and the second term represents the model error due to the uncertainty of the parameter estimates. p is the number of model parameters, $\widehat{\text{Cov}}(\hat{\alpha}_d, \hat{\alpha}_e)$ is the estimated covariance between the model parameter estimates, and $\hat{T}'_d \hat{T}'_e$ are the estimated average values of the first order partial derivatives of the function used to estimate the target variable. The first-phase sampling variability was estimated as:

$$s_{Y_{VOL}}^2 = \left(1 - \frac{a}{A}\right) \frac{\sum_{k=1}^{M_c} (\hat{T}_k - \hat{\mu}_{Y_{VOL}} \hat{a}_k)^2}{M_c \bar{a}^2 (M_c - 1)} \quad (5)$$

where a represents the area covered by the strips, A represent the total area of the population (stand), and \bar{a} is the mean strip area.

To provide an estimate of mean bias, the estimated stand means ($\hat{\mu}_{Y_l}$) were compared with the reference values μ_Y from the harvester, and the mean population bias for all M_d stands was estimated as

$$\hat{B} = \frac{1}{M_d} \sum_{l=1}^{M_d} (\hat{\mu}_{Y_l} - \mu_{Y_l}) \quad (6)$$

The RMSE was used as accuracy measure for all stands, and it was estimated as

$$\widehat{\text{RMSE}} = \sqrt{\frac{1}{M_d} \sum_{l=1}^{M_d} (\hat{\mu}_{Y_l} - \mu_{Y_l})^2} \quad (7)$$

using the same notations as earlier. The standard error was calculated as the square root of the variance:

$$\widehat{SE} = \sqrt{\widehat{Var}(\hat{\mu}_Y)}. \quad (8)$$

4. Results

The results showed that an increasing number of strips lowered the RMSE, both in absolute and relative terms (Table 1), and the bias showed a similar trend. The trend can also be seen in the scatter plots (Figure 1). The proportion sampled area increased with more strips from $n=1$ until $n=3$, where it plateaued. The proportion corresponded to about 30%, but higher n decreased the RMSE further, without sampling a larger proportion of the stands. This indicates that it would be more cost efficient to collect more, shorter strips, rather than fewer but larger strips. The standard error was rather stable in the range of 9% to 17%, but without correlation to the number of strips. Since the variance estimator depends on the covered proportion, larger differences and repeated simulations would be needed to investigate this further.

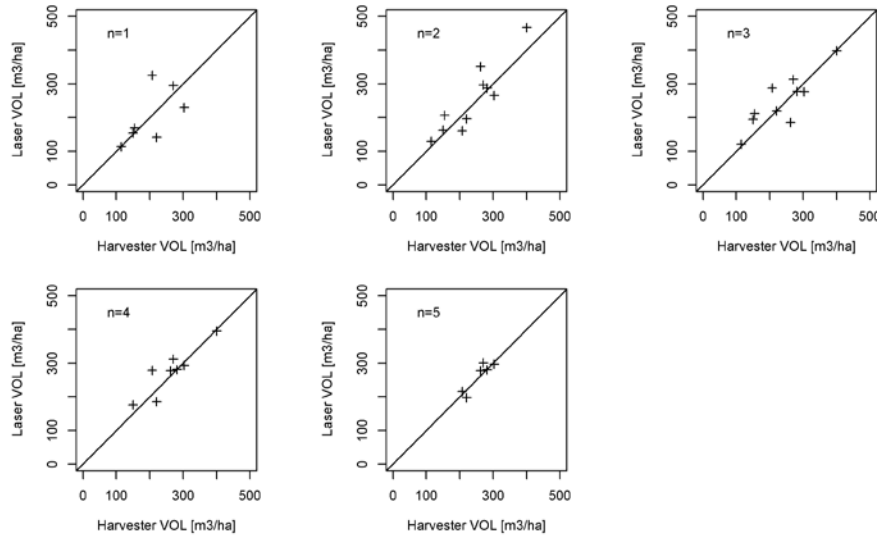


Figure 1: Estimated vs. reference VOL for different number of flight lines.

Table 1. Accuracies results

n	RMSE	Bias	Standard Error	Proportion of Tot Area	Stands
1	77.7 (34.2%)	19.6 (8.64%)	-	10.6%	8
2	45.0 (19.0%)	16.1 (6.82%)	36.2 (15.3%)	21.6%	10
3	45.1 (19.1%)	12.3 (5.18%)	21.4 (9.06%)	32.5%	10
4	33.7 (12.9%)	13.3 (5.09%)	35.2 (13.5%)	29.3%	8
5	17.3 (6.73%)	4.12 (1.60%)	45.0 (17.5%)	30.1%	6

Acknowledgements

The work was funded by the Bo Rydin's foundation for scientific research (award no F19/17) and Mistra Digital Forest. The HPC2N is acknowledged for providing data resources for the TLS processing.

References

- Finney, D. J. 1941. "On the Distribution of a Variate Whose Logarithm Is Normally Distributed." *Supplement to the Journal of the Royal Statistical Society* 7(2):155–61.
- Holmgren, Johan and Eva Lindberg. 2019. "Tree Crown Segmentation Based on a Tree Crown Density Model Derived from Airborne Laser Scanning." *Remote Sensing Letters* 10(12):1143–52.
- Huber, P. J. 1981. *Robust Statistics*. Wiley, New York.
- Olofsson, K. and J. Holmgren. 2017. "Tree Stem and Canopy Biomass Estimates from Terrestrial Laser Scanning Data." Pp. 157–60 in *International Archives of the Photogrammetry, Remote Sensing and Spatial Information Sciences - ISPRS Archives*. Vol. 42.
- Olofsson, Kenneth and Johan Holmgren. 2016. "Single Tree Stem Profile Detection Using Terrestrial Laser Scanner Data, Flatness Saliency Features and Curvature Properties." *Forests* 7(9).
- Ståhl, Göran, Sören Holm, Timothy G. Gregoire, Terje Gobakken, Erik Næsset, and Ross Nelson. 2011. "Model-Based Inference for Biomass Estimation in a LiDAR Sample Survey in Hedmark County, Norway." *Canadian Journal of Forest Research* 41(1):96–107.

Quantifying TLS Data and Diameter Estimation Uncertainty

Vincent B. Verhoeven¹, Markku Åkerblom¹, and Pasi Raumonon¹

¹Unit of Computing Sciences, Tampere University; Korkeakoulunkatu 7, 33720 Tampere, Finland

1 Introduction

Uncertainties in vegetation volume and biomass account for a large part of the uncertainty of terrestrial carbon cycle models (Bloom et al., 2016). Biomass is frequently calculated with allometric equations using the tree diameter (Asner et al., 2013; Paul et al., 2013), meaning that errors in the tree diameter propagate into quantities used in environmental modelling. Terrestrial laser scanning (TLS) with geometrical tree reconstruction is a useful technology to measure vegetation volume and biomass, thus it is important to quantify the uncertainty of tree diameter estimation using TLS data.

Studies have shown that uncertainties in the laser scanning data and methodologies applied to it result in errors in the properties derived with it (Boehler et al., 2003; Lichti et al., 2005). Additionally, studies have been performed that assess the uncertainty of results obtained with TLS data of trees (Disney et al., 2018; Wang et al., 2019), however the consideration of uncertainty for the reconstruction of trees is rare. Furthermore, to the authors' best knowledge no study exists that quantifies this uncertainty and accounts for it prior to the determination of tree properties, i.e. during data processing and the reconstruction of tree geometry.

The uncertainty in the detected hit location comes primarily from the finite laser beam width which widens with range and beam divergence angle, as well as the incidence angle of the beam with the object (Hartzell et al., 2015). It is thus affected by the scanner's specifications, the object's surface and the locations of the scanner. This study views the point cloud not as discrete locations, but instead as a set of continuous probability distributions centred on their reported hit locations. In particular, this means that it is possible to rigorously account for points from separate scanning positions with significantly different uncertainties.

The uncertainty is propagated to the diameter estimate through Monte Carlo sampling, where with each iteration the point cloud is shifted randomly according to the computed probability distributions of each point. Moreover, a maximum likelihood based circle fitting method that uses the distribution information directly is presented.

2 Data & Methods

For this paper simulated laser scanning data are used, enabling a sensitivity analysis of the uncertainty and the algorithm's performance with changing scanning parameters. The simulated data are generated by creating a deterministic point cloud which assumes there is no uncertainty, after which they are randomly shifted in their respective radial and propagation (range) directions according to their respective probability distributions (Hartzell et al., 2015). The resulting stochastic point cloud is used for the remainder of the algorithm, and the true hit locations and geometry are assumed to be unknown.

The uncertainty of the tree stem - or branch - centre and diameter is determined through Monte Carlo sampling, akin to (Shapiro & Philpott, 2007). A schematic overview of the method is given in Figure 1. The sampling revolves around the same principle as the creation of the synthetic point cloud, however without prior knowledge of the geometry. The point cloud uncertainty estimated from the initial shape fit is used to shift the original point cloud randomly for each Monte Carlo iteration. The uncertainty of the shape parameters is computed by taking the α and $1 - \alpha$ quantiles of the resulting series of geometrical parameters.

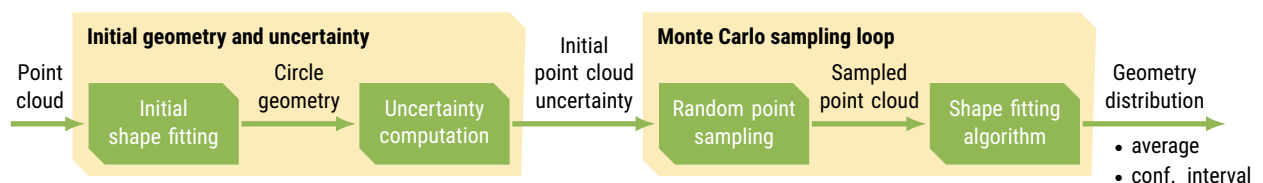


Figure 1: Overview of the method used to determine the tree stem shape parameters and their uncertainty.

The sampled point cloud is used as the basis for shape fitting, however to compute the probability distribution around each point the geometry of the object has to be assumed. To reduce the effect of errors in the initial geometry estimate, initial shape fitting is performed for each Monte Carlo iteration as well. Next, the optimal shape parameters are determined by maximising the likelihood of the circle, given the point cloud's probability distributions computed according to the initial shape fit. An example of this is shown in Figure 2a. This enables the shape fitting algorithm to more effectively use points originating from different scanners or striking the object with a higher incidence angle, as it considers the differences in their uncertainty. A schematic example of this is given in Figure 2b. It should be noted that these probability distributions are not changed by the optimiser's estimates, to prevent the optimiser from changing the geometry to alter the uncertainty rather than to more accurately resemble the underlying shape.

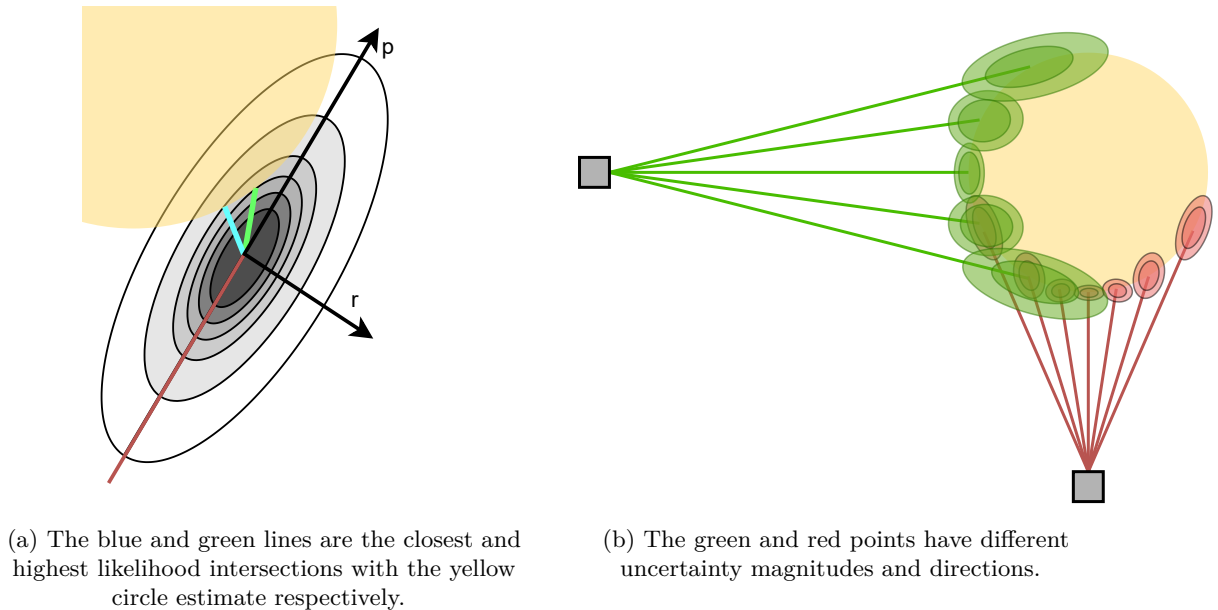


Figure 2: Schematic overview of the probability distribution of a single point (a) and the point clouds from two scanners (b).

If the initial geometry estimate is poor, points that are further away have a negligible and near-constant likelihood, and are thus ignored by the optimiser. As such, the second objective of the shape fitting algorithm is to minimise the expected squared distance of the points to the circle, given their respective probability distributions. This second objective is intentionally affected by points that are distant to the estimated geometry, which necessitates outlier filtering before shape fitting.

3 Results & Discussion

The method proposed above has been tested on a scanning setup akin to Figure 2b, where the left and bottom scanners are at 100 and 50 metres distance from a 0.1 metre diameter tree stem. The specifications of the Faro Focus (FARO, 2020) were used, with both the normal (0.30 mrad) and double (0.60 mrad) the beam divergence δ , to show the effect of greater uncertainty. The results of 100 Monte Carlo iterations are shown in Table 1 for linear least squares (LS), linear least squares weighted by the inverse distance between scanner and tree stem (WLS), and the maximum likelihood method (ML).

The estimate from the maximum likelihood method is closest to the true solution, with least squares having the greatest error. The performance difference between maximum likelihood and (weighted) linear least squares increases with uncertainty. The ML method is thus able to estimate geometry with lower quality data, however the performance benefit is small if the data quality is high. ML further has the thinnest confidence intervals, aside from the radius estimate with greater uncertainty where WLS outperforms it.

Table 1: The results for two beam divergence angles δ and three shape fitting methods. The errors of the estimated radius and centroid location, as well as the width of the 95% confidence interval (CI), are relative to the true radius.

δ [mrad]	Method	Radius		Centroid	
		Error [%]	CI width [%]	Error [%]	CI width [%]
0.30	LS	11.2	27.5	7.9	46.0
	WLS	9.1	23.0	6.3	37.2
	ML	4.2	22.0	2.5	28.3
0.60	LS	27.3	80.2	18.5	159.0
	WLS	23.1	58.4	16.3	117.3
	ML	7.6	69.6	2.7	88.0

4 Conclusion

Key tree parameters can be computed using geometrical tree models reconstructed from TLS data. The data and geometry derived from TLS data can contain significant uncertainty however, which this paper quantifies for diameter estimation and utilises to reconstruct the diameter more accurately.

The input data uncertainty is quantified through analytical computations of the laser beam properties, after which the circle is fitted to maximise the likelihood taking the probability distribution of each point into account. This enables the shape fitting method to distinguish between points that come from different scanners and have different directions and magnitudes of uncertainty.

A comparison was performed between the maximum likelihood method and (distance weighted) linear least squares for two scenarios of different uncertainty. The maximum likelihood had the lowest errors in radius (4.2 and 7.6%) and location of the centroid (2.5 and 2.7%), with the performance difference to the least squares approaches increasing with higher uncertainty.

Further research is planned to extend the presented methodology to the 3rd dimension by fitting cylinders to 3-dimensional point clouds. Additionally, the robustness of the method to surface roughness and non-circular cross-sections will be analysed.

References

- Asner, G. P., Mascaro, J., Anderson, C., Knapp, D. E., Martin, R. E., Kennedy-Bowdoin, T., van Breugel, M., Davies, S., Hall, J. S., Muller-Landau, H. C., et al. (2013). High-fidelity national carbon mapping for resource management and redd+. *Carbon balance and management*, 8(1), 1–14.
- Bloom, A. A., Exbrayat, J.-F., Van Der Velde, I. R., Feng, L., & Williams, M. (2016). The decadal state of the terrestrial carbon cycle: Global retrievals of terrestrial carbon allocation, pools, and residence times. *Proceedings of the National Academy of Sciences*, 113(5), 1285–1290.
- Boehler, W., Vicent, M. B., Marbs, A., et al. (2003). Investigating laser scanner accuracy. *The International Archives of Photogrammetry, Remote Sensing and Spatial Information Sciences*, 34(Part 5), 696–701.
- Disney, M. I., Boni Vicari, M., Burt, A., Calders, K., Lewis, S. L., Raunonen, P., & Wilkes, P. (2018). Weighing trees with lasers: Advances, challenges and opportunities. *Interface Focus*, 8(2), 20170048.
- FARO. (2020). *Faro focus laser scanner*. Retrieved May 19, 2021, from <https://media.faro.com/-/media/Project/FARO/FARO/FARO/Resources/2021/01/15/22/34/Tech-Sheet-FARO-Focus-Laser-Scanners-ENG.pdf?rev=cb02264ffcbd4123b82a5c42f29b14be>
- Hartzell, P. J., Gadowski, P. J., Glennie, C. L., Finnegan, D. C., & Deems, J. S. (2015). Rigorous error propagation for terrestrial laser scanning with application to snow volume uncertainty. *Journal of Glaciology*, 61(230), 1147–1158.
- Lichti, D. D., Gordon, S. J., & Tipdecho, T. (2005). Error models and propagation in directly georeferenced terrestrial laser scanner networks. *Journal of surveying engineering*, 131(4), 135–142.
- Paul, K. I., Roxburgh, S. H., England, J. R., Ritson, P., Hobbs, T., Brooksbank, K., Raison, R. J., Larmour, J. S., Murphy, S., Norris, J., et al. (2013). Development and testing of allometric equations for estimating above-ground biomass of mixed-species environmental plantings. *Forest Ecology and Management*, 310, 483–494.
- Shapiro, A., & Philpott, A. (2007). A tutorial on stochastic programming. *Manuscript*. Available at www2.isye.gatech.edu/ashapiro/publications.html, 17.
- Wang, Y., Lehtomäki, M., Liang, X., Pyörälä, J., Kukko, A., Jaakkola, A., Liu, J., Feng, Z., Chen, R., & Hyypä, J. (2019). Is field-measured tree height as reliable as believed—a comparison study of tree height estimates from field measurement, airborne laser scanning and terrestrial laser scanning in a boreal forest. *ISPRS journal of photogrammetry and remote sensing*, 147, 132–145.

Using Stochastic Geometry and Sequential Spatial Point Process Model for Estimation of Stand Density Based on ALS-ITD.

L. Mehtätalo¹, A. Yazigi², K. Kansanen², P. Packalen², T. Lähivaara³, M. Maltamo², M. Myllymäki⁴ and A. Penttinen⁵

¹Natural Resources Institute Finland (Luke), Yliopistokatu 6, 80100 Joensuu, Finland
Email: lauri.mehtatalo@luke.fi

²University of Eastern Finland, Joensuu campus, Yliopistokatu 2, 80101 Joensuu, Finland
Email: adil.yazigi@uef.fi, kasperkansanen@gmail.com, petteri.packalen@uef.fi, matti.maltamo@uef.fi.

³University of Eastern Finland, Kuopio campus, Yliopistonranta 1, 70600 Kuopio
Email: timo.lahivaara@uef.fi

⁴Natural Resources Institute Finland (Luke), Latokartanonkaari 9, 00790 Helsinki, Finland
Email: mari.myllymaki@luke.fi

⁵University of Jyväskylä, PO Box 35, Seminaarinkatu 15, 40014 University of Jyväskylä
Email: antti.k.penttinen@jyu.fi

1. Introduction

In individual tree detection (ITD), trees are delineated from a pre-processed ALS point cloud. A problem in ITD is that all trees are not visible when forest is seen from above. Here we focus on estimation of the hidden trees. Mehtätalo (2006) proposed a Horvitz-Thompson-like estimator for stand density (N , trees per ha) in ITD. The estimator was based on a sequential construction of the detected crown discs. The crown discs are ordered with respect to their diameter from the largest to the smallest. The largest tree is observed for sure. The other trees are observed from above only if they are not hidden below the crowns of the larger trees. Therefore, the probability to detect the i :th largest detected tree with radius r_i was computed by using the union of larger crown segments. Especially, it was assumed that the tree is not detected if the center point of the crown is within the union of larger tree crowns.

Kansanen et al. (2016, 2019) generalized the detection condition by defining a set A_i , which was obtained by removing a buffer of width αr_i from the union of larger crown segments. Here α is a tuning parameter that can be estimated either based on the properties of the applied ITD algorithm or empirically by using error of stand density as a criterion. If tree locations follow complete spatial randomness, the detection probability for tree i can be approximated as the proportion of the whole plot area that was not covered by A_i ,

$$\hat{\pi}_i = 1 - \frac{|A_i \cap W|}{|W|}, \quad (1)$$

where W is the sample plot of interest. After computing the detection probabilities, stand density (trees per plot) was estimated using a Horvitz-Thompson-like estimator

$$\hat{N} = \sum \frac{1}{\hat{\pi}_i} = N_{\text{detected}} + \sum \left(\frac{1}{\hat{\pi}_i} - 1 \right), \quad (2)$$

where the summation runs from 1 to the detected tree count. The latter form explicitly shows that the estimator is a sum of detected tree count N_{detected} and an estimated hidden tree count $\sum \left(\frac{1}{\hat{\pi}_i} - 1 \right)$.

An implicit assumption in the above constructions is that the density of trees of a given size in the parts that are not visible to the scanner is similar to the density in the visible parts. This assumption may not be realistic because the parts that are hidden provide worse growing conditions for small trees than the visible parts. This problem is implicitly taken into account if the tuning parameter α is estimated empirically so that the estimated stand densities match with the field measurements. However, a better solution might be to model the variability in stand density explicitly.

A finite sequential spatial point process model (SSPP) was recently proposed for forest data in Yazigi et al (2021). A similar model has been previously applied with eye movement data (Penttinen and Ylitalo 2016). In SSPP, the points are ordered according to the time and the locations of the latter points are affected by the earlier points. In the forestry context, it is realistic to assume that the order in terms of

tree age is well approximated by the order of trees in terms of size. The model is based on an accept-reject construction as follows. The first tree location is generated uniformly at random. For each of the latter trees, a uniform location is proposed. The proposal is accepted with probability θ , ($0 < \theta < 1$) if the proposed location is within a r -radius neighbourhood of at least one of the previous locations, and with probability $1 - \theta$ if the proposed location is not within any neighbourhood. The acceptance probability θ and interaction radius r are parameters of the model, which were estimated using maximum likelihood. The model allows a wide range of spatial point patterns. Especially $\theta = 1/2$, leads to complete spatial randomness, $\theta < 1/2$ a regular tree pattern and $\theta > 1/2$ a clustered pattern.

If the parameter r is selected so that it corresponds to the applied detection condition, the ratio $\frac{\theta}{1-\theta}$ describes the ratio of stand densities in the hidden and visible parts of the forest in the estimation method of Kansanen et al (2016, 2019). However, application of the model requires an estimate of θ be available. It might be possible to model parameter θ empirically using such predictors based on the ALS data which include information of the spatial pattern of tree locations, see Häbel et al. (2021).

In this paper, we apply the model of Yazigi et al. (2021) in the context of the method of Kansanen et al. (2016) to allow different stand densities in the hidden and visible parts of the plot. The developed model is evaluated with empirical data and compared with the previous methods.

2. Data and methods

A data set of 111 square fixed-area plots of size 30 by 30 meters from Liperi, North Carelia, Finland is used. The number of stems, quadratic mean diameter and basal area of the plots varied within 211-3900 trees per ha, 8.2-37.2 cm, and 7.84-46.19 m²/ha, respectively. 39% of the plots were dominated by Scots pine, 43% by Norway spruce, and 18% by birch species. All trees were measured for location, diameter (DBH) and height. ALS data were acquired using an Optech Titan instrument on July 2-10, 2016. Although this scanner operates in three wavelengths, we used only the 1064 nm channel in this study. The scanning altitude was 850 meters, the scanning half angle 20 degrees, pulse repetition frequency 250 kHz and sampling density 4.8 pulses per m².

We assume that a tree is detected if the center point of the crown is not within the union of larger tree crowns so that the detectability is given by Equation (1) where $A = \bigcup_{j=1}^{i-1} C_j$ and C_j is the crown disc of tree j . However, we assume that for each tree i , the density in the hidden part relative to the density in the visible part is $\frac{\theta}{1-\theta}$. Therefore, we propose here the following new estimator for the stand density:

$$\hat{N} = N_{\text{detected}} + \frac{\theta}{1-\theta} \sum \left(\frac{1}{\hat{\pi}_i} - 1 \right). \quad (3)$$

Notice that the estimator provides weights for every tree, so extension to estimation of other population characteristics (such as basal area) is straightforward.

The estimator was evaluated by using an analysis with the following steps:

1. Individual tree detection was conducted using a method that provided estimates of tree locations and (maximum) tree crown radius (Lähivaara et al. 2014).
2. The detected trees were matched with field-measured trees with a manual procedure. A linear mixed-effect model (see e.g. Mehtätalo and Lappi 2020) was fitted to model the crown width (based on ALS) on the field-measured tree DBH. The model was used to predict crown radius for all field-measured trees.
3. Using the predicted crown radii from step (2) as a known interaction radii, the “true” value of θ of in the SSPP model (Yazigi et al. 2021) was estimated separately for each plot.
4. The estimate of θ was modeled using different plot-level characteristics proposed by Häbel et al. (2021). Prediction based on that model was used in step 5.
5. Stand density was estimated for each plot using the estimator (3).

For comparison, the estimator of Kansanen et al. (2016) was also implemented. The tuning parameter α was estimated by finding for each sample plot such a value of α that provided minimum difference between the field-measured N and ALS-estimated N . The estimates were modeled using the same predictors as used in step 4 above and predicted for all plots for a procedure comparable with steps 4 and 5 above. Estimation using $\alpha = 0$ based on Mehtätalo (2006) was also implemented.

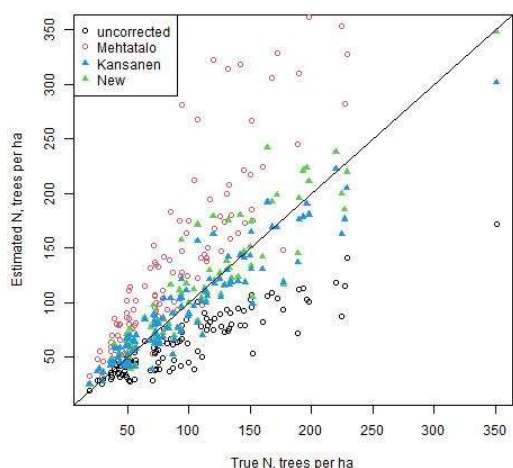


Figure 1. The estimated stand density using the four applied methods against field measurement

The new method. The new method was comparable with that of Kansanen (2016) with respect to bias, but slightly worse in terms of RMSE. Figure 1 shows the plot-specific estimates of different methods against the true stand density.

The presented results are only tentative. For example, a leave-one-out cross-validation should be implemented to confirm the findings. In addition, the applied correction method uses either θ or α in estimation, but also a method that utilizes both of them is possible and of interest. Furthermore, instead of the MLE of θ in step 4, an estimate based on similar N -matching could be used as we used for α .

Acknowledgements

This research was financially supported by the Academy of Finland through the Finnish Centre of Excellence of Inverse Modeling and Imaging, the flagship program “Forest-Human-Machine Interplay - Building Resilience, Redefining Value Networks and Enabling Meaningful Experiences (UNITE, decision number 337655)” and research projects 295100, 310073, 321761 and 327211.

References

- Häbel, Henrike; Balazs, Andras; Myllymäki, Mari. 2021. Spatial analysis of airborne laser scanning point clouds for predicting forest structure. *Mathematical and Computational Forestry & Natural Resource Sciences* 13(1): 15-28.
- Kansanen, K., J. Vauhkonen, T. Lähivaara, and L. Mehtätalo. 2016. Stand density estimators based on individual tree detection and stochastic geometry. *Canadian Journal of Forest Research* 46(11):1359–1366.
- Kansanen, K., J. Vauhkonen, T. Lähivaara, A. Seppänen, M. Maltamo, and L. Mehtätalo. 2019. Estimating forest stand density and structure using Bayesian individual tree detection, stochastic geometry, and distribution matching. *ISPRS Journal of Photogrammetry and Remote Sensing* 152:66–78.
- Lähivaara, T., A. Seppänen, J. Kaipio, J. Vauhkonen, L. Korhonen, T. Tokola, and M. Maltamo. 2014. Bayesian approach to tree detection based on airborne laser scanning data. *IEEE Transactions on Geoscience and Remote Sensing* 52(5):2690–2699.
- Mehtätalo, L. 2006. Eliminating the effect of overlapping crowns from aerial inventory estimates. *Canadian Journal of Forest Research* 36(7):1649–1660.
- Mehtätalo, L. and Lappi, J. 2020. *Biometry for Forestry and Environmental Data: with examples in R*. New York: Chapman and Hall/CRC. 426 p.
- Penttinen, A. and Ylitalo, A-K. Deducing self-interaction in eye movement data using sequential spatial point processes. *Spatial Statistics* 17: 1-21.
- Yazigi, A., A. Penttinen, A.K. Ylitalo, M. Maltamo, P. Packalen, and L. Mehtätalo. 2021. Sequential spatial point process models for spatio-temporal point processes: A self-interactive model with application to forest tree data. arXiv preprint.

Table 1. The relative bias and RMSE of the four applied methods.

Method	bias, %	RMSE, %
uncorrected	-35	48.8
Mehtatalo	57	80.9
Kansanen	-3.5	20.0
New	3.5	22.5

3. Results and discussion

From among the variables proposed by Häbel et al (2021) the total number of distinct patches in the CHM at 80% height of the total height and integrated deviation of the F-function from the theoretical reference were the best predictors of both θ and α . The R-square was 16% in the model of θ and 10% in the model of α .

Table 1 shows the relative bias and RMSE of the

Crown shape and size of Scots pine affected by thinning?

N Saarinen¹, T. Yrttimaa¹, V. Kankare¹, V. Luoma², J. Pyörälä², S. Bianchi³, S. Huuskonen³, J. Hynynen³, M. Holopainen², J. Hyypä⁴, M. Vastaranta¹

¹School of Forest Sciences, University of Eastern Finland, P.O. Box 111, 80101 Joensuu, Finland
Email: {ninni.saarinen; tuomas.yrttimaa; ville.kankare; mikko.vastaranta}@uef.fi

²Department of Forest Sciences, University of Helsinki, P.O. Box 27, 00014 University of Helsinki, Finland
Email: {ville.luoma; jiri.pyorala; markus.holopainen}@helsinki.fi

³Natural Resources Institute Finland, Latokartanonkaari 9, 00790 Helsinki, Finland
Email: {simone.bianchi; saija.huuskonen; jari.hynynen}@luke.fi

⁴Department of Remote Sensing and Photogrammetry, Finnish Geospatial Research Institute, National Land Survey of Finland, Geodeetinrinne 2, FI-02430 Masala, Finland
Email: juha.hyypa@nls.fi

1. Introduction

Trees adapt to their growing conditions by regulating size of their parts and their relationships. For example, removal or death of adjacent trees increases the amount of light to the remaining trees and their crown can expand. Trees of different species require differing amount of growing space; for example, Scots pine (*Pinus sylvestris* L.) is more demanding for space than Norway spruce (*Picea abies* (H. Karst) L.) (Aaltonen 1925).

In dense forests, lower branches die due to the limited amount of light (Heikinheimo 1953, Flower-Ellis et al. 1976, Kellomäki 1980). Live-crown ratio (proportion of live crown from tree height) is used in assessing vitality of trees. Removal or death of trees enhances the light regime and photosynthesis for the remaining trees, and this is particularly evident in near the lowest limit of live crown where changes in the amount of light increases considerably more compared to the top of a tree.

There is also a relationship between tree size and growing conditions that can be assessed through the light regime. Removal or death of trees increases the light for various parts of and below crown of remaining trees. According to Oker-Blom & Kellomäki (1982), self-shading is greater for large trees compared to medium or small trees.

Thinning is aimed at improving growing conditions of remaining trees and maximize their economic value. Thinning decreases the shadowing leaf mass, increases the amount of light, and thus enhances the growth of the remaining trees (White 1980). Thinning intensity affects the number of removed trees, whereas thinning type defines what kind of trees are removed, and thus left to grow. Intermediate and suppressed as well as overgrown trees are removed with thinning from below, whereas dominant and overgrown trees are removed with thinning from below.

Although, forest growth and yield research have a long history in studying effects of forest management, measuring tree crown has mainly been limited to live-crown proportion that can easily be measured together with tree height. Terrestrial laser scanning (TLS) offers a means for characterizing individual trees with a detail (Calders et al. 2020, Liang et al. 2018).

Thus, the aim of the study was to investigate how crown size and shape of individual Scots pine trees generated from TLS data differed between thinning intensity and type. Furthermore, we studied how thinning affected crown size and shape of dominant trees (i.e., the 100 thickest trees per hectare) only.

2. Data and Methods

2.1 Study area and data acquisition

The study area is located in southern boreal forest zone in Finland and consists of three study sites with relatively flat terrain (elevation above sea level ~137 m±17 m) in mesic heath forest dominated by Scots pine. The study sites were established in 2005 and 2006 when nine rectangular sample plots (sized 1000-1200 m²) were placed on each study site (27 plots in total). At the same time, first in situ measurements were carried out and the plots were also thinned according to the experimental study design that included two levels of thinning intensity (i.e., moderate and intensive) and three thinning types (i.e., from below,

from above, and systematic) resulting in six different thinning treatments: moderate thinning from below (3 plots), moderate thinning from above (4 plots), moderate systematic thinning (5 plots), intensive thinning from below (3 plots), intensive thinning from above (5 plots), and intensive systematic thinning (5 plots).

One plot at each study site was left as a control plot where no thinning has been carried out since the establishment of the sites. Suppressed and co-dominant trees were removed with thinning from below, whereas dominant trees were mainly removed with thinning from above. Additionally, unsound and damaged trees (e.g., crooked, forked) were removed. With intensive thinning, the remaining basal area was ~50% lower compared to moderate thinning. Stem density per hectare varied between 1160 and 1390 before thinning and between 290 and 1030 after thinning (see more information on plot structure before and after thinning in Saarinen et al. 2020).

TLS data acquisition was carried out with Trimble TX5 3D laser scanner between September and October 2018. Eight scans were acquired from each plot, and they were co-registered into a single, aligned coordinate system with mean distance error of 2.9 ± 1.2 mm (more description in Saarinen et al. 2020).

Points originated from a crown of individual Scots pine trees with diameter at breast height varying between 7.6 cm and 36.4 cm were identified by utilizing a fully automatic method developed by Yrttimaa et al. (2019, 2020). The methodology includes point cloud normalization, tree segmentation, and point cloud classification. Points representing planar, vertical, and cylindrical surfaces were assumed to have originated from stem and rest of the tree-level points were classified as crown points.

Table 1. Crown attributes.

Attribute	Definition/calculation
Crown volume	Volume of the 3D convex hull
Surface area	Surface area of the 3D convex hull
Maximum diameter	Crown points were divided in height percentiles (i.e., slices) of 10% starting from the lowest part and their diameter was calculated using 2D convex hull -> maximum
Projection area	Area of the maximum crown diameter
Live crown base height	Height of the maximum crown diameter; Defined from the crown slices
Mean diameter	Mean diameter of the crown slices
Live-crown ratio	Proportion of live crown (i.e., length between live crown base height and tree height) from the tree height

2.2 Crown attributes and statistical analyses

Attributes characterizing tree crowns were generated from the classified point originated from individual tree crown. A 3D convex hull was fitted to envelope the crown points of each tree of which crown volume and surface area were derived (Table 1). Crown points were divided in slices based on height by utilizing 10% percentiles and a 2D convex hull was fitted to all these slices to obtain maximum and mean crown diameter. Crown projection area was defined at the height of the maximum crown diameter. Similarly, the height of the maximum crown diameter was defined as the live crown base height, which was used, together with tree height, to define live-crown ratio.

A nested- two-level linear mixed-effects model was utilized to find possible statistically significant differences in crown attributes between different thinning treatments (including the control plots). The analyses were carried out with i) all Scots pines within the sample plots (n=1919), and ii) with dominant trees only (n=290). Dominant trees from each sample plot were defined based on their diameter at breast height, in other words the trees representing the 100 thickest trees per hectare that would have been used for calculating top height.

3. Results and Discussion

When all Scots pine trees were considered, crown volume, projection area, maximum and mean diameter, live-crown ratio, and diameter at 10-80 crown height percentiles were statistically significantly larger ($p < 0.05$) due to intensive thinning from below compared with moderate thinning from below. Between moderate and intensive thinning from above, live crown base height, live-crown ratio, and diameter at 10-30 crown height percentiles increased significantly ($p < 0.05$). Crown volume, surface area, projection area, and maximum diameter increased when thinning from below was

compared with other thinning types, however, there was statistically significant difference ($p < 0.05$) only within intensive thinnings.

When only dominant trees were included in the analyses, crown volume, projection area, maximum diameter, and diameter of 10-70 crown height percentiles increased statistically significantly ($p < 0.05$) between moderate and intensive thinning from below. With thinning from above, only diameter of 10-20 crown percentile heights of the dominant trees increased statistically significantly between moderate and intensive thinning. Similarly to all Scots pine trees, crown volume and surface area of dominant trees were statistically significantly larger between thinning from below and other thinning types, but only within intensive thinnings.

The crown attributes generated here from TLS have been challenging to obtain with traditional means. Here, diameter of crown height percentiles, for example, that characterize crown shape has not been possible to measure before the utilizations of TLS. Only maximum diameter has been measured, when needed, with a measuring tape on the ground underneath a tree crown. Thus, it is challenging to assess the accuracy of the presented crown attributes based on TLS.

There are no studies on the effects of thinning on conifers but there is an increasing body of literature studying European beech (*Fagus sylvestris*) trees. Juchheim et al. (2017), for example, found that increasing thinning intensity increased crown surface area and crown length.

This study contributed to understanding how Scots pine trees adapt to their increased growing space due to management activities by investigating their crown shape and size.

4. Conclusions

Thinning intensity increased crown shape and size of individual Scots pine trees, whereas thinning type mainly increased crown size. The results were similar when the largest trees by their diameter at breast height (i.e., dominant trees) were considered. Thus, it can be concluded that thinning intensity increased both crown shape and size of Scots pine trees of different sizes.

Acknowledgements

The study was funded by the Academy of Finland (project numbers 315079, 345166, and 327861).

References

- Aaltonen VT, 1925, Metsikön itseharvenemisesta ja puiden kasvutilasta luonnonmetsissä, *Communicationes Ex Instituto Quaestionum Forestalium Finlandiae* 9: 1-17. [Ber der Selbstabscheidung un den Wuchsraum de Bäume in Naturbeständen]. In Finnish with German summary.
- Calders K, et al, 2020, Terrestrial laser scanning in forest ecology: Expanding the horizon, *Remote Sensing of Environment* 251: 112102.
- Flower-Ellis J, Albrektsson A, Olsson L, 1976, Structure and growth of some young Scots pine stands: (1) dimensional and numerical relationships. Swedish Conifer Project, *Technical Report* 3: 1-98.
- Heikinheimo O, 1953, Puun rungon luontaisesta karsitumisesta, *Communtiones Instituti Forestalis Fenniae* 41(5): 1-39. [On natural pruning of tree stems]. In Finnish with English summary.
- Juchheim, J., et al. 2017. How management intensity and neighborhood composition affect the structure of beech (*Fagus sylvatica* L.) trees. *Trees* 31:1723-1735.
- Kellomäki S, 1980, Growth dynamics of young Scots pine crowns, *Communicationes Instituti Forestalis Fenniae* 98(4): 1-50.
- Liang X, et al, 2018, International benchmarking of terrestrial laser scanning approaches for forest inventories, *ISPRS Journal of Photogrammetry and Remote Sensing* 144:137-179.
- Oker-Blom P, Kellomäki S, 1982, Metsikön tiheyden vaikutus puun latvuksen sisäiseen valoilmastoon ja oksien kuolemiseen – Teoreettinen tutkimus, *Folia Forestalia* 509: 1-14. [Effect of stand density on the within-crown light regime and dying-off of branches – Theoretical study]. In Finnish.
- Saarinen N, et al, 2020, Assessing the effects of thinning on stem growth allocation of individual Scots pine trees. *Forest Ecology and Management* 474: 118344.
- White J, 1980, Demographic factors in population of plants, In: Solbrig OT (Ed.), *Demography and Evaluation in Plant Populations*. Botanical Monographs 15. Los Angeles, USA, 21-48.
- Yrttimaa T, et al, 2019, Investigating the feasibility of multi-scan terrestrial laser scanning to characterize tree communities in southern boreal forests, *Remote Sensing* 11(12): 1423.
- Yrttimaa, T., et al. 2020. Multisensorial close-range sensing generates benefits for characterization of managed Scots pine (*Pinus sylvestris* L.) stands, *ISPRS International Journal of Geo-Information* 9(5): 309.

Using ICESat-2 to Characterize Coastal Ecosystems

Nathan Thomas^{1,2}, Lola Fatoyinbo², Avi Putri Pertiwi³, Dimosthenis Traganos³, David Lagomasino⁴, Dimitris Poursanidis⁵, Shalimar Moreno⁴, Isamar Cortes⁶

¹Earth System Science Interdisciplinary Center, University of Maryland College Park, MD 20740, USA

²NASA Goddard Space Flight Center, Greenbelt, MD 20771, USA

³German Aerospace Center (DLR), Berlin, Germany

⁴Coastal Studies Institute, East Carolina University, Wanchese, NC 27981, USA

⁵Foundation for Research and Technology, Institute of Applied and Computational Mathematics, The Remote Sensing Lab, Heraklion, Crete, Greece

⁶Montclair State University, Montclair, NJ 07043

Email: nathan.m.thomas@nasa.gov

1. Introduction

Coastal seascapes (seagrasses, mangroves, coral reefs, tidal flats) support the livelihoods of over 3 billion people in 100+ countries and billions in revenue; offer protection from extreme weather events; provide 25% of the oceanic carbon pool and support 25% of global biodiversity. Despite this, the extent of coastal benthic ecosystems, such as seagrasses, are poorly quantified (Macreadie et al. 2019). This is particularly pertinent in tropical and developing nations and so called “Big Ocean States” (or Small Island Nations) which do not have the financial capacity to conduct extensive bathymetric surveys but depend upon coastal resources, to sustain their economies (Burke et al. 2001). Furthermore, the distribution of mangrove forest height is well known, but is derived from often static and outdated elevation data, particularly at the global level. With the increased availability of global elevation data (eg. TanDEM-X) ICESat-2 lidar data provides a means for measuring and calibrating estimates of canopy height.

2. Methods

Our aim was to evaluate the ability of ICESat-2 to characterize ecosystem structure in coastal environments. We used ICESat-2 to retrieve estimates of i) mangrove forest canopy height and aboveground structure and ii) bathymetry in shallow water environments. This utilized currently available ICESat-2 ATL08 and ATL03 data.

2.1 Coastal Forest Structure

We used existing accurate elevation datasets to assess the performance of ICESat-2 to estimate mangrove canopy height. Specifically, in Everglades National Park, Florida, 5 m NASA GLiHT CHMs and DTMs were compared against ICESat-2 ATL08 canopy height and terrain height, respectively. GLiHT height was extracted for each ICESat-2 ATL08 segment, as well as dominant mangrove type using an existing species map. Regression analysis was used to measure the agreement between the two height estimates. Furthermore, species data was used to assess the impact of variable mangrove structure on the accuracy of the canopy and ground height estimations.

2.2 Benthic Surface Retrieval

ICESat-2 ATL03 geolocated photon data were used to target sub-aquatic surfaces and were used to train 3 Sentinel-2 SDB models in the Google Earth engine cloud computing environment. The models of Stumpf et al. (2003) (CBS), Lyzenga et al. (2006) (CBL) and a Support Vector Machine (SVM) were trialed in Bermuda, Biscayne Bay in Florida and Gulf of Chania in Crete. Sentinel-2 composites were generated, using the 20th percentile of the composite data cube to remove effects, such as glint and waves. Sub-aquatic surface depths were calibrated following Parrish et al. (2019) to account for the refraction of the photons at the water surface.

To validate these depth estimates we used a locally sourced NOAA bathymetric DEM, single beam sonar (SBS) data and independent ICESat-2 depths, dependent on availability at each location. The use of independent ICESat-2 data was used to demonstrate a wholly spaceborne approach for mapping nearshore coastal bathymetry.

3. Results

3.1. Coastal Forest Structure

We measured a strong agreement ($r^2:0.94$; Figure 1) between ICESat-2 ATL08 and GLiHT canopy height at everglades National Park, Florida. Mangrove trees were correctly characterized as taller mangrove types than scrub and shrub type mangroves. Less agreement was found between terrain height estimates, with mangrove types with increased aboveground structural complexity driving this disagreement.

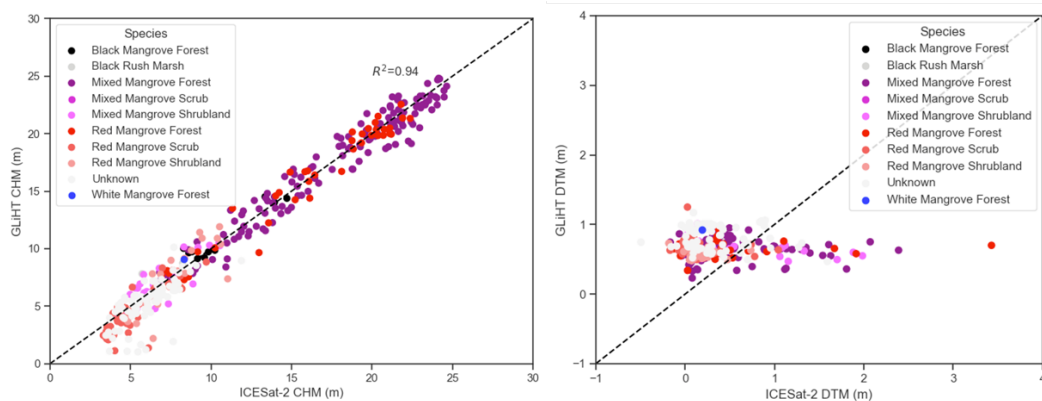


Figure 1. Left: Strong agreement between ICESat-2 ATL08 and NASA GLiHT CHMs, with forest type mangroves proving to be taller than shrub and scrub types. Right: Disagreement between ICESat-2 and GLiHT terrain heights, with mangrove forest types driving greater uncertainty.

3.1. Benthic Surface Retrieval

ICESat-2 ATL03 geolocated photon data was successfully used to train 3 Sentinel-2 SDB models at each of the study site locations, improving the spatial resolution (10 m) and detail over openly existing available data (Figure 2). The CBL method produced the most reliable SDB estimates at all sites. RMSE values of 2.62 m, 0.83 m, and 2.19 m, and MAE of 2 m, 0.65 m, and 2.02 m were calculated for Bermuda, Biscayne Bay, and Crete, respectively. The RMSEs of the CBL were approximately 10% of the maximum depth for the Bermuda (26 m) and Crete (22 m) models, but 17% for the Biscayne Bay model where the maximum depth was much lower (5 m). The R^2 of the models for Bermuda, Biscayne Bay, and Crete were 0.68, 0.79, and 0.83, respectively. The reference and the modeled depths of Bermuda were in good agreement between the depths of 11-17 m, whereas for the shallower Biscayne Bay it was between the depths of 1.2-3 m.

3.1. Discussion and Conclusion

In this study, we have demonstrated that ICESat-2 is able to accurately characterize mangrove forest canopy height in a mixed species mangrove forest in Florida, validating its wider use in studies of mangrove structure and its potential use in biomass estimation. However, terrain height was found to be more variable, with mangrove type driving increased disagreement between the two measurements. This is interpreted to be due to the increased sub-canopy complexity of taller mangrove trees which may lead to false ground detections.

We also demonstrate the unique fusion of openly available ICESat-2 and Sentinel-2 data for retrieving openly available shallow water bathymetry DEMs, from coastline to island nation scales. We developed adaptive bathymetry estimation methods derived solely from space-borne observations over coastal waters in Bermuda, Biscayne Bay, and Crete at high-resolution and with low error. The high resolution of Sentinel-2 and ICESat-2 data allows us to map benthic variability in detail, improving upon freely available bathymetry maps. Our demonstrated method could enable the development of a global

map of coastal submerged ecosystems, which continues to be a critical need of the Blue Economy community. This would be the foundation of global habitat accounting for currently poorly mapped sub-aquatic ecosystems as seabed morphology is a usual and helpful parameter in aiding underwater coastal habitat monitoring.

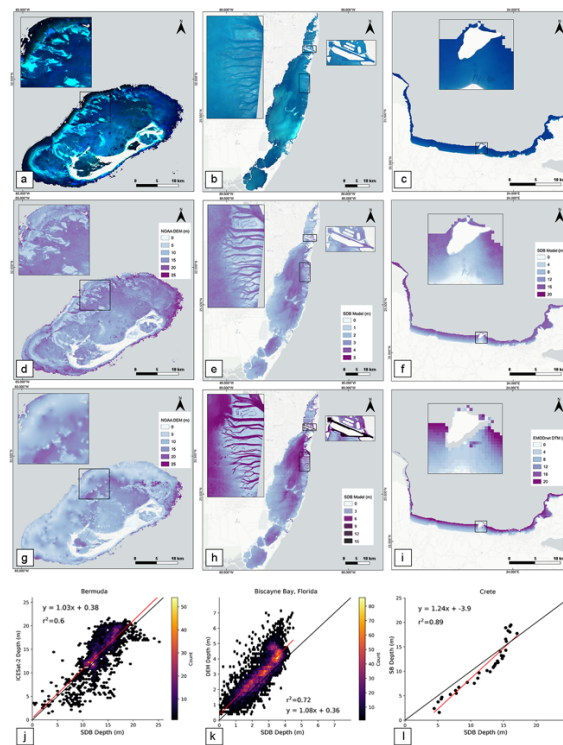


Figure 2. (a, b, c) Sentinel-2 RGB synthesis. (a) Bermuda: 53 L2A Surface Reflectance tiles, 597 km² (March 28, 2017 – April 20, 2020); (b) Biscayne Bay: 583 L1C Top-Of-Atmosphere tiles, 689 km² (January 1, 2015 – December 31, 2019); (c) Crete: L1C 403L1C Top-Of-Atmosphere, 61 km² (January 1, 2015 – December 31, 2019). (d, e, f) CBL Bathymetry SDB at Bermuda, Biscayne Bay and Crete. (g, h, i) NOAA DEM at Bermuda and Biscayne Bay and EMODnet at Crete, j, k, l) SDB-ICESat-2 depth comparison at Bermuda, Biscayne Bay and Crete.

Acknowledgements

This research was funded by NASA Studies with ICESat-2 Program (Grant No. 80NSSC20K0968). A. Pertiwi and D. Traganos acknowledge funding for their efforts from the German Aerospace Center (DLR) through the Global Seagrass Watch project. Dimitris Poursanidis acknowledges terra Solutions marine environment research for the support in bathymetry data collection, funded by MEDPAN.

References

- Burke, L. M. and World Resources Institute. (2001) *Pilot analysis of global ecosystems : coastal ecosystems*. World Resources Institute. Available at: <https://www.wri.org/publication/pilot-analysis-global-ecosystems-coastal-ecosystems> (Accessed: 6 October 2019)
- Lyzenga, D.R. et al. 2006. Multispectral bathymetry using a simple physically based algorithm. *IEEE Transactions on Geoscience and Remote Sensing*, 44, pp. 2251-2259.
- Macreadie, P. I. et al. (2019) “The future of Blue Carbon science”, *Nature Communications*, Nature Publishing Group, 10 (1), p. 3998
- Parrish, C. E. et al. (2019) “Validation of ICESat-2 ATLAS Bathymetry and Analysis of ATLAS’s Bathymetric Mapping Performance”, *Remote Sensing*, MDPI, 11 (14), p. 1634
- Stumpf, R. P. et al. (2003). Determination of water depth with high-resolution satellite imagery over variable bottom types. *Limnology & Oceanography*, 48, 547–556.

Estimating Surface Fuel Density from TLS and ALS: A Two-Tiered Approach that Accounts for Sampling Scale

A. T. Hudak¹, B. C. Bright¹, E. Rowell², K. Robertson², S. Pokswinski², K. Hiers², S. Prichard³,
H. Nowell⁴, C. Holmes⁴, E. M. Gargulinski⁵, A. J. Soja⁵

¹USDA Forest Service, Rocky Mountain Research Station, 1221 South Main St., Moscow, ID 83843
Email: andrew.hudak@usda.gov, benjamin.c.bright@usda.gov

²Tall Timbers Research Station & Land Conservancy, 13093 Henry Beadel Drive, Tallahassee, FL 32312
Email: erowell@talltimbers.org, krobertson@talltimbers.org, spokswinski@talltimbers.org, jkhiers@talltimbers.org

³University of Washington, School of Environmental and Forest Sciences, Anderson Hall, Box 352100, Seattle, WA 98195-2100
Email: sprich@uw.edu

⁴Florida State University, Dept. of Earth, Ocean, and Atmospheric Science, 1011 Academic Way, Tallahassee, FL 32306-4520,
Email: hak07@my.fsu.edu, cdholmes@fsu.edu

⁵NASA Langley Research Center, 21 Langley Boulevard, Mail Stop 420, Hampton, VA 23681-2199,
Email: emily.m.gargulinski@nasa.gov, amber.j.soja@nasa.gov

1. Introduction

Terrestrial Laser Scanning (TLS) and Airborne Laser Scanning (ALS) collect 3D point cloud data that have been related to destructive harvest plot measures of surface fuel densities using regression models (Hudak et al. 2016, Rowell et al. 2020). Higher resolution makes TLS data well suited for characterizing surface fuel components at plot scale, whereas synoptic coverage makes ALS data well suited for surface fuel density mapping at landscape scale. We tested a two-tiered modelling approach, where surface fuel density was estimated with TLS metrics in large plots; these estimates were in turn used to train a second model to map fuel density from ALS metrics across an ~1000 ha area in the 102,716 ha Blackwater River State Forest (BRSF) in the Florida panhandle, USA. There, 362 ha was burned on 30 August 2019, in coordination with the NOAA/NASA Fire Influence on Regional to Global Environments and Air Quality (FIREX-AQ) campaign to measure smoke emissions from a DC-8 aircraft that flew multiple transects through the smoke plume. Our larger goal for this paper and in support of FIREX-AQ was to accurately characterize fuels on the ground, to help constrain the two largest sources of uncertainty in emissions estimates: fuel load and fuel consumption. This analysis focused on fuel load.

2. Methods

TLS data was collected across six large plots ranging in size from 39-351.5 m² that were comprised primarily of three surface fuel components: shrubs, wiregrass, and litter. Bulk densities of these components were measured in 3D destructive harvest plots, following the methods of Hawley et al. (2018). These component fuel density estimates were used as the response variables to predict fuel densities from height, surface area, volume, and porosity metrics derived from TLS, following Rowell et al. (2020). In turn, these TLS estimates were used as the response variables to predict component fuel densities from ALS-derived canopy height and density metrics, per Hudak et al. (2016). The predictive ALS models were subsequently applied to the same selected ALS metrics to generate surface fuel density maps of each fuel component. The mapped surface fuel estimates were subsequently adjusted upwards in proportion to overstory canopy cover to correct for overstory occlusion of the ALS signal (Hudak et al. 2016). Multiple linear regression was used for all models, and only two variables were selected per model due to the small sample size of only six plots. Total fuel densities were calculated as the sum of the shrub, grass, and litter fuel density estimates at all three levels (i.e., field measures, TLS estimates, and ALS estimates).

3. Results and Discussion

TLS and ALS metrics selected as predictors in the models are shown in Table 1. Although not all predictors were significant, the models predicting shrub, grass, and litter fuel densities were all

significant, for both TLS (Figure 1) and ALS (Figure 2). Based on the relatively low RMSE for the models at each step, the two-tiered approach appears to have worked well for mapping densities of surface fuel components at the BRSF burn, despite having only six sample plots. We believe that the large size of the six training plots was highly conducive to both TLS and ALS characterization, as evidenced by the high Adj. R^2 statistics (Figure 2).

Table 1. Linear regression models predicting shrub, grass, and litter fuel density (g/m^3) from A) TLS and B) ALS metrics. Models were limited to two predictors given that there were only six field plots.

Sensor	Fuel Component	Selected Metric	Estimate	Std. Error	t value	Pr(> t)	Significance
A) TLS							
	Shrub	(Intercept)	20.8800	6.7640	3.087	0.00314	**
		Surface area sum	1.04E-05	3.02E-06	3.456	0.00105	**
		Porosity mean	-21.0300	6.8290	-3.079	0.00321	**
	Grass	(Intercept)	-5.9570	5.0890	-1.171	0.2523	
		Surface area sum	5.73E-06	1.22E-05	0.472	0.6411	
		Vertical plant area density	0.3183	0.1170	2.72	0.0115	*
	Litter	(Intercept)	11.7570	57.7820	0.203	0.842	
		Porosity standard deviation	365.0640	205.9290	1.773	0.102	
		Horizontal plant area density	2.9720	2.1390	1.389	0.19	
B) ALS							
	Shrub	(Intercept)	127.2032	21.7838	5.839	0.01001	*
		Understory height 90 th percentile	-164.5434	27.7899	-5.921	0.00962	**
		Understory density, 0-15 cm	1.5737	0.5817	2.705	0.07344	.
	Grass	(Intercept)	200.1723	6.1741	32.421	6.45E-05	***
		Understory density, 15-50 cm	-5.7682	0.3455	-16.695	0.000468	***
		Canopy skewness	-10.4343	1.1893	-8.773	0.003119	**
	Litter	(Intercept)	440.8075	17.3401	25.421	0.000133	***
		Understory density, 15-50 cm	-7.8391	1.1797	-6.645	0.006945	**
		Canopy density, 0-15 cm	-1.9054	0.9672	-1.97	0.143444	

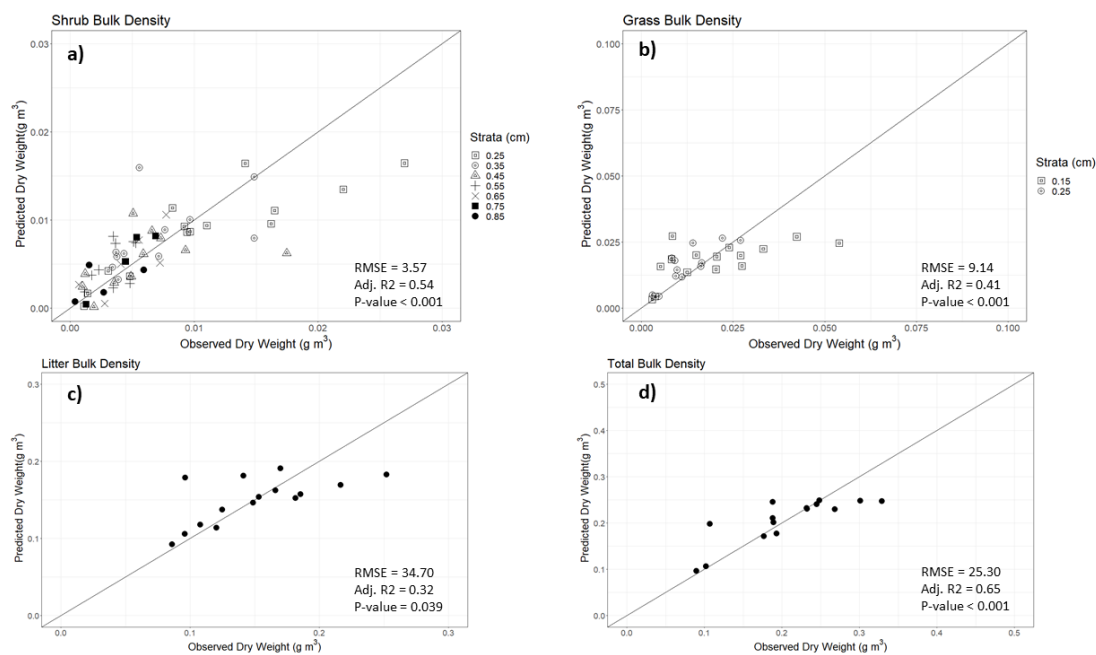


Figure 1: Linear regression models predicting destructive harvest plot measurements of a) shrub, b) grass, and c) litter fuel density (g/m^3) from two TLS metrics (Table 1a), and d) total surface fuel density, calculated as the sum of the shrub, grass, and litter components. Plot symbols in a) and b) legends indicate the midpoints of 10 cm interval height strata above the ground.

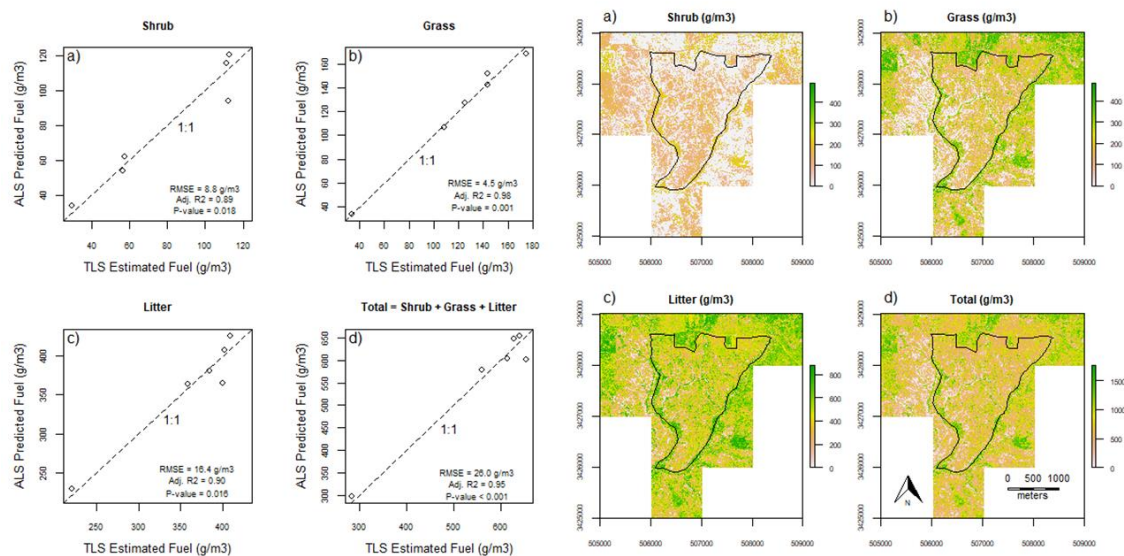


Figure 2: At left are linear regression models (left) predicting TLS estimates of a) shrub, b) grass, and c) litter fuel density (g/m³) from two ALS metrics (Table 1b), and d) total surface fuel density, calculated as the sum of the shrub, grass, and litter components. At right are the corresponding maps, with the planned burn perimeter overlaid in black.

4. Conclusion and Ongoing Work

These ALS-derived surface fuel density maps, trained with TLS data that serves to bridge the scaling gap between ALS and locally collected destructive harvest plot datasets, provide more refined estimates of surface fuel component densities than can be estimated by any other current method. We are currently validating these maps with independent estimates of fuel loads and consumption collected pre- and post-fire at 25 paired sample plots within the burn area. These data will be used to assess biases and constrain the uncertainties in estimating smoke emissions measured with instruments on board the DC-8. Lessons learned at this BRSF burn, which was well characterized from both a fuels and emissions standpoint, will help guide analyses on other FIREX-AQ fires sampled in 2019.

Acknowledgements

Funding was provided by NASA FIRECHEM Award 80NSSC18K0685, JFSP FASMEE Award 15-S-01-01, and DOD SERDP Award RC19-1064.

References

- Hawley CM, Loudermilk EL, Rowell EM and Pokswinski S, 2018, A novel approach to fuel biomass sampling for 3D fuel characterization. *MethodsX*, 5:1597-1604.
- Hudak AT, Dickinson MB, Bright BC, Kremens RL, Loudermilk EL, O'Brien JJ, Hornsby B and Ottmar RD, 2016, Measurements relating fire radiative energy density and surface fuel consumption—RxCADRE 2011 and 2012. *International Journal of Wildland Fire*, 25:25-37.
- Rowell E, Loudermilk EL, Hawley C, Pokswinski S, Seielstad C, Queen L, O'Brien JJ, Hudak AT, Goodrick S and Hiers JK, 2020, Coupling terrestrial laser scanning with 3D fuel biomass sampling for advancing wildland fuels characterization. *Forest Ecology and Management*, 462:117945.

Estimation of nature conservation value using airborne laser scanning data by deadwood recognition

L. Huo¹, J. Strengbom¹, E. Lindberg¹

¹ Swedish University of Agriculture Sciences, Sweden
Email: langning.huo@slu.se, joachim.strengbom@slu.se, eva.lindberg@slu.se

1. Introduction

Planning of forest management operations in boreal forests requires assessment of the biodiversity potential of the forest stands to determine if they can be harvested or should be set aside due to high conservation values, and to identify patches with high conservation values for retention of biodiversity. The latter includes the preservation of deadwood and trees with high conservation values, often of uncommon species (Gustafsson et al. 2020). There is currently no way to acquire this information automatically and objectively for large areas.

Information relevant for habitat studies that can be derived from airborne laser scanning (ALS) data includes canopy openness and foliage height diversity as well as the height and species of individual trees (Müller and Vierling 2014). Dense ALS data have the potential to provide information about structures in the forest relevant for biodiversity such as standing and downed deadwood and trees with high conservation values (i.e., biodiversity indicators). The full 3D representation of the forest from laser scanning data provides insights into ecologically relevant features of the forest (Onojeghuo and Onojeghuo 2017).

The amount of deadwood is important for the maintenance of biodiversity since hundreds of Fennoscandian forest-dwelling species depend on deadwood (ArtDatabanken 2020). Deadwood has been the focus of many studies of retention forestry (Gustafsson et al. 2020). Downed deadwood has been detected from ALS data with 3D reconstruction methods (Lindberg et al. 2013; Mücke et al. 2013) as well as with statistical methods based on the canopy structure (Tanhuanpaa et al. 2015).

This study presents a new method to detect downed deadwood from dense ALS data. The results from the method are compared with biodiversity indicators that have been assessed in the field. The method for detecting dead wood is planned to be a part of a processing chain to estimate the amount of structures relevant for biodiversity that can be used for creating maps of biodiversity indicators for laser-scanned forest stands to determine if a forest stand should be harvested or set aside for conservation and to guide retention in the forest stand in connection to forest management operations.

2. Data and Methods

2.1 Data

The study area Siljansfors is located in mid-Sweden (Lat. 60.9° N, Long. 14.3° E). Most of the area is covered with managed hemi-boreal forest. The most common tree species are Scots pine (*Pinus sylvestris*), Norway spruce (*Picea abies*), and birch (*Betula spp.*).

During the summer of 2019, a field inventory was done to assess the forest biodiversity potential in 19 forest stands in the study area. The inventory was done in 1 ha field plots according to the methodology developed by Skogsbiologerna AB (Drakenberg and Lindhe 2001). The assessment is based on a field form with eighty questions in different categories: site, dynamics, habitats, trees, structure and deadwood. The scores from the questions are then combined into site score and stand score, and the total biodiversity potential score is calculated as the sum of them for each field plot.

ALS data were collected on June 28, 2019, with a Riegl VQ 1560i-DW (Riegl, 2020) scanner at 800 m above the ground. The scanner records two channels (CH): CH1 with 532 nm (Green) and CH2 with 1064 nm (near infrared (NIR)). The average density of first returns was 26.5 m⁻².

2.2 Methods

Downed deadwood trunks were detected using a template matching algorithm. The steps were as follows.

Step 1. Rasterization. Point clouds were sliced into [0.2, 0.5], [0.4 – 0.7], [0.6 – 0.9] and [0.2 – 1.0] m height intervals, and rasterized with 0.25 m resolution.

Step 2. Creation of templates. Linear filters with 0.25 m resolution were designed with 6 m length and 0.25 m or 0.50 m width. The filters have $0 - \pi$ horizontal angle with 0.01π intervals (Denoted as directions of templates, examples in Figure 1).

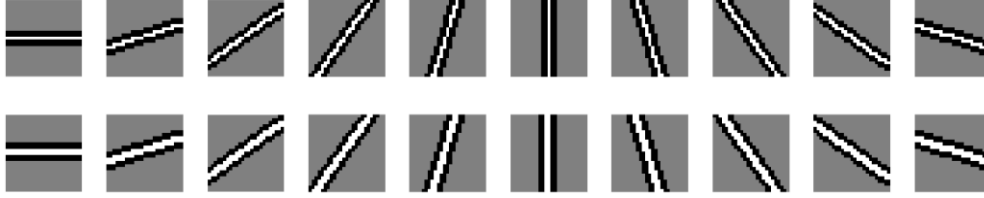


Figure 1. Examples of the linear filters (templates). The templates have 0.25 m width (first line) and 0.50 m width (second line). The pixel values are 1, -1, and 0 for the white, black, and grey pixels.

Step 3. Template matching. The rasters of the sliced point clouds were convoluted using the templates. After the convolution, all the pixels with values larger than Th were marked as potential positions (denoted as *Set A*) of the deadwood, and the directions of the templates were recorded for the next step (*Set A* $\{(x, y, \alpha)\}$, where x and y were the relative coordination and α was the direction of the templates which resulted in a convoluted pixel value larger than Th). Th was set to 0.4 times the length \times width (24×1 or 2 pixel) of the templates.

Step 4. Determination of the deadwood positions. After Step 3, *Set A* included the positions from the downed deadwood (denoted as *Set A1*), and other linear objects on the ground such as bushes (*Set A2*). We observed that *Set A1* usually contained positions with the same x and y and similar α , while *Set A2* usually contained isolated positions. We set a standard to separate *Set A2* from *Set A1*, e.g. the isolated positions within 1 m radius circular range with α differences no larger than 0.02π . Then we merged elements in *Set A1* which belong to the same deadwood trunk. We used the Mean Shift Clustering algorithm on *Set A1*, which clustered the elements with similar x , y , and α . The average x , y of each cluster were determined as the positions of the deadwood.

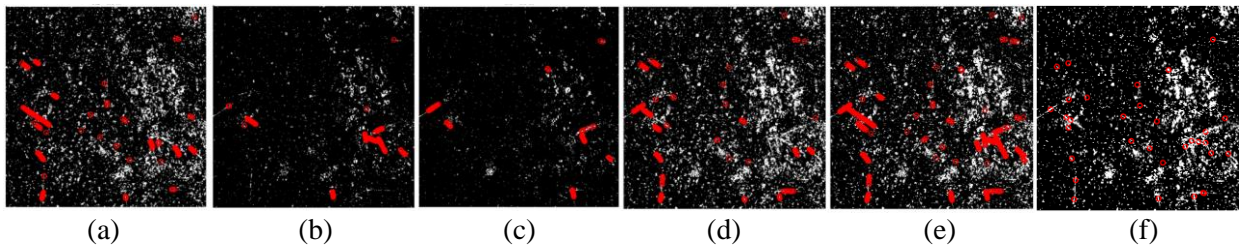


Figure 2. Process of detecting downed dead wood. (a - d) Detection from rasters of [0.2, 0.5], [0.4 – 0.7], [0.6 – 0.9] and [0.2 – 1.0] height intervals. (e) The potential positions from all rasters (*Set A*). (f) Final positions of the dead wood.

3. Results and discussions

Among the 19 plots, 228 deadwood trunks were recorded from the field measurement, with 219 trunks detected by the algorithm. The detection yielded 1.55 RMSE (12.9%) on estimating the number of deadwood trunks, with underestimation for the plots with large numbers of deadwood trunks (Figure (a)).

The number of deadwood trunks was used to classify plots with high and low conservation values. Based on the field observation, a threshold of 8 trunks was used for the classification, e.g. plots with ≥ 8 deadwood trunks were classified as high conservation value plots ($CV \geq 15$), and plots with < 8 deadwood trunks were classified as low conservation value plots ($CV < 15$). Based on the criteria, six out of 19 plots in the study area have high conservation value. By using the detected number of deadwood trunks from laser data, seven plots were classified as high conservation value. The overall classification accuracy was 0.89 (Table 1), and the Kappa coefficient was 0.78.

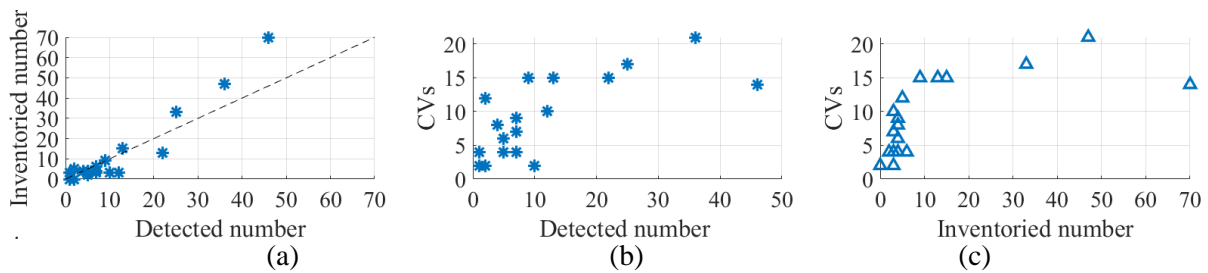


Figure 3. (a) Inventoried and detected number of deadwood trunks. (b) Detected number of deadwood trunks from each plot and the CVs. (c) Inventoried number of deadwood trunks from each plot and the CVs

Table 1. The classification accuracy of estimation of the conservation values.

		Actual class			User's accuracy
		Low CV (<15)	High CV (≥ 15)	Total	
Predicted class	Low CV (<15)	11	0	11	1.00
	High CV (≥ 15)	2	6	8	0.75
	Total	13	6		Overall accuracy
Producer's accuracy		0.85	1.00		0.89

4. Conclusions

This study used a template matching method to detect downed dead wood from ALS data. It obtained a 1.55 RMSE (12.9%) on estimating the number of deadwood trunks for each plot. The results illustrated the potential of ALS data for deadwood recognition. The number of deadwood trunks was used as a feature to classify forest stands with high and low conservation values, with 0.94 overall classification accuracy and 0.88 kappa coefficient. We conclude that the amount of deadwood is a crucial indicator of habitat quality in boreal forests, and ALS data is an efficient tool to estimate the conservation value. The proposed method could be used to map the forest conservation value in large areas in the future.

Acknowledgements

This research was financed by the Swedish Foundation for Strategic Environmental Research with the research program Mistra Digital Forest. The ALS data and the field inventory were financed by the forest company Stora Enso and by the Swedish University of Agricultural Sciences.

References

- ArtDatabanken, S. (2020). Rödlistade arter i Sverige 2020. In. Uppsala, Sweden: SLU
- Drakenberg, B., & Lindhe, A. (2001). Field Assessment of Forest Ecological Values - a structures and substrates approach at the stand level. In (p. 5). Stockholm, Sweden: Skogsbiologerna AB
- Gustafsson, L., Hannerz, M., Koivula, M., Shorohova, E., Vanha-Majamaa, I., & Weslien, J. (2020). Research on retention forestry in Northern Europe. *Ecological Processes*, 9, 13
- Lindberg, E., Hollaus, M., Mücke, W., & Pfeifer, N. (2013). Detection of Lying Tree Stems from Airborne Laser Scanning Data Using a Line Template Matching Algorithm. In, *International Archives of the Photogrammetry, Remote Sensing and Spatial Information Sciences* (pp. 169-174). Antalya, Turkey: ISPRS - International Society for Photogrammetry and Remote Sensing
- Mücke, W., Deák, B., Schroiff, A., Hollaus, M., & Pfeifer, N. (2013). Detection of fallen trees in forested areas using small footprint airborne laser scanning data. *Canadian Journal of Remote Sensing*, 39, S1-S9
- Müller, J., & Vierling, K. (2014). Assessing Biodiversity by Airborne Laser Scanning. In M. Maltamo, E. Naesset, & J. Vauhkonen (Eds.), *Forestry Applications of Airborne Laser Scanning: Concepts and Case Studies* (pp. 357-374). Dordrecht, Netherlands: Springer
- Onojeghuo, A.O., & Onojeghuo, A.R. (2017). Object-based habitat mapping using very high spatial resolution multispectral and hyperspectral imagery with LiDAR data. *International Journal of Applied Earth Observation and Geoinformation*, 59, 79-91
- Tanhuanaa, T., Kankare, V., Vastaranta, M., Saarinen, N., & Holopainen, M. (2015). Monitoring downed coarse woody debris through appearance of canopy gaps in urban boreal forests with bitemporal ALS data. *Urban Forestry & Urban Greening*, 14, 835-843

Explore the structural diversity of forest edges using spaceborne lidar

Mengxi Wang^{1,2}; Kim Calders²; Hans Verbeeck²; Fricke Van Coillie¹; Pieter De Frenne³; Camille Meeussen³; John Armston⁴; Atticus Stovall^{4,5}

¹Remote Sensing & Spatial Analysis laboratory, Department of Environment, Faculty of Bioscience Engineering, Ghent University, Belgium;

²Computational & Applied Vegetation Ecology Laboratory, Department of Environment, Faculty of Bioscience Engineering, Ghent University, Belgium;

³Forest & Nature Lab, Department of Environment, Faculty of Bioscience Engineering, Ghent University

⁴Department of Geographical Sciences, University of Maryland, College Park, MD, USA

⁵Biospheric Sciences Laboratory, NASA Goddard Space Flight Center, Greenbelt, MD, USA

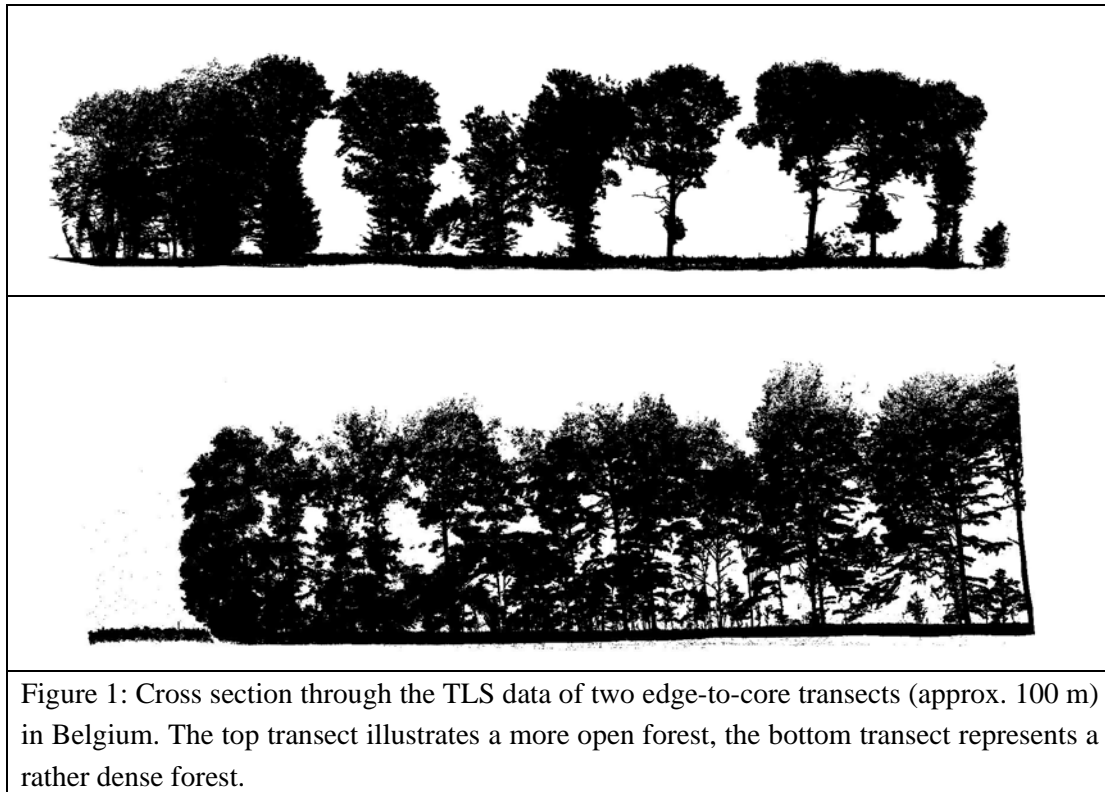
1. Introduction

Forest edges represent approximately 20% of the global forested area, and the total area of forest edges continues to increase due to forest fragmentation (Haddad et al., 2015). Forest edges have different communities than forest interiors and provide suitable habitats for a variety of animals (Honnay et al., 2002). Forest edges and the forest core are structurally different, yet there is relatively limited description of forest edge structural variation and its drivers, especially at large spatial scales (Meeussen et al., 2020). Quantifying structural variation using traditional inventory techniques, such as measuring the variation of tree height and canopy cover, are laborious, time consuming and hard to scale up to larger areas. Meeussen et al. (2020) used terrestrial laser scanning (TLS) to study structural variation of forest edges across Europe, this was the first study on forest edge structure at the continental scale. Representative sampling of forest edges across forest types and regions using TLS alone remains a challenge, therefore extending the sampling of forest edge types and locations could improve our knowledge on forest edge structure. NASA's Global Ecosystem Dynamics Investigation (GEDI) is designed for the measurement of forest structure and has the potential to address this challenge (e.g., Spracklen, B., 2021). GEDI produces high resolution laser ranging observations of the vertical structure of the Earth tropical and temperate forests, with elevation and height metrics available from the GEDI L2A data product and canopy cover and vertical profile metrics from the GEDI L2B data product (Dubayah et al., 2020).

2. Objectives

In this work, we investigate structural variation of forest edges in different regions of Europe, determining whether this variation is related to different regions and how structure changes from the forest edge to the forest core. We use 60 edge-to-core transects that are distributed across 9 different countries and regions in Europe. They were designed along latitudinal, elevational and management gradients across Europe and TLS data was collected in each transect in 2018. We used a RIEGL VZ-400 instrument (see Figure 1 for a cross-section through two transects). In these 60 transects, 36 of them are covered by GEDI. We calculated GEDI-

related structural metrics such as plant area index (PAI), fraction of vegetation cover (FVC) and foliage height diversity (FHD). We will subsequently use our detailed TLS data to validate equivalent metrics derived from GEDI data. Our results will show the potential of exploring the structural variation of forest edges from space, and highlights the potential of monitoring structural diversity gradients at a continental scale.



Acknowledgements

Mengxi Wang was funded by the Chinese Scholarship Council (CSC) personal programme. We thank Tom Verhelst and Barbara D’hont for their help with TLS fieldwork. PDF and CV received funding from the European Research Council (ERC) under the European Union’s Horizon 2020 research and innovation programme (ERC Starting Grant FORMICA 757833).

Reference

- Dubayah, R. O., Blair, J. B., Goetz, S. J., Fatoyinbo, L., Hansen, M., Healey, S., Hofton, M., Hurtt, G., Kellner, J., Luthcke, S., Armston, J., Tang, H., Duncanson, L., Hancock, S., Jantz, P., Marselis, S., Patterson, P. L., Qi, W., & Silva, C. (2020). The Global Ecosystem Dynamics Investigation: High-resolution laser ranging of the Earth’s forests and topography. *Egyptian Journal of Remote Sensing and Space Sciences*, 1, 100002.
- Haddad, N.M. et al. (2015). Habitat fragmentation and its lasting impact on Earth’s ecosystems. *Sci. Adv.* 1, e1500052.
- Honnay, O. et al. (2002). Permeability of ancient forest edges for weedy plant species invasion. *For. Ecol. Manage.* 161, 109–122

Meeussen, C. et al. (2020) Structural variation of forest edges across Europe. *For. Ecol. Manage.* 462, 117929.

Spracklen, B. (2021) Determination of Structural Characteristics of Old-Growth Forest in Ukraine Using Spaceborne Lidar. *Remote Sens.* 2021, 13(7), 1233

The Potential of ALS Data for Habitat Classification in Forest Landscapes – First Results

A. Iglseder¹, N. Pfeifer¹, M. Hollaus¹

¹Department of Geodesy and Geoinformation, TU Wien, 1040 Vienna, Austria
Email: {anna.iglseder, norbert.pfeifer, markus.hollaus}@geo.tuwien.ac.at

1. Introduction

The preservation and protection as well as the improvement of the environment are stated as essential objectives of general interest. This includes the conservation of natural habitats of wild fauna and flora (European Commission 1992). The European Union's Habitats Directive (HD) and the Natura 2000 network provide a framework for classification and monitoring of different habitat types (Requena-Mullor et al. 2018). By date, these HD classifications are mainly expert-based investigations in the field. Within the presented study, a data-driven approach based on airborne laser scanning (ALS) data for HD classification in forest landscapes is tested. The aim is to reproduce the latest available HD classification for two study sites in the municipality of Vienna using supervised classification. Habitat types are basically defined by the occurring vegetation, terrain and soil characteristics. Previous studies show the potential of airborne ALS data for deriving forest structure (Hollaus et al. 2006, Lindberg et al. 2012) and species classification (Hollaus et al. 2009, Koenig and Höfle 2016). Furthermore, the suitability of ALS data for detailed terrain modelling, in particular in forested areas, is shown by Kraus and Pfeifer (1998). ALS data for different approaches of habitat classification or biodiversity monitoring are used e.g. in Räsänen et al. (2014), Coops et al. (2016) and Guo et al. (2017). For the HD classification, different features describing terrain, location and vegetation structure are derived from ALS point cloud data and rasterized to a 1 m grid. The features are examined with regard to their discriminant power for different HD classes and usability for random forest classification on 1 m pixel scale.

2. Data and Methods

2.1 Habitats Directive Classification

The HD classification scheme differentiates nine major habitat groups with a total of 229 habitat types (European Commission 2006). Within the two study sites, 22 different habitat out of five major habitat groups occur. The mapping of the HD classification of the green areas within the municipality of Vienna is provided as open data (Stadt Wien – <https://data.wien.gv.at>, 2020). After excluding ten habitat types due to low incidence, twelve habitat types out of three major habitat groups (freshwater habitats, natural and semi-natural grassland formations and forests) are considered. For this study, the habitat types were further limited to forests. Table 1 shows a summary and description of the considered habitat types.

2.2 Study Sites

Two different areas representing the two main green landscapes in Vienna are chosen for investigation: (A) hilly, primary forested areas in the west of Vienna and (B) river meadows and riparian forests along the Danube River. Study site A, located in the Vienna Woods and part of the Wienerwald Biosphere Reserve, covers 21.8 km². The altitude of study site A varies between 214 m and 515 m a.s.l., is hilly and cut by three major valleys. Study site B is located in the southeast of Vienna, along the riparian forests of the Danube River. The 10.3 km² of study site B cover the Viennese part of the Donau-Auen National Park. The mainly flat area stretches from 147 m to 163 m a.s.l. and shows incidences of a former dominant and now partly regulated braided river system and a floodplain landscape. The detailed distribution of the habitat types within the two study sites is shown in Table 1.

Table 1. HD types occurring in the study sites within the municipality of Vienna, according to European Commission (2006). The sign * prior to the name indicates priority habitat types.

Habitat group	NATURA 2000 Code	Covering study site	Description
Forests	9110	A (1%)	Luzulo-Fagetum beech forests
	9130	A (31.3%)	Asperulo-Fagetum beech forests
	9170	A (62.7%)	Galio-Carpinetum oak-hornbeam forests
	9180	A (0.8%)	* Tilio-Acerion forests of slopes, screes and ravines
	91E0	A (2.4%)	* Alluvial forests with <i>Alnus glutinosa</i> and <i>Fraxinus excelsior</i> (<i>Alno-Padion</i> , <i>Alnion incanae</i> , <i>Salicion albae</i>)
		B (10%)	Riparian mixed forests of <i>Quercus robur</i> , <i>Ulmus laevis</i> and <i>Ulmus minor</i> , <i>Fraxinus excelsior</i> or <i>Fraxinus angustifolia</i> , along the great rivers (<i>Ulmion minoris</i>)
	91F0	B (90%)	
91G0	A (1.8%)	*Pannonic woods with <i>Quercus petraea</i> and <i>Carpinus betulus</i>	

2.3 ALS data and feature extraction

The ALS data for the whole municipality of Vienna was acquired between November 9th and November 24th 2015 under leaf-off conditions. Two different sensors providing full waveform analysis were used: a Riegl LMS-Q680i and a Riegl LMS-Q560 (RIEGL Laser Measurement Systems, Horn, Austria). The acquisition resulted in a point density of > 16 echoes/m² for 97% of the whole city area.

The ALS features derived from the point cloud are grouped in terrain features, structure features, insolation features and full waveform features. In total, 22 features were derived on a 1 m grid.

2.4 Exploratory statistics and classification

Primarily, the distributions of the feature values grouped by the different habitat types were analysed for each study site. For the assessment of the feature performance for classification, a random forest model with recursive feature elimination was trained and a 10 fold spatial cross validation (CV) was performed to classify the whole study areas.

3. Results and Discussion

Chosen distributions of the feature values amongst the different habitat types are shown in Figure 1. Exemplarily, the horizontal distance to the closest water surface shows clear differences between some forest groups. The median TWI shows varies between the classes 9170 and 9180, which show similar distributions most other features. The first visual interpretation indicates potential of the derived features for classification of the different forest habitat types. The leave-off condition of the data acquisition limits the direct species determination of the trees to examination of the branch structures. Leave-on data could add valuable information about crown and canopy. Random forest classification with a mapping unit of 1 m² using samples of max. 2500 pixels per HD type and recursive feature selection results in OOB errors of 19.5% (study site A) and 16.7% (study site B). The overall accuracies determined by the predictions of the 10 fold spatial CV are 66% (study site A) and 80% (study site B).

4. Conclusion and Outlook

The current study shows that features derived from ALS point cloud data have high potential for classification of different habitat types of the European Union's Habitats Directive in forest landscapes. Chosen features, like horizontal distance to closest water surface, are useful for classification of different forest habitat types. Integration of further data sets with high temporal resolution for identification of phenological characteristics as well as spectral information (Sentinel-1 and Sentinel-2) and point clouds from image matching are subject of ongoing investigations.

Acknowledgements

The ALS data are provided by the municipality of Vienna. The ALS processing and classification work is funded by the FFG Austrian Space Applications Programme ASAP 15, grant agreement number 881400, Anwendungsmöglichkeiten von Sentinel-Daten für ein Monitoring im Umwelt- und Naturschutz in Städten am Beispiel Wien, SeMoNa22.

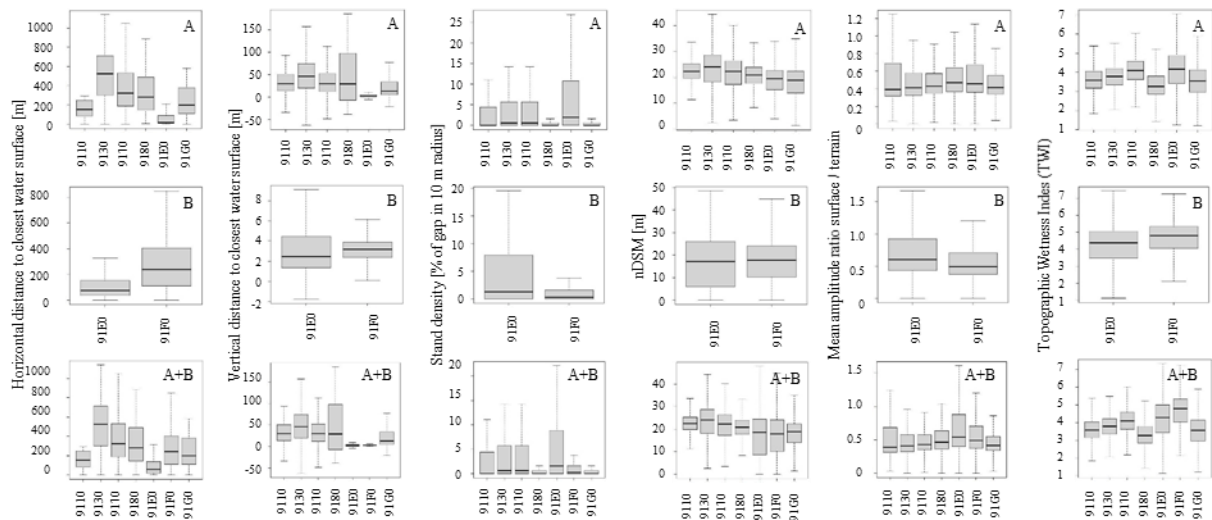


Figure 1: Boxplots of the distribution of chosen features of different HD types (Natura 2000 Code, see Table 1) for both study sites A and B and in combination.

References

- Coops N, Tompaski P, Nijland W, Rickbeil GJM, Nielsen SE, Bater, CW, Stadt J, 2016, A forest structure habitat index based on airborne laser scanning data. *Ecological Indicators*, 67:346-357. doi.org/10.1016/j.ecolind.2016.02.057.
- European Commission, 1992, *Council Directive 92/43/EEC of 21 May 1992 on the conservation of natural habitats and of wild fauna and flora*. <https://eur-lex.europa.eu/legal-content/EN/TXT/HTML/?uri=CELEX:31992L0043&from=EN> (25. May 2021).
- European Commission, 2006, *Council Directive 2006/105/EC of 20 November 2006 adapting Directives 73/239/EEC, 74/557/EEC and 2002/83/EC in the field of environment, by reason of the accession of Bulgaria and Romania*. <https://eur-lex.europa.eu/legal-content/EN/TXT/PDF/?uri=CELEX:32006L0105&from=EN> (12. April 2021).
- Guo X, Coops NC, Tompalski P, Nielsen SE, Bater CW, Stadt JJ, 2017, Regional mapping of vegetation structure for biodiversity monitoring using airborne lidar data. *Ecological Informatics*, 38:50-61.
- Hollaus M, Mücke W, Höfle B, Dorigo W, Pfeifer N, Wagner W, Bauerhansl C and Regner B, 2009, Tree species classification based on full-wave-form airborne laser scanning data. *9th International Silvilaser Conference*, October 14–16, 2009, Texas A&M University, College Station, TX, USA, 54–62.
- Hollaus M, Wagner W, Eberhöfer C and Karel W, 2006, Accuracy of large-scale canopy heights derived from LiDAR data under operational constraints in a complex alpine environment. *ISPRS Journal of Photogrammetry and Remote Sensing*, 60(5):323-338. doi.org/10.1016/j.isprsjprs.2006.05.002.
- Koenig C and Höfle B, 2016, Full-Waveform Airborne Laser Scanning in Vegetation Studies—A Review of Point Cloud and Waveform Features for Tree Species Classification. *Forests*, 7(9):198. doi.org/10.3390/f7090198.
- Kraus K and Pfeifer N, 1998, Determination of terrain models in wooded areas with airborne laser scanner data. *ISPRS Journal of Photogrammetry and Remote Sensing*, 53(4):193-203. doi.org/10.1016/S0924-2716(98)00009-4.
- Lindberg E, Olofsson K, Holmgren J and Olsson H, 2012, Estimation of 3D vegetation structure from waveform and discrete return airborne laser scanning data. *Remote Sensing of Environment*, 118:151-161. doi.org/10.1016/j.rse.2011.11.015.
- Mikita T, Klimánek M and Cibulka M, 2013, Evaluation of airborne laser scanning data for tree parameters and terrain modelling in forest environment. *Acta Universitatis Agriculturae et Silviculture Mendelianae Brunensis*, 61(5):1339-1347. doi.org/10.11118/actaun201361051339
- Räsänen A, Kuitunen M, Tomppo E, Lensu A, 2014, Coupling high-resolution satellite imagery with ALS-based canopy height model and digital elevation model in object-based boreal forest habitat

type classification. *ISPRS Journal of Photogrammetry and Remote Sensing*, 94:169-182. doi.org/10.1016/j.isprsjprs.2014.05.003.

Requena-Mullor JM, Reyes A, Escribano P, Cabello J, 2018, Assessment of ecosystem functioning from space: Advancements in the Habitats Directive implementation. *Ecological Indicators*, 89:893-902. doi.org/10.1016/j.ecolind.2017.12.036.

Stadt Wien – <https://data.wien.gv.at>, 2020, *Mapping of biotope types in Vienna: selective mapping of habitats and biotopes as defined by the Vienna according to the Vienna Nature Protection Ordinance and the EU Directive on the conservation of natural habitats and wild fauna and flora.* https://www.data.gv.at/katalog/dataset/stadt-wien_biotoptypenkartierungwien (28 January 2021).

Unit-level Small Area Estimation of Forest Inventory with GEDI Auxiliary Information

Shaohui Zhang^{1,2}, Cédric Vega³, Olivier Bouriaud³, Sylvie Durrieu⁴, Jean-Pierre Renaud^{2,3}

¹University of Eastern Finland, Yliopistokatu 7, 80130 Joensuu, Finland
Email: shaohui.zhang@uef.fi

²Office National des Forêts, 8 Allée de Longchamp, 54600 Villers lès Nancy, France
Email: jean-pierre.renaud-02@onf.fr

³The Institut National de L'information Géographique et Forestière, 14 Rue Girardet, 54000 Nancy, France
Email: {cedric.vega; olivier.bouriaud}@ign.fr

⁴UMR TETIS, INRAE, Univ Montpellier, 500 Rue Jean-François Breton, 34196 Montpellier, France
Email: sylvie.durrieu@inrae.fr

1. Introduction

National Forest Inventories (NFIs) play an important role in understanding the state of forests at the national and regional levels. Forest inventory for small territorial areas, such as municipalities, is also important for decision-makers. However, information is relatively limited at this level. As a result, developing small area estimation (SAE) approaches has gained increasing popularity in the field of forest inventory. It enables prediction of forest attributes for sub-populations using regression models based on auxiliary data commonly derived from remote sensing techniques over an area of interest (AOI). It has been reported that SAE can improve the precision of forest inventory without increasing costs (Mandallaz, Breschan and Hill 2013) and may produce reliable predictions of forest attributes locally, even when field plots are not available (Rao 2014).

Tomppo (2006) is a pioneer in the use of auxiliary data for multi-source forest inventory. Previously, common sources of auxiliary data often came from satellite-based imagery (McRoberts et al. 2007), digital aerial photogrammetry (Breidenbach et al. 2018), and airborne laser scanning (Magnussen et al. 2014). NASA's newly-launched Global Ecosystem Dynamics Investigation (GEDI) is a full waveform LiDAR instrument aboard the International Space Station (ISS). Its products consist of footprint measurements projected to cover 4% of the global land surface by the end of its mission (Dubayah et al. 2020). This will provide an unprecedented opportunity to systematically collect samples of forest information that can be used in SAE on a large scale.

The objective of this study is to explore the possibility of using GEDI auxiliary data to improve the accuracy of forest inventory for a large natural area in central France (Sologne), as well as for smaller sub-areas defined by French administrative boundaries (departments). The results will then be compared against estimates obtained from simple random sampling (SRS), to assess the efficiency of the auxiliary data.

2. Data and Methods

2.1 Study Area

Our study is based in Sologne, central France, which covers an area of approximately 6000km². The topography is mostly flat, with most elevations within the range of 110–250m, except the south-eastern part, where undulating terrain reaches 400m. Forests cover approximately 48% of the area and are dominated by pure broadleaved species (75.3%). Conifer and mixed stands account for 15.5% and 9.2% of the forest areas respectively. The climate is temperate Atlantic, with mean annual temperature and precipitation of 11°C and 725mm.

2.2 NFI Data

For the study area, 902 permanent NFI plots, surveyed between 2015 and 2019, were available. This five-year timeframe is routinely used in official French NFI statistics. Each plot contains detailed inventory information, including density (trees/ha), quadratic mean diameter (cm), basal area (m²/ha),

dominant height (m), and volume (m³/ha). However, this paper focuses solely on the aspect of forest volume estimations. Details of inventory schemes and methods can be found in Hervé et al. (2014).

2.3 Auxiliary Data Sources and Processing

GEDI Level 2A products, acquired between 2019-04-22 and 2020-04-14, were used as auxiliary data. Each footprint is of 25-meter diameter and has the information of beam types (i.e., full or half power), sensitivity, geo-located elevation and height metrics.

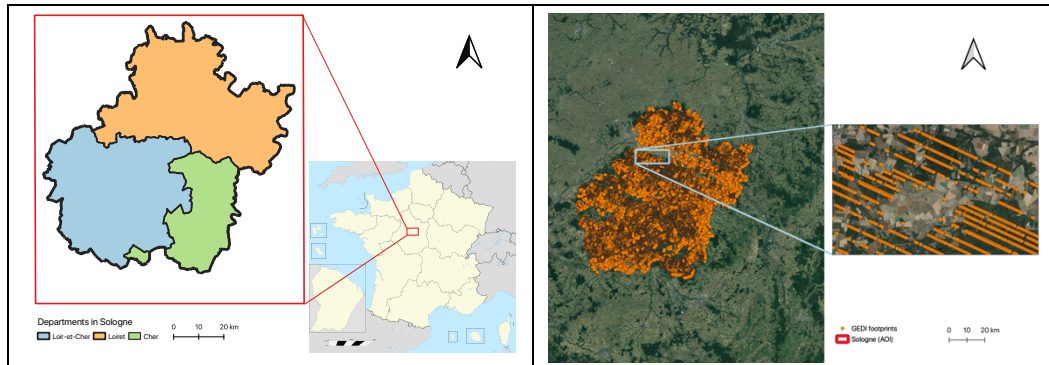


Figure 1: Location of the Study Area (departments have different colours) and availability of GEDI footprints over the AOI.

Only the best quality footprint data were retained based on the following filtering criteria: Firstly, we only kept footprints whose quality flag is 1, degrade flag is 0, and sensitivity is ≥ 0.9 . This is a standard filtering criterion applied to select suitable GEDI footprints, which also ensures that the beam power is strong enough to penetrate the canopy and reach the ground with 90% probability (Hancock et al. 2019). Next, we followed the definition of forest from FAO, which states that “trees in a forest reach a minimum height of 2-5 m at maturity” (FAO 2021). Therefore, we used an average height of 3m as threshold and removed those footprints whose RH_{100} values were smaller than 3 and thus did not qualify as forest. As a result, a total number of 112,569 footprints were included for further analysis. In addition, the footprints were intersected with forest masks to determine in which types of forest they were located. Height metrics and forest types were then extracted from the footprints and formed the auxiliary data frame.

Lastly, seven nearest neighbouring GEDI footprints around individual NFI plots were identified based on their Euclidean distances. We set an additional distance threshold of 200m to filter out those NFI plots that had neighbouring footprints located farther than the threshold and thus may misrepresent the plot information. Based on the identified shot numbers, the remaining 105 NFI plots were then joined with one of the seven neighbouring footprints that shared the closest forest height, as defined by the smallest value of $|\text{NFI dominant height} - RH_{100}|$. This formed the calibration data frame.

2.4 Unit-level Small Area Estimation

Unit-level SAE was performed using the two-phase estimation procedure provided in R package “forestinventory” and described in Hill, Massey and Mandallaz (2021). The first phase of auxiliary GEDI information was used to generate model predictions based on linear regression using the method of ordinary least square. The second phase contains the targeted NFI plot attributes, i.e., forest volume alone in this case, that is used to generate model coefficients and correct bias.

3. Results and Discussion

A total of 101 auxiliary GEDI variables (100 height metrics and one forest type) were available and tested to predict forest volumes. Variable selection was done using an exhaustive search with the help of “randomForestSRC” R-package (Ishwaran and Kogalur 2021). The most relevant variables were manually verified to yield the best model fit and a low variance inflation factor (< 5). The final linear model retained was:

$$\hat{Y} = \beta_0 + \beta_1 * RH_{100} + \beta_2 * RH_{20} + \beta_3 * \text{Forest Type} \quad (1)$$

Where \hat{Y} is the predicted volume, β_0 is the intercept, β_1 , β_2 and β_3 represent coefficients. RH_{100} and RH_{20} represent respectively the relative heights at which the maximum and the 20th percentile of waveform energy above the ground peak are reached.

Based on this model formulation, SAE of forest volume was performed at the Sologne and sub-area levels. Results showed that GEDI auxiliary information significantly improved estimate accuracy compared with results obtained without this auxiliary information (Table 1). At the whole AOI level, the variance was significantly reduced and an increase in relative efficiency by a factor of 2.6 was obtained. In each sub-area, similar results were achieved, with reduced variance and an increase in relative efficiency by factors varying between 1.6 and 2.6. However, the mean forest volume was somehow underestimated using SAE estimation with the help of GEDI auxiliary data at both AOI and sub-area levels. We further calibrated the model and discovered that this was likely caused by model extrapolation, as a considerable number (16%) of predicted forest volumes fell outside the model calibration domain.

Table 1. Volume estimations of SAE and SRS at both AOI and department levels

Area	Plot N	SRS Estimation	SRS Variance	SAE Estimation	SAE Variance	Relative Efficiency
Overall AOI	105	192.0 ± 25.6	164.3	170.2 ± 15.8	62.4	2.6
Cher	20	198.0 ± 51.1	653.0	185.3 ± 40.2	404.0	1.6
Loiret	46	224.1 ± 43.6	475.5	181.7 ± 27.2	224.1	2.6
Loir-et-Cher	39	151.1 ± 34.8	302.2	150.6 ± 22.0	120.4	2.5

4. Conclusions

This paper performed unit-level small area estimation using GEDI Level 2A as auxiliary data. We associated GEDI auxiliary information with NFI plots based on Euclidean distance to assess forest volume estimation. It is shown that GEDI auxiliary information can help improve forest volume estimation significantly when compared to simple random sampling alone. The fact that GEDI data are open-access and cover the entire country makes it a particularly attractive tool for improving forest inventory at regional and local levels.

References

- Breidenbach J et al., 2018, Unit-level and area-level small area estimation under heteroscedasticity using digital aerial photogrammetry data, *Remote Sensing of Environment*, 212, 199–211.
- Dubayah R et al., 2020, The Global Ecosystem Dynamics Investigation: High-resolution laser ranging of the Earth's forests and topography, *Science of Remote Sensing*, 1, 100002.
- FAO, 2021, Comparative framework and Options for harmonization of definitions: <http://www.fao.org/3/Y4171E/Y4171E10.htm>. Accessed 16 March 2021.
- Hancock S et al., 2019, The GEDI Simulator: A Large-Footprint Waveform Lidar Simulator for Calibration and Validation of Spaceborne Missions, *Earth and Space Science*, 6(2): 294–310.
- Hervé JC et al., 2014, L'inventaire des ressources forestières en France: un nouveau regard sur de nouvelles forêts, *Revue Forestière Française*, (3): 247-260.
- Hill A, Massey A and Mandallaz D, 2021, The R Package forestinventory: Design-Based Global and Small Area Estimations for Multiphase Forest Inventories, *Journal of Statistical Software*, 97(1): 1–40.
- Ishwaran H and Kogalur UB, 2021, *RandomForestSRC: Fast Unified Random Forests for Survival, Regression, and Classification (RF-SRC)*, R package version 2.11.0.
- Magnussen S et al., 2014, National forest inventories in the service of small area estimation of stem volume, *Canadian Journal of Forest Research*, 44(9): 1079–1090.
- Mandallaz D, Breschan J and Hill A, 2013, New regression estimators in forest inventories with two-phase sampling and partially exhaustive information: a design-based monte carlo approach with applications to small-area estimation. *Canadian Journal of Forest Research*, 43(11): 1023-1031.
- McRoberts RE et al., 2007, Estimating areal means and variances of forest attributes using the k-Nearest Neighbors technique and satellite imagery, *Remote Sensing of Environment*, 111(4): 466–480.
- Rao JNK, 2014, Small-area estimation, in *Wiley StatsRef: Statistics Reference Online*, 1–8.
- Tomppo E, 2006, The Finnish multi-source national forest inventory-small area estimation and map production, in *Forest Inventory – Methodology and Applications*, 195–224.

Distinguishing tropical forest typologies with UAV LiDAR

J. E. Scheeres¹, B. Brede¹, J. de Jong², P. G. Molin³, F. Miranda⁴, C. Almeida⁴, E. Broadbent⁵,
A. M. Almeyda Zambrano⁶, P. Brancalion⁴, D. R. A. de Almeida⁴

¹Laboratory of Geo-Information Science and Remote Sensing, Wageningen University & Research, Wageningen, The Netherlands
Email: {janneke.scheeres; benjamin.brede}@wur.nl

²Forest Ecology and Forest Management Group, Wageningen University & Research, Wageningen, The Netherlands
Email: johan1.dejong@wur.nl

³Center for Nature Sciences, Federal University of São Carlos (UFSCar/CCN), Buri, SP, Brazil
Email: pgmolin@ufscar.br

⁴Department of Forest Sciences, “Luiz de Queiroz” College of Agriculture, University of São Paulo (USP/ESALQ), Piracicaba, SP, Brazil
Email: {fredtsmiranda; cathe.torres; pedrobrancalion; daniloflorestas}@gmail.com

⁵School of Forest Resources and Conservation, University of Florida, Gainesville, FL, USA
Email: eben@ufl.edu

⁶Center for Latin American Studies, University of Florida, Gainesville, FL, USA
Email: aalmeyda@ufl.edu

1. Introduction

There is a gap in knowledge regarding the outcomes of different forest restoration strategies and the processes that occur within these new forests to effectively implement restoration strategies (Crouzeilles et al., 2016). To bridge this gap, it is important to identify the different forest typologies at a landscape scale, and subsequently to monitor restoration outcomes, such as forest composition, health, and functioning (Almeida et al., 2019a).

LiDAR is receiving much attention as an effective tool for forest monitoring due to its ability to capture forest structure efficiently (Almeida et al., 2019a). Due to recent technical advances, Unoccupied Aerial Vehicle (UAV)-LiDAR has become more available for forest monitoring. These systems are lightweight, field-portable, have a relatively low cost, can acquire data at fine spatial and temporal resolutions, and are more flexible in use than other LiDAR systems (Zahawi et al., 2015). In this way UAV-LiDAR could replace costly and time intensive field inventories (Almeida et al., 2019c). Nevertheless, little is known of the potential of UAV-LiDAR in a forest restoration context, or their ability to distinguish structural attributes in mixed-species plantations (Almeida et al., 2019b). The objective of this study was to explore the potential of UAV-LiDAR to distinguish tropical forest typologies at a plot level with classification, and to identify the most effective metrics for classification.

2. Data and Methods

The sample sites were 150 forest plots of 800-900 m² in the Atlantic Forest of Brazil of six forest typologies. The typologies were monoculture plantation (N = 56), abandoned monoculture (N = 25), and mixed plantation (N = 8) – which were simplified as ‘plantation’; forest remnant (N = 7), natural regeneration (N = 24), and restoration plantation (N = 30) – simplified as ‘natural’. LiDAR data was acquired with the GatorEye system in August 2019 with a Velodyne VLP-16 dual-return sensor (Almeida et al., 2019c). The pulse density was 216.14 ± 94.3 points m⁻².

Thirty-three metrics in total were extracted per forest plot point cloud. Mean CHM, CHM rugosity, and gap fraction were extracted from canopy height models (CHM). CHM contain the absolute vegetation height above ground. Twenty five metrics were extracted from the normalised point clouds: height percentile cloud metrics hp.nmean and hp.nSD, where n = [5,10,25,50,75,90]; cloud return density above quantile metrics dq.imean and dq.iSD, where i = [20,40,60,80]; minimum return height C_{min}mean and C_{min}SD; maximum return height C_{max}mean and C_{max}SD; and Gini coefficient (GC). The height percentile metrics represent the distribution of vegetation through the canopy, specifically at which height a proportion of vegetation is concentrated. Five metrics were extracted from three-dimensional voxel matrices: leaf area index (LAI) mean, LAI SD, LAI understory, Leaf Area Height Volume (LAHV), and Foliage Height Diversity (FHD). Voxel matrices, which represent square units of canopy volume, were computed per normalised height point cloud with the LeafR package (Almeida, 2019). Then Leaf Area Density (LAD) profiles were calculated, which are vertical distributions of the leaf area in voxels. LAI understory was computed as the sum of LAD at all heights below five metres

(Almeida et al., 2019a). LAHV was calculated as the sum of vegetation volume over all heights, where z is the height in the canopy ($z = 1, 2, 3, \dots, \max z$) and LAD_z is the mean LAD at that height. FHD was calculated with Shannon's index applied to the plot mean LAD profile.

To distinguish the six non-simplified typologies, and the two simplified typologies, random forest was used to build supervised classification models. The models were tuned by iteratively removing the metric with the lowest importance until stabilisation of the accuracy was reached. The two random forest models were validated with Leave-one-out-cross-validation and their performance was assessed with confusion matrices. The importance of UAV-LiDAR metrics was assessed with their mean increase in MDA per standard deviation.

3.Results

3.1 Performance assessment of classification models

The six-typology classification model performed with a kappa statistic of 0.46 and overall accuracy (OA) of 58.7% (Table 1). Monoculture plantation and restoration plantation were most accurately classified, and mixed planation was never correctly classified (Table 1). Forest remnant, natural regeneration, and restoration plantation were most difficult to distinguish from each other. 48% of the abandoned monoculture plots were mis-classified as monoculture plantation. The simplified classification model performed better with a kappa statistic of 0.78 and OA of 90.0% (Table 2).

Table 1. Confusion matrix for classification of non-simplified typologies with User's Accuracy (UA), Producer's Accuracy (PA), and overall accuracy. The correctly classified plots are in bold.

		Predicted						PA(%)
		Forest remnant	Natural re-generation	Restoration plantation	Mixed plantation	Abandoned mono-culture	Monoculture plantation	
Reference	Forest remnant	2	2	2		1		28.6
	Natural regeneration	1	13	8		2		54.2
	Restoration plantation		7	21		1	1	70.0
	Mixed plantation	1		1		4	2	0
	Abandoned monoculture	1	2	1		9	12	36.0
	Monoculture plantation		1	2		10	43	76.8
	UA(%)	40.0	52.0	60.0	0	33.3	74.1	58.7

Table 2. Confusion matrix for classification of the simplified typologies.

		Predicted		PA(%)
		Natural	Plantation	
Reference	Natural	56	5	91.8
	Plantation	10	79	88.8
UA(%)		84.8	94.0	90.0

3.2 Analysis of metric importance

The metrics included in the final non-simplified typologies model (in order of importance) were (LAI) understory, hp.50SD, dq.40SD, and CHM rugosity. LAI understory and hp.50SD were the two metrics

used in the simplified classification model. LAI understory showed most variation between all typologies, and hp.50SD clearly distinguished the natural- from the plantation typologies.

4. Discussion

The successful classification of the simplified natural and plantation typologies is important, because in large scale restoration initiatives or forest assessments this distinction is often not made and forest cover is the primary indicator used (Chazdon et al, 2016). LAI understory and hp.50SD were able to capture the difference in active removal of undergrowth and regular planting structure of plantations from the natural typology growth forms. The overall lower accuracy in the non-simplified typology classification was due to low sample sizes, broad variation of growth forms within typologies, the difference in forest structure of early succession and later successional stages, and similarity of all typologies in an early successional stage. Nevertheless, the LAI understory metric showed potential for distinction of similar types. Furthermore, understory vegetation is used as an ecological indicator for forest health, biodiversity, and regeneration potential, but is laborious to measure in the field and inaccurate with low LiDAR point densities (Campbell et al., 2018). Therefore, UAV-LiDAR has potential for measuring understory vegetation as a useful restoration outcome indicator. For further distinction of similar typologies, and avoiding noise from different successional stages, future research should explore LiDAR fusion with optical sensors.

5. Conclusions

Plantation typologies were successfully discerned from natural typologies, but other non-structural features may be needed to separate similar typologies. The metric LAI understory showed the most potential as a unique feature to distinguish typologies, and it should be further explored. Overall, UAV-LiDAR can be used to identify structural differences in a broad range of forest restoration sites and can be of good use for existing and future forest restoration projects.

Acknowledgements

The São Paulo Research Foundation (FAPESP, grants #2018/21338-3, #2018/18416-2, #2019/14697-0 and #2020/06734-0) is acknowledged for financial support. Thanks to the NewFor project team for the field data, and to the (SPEC) Lab at the University of Florida who funded and collected the GatorEye LiDAR data. B.B. is supported by the IDEAS-QA4EO and ForestScan contracts funded by ESA-ESRIN.

References

- Almeida, D. R. A. d. (2019). LeafR: Provides a set of functions for analyzing the ecological structure of forests based on lai and lad measures derived from lidar data. [R package version 0.3]
- Almeida, D. R. A. d., Stark, S. C., Chazdon, R., Nelson, B. W., Cesar, R. G., Meli, P., Gorgens, E. B., Duarte, M. M., Valbuena, R., Moreno, V. S., Mendes, A. F., Amazonas, N., Gonçalves, N. B., Silva, C. A., Schiatti, J., & Brancalion, P. H. (2019a). The effectiveness of lidar remote sensing for monitoring forest cover attributes and landscape restoration. *For. Ecol. Manage.*, 438, 34–43.
- Almeida, D. R. A. d., Stark, S. C., Shao, G., Schiatti, J., Nelson, B. W., Silva, C. A., Gorgens, E. B., Valbuena, R., Papa, D. d. A., & Brancalion, P. H. S. (2019b). Optimizing the remote detection of tropical rainforest structure with airborne lidar: Leaf area profile sensitivity to pulse density and spatial sampling. *Remote Sens.*, 11(1), 92.
- Almeida, D. R. A. d., Broadbent, E. N., Zambrano, A. M. A., Wilkinson, B. E., Ferreira, M. E., Chazdon, R., Meli, P., Gorgens, E. B., Silva, C. A., Stark, S., Valbuena, R., Papa, D., & Brancalion, P. (2019c). Monitoring the structure of forest restoration plantations with a drone-lidar system. *Int. J. Appl. Earth Obs. Geoinf.*, 79(April), 192–198.
- Campbell, M. J., Dennison, P. E., Hudak, A. T., Parham, L. M., & Butler, B. W. (2018). Quantifying understory vegetation density using small-footprint airborne lidar. *Remote Sens. Environ.*, 215, 330–342.
- Chazdon, R. L., Brancalion, P. H. S., Laestadius, L., Bennett-Curry, A., Buckingham, K., Kumar, C., Moll-Rocek, J., Vieira, I. C. G., & Wilson, S. J. (2016). When is a forest a forest? Forest concepts and definitions in the era of forest and landscape restoration. *Ambio*, 45(5): 538–550.
- Crouzeilles, R., Curran, M., Ferreira, M. S., Lindenmayer, D. B., Grelle, C. E. V., & Rey Benayas, J. M. (2016). A global meta-Analysis on the ecological drivers of forest restoration success. *Nat. Commun.*, 7(1), 1–8.
- Zahawi, R. A., Dandois, J. P., Holl, K. D., Nadwodny, D., Reid, J. L., & Ellis, E. C. (2015). Using lightweight unmanned aerial vehicles to monitor tropical forest recovery. *Biol. Conserv.*, 186, 287–295.

Comparing portable MLS to TLS and UAV-LS derived individual tree parameters

H.M. Bartholomeus¹, A. Lau Sarmiento¹, B. Brede¹
K. van Hove¹, N. Koelewijn¹

¹ Wageningen University & Research, Laboratory of Geo-Information Science and Remote Sensing, Droevendaalsesteeg 3, 6708 PB Wageningen, the Netherlands
Email: {harm.bartholomeus; alvaro.lausarmiento; benjamin.brede; kim.vanhoeve; niek.koelewijn@wur.nl}

1. Introduction

LiDAR is becoming an important technique for forest monitoring. The 3D representation through LiDAR scans can give valuable insight in to forest functioning and changes there in (Calders et al., 2020) or give us individual tree biomass (Gonzalez de Tanago et al., 2018).

LiDAR can be used to derive forestry parameters in different setups. Terrestrial Laser Scanning (TLS) has been used to measure and monitor forests for many years, and is especially valued for the high accuracy of TLS measurements and derived parameters. Unoccupied Aerial Vehicle laser scanning (UAV-LS) has become available over the last years and has shown to be an effective system to investigate forests that cannot be entered by foot, or facilitates covering larger areas in a shorter time. Mobile laser scanning (MLS) is one of the techniques to acquire forest understory 3D data (Liu et al., 2021). The technique uses the simultaneous localization and mapping (SLAM) algorithm to efficiently create 3D point clouds.

Mobile LiDAR scanners could prove very useful in circumstances where traditional TLS systems face difficulty, and where UAV-LS is prohibited or too costly. However, the precision of MLS in comparison to TLS and UAV-LS dictates the usefulness of the mobile systems to measure and monitor trees in forests and urban environments. Further testing is required to show the applicability of MLS in forests (Calders et al., 2020).

Different platforms all have their pros and cons, where mainly the acquisition speed is a point of interest. The practical problem is that for subsequent sampling (e.g. for forest monitoring), TLS is too slow and labour intensive. UAV-LS could partly fill this gap, but the operation is complicated and costly in comparison to MLS. A UAV-LS vs TLS comparison was done by Brede et al. (2017), who showed that both techniques have the potential to derive tree metrics, like tree height and diameter breast height (DBH). Previously, MLS and TLS were compared by Bauwens et al. (2016), but the MLS technique has further developed, which has resulted in increased measurement range and point densities.

The objective of this paper is to benchmark the performance of a backpack MLS system against TLS and UAV-LS for the estimation of some common tree parameters. This is done in two case studies: the MLS vs UAV-LS comparison is done for a small forest area, while a comparison of MLS and TLS is done for trees in an urban area.

2. Data and Methods

The data for the MLS vs UAV-LS comparison has been acquired in the Oostereng, a forest in the Veluwe area, the Netherlands. The trees in the investigated forest plot are of the species Douglas fir (*Pseudotsuga menziesii*), and all data has been acquired in February 2021. MLS data were collected with the Greenvalley LiBackpack DGC-50, a dual LiDAR backpack system, composed of two Velodyne VLP-16 scanners, Inertial Measurement Unit, GNSS, 360 degree camera and processing unit. Initial data processing through SLAM is done on the processing unit itself, but integration of GNSS data and data point coloring is done during post-processing. UAV-LS data were acquired on the same day using a Riegl Ricopter with a VUX-1UAV scanning system. Flights were conducted at 90 m above ground level and processing to a geo-rectified pointcloud was done following the procedures described in Brede et al. (2017). A 25 m x 25 m subset of the forest plot was selected for further analysis, where 12 trees were visually identified and manually segmented using CloudCompare (Cloudcompare, 2020). Tree height was calculated by subtracting the minimal z value from the maximal z value for each of the tree segments. The DBH was calculated with ordinary least squares circle fitting implemented in the

lsfit.circle function from the R package “circular”. The DBH was calculated at 1.3 m above ground, with a 5 cm buffer. The subsets were visually inspected to filter out points that were not situated around the trunk of the trees. Two trees needed adjustments to create a correct subset of the trunk at DBH height.

Data for the MLS vs TLS comparison were collected in January 2021 on the Wageningen University and Research campus in Wageningen, The Netherlands. The 22 selected deciduous trees, growing next to a road, were scanned with the Riegl VZ-400. Ten scan locations were chosen and for co-registration of the individual scans, six reflectors were installed on both sides of the road. MLS data of the same area were acquired using the Greenvalley LiBackpack DGC-50 system. Extraction of individual tree point clouds was done with Cloud Compare software in a manner similar to Lau et al. (2018). Tree height was deduced by taking the distance between the top and bottom point. Crown diameter was calculated the average of the the largest lengths of the crown in the North-South and East-West directions.

For both cases the different point clouds were first coarse registered by manually selecting corresponding points and performing a rigid body transformation. Fine registration was done with the Iterative Closest Point algorithm in CloudCompare.

3. Results and Discussion

In the forest plot the MLS measured tree height of most trees is within 0.5 m of the UAV-LS tree height (Figure 1). However, when the canopy is denser the MLS system has difficulties to reach the top of the canopy, which is shown by a lower tree height measured with MLS compared to UAV-LS. For the 12 trees in the subplot this results in an RMSE for the tree height of 1.61 m, which is almost solely a result of the 4 trees of which the upper canopy was not properly sampled.

The DBH calculated from the UAV-LS point clouds is generally larger than for the MLS data, which is summarized in an RMSE of 9 cm between both acquisition methods. This is largely the result of one tree where the DBH estimates had a great deviation.

Differences between calculated tree height and DBH of MLS and UAV-LS datasets were statistically analysed using linear regression and paired t-tests. The calculated tree height was significantly larger for a tree from the UAV-LS dataset compared to the MLS dataset ($t = 2.254$, $df = 11$, $p = 0.0456$). The same pattern was observed for DBH ($t = 3.619$, $df = 11$, $p = 0.0040$).

For the campus site the tree height and crown diameter were compared, and MLS and TLS give very comparable results in this case (Figure 2). Since all trees are free standing and relatively low there is very low occlusion, and as a result the estimated height of the trees is almost identical (RMSE = 0.01 m). Also the crown dimensions are comparable between the systems.

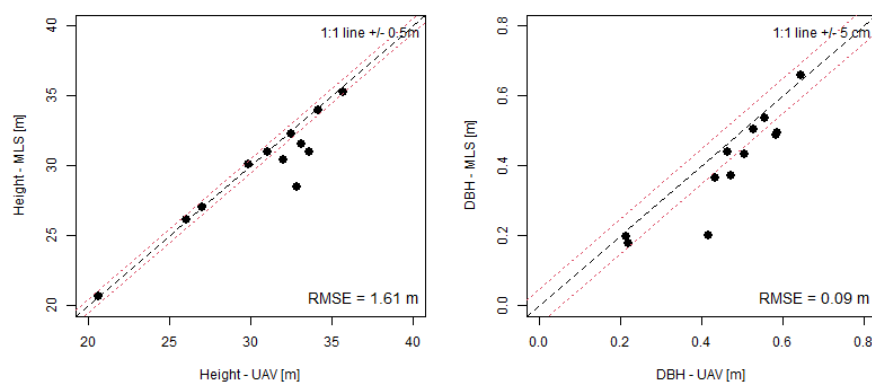


Figure 1: scatterplots of MLS vs UAV-LS derived individual tree height (left) and DBH (right). The dashed black line indicates the 1:1 line and the dashed red lines show the 1:1 line +/- 0.5m or 0.05m respectively.

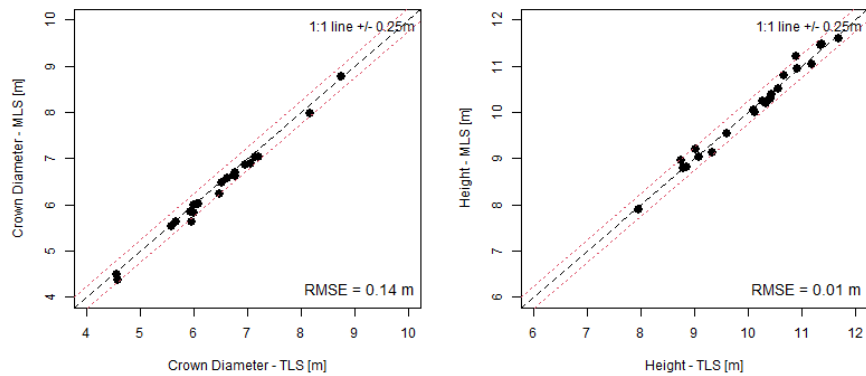


Figure 2: scatterplots of MLS vs TLS derived individual crown diameter (left) and tree height (right). The dashed black line indicates the 1:1 line and the dashed red lines show the 1:1 line +/- 0.5 m or 0.05 m respectively.

In terms of acquisition time, the LiBackPack DGC-50 MLS system outperforms both other systems. The point cloud quality of the TLS is better, but for the derived tree parameters it does not make a large difference. MLS shows to be an acceptable alternative to UAV-LS in forested areas, but with dense canopies data are to be treated with care. An improvement of the measurement strategy could still lead to better sampling of the upper parts of the canopy.

4. Conclusions

In a more open environment, the MLS and TLS tree height and crown diameter are comparable, but for a more dense canopy MLS tends to miss the treetops regularly, when compared to UAV-LS. For DBH differences are observed between systems, but evaluation against ground truth measurements has to show which is more accurate. The MLS system shows much potential in terms of usability. The scans made with the Greenvalley LiBackpack DGC-50 were made more quickly and with more ease than those made with the Riegl VZ-400 and the Riegl Ricopter.

References

- Bauwens, S., H. Bartholomeus, K. Calders, and P. Lejeune (2016). Forest inventory with terrestrial LiDAR: A comparison of static and hand-held mobile laser scanning. *Forests* 7(6).
- Brede, B., Lau, A., Bartholomeus, H.M., & Kooistra, L. (2017). Comparing RIEGL RiCOPTER UAV LiDAR derived canopy height and DBH with terrestrial LiDAR. *Sensors*, 17, 2371
- Calders, K., J. Adams, J. Armston, H. Bartholomeus, S. Bauwens, L. P. Bentley, J. Chave, F. M.Danson, M. Demol, M. Disney, R. Gaulton, S. M. Krishna Moorthy, S. R. Levick, N. Saarinen, C. Schaaf, A. Stovall, L. Terry, P. Wilkes, and H. Verbeeck (2020). Terrestrial laser scanning in forest ecology: Expanding the horizon. *Remote Sensing of Environment* 251, 112102.
- CloudCompare (version 2.11.3) [GPL software]. (2020). Retrieved from <http://www.cloudcompare.org/>
- Fernández-Sarría, A., L. Martínez, B. Velázquez-Martí, M. Sajdak, J. Estornell, and J. A. Recio (2013). Different methodologies for calculating crown volumes of *Platanus hispanica* trees using terrestrial laser scanner and a comparison with classical dendrometric measurements. *Computers and Electronics in Agriculture* 90, 176–185.
- Gonzalez de Tanago, J., A. Lau, H. Bartholomeus, M. Herold, V. Avitabile, P. Raunonen, C. Martius, R.C. Goodman, M. Disney, S. Manuri, A. Burt, K. Calders (2018). Estimation of Above-Ground biomass of Large tropical trees with terrestrial LiDAR. *Methods in Ecology and Evaluation* 9-2, 223-234.
- Lau, A., L. P. Bentley, C. Martius, A. Shenkin, H. Bartholomeus, P. Raunonen, Y. Malhi, T. Jackson, and M. Herold (2018). Quantifying branch architecture of tropical trees using terrestrial LiDAR and 3D modelling. *Trees - Structure and Function* 32(5), 1219–1231.
- Liu, L.L., Zhang, A.W., Xiao, S., Hu, S.X., He, N.P., Pang, H.Y., Zhang, X.Z., & Yang, S.K. (2021). Single Tree Segmentation and Diameter at Breast Height Estimation With Mobile LiDAR. *IEEE Access*, 9, 24314-24325

Understanding phenological changes of coniferous forests in Cyprus using time-series of SAR data from 2015 till 2020

M. Miltiadou^{1,2}, C. Theocharidis^{1,2}, V. Karathanassi³, A. Agapiou^{1,2}, M. Nikolaidis^{1,2}, C. Danezis^{1,2}

¹ Department of Civil Engineering and Geomatics, Faculty of Engineering and Technology, Cyprus University of Technology, 3036 Lemesos, Cyprus

²Eratosthenes Centre of Excellence, 3036 Lemesos, Cyprus

³School of Rural and Surveying Engineering, National Technical University of Athens, Athens, Greece

1. Introduction

Recent reports stressed the vulnerability of the forest ecosystem in the European Union (EU), especially to the south [1] [2]. Climate change alters our environment by shifting weather conditions, rising sea levels, increasing flood risks and threatening food production. Shoukri and Zachariadis, 2012, highlighted that Mediterranean Europe is expected to experience the most adverse climate change effects compared to other European regions [3]. Furthermore, Cleland et al., 2017 showed that climate change confers shifts to blooming time [4]. According to Wolkovich et al., 2012, the phenological responses (i.e., alternations in blooming timing) of plants to warmer conditions are unpredicted [5]. According to the US committee on phenology, phenology is "the study of the timing of recurring biological events, the causes of their timing with regard to biotic and abiotic forces and the interactions among phases of the same or different species"[6]. This includes structural changes – e.g., relating to how leaves of trees change seasonally – that can be identified by observing the backscattered coefficient of SAR data. The overarching aim of this study is to understand the phenological changes of a coniferous forest over time in Cyprus by analysing time series of SAR data.

2. Study Area

The study area is a coniferous state forest dominated by *Pinus Brutia*. It is located on the Troodos mountains range in Cyprus; it covers the Paphos forest and its surrounding forested areas. Cyprus is an island in the north-eastern end of the Mediterranean Sea [7]. While according to the literature, 18.7% was covered by forests in 2008 [8], ancient statements reveal that the entire inland including its plains used to be covered by forests [9]. In Cyprus, the summers start in mid-May and last till mid-September and they are dry and warm. Winters start in mid-November and end in mid-March and are mild [10].

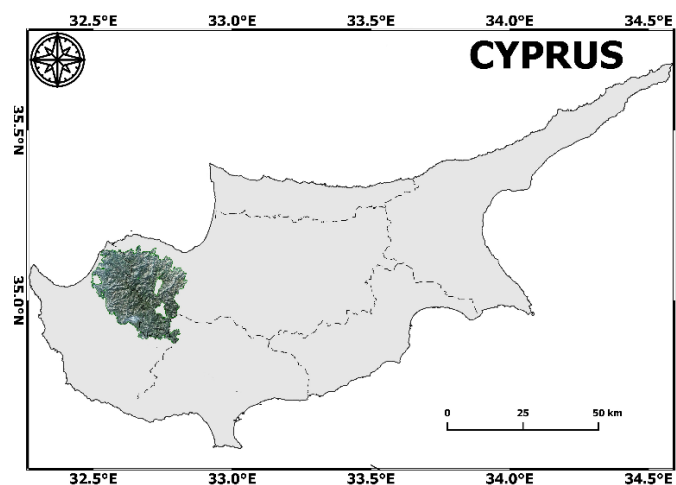


Figure 1. Study Area on the west-north end of Troodos Mountains range.

3. Data

The study interprets Sentinel-1 data from the timeframe Oct 2014 till Dec 2020. A total number of 304 images were downloaded but after filtering images acquired during high rainfall, 252 images remained for interpretation. This corresponds to an average of 42 images per year.

4. Methods

Pre-processing was done in SNAP ESA tool, while the extraction of the phenological graphs was automated in Python with specialised implemented tools for extracting the average backscattered coefficient from a given mask defining the area of interest. The tools then gather the average backscattered coefficients, clean the data from noise and create the phenological graphs. There is work in progress for generating forecasting and predicting models that will be trained by extracting feature (e.g., peak backscattered coefficient amplitude that represents peak structural blooming timing). Evaluation will be done using four years (2015-2018) as the training dataset and the other 2-years (2019-2020) as the testing dataset.

5. Preliminary Results, Discussion and Conclusions

Figure 2 shows a time-series of the normalised Backscattered coefficient (σ_0) of the VH and VV polarizations of Sentinel-1. It shows that the phenological cycle of the coniferous forest starts in November each year and contains on average two peaks: one in January and one in July. The first one correlates with the rainy season, and it should, therefore, relate to increased Leaf Area Index. The 2nd peak comes a couple of months after the blossoming time of the Pines during the cone growing period. It seems that monitoring both peaks by SAR could contribute into identifying forest degradation and its ability to regenerate itself as its regeneration depends on seeds. This is extremely important considering that in recent survey research 65.65% of Cypriot participants stated that they observed moderate to very much forest degradation including difficulty of regeneration [11].

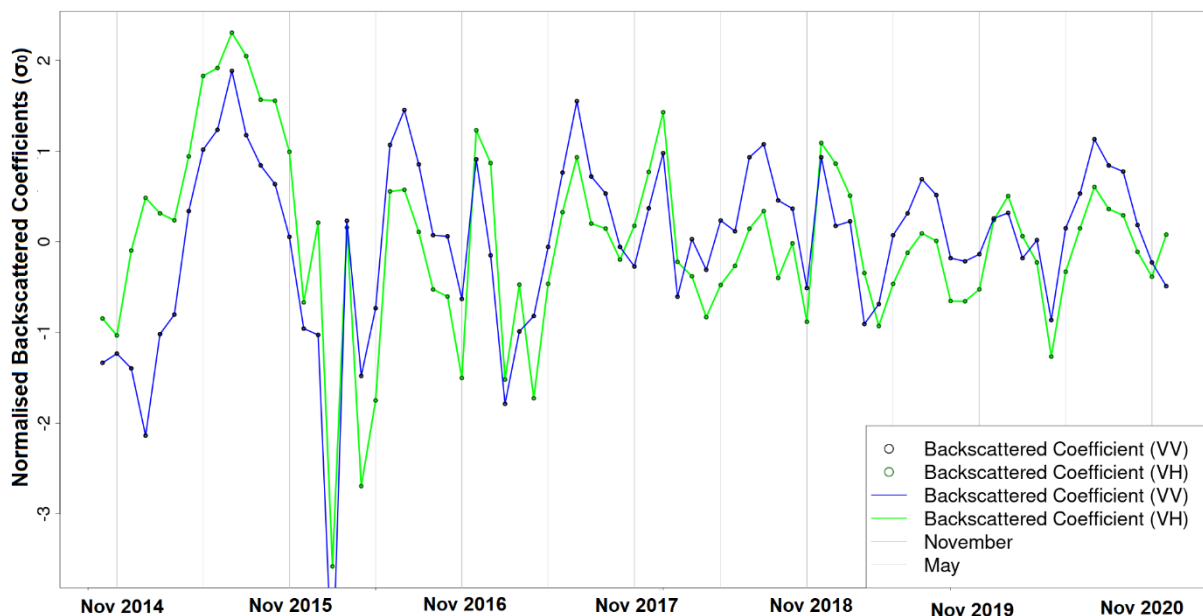


Figure 2. Normalised Backscattered Coefficients of VV and VH polarizations

Acknowledgements

The study is part of the project "ASTARTE" (EXCELLENCE/0918/0341) that is co-financed by the European Regional Development Fund and the Republic of Cyprus through the Research Innovation Foundation.

References

- [1] M. Hildén and A. Marx, “Evaluation of climate change state, impact and vulnerability indicators,” *ETC CCA Tech. Pap.*, vol. 2, p. 2013, 2013.
- [2] CYPADAPT, “Report on the future climate change impact, vulnerability and adaptation assessment for the case of Cyprus,” 2012.
- [3] E. Shoukri and T. Zachariadis, “Climate change in Cyprus - Impacts and adaptation policies,” *Cyprus Univ. Technol.*, 2012.
- [4] E. E. Cleland, I. Chuine, A. Menzel, H. A. Mooney, and M. D. Schwartz, “Shifting plant phenology in response to global change,” *Trends Ecol. Evol.*, vol. 22, no. 7, pp. 357–365, 2007.
- [5] E. M. Wolkovich *et al.*, “Warming experiments underpredict plant phenological responses to climate change,” *Nature*, vol. 485, no. 7399, p. 494, 2012.
- [6] I. L. Hudson and M. R. Keatley, “Phenological research,” *Methods Environ. Clim. Chang. Anal.*, 2010.
- [7] J. V Thirgood and others, *Cyprus: a chronicle of its forests, land and people*. University of British Columbia Press, 1987.
- [8] I. N. Vogiatzakis, G. Pungetti, and A. M. Mannion, *Mediterranean island landscapes: natural and cultural approaches*, vol. 9. Springer Science & Business Media, 2008.
- [9] J. Holmboe, *Studies on the vegetation of Cyprus: Based upon researches during the spring and summer 1905*, vol. 10, no. 2. Bergens Museums, 1914.
- [10] C. Nicolaou, *Wild Mammals of Cyprus*. CYPRUS FORESTRY ASSOCIATION, 2007.
- [11] M. Miltiadou, E. Antoniou, C. Theocharidis, and D. Chris, “Do People Understand and Observe the Effects of Climate Crisis on Forests ? The Case Study of Cyprus,” *Forests*, vol. 12, no. 9, p. 1152, 2021.

Close-Range Remote Sensing for National Forest Inventory Applications – A Comparison of Terrestrial and Airborne Approaches

D. Kükenbrink¹, M. Marty¹, R. Bösch¹, C. Ginzler¹

¹Swiss Federal Institute for Forest, Snow and Landscape Research, Zürcherstrasse 111, CH-8903 Birmensdorf
Email: {daniel.kuekenbrink; mauro.marty; ruedi.boesch; christian.ginzler}@wsl.ch

1. Introduction

Evaluation of the state and dynamics of forest ecosystems requires accurate, repeated and robust measurements of important forest biophysical parameters. Such measurements and forest assessments are traditionally performed within the framework of National Forest Inventories (NFI), where established field measurement methodologies are often time-consuming and sometimes subject to observer bias. New methodologies for accurate and quantitative, wall-to-wall acquisitions of different forest parameters could potentially advance the way NFIs are performed. With the recent developments in the field of terrestrial, mobile and drone-based laser scanning (TLS, MLS, UAVLS) as well as new advances in terrestrial and aerial structure from motion (SfM) applications, close-range remote sensing could play an important role in supporting traditional NFIs. However, in order to include these technologies within the framework of an operational NFI, its robustness and applicability needs to be assessed and evaluated.

In this contribution, we evaluate multiple close-range remote sensing technologies for the potential to support NFIs. We evaluate the performance to extract important forest inventory parameters such as tree position and diameter at breast height (DBH) and analyse the coverage and completeness of acquired datasets in respect to three 50x50 m² plots within a Swiss temperate mixed forest.

2. Data and Methods

The study area is located in a temperate mixed forest close to Zurich, Switzerland. For a 1 ha large plot, tree positions and DBH of all trees with a DBH ≥ 7 cm as well as a TLS campaign under leaf-off conditions using a FARO Focus3D scanner were acquired. Within the 1 ha plot, three 50x50 m² plots were defined, following the plot size definition of the Swiss NFI. These three plots were used to test multiple sensors with varying characteristics and acquisition patterns. The three plots showed varying tree densities (340, 440, and 564 trees/ha with DBH ≥ 7 cm) with varying species compositions and structural complexity (e.g. dense understorey vegetation). A set of TLS, MLS, UAVLS sensors as well as a terrestrial structure from motion (SfM) image acquisition was tested on these three plots, which are summarized in Table 1. All datasets were analysed regarding their point density distribution within the canopy, the coverage of the 50x50 m² plots and the extraction of the digital terrain model, where the DTM derived from the FARO TLS scan served as the reference. Tree positions and DBH were also extracted from all datasets and compared to reference acquisitions using a tachymeter and a calliper. We restricted the tree position and DBH comparison to trees with DBH ≥ 12 cm, following the methodology of the Swiss NFI. Tree positions and DBH were extracted using the R-package TreeLS (De Conto et al. 2017). Tree detection and DBH extraction performance was evaluated regarding their correctness (fraction of matched trees to number of detected trees), completeness (fraction of matched trees to number of reference trees), and the BIAS and RMSE of the DBH extraction. A detected tree was labelled as matched if a reference tree was found within 2 m from the detected position and the estimated DBH did not deviate more than 20% from the reference.

3. Results and Discussion

The analysed 3D point-cloud datasets differ substantially in terms of point density as well as point density distribution (Table 2 and Figure 1). Table 2 summarises the results from the dataset comparison.

Table 1: Acquired dataset specifications. Acquisition times refer to the 50x50 m² interpretation area unless otherwise stated (i.e. UAVLS and FARO acquisitions). Approximate distance between scan positions for TLS acquisition are specified with Δd .

Sensor	Sensor Type	Acquisition Date	Acquisition Pattern	Acquisition Time
FARO Focus3D	Phase Shift TLS	January 2020 (Leaf-Off)	Regular grid $\Delta d \approx 10$ m	6 days (for 1 ha)
Leica BLK 360	Time of flight TLS	September 2020 (Leaf-On)	Regular grid $\Delta d \approx 5$ m	6 hours
Riegl VUX1-UAV	UAVLS	March 2020 (Leaf-Off)	Regular grid	≈ 2 hours (for 52 ha)
Riegl miniVUX2	UAVLS	September 2020 (Leaf-On)	Regular grid	20 minutes (for 1 ha)
ZebRevo	MLS	October 2020 (Leaf-On)	Snake pattern	≈ 20 minutes
GoPro Hero 8 Black (12MP)	Terrestrial SfM	September 2020 (Leaf-On)	Circular Pattern	≈ 20 minutes

The average over all three plots is given, however the DTM accuracy as well as the tree detection and DBH extraction performance is highly dependent on the structural complexity of the plots. The two denser plots show multiple patches of very dense undergrowth, making data acquisition and the extraction of terrain and tree parameters in these areas difficult. Compared to the reference datasets, the leaf-on acquired BLK360 TLS acquisition performed best. However, the faster acquired and processed ZebRevo point-cloud performs similarly as the BLK360, even with the lower precision of the instrument. However, some trees were missed by the ZebRevo. The GoPro camera was able to detect more than 50% of the reference trees, however, it also only covered in average 80% of the entire plot area. Nevertheless, the estimated DBH of the detected trees show quite accurate results, even outperforming those extracted from the BLK360 acquisitions. However, further investigations are needed to fully evaluate the performance of each approach. The quality of extracted point-clouds from SfM acquisitions is highly dependent on the acquisition pattern, structural complexity (undergrowth vegetation) as well as the conditions during the acquisitions (light, wind). Further investigations are needed to analyse the robustness of such acquisitions for the use within NFIs.

UAVLS acquisitions, especially under leaf-on conditions (miniVUX2), showed some difficulties in accurately extracting terrain and tree information. The often dense overstorey vegetation resulted in substantially occluded areas in the lower canopy regions as also depicted in Figure 1. Further analysis on best acquisition patterns (e.g. Bruggisser et al., 2020) to acquire data or the possibilities to use within canopy UAVLS flights (e.g. Hyypä et al., 2020) could possibly help in this regard.

Table 2: Summary of extracted point-cloud acquisitions and the performance for DTM extraction and tree detection and DBH extraction from the different point-clouds. The average over all three analysed plots is given for all metrics.

Sensor	Point Density [pts/m ²]	DTM Coverage [%], Mean [m], std [m]	Tree detection [Correctness, Completeness]	DBH Difference Bias, RMSE [cm]
FARO	869'862	Reference	0.91/0.83	0.13/2.42
BLK 360	1'203'548	100/0.03/0.11	0.76/0.77	1.45/4.43
VUX1-UAV	4'372	100/-0.12/0.12	0.75/0.43	1.67/3.7
miniVUX2	1'888	100/0.18/0.92	0.44/0.14	-2.94/4.45
ZebRevo	15'777	100/-0.06/0.13	0.73/0.59	0.5/3.92
GoPro8	29'523	80.3/0.3/1.5	0.87/0.51	0.5/2.59

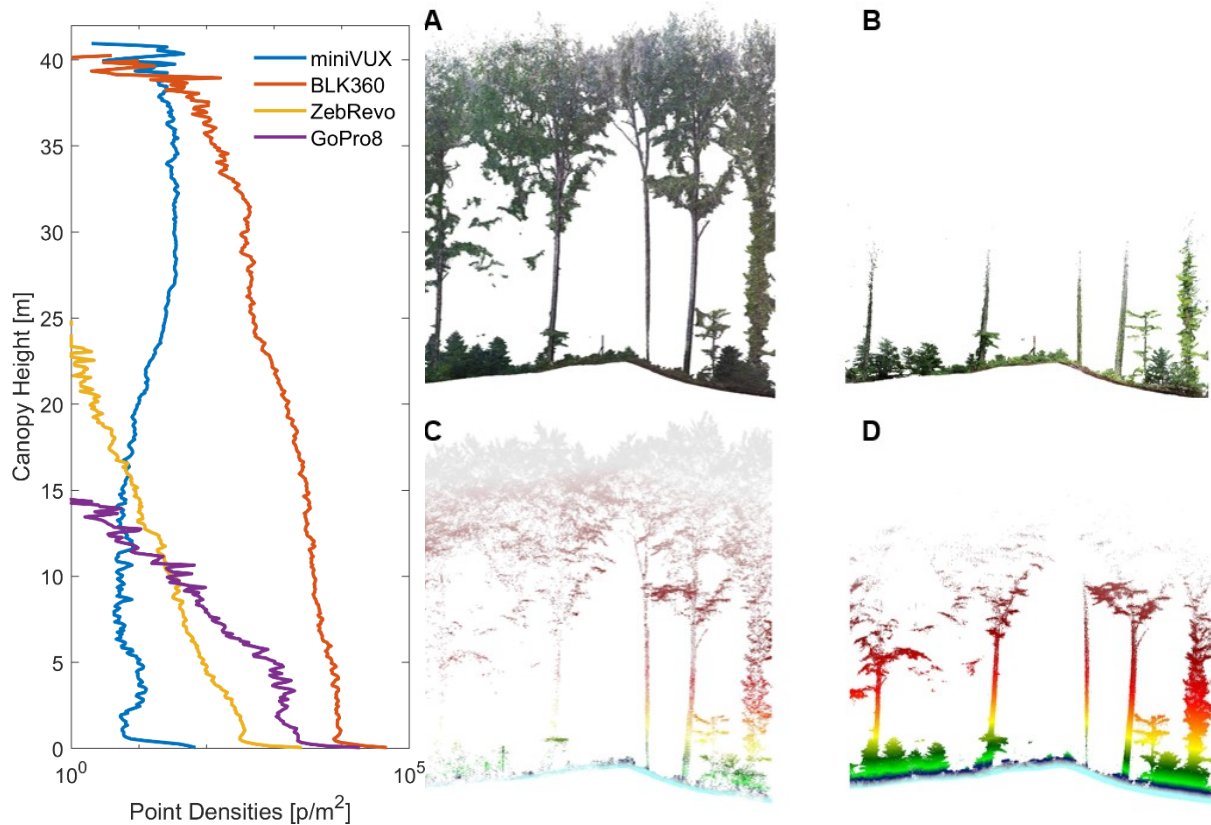


Figure 1: Vertical point density distribution and transects through point-clouds for BLK360 (A), GoPro 8 (B), miniVUX2 (C) and ZebRevo (D) acquisitions. BLK360 and GoPro point-clouds colored based on RGB camera information, miniVUX2 and ZebRevo point-clouds colored according to height above ground.

4. Conclusions

Close range remote sensing technologies are increasingly investigated regarding their potential for an operational application within NFIs. TLS reign as the high standard for acquiring high detailed 3D information at the single tree level. However, long and complicated acquisition procedures often neglect an operational inclusion within NFIs. Technologies allowing for faster data acquisition, however often at the price of a loss in precision and accuracy, such as MLS, UAVLS or even terrestrial or UAV SfM, therefore become increasingly more popular. In this study we analysed multiple sensor and acquisition approaches to extract terrain and tree information in three plots of varying complexity. Further analysis is needed to analyse the robustness of each approach in terms of applicability within a national forest inventory. Nevertheless, close range remote sensing shows high potential for forest structure assessment within the framework of a NFI.

Acknowledgements

This work was supported by the Swiss National Forest Inventory (LFI).

References

- Bruggisser M, Hollaus M, Otepka, J. and Pfeifer N. 2020, Influence of ULS acquisition characteristics on tree stem parameter estimation. *ISPRS J. Photogrammetry*, 168: 28-40.
- De Conto T, Olofsson K, Gørgens E B, Rodriguez L C E and Almeida G, 2017, Performance of stem denoising and stem modelling algorithms on single tree point clouds from terrestrial laser scanning. *Computers and Electronics in Agriculture*, 143:165-176.
- Hyypä E, Hyypä J, Hakala T, Kukko A, Wulder M A, White J C, Pyörälä J, Yu X, Wang Y, Virtanen J P, Pohjavirta O, Liang X, Holopainen M, Kaartinen H, 2020, Under-canopy UAV laser scanning for accurate forest field measurements. *ISPRS Journal of Photogrammetry and Remote Sensing*, 164: 41–60.

A pan-tropical campaign to link architectural and biophysical traits

Phil Wilkes^{1,2}, Alexander Shenkin³, Harm Bartholomeus⁴, Benjamin Brede⁴, Andrew Burt¹, Kim Calders⁵, Toby Jackson⁶, Alvaro Lau⁴, Eduardo Maeda⁷, Matheus Nunes⁷, Louise Terryn⁵, Matheus Boni Vicari¹, Hans Verbeeck⁵, Mathias Disney^{1,2}, Lisa P. Bentley⁸ and Yadvinder Malhi³

¹University College London, Department of Geography, Gower Street, London, WC1E 6BT, UK
Email: {p.wilkes, mathias.disney, a.burt}@ucl.ac.uk

²NERC National Centre for Earth Observation (NCEO)

³Environmental Change Institute, School of Geography and Environment, University of Oxford, South Parks Road, Oxford OX1 3QY, UK
Email: {alexander.shenkin, yadvinder.malhi}@ouce.ox.ac.uk

⁴Laboratory of Geo-Information Science and Remote Sensing, Wageningen University, P.O. Box 47, Wageningen 6700 AA, the Netherlands
Email: {alvaro.lausarmiento, harm.bartholomeus, benjamin.brede}@wur.nl

⁵CAVElab - Computational & Applied Vegetation Ecology, Department of Environment, Ghent University, Belgium
Email: {kim.calders, louise.terryn, hans.verbeeck}@ugent.be

⁶Department of Plant Sciences, University of Cambridge, Downing Street, Cambridge, CB2 3EA
Email: tj312@cam.ac.uk

⁷Department of Geosciences and Geography, University of Helsinki, Helsinki, Finland
Email: {eduardo.maeda, matheus.nunes}@helsinki.fi

⁸Department of Biology, Sonoma State University, 1801 E. Cotati Ave., Rohnert Park, CA 94928, USA
Email: lisa.bentley@sonoma.edu

1. Introduction

The variation in structure and form of trees is critical in linking leaf and tree physiology to tree function and to coordinate constraints on tree growth and mortality. Measurement of tree architecture is being revolutionized by ground-based 3D terrestrial laser scanning (TLS) in combination with new theoretical frameworks.

Here we present preliminary results from a project that has captured TLS data from forest plots spanning the tropics; from Peruvian cloud forest, to Ghanaian savanna, to Malaysian dipterocarp upland. Following leaf and wood trait campaigns previously conducted across a bottom-up forest carbon cycling network (GEM, Malhi et al. 2021), our goal is to understand the functional role of tree architecture in tree and forest demographics, resilience, and growth and reproduction strategy. This is crucial for predicting forest response to climate change.

We have so far constructed 3D tree models from 19 plots and ~250 species. Linking tree architecture with leaf and wood traits has resulted in an unprecedented database of tree 3D structural, demographic, and functional trait data.

2. Methods

A leaf traits campaign was conducted (see Asner et al. 2016) where a suite of physiological traits were measured for a subsample of trees (Shenkin et al. 2021). Plots cover a range of forest types and conditions spanning the tropics (Table 1 and Figure 1). For the same subsample of trees TLData were captured with a RIEGL VZ-400 (UCL, WU and Ghent) or VZ-400i (University of Helsinki) on a regular grid. (Wilkes et al. 2017). Each trait tree was tagged with a qrDAR code (<https://github.com/philwilkes/qrdar>) to enable post-scan identification.

Trees were automatically extracted in post processing and manually “cleaned” to remove neighbouring trees or add missing canopy sections. TLSeparation (Vicari et al. 2018) was run to remove leaf points; the remaining wood points were then enclosed using TreeQSM v.2.3 which produces a 3D, topologically coherent volume model for each tree. Analysis of tree structure was performed on QSMs using treestruct (<https://github.com/ashenkin/treestruct>).

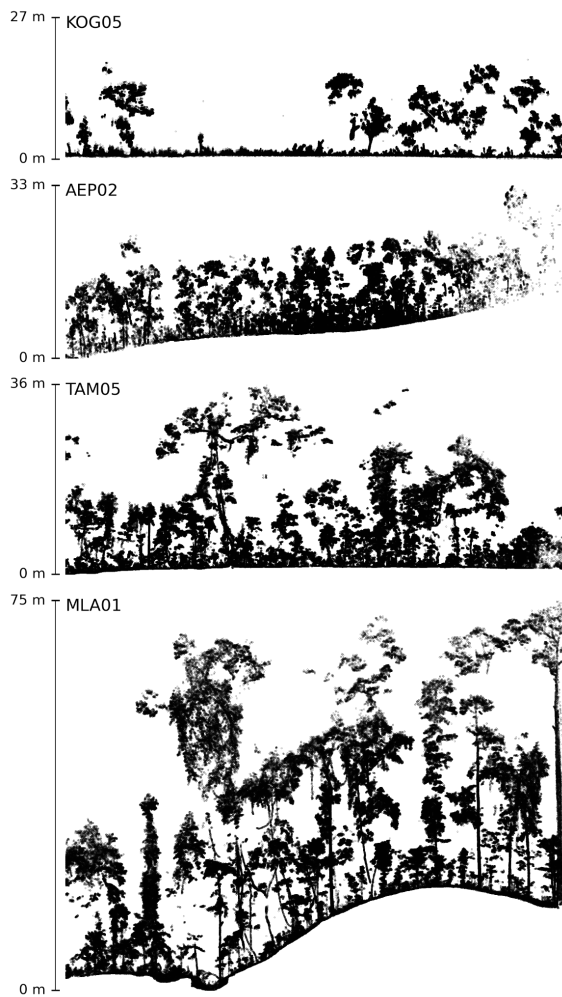


Figure 1. 1 m slices through TLS data for a subset of plots highlighting differences in forest structure and terrain.

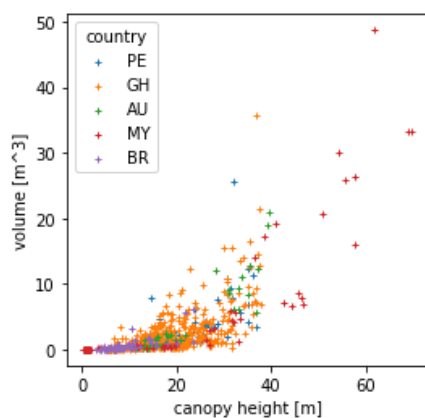


Figure 2. Tree height vs. volume for N=730 trees

3. Results and Discussions

So far, across the 19 plots, over 730 trees from 250 species have been extracted, modelled and linked with the trait database. This represents the largest architecture-trait database currently compiled spanning the tropics. Trees range in height from 2 - 100 m, including the tallest tropical tree yet discovered (Shenkin et al. 2019), and volume from 0.01 - 48.7 m³ (Figure 2).

Initial analysis indicates that the finer structures in tree crowns play a significant role in tree function, especially where surface area (as opposed to volume) is the critical scalar. We also find that tree and branch architecture lie on orthogonal axes suggesting that the former is determined by life-history and the latter by phylogeny. Finally, we find that wind, rather than gravitational stability, is likely a controlling determinant of tree height.

Branches were also harvested and modelled for a subsample of trees (Wilkes et al. in review). Early results suggest that branch architecture and tree shape comprise orthogonal axes in trait ordination analysis. New tools are required to analyse these smaller branch structures, due to the inherent limitations of TLS data and QSM reconstruction at these scales.

4. Conclusions

This project represents a coordinated collaboration between a number of institutions across the globe spanning nearly a decade of functional trait and TLS campaigns. The results coming from these coordinated efforts underscore the importance of collaboration and continuous funding streams. Furthermore, while these campaigns benefit science, they have also served to strengthen institutional ties across countries. We endeavour to offer these campaigns as models for those seeking to generate large, deep, and connected datasets across disparate ecosystems.

Table 1. List of plots. ISO country codes used. Team codes; WU Wageningen University, UCL University College London and UoH University of Helsinki. *N trees* is trees extracted so far.

Plot	Country	Year	Lat	Lon	Area (ha)	Grid (m)	Angular step	Team	N trees
ESP-01	PE	2014	-13.175	-71.595	1	20	0.06	WU	26
ANK-01	GH	2016	5.268	-2.694	1	10	0.04	UCL/WU	96
KOG-02	GH	2016	7.262	-1.150	1	20	0.04	WU	73
KOG-04	GH	2016	7.303	-1.180	1	20	0.04	WU	74
KOG-05	GH	2016	7.305	-1.165	1	20	0.04	WU	121
TAM-05	PE	2017	-12.831	-69.271	1	10	0.04	UCL	38
TAM-06	PE	2017	-12.839	-69.296	1	10	0.04	UCL	24
AEP-02	AU	2018	-17.147	145.587	0.5	10	0.04	UCL	27
AEP-09	AU	2018	17.121	145.634	1	10	0.04	Ghent	57
AEP-33	AU	2018	-17.285	145.571	0.5	10	0.04	UCL	27
AEP-41	AU	2018	-16.136	145.441	0.5	10	0.04	Ghent	32
MLA-01	MY	2018	4.747	116.970	1	10	0.04	UCL	48
SAF-03	MY	2018	4.691	117.588	0.5	10	0.04	UCL	35
SAF-05	MY	2018	4.716	117.610	0.5	10	0.04	UCL	10
CBN-01	MY	2019	4.951	117.792	1	10	0.04	UoH	43
CRP-01	BR	2019	-14.712	-52.352	0.25	10	0.04	UoH	5
CRP-02	BR	2019	-14.712	-52.352	0.25	10	0.04	UoH	7
NXV-01	BR	2019	-14.423	-52.210	1	10	0.04	UCL	60
VCR-02	BR	2019	-14.832	-52.168	1	10	0.04	UCL	14

5. Acknowledgements

Data collection Malaysia was conducted under permit JKM/MBS.1000-2/2 JLD.7 (87). Funding sources include Natural Environment Research Council (NERC) NE/P011780/1 and [weighing trees with lasers] and we acknowledge capital support from NERC National Centre for Earth Observation (NCEO) and UCL Geography. YM is supported by the Frank Jackson Foundation. EM and MN are funded by the Academy of Finland (318252, 319905). We are hugely grateful to our project partners; Sabah Biodiversity Center, Chief Minister's Department Office of Internal Affairs & Research, Land & Survey Department, Sabah Forestry Department, the Maliau Basin and Danum Valley Management Committees, Forest Research Center (Sabah), SEARRP, Lucas Cernusak and team at James Cook University and the Daintree Rainforest Observatory, Matt Bradford and CSIRO Atherton, the Jabalbina Yalanji Aboriginal Corporation, the Kuku Yalanji Traditional Owners, Ben Hur Marimon, Beatriz Marimon, Wesley Jonatar and Universidade do Estado de Mato Grosso (UNEMAT), Brienne Forbes, Esteban Velasquez and Cecilia Chavana-Bryant.

6. References

- Asner, Gregory P., et al. "Scale Dependence of Canopy Trait Distributions along a Tropical Forest Elevation Gradient." *New Phytologist*, 2016. <https://doi.org/10.1111/nph.14068>.
- Boni Vicari, M., et al., 2019. Leaf and wood classification framework for terrestrial LiDAR point clouds. *Methods Ecol. Evol.* 10, 680–694.
- Shenkin, A., et al., 2020. The Influence of Ecosystem and Phylogeny on Tropical Tree Crown Size and Shape. *Front. For. Glob. Chang.* 3, 109.
- Shenkin, A., et al., 2019. The World's Tallest Tropical Tree in Three Dimensions. *Front. For. Glob. Chang.* 2, 1–5.
- Wilkes, P., et al., 2017. Data Acquisition Considerations for Terrestrial Laser Scanning of Forest Plots. *Remote Sens. Environ.* 196, 140–153.

Influence of distance to the sensor on stem detection with car-mounted mobile laser scanner

R. de P. Pires¹, J. Holmgren¹, K. Olofsson¹, E. Lindberg¹, H. J. Persson¹

¹Dept. of Forest Resource Management, Swedish University of Agricultural Sciences, Umeå, Sweden -
Emails: {raul.de.paula.pires; johan.holmgren; kenneth.olofsson; eva.lindberg; henrik.persson}@slu.se

1. Introduction

The use of Mobile Laser Scanners (MLSs) has been studied in the last decades as an alternative to traditional forest inventory, providing accurate measurements of stem profiles and diameter at breast height (DBH) at tree level in relatively short time (Hyypä et al., 2020; Liu et al., 2021; Puliti et al., 2020).

There are only a few studies assessing the accuracy to measure forest structure for car- or vehicle-mounted MLS. For instance, Forsman, Holmgren, and Olofsson (2016) proposed an algorithm to detect stem points in an MLS point cloud acquired from a car, yielding an RMSE (Root Mean Squared Error) of 3.7 cm for DBH estimations. Later, Čerňava et al. (2019) tested the performance of a MLS mounted on a tractor used under heavy canopy conditions. They reported an RMSE of 3.06 cm for DBH estimates. Both studies suggest that vehicle-mounted MLSs could be used to conduct forest measurements.

However, car-mounted MLSs might be restricted to the road or skid networks and cannot cover areas inside the forest. Before such MLSs could be used at large scale, it is important to understand the limitations. The main objective of this study is to assess the suitability of a car-mounted MLS to retrieve field reference data from the forest roads. In this study, we refer to distance to the road to express the distance from a specific tree or plot to the sensor's trajectory. The specific objectives are: (1) to propose an algorithm for ITD (Individual Tree Detection) with MLS data and (2) to assess the influence of the distance to the roadside on ITD.

2. Data and Methods

2.1 Study area and MLS system

The algorithm was validated on the Remningstorp test site, in southern Sweden (lat. 58°N, lon. 13°E). In total, we measured the position and DBH of the trees in 18 circular plots with 10 m radius, organized in 6 groups. In each group, three plot centers were aligned perpendicular to the road. In order to evaluate the effect of the distance from the road on the proposed method's accuracy, we divided the plots in 3 groups: the first group with the plots closer to the road, from 0 – 20 m, the intermediate group with the plots from 20 – 40 m from the road and last group, from 40 – 60 m. The plots had around 600 trees/ha (80% Norway spruce, 15% pine and 5% broadleaved) and a mean DBH of 27.5 cm.

The MLS data were collected with a car-mounted Riegl VUX-1LR sensor. The car operated with a speed of 5 km/h and the sensor was leaning 30 degrees from the horizontal plane. The sensor emitted near infrared pulses (1550 nm) at a repetition frequency of 820 Hz. The footprint was 5 cm at 100 m from the sensor. This setup yields point clouds with high resolution within scan lines (angular step width of 0.0066 degrees), but large distances between two consecutive scan lines (at least 10 cm). The point density varied according to the distance from the road, as in Figure 1.

2.2 Individual Tree Detection

The proposed ITD algorithm assumes that points belonging to the same stem appear in the point cloud as arcs, and identifies point clusters with a circular shape within scanlines, as in Forsman et al. (2016). Next, we fit circles to the identified arcs in order to eliminate point clusters that do not have a circular shape, using the modified version of Random Sample Consensus (RANSAC) algorithm described by Olofsson et al. (2014). Finally, since the trees were detected independently in each scan line, we needed to vertically aggregate the arcs in order to build individual tree stems. Thus, in the stem segmentation, we associated several arcs to a single stem from the circle center locations obtained in the

previous step, using an adaptation of the tree stem segmentation proposed by Holmgren et al. (2019). Once the arcs were segmented into stems, we recorded the position of the lowest arc as being the position of the stem.

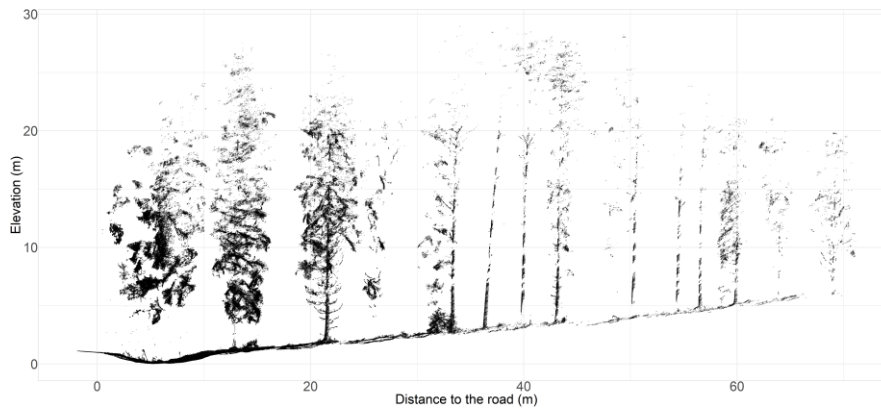


Figure 1: Representation of 3D point cloud, where the point density varies according to the distance from the sensor. The left side is closer to the sensor than the right side and has more points in the canopy and stem than the trees in the right side of the figure.

2.3 Accuracy Assessment

The accuracy of the ITD was assessed zone-wise by matching the MLS-detected trees with the field-recorded tree positions by conducting a search on the surroundings of each MLS-detected tree using a 30 cm radius. If an MLS-detected tree corresponded to a field-recorded one, the tree was considered a true positive. If it did not correspond to any field-recorded tree, it was considered as a false positive. Finally, we considered omission when a field-recorded tree position did not have any correspondence with the MLS-detected individuals. To better understand the performance of the ITD of trees with different size, they were grouped in three DBH classes: $DBH < 15$ cm, $15 \text{ cm} \leq DBH < 30$ cm and $DBH \geq 30$ cm. In each DBH class, we computed the precision (1) and sensitivity (2).

$$Precision = \frac{\text{Number of true positives}}{\text{Number of trees found}} \quad (1)$$

$$Sensitivity = \frac{\text{Number of true positives}}{\text{Number of true positives} + \text{Number of omissions}} \quad (2)$$

3. Results

Table 1. Individual tree detection's (ITD) accuracy according to the distance range from the road.

Zone	0 – 15 cm		15 – 30 cm		≥ 30 cm	
	Precision	Sensitivity	Precision	Sensitivity	Precision	Sensitivity
First (0 – 20 m)	0.0%	0.0%	92.2%	93.7%	85.0%	85.8%
Intermediate (20 – 40 m)	-	0.0%	98.1%	91.2%	93.3%	100%
Last (40 – 60 m)	-	0.0%	100%	71.9%	100%	87.0%

The ITD performance varied according to the tree's distance to the road and DBH class. No trees with $DBH < 15$ cm were detected correctly, regardless of the zone. We noticed the lowest precision in the study (Table 1) in the first zone, from 0 – 20 m, where more than 10% of the trees with $DBH \geq 30$ cm were false positives. The high number of heavy branches and the proximity to the sensor, which makes branches close to the road have a high point density, appears as the main reason for the observed false positives from 0 – 20 m.

The best overall ITD performance was obtained from 20 – 40 m, where the branches were smaller when compared to the ones in first zone, thus, being more easily separated from stems. In the intermediate zone, the point density was not as high as in the first zone, causing less false positives amongst the found trees with $DBH \geq 15$ cm (Table 1).

Finally, in the third zone, from 40 – 60 m, no false positives were noticed (Table 1). However, the sensitivity in the area was the lowest in the study: 71.9% on trees with DBH between 15 – 30 cm. This

may be explained by the fact that the point density decreases significantly in areas further from the road, consequently, it is more likely to have fewer returns from the trees in the last zone. However, the sensitivity increased to 87.0% for trees with DBH \geq 30 cm, which implies that trees with larger DBHs are found more easily at 40 – 60 m from the road.

4. Discussion

A benchmark of different MLS systems used for forest inventory was reported by Hyyppä et al. (2020), where backpack, handheld and under-canopy MLSs were compared. The authors obtained 100% precision with all the systems. Depending on the forest conditions and the sensor used, the sensitivity ranged from 79.0% to 95.2% with the backpack MLS, 76.7% to 92.9% with a handheld MLS and 81.4% to 92.9% with an under-canopy ULS (Unmanned aerial vehicle Laser Scanner). Our method yielded comparable sensitivities in the first and intermediate zones when considering trees with DBH \geq 15 cm. For small trees (DBH < 15 cm), the branches often occluded the stems, especially for Norway spruce trees which was the dominant species. The occlusion combined with the distance from the sensor prevented the detection of stems with DBH < 15 cm. The method we propose can be used at an optimal distance range in which the system is able to detect trees with good accuracy.

MLS systems have been studied for more than one decade as alternatives to manual forest inventories, but still they are not operationally used. The MLS system we tested can be used for automatic large-scale forest assessments, since it can take advantage of the forest roads and skid trails to make measurements on the go during field visits. In terms of autonomy, a vehicle-mounted MLS can operate for a longer time than, e.g., an ULS. Future studies may explore the potential of such system to obtain more measurements of the tree stems, capturing DBH, stem profile and volume. In addition, other methods to improve the ITD's precision in the first zone may be developed.

5. Conclusions

In this study, we proposed a method capable of identifying tree stems from car-mounted MLS point clouds, collected from the roadside. We could detect trees with a sensitivity and precision comparable with other MLSs that were located in the forest. We observed that the accuracy of ITD decreased as the distance from the trees to the road increased. We recommend establishing an optimal distance range where it is possible to obtain the highest precision and sensitivity.

Acknowledgements

This work was financed by Stora Enso as part of a strategic collaboration with the Swedish University of Agricultural Sciences.

References

- Forsman, M., Holmgren, J., & Olofsson, K. (2016). Tree stem diameter estimation from mobile laser scanning using line-wise intensity-based clustering. *Forests*, 7(9). <https://doi.org/10.3390/f7090206>
- Holmgren, J., Tulldahl, M., Nordlöf, J., Willén, E., & Olsson, H. (2019). Mobile laser scanning for estimating tree stem diameter using segmentation and tree spine calibration. *Remote Sensing*, 11(23), 1–18. <https://doi.org/10.3390/rs11232781>
- Hyyppä, E., Yu, X., Kaartinen, H., Hakala, T., Kukko, A., Vastaranta, M., & Hyyppä, J. (2020). Comparison of backpack, handheld, under-canopy UAV, and above-canopy UAV laser scanning for field reference data collection in boreal forests. *Remote Sensing*, 12(20), 1–31. <https://doi.org/10.3390/rs12203327>
- Liu, L., Zhang, A., Xiao, S., Hu, S., He, N., Pang, H., Zhang, X., & Yang, S. (2021). Single Tree Segmentation and Diameter at Breast Height Estimation with Mobile LiDAR. *IEEE Access*, 9, 24314–24325. <https://doi.org/10.1109/ACCESS.2021.3056877>
- Olofsson, K., Holmgren, J., & Olsson, H. (2014). Tree stem and height measurements using terrestrial laser scanning and the RANSAC algorithm. *Remote Sensing*, 6(5), 4323–4344. <https://doi.org/10.3390/rs6054323>
- Puliti, S., Breidenbach, J., & Astrup, R. (2020). Estimation of forest growing stock volume with UAV laser scanning data: Can it be done without field data? *Remote Sensing*, 12(8). <https://doi.org/10.3390/RS12081245>

Estimating canopy cover from ICESat-2

Lana Narine^{1*}, Lonesome Malambo² and Sorin Popescu³

¹Auburn University, Auburn, AL 36849
Email: lln0005@auburn.edu

^{2,3}Texas A&M University, College Station, TX 77843
Email: mmoonga@tamu.edu; s-popescu@tamu.edu

1. Introduction

Canopy cover is a fundamental vegetation structural parameter that is used to define a forest and support a range of vegetation applications, including habitat mapping (Lerman et al. 2014), modeling forest aboveground biomass (Narine et al. 2020) and assessing forest degradation (McCarley et al. 2017). NASA's Ice, Cloud, and land Elevation Satellite-2 (ICESat-2) mission offers an extraordinary capability to capture up-to-date information about forest ecosystems with data acquired by its Advanced Topographic Laser Altimeter System (ATLAS) since 2018. The capability of a spaceborne lidar to contribute to estimating biophysical forest parameters has been proven with ICESat-2's predecessor, ICESat, which operated from 2003 to 2009. For example, observations from ICESat's Geoscience Laser Altimeter System (GLAS) were used to map global canopy heights (Lefsky, 2010; Simard et al., 2011) and AGB (Hu et al. 2016), and characterize forest volume (Pourrahmati et al. 2015), and canopy cover (Tang et al. 2016). With the enhanced capability to provide greater spatial coverage and observations at higher spatial resolutions with ICESat-2, there are exceptional opportunities to derive up-to-date vegetation information as well as spatially comprehensive products through synergistic approaches with data from longstanding space-based programs like Landsat. As a first step to generating a wall-to-wall canopy cover product, the overall goal of this study was to examine ICESat-2's vegetation product data, ATL08, and custom-processed geolocated photon data, ATL03, for characterizing canopy cover. For this study, comparisons with reference canopy cover were made at the 100-m segment level (ATL08) and canopy parameters were examined for the development of predictive models. Relationships were also examined at the 30-m pixel scale, consistent with Landsat imagery and National Land Cover Database (NLCD) products (Homer et al. 2015).

2. Data and Methods

2.1. Study area

Data over a study site located in southeast Texas in the Sam Houston National Forest (SHNF) (30° 42' N, 95° 21' W) were examined for this study. The area exhibits vegetation conditions that are typical for the southeastern United States, consisting primarily of longleaf pine (*Pinus palustris*) stands, stands of loblolly pine (*Pinus taeda*), slash pine (*Pinus elliottii*), bottomland hardwoods, mixed hardwoods and pine hardwoods. This site was used for an initial aboveground biomass mapping study with ICESat-2 and pre-launch investigations with simulated ICESat-2 data.

2.2. Airborne lidar

Airborne lidar data acquired in 2018-2019 from USGS 3D Elevation program (3DEP) were used. Point clouds were clipped based on ICESat-2 tracks, processed to derive aboveground level heights (vegetation) and to calculate canopy cover as the proportion of returns above 4.6 m (USDA Forest Service 2014) for each matching ATL08 segment (Narine et al. 2019). For pixel-level comparisons, the normalized point clouds were clipped to match selected 30-m NLCD pixels and canopy cover was computed at this scale.

2.3. ICESat-2 data and processing

ICESat-2 ATL08 and corresponding ATL03 data from release 003 were downloaded from the National Snow and Ice Data Center (NSIDC). The ATL03 granule examined for this study was

ATL03_20181203072948_10030106_003_01. Using data from one strong beam (gt3r), custom noise filtering and photon classification algorithms (Popescu et al. 2018) were applied and ATL08 data were used to extract segments. Classified photons (noise, ground, canopy and top-of-canopy) in the ATL08 product were traced back to ATL03 and processed to compute canopy cover as the percentage of photons above 4.6 m withing a segment. Similarly canopy cover was computed from the custom-processed data and combined with corresponding ATL08 variables (Neuenschwander and Pitts 2019). To explore canopy cover at the 30 m pixel level, where ICESat-2 track lengths were at least 30 m across a pixel, photons from ATL08 and custom-processed data were used to compute canopy cover for those 30 m cells and were combined with reference estimates.

2.4. Data analysis

Canopy cover extracted from the custom processed ATL03 and ATL08 segments were compared with airborne lidar-derived canopy cover (reference) and the coefficient of determination (R^2) and RMSE values were used to assess the relationships. To understand the application of canopy parameters, linear regression models were used to relate canopy metrics (ATL08 and custom-processed ATL03) with reference canopy cover at the segment scale; 111 segments were used for model building and remaining 55 segments, for model evaluation. Comparisons at the 30-m scale were made with reference airborne lidar-derived canopy cover and NLCD canopy cover.

3. Results and Discussion

Segment-level comparisons between ICESat-2 derived canopy cover and reference airborne lidar estimates for the SHNF site, are shown in Figure 1.

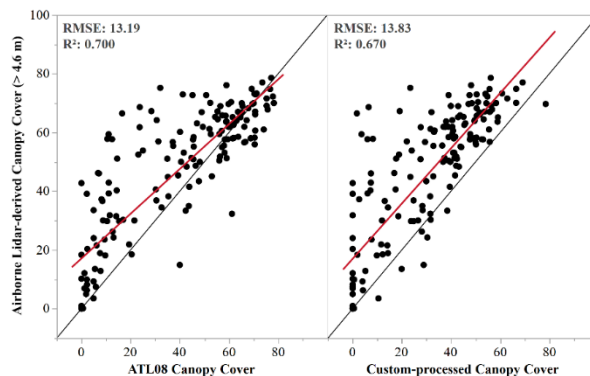


Figure 1: Airborne-lidar derived canopy cover versus ATL08 and custom-processed ATL03 canopy cover for segments over SHNF, Texas.

Canopy cover estimation using relative canopy height metrics from custom-processed dataset resulted in a model containing canopy cover (> 4.6 m) and maximum height (p -values < 0.001), which explained 70% variance of the airborne lidar-derived canopy cover (RMSE = 12%) with the test set (Figure 2). Similarly, ATL08 maximum height and canopy cover remained in the final canopy cover and yielded a R^2 and RMSE of 0.69 and 10% respectively (Table 1) (p -values < 0.001).

Table 1. Linear regression results for estimating canopy cover

Dataset	RMSE		R^2		Model
	Training	Test	Training	Test	
ATL08	9.17%	11.67%	0.80	0.70	$-1.34 + 1.65*\text{maximum height} + 0.41*\text{canopy cover}$
Custom-processed	12.05%	10.07%	0.77	0.69	$6.51 + 1.37*\text{maximum height} + 0.50*\text{canopy cover}$

Considering the full range of canopy cover computed at the pixel scale, ICESat-2-derived values were less correlated with reference airborne lidar estimates and weaker relationships were observed with NLCD canopy cover (2016 product) (Figure 2).

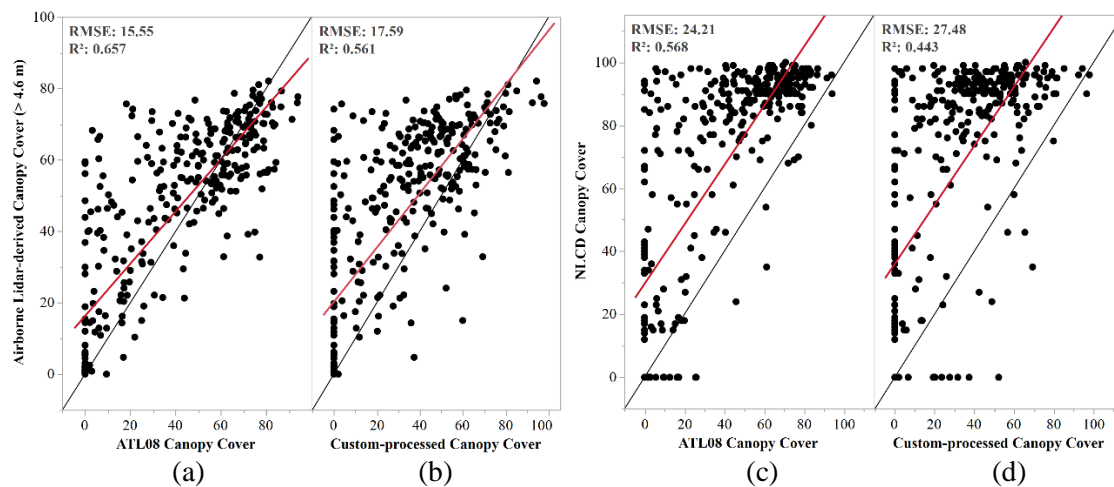


Figure 2: Airborne-lidar derived canopy cover versus ATL08 (a) and custom-processed ATL03 canopy cover (b); NLCD canopy cover versus ATL08 (a) and custom-processed ATL03 canopy cover (b) ($n = 339$).

4. Conclusions

While further investigations are needed to develop canopy cover characterizations with ICESat-2, current results for temperate forest conditions in the southern US highlight good agreements between ICESat-2-derived canopy cover from segments and reference airborne lidar estimates. Ongoing research serves to develop approaches for computing canopy cover over vegetated sites in the southern US and an examination of methods for developing a 30-m wall-to-wall product.

5. References and Citations

- Homer, C., Dewitz, J., Yang, L.M., Jin, S., Danielson, P., Xian, G., Coulston, J., Herold, N., Wickham, J., & Megown, K. (2015). Completion of the 2011 National Land Cover Database for the Conterminous United States - Representing a Decade of Land Cover Change Information. *Photogrammetric Engineering and Remote Sensing*, 81, 345-354
- Lerman, S.B., Nislow, K.H., Nowak, D.J., DeStefano, S., King, D.I., & Jones-Farrand, D.T. (2014). Using urban forest assessment tools to model bird habitat potential. *Landscape and Urban Planning*, 122, 29-40
- McCarley, T.R., Kolden, C.A., Vaillant, N.M., Hudak, A.T., Smith, A.M.S., & Kreitler, J. (2017). Landscape-scale quantification of fire-induced change in canopy cover following mountain pine beetle outbreak and timber harvest. *Forest Ecology and Management*, 391, 164-175
- Narine, L.L., Popescu, S., Neuschwander, A., Zhou, T., Srinivasan, S., & Harbeck, K. (2019). Estimating aboveground biomass and forest canopy cover with simulated ICESat-2 data. *Remote Sensing of Environment*, 224, 1-11
- Narine, L.L., Popescu, S.C., & Malambo, L. (2020). Using ICESat-2 to Estimate and Map Forest Aboveground Biomass: A First Example. *Remote Sensing*, 12, 1824
- Neuschwander, A., & Pitts, K. (2019). The ATL08 land and vegetation product for the ICESat-2 Mission. *Remote Sensing of Environment*, 221, 247-259
- Popescu, S.C., Zhou, T., Nelson, R., Neuschwander, A., Sheridan, R., Narine, L., & Walsh, K.M. (2018). Photon counting LiDAR: An adaptive ground and canopy height retrieval algorithm for ICESat-2 data. *Remote Sensing of Environment*, 208, 154-170

Acknowledgements

This study was funded by NASA ICESat-2 Science Team, Studies with ICESat-2 NNH19ZDA001N grant.

Deep Learning-based classification of tree species and standing dead trees using Silvi-Net

S. Briechle¹, P. Krzystek¹, G. Vosselman²

¹Munich University of Applied Sciences, Munich, Germany
Email: {sebastian.briechle; peter.krzystek}@hm.edu

²Faculty of Geo-Information Science and Earth Observation (ITC), University of Twente, Enschede, the Netherlands
Email: george.vosselman@utwente.nl

1. Introduction

Conservationists and forest managers rely on the precise mapping of individual trees from remote sensing data to efficiently derive forest attributes. In recent years, the additional quantification of deadwood in particular has attracted interest. However, tree-level approaches using segmented individual trees are still limited in their accuracy and their application is therefore mostly restricted to research studies. Furthermore, the combined classification of pre-segmented individual trees in terms of tree species and health status is important for practice, but has been insufficiently investigated so far.

In addition, the application of Deep Learning (DL)-based methods for the classification of pre-segmented individual trees based on lidar data has hardly been investigated so far. Hamraz et al. (2019) used a convolutional neural network (CNN) to classify coniferous and deciduous trees in a natural forest (330 stems/ha). By generating images from airborne laser scanning (ALS) point clouds (50 points/m²), a classification accuracy of 92% for conifers and 87% for deciduous trees was achieved. In a tropical wetland in southern China, Sun et al. (2019b) developed a patch-based classification algorithm for seven classes, including six individual tree classes (1,388 training samples, 362 test samples). Their most effective model classified image patches with an OA of 90%. In the same research area, Sun et al. (2019a) mapped 18 tree species using ALS data and high-resolution RGB imagery and achieved an overall accuracy (OA) of 73% at the individual tree level. Recently, Briechle et al. (2020) classified three tree species (pine, birch and alder) and standing dead pine trees with crowns using PointNet++ together with drone-based lidar data and multispectral (MS) imagery. In addition to 3D geometry, laser intensity values and MS features were also integrated into the classification process. Overall, their DL-based method (OA = 90%) was successful using raw 3D data and superior to a baseline method using an RF classifier and hand-crafted features (OA = 85%).

In this work, we introduce Silvi-Net, a dual CNN-based approach fusing airborne lidar data and MS images for 3D object classification.

2. Data and Methods

In our studies, we analysed the performance of Silvi-Net using data collected in two study areas, the Chernobyl Exclusion Zone (ChEZ) and the Bavarian Forest National Park (BFNP). For both study areas, the lidar point density was about 55 points/m² and the ground sampling distance values of the true orthophotos were 10 cm (ChEZ) and 20 cm (BFNP).

Using an interactive tool, single tree segments were manually labeled based on visual interpretation. In order to make our classification results independent of the segmentation quality, incorrect segments were generally not considered in the labeling process. In detail, the trees in the ChEZ were manually subdivided into the classes “pine”, “birch”, “alder”, and “dead tree”. In the BFNP, we labeled the trees with the categories “coniferous” (mostly spruce), “deciduous” (mostly beech and larch), “snag”, and “dead tree”. Here, “snag” refers to a partly or completely dead tree missing a crown or most of the smaller branches, whereas trees labeled “dead tree” are dead trees with crowns. The distinction between “snag” and “dead tree” was based on the subjective perception of three different research assistants. Finally, the labeled samples were randomly sorted into training, validation, and test datasets (Tables 1 and 2). Note that we also included class balancing for both training and validation data.

Table 1: Number of samples for study area ChEZ; train/val/test split: 56%/14%/30%.

Tree class	Training samples	Validation samples	Test samples
<i>pine</i>	93	23	51
<i>birch</i>	93	23	51
<i>alder</i>	93	23	51
<i>dead tree</i>	93	23	51
Σ	372	92	204

Table 2: Number of samples for study area BFNP; train/val/test split: 51%/22%/27%.

Tree class	Training samples	Validation samples	Test samples
<i>coniferous</i>	345	149	259
<i>deciduous</i>	345	149	202
<i>snag</i>	345	149	139
<i>dead tree</i>	345	149	145
Σ	1380	596	745

The methodology (Figure 1) is as follows: Initially, individual 3D trees are segmented from the lidar point cloud, and 12 silhouette-like side views are rendered and enriched with calibrated laser echo characteristics. Then, the projected outlines of the segmented trees are used to mask the MS orthomosaic and generate one image patch per tree. Next, two independent ResNet-18 networks are trained to learn relevant features from both datasets. This optimisation process is based on pre-trained CNN weights and recursive retraining of the model parameters. Subsequently, the extracted features are fused and fed to the final classification step. Here, we use a standard multi-layer perceptron that outputs 12 predictions per tree. Finally, we utilize majority voting to outvote individual misclassifications.

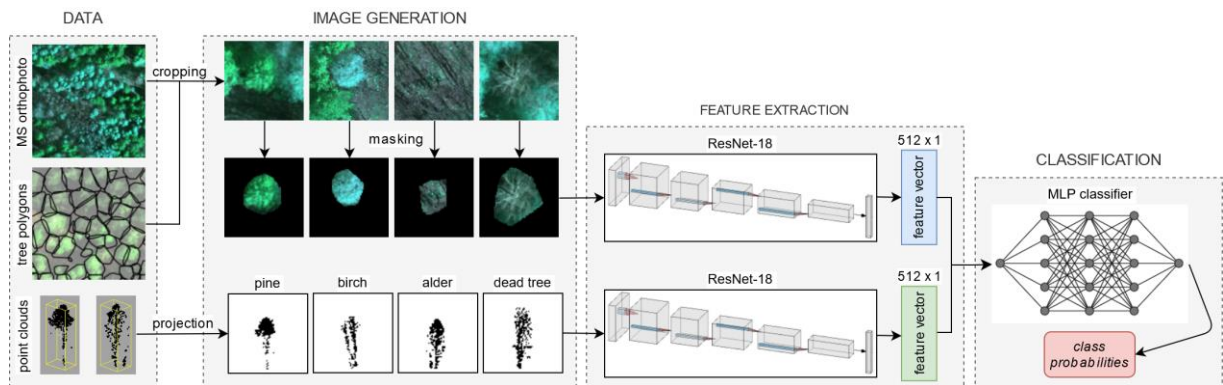


Figure 1: Outline of the proposed method, Silvi-Net.

3. Results and Discussion

In general, the trained models showed a high generalisation capacity on independent test data and achieved an OA of 96.1 % for the classification of pines, birches, alders and dead trees in the ChEZ and 91.5 % for conifers, deciduous trees, snags and dead trees in the BFNP (Figure 2). Interestingly, lidar-based imaging increased OA by 2.5 % (ChEZ) and 5.9 % (BFNP) compared to experiments using MS images only. Furthermore, Silvi-Net showed 11.3 % (ChEZ) and 2.2 % (BFNP) better OA compared to the baseline method PointNet++.

It should be noted that the datasets differ in terms of forest types and sensor models as well as geometric and spectral resolution. Both the ground resolution and the number of spectral channels of the MS images are clearly higher in the ChEZ. Thus, the MS images in this study area contain more extractable information for tree classification which mainly explains the superior results in the ChEZ.

Overall, Silvi-Net enables a convenient fusion of 2D and 3D data acquired by different sensor types. This allows information from the object geometry, laser intensity and reflection in the visible and NIR spectrum to be combined. Crucial here is the automatic extraction of meaningful features from previously generated 2D representations. The technique of transfer learning with pre-trained weights also enables fast model convergence, even with relatively small data sets.

Nevertheless, we want to make clear that a well-functioning upstream segmentation of single trees is mandatory for Silvi-Net to work well. In our study, we used almost perfectly delineated single trees. These were generated by the normalised cut segmentation algorithm by manually labelling optimal segments. This minimised the effect of under- or over-segmentation. From a practical point of view,

however, many tree segmentation methods will cause problems in forests with even higher stand density and more canopy complexity.

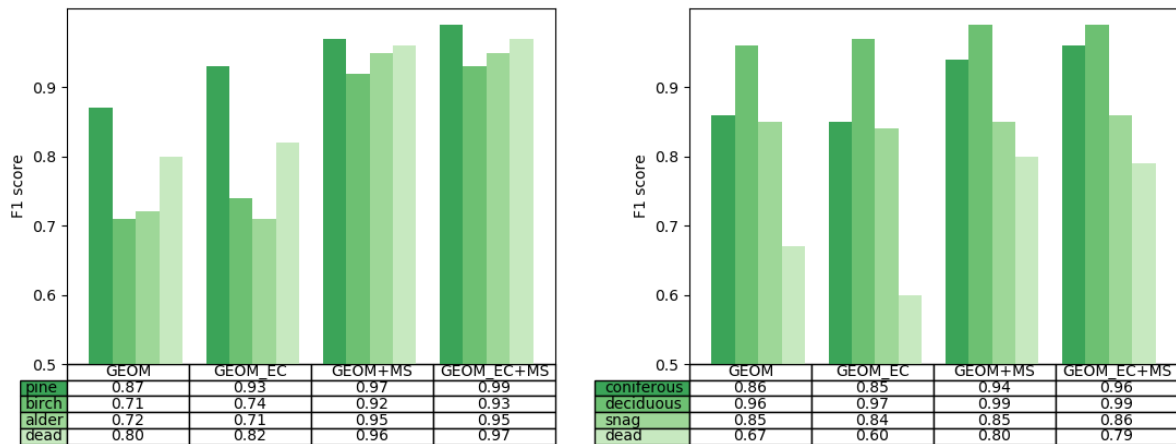


Figure 2: F1 scores per class for Silvi-Net in the ChEZ (left) and in the BFNP (right), using different feature sets.

4. Conclusions

In this paper, we presented Silvi-Net, a dual CNN-based approach for the combined classification of pre-segmented 3D tree objects, especially with respect to tree species and deadwood. The innovative contribution of our study is the fusion of MS image patches and multiple side views rendered from 3D lidar data in a CNN-based approach. Using the transfer learning technique, Silvi-Net enables fast model convergence, even for datasets with a reduced number of samples.

The effectiveness of our approach has been demonstrated using 2D and 3D datasets from two natural forest areas (400-530 trees/ha) collected with different sensor models and different geometric and spectral resolution. Consequently, users can produce reliable maps, which are of great importance for applications such as automated inventory and monitoring projects.

In future work, the challenge will be to reliably classify ten or more individual tree species and structurally complex forests. This objective can be supported by improved optical sensors providing high-quality lidar point clouds and high-resolution multi-channel images. In addition, off-the-shelf CNNs and transfer learning can be applied to the specific task of tree species classification, even for relatively small datasets.

Acknowledgements

The authors would like to thank Prof. Dr. Marco Heurich, for providing the remote sensing data in the study area BFNP. We also highly appreciate the support from Dr. Norbert Molitor for organizing the field trips in the ChEZ. This research was funded by Federal Ministry of Education and Research (BMBF), Germany (Grant No. 03FH004IX6).

References

- Briechle, S., Krzystek, P., Vosselman, G., 2020. Classification of tree species and standing dead trees by fusing UAV-based lidar data and multispectral imagery in the 3D deep neural network PointNet++. *ISPRS Ann. Photogramm. Remote Sens. Spatial Informat. Sci.*, V-2-2020, 203–210. <https://doi.org/10.5194/isprs-annals-V-2-2020-203-2020>.
- Hamraz, H., Jacobs, N., Contreras, M., Clark, C., 2019. Deep learning for conifer/deciduous classification of airborne lidar 3D point clouds representing individual trees. *ISPRS J. Photogramm. Remote Sens.* 158, 219–230. <https://doi.org/10.1016/j.isprsjprs.2019.10.011>.
- Sun, Y., Huang, J., Ao, Z., Lao, D., Xin, Q., 2019a. Deep learning approaches for the mapping of tree species diversity in a tropical wetland using airborne lidar and high-spatial-resolution remote sensing images. *Forests* 10. <https://doi.org/10.3390/F10111047>.
- Sun, Y., Xin, Q., Huang, J., Huang, B., Zhang, H., 2019b. Characterizing tree species of a tropical wetland in southern china at the individual tree level based on convolutional neural network. *IEEE J. Sel. Top. Appl. Earth Obser. Remote Sens.* 12, 4415–4425. <https://doi.org/10.1109/JSTARS.2019.2950721>.

Species classification of cork oak and stone pine trees using airborne laser scanning and individual tree detection

D. N. Cosenza¹, P. Soares¹, M. Tomé¹, J. M. C. Pereira¹, J. M. N. Silva¹

¹Forest Research Centre, School of Agriculture, University of Lisbon, Tapada da Ajuda, 1349-017 Lisbon, Email: dncosenza@gmail.com; {paulasoares; magatome; jmcperreira; joaosilva}@isa.ulisboa.pt

1. Introduction

Cork oak (*Quercus suber* L.) woodlands are important ecosystems in Mediterranean countries. They provide wood and non-wood materials, regulate water quality, prevent soil erosion, and provide cultural services for the community (Bugalho et al. 2011). This ecosystem is particularly valuable for Iberian economies, where 80% of global cork are produced (50% in Portugal, and 30% in Spain, APCOR 2019). Such importance made Portugal implement rigid protection laws to control exploitation of the cork oaks. The felling of cork oaks might be punishable by a fine, and authorized cuts (e.g., for road construction) must be compensated by the plantation of trees in an area 1.25 times larger than the intervened area. However, cork oak trees are frequently mixed with stone pines (*Pinus pinea* L.), which are used for cone and pine kernel production. The spatial heterogeneity of both species in the stands creates difficulties to traditional forest inventory. An alternative is using remote sensing techniques to collect tree-level data. In this case, individual tree detection (ITD) using remote sensing must be used along with species classification algorithms.

Airborne laser scanning (ALS) and ITD data are widely applied for tree species classification (Fassnacht et al. 2016). The process involves isolating trees in the point clouds and computing metrics to be used as predictors in classification models. Different approaches can be used for supervised classification, namely the linear discriminant analysis (LDA), k-nearest neighbors (kNN), random forest (RF), artificial neural networks (ANN), and support vector machines (SVM) – see Korpela et al. (2010) and Deng et al. (2016). Most research compared these approaches for the case of boreal and temperate forests. However, to the best of our knowledge, there is still limited information regarding their effectiveness in Iberian woodlands. Thus, this study aims to benchmark different classification approaches to distinguish between cork oak and stone pine trees in pure and mixed stands. We tested LDA, kNN, RF, ANN, and SVM assessing for classification accuracy with different training data sizes.

2. Methods

The study area was in the Alentejo region, in mid-south Portugal. The forest stands were in powerline wayleaves (Figure 1a). High-density ALS data (>45 returns m⁻²) were collected using a helicopter flying at low altitude. ALS data analysis was conducted using *lidR* package (Roussel et al. 2020), so please see the package documentation for further details about ALS data processing. Trees were segmented based on Silva et al. (2016) algorithm. Visual inspection was conducted to select 1000 cork oaks and 1000 stone pines trees to build the training data (Figure 1b). Packalén et al. (2012) simulated annealing algorithm was used to select 15 predictor metrics (Table 1). The selections were based on the Kappa coefficient, where $Kappa = (p_o - p_e) / (1 - p_e)$, p_o is the relative observed agreement, and p_e is the probability of chance agreement. LDA was trained using the *MASS* package (Venables and Ripley 2002), kNN with *yaImpute* (Crookston and Finley 2008), RF with *randomForest* (Liaw and Wiener 2002), ANN with *nnet* (Venables and Ripley 2002), and SVM with *e1071* (Meyer et al. 2020). kNN was trained using $k=5$, inverse distance weighting, and distance metric computed using Euclidean distance (kNN_Euc), Mahalanobis (kNN_Mah), most similar neighbor (kNN_MSN), and random forest (kNN_RF). ANN was trained using a single hidden layer with 10 neurons. All other model hyperparameters were set to package default.

Random and balanced samples of the original dataset were used to compare models. We tested training data sizes of 40, 60, 80, 100, 150, 200, 250, 300, 350, 400, 600, 800, 1000, 1500, and 2000 trees. The models were compared using the Kappa statistic and overall accuracy (i.e., percentage of agreement) computed by 10-fold cross-validation repeated 100 times for each training data size.

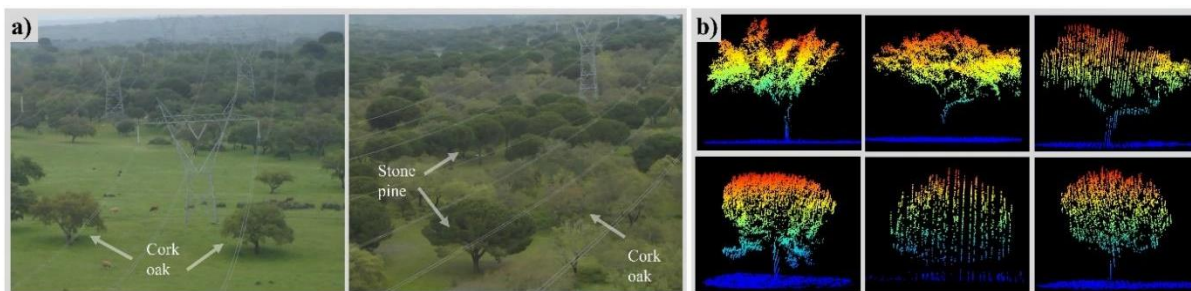


Figure 1: a) Images of the area; b) Examples of cork oak (top row) and stone pine (bottom row) trees.

Table 1. ALS metrics used in the models.

Type	Metrics*
LDA	$h_{35}, h_{45}, h_{60}, h_{80}, h_{95}, h_{d3}, h_{d8}, h_{smean}, h_{max}, h_{sd}, h_{kurt}, i_{dq90}, i_{sd}, curv, line$
kNN_Euc	$h_{20}, h_{45}, h_{55}, h_{85}, h_{90}, h_{d4}, h_{d6}, h_{sd}, h_{amean}, h_{smean}, h_{cmean}, h_{skew}, i_{max}, i_{dq90}, plan$
kNN_Mah	$h_{10}, h_{45}, h_{75}, h_{85}, h_{90}, h_{d1}, h_{d4}, h_{d6}, h_{d7}, h_{d8}, h_{a2m}, i_{dq30}, i_{mean}, i_{skew}, sphe$
kNN_MSN	$h_{d5}, h_{d7}, h_{d8}, h_{d9}, h_{mean}, h_{amean}, h_{cmean}, h_{sd}, h_{a2m}, i_{mean}, i_{sd}, i_{skew}, \lambda_m, line, sphe$
kNN_RF	$h_5, h_{15}, h_{60}, h_{85}, h_{d2}, h_{d3}, h_{max}, h_{a2m}, i_{dq10}, i_{kurt}, i_{mean}, i_{sd}, line, sphe, hori$
RNA	$h_5, h_{10}, h_{20}, h_{40}, h_{75}, h_{d1}, h_{d2}, h_{d6}, h_{d7}, h_{d9}, h_{dq70}, i_{sd}, i_{skew}, hori, plan$
RF	$h_{30}, h_{40}, h_{85}, h_{90}, h_{d2}, h_{d6}, h_{d7}, h_{mean}, i_{sd}, h_{cv}, i_{dq10}, i_{dq90}, i_{kurt}, i_{sd}, line$
SVM	$h_{30}, h_{35}, h_{50}, h_{60}, h_{65}, h_{85}, h_{d8}, h_{skew}, i_{max}, i_{sd}, i_{dq10}, \lambda_b, line, sphe, anis$

*Prefixes h and i indicate return height and intensity metrics and subscripts indicate the following statistics: x -th percentile (x), maximum (max), mean ($mean$), square mean ($smean$), cubic mean ($cmean$), kurtosis ($kurt$), skewness ($skew$), standard deviation (sd), coefficient of variation (cv), interquartile distance range (iqr), percentage below the x -th height fraction (dx) in a total of 10 fractions, percentage of returns above 2 m ($pa2m$), percentage of returns above mean ($amean$), percentage below the x -th height percentile (qx); vertical complexity index (vci); eigen-based metrics: λ_s , medium (λ_m), and largest (λ_l) eigen values, anisotropy ($aniso$), curvature ($curv$), horizontality ($horiz$), linearity ($line$), planarity ($plan$), and sphericity ($spher$).

3. Results and discussion

Each approach had similar patterns for Kappa and overall accuracy (Figure 2). kNN_RF performed the best but comparable to RF and SVM. ANN had an intermediary performance. LDA, kNN_Mah, and kNN_MSN had poor and similar performances, while kNN_Euc performed the poorest. All approaches improved performance rapidly when more training data were used, but marginal improvements were noted after 400-600 training trees. For instance, when using >600 trees kNN_RF, RF, and SVM had Kappa values between 0.70-0.75 and 85-87% of accuracy, ANN had between 0.65-0.70 for Kappa and 82-84% of accuracy, and the others between 0.48-0.58 and 74-79%.

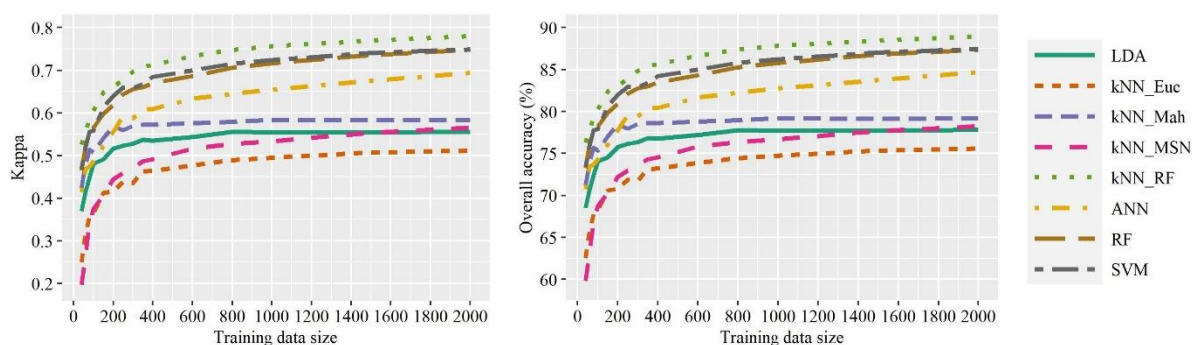


Figure 2: Kappa coefficient (left) and overall accuracy (right) for different training data sizes.

kNN_RF has been successfully used to classify tree species in boreal forests (Vauhkonen et al. 2010), and SVM, RNA, and RF in temperate forests (Deng et al. 2016). The advantage of RF and kNN_RF is their ability to handle high-dimensional datasets. However, Åkerblom et al. (2017) obtained better results with kNN_Euc distance than with SVM. Differently from Åkerblom et al. (2017), we did not tune the model hyperparameters, which might explain our poor performance for kNN_Euc. The minimal training data size was in line with the literature, where Korpela et al. (2010) found accuracies around 87% using kNN_MSN and just 300 training trees in boreal forests. Other factors might affect

the accuracy of the classification algorithms, such as the point density, ALS metrics, and forest structure. Our analysis involved only two classes, so it is likely that less effective results are achieved if more species are included. The effect of the ITD algorithm was also not considered, but the experience suggests this would not be significant if well-calibrated algorithms are used. Furthermore, our study involves sparse broad leaf and conifer trees, so it is possible that analyses based on satellite images also provide satisfactory results for a more cost-effective inventory. All these topics must be addressed in further studies for the case of woodlands and mixed stands of cork oak and other species.

4. Conclusion

kNN_RF, RF, and SVM were the best models to distinguish cork oak from stone pine trees using ALS and ITD. Balanced training data of 400 trees allowed training models with Kappa ≥ 0.7 and overall accuracy $> 83\%$.

Acknowledgments

We thank Rede Elétrica Nacional, SA (REN) for the datasets. This research was funded by the Forest Research Centre, a research unit funded by Fundação para a Ciência e a Tecnologia I.P. (FCT), Portugal (UIDB/00239/2020). D. N Cosenza was also supported by FCT [PD/BD/128489/2017].

References

- Åkerblom, M., Raunonen, P., Mäkipää, R., and Kaasalainen, M. 2017. Automatic tree species recognition with quantitative structure models. *Remote Sensing of Environment* 191: 1–12. doi:10.1016/j.rse.2016.12.002.
- APCOR [Portuguese Cork Association]. 2019. Information bureau: cork sector in numbers. Available from https://www.apcor.pt/wp-content/uploads/2019/02/CORK-SECTOR-IN-NUMBERS_EN.pdf [accessed 5 June 2021].
- Bugalho, M.N., Caldeira, M.C., Pereira, J.S., Aronson, J., and Pausas, J.G. 2011. Mediterranean cork oak savannas require human use to sustain biodiversity and ecosystem services. *Frontiers in Ecology and the Environment* 9(5): 278–286. doi:10.1890/100084.
- Crookston, N.L., and Finley, A.O. 2008. yaImpute: an R package for κ NN imputation. *Journal of Statistical Software* 23(10): 1–16. doi:10.18637/jss.v023.i10.
- Deng, S., Katoh, M., Yu, X., Hyypä, J., and Gao, T. 2016. Comparison of tree species classifications at the individual tree level by combining ALS data and RGB images using different algorithms. *Remote Sensing* 8(12): 1034. doi:10.3390/rs8121034.
- Fassnacht, F.E., Latifi, H., Stereńczak, K., Modzelewska, A., Lefsky, M., Waser, L.T., Straub, C., and Ghosh, A. 2016. Review of studies on tree species classification from remotely sensed data. *Remote Sensing of Environment* 186: 64–87. doi:10.1016/j.rse.2016.08.013.
- Korpela, I., Ørka, H., Maltamo, M., Tokola, T., and Hyypä, J. 2010. Tree species classification using airborne LiDAR – effects of stand and tree parameters, downsizing of training set, intensity normalization, and sensor type. *Silva Fennica* 44(2): 319–339. doi:10.14214/sf.156.
- Liaw, A., and Wiener, M. 2002. Classification and regression by randomForest. Available from <https://cran.r-project.org/package=randomForest> [accessed 14 September 2019].
- Meyer, D., Dimitriadou, E., Hornik, K., Weingessel, A., and Leisch, F. 2020. e1071: misc functions of the Department of Statistics, Probability Theory Group (Formerly: E1071), TU Wien. Available from <https://cran.r-project.org/package=e1071> [accessed 4 March 2021].
- Packalén, P., Temesgen, H., and Maltamo, M. 2012. Variable selection strategies for nearest neighbor imputation methods used in remote sensing-based forest inventory. *Canadian Journal of Remote Sensing* 38(5): 557–569. doi:10.5589/m12-046.
- Roussel, J.-R., Auty, D., Coops, N.C., Tompalski, P., Goodbody, T.R.H., Meador, A.S., Bourdon, J.-F., de Boissieu, F., and Achim, A. 2020. lidR: an R package for analysis of Airborne Laser Scanning (ALS) data. *Remote Sensing of Environment* 251: 112061. Elsevier. doi:10.1016/j.rse.2020.112061.
- Silva, C.A., Hudak, A.T., Vierling, L.A., Loudermilk, E.L., O'Brien, J.J., Hiers, J.K., Jack, S.B., Gonzalez-Benecke, C., Lee, H., Falkowski, M.J., and Khosravipour, A. 2016. Imputation of individual longleaf pine (*Pinus palustris* Mill.) tree attributes from field and LiDAR data. *Canadian Journal of Remote Sensing* 42(5): 554–573. doi:10.1080/07038992.2016.1196582.
- Vauhkonen, J., Korpela, I., Maltamo, M., and Tokola, T. 2010. Imputation of single-tree attributes using airborne laser scanning-based height, intensity, and alpha shape metrics. *Remote Sensing of Environment* 114(6): 1263–1276. Elsevier Inc. doi:10.1016/j.rse.2010.01.016.
- Venables, W.N., and Ripley, B.D. 2002. Modern applied statistics with S. *In* 4th edition. Springer New York, New York, USA. doi:10.1007/978-0-387-21706-2.

Exploring the innovation potential of single photon lidar for operational large-area forest inventories

Joanne White¹, Murray Woods²

¹ Canadian Forest Service, Canada
Email: joanne.white@canada.ca

² retired from Ontario Ministry of Natural Resources and Forestry, Canada
Email: woods.murray@gmail.com

Abstract

The use of lidar in operational forest inventories continues to proliferate. For the current forest inventory cycle, the province of Ontario, Canada has committed to the acquisition of single photon lidar (SPL) for approximately 550,000 km² of forest area over the next decade. We report on recent and ongoing investigations that explore the capacity of SPL to provide data that can effectively support area-based forest inventories and provide quality digital elevation products. We share results of our assessments of both forest inventory outputs and digital elevation models, informed by comprehensive independent reference data, and provide insights on lessons learned for large area implementation and opportunities for innovations to address other forest inventory information needs with the SPL data.

ICESat-2 data classification and canopy height validation--a case study in the northern region of China

Li He^{1,3}, Yong Pang^{2,3,*}, Zhongjun Zhang¹, Xiaojun Liang^{2,3}, Bowei Chen⁴

¹School of Artificial Intelligence, Beijing Normal University, Beijing 100875, China
Email: allen_he1996@outlook.com; zzj@bnu.edu.cn

²Institute of Forest Resource Information Technique, Chinese Academy of Forestry, Beijing 100091, China

³Key Laboratory of Forestry Remote Sensing and Information System, National Forestry and Grassland, Beijing 100091, China
Email: pangy@ifrit.ac.cn; Stanfordlxj@163.com

⁴Key Laboratory of Digital Earth Science, Aerospace Information Research Institute, Chinese Academy of Sciences, Beijing 100094, China
Email: rs.cbw@foxmail.com

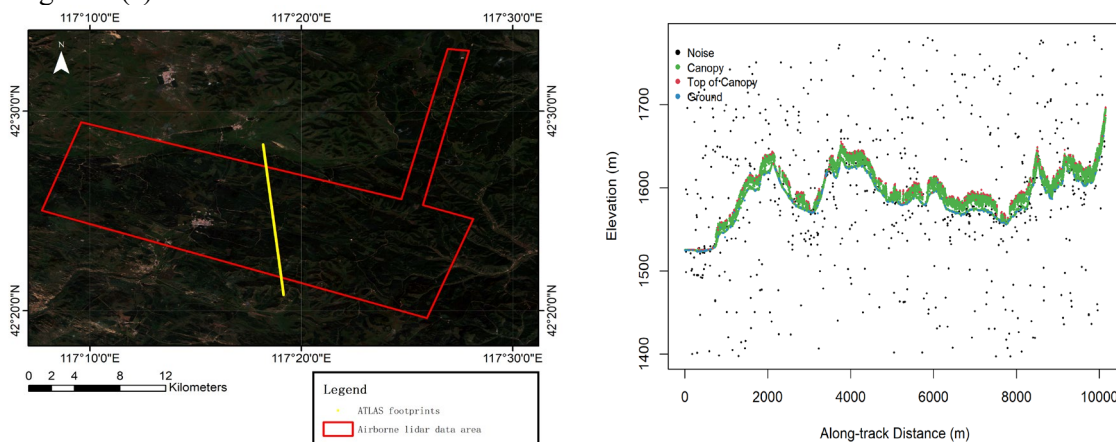
1. Introduction

NASA's ICESat-2 was launched in the fall of 2018 and is collecting a huge amount of data globally. One of ICESat-2 Level-2 products, ATL03, provides time, latitude, longitude, and ellipsoidal height for each photon downlinked from Advanced Topographic Laser Altimeter System (ATLAS) (Neumann et al., 2021). However, noise could seriously affect the observation results, accurate classification of photons is the basis of subsequent study. Some photon classification algorithms have been proposed in the past. Zhang's algorithm based on DBSCAN (2014) and Zhu's algorithm based on OPTICS (2021) use density clustering to distinguish photons. Their methods are affected by parameters and need to be verified in large-scale study area. ATL08, one of ICESat-2 products, is using the Differential, Regressive, and Gaussian Adaptive Nearest Neighbor (DRAGANN) filtering technique by adaptive neighborhood search to identify and remove noise photons (Neuenschwander et al., 2021). According to the distribution features of photons, Chen modified Local Outlier Factor (LOF) algorithm by defining the ellipse search area to filter the noise (Chen et al., 2019a).

Based on Chen's research, we proposed some methods to adapt the algorithm for large scale ATLAS data processing. Using ATL03 data in our study area, we classified photons by our improved algorithm. Then we used signal photons to predict heights of canopy. Results show that our improved algorithm could effectively remove noise photons.

2. Data and Methods

Our study area is located in the Saihanba Forest Farm, Hebei Province, north of China. We used the ATL03 data acquired at the night of June, 2019 by strong beam in this area as the original data for photon classification. The data of airborne lidar was used as reference data (Pang et al., 2021), and the acquisition time of airborne lidar data was the summer of 2018. The location of our study area is shown in Figure 1 (a).



(a) The location of our study area.

(b) The classification result of our algorithm.

Figure 1: The location of our study area and the classification result of our algorithm.

Firstly, based on LOF with Ellipse Searching Area, our methods proposed to adapt the algorithm for large scale ATLAS data processing are as followed:

(1) Coarse Denoising by LOF with Horizontal Ellipse Searching Area. After the signal interval is determined by the elevation histogram, coarse denoising is carried out. The purpose of this method is to use the algorithm to find ground photons, so as to filter out noise photons far away from ground surface. Because the density of ground photons is usually larger than others, and ground photons is always distributed in the lower part of signal photons, it is not hard to extract coarse ground photons by LOF algorithm. Then we can get coarse terrain in the area. In order to avoid local dense photons affecting the extraction of ground photons, the number of domain members can be selected larger in LOF algorithm.

(2) Accurate Denoising by LOF with Rotating Ellipse Searching Area. The purpose of this method is to reduce the influence of terrain slope on LOF algorithm by ellipse searching area adapted to terrain. Photons after coarse denoising are divided into several intervals along the track. We calculate the terrain slope by coarse ground photons in the interval. In each interval, rotating angle of ellipse searching area is equal to the terrain slope. Then, we calculate LOF scores for photons in the interval to classify signal photons and noise. In order to avoid the influence of boundaries on LOF, we set buffers on the left and right sides. Finally, according to the spatial distribution, the signal photons are classified as Top of Canopy photons, Canopy photons and Ground photons.

Secondly, we used airborne lidar data as the reference to analyze accuracy of our algorithm in different scales. We generated DTM and CHM with 1m resolution by airborne data, then extracted corresponding region by UTM coordinates of photons. The length of this region is the same as that of track about 10000 m, and the width is 17m, which is similar to the diameter of footprints. In this region, we calculated mean terrain height per meter along the track in DTM as the reference terrain height, and calculated the canopy heights of ATL data. CHM was used to compute canopy heights from airborne lidar data. Referring to the work by Neuenschwander et al. (2020), we regarded the 98th percentile of the reference heights (RH98) as evaluation metric, and set up nine different scales ranging 20 m to 100 m. ATL_RH98 means 98th percentile of signal photon heights, and ALS_RH98 means 98th percentile of all return heights.

3. Results and Discussion

According to the methods mentioned above, the result of classification of our algorithm is shown in Figure 1 (b). We could find that most signal photons can be classified correctly, and our method can adapt to terrain changes and accurately extract signal photons in steep terrain areas. A small number of signal photons close to the ground (higher than the ground) would be misclassified as noise due to their lower local density.

The results of canopy heights comparison are shown in Table 1 and Figure 2. The results show that canopy heights calculated from classified photons have good consistency with airborne lidar data, and we get the minimal Root Mean Squared Error and the maximal R-square at 70 m. When research scale goes beyond 50 m, canopy heights from classified photons are in better consistency with ALS data. At the same scale, canopy heights have smaller RMSE, which shows that our improved algorithm can effectively remove part of noise photons which are difficult to be removed by the original algorithm in Chen's research (Chen et al., 2019b).

The goal of this study is to verify the accuracy of photon classification algorithm by canopy heights. The following two reasons might contribute to those points with large errors of canopy height. Firstly, the noise with large local density are hard to be filtered by our methods and are misclassified as signal photons, resulting in the errors of canopy height. Secondly, the ATL03 data contains photons from land buildings, while the ALS data filters the data of land buildings. This difference will lead to errors. In future study, we will further improve our methods and reduce the errors caused by inconsistent data.

Table 1. The evaluation in the RH98 between our algorithm and airborne lidar data for different scales.

Scales	20 m	30 m	40 m	50 m	60 m	70 m	80 m	90 m	100 m
R ²	0.74	0.80	0.80	0.84	0.83	0.92	0.81	0.85	0.84
RMSE (m)	2.76	2.30	2.22	1.84	1.88	1.18	1.89	1.65	1.54

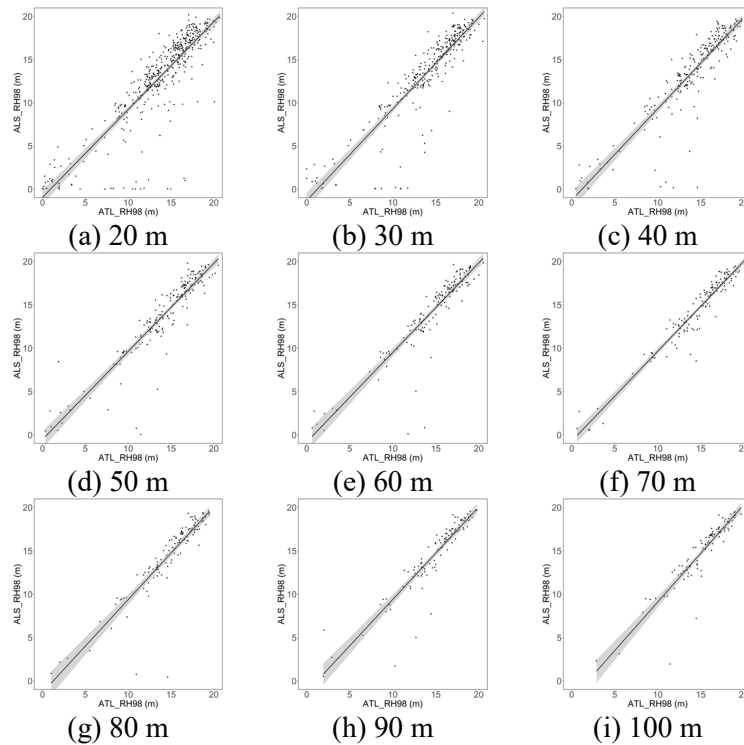


Figure 2: The comparison results in the RH98 between our algorithm and airborne lidar data for different scales.

4. Conclusions

In this study, we made some improvements to adapt the algorithm for large scale ATLAS data processing. We classified photons as Noise, Top of Canopy photons, Canopy photons and Ground photons in ATL03 data and by comparing canopy heights calculated by classified photons with that calculated by ALS data, the results indicate that our method can effectively separate signal photons and noise in different terrain.

Acknowledgements

This study was funded by the Natural Science Foundation of China (41871278) and National Key Research and Development Program of China (2017YFD0600404).

References

- Chen B W, Pang Y, Li Z Y, *et al*, 2019a. Ground and Top of Canopy Extraction From Photon-Counting LiDAR Data Using Local Outlier Factor With Ellipse Searching Area. *IEEE Geoscience and Remote Sensing Letters*, 16(9):1447-1451.
- Chen B W, Pang Y, Li Z Y, *et al*, 2019b. Potential of Forest Parameter Estimation Using Metrics from Photon Counting LiDAR Data in Howland Research Forest. *Remote Sensing*, 11(7):856-877.
- Neuenschwander A, Guenther E, White J C, *et al*, 2020. Validation of ICESat-2 terrain and canopy heights in boreal forests. *Remote Sensing of Environment*, 251 (2020) 112110.
- Neuenschwander A, Pitts K, Jelley B, *et al*, 2021. Ice, Cloud, and Land Elevation 1 Satellite 2 (ICESat-2) Algorithm Theoretical Basis Document (ATBD) for Land-Vegetation Along-Track Products (ATL08). National Aeronautics and Space Administration, Goddard Space Flight Center.
- Neumann T, Brenner A, Hancock D, *et al*, 2021. Ice, Cloud, and Land Elevation Satellite-2 (ICESat-2) Project: Algorithm Theoretical Basis Document (ATBD) for Global Geolocated Photons (ATL03). National Aeronautics and Space Administration, Goddard Space Flight Center.
- Pang Y, Liang X J, Jia W, *et al*, 2021. The comprehensive airborne remote sensing experiment in Saihanba forest farm. *National Remote Sensing Bulletin*, 25(4):904-917.
- Zhang J, Kerekes J, Csatho B, *et al*, 2014. A clustering approach for detection of ground in micropulse photon-counting lidar altimeter data. *2014 IEEE Geoscience and Remote Sensing Symposium*.
- Zhu X X, Nie S, Wang C, *et al*, 2021. A noise removal algorithm based on OPTICS for photon-counting LiDAR data. *IEEE Geoscience and Remote Sensing Letters*, 18(8):1471-1475.

GEDI data evaluation and canopy height change analysis--a case study in the Northeast of China

Xiaojun Liang^{1,2}, Yong Pang^{1,2*}, Zengyuan Li^{1,2}

¹Institute of Forest Resource Information Technique, Chinese Academy of Forestry, Beijing 100091, China;

²Key Laboratory of Forestry Remote Sensing and Information System, National Forestry and Grassland, Beijing 100091, China
Email: Stanfordlxj@163.com; pangy@ifrit.ac.cn

Highlight:

In order to evaluate the effectiveness and accuracy of Global Ecosystem Dynamics Investigation (GEDI) in canopy height measurement, a set of rules was designed to filter the GEDI L2A version 2 data and compare the consistency with airborne observation data. Then, the airborne data of two periods were combined to evaluate canopy height growth.

Key words: *GEDI, canopy height, data filter, Change of tree growth*

1. Introduction

A new generation of satellite mission of LiDAR observations Global Ecosystem Dynamics Investigation (GEDI) has launched and a member of data has released publicly (Dubayah et al., 2020), in which the Relative Height(RH) energy metrics were used to calculate canopy height. We conducted experiments to evaluate the effectiveness of GEDI canopy height inversion in low slope topography in the northern forest region of China. The 99th quantile height (H99) of airborne laser scanning (ALS) data was used to evaluate the accuracy of RH, and the changes in canopy height of larch forest were evaluated based on RH index combined with ALS data of two periods.

2. Content

First, GEDI data was filtered based on the method of the latest research results (Dorado-Roda et al., 2021; Guerra-Hernández et al., 2021; Rishmawi et al., 2021; Potapov et al., 2021). In addition, under the premise of satisfying the filter rules, it should be synchronized with ALS observation time as much as possible.

The screening rules are as follows: (1) Footprints located in the forest area, no forest management activities; (2) Value of quality flag was 1, do not affected by clouds and rain; (3) Different types of beams effectively covered the ALS observation area; (4) GEDI RH99 was greater than 2 m; (5) The subcompartment was buffered inward by 25 m to reduce the impact of positioning errors and stand edge effects.

The distribution of footprints filtered is shown in Figure 1, and the data collection time of GEDI and ALS is shown in Table 1.

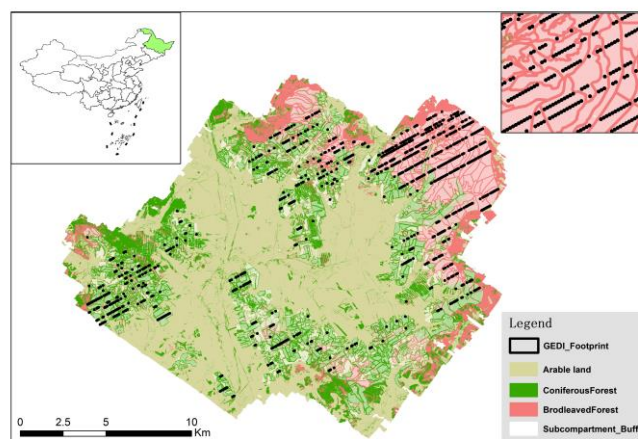


Figure 1: Distribution of filtered GEDI footprint for canopy height assessment

Table 1. Data acquisition description.

Data	Time(YYYY.M.D H)	Description
GEDI L2A	2020.5.2 2	Chinese time
	2020.5.6 1	Used for canopy height assessment
	2020.7.26 17	
	2019.7.4 2	Used to assess canopy height changes
	2019.5.11 23	
ALS data	2017.6	Used to assess canopy height changes
	2020.9	Used to evaluate the inversion and change of canopy height

Secondly, we used the method in the literature (Potapov et al., 2021) to calculate the H99 in the footprint level based on ALS data, and combined with the forest types in the footprint level covered area marked by hyperspectral image (HSI).

Then, we evaluated the GEDI canopy height based on the data of the filtered and marked. Based on the data usage instructions published by NASA LPDAAC (Dubayah et al., 2020), the difference of night and day acquisition time of GEDI L2A data on the data accuracy were analysed firstly. Then the full power beam and the "cover" beam were analysed. Secondly, based on the above analysis results, the inversion results were analysed by forest types. The analysis results based on determination coefficient R^2 were shown in Figure 2 below.

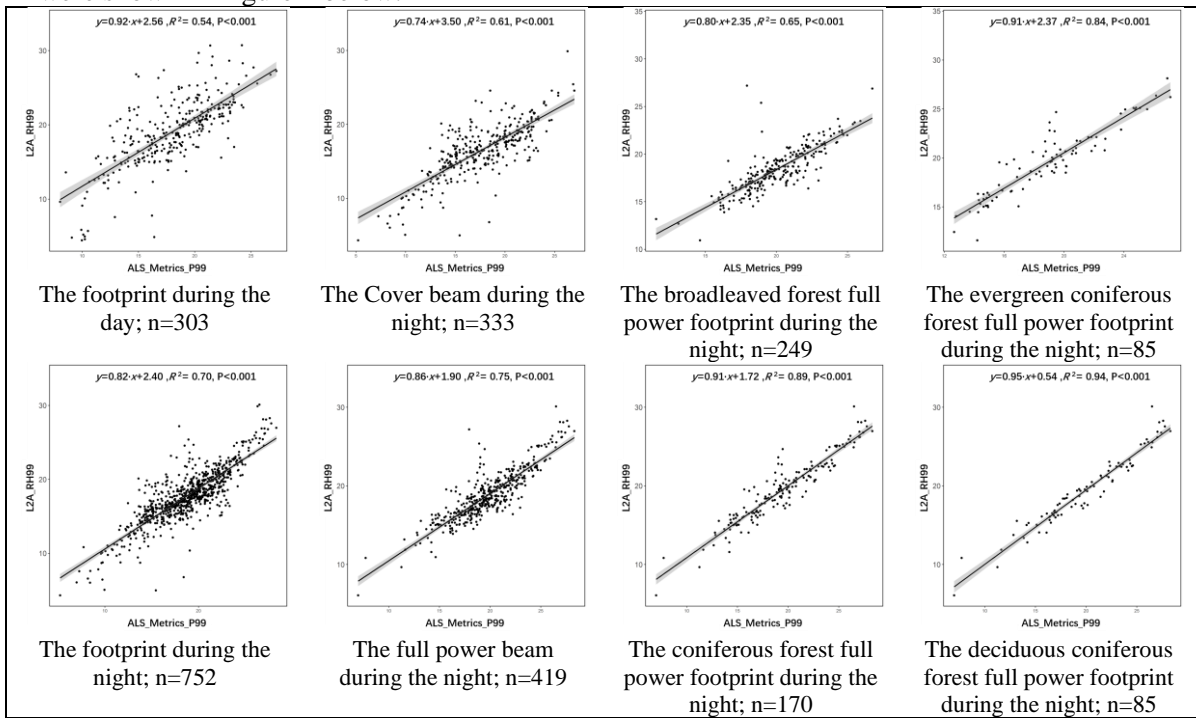


Fig. 2. Effectiveness and accuracy evaluation of canopy height inversion using GEDI RH index

According to the analysis results above, the footprints of full power beam during the night have the best inversion capability for the canopy height of deciduous coniferous forest. In further study, the results showed that the R^2 of 75th percentile height (usually used to describe mean canopy height) between ALS and GEDI were 0.8196 and 0.8165 for evergreen and deciduous forests, respectively.

Finally, the GEDI data in 2019 were filtered based on the above filtered rules, and the canopy height change analysis was made by combining the ALS point cloud data in 2017 and 2020. As shown in Fig.3, the change value from 2017 ALS to 2019 GEDI was 2.394m, and 1.298m from 2017 ALS to 2020 ALS, among all selected larch forest canopy height changes at footprint level.

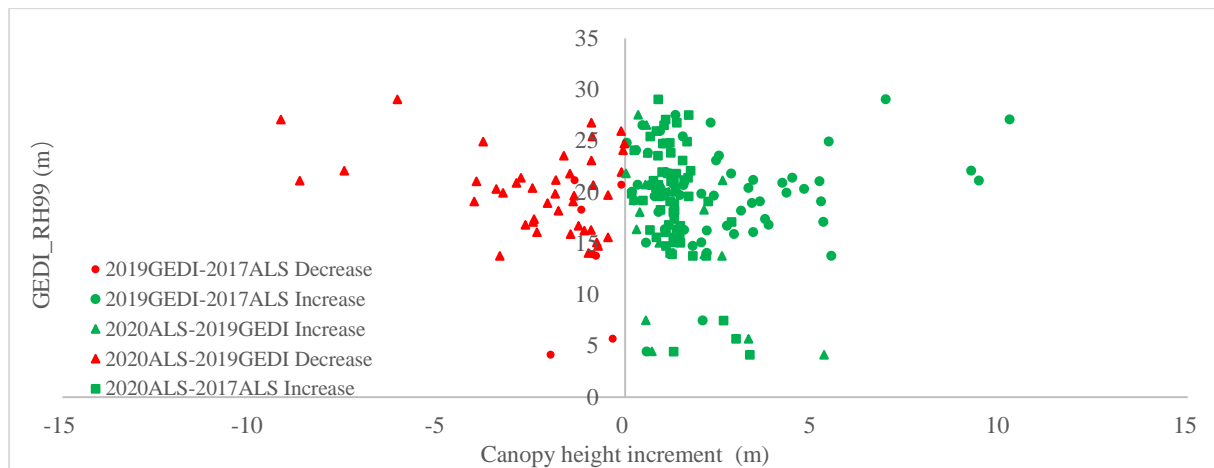


Fig. 3 Distribution of canopy height change in footprint level

As the results shown in Figure 3, GEDI overestimated coniferous forest change. However, the mean canopy height (calculated by H75 of ALS and RH75 of GEDI, respectively) was underestimated.

Acknowledgements

This study was supported by National Key Research and Development Program (2020YFE0200800 & 2017YFD0600404).

References

- Dorado-Roda I., Pascual A., *et al.* 2021. Assessing the Accuracy of GEDI Data for Canopy Height and Aboveground Biomass Estimates in Mediterranean Forests. *Remote Sensing*, (2021) 13:2279.
- Dubayah R., Scott G., Blair J B., *et al.* 2020. GLOBAL Ecosystem Dynamics Investigation (GEDI) Level 02 User Guide, 2020: Version 1.
- Dubayah R., Blair J B., Scott G., *et al.* 2020. The Global Ecosystem Dynamics Investigation: High-resolution laser ranging of the Earth's forests and topography. *Science of Remote Sensing*, 1(2020): 100002.
- Guerra-Hernández J., Pascual A. 2021. Using GEDI lidar data and airborne laser scanning to assess height growth dynamics in fast-growing species: a showcase in Spain. *Forest Ecosystems*, (2021) 8:14.
- Potapov P., Li X Y., Hernandez-Serna A., *et al.* 2020. Mapping and monitoring global forest canopy height through integration of GEDI and Landsat data. *Remote Sensing of Environment*, 253 (2021) 112165.
- Rishmawi K., Huang C Q., and Zhan X W. 2021. Monitoring Key Forest Structure Attributes across the Conterminous United States by Integrating GEDI LiDAR Measurements and VIIRS Data. *Remote Sensing*, (2021) 13:442.

Estimation of Spatial Distribution of Leaf Area Density in Canopies from Terrestrial LiDAR Point Clouds

M. Soma^{1,2}, F. Pimont¹, S. Durrieu², J-L. Dupuy¹

¹ UR 629 Ecologies des Forêts Méditerranéennes (URFM), INRAe, 84914 Avignon, France
Email: {maxime.soma;francois.pimont;jean-luc.dupuy}@inrae.fr

² UMR Territoires, Environnement, Télédétection et Information Spatiale (TETIS), INRAe, 34196 Montpellier, France
Email: {sylvie.durrieu}@inrae.fr

1. Introduction

Leaf area is a key variable of forest ecosystems functioning, as it controls energy, water and carbon exchanges between canopy and atmosphere. Quantifying and understanding these fluxes require a fine scale 3D description of vegetation structure, including the spatial distribution of leaf area density.

Leaf Area Densities (LAD, m^2/m^3) are the one-sided areas of leaves per unit of volume. Their vertical integration provides leaf areas per unit of ground surface, i.e. the Leaf Area Index (LAI, m^2/m^2), which is key variable for parametrization of ecophysiological and 3D radiative transfer models in forests. Yet, measuring LAD manually is complex and time-consuming and hemispherical photos methods are limited by vegetation clumping and are not designed for 3D estimations.

LiDAR technology has the potential to capture at high-throughput the required level of details for 3D description of canopy structure. While space-based or aerial LiDAR cover large areas, the size of their footprints and occlusion of signal limit the fine quantification of 3D spatial distribution of canopy components, in particular in medium to low vegetation. Terrestrial LiDAR operates from the ground level and provides high-density point clouds. This sensor has been widely used to assess wood volumes in forest inventories, generally relying on a discrete reconstruction of trunks and large branches.

The use of terrestrial LiDAR to quantify leaf area is limited by significant bottlenecks. First, the appropriate choice of variables and statistics of interest for relating point cloud to LAD is still debated. Second, beam divergence affects the sampling of heterogeneous surfaces (Béland et al., 2011), while interactions between impulsions and canopy elements depend on laser characteristics and vegetation material properties, involving complex physical processes. Third, a low number of sampling beams can bias LAD estimators, and may even preclude providing estimations in some areas of the scene (Pimont et al., 2018). The present work aimed at disentangling these various sources of biases and errors, and proposed unbiased methods for LAD estimations in forest plots from terrestrial LiDAR point clouds.

2. Methods and data

We relied on a statistical approach relating metrics from TLS point-clouds and attenuation coefficient of vegetation within elementary volumes called ‘voxels’. Our work characterised and limited the sensitivity of this approach to statistical biases, vegetation structure and sensor properties.

2.1 Theoretical estimation of LAD

The first step focussed on the evaluation and correction of statistical biases inherent to the various inversion methods of transmittance described in the literature. We relied on a theoretical framework to control vegetation properties and sampling with numerical references for LAD (Pimont et al., 2019).

Such simulations allowed testing promising variables, and formalizing biases in order to rigorously develop and compare unbiased estimators. A specific effort was put in making use of all geometric information available from TLS data, i.e. free path explored by beams within voxels before interception.

A maximum likelihood for the coefficient of attenuation within a given voxel was rigorously retrieved and corrections for both low sampling configurations and size of leaf elements were implemented (Pimont et al., 2018). Confidence intervals associated with this unbiased estimator were also provided.

2.2 Test of LAD estimators on actual tree branches

Theoretically unbiased estimators were tested at branch scale in laboratory conditions under various scanning conditions and compared with destructive references (Soma et al., 2018).

Three tree species of distinct leaf morphology were selected to evaluate the quality of LAD estimators in a range of structural diversity. Branches were scanned with two LiDAR instruments relying on two different technologies, namely phase-shift and time-of-flight instruments. Scans were performed from distances ranging from 2.5 m to 20 m. Series of scans were conducted on fully foliated branches, half-foliated and defoliated branches in order to extend the range of sampled LAD.

Leaves were manually harvested, weighted and 2D flat-scanned after each step to retrieve reference biomass and area of leaves for each branch. This step allowed testing robustness of LAD estimators regarding biases related with actual vegetation structure (clumping effect/voxel size, leaf size and morphology) and with instrument limitations (sampling variations, beam divergence and noise). An empirical correction factor H was estimated to account for these effects in the various tested configuration, resulting in the LAD estimate \widetilde{LAD} :

$$\widetilde{LAD} = \frac{H}{G} \tilde{\Lambda} = \frac{H}{G \sum z_e} \left(N_i - \frac{\sum_{hits} z_e}{\sum z_e} \right) \quad (1)$$

with z_e the effective free path of beams within a voxel, $\sum_{hits} z_e$ the sum of z_e for intercepted beams only, and G the effective area of interception of leaves, generally assumed to be equal to 0.5.

2.3 Field estimation of LAD at tree scale

The developed LAD estimators were applied to 15 isolated trees, scanned from 6 viewpoints.

We used LAD unbiased estimators and calibrations developed in previous steps to estimate total tree leaf areas and LAD profiles. Absolute references were obtained from manual harvest. This field campaign allowed evaluating our method, test the robustness of the approach and identify its limits.

2.4 Influence of sampling and estimations in occluded volumes with kriging

Further analyses were conducted with a virtual scene representative of a forest plot in which the reference 3D distribution of LAD is known -contrary to field experiments (Soma et al., 2021).

First, the aim of this numerical experiment was to evaluate the magnitude of biases and errors resulting from vegetation heterogeneity and sampling limitations at plot scale. Regarding references and confidence intervals, we disentangled the role of number of scans and voxel size on LAD estimations.

Second, we used this scene to develop a specific kriging method to provide an unbiased estimator for LAD estimation in poorly sampled and occluded areas (Soma et al., 2020).

3. Results and discussion

3.1 A theoretically unbiased LAD estimator

The numerical framework allowed the comparison of several LAD estimators regarding their potential biases and variances (Pimont et al., 2018). They are valid under several major assumptions, in particular a random sampling with infinitely thin beams. The newly proposed formulations are robust in a wider range of LAD values, elements size and number of beams than the usually used LAD estimators.

We recommend using the LAD estimator relying on the maximum likelihood approach because it was the less sensitive to the various sources of bias.

3.2 Voxel size and distance effects

Branch scale experiment revealed higher underestimations of LAD when voxel size increased whatever the type of vegetation or instrument. Such effect might result from heterogeneity of vegetation distribution within a given voxel. Additionally, with the phase shift instrument, raising the distance between the sensor and the measured branch yielded large overestimations, which might be related to beam divergence, which affects the effective footprint of the instrument.

Correction factors for these effects were provided for the studied species and according to voxel size. After these corrections, we obtained LAD estimations with 20% errors compared to actual vegetation using the recommended estimator with the tested instruments (Soma et al., 2018).

3.3 Tree scale estimation

Application of the method to individual trees showed that corrections developed in previous steps produced reliable estimations providing the canopy is appropriately sampled (Fig. 1).

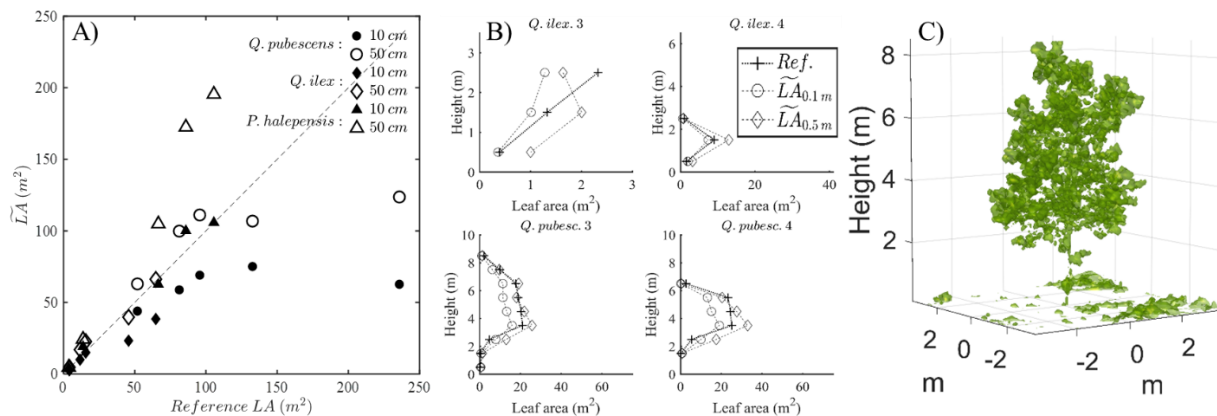


Figure 1. A) Comparison of LiDAR estimations of total tree leaf areas *versus* references for 3 species and 2 voxel sizes. B) Comparison of LAD profiles obtained from LiDAR with 0.1 m and 0.5 m voxels *versus* references. C) 3D distribution of leaf areas with 0.1 m voxel size.

3.4 Sampling limitations at plot-scale

At stand scale, the oversampling of voxels containing few vegetation compared to dense voxel negatively biased the computation of mean LAD profile. The magnitude of this bias depends on height in canopy, vegetation structure, scan design and voxel size. We found that using 0.5 m voxels was more appropriate because it eased corrections of other biases.

The developed LAD kriging method provided correct estimations in occluded voxels, and yielded better results at stand level than ignoring these areas. This method was validated in an actual forest plot.

4. Conclusions

The combination of theoretical analyses, field experiments and numerical experiments allowed to get a comprehensive understanding of processes involved in remote sensing of LAD with terrestrial LiDAR. In this study, the different sources of bias in LAD assessment were disentangled and ranked. Solutions to correct those biases at different scales, from branch to forest plots, have also been suggested.

References

- Béland, M., Widlowski, J.L., Fournier, R.A., Cote, J.F., Verstraete, M.M., 2011. Estimating leaf area distribution in savanna trees from terrestrial LiDAR measurements. *Agric. For. Meteorol.* 151, 1252–1266. <https://doi.org/10.1016/j.agrformet.2011.05.004>
- Pimont, F., Allard, D., Soma, M., Dupuy, J.-L., 2018. Estimators and confidence intervals for plant area density at voxel scale with T-LiDAR. *Remote Sens. Environ.* 215, 343–370. <https://doi.org/10.1016/j.rse.2018.06.024>
- Pimont, F., Soma, M., Dupuy, J.L., 2019. Accounting for wood, foliage properties, and laser effective footprint in estimations of leaf area density from multiview-LiDAR data. *Remote Sens.* 11. <https://doi.org/10.3390/rs11131580>
- Soma, M., Pimont, F., Allard, D., Fournier, R., Dupuy, J.-L., 2020. Mitigating occlusion effects in Leaf Area Density estimates from Terrestrial LiDAR through a specific kriging method. *Remote Sens. Environ.* 245, 111836. <https://doi.org/10.1016/j.rse.2020.111836>
- Soma, M., Pimont, F., Dupuy, J.-L., 2021. Sensitivity of voxel-based estimations of leaf area density with terrestrial LiDAR to vegetation structure and sampling limitations: A simulation experiment. *Remote Sens. Environ.* 257, 112354. <https://doi.org/10.1016/j.rse.2021.112354>
- Soma, M., Pimont, F., Durrieu, S., Dupuy, J.-L., 2018. Enhanced Measurements of Leaf Area Density with T-LiDAR: Evaluating and Calibrating the Effects of Vegetation Heterogeneity and Scanner Properties. *Remote Sens.* 10, 1580. <https://doi.org/10.3390/rs10101580>

Terrestrial Laser Scanning Reveal Connection Between Changes in Tree Stem Dimensions and Crown Structure

T. Yrttimaa ¹, V. Luoma ², N. Saarinen ¹, V. Kankare ¹, S. Junntila ¹, M. Holopainen ², J. Hyyppä ³, M. Vastaranta ¹

¹ School of Forest Sciences, University of Eastern Finland, 80101 Joensuu, Finland
Email: {tuomas.yrttimaa; ninni.saarinen; ville.kankare; samuli.junntila; mikko.vastaranta}@uef.fi;

² Department of Forest Sciences, University of Helsinki, 00790 Helsinki, Finland
Email: {ville.luoma; markus.holopainen}@helsinki.fi

³ Department of Photogrammetry and Remote Sensing, Finnish Geospatial Research Institute, National Land Survey of Finland, 02430 Masala, Finland
Email: juha.hyyppa@nls.fi

1. Introduction

Tree growth is a physio-ecological phenomena of high interest among researchers across disciplines. It is known that the growth of trees is affected by the availability of growth resources such as temperature, nutrients, water and sunlight as well as competition between trees (e.g. Tomé and Burkhart 1989; Ericsson et al. 1996). With limited growth resources, a tree aims to reach its living crown upwards for enhanced lighting conditions before allocating growth to its supporting structures (Oliver and Larson 1996). Therefore the allometric relationship between primary and secondary growth of trees has been considered as an indicator of trees' adaptation to the environment (King et al. 2006; Bartholomé et al. 2013).

Observing changes in tree characteristics has conventionally required either retrospective measurements of destructively sampled trees or modeling (Weiskittel et al. 2011; Kershaw et al. 2016). The use of close-range sensing techniques such as terrestrial laser scanning (TLS) have today enabled non-destructive approaches to reconstruct the three-dimensional (3D) structure of trees and tree communities in space and time (e.g. Dassot et al. 2011; Liang et al. 2016). Prior studies have shown that the characteristics of both stem (e.g. Liang et al. 2013; Olofsson and Holmgren 2016; Saarinen et al. 2017) and crown (e.g. Henning and Radke 2006; Seidel et al. 2011, 2015; Metz et al. 2014) can be characterized using point cloud-based methods. Changes in the structure of trees and tree communities can then be analysed when the point cloud acquisition campaign is repeated to cover a few years monitoring period (e.g. Luoma et al. 2019, 2021; Yrttimaa et al. 2020a).

This study aims at improving the understanding of tree allometry in general and the relationship between tree stem and crown dynamics in particular using bitemporal TLS point clouds. As presented in prior studies (e.g. Seidel et al. 2015; Pretzsch 2021), tree growth is seemingly affected by stem and crown structure that can be accessed using point cloud-based methods. The objective of this study was thus to investigate how tree crown structure and its dynamics reflect changes in stem characteristics. We hypothesize that the growth of attributes characterizing tree stem dimensions (i.e., basal area and stem volume) is related to the attributes characterizing tree crown structure and its changes (i.e., projection area, perimeter, surface area, volume, length, center of mass). The findings of this study are assumed to be beneficial in justifying upscaling applications where detailed ground-sampled information from the target tree characteristics of interest is generalized at the entire forest landscape level by making use of the allometric relationship between the target characteristics and features obtained from airborne remote sensing techniques.

2. Materials and methods

The experimental design of this study consists of 37 circular sample plots ($r = 11$ m) and 1280 trees and is located in Evo, southern Finland ($61^{\circ}19.6' N$ $25^{\circ}10.8' E$). The study site encompasses diverse southern boreal forest structures including both managed and single-layered as well as unmanaged and multi-layered forests. A multi-scan TLS campaign was first carried out in the spring/summer of 2014 (T1) and repeated in the autumn of 2019 (T2) to capture at least a five-year monitoring period in between the observations (for more details, see Yrttimaa et al. 2020a). A point cloud classification procedure presented in Yrttimaa et al. (2020b) was applied to detect trees and to separate points

originating from tree stem (i.e. stem points) from points originating from branches and foliage (i.e., non-stem points). The stem points and a point cloud processing method developed in Yrttimaa et al. (2019) were used to derive stem attributes such as basal area and stem volume at T1 and T2. Attributes characterizing crown structure were obtained by enveloping the non-stem points with a 2D/3D-convex hull object for which a set of features, such as projection area, perimeter, surface area, volume, length, and center of mass, were derived. Changes in the examined stem and crown attributes were computed by subtracting the T1-attributes from the T2-attributes (see Figure 1). Correlation coefficient (r) was utilized in assessing the relationship between the stem and crown attributes.

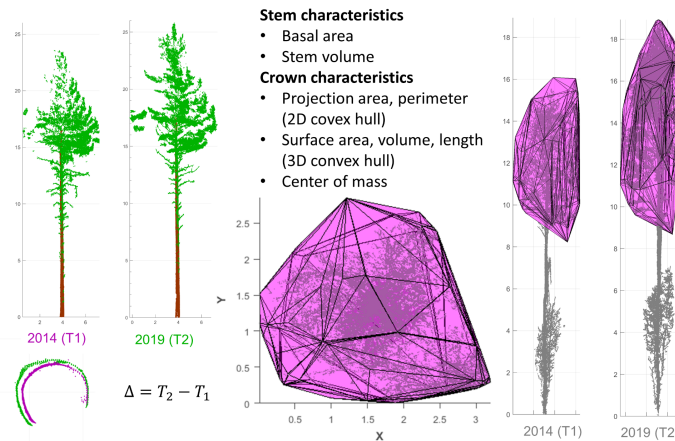


Figure 1. Illustration of the tree characteristics derived from the classified point clouds.

3. Results and discussion

A total of 736 trees could be detected from the point clouds at both time points with their stem and crown characteristics derived using the point cloud-based methods. Investigations of the relationships between stem growth and crown dynamics revealed that basal area increment and stem volume increment were best correlated with attributes characterizing the crown dimensions at T1 and T2. Correlation coefficient of 0.37-0.46 was obtained depending on the crown attribute in question (see Table 1). The relationship was noticed to be stronger ($r = 0.65-0.77$) for trees in managed sample plots with sparse and even canopy structure. This finding is in line with that reported by Seidel et al. (2015) that the physical dimensions of a tree crown are closely related with radial tree growth. However, seemingly lower correlations were recorded between stem growth and changes in the crown characteristics (Table 1). Changes in the center of mass of the crown as well as crown length were the most correlating crown characteristics with $r = 0.17-0.23$. This can be explained by the fact that, in general, tree growth is affected by competition between trees that can be captured through the structural status of a tree crown (Metz et al. 2013; Seidel et al. 2015). Here, the monitoring period covered a relatively short period of time with respect to the lifespan of trees in boreal forests. As per the general knowledge, a tree prioritizes reaching its living crown upwards for enhanced lighting conditions before allocating growth to its supporting structures (Oliver and Larson 1996). Thus, changed growing conditions first affect the dynamics of crown structure with stem growth following with a delay. More prediction power for estimating stem growth through the structure of tree crown is assumed to be gained by taking neighbourhood competition into account (see e.g. Metz et al. 2013).

Table 1. Correlation coefficient (r) indicating the relationship between increments in stem dimensions (basal area and volume) and crown characteristics derived at T1/T2 and their change (in parenthesis).

Crown characteristics	Basal area increment	Stem volume increment
<i>Projection area</i>	0.45 (0.05)	0.38 (0.10)
<i>Perimeter</i>	0.46 (0.04)	0.37 (0.09)
<i>Surface area</i>	0.46 (0.11)	0.40 (0.25)
<i>Volume</i>	0.45 (0.06)	0.42 (0.25)
<i>Center of mass</i>	0.40 (0.19)	0.36 (0.23)
<i>Length</i>	0.33 (0.17)	0.30 (0.23)

Acknowledgements

The study was funded by the Academy of Finland (grant numbers 31507, 345166, 331711 and 334001) and carried out within the SCAN FOREST research infrastructure (www.scanforest.fi).

References

- Bartholomé J, Salmon F, Vigneron P, Bouvet JM, Plomion C, Gion JM. 2013. Plasticity of primary and secondary growth dynamics in Eucalyptus hybrids: a quantitative genetics and QTL mapping perspective. *BMC plant biology*, 13(1), 1-14.
- Dassot M, Constant T, Fournier M. 2011. The use of terrestrial LiDAR technology in forest science: application fields, benefits and challenges. *Annals of forest science*, 68(5), pp.959-974.
- Ericsson T, Rytter, L, Vapaavuori E. 1996. Physiology of carbon allocation in trees. *Biomass and Bioenergy*, 11(2-3), 115-127.
- Henning JG, Radtke PJ. 2006. Ground-based laser imaging for assessing three-dimensional forest canopy structure. *Photogrammetric Engineering & Remote Sensing*, 72(12), 1349-1358.
- Kershaw Jr, JA, Ducey MJ, Beers TW, Husch B. 2016. Forest mensuration. *John Wiley & Sons*.
- King DA, Davies SJ, Noor NSM. 2006. Growth and mortality are related to adult tree size in a Malaysian mixed dipterocarp forest. *Forest Ecology and Management*, 223(1-3), 152-158.
- Liang X, Kankare V, Yu X, Hyypä J, Holopainen M. 2013. Automated stem curve measurement using terrestrial laser scanning. *IEEE Transactions on Geoscience and Remote Sensing*, 52(3), 1739-1748.
- Liang X, Kankare V, Hyypä J, Wang Y, Kukko A, Haggrén H, Yu X, Kaartinen H, Jaakkola A, Guan F, Holopainen M, Vastaranta M. 2016. Terrestrial laser scanning in forest inventories. *ISPRS Journal of Photogrammetry and Remote Sensing*, 115, 63-77.
- Luoma V, Saarinen N, Kankare V, Tanhuanpää T, Kaartinen H, Kukko A, Holopainen M, Hyypä J, Vastaranta M. 2019. Examining Changes in Stem Taper and Volume Growth with Two-Date 3D Point Clouds. *Forests* 10 (5), 382.
- Luoma V, Yrttimaa T, Kankare V, Saarinen N, Pyörälä J, Kukko A, Kaartinen H, Hyypä J, Holopainen M, Vastaranta M 2021. Revealing Changes in the Stem Form and Volume Allocation in Diverse Boreal Forests Using Two-Date Terrestrial Laser Scanning. *Manuscript submitted in publication*.
- Metz J, Seidel D, Schall P, Scheffer D, Schulze ED, Ammer C. 2013. Crown modeling by terrestrial laser scanning as an approach to assess the effect of aboveground intra-and interspecific competition on tree growth. *Forest Ecology and Management*, 310, 275-288.
- Oliver CD, Larson BC. 1996. Forest stand dynamics: updated edition. *John Wiley and sons*.
- Olofsson K, Holmgren J. 2016. Single tree stem profile detection using terrestrial laser scanner data, flatness saliency features and curvature properties. *Forests*, 7(9), p.207.
- Saarinen N, Kankare V, Vastaranta M, Luoma V, Pyörälä J, Tanhuanpää T, Liang X, Kaartinen H, Kukko A, Jaakkola A, Yu X, Holopainen M, Hyypä, J. 2017. Feasibility of Terrestrial laser scanning for collecting stem volume information from single trees. *ISPRS Journal of Photogrammetry and Remote Sensing*, 123, 140-158.
- Seidel D, Leuschner C, Müller A, Krause B. 2011. Crown plasticity in mixed forests—quantifying asymmetry as a measure of competition using terrestrial laser scanning. *Forest Ecology and Management*, 261(11), 2123-2132.
- Seidel D, Schall P, Gille M, Ammer C. 2015. Relationship between tree growth and physical dimensions of *Fagus sylvatica* crowns assessed from terrestrial laser scanning. *iForest-Biogeosciences and Forestry*, 8(6), 735.
- Tomé M, Burkhart HE. 1989. Distance-dependent competition measures for predicting growth of individual trees. *Forest Science*, 35(3), 816-831.
- Weiskittel AR, Hann DW, Kershaw Jr JA, Vanclay JK. 2011. Forest growth and yield modeling. *John Wiley & Sons*.
- Yrttimaa T, Saarinen N, Kankare V, Liang X, Hyypä J, Holopainen M, Vastaranta M. 2019. Investigating the feasibility of multi-scan terrestrial laser scanning to characterize tree communities in southern boreal forests. *Remote Sensing*, 11(12), 1423.
- Yrttimaa T, Luoma V, Saarinen N, Kankare V, Junttila S, Holopainen M, Hyypä J, Vastaranta, M. 2020a. Structural Changes in Boreal Forests Can Be Quantified Using Terrestrial Laser Scanning. *Remote Sensing*, 12(17), 2672.
- Yrttimaa T, Saarinen N, Kankare V, Hynynen J, Huuskonen S, Holopainen M, Hyypä J., Vastaranta, M. 2020b. Performance of terrestrial laser scanning to characterize managed Scots pine (*Pinus sylvestris* L.) stands is dependent on forest structural variation. *ISPRS Journal of Photogrammetry and Remote Sensing*, 168, 277-287.

Improving GEDI Footprint Geolocation using a High Resolution Digital Terrain Model

A. Schleich¹, M. Soma¹, S. Durrieu¹, C. Véga², J.P. Renaud^{2,3}, O. Bouriaud²

¹UMR Territoires, Environnement, Télédétection et Information Spatiale (TETIS), INRAE, Univ Montpellier, 500 Rue Jean-François Breton
34196 Montpellier, France

Email: {anouk.schleich; maxime.soma; sylvie.durrieu}@inrae.fr

²Laboratoire d'Inventaire Forestier, IGN, 14 Rue Girardet 54042 Nancy, France

Email: {cedric.vega; olivier.bouriaud}@ign.fr

³Office National des Forêts, 8 Allée de Longchamp 54600 Villers-les-Nancy, France

Email: jean-pierre.renaud-02@onf.fr

1. Introduction

In 2018, NASA launched the Global Ecosystem Dynamics Investigation (GEDI) mission, a high resolution lidar system installed onboard the International Space Station (ISS). It is producing high quality 3D observations of the Earth surface structure, which are highly relevant to study forest ecosystems at a global scale (Qi et al. 2019). GEDI data is composed of 25 m diameter circular footprints for which the waveform of the received energy intensity returned by the ground is recorded. Each GEDI footprint is georeferenced and its positioning accuracy (for version 1 releases) is estimated at 15-20 m in planimetry with a systematic component of 8-10 m and a noise of the order of 8 m (1σ). A final horizontal geolocation accuracy of 8 m is expected after further processing in the final version (Dubayah et al. 2020).

Compared to most other spatial satellites the ISS is much closer to earth, causing more variations in its orientation and altitude. Therefore, geolocating data acquired by ISS sensors is more difficult than geolocating data acquired by satellites (Dou et al. 2014). An improved geolocation of GEDI data is mandatory to evaluate their quality, by comparison with other earth observation data or field measurements, and to further facilitate their integration in ecosystem monitoring approaches. We propose a method to improve the georeferencing of GEDI footprints using a precise Digital Terrain Model (DTM).

2. Data and Methods

2.1 Data

The study site is located in south-western France and includes the Landes forest, the largest metropolitan French forest. All GEDI data of the study site has been downloaded from NASA's archive center. However, for this study, we will focus on version 1 of the level 2A product of the orbit N°3709, acquired during daytime on August 8th 2019. The area intersected by this orbit is mainly agricultural with several small tree patches. To avoid issues with ground elevation estimation, only high quality and full power data are used (Duncanson et al. 2020). The latitude, longitude and elevation of the lowest mode (i.e. ground peak) are respectively assimilated to the footprint centre coordinates and the mean ground elevation within the area covered by the footprint. The height of the highest canopy return (i.e. RH 100) is also extracted.

The reference DTM used is a 1 m resolution DTM (RGE Alti©) of the National Institute of Geographic and Forest Information (IGN) derived from both airborne lidar data and airborne stereoscopic images. The vertical accuracy (Root Mean Square Error, RMSE) is either 30 cm or 70 cm, depending on the data source. To allow comparison with GEDI, a moving window algorithm was applied to the DTM, by computing for each pixel the average DTM value in a 25 m circular window. The resulting 1 m resolution focal DTM was referred to as DTMref.

A photogrammetric digital surface model (DSM) derived from aerial photographs (1 m resolution) acquired in summer 2018 was also provided by IGN. As for the DTM, a DSMref is created using the same moving window algorithm and the maximum focal statistic. For each 1 m grid cell, the maximum

height value of the surrounding 25 m diameter circle of the DSM is assigned, which is assumed to be comparable to the elevation of the highest canopy return of a GEDI footprint.

2.2 Methods

The geolocation adjustment method assumes that, 1) errors between GEDI ground elevations and DTMref are minimal when the footprints are shifted by a distance in latitude (Y) and longitude (X) corresponding to the effective geolocation of the GEDI footprints and 2) the shift remains optimal for a subset of contiguous footprints acquired within a time period and despite possible abrupt changes in ISS orientation and altitude; the maximum length of such subset needs to be defined.

The optimal shift is obtained by testing all possibilities (by 2 m steps) within a range of shifts of ± 50 m in X and Y, and identifying the position which minimizes the difference between DTMref and GEDI elevations. Considering all potential shifts, leads to 2601 vectors of N elevation differences, N being the number of footprints of the considered orbit segment. For each vector, two statistic indicators were tested, the RMSE and the Mean Absolute Error (MAE), and were used to produce the corresponding error maps of the search area.

An accumulation flow algorithm is then applied to the error maps. A simple divergent flow algorithm, called FD8 (Freeman 1991), commonly used for watershed computations, is used. Thus, the lowest grid values should have the highest flow accumulation values (see Figure 1).

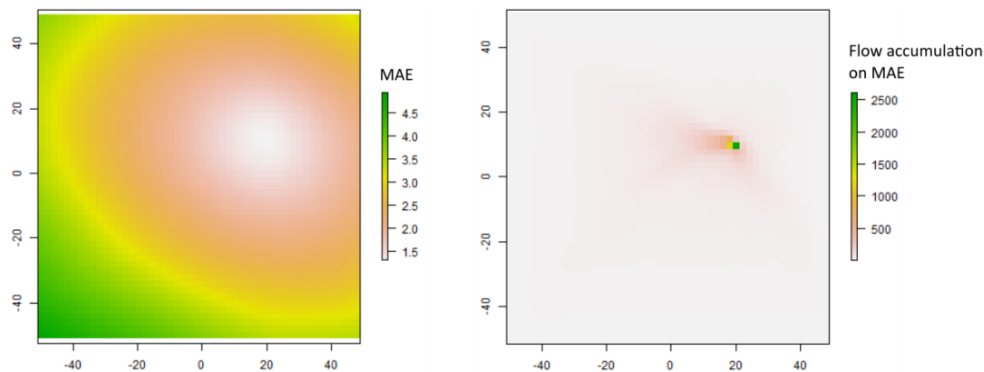


Figure 1: Example of error map showing the MAE for each tested shift (left) and the flow accumulation results applied to the error map (right).

Next, two approaches were tested. The first consists in defining the maximum value in the accumulation grid, as the optimal adjustment, i.e. the shift in Y and X that has to be applied to the GEDI footprint coordinates to improve their geolocation. The second approach is to keep the 1% of the highest accumulation values in the accumulation grid, and to calculate a weighted average of the coordinates to define the final optimal shift. This barycentre method is assumed to be less sensitive to outliers. In total, four methods were tested: maximum flow accumulation on RMSE and MAE error maps, and barycentre of maximum flow accumulation on RMSE and MAE error maps.

The number of footprints taken into account for the statistic indicator can be modulated. All footprints of an orbit that are within the study area can be used to find one global optimal shift. To take better account of ISS instability, one optimal shift can also be computed for each footprint individually, using a certain number of neighbouring footprints, which are selected based on GPS time and for a time interval centred on the single given footprint. In this study, a time interval of 0.215 seconds was chosen, resulting in about 200 neighbouring footprints, covering a zone of 3 by 2 km².

To evaluate our results the final RMSE and MAE before and after shifting are compared. An independent method is also used by applying the shifts to the DSMref and comparing the vegetation heights before and after applying the shifts.

3. Results and Discussions

When calculating a shift for each footprint individually, an important variability is observed. For the studied orbit, all shifts are positive, from 4 to 34 m for X and from 4 to 26 m for Y. The improved GEDI geolocations are oriented north-eastern from the original positions. There are gradual variations as well as abrupt changes.

As quick changes in the shift values are observed, computing only one shift for all data of an orbit seems less appropriate. Nevertheless it could be considered if a rough geolocation is sufficient.

The four methods give very similar results when looking at the overall RMSE (2.50 before and 2.10 m after adjustment) and MAE (1.45 before and 1.07 m after adjustment). Considering only ground elevation data, it is difficult to evaluate which method adjusts best the geolocation of the GEDI data.

When GEDI vegetation height (RH100) and the photogrammetric DSMref were compared with and without shifts, the MAE barycentre method was found to perform better. Before correction, the RMSE was 5.55 m and the MAE was 3.82 m. After correction, it respectively passed to 3.81 m and 2.66 m. The geolocation adjustment considerably improved the vegetation elevation estimation of GEDI (see Figure 2).

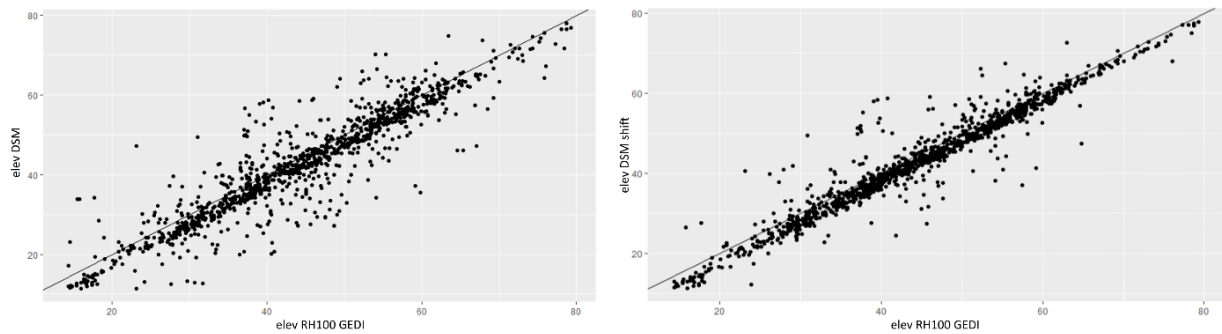


Figure 2: GEDI and DSM elevation without (left) and with the geolocation correction (right).

4. Conclusions

GEDI data provide information about forest structure at large scale and with a high sampling density, but their lack of georeferencing accuracy can be detrimental to their use in building models on forest attributes. The proposed method proved successful to improve footprint geolocation based on an orbit, but has to be further evaluated on more orbits and over more forests. Although the next generation of GEDI releases should have improved geolocation, the presented method, which can be performed in areas having high resolution DTM, could still be used to further improve footprint positioning.

Preliminary results show that the methodology provides corrections in the same direction than GEDI v2, but with lower RMSE and MAE values. The method will be applied on GEDI v2 and ICESat-2 data and in more complex environment (vegetation and topography) to assess the impact of elevation heterogeneity on lidar products and on the performance of the algorithm.

Acknowledgements

This research was funded by CNES within the TOSCA SLIM project, the financial support of CNES for the postdoctoral position of Maxime Soma and the cofounding of INRAE and IGN for the thesis of Anouk Schleich. We would also like to thank IGN for providing the photogrammetric DSM data.

References

- Dou C, Zhang X, Guo H, Han C and Liu M, 2014, Improving the Geolocation Algorithm for Sensors Onboard the ISS: Effect of Drift Angle, *Remote Sensing*, 6:4647-4659.
- Dubayah R, Luthcke S, Blair J, Hofton M, Armston J, Tang H. GEDI L1B Geolocated Waveform Data Global Footprint Level V001, 2020, distributed by NASA EOSDIS Land Processes DAAC
- Dubayah R, Blair J, Goetz S, Fatoyinbo L, Hansen M, Healey S, Hofton M, Hurtt G, Kellner J and Luthcke S, 2020, The Global Ecosystem Dynamics Investigation: High-resolution laser ranging of the Earth's forests and topography, *Science of remote sensing*, 1:100002.
- Duncanson L, Neuenschwander A, Hancock S, Thomas N, Fatoyinbo T, Simard M, Silva C, Armston J, Luthcke S, Hofton M, Kellner J and Dubayah R, 2020, Biomass estimation from simulated GEDI, ICESat-2 and NISAR across environmental gradients in Sonoma County, California, *Remote Sensing of Environment*, 242: 111779.
- Freeman T, 1991, Calculating catchment area with divergent flow based on a regular grid, *Computers and Geosciences*, 17:413-422.
- Qi W, Lee S, Hancock S, Luthcke S, Tang H, Armston J, and Dubayah R, 2019, Improved forest height estimation by fusion of simulated GEDI Lidar data and TanDEM-X InSAR data, *Remote Sensing of Environment*, 221: 621-34.

Stem Volume Modeling in Eastern Texas Loblolly Pine Forests

L. Malambo¹, S. Popescu¹

¹Ecology and Conservation Biology, Texas A&M University, College Station TX 77843, USA
Email: mmoonga@tamu.edu

1. Introduction

Stem volume is a key variable in forest inventory that is useful in the assessment of forest productivity. Accurate estimation of stem volume is therefore critical to support sound economic applications such as timber production (Radtke et al. 2017). Airborne LiDAR data are increasingly being applied for the quantification of forest resource volumes (Wulder et al. 2012). Measures derived from airborne lidar data such as tree heights and crown diameters together with relevant indirectly derived parameters such as diameter at breast height (DBH) are used to estimate stem volumes at tree or stand level based on published allometric equations or using regression analyses (Oono and Tsuyuki 2018). Increasingly, estimates of forest stem volumes are needed over large areas for resource managers to evaluate expected amount of timber from a woodshed for timber marketing and management planning. Airborne lidar, although effective for such a purpose, is usually not available over large areas. With the goal of developing wall to wall stem volume product, this study evaluated regression models relating lidar-based stem volume estimates and multitemporal Landsat 8 image data and ancillary existing vegetation height (EVH) datasets from the LANDFIRE program (Rollins 2009) in Loblolly pine (*Pinus spp.*) forests in eastern Texas. We developed reference stem volume estimates by applying published stem volume allometric equations to lidar derived individual tree measurements, which were then aggregated to 30 m Landsat spatial resolution. XGBoost (Chen et al. 2015) regression models were then set up between reference stem volume, as dependent variable, and Landsat data and ancillary EVH data, as predictors. We tested the performance of the regression models against test data at three Landsat image dates and assessed the benefit of combining multitemporal Landsat data in improving the accuracy of the developed models.

2. Data and Methods

2.1 Study site and data

Our study site (centered on Latitude 30° 27' 14.77" N, Longitude 94° 35' 54.54" W) is in southeastern Texas covering the area between the Texas-Louisiana border on one side and the Sam Houston National Forest on the other side. Several datasets were collected to support the development and evaluation of models for estimating volume including airborne lidar, Landsat, land cover and disturbance data. Airborne lidar data acquired in 2016 under the 3DEP program (Thatcher, Lukas and Stoker 2020) were obtained from OpenTopography.com. These data did not cover the entire study site but provided the needed near-ground truth data for estimating individual tree attributes including tree height and crown width. Landsat 8 surface reflectance data acquired on 03 Jan 2018, 24 May 2017 and 29 September 2017 were obtained from the USGS Earth Explorer website and enabled the development and scaling up of stem volume models to the entire study area. We also obtained 2016 LANDFIRE EVH to provide height information. EVH represents the average height of the dominant vegetation for a 30-m cell and is estimated by combining existing airborne lidar measurements and Landsat data (Rollins 2009). The National Land Cover Dataset (NLCD) was also used to provide species cover data, which enabled development of separate volume models for pines species. Forest cover disturbance data were generated over the study site using the LandTrendr algorithm (Kennedy et al. 2018) as implemented in the Google Earth Engine to facilitate exclusion of changed areas from the analysis.

2.2 Processing airborne lidar data

For adequate processing 100 330 m by 330 m sites in Pine forested areas were randomly selected. Airborne lidar data in each of these sites were processed to remove noise and normalized to aboveground level to enable the estimation of individual tree heights. The aboveground level data were then used for individual tree detection and crown segmentation using automated routines implemented in the lidR

package (Roussel et al. 2020). Local Variable Filtering method (Popescu and Wynne 2004) was applied for individual tree segmentation while a method developed by Silva et al (2016) was used for tree crown segmentation.

2.3 Generating reference volume data

Published allometric equations were used to estimate tree attributes not directly estimable from airborne lidar and tree-level stem volume. A critical attribute to estimating tree-level stem volume is tree diameter. An allometric equation for Loblolly Pines developed by Popescu (2007) was applied to estimate diameter and breast height (DBH). Given the crown diameter (CD) and tree height both in meters, DBH was calculate per tree according to (1) as:

$$DBH(cm) = 0.16 + CD + 1.22H \quad (1)$$

Having determined DBH for each tree, stem volume was calculated based on allometric equations in Radke et (2017), which we do not list here due to space limitation. All stem volume estimates at a tree level were then aggregated at the Landsat scale to facilitate retrieval of matching Landsat and EVH data.

2.4 Stem volume modelling using XGBoost

In our preliminary analyses, we evaluated several regression methods approaches including multiple linear regression, machine learning algorithms such as Random Forests, XGBoost and neural networks for predicting stem volume. XGBoost showed better performance and was adopted for this study. XGBoost, for Extreme Gradient Boosting, is an optimized distributed gradient boosting library which provides a parallel tree boosting to solve many data science problems in a fast and accurate way (Chen et al. 2015). Unlike Random Forests which builds independent trees, XGBoost builds trees sequentially, which provides opportunities for accuracy improvement. To facilitate model building, stem volume data from the 100 sites together with corresponding Landsat and EVH data were combined into one dataset. Non-pine and disturbed samples were removed prior to fitting models. To assess the benefit of multitemporal Landsat data, separate regression models were built using reference stem volume, as dependent variable, and each of the three Landsat images and EVH, as independent variables. A fourth model was built that combined all the Landsat 8 data and EVH. For both models, hyper-parameter tuning was carried out using a grid search approach to select optimal values for the learning rate, number of estimates and the maximum depth of the trees. For each of the models, 85% of the data was used for training and 15% for testing the accuracy of the prediction. The performance of the models was evaluated based on coefficients of variation (R^2), mean absolute error (MAE) and mean absolute percent error (MAPE).

3. Results and Discussion

The total number of samples collected from the 100 sites was 8454. Of this, 7186 were used for training the models and 1268 for testing. Table 1 summarizes the performance of the four regression models trained for predicting stem volume. Model performance varied by Landsat 8 date with the model II trained with data acquired on 05/24/2017 showing the best performance among separate models in terms of R^2 and MAE values. R^2 values ranged from 0.71 to 0.77 and MAE values ranged from 71.4 cubic feet (cu.ft.) to 81.7 cu.ft. estimates. Model performance improved when combined Landsat data were used. All model predictions were within 24 -29% of corresponding reference stem volume.

Table 1: Summary of model performance

Model	Landsat 8 data	R^2	MAE (cu.ft.)	MAPE (%)
1	3-Jan-18	0.71	81.7	29.79
11	24-May-17	0.74	74.5	26.36
111	29-Sep-17	0.72	79.3	28.19
1V	Combined data	0.77	71.4	24.44

In terms of variable importance, the EVH variable was overwhelming significant in all models. However, the variable importance for individual Landsat bands fluctuated with time which is indicative of impact of seasonal changes on forest structure.

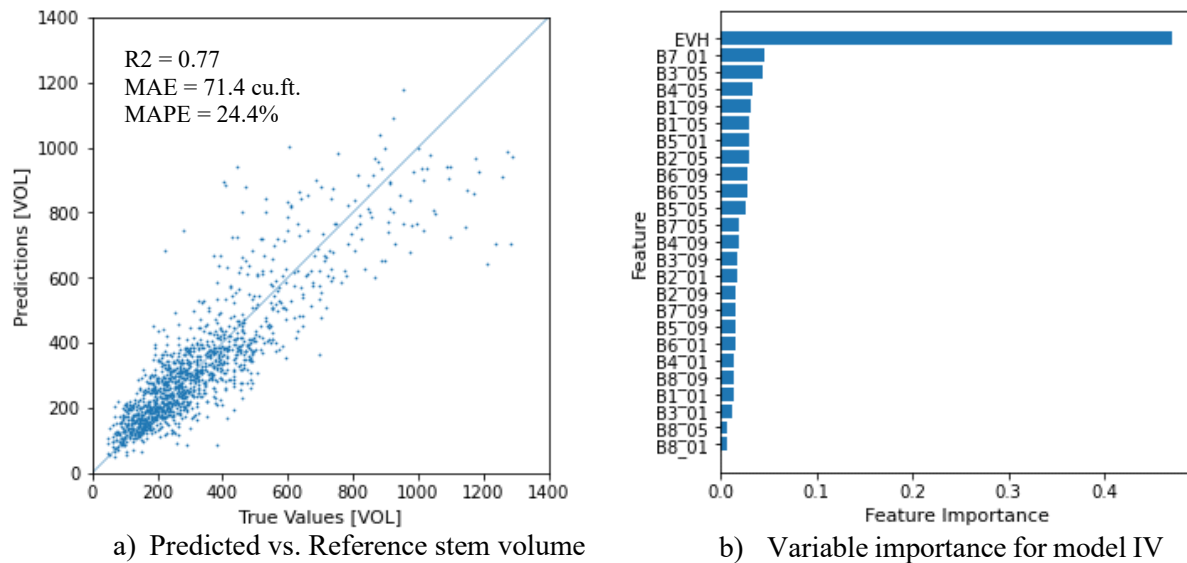


Figure 1: Combined Regression Model Performance. a) Scatter plot of predicted vs reference stem volume values, b) Variable importance for combined model. B indicates Landsat bands, suffixes _01, _05 and _09 indicate the respect image dates (Jan, May and September)

4. Conclusion

Results from this study show that there is a high potential for developing wall to wall product by leveraging available airborne lidar and multitemporal image data. The improved performance of the developed stem volume models indicates that there is a benefit in applying multitemporal image data, though the gain was not that large in our case. While promising results were obtained in this study, it is expected that even better performance could be achieved by extraction of more features from the EVH and Landsat data such as spectral indices, principal components and other transformations.

References

Chen, T., T. He, M. Benesty, V. Khotilovich, Y. Tang & H. Cho (2015) Xgboost: extreme gradient boosting. R package version 0.4-2, 1.

Kennedy, R. E., Z. Yang, N. Gorelick, J. Braaten, L. Cavalcante, W. B. Cohen & S. Healey (2018) Implementation of the LandTrendr algorithm on google earth engine. *Remote Sensing*, 10, 691.

Oono, K. & S. Tsuyuki (2018) Estimating individual tree diameter and stem volume using airborne LiDAR in Saga Prefecture, Japan. *Open Journal of Forestry*, 8, 205.

Popescu, S. C. & R. H. Wynne (2004) Seeing the trees in the forest. *Photogrammetric Engineering & Remote Sensing*, 70, 589-604.

Radtke, P., D. Walker, J. Frank, A. Weiskittel, C. DeYoung, D. MacFarlane, G. Domke, C. Woodall, J. Coulston & J. Westfall (2017) Improved accuracy of aboveground biomass and carbon estimates for live trees in forests of the eastern United States. *Forestry: An International Journal of Forest Research*, 90, 32-46.

Rollins, M. G. (2009) LANDFIRE: a nationally consistent vegetation, wildland fire, and fuel assessment. *International Journal of Wildland Fire*, 18, 235-249.

Roussel, J.-R., D. Auty, N. C. Coops, P. Tompalski, T. R. Goodbody, A. S. Meador, J.-F. Bourdon, F. de Boissieu & A. Achim (2020) lidR: An R package for analysis of Airborne Laser Scanning (ALS) data. *Remote Sensing of Environment*, 251, 112061.

Silva, C. A., A. T. Hudak, L. A. Vierling, E. L. Loudermilk, J. J. O'Brien, J. K. Hiers, S. B. Jack, C. Gonzalez-Benecke, H. Lee & M. J. Falkowski (2016) Imputation of individual longleaf pine (*Pinus palustris* Mill.) tree attributes from field and LiDAR data. *Canadian journal of remote sensing*, 42, 554-573.

Thatcher, C. A., V. Lukas & J. M. Stoker. 2020. The 3D Elevation Program and energy for the Nation. US Geological Survey.

Wulder, M. A., J. C. White, R. F. Nelson, E. Næsset, H. O. Ørka, N. C. Coops, T. Hilker, C. W. Bater & T. Gobakken (2012) Lidar sampling for large-area forest characterization: A review. *Remote Sensing of Environment*, 121, 196-209.

LEAF-WOOD SEPARATION AND TREE SKELETONIZATION FROM LOW RESOLUTION AND NOISY 3-D POINT CLOUDS

Tian Zhang, Sagi Filin

Mapping and Geo-Information Engineering, Technion – Israel Institute of Technology, Haifa, Israel
Email: {tianz,filin}@technion.ac.il

1. Introduction

Three-dimensional characterization of trees and their structure plays a pivotal role in forestry-related applications. It facilitates the estimation of biomass, monitoring of forest inventory, and helps to assess forest-fire risks (Vicari et al., 2019; Terryn et al., 2020). For tree-specific studies, e.g., phenotyping-related or orchard yield measurement, localized acquisition by terrestrial laser scans (TLS) is a common choice (Ferrara et al., 2018; Li and Liu, 2019). However, such data acquisition source is inefficient and related analyses are challenged by the volume of data as well as the non-uniform shape of trees.

It is customary to approach point-cloud based tree-modeling by reconstructing their shape and then applying geometric completion steps through predefined rules and heuristics (Livny et al., 2010). However, some have identified the separation of leaves from branches as the preparatory step that precedes such reconstruction (Danson et al., 2014; Chaudhury and Godin, 2020). Though the separation of that kind has been approached by classifying the intensity channel (Danson et al., 2014), it is common to use local geometric cues, such as normal similarity, point density, and arrangement to facilitate this task (Vicari et al., 2019; Krishna Moorthy et al., 2020; Wang, 2020). When considering reconstruction, the scanned trees would generally appear bare of leaves leaving the focus to its structure. Capitulating on its cylindrical form, local fitting has seen some popularity (e.g., Burt et al., 2019), while others have attempted to identify a skeletal form by using node connectivity approaches, with the aid of octree- or voxel-based structures (Bucksch and Lindenbergh, 2008; Zhao et al., 2015). As they encode sophisticated logic, they may exhibit sensitivity to varying point densities. Alternative approaches iteratively converge to the skeletal form, where a Laplacian-based contraction has been applied by Cao et al. (2010), and L1-median skeleton form by Wang et al. (2016); Mei et al. (2017).

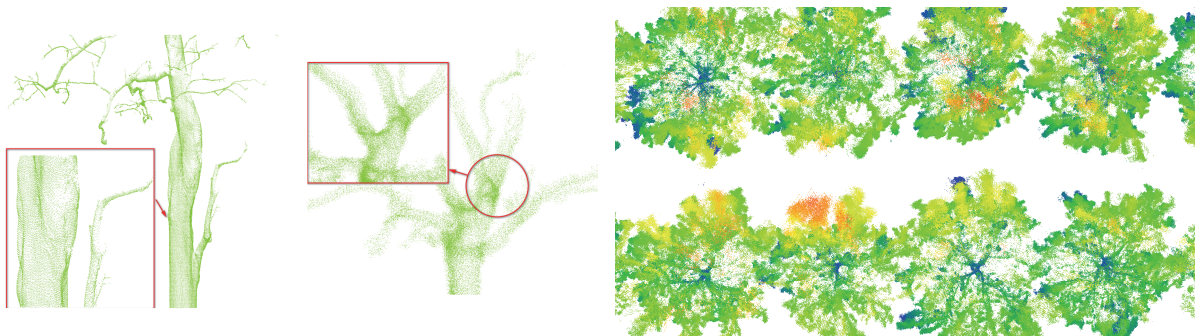


Figure 1: Tree related point-clouds, (left) TLS data acquired ~ 50 m from object, (middle) handheld scanner (GEO-SLAM ZEB Revo RT), acquired 2 m from object; (right) bird view of the collected data, colored by elevation.

Most approaches utilize TLS data as their source, suggesting that the point clouds they process are dense and that the noise level is limited. When considering actual tree modeling on a larger scale, the use of stationary TLS is cumbersome and non-scalable. Instead, we consider in this paper a model that is driven by *handheld* scanning devices, which offer greater flexibility yet come at a cost of decreased resolution and accuracy (Figure. 1). Such characteristics limit the ability to perform leaf-wood separation in a simple manner and to identify the tree directly from the point cloud. They also require a greater focus on density-related effects and the impact of noise on the reconstruction.

2. Data and Methods

For our evaluation handheld scanning data of an almond orchard was collected (Figure 1). For the modelling, our proposed approach is structure-based where due to the noisy data, we consider the L1-median curve extraction (Equation 1) as our framework.

Given a pointset Q , our aim is to identify a set of characteristic skeleton points X subject to:

$$\operatorname{argmin} |x_i - q_j| \theta(|x_i - q_j|) + R(X) \quad (1)$$

where $\theta(r) = \exp\left(-\frac{r^2}{h^2}\right)$ is a weight function and h is a density related term, $q_j \in Q$ is a point in the original set Q and $R(X)$ is regularization term (Huang et al., 2013). In evaluating affecting factors on the reconstruction, we demonstrate in Figure (2) how a direct application of a size-adaptive version of this form, where the value of h is increased between cycles, exhibits sensitivity in the presence of clutter. To filter the foliage, we evaluate leaf-removal models, particularly the recent one by Wang (2020), where local normal and proximity are considered as differentiating attributes. Figure (3) shows that because of the high-level of noise, results are partial, even when the normal similarity criterion is relaxed. Realizing these limiting factors when considering sparser and noisy data than that provided by TLS, our proposed approach places greater focus on robust measures and functions when quantifying features, while limiting the effect of derivatives in our evaluation. For that, we derive a shape-preserving model to attenuate the noise. Then, we show have a focus on neighborhood definition allows to robustify the feature computation for the presence of noise, clutter, and shape variation. In addition, and under the realization that the wood-leaf separation is a binary clustering form, we cast this problem as a graph-cuts formulation, demonstrating how it allows us to yield an optimal form. Using content aware modeling of both the overall tree point-cloud and then of its geometry, we provide a computationally efficient and reliable characterization of the sought form.

3. Results and Discussion

The application of our model is demonstrated in Figure (4) where we show how the trunk and branches are separated from the rest of the data and eliminate the clutter from the pointset. Additionally, in adapting the L1-median form, we demonstrate the application of a regularization form that encourages compliance with the overall trend of the surrounding neighborhood points. This facilitates convergence to the skeletal form within a small number of iterations.

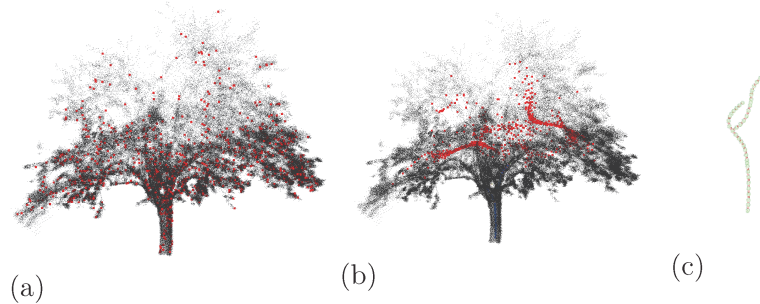


Figure 2: Skeleton extraction from the raw data using L1-median approach, a) seed points, b) intermediate results showing lack of convergence, c) extracted skeleton.

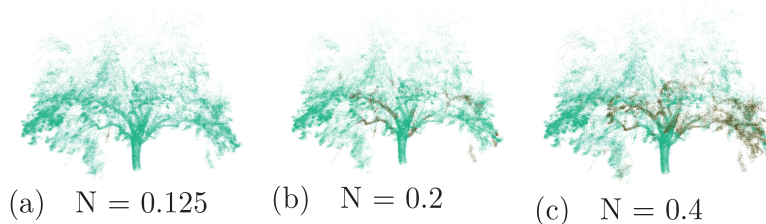


Figure 3. Wood-Leaf separation using Wang (2020). Thresholds are given according to the optimized configuration (0.1-0.2). Leaves and wood points are colored green and brown, respectively.

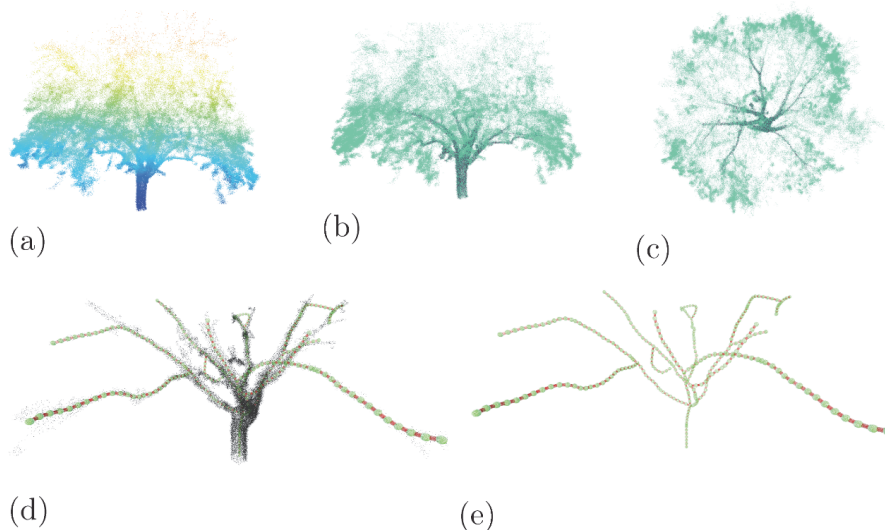


Figure 4. Our approach – (a-c) Wood-Leaf separation (leaves – green, trunk – black), (d-e) skeletonization results.

References

- Bucksch, A., Lindenbergh, R., 2008. CAMPINO—A skeletonization method for point cloud processing. *ISPRS journal of photogrammetry and remote sensing*, 63(1), 115–127.
- Burt, A., Disney, M., Calders, K., 2019. Extracting individual trees from lidar point clouds using TreeSeg. *Methods in Ecology and Evolution*, 10(3), 438-445.
- Cao, J., Tagliasacchi, A., Olson, M., Zhang, H., Su, Z., 2010. Point cloud skeletons via Laplacian based contraction. *2010 Shape Modeling International Conference*, 187–197.
- Chaudhury, A., Godin, C., 2020. Skeletonization of Plant Point Cloud Data Using Stochastic Optimization Framework. *Frontiers in Plant Science*, 11, 773. <https://www.frontiersin.org/article/10.3389/fpls.2020.00773>.
- Danson, F. M., Gaulton, R., Armitage, R. P., Disney, M., Gunawan, O., Lewis, P., Pearson, G., Ramirez, A. F., 2014. Developing a dual-wavelength full-waveform terrestrial laser scanner to characterize forest canopy structure. *Agricultural and Forest Meteorology*, 198-199, 7 - 14.
- Ferrara, R., Virdis, S. G., Ventura, A., Ghisu, T., Duce, P., Pellizzaro, G., 2018. An automated approach for wood-leaf separation from terrestrial LIDAR point clouds using the density based clustering algorithm DBSCAN. *Agricultural and Forest Meteorology*, 262, 434-444.
- Huang, H., Wu, S., Cohen-Or, D., Gong, M., Zhang, H., Li, G., Chen, B., 2013. L1-Medial Skeleton of Point Cloud. *ACM Trans. Graph.*, 32(4).
- Krishna Moorthy, S. M., Calders, K., Vicari, M. B., Verbeeck, H., 2020. Improved Supervised Learning-Based Approach for Leaf and Wood Classification from LiDAR Point Clouds of Forests. *IEEE Transactions on Geoscience and Remote Sensing*, 58(5), 3057-3070.
- Li, L., Liu, C., 2019. A new approach for estimating living vegetation volume based on terrestrial point cloud data. *PLOS ONE*, 14(8), 1-22. <https://doi.org/10.1371/journal.pone.0221734>.
- Livny, Y., Yan, F., Olson, M., Chen, B., Zhang, H., El-Sana, J., 2010. Automatic Reconstruction of Tree Skeletal Structures from Point Clouds. *ACM Trans. Graph.*, 29(6).
- Mei, J., Zhang, L., Wu, S., Wang, Z., Zhang, L., 2017. 3D tree modeling from incomplete point clouds via optimization and L1-MST. *International Journal of Geographical Information Science*, 31(5), 999–1021.
- Terryn, L., Calders, K., Disney, M., Origo, N., Malhi, Y., Newnham, G., Raunonen, P., Åkerblom, M., Verbeeck, H., 2020. Tree species classification using structural features derived from terrestrial laser scanning. *ISPRS Journal of Photogrammetry and Remote Sensing*, 168(June), 170–181.
- Vicari, M. B., Disney, M., Wilkes, P., Burt, A., Calders, K., Woodgate, W., 2019. Leaf and wood classification framework for terrestrial LiDAR point clouds. *Methods in Ecology and Evolution*, 10(5), 680-694.
- Wang, D., 2020. Unsupervised semantic and instance segmentation of forest point clouds. *ISPRS Journal of Photogrammetry and Remote Sensing*, 165(1), 86 - 97.
- Wang, Z., Zhang, L., Fang, T., Tong, X., Mathiopoulos, P. T., Zhang, L., Mei, J., 2016. A Local Structure and Direction-Aware Optimization Approach for Three-Dimensional Tree Modeling. *IEEE Transactions on Geoscience and Remote Sensing*, 54(8), 4749–4757.
- Zhao, G., Shi, Y., Wang, M., Xu, Y., 2015. Rapid reconstruction of tree skeleton based on voxel space. *Proceedings of the 2015 International Conference on Electrical, Electronics and Mechatronics*, Atlantis Press, 97–100.

Effect of variability of normalized differences calculated from multi-spectral lidar on individual tree species identification

B. C. Budei¹, B. St-Onge², R. A. Fournier³, D. Kneeshaw¹

¹University of Quebec at Montreal, Case postale 8888, succ. Centre-ville, Montreal (Quebec), H3C 3P8, Canada
Email: budei.brindusa_cristina@courrier.uqam.ca, kneeshaw.daniel@uqam.ca

²Geophoton Inc., 6310 Clanranald Ave., Montreal (Quebec), H3X 2T3, Canada. Email: bso@geophoton.ca

³University of Sherbrooke, 2500, boulevard de l'Université, Sherbrooke (Quebec), J1K 2R1, Canada
Email: Richard.Fournier@USherbrooke.ca

1. Introduction

Individual tree species identification is a key information in precision forest inventories and forest management. Multispectral airborne laser scanners (MALS) offer the opportunity to improve species identification compared to monospectral ALS, by opening the possibility of computing intensity features from two channels, each having different spectral information. Intensity features like ratios of channels or normalised differences (ND) are potentially less variable for a given species than the single channel absolute intensities, i.e., less prone to variations caused by external factors, such as scan angle, or variations in tree characteristics, such as tree height. The multispectral lidar Titan of Teledyne Optech Inc. incorporates three lasers (channels C1, C2, C3) that scan with different wavelengths (respectively 1550, 1064 and 532 nm), different scanning plane tilt angles (respectively 3.5°, 0° and 7°) and different beam divergence (0.35 mrad in C1 and C2, 0.7 mrad in C3). The objectives are 1) to analyse the variability of NDs calculated from multispectral lidar due to viewing geometry, 2) to evaluate the effect of intensity normalisation on ND values as well as on single tree species identification accuracy using ND features, 3) to evaluate the variability of ND related to tree characteristics such as the tree height.

2. Data and Methods

The multispectral lidar data were acquired in July 2015 in the York Regional Forest (YRF), Ontario, Canada using the Titan system. The flight height was about 800 m above ground, with 10 first returns m⁻² for all three channels within each single flight line, and a mean of 20 first returns m⁻² for overlapping flight lines. The data were captured with a maximum mirror lateral scan angle of 15 degrees. This resulted in a maximum net scan angle of 20 degrees due to the combination of the scanning plane tilt and the lateral scan angles. Reference data were acquired for six needleleaf tree species through field identification and photointerpretation of high-resolution images. Manual delineation of the sampled crowns was performed on the canopy height model. A large number of point cloud 3D features were calculated from normalized return heights. Moreover, intensity features were computed from the raw as well as from the range-normalized intensities of returns (Budei et al. 2018, Budei and St-Onge 2018). We here focus on ND intensity features that are calculated as combinations of two channels: NDG1 as $(C2+C3)/(C2-C3)$; NDG2 as $(C1+C3)/(C1-C3)$ and NDIR as $(C1+C2)/(C1-C2)$. Several ND versions were calculated from different statistics (50th, 75th, 90th, 95th percentiles of the intensity distribution or mean of return intensities in each channel) applied on selections of return types (all returns, single returns or first returns). These were computed for the returns falling within 60% of the upper crown length. Random forest classification was used for tree species identification.

Because of the variations in viewing geometry caused by differences in net scan angles and beam divergence, the multispectral lidar NDs do not meet the assumptions generally accepted for indices

calculated from optical satellite images, where spectral values of the same pixel (e.g., the red and near infrared values of a given pixel) have the same footprint, the same resolution and the same viewing angle. Increase in scan angle causes a decrease in return intensity, a change in return distribution and a decrease in number of returns per pulse. These scan angle effects might concern ND values. For each of the three ND types, a mean scan angle was calculated between the averages of scan angle values of returns in corresponding channels for each tree crown. For the first objective, we computed ND values from individual flight lines and evaluated their correlation with corresponding mean scan angles. We trained a random forest algorithm with all trees and then compared the identification accuracy for three classes of mean scan angle values. For the second objective, we computed ND values from individual flight lines using first the raw intensities and second the normalized intensities. We compared the change in correlation values of NDs with mean scan angles between NDs using raw and normalized intensities. Moreover, after species identification, we compared identification results obtained respectively with raw and normalized intensities. For the third objective, ND values vary with intra-specific properties affected by age, such as tree size and shape. We therefore calculated the correlation of ND, computed from returns from all flight lines, with tree height and then evaluated whether this correlation influences identification accuracy.

3. Results

A scan angle below 20 degrees (and in the case of a topography having only small variations) had a low influence on ND values, with correlations remaining below $|\pm 0.2|$. Figure 1 presents results of species identification with different feature selections from individual channels and pairs of channels (including ND and channel ratios). Results are given by scan angle class.

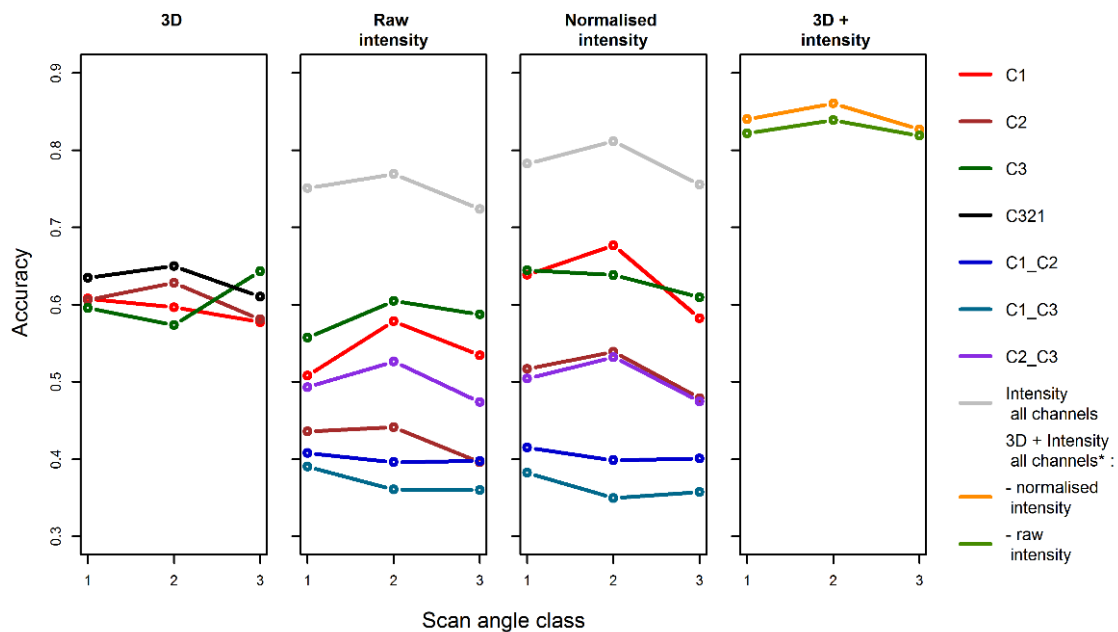


Figure 1: Random forest species identification accuracy by scan angle class: 1 = small scan angles near nadir, 2 = middle class scan angles, 3 = large scan angles. The classifications related to C1, C2, C3 used features from single channels, while those related to C1_C2, C1_C3, C2_C3 used NDs and ratios of intensity. C321 used 3D features with returns from all channels.

There is no significant difference between ND values computed from raw intensities compared to normalized intensities, and consequently, between identification accuracy using only NDs and channel ratios from raw and normalized intensities. By contrast, range normalization improved the accuracy of tree species identification by 8% when only single channel intensity features were used.

Even if ND features presented high correlation to tree height (Figure 2), these features are selected by the random forest model as within the best features for species identification.

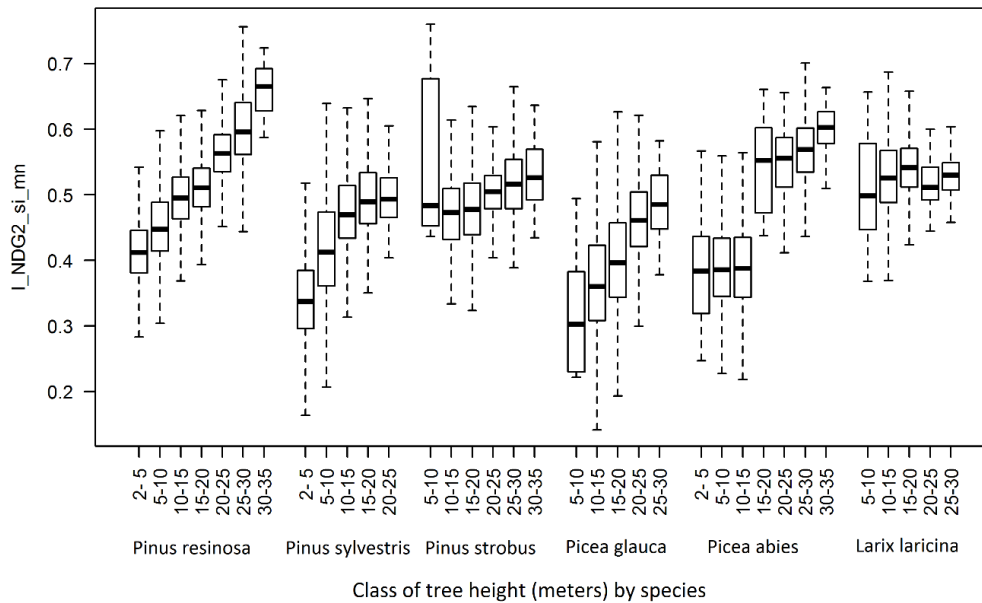


Figure 2: Variation of the feature $I_NDG2_si_mn$ by height classes of 5 m. $I_NDG2_si_mn$ represents the ND calculated between the mean (mn) intensity of the single (si) returns of middle IR (C1) and the green (C3) channels.

4. Discussion and conclusion

The inherent normalization formula of ND compensated to a certain measure for scan angle variation and for the lack of intensity normalization. This finding is useful since the intensity normalization of laser returns is often difficult, as necessary range information is lacking in the generally used LAS format.

The ND features presented a high variability as tree height changed. However, in an automatic ranking of variables using a random forest algorithm, ND features appeared to be among the most important ones for species classification, despite their variation with tree height. Even if random forest handled the high variability with tree height, attention must be given to sample representativity in each tree height class.

We conclude that NDs are robust variables that allow for an improvement in tree species identification even for a large range of tree heights, while at the same time reducing the need for intensity normalization.

Acknowledgements

We express our thanks to Teledyne Optech Incorporated (Vaughan, Canada) for graciously providing the Titan MALS dataset. This study was partially funded by the National Sciences and Engineering Research Council of Canada, by the AWARE project (NSERC File: CRDPJ 462973 – 14, Grantee: N.C. Coops, FRM, UBC), in collaboration with Canadian Wood Fiber Centre (CWFC) and FP-Innovations.

References

- Budei BC, St-Onge B, Hopkinson C, and Audet FA, 2018, Identifying the genus or species of individual trees using a three-wavelength airborne lidar system, *Remote Sensing of Environment*, 204:632-647.
- Budei BC, and St-Onge B, 2018, Variability of multispectral lidar 3D and intensity features with individual tree height and its influence on needleleaf tree species identification, *Canadian Journal of Remote Sensing*, 44 (4):263-286.

Can iPad Pro be as reliable as TLS for urban forest inventories?

P. Wężyk¹, R. Bobrowski², K. Zięba-Kulawik¹, M. Winczek

¹University of Agriculture in Kraków, Poland, Al. 29-listopada 46, 31-425
Email: {piotr.wezyk; karolina.zieba}@urk.edu.pl

²Midwestern State University, Brazil, Rua Profa. Maria R. Z. Almeida, 84.505-677
Email: rogerio@unicentro.br

1. Introduction

The labour cost and the time spent of experts are two main problems performing detailed urban forest (UF) inventories. So, different strategies have been adopted to reduce them while keeping or improving the data quality to generate information for urban planners and urban forest managers.

These strategies can be a more sophisticated technique to get faster and precise information using Light Detection and Ranging (LiDAR) technology. The most used methods include airborne (ALS), terrestrial (TLS), and mobile laser scanning (MLS) to obtain dense 3D point clouds for the analysis of vegetation 3D structure (Tanhuanpää et al. 2014; Wężyk et al. 2016; Chen et al., 2019).

Although methods based on LiDAR are more precise and faster for data acquisition, costs related may not be interesting for public administration because its costs are not related only to acquisition campaign but also to the costs of software for data processing and specialist (Ciesielski, Sterenczak, 2019; Li et al., 2019).

For data acquisition at a tree level, one option to surpass the costs of a traditional laser scanner technology could be the use of mobile applications available for tablets or smartphones equipped with a scanner.

The first mobile applications based on built-in laser scanner (LiDAR sensor) and image matching approach appeared in 2020 with the new model of iPad Pro 2020 and iPhone 12 Pro (iOS). The LiDAR sensor allows 3D precise scanning of objects located up to 5.0 m from the device and works by measuring the travel time of laser light photons sent from the device and reflected from the object (Narain, 2020).

Our main goal was to test the applicability and preciseness of the iPad Pro 2020 to acquire data for tree DBH and distances compared to a traditional terrestrial laser scanner used in urban forest inventory.

2. Materials and Methods

We measured the DBH and distance among 100 trees of different species at Park Lotników Polskich, in Kraków, Poland (Figure 1A). This park is one of the main green infrastructures of the city, important for delivering ecosystem services and promoting leisure and social recreation.

Tree trunks of ten different groups of trees were marked at DBH height (1.30 m) with a white line, to better promote the visualization of DBH slice and its point clouds, while processing data from iPad Pro and TLS scanner (Figure 1B and 1C).

We used an iPad Pro 2020 (12.4") and *Capture* app. to collect the inventory data. While scanning tree trunks, we kept approximately 2.0 m distance between the trunk and iPad Pro cameras, as this device has a limitation to scan objects up to 5.0 m. During scanning the device was kept at 1.40 m high in an upright position.

A terrestrial laser scanner - FARO FOCUS 3D 130 was used to scan the same groups of trees from 5 TLS stations per group of 10 trees scanned. We kept < 12.0 m distance from scanner to targets (spheres 7.5 cm radius) used as objects for single scans matching.



Figure 1: Distribution of groups of trees scanned in Park Lotników Polskich (A), marks made on trees at DBH level (B), iPad Pro screen after scanning a tree (C), point cloud of scanned tree at DBH level displayed in TerraScan (Terrasolid) software (D).

Point clouds acquired with iPad Pro and TLS FARO were processed in Microstation V8i (Bentley) and TerraScan (Terrasolid) software aiming to measure the distance among tree trunks and to extract the point clouds from each DBH slice. Point clouds extracted were analyzed in QGIS software by means of the Convex Hull algorithm to get the value of the perimeter at breast height (PBH) that was converted in the mean DBH value for each tree scanned. Tree distances were measured from the middle of the bottom of each tree trunk to the exact position of the other three trees.

We performed the Fligner-Killeen test for equal coefficients of variation and linear regression to describe the relationship between iPad Pro and TLS FARO data and their RMSE values from groups of DBH data and distance

3. Results and discussion

Among groups of species scanned, DBH varied between 15.01 and 72.57 cm for iPad Pro and from 17.34 cm and 73.40 cm for TLS FARO, due to different tree species, sizes and ages. Distances between trees varied from 2.70 m and 20.52 m for iPad Pro and from 2.66 m and 20.17 m in case of TLS FARO.

We found no significant difference between data collected with iPad Pro and TLS FARO, nor for DBH nor distances ($p > 0.05$). At a 95% level, confidence intervals varied in the same manner (Table 1), and coefficients of variation varied from 39.63% to 37.78% and from 43.85% to 43.94%, respectively for DBH and distance values measured.

Table 1. Confidence intervals (CI) for each variable measured with iPad Pro and TLS FARO, with indication of the number of observations (N) and p -values.

Variable	N	CI (iPad Pro)	CI (TLS FARO)	p -value
DBH	100	36.19 – 43.91	34.41 – 41.86	0.3584
Distance	300	4.01 – 4.74	4.03 – 4.77	0.9198

Regressions fitted have shown that iPad Pro can deliver precise data for distance among trees and quite good ones for DBH measurements, as RMSE kept under low values (Figure 2). When comparing the RMSE values with those from forest inventories based on TLS cloud points, we noticed that we can achieve not different values from the ones obtained in forest conditions with varying TLS devices accuracies and scanning methods (Pueschel et al., 2013; Ryding et al., 2015). So, iPad Pro can be useful for calculating tree registration in urban forest inventories, mainly where GNSS signals can be lost or weakened due to canopy cover or multipath issues caused by thick trunks or buildings.

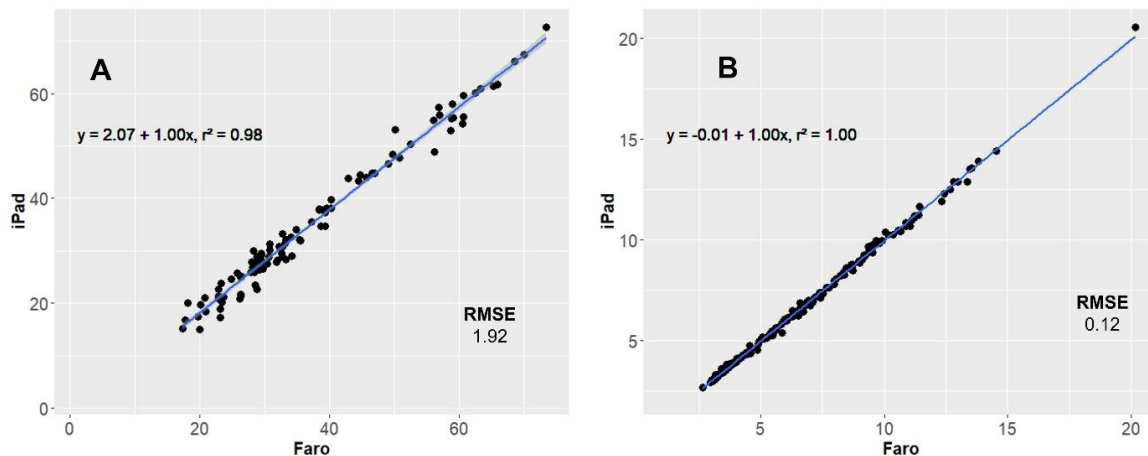


Figure 2: Regressions fitted for DBH (A) and distance values (B) between iPad Pro and TLS FARO 3D data, with RMSE values (cm) for DBH and distance (m).

4. Conclusions

For UF inventories regarding DBH measurements and distance among trees for positioning them, iPad Pro seems to be a reliable device to gather data quickly and cheaper, which can help small communities and improve public engagement in this activity.

References

- Chen, Y, Wang, S, Li, J, Ma, L, Wu, R, Luo, Z, Wang, C, 2019, Rapid Urban Roadside Tree Inventory Using a Mobile Laser Scanning System. *IEEE Journal of Selected Topics in Applied Earth Observations and Remote Sensing*, 12(9):3690-3700.
- Ciesielski, M, Sterenczak, K, 2019, Accuracy of determining specific parameters of the urban forest using remote sensing. *iForest*, 12:498-510.
- Li, Q, Yuan, P, Liu, X, Zhou, H, 2020, Street tree segmentation from mobile laser scanning data. *International Journal of Remote Sensing*, 41(18):7145-7162.
- Narain, A, 2020, Apple's LiDAR Scanner a game-changer in scanning technology? *Geospatial world*, URL: <https://www.geospatialworld.net/blogs/apples-lidar-scanner/> (Accessed 18.12.2020).
- Pueschel, P, Newnham, G, Rock, G, Udelhoven, T, Werner, W, Hill, J, 2013, The influence of scan mode and circle fitting on tree stem detection, stem diameter and volume extraction from terrestrial laser scans. *ISPRS Journal of Photogrammetry and Remote Sensing*, 77:44-56.
- Ryding, J, Williams, E, Smith, M J, Eichhorn, M P, 2015, Assessing Handheld Mobile Laser Scanners for Forest Surveys. *Remote Sensing*, 7:1095-1111.
- Tanhuanpää, T, Vastaranta, M, Kankare, V, Holopainen, M, Hyppä, J, Hyppä, H, Alho, P, Raisio, J, 2014, Mapping of urban roadside trees - A case study in the tree register update process in Helsinki city. *Urban Forestry and Urban Greening*, 13:562-570.
- Wężyk P, Hawryło P, Szostak M, 2016, Determination of the number of trees in the Bory Tucholskie National Park using crown delineation of the canopy height models derived from aerial photos matching and airborne laser scanning data. *Archiwum Fotogrametrii, Kartografii i Teledetekcji*, 28:137-156.

Monitoring of urban forests using 3D spatial indices based on ALS point clouds: a city-level analysis

Karolina Zięba-Kulawik^{1,2}, Konrad Skoczylas², Piotr Wężyk¹, Hichem Omrani²

¹University of Agriculture in Krakow, Faculty of Forestry, Department of Forest Resource Management, al. 29 Listopada 46, 31-425 Kraków, Poland

²Urban Development and Mobility Department, Luxembourg Institute of Socio-Economic Research, 11 Porte des Sciences, 4366 Esch-sur-Alzette, Luxembourg

By 2050, nearly 70% of the entire population will live in urban areas. Therefore cities must be appropriately shaped to be as resident-friendly as possible, paying particular attention to urban vegetation, which is an essential component of the suitable quality of life. So far, research often relied on two-dimensional (2D) mapping of urban vegetation using remote sensing imageries and vegetation indicators, where the greenery was evenly distributed, regardless of the cubature. In reality, the spatial and vertical structure of vegetation varies, and the layers often overlap. As novelty, we propose in this paper a 3D approach that explores: Vegetation 3D Density (V3DI) and Vegetation Volume to Building Volume (VV2BV) indices in Luxembourg City. The goal of the study was to investigate the relationship between the volume of vegetation and buildings in a rapidly developed Luxembourg City. The vegetation volume was calculated using airborne laser scanning point clouds (ALS LiDAR) processed into voxels (0.5 m). The volume of the buildings was calculated based on the results of 3D ALS LiDAR point cloud modeling.

We used ALS LiDAR point clouds from airborne mission obtained in February 2019 for entire Luxembourg City with mean point density: 25 points/m².

These indices have been estimated for districts, cadastral parcels, in a cell grid of 100 m and for each building individually, with a 100 m buffer. We found that in 2019 in Luxembourg City, the urban forests covered 1689 ha, which makes 33% of the entire administrative area. The 3D analyzes showed that the total volume of vegetation (> 1.0 m above ground) is about 40 million m³, indicating 328 m³ of greenery per resident. The V3DI was 0.77 m³/m². The overall VV2BV(%) index for Luxembourg showed 41.6%, and only in four districts of Luxembourg showed a high value of VV2BV index > 67%, which indicates areas with high levels of green infrastructure to contribute to the health and better quality of life.

A case study for detection and modelling of submerged deadwood from UAV-borne topo-bathymetric LiDAR point clouds

G. Mandlbürger¹, D. Monetti², M. Hollaus¹, M. Wimmer¹, J. Otepka-Schremmer¹, N. Pfeifer¹

¹TU Wien, Department of Geodesy and Geoinformation, Wiedner Hauptstr. 8-10, 1040 Vienna, Austria
Email: {gottfried.mandlbuerger; markus.hollaus; michael.wimmer; johannes.oteпка; norbert.pfeifer}@geo.tuwien.ac.at

²Skyability GmbH, GZO – Dienstleistungszentrum 4, Top 3, 7011 Siegendorf, Austria
Email: david.monetti@skyability.com

1. Introduction

Alluvial forests constitute an important and ecologically sensitive habitat. Diseases of endemic tree species like ashes have increased the amount of dead wood in alluvial forests in Austria in the recent past (Kessler et al. 2012). During seasonal flood peaks, the increased discharge carries deadwood stems into the active river channels, where they are floating downstream until either natural or artificial barriers (river bends, bridge piers, hydropower stations, etc.) stop their movement. On the one side, stranded driftwood plays an important role in aquatic ecosystems, e.g. as shelter for juvenile fish stages, but on the other side, it can cause severe problems like log jams potentially resulting in flooding of residential areas. For these reasons, monitoring of the volume and distribution of driftwood within rivers and lake outlets is an important topic from both an ecologic and socio-economic point of view.

In the recent past, airborne topo-bathymetric LiDAR (Light Detection And Ranging) has gained increased importance for mapping the littoral zone of both coastal and inland water areas. Bathymetric LiDAR uses short laser pulses in the green domain of the electro-magnetic spectrum for measuring objects above and below the water table. One of the main issues in bathymetric LiDAR is eye safety, as the green radiation also penetrates the human eye potentially causing severe injuries. For this reason, a larger beam divergence is used in bathymetric LiDAR resulting in typical footprint diameters in the range of about 50 cm for data acquisition from manned platforms. This, however, hampers the detectability of submerged tree stems and branches, especially for stem diameters < 30 cm. The advent of UAV-borne topo-bathymetric LiDAR sensors has changed this situation fundamentally, as these systems provide small laser footprint diameters of around 10 cm and a high laser pulse density of > 200 points/m².

In this case study we present early results of using 3D point clouds acquired with a survey-grade topo-bathymetric laser scanner for detecting and modelling submerged driftwood. We demonstrate that stems and even branches are well recognizable in the point cloud and that the achieved point density and measurement precision allows derivation of the driftwood skeleton parameters like tree length and diameter. This enables quantitative analysis of submerged biomass.

2. Study area and data sets

The flight campaign took place on March 9, 2021 at the Pielach River, a pre-Alpine, right hand tributary of the Danube river in Lower Austria (48° 12' 50"N, 15° 22' 30"E) with a lightweight *RIEGL VQ-840-G* topo-bathymetric laser scanning system mounted on an octocopter UAV platform. The sensor operates at pulse repetition rates (PRR) of 50-200 kHz and enables arbitrary choice of the laser beam divergence within a range of 1-6 mrad (Mandlbürger et al. 2020). This allows balancing the achievable depth penetration and spatial resolution. The employed sensor provides a maximum depth penetration of 1-2 times the Secchi depth (Effler 1998) and a laser footprint diameter of 5-30 cm for a typical flying altitude of 50 m above ground level (agl) (Mandlbürger et al. 2020). To test the detection and modelling of driftwood, a 750 m long section of the meandering river course was captured with 17 short strips (cf. Figure 1) in two separate flights using the flight mission parameters reported in Table 1. Because of

the green wavelength, the canopy of the alluvial forest, ground below it, and the mid-storey were captured, as well as water surface, riverbed, and reflections in the water column in between.

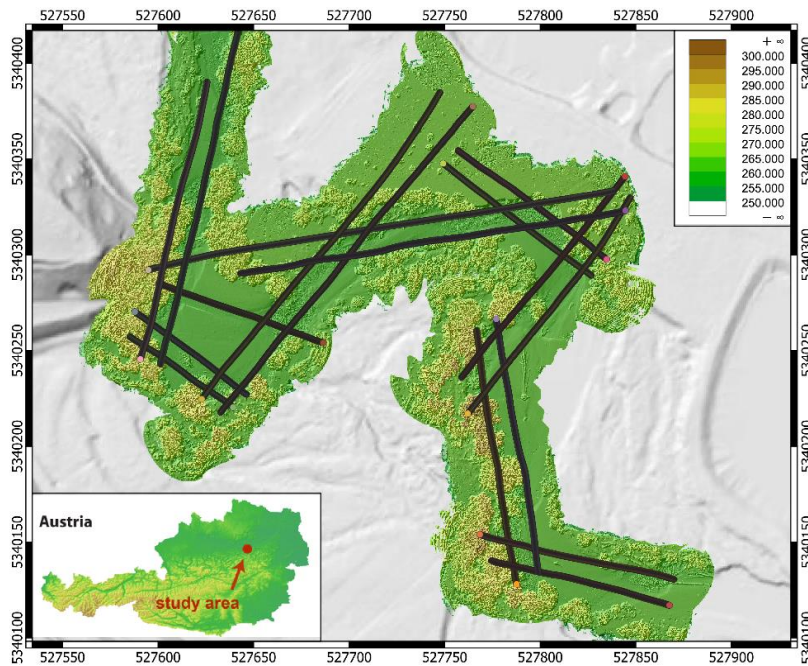


Figure 1: Study area Pielach river: superposition of shaded and color coded DSM map, image background: basemap.at (terrain); UAV flight trajectory (black framed dots), Coordinate Reference System: ETRS89/UTM33 (EPSG:25833); lower left: location of study area within

Table 1. UAV flight mission parameters.

PRR	Flying altitude	Beam divergence	Footprint diameter	Laser pulse density
50 kHz	50 m agl	2 mrad	10 cm	200 points/m ²
200 kHz	60 m agl	1 mrad	6 cm	600 points/m ²

3. Methods

After alignment and georeferencing of the laser strips, a standard quality assessment was performed to evaluate the achieved precision (< 3 cm) and point density (> 200 points/m²). After modelling the water surface and refraction and run-time correction of the raw laser measurements, a Digital Elevation Model (bare ground + submerged bottom) was derived using hierarchical robust interpolation (Pfeifer and Mandlburger 2018). In a subsequent processing step, the volumetric point density of all submerged points within the water column (i.e., points classified neither as riverbed nor as water surface) was calculated. Points meeting a certain minimum 3D point density were classified as underwater vegetation. Visual analysis revealed that there are two categories of submerged vegetation: (i) single broad tree stems, and (ii) bunches of smaller branches. Especially for the prior, the high point density enabled semi-automatic estimation of stem diameters using the approach of Wieser et al. (2019).

4. Results and discussions

Figure 2 shows 3D point clouds of submerged driftwood in perspective views. Figure 2a exhibits a large individual stem colored by RGB and Figure 2b features many thin branches of an entire willow tree colored by class ID (red=submerged vegetation). While the trunk of the larger stem in Figure 2a is already buried into the riverbed gravel, the small willow tree just recently broke off the steep bank side and is not anchored in the ground. Both examples prove the feasibility of (i) detecting and (ii) automatically classifying underwater vegetation from UAV-borne topo-bathymetric point clouds. For

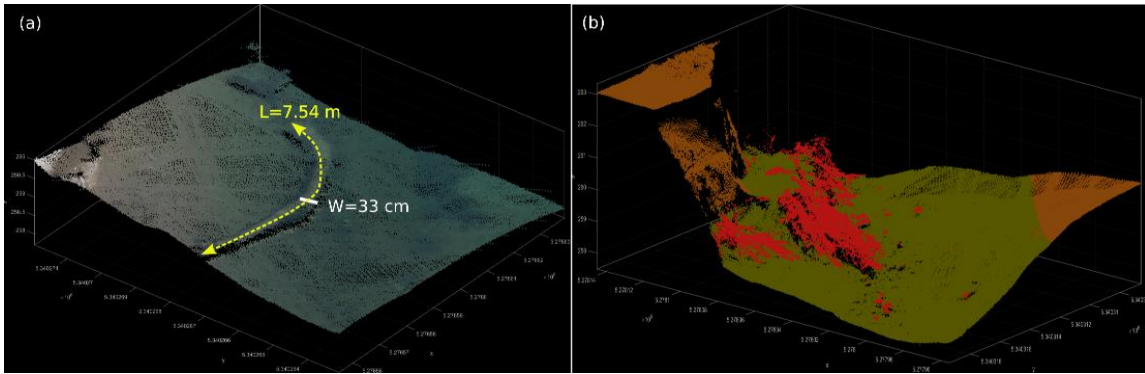


Figure 2: Examples of 3D point clouds of submerged driftwood. (a) single stem (colored by RGB); (b) bunch of willow tree branches (colored by class ID; red=submerged driftwood)

larger stem, semi-automatic width estimation resulted in a stem diameter of 33 cm. In addition, a length of 7.54 m was derived via manual digitization in a 3D viewer. In contrast to deadwood detection in dry forests (Mücke et al. 2013, Lindberg et al. 2013), submerged driftwood is often sparser and the absence of understorey facilitates detection. On the other hand, forward scattering of the laser signal underwater leads to blurring of the points clouds, which complicates (i) automatic detection of dense small structures (branches) and (ii) precise estimation of stem widths due to progressive broadening of submerged driftwood point clouds with increasing water depth.

5. Conclusions and outlook

In this study, we demonstrated that UAV-borne topo-bathymetric LiDAR is a suitable tool for detecting submerged driftwood. The automatically classified 3D points enabled the quantification of relevant stem parameters like length and width via either semi-automatic analysis or manual digitization. With these promising early results, ongoing research focuses on (i) improving the classification of driftwood, (ii) automatic segmentation of individual stems, and (iii) further automation of parameter retrieval, and (iv) accuracy assessment of the derived metrics w.r.t. reference data with special emphasis on unbiased stem width estimation.

References

- Effler S.W, 1988, Secchi Disc Transparency and Turbidity. *Journal of Environmental Engineering*, 114(6): 1436-1447.
- Kessler M, Cech T.L, Brandstetter M, Kirisits T, 2012, Dieback of ash (*Fraxinus excelsior* and *Fraxinus angustifolia*) in Eastern Austria: disease development on monitoring plots from 2007 to 2010. *Journal of Agricultural Extension and Rural Development*, 4(9), 223-226.
- Lindberg E, Hollaus M, Mücke W, Fransson J. E. S., Pfeifer N, 2013, Detection of lying tree stems from airborne laser scanning data using a line template matching algorithm. *ISPRS Annals of the Photogrammetry, Remote Sensing and Spatial Information Sciences*, II-5/W2, 169-174.
- Mandlbürger G, Pfennigbauer M, Schwarz R, Flöry S and Nussbaumer L, 2020, Concept and Performance Evaluation of a Novel UAV-Borne Topo-Bathymetric LiDAR Sensor. *Remote Sensing*, 12(6), 986: <https://doi.org/10.3390/rs12060986>.
- Mücke W, Hollaus M, Pfeifer N, Schroiff A, Deák B, 2013. Comparison of discrete and full-waveform ALS features for dead wood detection. *ISPRS Annals of the Photogrammetry, Remote Sensing and Spatial Information Sciences*, II-5/W2, 199-204.
- Pfeifer N and Mandlbürger G, 2018, LiDAR data filtering and digital terrain model generation; in: *Topographic Laser Ranging and Scanning - Principles and Processing*, Second Edition, J. Shan, C. Toth (ed.), CRC Press, Boca Raton, 2018, ISBN: 9781498772273, 349 - 378.
- Wieser M, Mandlbürger G, Hollaus M, Otepka, J, Glira P and Pfeifer N, 2018, A Case Study of UAS Borne Laser Scanning for Measurement of Tree Stem Diameter. *Remote Sensing*, 9(11), 1154.

Terrestrial laser scanning for forest inventories: Tree volume and biomass estimation using extended allometric models

Aline Bornand^{1,2}, Meinrad Abegg¹, Felix Morsdorf²

¹ Swiss Federal Institute for Forest, Snow and Landscape Research WSL, Zürcherstrasse 111, CH-8903 Birmensdorf, Switzerland
Email: {aline.bornand; meinrad.abegg}@wsl.ch

²Remote Sensing Laboratories, Department of Geography, University of Zurich, Winterthurerstr 190, CH-8057 Zürich, Switzerland
Email: felix.morsdorf@geo.uzh.ch

1. Introduction

Forest inventories deliver information on forest area, the amount and change of forest resources, the development of the biotope forest in general and the carbon balance of a country. Single tree volume is the basis for many estimates provided by forest inventories and is not directly measurable in the field up to now. In the Swiss National Forest Inventory (NFI), wood volume and changes in wood volume are estimated based on the stem volume of individual trees using various models. For a sub-sample of tally trees, single stem volume is estimated by allometric models using three measured tree dimensions: diameter at breast height (DBH), upper diameter at 7 m height (d7) and tree height. Based on these three variables the volume of the stem, which usually is of a conical shape, can be calculated with a very high precision ($R^2 > 98.7$) (Herold et al. 2019). On the other hand, total tree volume, needed e.g., for biomass estimation, is far more complex to model, making the prediction of branch wood more prone to unexplained variation. Moreover, these allometric models for total tree volume (including branches) are based on destructively sampled trees from experimental sites and are currently not completely representative for the whole country.

Close range remote sensing technologies such as terrestrial laser scanning (TLS), present a possibility to address the need for more direct measurements. Currently, no operational application exists for TLS in forest inventories, due to open questions concerning precision and accuracy. Nevertheless, many TLS-based approaches contributing to individual tree volume or above-ground biomass estimation have been proposed and developed. A straightforward application is to retrieve simple tree structure metrics, such as stem and crown diameters, from point clouds instead of manual measurements (Holopainen et al. 2011). Tree volume can also be approximated by the voxel representation of an individual tree point cloud (Vonderach et al. 2012). The most detailed volume estimation is commonly achieved by quantitative structure models (QSM) (e.g. Raumonen et al. 2013) which estimate tree volume based on a real morphological structure model of a specific tree. However, in the context of a large-scale or national inventory, computing a QSM for every sampled tree still remains less effective than traditional inventory methods due to demands on point cloud quality and cost of data acquisition. Instead, QSMs have been proposed as non-destructive reference data for training (traditional) allometric models (Stovall et al. 2018). Another possible way of integrating TLS into forest inventories is to extend allometric models by including TLS-derived variables, such as crown diameter (Lau et al. 2019).

In order to assess these possibilities, the objectives of this study include (1) to evaluate the explanatory power of TLS-derived tree metrics regarding tree volume and biomass (total, coarse wood and fine wood), and (2) incorporating them into preliminary allometric models based on 60 sample trees. (3) Additionally, we will compare the estimated volumes to operational allometric models and to quantitative structure models.

2. Data and Methods

The study area consists of two managed mixed temperate forest sites located on the Swiss Plateau. The main tree species on site 1 are: *Fagus sylvatica*, *Picea abies*, *Acer pseudoplatanus* and *Fraxinus*

excelsior, while the following species are present on site 2: *Fagus sylvatica*, *Fraxinus excelsior*, *Acer pseudoplatanus*, *Pinus sylvestris*, *Pinus nigra* and *Larix decidua*. From each site, approximately 30 sample trees were chosen, aiming to represent the respective species range and height distribution. DBH, d7, tree height and crown parameters were measured on the standing trees following inventory procedure. After harvesting, trees were weighed using a crane scale. The total weight was further divided into coarse wood (trunk and branches with diameter >7 cm) and fine wood (branches and twigs with diameter <7 cm). Wood disc samples were taken every 2 m along each stem to determine wood density, which was then used to convert tree weight to biomass and volume.

The TLS data were collected in winter 2020/2021 using a Leica BLK360 terrestrial laser scanner (Leica Geosystems, Heerbrugg, Switzerland), while distributing scan positions across the site so that every tree of interest was included in at least three different scans from different directions. The raw point clouds from different scan positions were co-registered using Cyclone REGISTER 360 (Leica Geosystems, Heerbrugg, Switzerland). Individual trees were segmented from the point cloud using the CompuTree software (Othmani et al. 2011), including manual filtering as the last step.

A set of tree structure metrics was then extracted from each individual tree point cloud. Besides DBH and crown diameter, multiple stem diameter values were taken between 2 m and 10 m and at 25%, 50% and 75% of tree height. To serve as metrics describing crown structure, crown projected area and volumes of different convex and concave hulls (alpha shapes) around both the crown and the whole tree were also calculated. Additionally, wood volume per compartment (diameter >7 cm and diameter ≤7 cm), was derived following the QSM approach as implemented in the TreeQSM tool (Raumonen et al. 2013).

Linear regression and correlation coefficients relating reference total, coarse and fine wood volume to the TLS-enabled tree metrics are subsequently used as a first indication of their respective explanatory power. In order to find effective combinations of the most relevant of these metrics, allometric models are then built and tested, along the lines of existing NFI stem volume models.

3. Results and Discussion

Regarding the power to predict tree volume, we observe that stem diameters up to approximately 10 m or 50% of tree height correlate well with total and coarse wood volume. TLS-based crown diameters on the other hand show lower values of correlation with total volume ($R^2 = 0.25 - 0.52$). We observe the various crown hulls to correlate with fine wood volume as derived by QSMs ($R^2 = 0.8 - 0.92$) but less so with total volume from QSMs and destructively measured volume ($R^2 = 0.2 - 0.5$). A possible reason for this is that TLS-based descriptors of crown shape can be heavily influenced by point cloud filtering and segmentation methods. Also, the accuracy of reference measurements needs to be considered, as some crowns were damaged during felling and weighing operations. Despite this, crown characteristics are a promising addition for allometric equations because they provide valuable information on branch volume and are also known to be sensitive to stand structure (Forrester et al. 2017).

As a next step, we will analyse interactions between the presented tree metrics as well as evaluate the feasibility of additive allometric models for coarse wood and fine wood. We expect coarse wood volume to be estimated reasonably well by a combination of “distance metrics” (tree height and various stem and crown diameters). Crown hulls in combination with echo density metrics could serve as a possible approximation for the volume of fine branches.

4. Conclusions

As the new allometric equations are fitted on a limited sample containing various species, they are not expected to be suitable for use outside the respective test sites (Duncanson et al. 2015). Rather, they provide an indication as to which parameter combinations should be further investigated and which metrics would be suitable to include in future inventories.

References

- Duncanson L, Rourke O and Dubayah R, 2015, Small Sample Sizes Yield Biased Allometric Equations in Temperate Forests. *Scientific Reports*, 5: 17153.
- Forrester D, Tachauer, I, Annighoefer P, Barbeito I, Pretzsch H, Ruiz-Peinado R, Stark H, Vacchiano G, Zlatanov T, Chakraborty T, Saha S and Sileshi G, 2017, Generalized biomass and leaf area allometric equations for European tree species incorporating stand structure, tree age and climate. *Forest Ecology and Management*, 396: 160–175.
- Herold A, Zell J, Rohner B, Didion M, Thürig E and Rösler E, 2019, State and Change of Forest Resources. In: Fischer C & Traub B (eds), *Swiss National Forest Inventory – Methods and Models of the Fourth Assessment*, Springer, 205–230.
- Holopainen M, Vastaranta M, Kankare V, Rätty M, Vaaja M, Liang X, Yu X, Hyyppä J, Hyyppä H, Viitala R and Kaasalainen S, 2011, Biomass estimation of individual trees using stem and crown diameter TLS measurements. *ISPRS - International Archives of the Photogrammetry, Remote Sensing and Spatial Information Sciences*, 3812: 91–95.
- Lau A, Calders K, Bartholomeus H, Martius C, Raunonen P, Herold M, Vicari M, Sukhdeo H, Singh J and Goodman R, 2019, Tree biomass equations from terrestrial LiDAR: A case study in Guyana. *Forests*, 10(6):527.
- Othmani A, Piboule A, Krebs M, Stolz C and Voon L, 2011, Towards automated and operational forest inventories with T-Lidar. In: *11th International Conference on LiDAR Applications for Assessing Forest Ecosystems (SilviLaser 2011)*.
- Raunonen P, Kaasalainen M, Åkerblom M, Kaasalainen S, Kaartinen H, Vastaranta M, Holopainen M, Disney M and Lewis P, 2013, Fast automatic precision tree models from terrestrial laser scanner data. *Remote Sensing*, 5(2):491–520.
- Stovall A, Shugart H and Anderson-Teixeira K, 2018, Assessing terrestrial laser scanning for developing non-destructive biomass allometry. *Forest Ecology and Management*, 427: 217–229.
- Vonderach C, Vögtle T, Adler P and Norra S, 2012, Terrestrial laser scanning for estimating urban tree volume and carbon content. *International Journal of Remote Sensing*, 33(21): 6652–6667.

Operationalizing multi-temporal stem volume assessment based on ALS data

M. Hollaus¹, N. Pfeifer¹, T. Gschwantner², A. Berger²

¹ TU Wien, Department of Geodesy and Geoinformation, Wiedner Hauptstraße 8-10, 1040 Vienna, Austria
Email: (markus.hollaus, Norbert.pfeifer)@geo.tuwien.ac.at

² Federal Research and Training Centre for Forests, Natural Hazards and Landscape (BFW), Seckendorff-Gudent-Weg 8, 1131 Vienna, Austria
Email: (thomas.gschwantner, ambros.berger)@bfw.gv.at

1. Introduction

Large area stem volume information, one of the most important parameters in forestry, can be derived from various types of remote sensing data, such as microwave remote sensing, satellite-based optical data or airborne acquired optical data, including Airborne Laserscanning (ALS). Currently the highest accuracy combined with the highest spatial resolution of the derived stem volume maps are obtained from ALS data. Furthermore, ALS data have the advantage that they are not influenced by topographic shadows which is a limiting factor in complex topographic environments for the majority of the remote sensing methods. One limiting factor of ALS is the reduced temporal resolution of country-wide data sets, e.g. currently in Austria time steps of ≥ 6 years.

To estimate stem volume from ALS data for large areas (e.g. >1000 km²), area-based approaches are commonly applied. In the majority, these approaches are based on regression models using in-situ forest inventory (FI) data, i.e. on plot level, as ground reference for calibration purposes. Especially for large scale applications there is normally a time gap between the ALS data acquisitions and the in-situ FI measurements. This leads to deviations with respect to harvested trees and forest growth between the date of ALS and FI data acquisitions. On the other hand, multiple epochs of ALS data are in the meantime available for many forested regions.

The aim of this study is to investigate the potential of country-wide, multi-temporal stem volume estimations based on ALS and national forest inventory (NFI) data. The study is done for the federal state of Vorarlberg, Austria. Three ALS data sets, acquired in the framework of country-wide ALS campaigns and NFI data are used for this study.

2. Study area and data

The study area is located in the western part of Austria and covers the federal state of Vorarlberg with an area of 2601 km². The altitude varies between 396 m a.s.l. at the Lake Constance and 3312 m a.s.l. at the Piz Buin in the Silvretta mountains. In addition to the large Rhine Valley the area is characterized by several smaller valleys forming a complex mountainous landscape. Forests cover $\sim 37\%$ (970 km²) of the total area and consist of 82.8% coniferous and 17.8% deciduous tree species. The dominant coniferous tree species are spruce (*Picea abies*) with $\sim 60.0\%$ and fir (*Abies alba*) with 20.4% of the standing volume (BFW, 2021).

The ALS data were acquired within operational country-wide ALS campaigns in the years 2002-2006, 2011, and 2017. In the following, the ALS data sets are named ALS_2004, ALS_2011 and ALS_2017, respectively. The point densities vary in the range of 4-20 echoes per m² for ALS_2004, 7-40 echoes per m² for ALS_2011 and 15-80 echoes per m² for ALS_2017. From the ALS_2017 data a detailed digital terrain model (DTM) with a spatial resolution of 0.5x0.5 m² was derived. This DTM was used as reference for all three ALS data sets. Additionally, a high resolution (1x1 m²) forest mask generated by the BFW (www.bfw.ac.at) from aerial images and ALS data was used.

To calibrate the stem volume models, data from the Austrian NFI was used as reference. The NFI data are extracted from the operational NFI periods 2000-02, 2007-09 and 2016-21. For each sample plot, information about sample tree positions, diameters at breast height (DBH), tree species, tree heights and stem volumes are available. Further details about the NFI data can be found in Gschwantner et al. (2016).

3. Methods

For each ALS data set a digital surface model (DSM) was calculated based on the land cover dependent approach described in Hollaus et al. (2010). This approach uses for rough surfaces the DSM calculated from the highest 3D point per raster cell and for smooth surfaces and for data gaps the DSM based on moving least squares interpolation of a local point cloud. Finally, the normalized digital surface model (nDSM) was calculated by subtracting the DTM from the DSM. The derived DSM and nDSM models have a spatial resolution of 1x1 m.

To use the NFI data as ground reference for ALS based regression models, the geolocation accuracy between ALS and NFI data has to be checked in a first step. This was done manually in a GIS environment by overlaying the nDSM with the NFI sample tree positions including the measured tree heights. As shown in Figure 1 the NFI sample tree positions were moved to the local maximas of the nDSM, which can be assumed as tree positions. Furthermore, Figure 1 shows that three sample trees

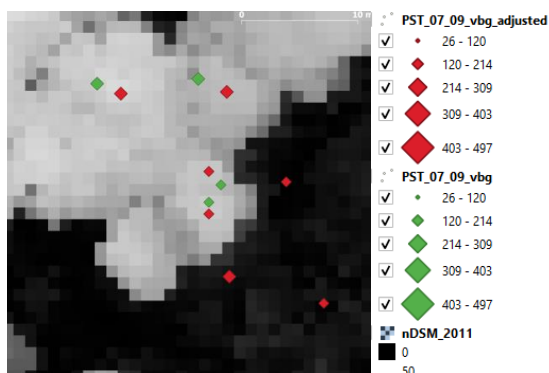


Figure 1: nDSM overlaid with NFI sample tree positions. The green diamonds represent the locations of the original positions and the red one the adjusted positions.

ALS data. Crown area was estimated for each sample tree (NFI) using an empirical function depending on tree species (NFI), tree height (ALS), and altitude (ALS). The estimated crown area was used as spatial reference for extracting the average nDSM value, which corresponds to the average crown height. These derived crown heights were used as explanatory variable in a polynomial function.

Finally, the derived stem volume model was applied to each ALS data set for the entire forest area of Vorarlberg. The derived stem volume maps with a spatial resolution of 5x5 m² were used to assess the amount of harvested areas and their corresponding stem volume amount as well as the increase of stem volume due to tree growth. The processing of the ALS data was done with the OPALS software (Pfeifer et al., 2014).

were harvested in the time between ALS and NFI data acquisition. All harvested trees were excluded from the calibration procedure. To consider the mentioned time gap between ALS and NFI data acquisition a tree growth model (Ledermann, 2006; Ledermann et al., 2017; Monserud und Sterba, 1996) was used to model tree height and stem volume for the date of ALS data acquisition. The stem volume for each sample tree was calculated based on the volume functions described in Braun (1969), Pollanschütz (1974), and Schieler (1988).

Adapted from the plot-based approach presented in Hollaus et al. (2009) it is assumed that the single tree stem volume can be correlated to the mean canopy surface height above the ground level derived from the

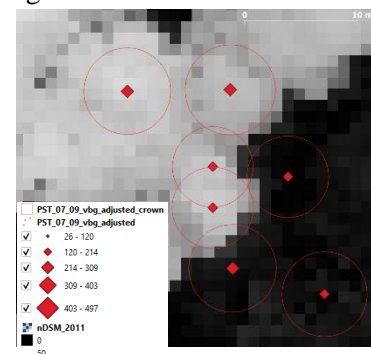


Figure 2: nDSM overlaid with adjusted NFI sample tree positions and the estimated crown areas.

4. Results and discussion

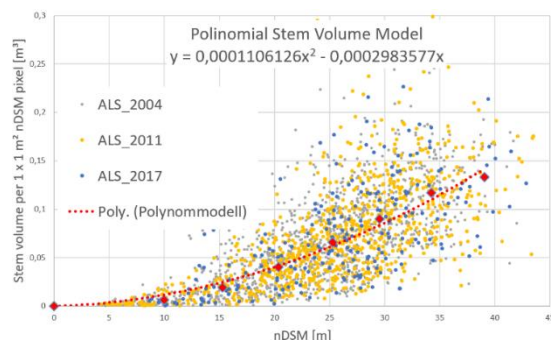


Figure 3: Scatterplots for stem volume and average crown height (nDSM). The three different colors represent the three ALS data sets. The red dashed line shows the fitted polynomial stem volume model.

Based on the described co-registration approach 1146, 857, and 222 sample trees respectively were useable for calibrating the polynomial model. The reason for the low number of sample trees for ALS_2017 is that this inventory is still ongoing and not all NFI plots are surveyed yet. Figure 3 shows the correlation between the NFI derived sample tree stem volumes and the ALS derived mean nDSM heights. As visible in Figure 3 there is no statistically significant difference of the correlations between the three ALS data sets. Therefore, only one polynomial model was calibrated for assessing the multi-temporal stem volume maps. The calibrated stem volume model was applied for all

three ALS data sets. In Figure 4 the changes of the stem volumes between ALS_2004 and ALS_2011, and ALS_2011 and ALS_2017 are shown. In total 3,36 Mio m³ stem volume was harvested between ALS_2004 and ALS_2011 and 2,50 Mio m³ between ALS_2011 and ALS_2017. In the same time periods the stem volumes increased by 4,42 Mio m³ and 5,56 Mio m³ respectively. The quantified changes are in good agreement with the federal state wide NFI statistics. The benefit of the ALS derived stem volumes map is the high spatial resolution of 5x5 m² and thus demonstrate the high potential of ALS data for large- as well as small-scale operational stem volume estimation.

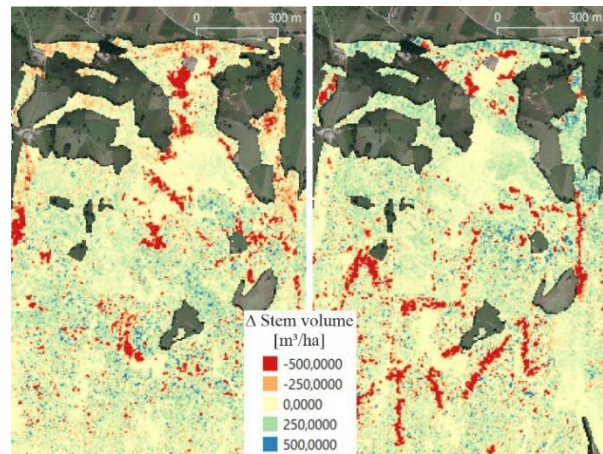


Figure 4: Derived stem volume maps. (Left) difference stem volume map ALS_2011 - ALS_2004 and (right) ALS_2017 - ALS_2011. The spatial resolution is 5x5 m².

5. Conclusion

This study shows the high potential of multi-temporal stem volume estimation based on country-wide ALS and NFI data. The derived stem volume maps allow detailed quantification of harvested forests as well as of stem volume increase with high spatial resolution. In further investigations the influence of different tree species and forest management practices (i.e. forest thinnings) will be investigated. Furthermore, the integration of image matching data to increase the temporal resolution will be studied.

Acknowledgements

The work has been supported by the “Landesamt für Vermessung und Geoinformation” Vorarlberg. They also provided the ALS data. The NFI data and the forest mask were provided by the BFW.

References

- BFW, 2021. ÖWI - interim results. https://bfw.ac.at/cms_stamm/500/images/OEWI/Vorarlberg_OEWI_16_18.pdf. Last accessed 05/21.
- Braun, R., 1969: Österreichische Forstinventur 1961-70. Methodik der Auswertung und Standardfehler-Berechnung. Mitteilungen der Forstlichen Bundesversuchsanstalt, Wien. Heft 84, 60 p.
- Gschwantner, T., Berger, A., Büchsenmeister, R. and Hauk, E., 2016: National Forest Inventories Reports: Austria. In: V.C.e.a. (Eds.) (Editor), National Forest Inventories – Assessment of wood availability and use. Springer, pp. 135-157.
- Hollaus, M., Mandlbürger, G., Pfeifer, N. and Mücke, W., 2010. Land cover dependent derivation of digital surface models from airborne laser scanning data, ISPRS Commission III Symposium PCV 2010 -- Photogrammetric Computer Vision and Image Analysis, Paris, pp. 221-226.
- Hollaus, M., Wagner, W., Schadauer, K., Maier, B. and Gabler, K., 2009: Growing stock estimation for alpine forests in Austria: a robust LiDAR-based approach. Canadian Journal of Forest Research 39 (7), 1387-1400. <https://doi.org/10.1139/X09-042>.
- Ledermann, T., 2006: Description of PrognAus for Windows 2.2. In: H. Hasenauer (Editor), Sustainable forest management – growth models for Europe. Springer, Berlin, pp. 71-78.
- Ledermann, T., Kindermann, G. and Gschwantner, T., 2017: Country report Austria. In: S.e.a. Barreiro (Editor), Forest Inventory-based projection systems for wood and biomass availability. Managing Forest Ecosystems 29. Springer International Publishing, pp. 79-95.
- Monserud, R.A. and Sterba, H., 1996: A basal area increment model for individual trees growing in even- and uneven-aged forest stands in Austria. Forest Ecology and Management 80, 57-80.
- Pfeifer, N., Mandlbürger, G., Otepka, J. and Karel, W., 2014: OPALS - A framework for Airborne Laser Scanning data analysis. Computers, Environment and Urban Systems 45, 125-136. <https://doi.org/10.1016/j.compenvurbsys.2013.11.002>.
- Pollanschütz, J., 1974: Formzahlfunktionen der Hauptbaumarten Österreichs. Allgemeine Forstzeitung 85 (12), 341-343.

Schieler, K., 1988: Methodische Fragen in Zusammenhang mit der Österreichischen Forstinventur. Diplomarbeit Universität für Bodenkultur Wien, 99 pp.

Modelling of Aboveground Biomass Change Using LiDAR Metrics and NFI Field Data: A Case Study of Southern Sweden

Ritwika Mukhopadhyay¹, Indu Indirabai¹, Mats Nilsson¹, Mikael Egberth¹, Emma Holmström¹, Magnus Ekström^{1,2}

¹Department of Forest Resource Management, Swedish University of Agricultural Sciences, Umeå, Sweden
Email: {ritwika.mukhopadhyay; indu.indirabai; mats.nilsson; mikael.egberth; emma.holmstrom; magnus.ekstrom}@slu.se

²Department of Statistics, USBE, Umeå University, Sweden
Email: magnus.ekstrom@umu.se

Keywords: Aboveground biomass, Airborne LiDAR, Categorical variables, Change estimation, GLS, Heteroscedasticity, Random forest.

1. Introduction

The estimation of forest state and change is crucial for the assessment of the changes in the carbon stocks which are necessary as per the requirements of the Kyoto Protocol (UNFCCC 2021). The estimation of the dynamics of forest aboveground biomass (AGB) is also important to study the impact of forest management towards climate change mitigation (e.g., Eggleston et al. 2006; Puliti and Astrup 2020). The field data from the National Forest Inventories (NFIs) are commonly used to estimate the state and change of forest attributes such as AGB and growing stock volume for countries and regions within countries (e.g., Tomppo et al. 2010). However the collection of the data is expensive, time consuming and sometimes also impossible in inaccessible areas (e.g., Saarela et al. 2020). To improve cost-efficiency of the forest attribute estimation, remotely sensed (RS) data are incorporated along with the field data. The use of RS data enables mapping of parameters across the landscape it covers as well as estimation of the target population mean and total (e.g., Saarela et al. 2020). Previous studies have been conducted combining field data with Light Detection and Ranging (LiDAR) data that proved to be efficient in monitoring AGB changes (e.g., Dubayah et al. 2010, Bollandsås et al. 2013, Næsset et al. 2013, Skowronski et al. 2014, McRoberts et al. 2015, Magnussen et al. 2015, Hopkinson et al. 2016, Ene et al. 2017, Puliti and Astrup 2020). Hudak et al. (2012) estimated the change in above ground biomass (Δ AGB, where Δ represents the change) through direct and indirect approaches from the changes in the predictor variables retrieved from the airborne laser scanning (ALS) data. McRoberts et al. (2015) presented direct and indirect estimation methods for Δ AGB using ALS data along with forest inventory data for a boreal forest in Våler Municipality, Norway.

Categorical variables have been implemented for the estimation of AGB using RS data and field inventory data in a number of studies (e.g., Ou et al. 2019, Li et al. 2019 and 2020). In Li et al. (2019) and Li et al. (2020) the categorical variables were formed based on the available field data and Landsat 8 data for different classes of forest crown densities. The categorical variables were used in the parametric models for the estimation of AGB. A comparative analysis between the models with and without categorical variables was performed proving the efficiency of the inclusion of categorical variables in modelling. In Ou et al. (2019), a comparative analysis of parametric models (linear model (LM) and LM with combined variables) and non-parametric methods (random forest (RF) and artificial neural network (ANN)) was conducted based on the inclusion of categorical variables for different age classes of *Pinus densata* forests. The models included categorical variables were observed to improve the overall accuracy of estimation by 14-42% and 32-44% for the training and testing plots based on the root mean-squared error (RMSE) values.

The objective of this study was to incorporate parametric models (LMs) and non-parametric (RF) methods along with categorical variables and using NFI field data and auxiliary LiDAR data for the estimation of Δ AGB. The study is mainly focused to observe the ability of LiDAR for Δ AGB estimation when different management practices of the forests are taken into account. The categorical variables were grouped based on the management practices such as, thinning and felling operations conducted in the plots.

2. Material and Methods

The study area is located in south of Sweden with a forest cover of 332171.8 ha and species composition with proportions such as, 24.6% Pine (*Pinus sylvestris*), 53.8% Spruce (*Picea abies*), 11.1% Birch (*Betula spp.*) and 24.5% of other broadleaved tree species. The Swedish NFI field data were available for 218 plots for two time periods, 2010-2014 and 2015-2019. The plots were circular with 10m radius sampled using the systematic cluster sampling method.

For each corresponding field plot the LiDAR metrics were retrieved using the Fusion software (McGaughey 2020). Laser returns above 1.5m height were retained in order to eliminate the non-vegetation returns. The LiDAR metrics used for the regression modelling were 80% height percentile (h_{p80}) and the vegetation ratio (vr) based on the previous studies (Nilsson et al. 2017, Saarela et al. 2020).

The ΔAGB was estimated directly from the plot-level NFI data available for time period 2 (2015-2019) and 1 (2010-2014). The data were grouped based on the silvicultural operations into three categories namely, plots with thinning operation, plots with clear felling operations and plots with no activity. The plot-level values for ΔAGB and the change in LiDAR metrics ($\Delta LiDAR$ metrics) were used for developing the relationship between the response variable (ΔAGB) and the predictor variables (Δh_{p80} and Δvr) along with the categorical variables (indicators I_1 and I_2). I_1 and I_2 represent the categories of plots with no activity and with thinning operation, respectively. Figure 1 presents an overview of the modelling workflow.

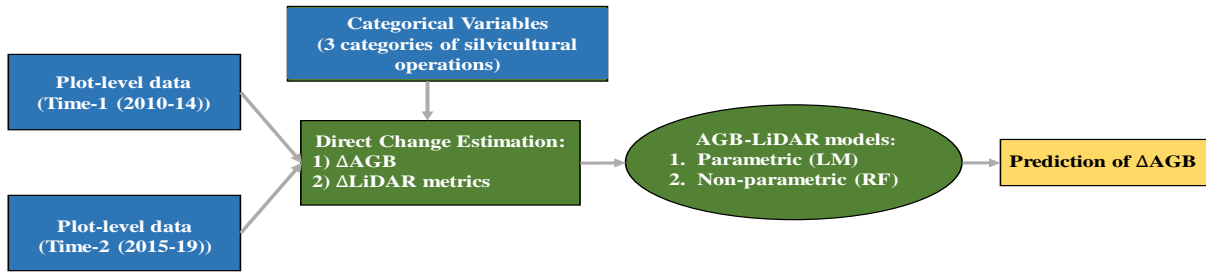


Figure 1: The methodological overview of this study.

For the parametric modelling, the LMs with and without accounting for heteroscedasticity were used along with the LiDAR metrics and categorical variables. For the model accounting for heteroscedasticity the *nlme* package in R was used (Pinheiro et al. 2021). The first model selected for the study was the LM with no intercept and with the LiDAR metrics and the categorical variables assuming that the random errors are homoscedastic. The second parametric model accounted for heteroscedasticity in random errors. To calculate weights, the variance function with the exponential form of the random error variance was selected from the *nlme* package in R (Pinheiro et al. 2021). The selection was based on the Akaike information criterion (AIC). The models have been represented in Table 1.

Table 1. The model forms of the parametric LMs, where, β and γ represent the coefficients and ε represents the random error for the first model. α and δ represent the coefficients and v represents the random error for the second model. And, I_1 and I_2 represent the first and the second group of the categorical variables.

Model type	Model form
LM (no account for heteroscedasticity)	$\Delta AGB = \beta_1 \Delta h_{p80} + \beta_2 \Delta vr + \gamma_1 (\Delta h_{p80} \cdot I_1) + \gamma_2 (\Delta vr \cdot I_1) + \gamma_3 (\Delta h_{p80} \cdot I_2) + \gamma_4 (\Delta vr \cdot I_2) + \varepsilon$
LM (account for heteroscedasticity)	$\Delta AGB = \alpha_1 \Delta h_{p80} + \alpha_2 \Delta vr + \delta_1 (\Delta h_{p80} \cdot I_1) + \delta_2 (\Delta vr \cdot I_1) + \delta_3 (\Delta h_{p80} \cdot I_2) + \delta_4 (\Delta vr \cdot I_2) + v$

For the non-parametric modelling, the RF method with and without categorical variables were used. The RF methods were formed using the *randomForest* package in R (Liaw and Wiener 2002). For this study, the default value of ' n_{tree} ' = 500 trees was used and the same dataset was used to fit the parametric models and the non-parametric methods for ΔAGB prediction.

3. Results and Discussion

The predicted Δ AGBs versus the field Δ AGBs were plotted for the four models, as seen in Figure 2. In case of the parametric models the under estimation of Δ AGB values for the plots for category 1 (plots with no activity) is higher compared to that of the non-parametric models where the underestimation is observed to be mostly in the positive range of the predicted Δ AGB values. The overestimation of the Δ AGB values for category 1 is observed to be clustered around 0 in case of the parametric models whereas, the RF model with categorical variables has a lower range of overestimated Δ AGB values. For category 2 (plots with thinning operation) the range of overestimation of Δ AGB values is observed to be lower and more spread out in case of the RF model with categorical variables compared to the other three models. The RMSE values of the four models have been listed in Table 2. The models with interactions with categorical variables have lower RMSE values. Out of the three models with categorical variable interactions, the LM model (with no account of heteroscedasticity) is observed to have a wider range of predicted Δ AGB values and the lowest RMSE value of 32.269 Mgha⁻¹ followed by the RF method with RMSE value of 34.608 Mgha⁻¹.

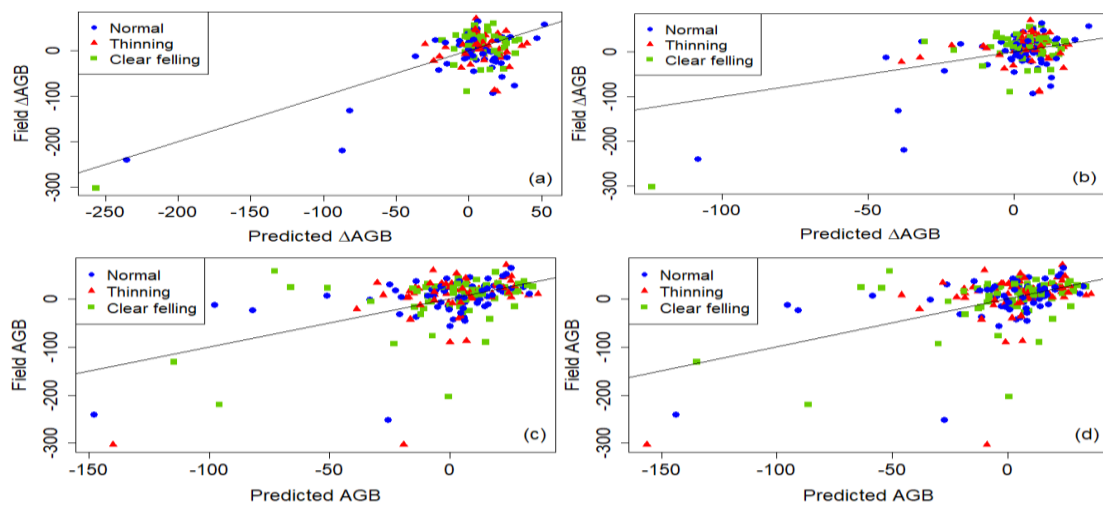


Figure 2: Predicted Δ AGB versus measured Δ AGB for: (a) LM without account for heteroscedasticity, (b) LM with account for heteroscedasticity, (c) RF without categorical variables, and, (d) RF with categorical variables.

The Δ AGB values can be predicted for the entire study area on the availability of the raster maps for the categorical variables based on the silvicultural operations conducted. From the trend in the above plots it can be expected to have a more heterogeneous map of predicted values of Δ AGB in case of the non-parametric RF method as the overestimation and underestimation of the smaller and larger Δ AGB values, respectively, is lesser compared to that of the parametric models.

Table 2. The models with their respective RMSE values in Mgha⁻¹.

Model/ Method	RMSE (Mgha ⁻¹)
LM (no account for heteroscedasticity)	32.269
LM (account for heteroscedasticity)	35.882
RF (without categorical variables)	43.708
RF (with categorical variables)	34.608

4. Conclusions

In this study, we incorporated the parametric and non-parametric models with categorical variables based on the different silvicultural operations conducted in the sample plots. The incorporation of the categorical variables along with LiDAR metrics was seen to improve the accuracy of Δ AGB prediction.

It was observed from this study that the models with interactions with categorical variables perform better, out of which the LM assuming the random errors are homoscedastic was observed to perform the best in terms of yielding the lowest RMSE value of 32.269 Mgha⁻¹. And, also the overestimation of lower Δ AGB values and underestimation of higher Δ AGB values was seen to improve in case of the non-parametric RF model along with the grouped factor of silvicultural operations.

Acknowledgements

Funding was provided by grants from the Swedish Research Council for Sustainable Development (FORMAS: FR-2019/0007), the Swedish Kempe Foundation (Kempestiftelserna: SMK-1847) and the Swedish National Space Agency (SNSA-171/19). We acknowledge the Swedish NFI for providing the field data used in the study.

References

- Bollandsås O M, Gregoire T G, Næsset E and Øyen B H, 2013, Detection of Biomass Change in a Norwegian Mountain Forest Area Using Small Footprint Airborne Laser Scanner Data. *Statistical Methods and Applications*, 22(1):113–29. doi: 10.1007/s10260-012-0220-5.
- Dubayah R O, Sheldon S L, Clark D B, Hofton M A, Blair J B, Hurt G C and Chazdon R L, 2010, Estimation of Tropical Forest Height and Biomass Dynamics Using Lidar Remote Sensing at La Selva, Costa Rica. *Journal of Geophysical Research: Biogeosciences*, 115(G2):n/a-n/a. doi: 10.1029/2009JG000933.
- Eggleston H S, Buendia L, Miwa K, Ngara T and Tanabe K, 2006, *2006 IPCC Guidelines for National Greenhouse Gas Inventories*. Institute for Global Environmental Strategies (IGES), Hayama, Japan.
- Ene L T, Næsset E, Gobakken T, Bollandsås O M, Mauya E W and Zahabu E, 2017, Large-Scale Estimation of Change in Aboveground Biomass in Miombo Woodlands Using Airborne Laser Scanning and National Forest Inventory Data. *Remote Sensing of Environment*, 188:106–17. doi: 10.1016/j.rse.2016.10.046.
- Hopkinson C, Chasmer L, Barr A G, Kljun N, Black T A and McCaughey J H, 2016, Monitoring Boreal Forest Biomass and Carbon Storage Change by Integrating Airborne Laser Scanning, Biometry and Eddy Covariance Data. *Remote Sensing of Environment*, 181:82–95. doi: 10.1016/j.rse.2016.04.010.
- Hudak A T, Strand E K, Vierling L A, Byrne J C, Eitel J U H, Martinuzzi S and Falkowski M J, 2012, Quantifying Aboveground Forest Carbon Pools and Fluxes from Repeat LiDAR Surveys. *Remote Sensing of Environment*, 123:25–40. doi: 10.1016/j.rse.2012.02.023.
- Li C, Li M and Li Y, 2020, Improving Estimation of Forest Aboveground Biomass Using Landsat 8 Imagery by Incorporating Forest Crown Density as a Dummy Variable. *Canadian Journal of Forest Research*, 50(4):390–98. doi: 10.1139/cjfr-2019-0216.
- Li C, Li Y and Li M, 2019, Improving Forest Aboveground Biomass (AGB) Estimation by Incorporating Crown Density and Using Landsat 8 OLI Images of a Subtropical Forest in Western Hunan in Central China. *Forests*, 10(2):104. doi: 10.3390/f10020104.
- Liaw A and Wiener M, 2002, *Classification and Regression by RandomForest*. Vol. 2.
- Magnussen S, Næsset E and Gobakken T, 2015, Lidar-Supported Estimation of Change in Forest Biomass with Time-Invariant Regression Models. *Canadian Journal of Forest Research*, 45(11):1514–23. doi: 10.1139/cjfr-2015-0084.
- McCaughy B, 2020, FUSION/LDV LIDAR Analysis and Visualization Software. *Pacific Northwest Research Station USDA Forest Service*, Retrieved May 14, 2021. (http://forsys.cfr.washington.edu/fusion/fusion_overview.html).
- McRoberts R E, Næsset E, Gobakken T and Bollandsås O M, 2015, Indirect and Direct Estimation of Forest Biomass Change Using Forest Inventory and Airborne Laser Scanning Data. *Remote Sensing of Environment*, 164:36–42. doi: 10.1016/j.rse.2015.02.018.
- Næsset E, Bollandsås O M, Gobakken T, Gregoire T G and Ståhl G, 2013, Model-Assisted Estimation of Change in Forest Biomass over an 11 year Period in a Sample Survey Supported by Airborne LiDAR: A Case Study with Post-Stratification to Provide ‘Activity Data. *Remote Sensing of Environment*, 128:299–314. doi: 10.1016/j.rse.2012.10.008.
- Nilsson M, Nordkvist K, Jonzén J, Lindgren N, Axensten P, Wallerman J, Egberth M, Larsson S, Nilsson L, Eriksson J and Olsson H, 2017, A Nationwide Forest Attribute Map of Sweden Predicted Using Airborne Laser Scanning Data and Field Data from the National Forest Inventory. *Remote Sensing of Environment*, 194:447–54. doi: 10.1016/j.rse.2016.10.022.
- Ou G, Li C, Lv Y, Wei A, Xiong H, Xu H and Wang G, 2019, Improving Aboveground Biomass Estimation of Pinus Densata Forests in Yunnan Using Landsat 8 Imagery by Incorporating Age Dummy Variable and Method Comparison. *Remote Sensing*, 11(7):738. doi: 10.3390/rs11070738.
- Pinheiro J, Bates D, DebRoy S, Sarkar D, Heisterkamp S, Willigen B V and Ranke J, 2021, *Package “nlme” Linear and Nonlinear Mixed Effects Models*.
- Puliti S and Astrup T F B, 2020, *Above-Ground Biomass Change Estimation Using National Forest Inventory Data with Sentinel-2 and Landsat 8*.
- Saarela S, Wästlund A, Holmström E, Mensah A A, Holm S, Nilsson M, Fridman J and Ståhl G, 2020, Mapping Aboveground Biomass and Its Prediction Uncertainty Using LiDAR and Field Data, Accounting for Tree-Level Allometric and LiDAR Model Errors. *Forest Ecosystems*, 7(1). doi: 10.1186/s40663-020-00245-0.
- Skowronski N S, Clark K L, Gallagher M, Birdsey R A and Hom J L, 2014, Airborne Laser Scanner-Assisted

Estimation of Aboveground Biomass Change in a Temperate Oak-Pine Forest. *Remote Sensing of Environment*. doi: 10.1016/j.rse.2013.12.015.

Tomppo E, Schadauer K, McRoberts R E, Gschwantner T, Gabler K and Ståhl G, 2010, *National Forest Inventories*. Springer, Netherlands.

UNFCCC, 2021, Kyoto Protocol - Targets for the First Commitment Period | UNFCCC. Retrieved May 12, 2021. (<https://unfccc.int/process-and-meetings/the-kyoto-protocol/what-is-the-kyoto-protocol/kyoto-protocol-targets-for-the-first-commitment-period>).

Terrestrial laser scanning reveals consistent dependencies between mean wood density and tree crown architecture

V. Kankare¹, N. Saarinen¹, J. Pyörälä², T. Yrttimaa¹, S. Huuskonen³, J. Hynynen³, M. Vastaranta¹

¹School of Forest Sciences, University of Eastern Finland, P.O. Box 111, 80101 Joensuu, Finland
Email: ville.kankare@uef.fi, ninni.saarinen@uef.fi, tuomas.yrttimaa@uef.fi, mikko.vastaranta@uef.fi

²Department of Forest Sciences, University of Helsinki, P.O. Box 27, 00014 University of Helsinki, Finland
Email: jiri.pyorala@helsinki.fi

³Natural Resources Institute Finland, Latokartanonkaari 9, 00790 Helsinki, Finland
Email: saiija.huuskonen@luke.fi, jari.hynynen@luke.fi

1. Introduction

Wood density is an important quality characteristic determining the suitability of raw material for a specific end use. In addition, the interest in wood density has considerably increased in recent years due to its importance in estimating forest biomass and carbon storage (Clough et al. 2017, Nam et al. 2018). Wood density of a tree species is widely expressed as a value from basic wood-density tables existing in scientific literature. However, it is known to be a site-specific parameter that can significantly vary within and between trees due to each individual tree adapting to its growing environment (Saranpää 2003). This has created a need to obtain wood density information over varying tree communities but there has not been a viable technological or methodological solution to characterize tree architecture (especially crown characteristics) sufficiently. Recently, the methodological development of terrestrial laser scanning (TLS) has reached a point where characterization of tree crown and branch properties is possible (e.g. Pyörälä et al. 2019). Therefore, the aim of this study was to evaluate the relationship between crown characteristics (shape and size) and wood density variation of Scots pine (*Pinus sylvestris* L.) trees in three different study sites. The main research questions were: (1) Are the dependencies between tree crown architecture and mean wood density consistent between different study sites? (2) What are the most influential crown characteristics explaining the wood density variation?

2. Data and Methods

The three study sites consist of even-aged (approximately 50 years) Scots pine dominated forests that are maintained by Natural Resources Institute Finland (detailed description in Saarinen et al. 2020). During the establishment, six different thinnings were conducted in addition to a control (i.e. no treatment). Treatments included three thinning types (thinning from below, above and systematic thinning) with two different thinning intensities (moderate and intensive). Wood density samples were collected using increment borer at fixed stem height of 1.3 m in March-April 2019 from 135 trees. Sample trees were selected based on the diameter distribution to represent different tree and stand characteristics. Bored samples were then analyzed with X-ray microdensitometry (Peltola et al. 2007) and following attributes

were calculated: ring basal area weighted mean values for wood density (WD_g) and mean ring width (RW_{mean}).

TLS data was collected with Trimble TX5 3D laser scanner (Trimble Navigation Limited, USA) with multiple scan setup to achieve best possible point coverage (see details Saarinen et al. 2020). The descriptive crown characteristics were derived from the point cloud data using algorithms originally developed by Yrttimaa et al. (2019, 2020) and Pyörälä et al. (2018). Derived characteristics included: crown height ($Crown_H$), area ($Crown_A$), volume ($Crown_V$), width ($Crown_W$), length ($Crown_L$), mean branch diameter ($Branch_D$), and mean whorl-to-whorl distance ($Whorl_D$).

The relationship between the crown characteristics, WD_g and RW_{mean} in the tree study sites were first investigated based on Pearson's correlation matrices. Then, a linear mixed effects model (LME) in package nlme (Pinheiro et al. 2016) of the R-software (R Core Team, 2019) was fitted and the analysis of variance was applied in testing the statistical significance of each crown attribute.

3. Results

Analysis showed that no strong (i.e. > 0.6) or statistically significant (p -value < 0.05) correlations between WD_g and crown characteristics were found in the three study sites. The highest correlation was found for $Branch_D$ (0.24). However, when evaluating correlations within thinning treatment wise, slightly higher correlations were visible. The highest correlations were found between $Crown_H$ (0.53) and $Branch_D$ (-0.53) from intensive thinning from below and control plots, respectively but overall the correlations were low. In contrast, when evaluating the correlations between crown characteristics and RW_{mean} , strong (i.e. > 0.6) and statistically significant (p -value < 0.05) correlations were observed for $Crown_A$, $Crown_V$ and $Crown_W$. Observed correlations were at similar levels between different study sites. The highest correlation (0.67) was observed between $Crown_V$ and RW_{mean} .

LME modelling showed that none of the crown characteristics had a statistically significant (p -values > 0.05) effect on WD_g in any of the tree study sites. In contrast, LME modelling showed that almost all of the crown characteristics had statistically significant effects (p -values < 0.05) on RW_{mean} . Only exceptions were $Branch_D$ and $Whorl_D$.

4. Discussion and conclusion

Results showed that the dependencies between crown characteristics and WD_g and RW_{mean} within the three study sites are consistent. Even though no strong correlations or statistical significant effects were observed between WD_g and evaluated TLS derived crown characteristics, the resulting correlations were similar between the study sites. Similar results have been reported previously and for example Jaakkola et al. (2005) concluded that intensive thinning is required to have considerable effect on WD_g . Results showed that the short timeframe since the establishment (approximately 15 years) affected more on crown characteristics than on wood density attributes. This indicates that the overall change in crown characteristic is faster compared to wood density attributes.

However, results showed that the crown characteristics tended to have a more significant effect and higher correlations on RW_{mean} than WD_g . The most influential characteristics were $Crown_W$, $Crown_A$ and $Crown_V$. These characteristics also had a statistically significant effect on RW_{mean} based on LME modelling. This result supports the fact that the increasing size of the tree crown causes trees to allocate their growth to stem size to increase the structural carrying capacity. Therefore, the future research should

focus on evaluating the development (i.e. growth) of crown characteristic in relation to mean density variation.

Acknowledgements

The study was funded by the Academy of Finland (project numbers 315079, 337127, 331711 and 337810).

References

- Clough B.J., Curzon M.T., Domke G.M., Russell M.B. and Woodall C.W., 2017, Climate-driven trends in stem wood density of tree species in the eastern United States: Ecological impact and implications for national forest carbon assessments. *Global Ecology and Biogeography*, 26(10): 1153–1164.
- Jaakkola T., Mäkinen H. and Saranpää P., 2005, Wood density in Norway spruce: changes with thinning intensity and tree age. *Canadian Journal of Forest Research*, 35: 1767–1778.
- Nam V.T., Anten N.P.R. and van Kuijk M., 2018, Biomass dynamics in a logged forest: the role of wood density. *Journal of Plant Research*, 131(4): 611–621.
- Peltola H., Kilpeläinen A., Sauvala K., Räsänen T. and Ikonen V.-P., 2007, Effects of early thinning regime and tree status on the radial growth and wood density of Scots pine. *Silva Fennica*, 41(3): 489-505.
- Pinheiro J., Bates D., DebRoy S., Sarkar D., R Core Team. 2016. nlme: Linear and Nonlinear Mixed Effects Models. Available: <https://cran.r-project.org/package=nlme> [Accessed September 21, 2020] R package version 3.1-143.
- Pyörälä, J., Liang, X., Vastaranta, M., Saarinen, N., Kankare, V., Wang, Y., Holopainen M. and Hyypä J., 2018, Quantitative assessment of Scots pine (*Pinus sylvestris* L.) whorl structure in a forest environment using terrestrial laser scanning. *IEEE Journal of Selected Topics in Applied Earth Observations and Remote Sensing*, 11(10): 3598-3607.
- Pyörälä J., Saarinen N., Kankare V., Coops N.C., Liang X., Wang Y., Holopainen M., Hyypä J. and Vastaranta M., 2019, Variability of wood quality studied using airborne and terrestrial laser scanning. *Remote Sensing of Environment*, 235.
- R Core Team, 2019, R: A language and environment for statistical computing. R Foundation for Statistical Computing, Vienna, Austria. URL <https://www.R-project.org/>.
- Saarinen N., Kankare V., Yrttimaa T., Viljanen N., Honkavaara E., Holopainen M., Hyypä J., Huuskonen S., Hynynen J. and Vastaranta M., 2020, Assessing the effects of thinning on stem growth allocation of individual Scots pine trees. *Forest Ecology and Management*, 474: 118344.
- Saranpää P., 2009, Wood density and growth. In: Barnett J. and Jeronimidis G. (eds) *Wood quality and its biological basis*, John Wiley & Sons, 87–117.
- Yrttimaa, T., Saarinen, N., Kankare, V., Liang, X., Hyypä, J., Holopainen, M., and Vastaranta, M., 2019, Investigating the feasibility of multi-scan terrestrial laser scanning to characterize tree communities in southern boreal forests. *Remote Sensing* 11(12): 1423.
- Yrttimaa, T., Saarinen, N., Kankare, V., Hynynen, J., Huuskonen, S., Holopainen, M., Hyypä, J., and Vastaranta, M., 2020, Performance of terrestrial laser scanning to characterize managed Scots pine (*Pinus sylvestris* L.) stands is dependent on forest structural variation. *ISPRS Journal of Photogrammetry and Remote Sensing* 168: 277-287.

Accuracy assessment of terrain and canopy height estimates from ICESat-2 and GEDI LiDAR missions in temperate and tropical forests: first results

M. Urbazaev¹, L. L. Hess², L. Sato³, J. P. Ometto³, C. Thiel⁴, C. Dubois¹, M. Adam¹,
C. Schmillius¹

¹Friedrich-Schiller-University Jena, Loebdergraben 32, 07743 Jena, Germany
Email: {mikhail.urbazaev; clemence.dubois; markus.adam; c.schmillius}@uni-jena.de

²University of California Santa Barbara, CA, USA, 93106

³Instituto Nacional de Pesquisas Espaciais (INPE), São José dos Campos, Brazil

⁴German Aerospace Center (DLR), Jena, Germany

1. Introduction

Two new NASA spaceborne Light Detection and Ranging (LiDAR) missions launched in late 2018 - the Ice, Cloud, and land Elevation Satellite 2 (ICESat-2) and the Global Ecosystem Dynamics Investigation (GEDI) - produce a new set of three-dimensional data of Earth's land surface. In this study we assessed the accuracy and precision of terrain and canopy height estimates from these two new LiDAR missions by examining the ICESat-2 ATL08 land and vegetation product, version 3 (Neuenschwander and Pitts 2019; Neuenschwander et al. 2020) and the GEDI L2A footprint elevation and canopy height metrics, version 1 (Dubayah et al. 2020a, Dubayah et al. 2020b). We conducted our analysis over temperate broadleaved and needleleaved forests as well as tropical rainforest. For assessment of terrain and canopy height estimates from spaceborne LiDAR data we used high-resolution airborne LiDAR (ALS) as reference data.

2. Methods and material

We investigated the accuracy of both sensors at three different study sites. The first two test sites are located in central Germany and covered by temperate broadleaved and needleleaved forests. The Amazon tropical forest site is a 2° x 2° region transected by the middle reaches of the Juruá river, a major tributary of the Amazon river in western Brazil. About 80% of the region consists of upland ("terra firme") hills, terraces, and interfluvial flats with the remainder occupied by seasonally inundated, largely forested floodplains.

As reference data we used small-footprint discrete-return airborne LiDAR data. The mean point density is around 4-20 returns per m². Terrain elevation, slope, canopy height and density estimates at a spatial resolution of 1 m were calculated with the LAStools software (version 200304).

For the accuracy assessment of ICESat-2 data we used the ATL08 product version 3 (Neuenschwander et al. 2020) acquired between October 2018 and July 2020. GEDI L2A version 1 data (Dubayah et al. 2020b) acquired between April 2019 and April 2020 over our study regions were used for the accuracy assessment of terrain and canopy height estimates.

Since the elevations in the ALS data are orthometric heights referenced to local geoids, a conversion to the WGS84 ellipsoid vertical reference as in GEDI and ICESat-2 data was applied. The Earth Gravitational Model (EGM) 2008 (Pavlis et al. 2012) geoid heights are provided in the GEDI L1B and ICESat-2 ATL03 products as auxiliary information. From the reference CHM we excluded those areas that are located outside forested areas. For this, we used a CHM threshold of 5 m for temperate and tropical forests (FRA 2015).

For terrain elevation comparison, we calculated a median value from reference data over GEDI and ICESat-2 footprints. For canopy height assessment, we extracted 95th percentile from CHM reference data over GEDI and ICESat-2 footprints. For statistical assessment of terrain and canopy height estimates, the following statistical metrics between spaceborne and reference data were calculated: R², mean error (ME), root mean square error (RMSE), median absolute deviation (MAD), linear error 90% (LE90).

3. Results and discussion

Our results show that both GEDI and ICESat-2 provide accurate terrain elevation estimates in three different biomes (broadleaved and needleleaved temperate forests, and tropical forest) (Figure 1). With the exception of ICESat-2 in tropical forests (with a small sample size though and one outlier), in all regions ME is lower than 1 m and R^2 is higher than 0.9 compared to the reference data.

ICESat-2 provides more precise estimates, e.g., LE90 from ICESat-2 is smaller than that from GEDI. The reason for this might be partly caused by a strong filtering (e.g., cloud, outlier removals) of ICESat-2 ATL08 data. On the other hand, there are many more GEDI samples (e.g., Figure 1), although only 12 months of GEDI data were used here (while ICESat 2 acquisition dates spanned 21 months).

The six GEDI algorithm setting groups perform differently in the three biomes. The default algorithm 1 is somewhat similar to the other four algorithms (2, 3, 4 and 6) and yielded one of the best results in temperate broadleaved and needleleaved forests. As expected, tropical forests represent the most challenging environment for both sensors to estimate terrain elevation. The number of reference samples in tropical forests is, however, much lower than in the other two environments, resulting in less robust statistics (Figure 1). Dense canopies with multiple vegetation layers cause a weak return from the ground, which complicates an accurate classification of the terrain. However, as shown here, GEDI terrain estimates from the algorithm 5 are quite accurate except for the areas over flooded forests. A lower signal end threshold helps to detect the ground more accurately below tropical forests with dense understory vegetation.

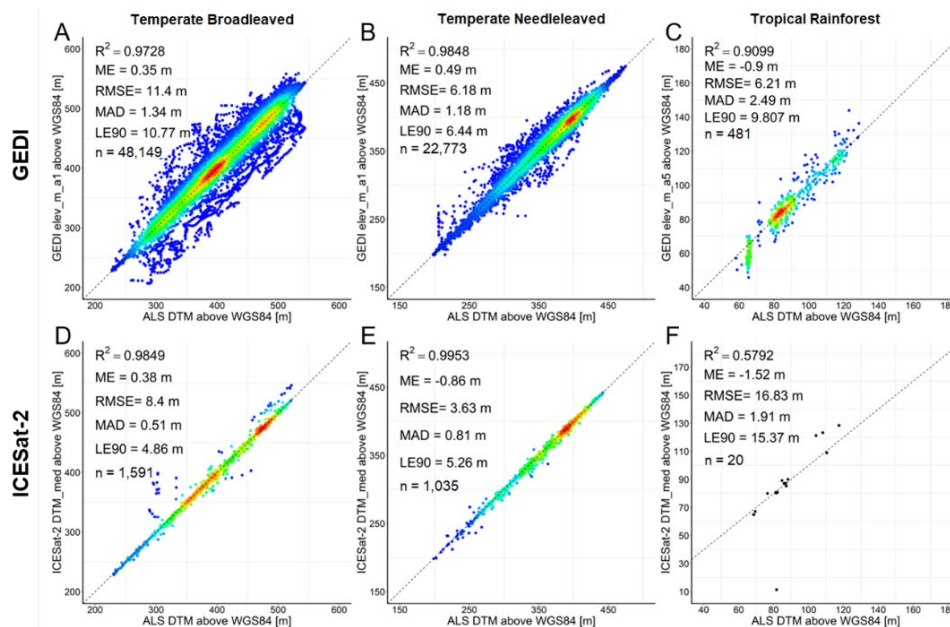


Figure 1: Terrain elevation estimates in temperate broadleaved (A, D), needleleaved (B, E) and tropical forests (C, F) from GEDI (upper figures) and ICESat-2 (bottom figures) vs. ALS DTM.

Canopy height estimates show much lower accuracy for both GEDI and ICESat-2 in all three biomes (Figure 2). Factors contributing to lower accuracy are 1) the canopy height estimate depends directly on the accuracy of terrain height; 2) vegetation canopies are much rougher than terrain, and are thus strongly influenced by the geolocation accuracy of spaceborne data.

In temperate forests the accuracies of the six GEDI algorithms for canopy height estimates differ in terms of R^2 and RMSE, with the most accurate algorithms 2 and 6. In this biome, algorithm 5 is the least accurate, due to underestimation of terrain elevation, which leads to an overestimation of canopy heights. The overestimation of GEDI and ICESat-2 canopy heights in temperate needleleaved forest can be partly caused by vegetation growth between the ALS and spaceborne acquisition dates. Finally, since current GEDI horizontal geolocation is around 10-20 m, it is difficult to conclude which algorithm performs best in temperate forests.

In contrast to the temperate forests, in the tropical forest area GEDI algorithm 5 provides the most accurate results compared to the ALS data, again thanks to more accurate estimation of terrain elevation. The other five GEDI algorithms underestimate canopy height with ME lower than 6 m. While the first

return might be detected correctly, an overestimation of terrain elevation leads to an underestimation of vegetation height.

The best results for canopy height estimation from ICESat-2 were found in temperate forests, with R^2 between 0.6-0.7 compared to the ALS CHM. In general, green lasers have a higher background solar noise and lower reflectance from vegetation as opposed to the near-infrared. Thus, a green laser might have problems when a canopy is dense and a low number of photons is collected (Swatantran et al. 2016), as it can be the case in tropical forests. In our temperate forests ICESat-2 canopy height estimates perform better than GEDI canopy height estimates, which can be caused by a strong filter of the ICESat-2 ATL08 product and a higher horizontal geolocation accuracy (5 m for ICESat-2 (Neuenschwander & Magruder 2019) and 10-20 m for GEDI (Dubayah et al. 2020a).

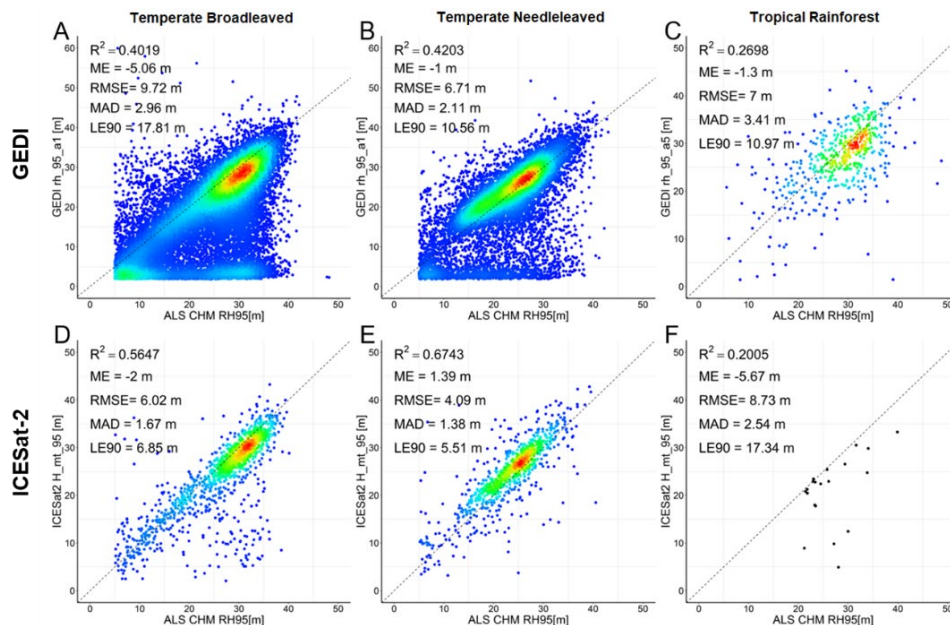


Figure 2: Canopy height estimates in temperate broadleaved (A, D), needleleaved (B, E) and tropical forests (C, F) from GEDI (upper figures) and ICESat-2 (bottom figures) vs. ALS CHM estimates.

Acknowledgements

M.U. was supported in part by the 2017–2018 Belmont Forum and BiodivERsA joint call for research proposals, under the BiodivScen ERA-Net COFUND program, and in part by the funding organization of the German Federal Ministry of Education and Research (BMBF) under grant no. 01LC1808A.

References

- Dubayah R., Blair JB, Goetz S, Fatoyinbo L, Hansen M, Healey S, Hofton M, Hurtt G, Kellner J and Luthcke S, 2020a, The Global Ecosystem Dynamics Investigation: High-resolution laser ranging of the Earth's forests and topography. *Science of Remote Sensing*, 1.
- Dubayah R, Hofton M, Blair JB, Armston J, Tang H and Luthcke S, 2020b, GEDI L2A Elevation and Height Metrics Data Global Footprint Level V001. DAAC, N.E.L.P.; https://doi.org/10.5067/GEDI/GEDI02_A.001.
- FRA (Forest Resources Assessment), 2015, *Terms and Definitions*. Food and Agriculture Organization of the United Nation.
- Höhle J and Höhle M, 2009, Accuracy assessment of digital elevation models by means of robust statistical methods. *ISPRS Journal of Photogrammetry and Remote Sensing*, 64: 398-406.
- Neuenschwander AL and Pitts KL, 2019, The ATL08 land and vegetation product for the ICESat-2 Mission. *Remote sensing of environment*, 221: 247-259.
- Neuenschwander AL and Magruder LA, 2019, Canopy and terrain height retrievals with ICESat-2: A first look. *Remote Sensing*, 11, 1721.
- Neuenschwander AL, Pitts KL, Jelley BP, Robbins J, Klotz B, Popescu SC, Nelson R.F, Harding D, Pederson D, and Sheridan R, 2020, ATLAS/ICESat-2 L2A Land and Vegetation Height, Version 3; <https://doi.org/10.5067/ATLAS/ATL08.003>.
- Pavlis NK, Holmes SA, Kenyon SC and Factor JK, 2012, The development and evaluation of the Earth Gravitational Model 2008 (EGM2008). *Journal of geophysical research: solid earth*, 117.
- Swatantran A, Tang H, Barrett T, DeCola P and Dubayah R, 2016, Rapid, high-resolution forest structure and terrain mapping over large areas using single photon lidar. *Scientific reports*, 6, 28277.
- Wessel B, Huber M, Wohlfart C, Marschalk U, Kosmann D and Roth A, 2018, Accuracy assessment of the global TanDEM-X Digital Elevation Model with GPS data. *ISPRS Journal of Photogrammetry and Remote Sensing*, 139: 171-182.

Forest Stand Delineation Using Airborne LiDAR and Hyperspectral Data

H. Xiong^{1,2}, Y. Pang^{1,2}, W. Jia^{1,2}, Y. Bai^{1,2}

¹ Institute of Forest Resource Information Techniques, Chinese Academy of Forestry, Beijing 100091, China
²Key Laboratory of Forestry Remote Sensing and Information System, National Forestry and Grassland, Beijing 100091, China
Email: 13545903512@163.com, pany@ifrit.ac.cn

1. Introduction

Forest stands are fundamental to forestry management. Forest stands are defined as large forested areas of homogeneous tree attributes and are traditionally delineated by operators through visual analysis of very high-resolution images, which is tedious and highly time-consuming. Therefore, this task could be automated for scalability and efficient updating purposes (Haara et al 2002).

With respect to existing methods, it appears that there are few studies focused on automatic delineation of forest stands based on multi-source remote sensing data. Also, tree species information with high accuracy is not fully used in recent methods. In this paper, a method based on the fusion of airborne LiDAR and hyperspectral data was proposed. The hyperspectral data give access to the dominant tree species of the forest stands while CHM derived from airborne LiDAR data provides geometric information of forest stands such as mean tree height and canopy closure.

2. Data and Methods

2.1 Study area

The study area is in Mengjiagang Forest Farm, Heilongjiang Province, China. The geographical coordinates are 130°32'-130°52'E and 46°20'-46°30'N. The major tree species of this farm include Korean pine (*Pinus koraiensis*), Spruce (*Picea asperata*), Mongolian pine (*Pinus sylvestris*), and larch (*Larix olgensis*), which approximately account for 80% of the forest area.

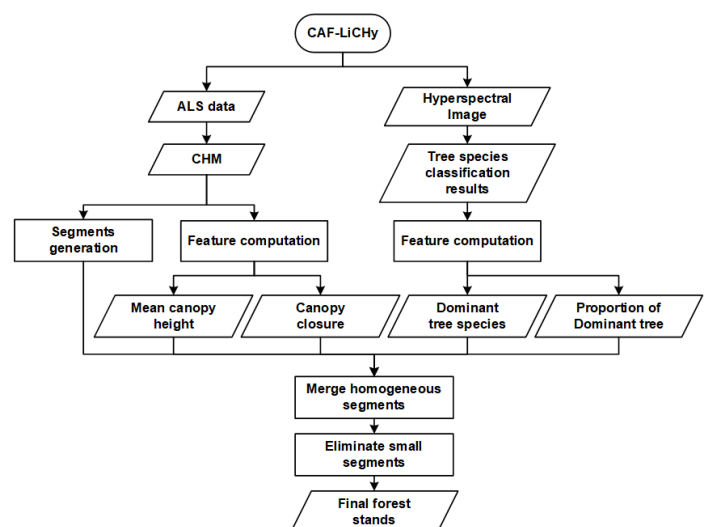
2.2 Data

The airborne data were collected in 2017 by LiCHy airborne observation system (Pang et al., 2016). The canopy height model (CHM) was obtained from the LiDAR point cloud data with 1 m spatial resolution. The tree species map was obtained by classification of hyperspectral images, with an overall accuracy of 91.28% and Kappa of 0.88. (Li et al., 2018).

2.3 Methods

There are three main steps of the stand delineating method: (i) the 1 m resolution CHM was down-sampled to 5 m, filtered by Minimum Variance Filter and over-segmented to get large amounts of segments smaller than the forest stand size; (ii) the attributes of segments were calculated, including mean canopy height, canopy closure, dominant tree species, the proportion of dominant tree species and so on; (iii) Two rules (merging homogeneous segments and eliminating small segments) were used to merge segments toward final forest stands. The workflow was presented in Figure 1.

Figure 1: The flowchart of automatic delineation of forest stands based on CHM and tree species.



To reduce the noise in homogeneous forest stands. The CHM was down-sampled to 3m, 5m, 7m, 10m respectively and filtered by several edge-remaining smoothing filters in different window sizes. Then the MVF filter was selected. The result was segmented by object-oriented multi-resolution segmentation with eCognition developer software.

Six attributes were derived from the CHM and the tree species map, which were mean tree height, canopy closure, dominant tree species, the proportion of dominant tree species, stand area, and length of common edge.

In the first merging step, a threshold of the maximum stand area was used to evaluate the sum of each segment and its neighbors. Then each pair of segments and neighbors would be judged whether they have the same dominant tree species, whether the difference of the two tree proportions was less than TP1 (Tree proportion threshold), the difference between their canopy closure was less than 0.2 and the difference between their CHM values was less than SH1 (Stand height threshold). The satisfactory segments were merged to their most suitable neighbors.

After that, there were still some segments that did not have any acceptable adjacent segment. A threshold value of minimum stand area was applied, and all of those smaller than the fixed threshold would be merged to one of their adjacent segments. Three attributes were used in this rule to ensure there was no repetition and no omission, including tree species, tree proportion, stand height, and length of common side.

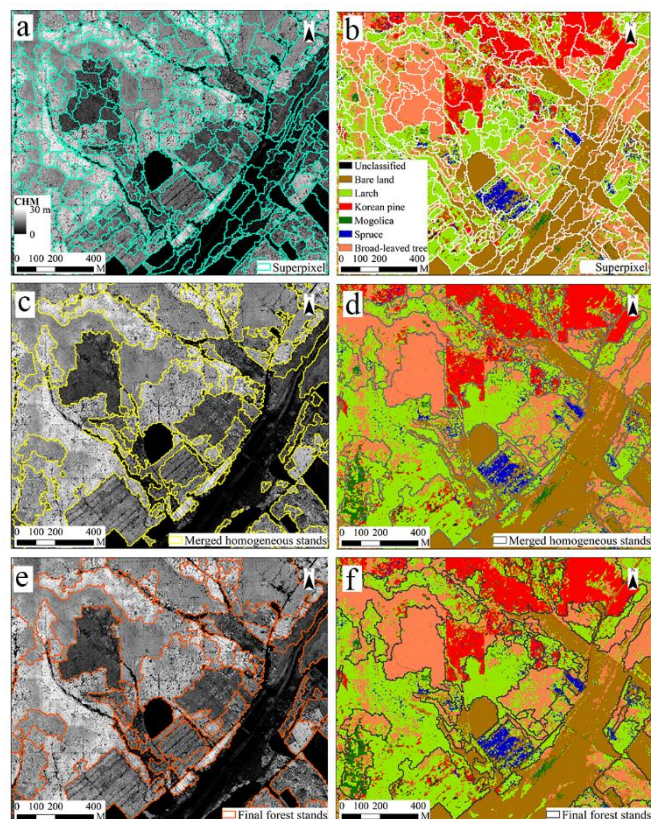
The delineating results were verified in two ways for accuracy. The manual forest stands, the logging forest stands and the forest stands delineated based on DOM of 0.1 m spatial resolution were used as reference data. The intersection over union ratio (IoU) (Nowozin et al., 2014) was introduced to compare the overlapping between automatically delineated forest stands and reference forest stands. The explained variance of mean DBH, mean tree height and mean canopy height of 5 m×5 m cells were used to evaluate the homogeneity of each forest stand and the heterogeneity between different forest stands (Pukkala et al., 2019a, 2019b; Jia et al., 2020). The closer the interpretable variance is to 1, the higher the forest stands' consistency are and the greater the variability among different forest stands are.

3. Results and Discussion

The delineating results of different scales were shown in Figure 2. The final automatically delineated forest stands were compared with the manual forest stands in Figure 3. The proportions of the final forest stands with IoU greater than 0.7 were 24%, 48%, and 64% for manual, logging and DOM mapping forest stands and 41%, 67%, and 82% for automatic forest stands with IoU greater than 0.5, respectively. The explained variances of mean DBH and mean height of the final forest stands were 97% and 98%, the same as manual forest stands. Our method explained 81.8% of the variation in mean canopy height in 5 m×5 m cells, which was 7.31% higher than the manual forest stands, 2.31% higher than the multiresolution segmentation results.

Figure 2: Segments, merged segments and final forest stands.

(a) Segments on CHM, (b) The merged segments on CHM, (c) The final forest stands on CHM, (d) Segments on tree species map, (e) The merged segments on tree species map (f) The final forest stands on tree species map.



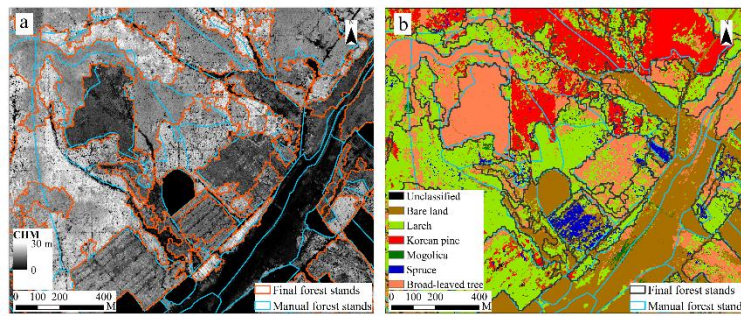


Figure 3: The final forest stands and manual forest stands.

(a)The final and manual forest stands on CHM, (b)The final and manual forest stands on tree species map.

4. Conclusions

It turned out that our results were generally similar to the manual forest stands. The forest stands automatically delineated by multiresolution segmentation method with CHM and tree species information derived from hyperspectral image have obvious advantages in terms of internal consistency, boundary accuracy and were more consistent with the distribution of trees at the boundaries. This method is timesaving and increases the accuracy of forest stand delineation, which can support fine forest management planning.

Acknowledgements

This study was supported by National Key Research and Development Program (2017YFD0600404 & 2020YFE0200800).

References

- Dechesne, C., C. Mallet, A. Le Bris and V. Gouet-Brunet, 2017, Semantic segmentation of forest stands of pure species combining airborne lidar data and very high resolution multispectral imagery. *ISPRS Journal of Photogrammetry and Remote Sensing* 126: 129-145.
- Haara A, Haarala M, 2002, Tree species classification using semi-automatic delineation of trees on aerial images. *Scandinavian Journal of Forest Research*, 17(6): 556-565.
- Koch, B., C. Straub, M. Dees, Y. Wang and H. Weinacker, 2009, "Airborne laser data for stand delineation and information extraction." *International Journal Of Remote Sensing* 30(4): 935-963.
- Leppänen, V., T. Tokola, M. Maltamo, L. Mehtätalo, T. Pusa and J. Mustonen, 2008, Automatic delineation of forest stands from lidar data. *GEOBIA*: 05-08.
- Li J, Pang Y, Li Z, et al. Tree Species Classification of Airborne Hyperspectral Image in Cloud Shadow Area, *International Symposium of Space Optical Instrument and Application*. Springer, Cham, 2018: 389-398.
- Mora, B., M. A. Wulder and J. C. White, 2010, Segment-constrained regression tree estimation of forest stand height from very high spatial resolution panchromatic imagery over a boreal environment. *Remote Sensing Of Environment* 114(11): 2474-2484.
- Mustonen, J., P. Packalen and A. Kangas, 2008, "Automatic segmentation of forest stands using a canopy height model and aerial photography." *Scandinavian Journal of Forest Research* 23(6): 534-545.
- Pang Y, Li Z, Ju H, et al, 2016, LiCHy: The CAF's LiDAR, CCD and hyperspectral integrated airborne observation system[J]. *Remote Sensing*, 8(5): 398.
- Pukkala, T., 2019a, Optimized cellular automaton for stand delineation. *Journal of Forestry Research* 30(1): 107-119.
- Pukkala, T., 2019b, Using ALS raster data in forest planning. *Journal of Forestry Research* 30(5): 1581-1593.
- Pukkala, T., 2020, Delineating forest stands from grid data. *Forest Ecosystems* 7(1): 1-14.
- Wu, Z., V. Heikkinen, M. Hauta-Kasari, J. Parkkinen and T. Tokola, 2014, ALS data based forest stand delineation with a coarse-to-fine segmentation approach. 2014 7th International Congress on Image and Signal Processing, IEEE.
- Wulder, M. A., J. C. White, G. J. Hay and G. Castilla, 2008, Towards automated segmentation of forest inventory polygons on high spatial resolution satellite imagery. *Forestry Chronicle* 84(2): 221-230.

High Resolution Mapping of Forest Resources and Prediction Uncertainty using Multisource Inventory Approach

Ankit Sagar^{1,2,3}, Cédric Vega², Christian Piédallu³, Olivier Bouriaud², Jean-Pierre Renaud^{2,4}

¹ Université de Lorraine, faculté des Sciences et Technologies - Campus Aiguillettes, 54506 Vandœuvre Les Nancy, France
ankitsagar240893@gmail.com

² Laboratoire d'Inventaire Forestier, Université de Lorraine, ENSG, IGN, INRA, 54000 Nancy, France
{Cedric.Vega; Olivier.Bouriaud}@ign.fr

³ UMR SILVA INRA-AgroParisTech-Université de Lorraine, 54000 Nancy, France
christian.piedallu@agroparistech.fr

⁴ Office National des Forêts, Pôle Recherche Développement Innovation, 54600 Villers-lès-Nancy, France
jean-pierre.renaud-02@onf.fr

1. Introduction

National forest inventory (NFI) provides precise forest resource estimates at national up to regional scale but could not support local estimates with high precision because of inadequate number of field plots. The forest managers and stakeholders prefer local estimates at fine spatial resolution (Chirici et al. 2020). Multi source-national forest inventory (MS-NFI) opens the possibility for wall-to-wall mapping of forest attributes with good precision at high spatial resolution. MS-NFI rely on the combination of NFI data with auxiliary data (remote sensing data, thematic map, etc.), and in many cases, this combination is modelled through a non-parametric k-nearest neighbour (k-NN) approach. k-NN is capable in predicting several attributes in a single model with a low prediction bias. The major drawbacks of k-NN are its inability to predict beyond the range of training data (Magnussen et al. 2010), the lack of well-established variance estimator (McRoberts et al. 2011) and its decreasing performance with increasing dimensionality.

The estimation maps for the forest resources are important (Tomppo et al. 2008; Chirici et al., 2020), but their prediction uncertainties have also to be taken into consideration. Methods have been proposed recently to map the prediction uncertainty (Esteban et al, 2019) and these maps have been included into an inferential framework (Saarela et al, 2020). In this study we propose a method building upon bootstrap model-based estimator (McRoberts et al. 2011) to estimate forest attributes of interest at pixel level and address the problem of extrapolation and precision of estimation by providing maps for both at high spatial resolution. For sake of concision, results were presented for growing stock volume (GSV) only.

2. Data and Methods

The study was conducted in oak-dominated French broadleaved forests of Sologne and Orleans (~7500 km²) in central France. NFI field data (819 plots) were collected from circular plots of 15-meter radius for a period of 5 year (2010 – 2014). The auxiliary data from ALS (2 point per m²) were acquired in winter of 2014 and three Level 2A Landsat 8 images were obtained during the summer of 2014. Forest map from National Institute of Geographic and Forest Information (IGN) was used to extract forest type information and for discarding pixels shared among forest and non-forest areas. A total of 56 metrics have been derived from these auxiliary data sources.

The k-NN model was built using Euclidean distance metrics with 5 nearest neighbours. Prior to modelling, an iterative feature deletion variable selection algorithm (Crookston and Finley 2008) had been used and the following 7 predictors had been selected: forest type from the forest map; mean and standard deviation of heights, canopy closure ratio (ratio between canopy and ground cover), percentage of returns above mean height, and 7th cumulative percentage of return from ALS data; and green band from the Landsat data.

The precision of each pixel estimation was assessed using 100 bootstraps. The prediction error was evaluated through the computation of relative Root Mean Square Error (RMSE_%) and bias for both training and testing sets. The prediction of each pixel was computed by taking mean of the boots.

The mean coefficient of variation (CV) of the boots were computed and used to classify pixels in three precision classes. The precision was considered high when the CV values were below the training RMSE%, intermediate in between the training and testing RMSE% and low otherwise. The uncertainty of the pixel prediction was assessed through the method of extrapolation, in which a convex hull (Barber et al. 1996) was built around the predictors from plot dataset and identifying pixels falling outside of the hull from population dataset as extrapolated pixels. The point to point distance of the extrapolated pixels to the calibration domain of the convex hull was also computed.

3. Results and Discussion

The mean plot level GSV used to train k-NN model was $160.6 (\pm 7.8) \text{ m}^3\text{ha}^{-1}$. The RMSE% of the model was 26.6% and 52% for training and testing sets, respectively. The model bias for the testing set was $-2.7 \text{ m}^3\text{ha}^{-1}$.

Table 1: Proportion of overall and extrapolated pixels partitioned into three precision classes, and the mean Euclidean distance of the extrapolated pixels from the convex hull. Numbers in parenthesis are standard deviation (SD) of the distance.

Pixel Type	Number of Pixels	High precision	Intermediate precision	Low precision
All	3,592,156 (100%)	77.3%	20.8%	1.8%
Extrapolated	1,337,000 (37%)	68.6%	27.5%	3.9%
Mean extrapolation distance and SD from the hull		1.15 (0.43)	1.41 (0.68)	2.06 (1)

Table 1 shows the bootstrap assessment of the GSV at pixel level. The study site constitutes ~ 3.6 million of forested pixels of 30-meter resolution. Based on the model RMSE%, the pixels were classified into three precision classes: 77.3% of the pixels were classified in high (bootstrapped $\text{CV} \leq 26.6\%$), 20.8% in intermediate ($26.6\% < \text{bootstrapped CV} < 52\%$) and 1.8% in low (bootstrapped $\text{CV} \geq 52\%$) precision classes. Overall, 37% of the pixels (~ 1.34 million) were found to be extrapolated of which 68.6%, 27.5% and 3.9% of these extrapolated pixels fall in high, intermediate and low precision classes, respectively.

It is observed from Table 1 that, as the distance of the extrapolated pixel to the convex hull increases, the pixel precision decreases. Figure 1 represents map products for a contrasted small subset of the study area. Overall, the map shows that low to intermediate precisions are often associated with extrapolation. In low volumes, such a combination is driven by the high variability in auxiliary data and the lack of measurements of small tree diameters on the field. Large volumes show some saturation (result not shown) which is masked by high precision, caused by the least variability in auxiliary data. In those values, extrapolation is the dominating factor. The Google imagery (Figure 1) further shows that extrapolation highlight transitions between forest and non-forest areas, forest stand limits, which are not fully covered in the field sample.

4. Conclusions

We provided a pixel level approach to map extrapolation and precision of k-NN predictions of GSV. The method will be extended to consider potential bias correction as a function of distances to the calibration domain of the extrapolated pixels. The map products will be further connected with the model-based bootstrap estimator (McRoberts et al. 2011) for inferring population mean and variances for either administrative or management units. Those map products could help stakeholders in their decision-making process.

5. Acknowledgements

We received the financial support of the French PIA project ‘‘Lorraine Universit  d’Excellence’’, reference ANR- 15-IDEX-04-LUE, through the project Impact DeepSurf. We thank the LABEX Arbre (ANR-11-LABX-0002-01, French National Research Agency (ANR)) for their long-term support. We thank J-R Roussel, C.B. Barber and D.C. Sterratt for their support with LidR and Geometry packages in R.

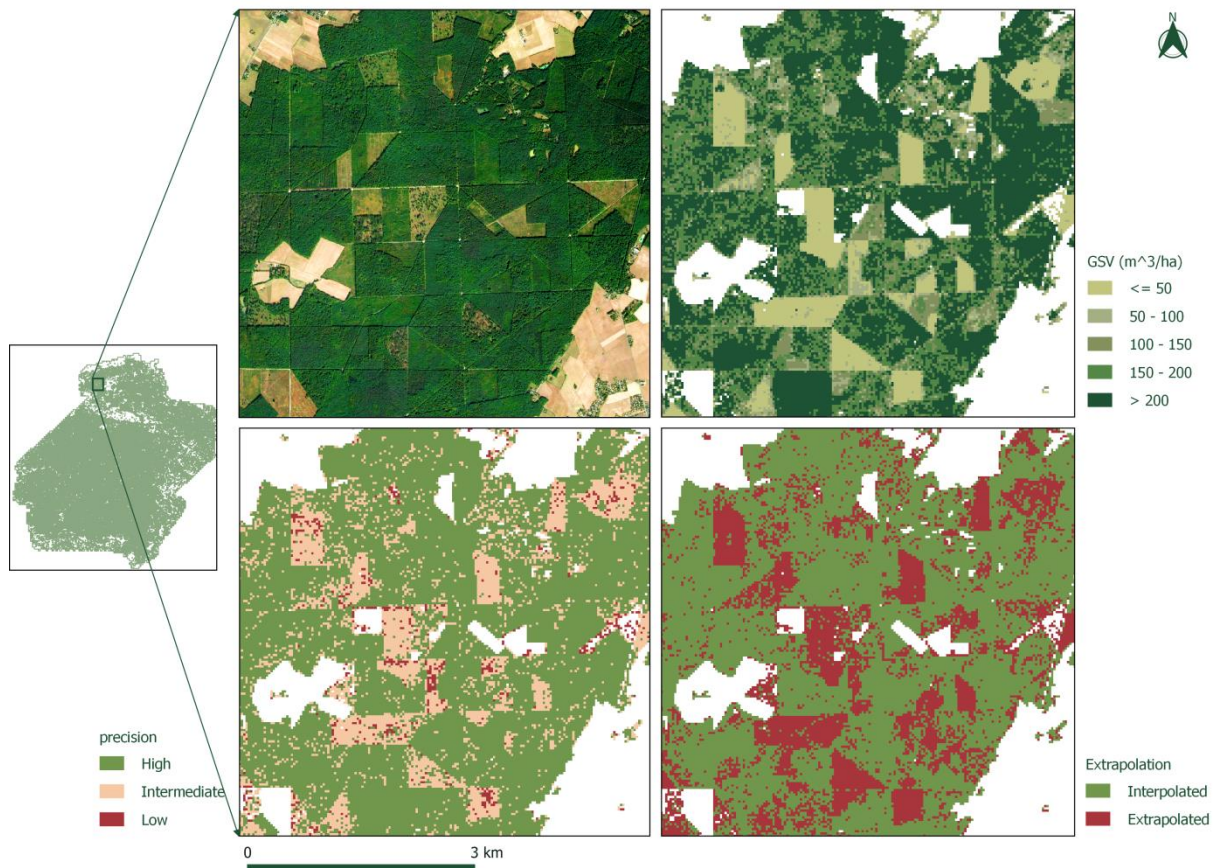


Figure 1: Map products for GSV: Google satellite image (top left), mean predicted volume (top right), precision class (bottom left) and extrapolation (bottom right).

6. References

- Barber C B, Dobkin D P and Huhdanpaa H, 1996, The quickhull algorithm for convex hulls. *ACM Transactions on Mathematical Software*, 22(4): 469–483.
- Chirici G, Giannetti F, McRoberts R E, Travaglini D, Pecchi M, Maselli F, Chiesi M and Corona P, 2020, Wall-to-wall spatial prediction of growing stock volume based on Italian National Forest Inventory plots and remotely sensed data. *International Journal of Applied Earth Observation and Geoinformation*, 84, 101959.
- Crookston N L and Finley A O, 2008, YaImpute: An R Package for KNN Imputation. *Journal of Statistical Software*, 23 (1): 1–16.
- Esteban J, McRoberts R, Fernández-Landa A, Tomé J and Næsset E, 2019. Estimating Forest Volume and Biomass and Their Changes Using Random Forests and Remotely Sensed Data. *Remote Sensing*, 11(16): 1944.
- Magnussen S, Tomppo E and McRoberts R E, 2010, A Model-Assisted k-Nearest Neighbour Approach to Remove Extrapolation Bias. *Scandinavian Journal of Forest Research*, 25 (2): 174–184.
- McRoberts R E, Magnussen S, Tomppo E O and Chirici G, 2011, Parametric, bootstrap, and jackknife variance estimators for the k-Nearest Neighbors technique with illustrations using forest inventory and satellite image data. *Remote Sensing of Environment*, 115(12): 3165–3174.
- McRoberts R E and Westfall J A, 2016, Propagating uncertainty through individual tree volume model predictions to large-area volume estimates. *Annals of Forest Science*, 73(3), 625–633.
- Saarela S, Wästlund A, Holmström E, Mensah A A, Holm S, Nilsson M, Fridman J and Ståhl G, 2020, Mapping aboveground biomass and its prediction uncertainty using LiDAR and field data, accounting for tree-level allometric and LiDAR model errors. *Forest Ecosystems*, 7(1): 43.
- Tomppo E, Haakana M, Katila M and Peräsaari J, 2008. Multi-source national forest inventory: Methods and applications (1. Ed). Springer Netherland.

Stem shape and volume of standing tree based on TLS point cloud inversion mixed-forest management

Yuan Sun^{1,2*}, Xiuyun Lin^{1,2*}, Cao Lin¹, Yanli Zhang³, Jiawen Jiang¹, Xiaorong Wen^{1,2}

¹ Co-Innovation Center for Sustainable Forestry in Southern China, Nanjing Forestry University, Nanjing 210037, China; yuan.sun@njfu.edu.cn;

² College of Forestry, Nanjing Forestry University, Nanjing 210037, China

³ Arthur Temple College of Forestry and Agriculture, Stephen F. Austin State University, Nacogdoches, TX 75962, [USA](#)

Abstract

Objects:

Agroforestry is a sustainable land management mode to solve the current problems of resource depletion and land use contradiction through planting mixed-forest. Mixed-forestry management can directly change the forest stand structure by adjusting the management allocation per unit area, and it has the multi-level characteristics composed by various vegetation types to achieve the corresponding management objectives. With the support of active remote sensing technology, three-dimensional point cloud scanned by TLS (Terrestrial laser scanning) can be quantitatively monitored in agroforestry environment.

Method:

This research took the Chinese fir mixed-forest in Gaofeng Forest Farm of Guangxi Province, South China as the research object, including four planting species: *Cunninghamia lanceolata* (Lamb.) Hook., *Phoebe bournei* (Hemsl.) Yang, *Manglietiastrum sinicum*, *Sarcandra glabra* (Thunb.) Nakai., with three mixed management: LP(*Cunninghamia lanceolata* (Lamb.) Hook. - *Phoebe bournei* (Hemsl.) Yang), LM(*Cunninghamia lanceolata* (Lamb.) Hook. - *Manglietiastrum sinicum*), and LS (*Cunninghamia lanceolata* (Lamb.) Hook. - *Sarcandra glabra* (Thunb.) Nakai.) A series of the height-related characteristic parameters were extracted from the scanned points of each tree stems, including a proposed new parameter and the height cumulative percentage (Hz%).

Then the differences of growth, stem shape, yield and height cumulative percentage (Hz) inflection point of Chinese fir under three mixed-forest modes were compared, and the stem taper equation and yield table of different mixed-forest modes were established.

Results:

1) The upper diameter accuracy obtained by multi-station scanning is high, and the correlation coefficient with manually measured data is 0.9864. The modified five-parameter Schumacher equation is the best stem form equation in this study. With R^2 0.963, 0.896, 0.919 for each mixed-forest.

2) Mixed management with *Manglietiastrum sinicum* shows more conducive to the growth of Chinese fir. The average diameter at breast height (DBH), tree height (H) and volume (V) of LM were the largest within the three mixed-forest, which were 25.7714cm, 20.3257m and 0.5195m³. And the cumulative length and volume of large timber, mid-length timber and short timber in the LM plot shows largest output, which were 28.18m, 92.69m and 259.20m, 1.93m³, 2.60 m³ and 2.67 m³.

3) The point cloud characteristic parameters (height cumulative percentage Hz) can reflect

the differences of each mixed-forest modes. The Hz curve of LM is higher than others. The cumulative height percentage curves of LM and LP shows significantly different after H15. The diameter at the height corresponding to the mutation point of LM remains the largest.

Conclusion:

Under different mixed-forest management, the three elements for forest mensuration (DBH, tree height, stem form fact) of standing trees have corresponding differences, and the status of living standing trees can be reflected through the high-precision point cloud data of TLS.

A NEW UAV LASER SCANNING BENCHMARK DATASET FOR CHARACTERIZATION OF SINGLE-TREE AND FOREST BIOPHYSICAL PROPERTIES

Stefano Puliti ¹, Grant Pearse ², Micheal Watt², Edward Mitchard ³, Iain McNicol ³, Magnus Bremer ^{4,8}, Martin Rutzinger ⁴, Peter Surovy ⁵, Luke Wallace ⁶, Markus Hollaus ⁷, Rasmus Astrup ¹

¹ Norwegian Institute for Bioeconomy Research (NIBIO), Division of Forest and Forest Resources, National Forest Inventory, Høgskoleveien 8, 1433 Ås, Norway (stefano.puliti@nibio.no; rasmus.astrup@nibio.no)

² Scion, 49 Sala Street, Private Bag 3020, Rotorua 3046 and 10 Kyle St, Christchurch 8011, New Zealand (Grant.Pearse@scionresearch.com; micheal.watt@scionresearch.com)

³ University of Edinburgh, School of GeoSciences, Crew Building, the King's Buildings, Edinburgh, Scotland (edward.mitchard@ed.ac.uk; magnus.bremer@uibk.ac.at, martin.rutzinger@uibk.ac.at)

⁴ University of Innsbruck, Institute of Geography Innrain 52f, A - 6020 Innsbruck (magnus.bremer@uibk.ac.at, martin.rutzinger@uibk.ac.at)
⁵ Faculty of Forestry and Wood Sciences, Czech University of Life Sciences, Prague, Kamýcká 129, 165 00 Praha, Czech Republic (psurovy@gmail.com)

⁶ School of Geography, Planning and Spatial Sciences, University of Tasmania, Hobart, Australia (luke.wallace@utas.edu.au)

⁷ TU Wien, Department of Geodesy and Geoinformation, E120-07, Wiedner Hauptstraße 8, 1040 Vienna, Austria (markus.hollaus@geo.tuwien.ac.at)

⁸ Austrian Academy of Sciences, Institute for Interdisciplinary Mountain Research, Innrain 25, 6020 Innsbruck, Austria (magnus.bremer@oeaw.ac.at)

1. Introduction

High resolution unmanned aerial vehicle laser based scanning (UAV-LS) data allows the identification of individual trees and has shown promising results in providing accurate key forestry variables comparable to in-situ observations. New and improved approaches for analyzing UAV-LS point clouds have to be developed to transform the vast and growing amounts of data from UAV-LS into actionable insights for decision making also advancing the derivation of essential biodiversity variables (e.g. Pereira et al. 2013).

The use of UAV-LS data for deriving single-tree measurements is a rapidly increasing field of research, and several studies investigated the possibility to obtain measurements of tree biophysical properties such as height (Brede et al. 2017, Hartley et al. 2020), crown dimensions (Wallace, Lucieer, and Watson, 2014), tree density (Sankey et al. 2017), diameter at breast height (Jaakkola et al. 2017, Wieser et al. 2017, Dalla Corte et al. 2020) and above ground biomass (AGB) or volume (Brede et al. 2019, Liang et al. 2019, Wang et al. 2019, Puliti, Breidenbach, and Astrup 2020). Despite the considerable efforts dedicated to developing automated ways to process UAV-LS data into useful data, current methods tend to be tailored to small datasets, and it remains challenging to evaluate the performance of different algorithms based on a consistent validation dataset. Furthermore, with the increased availability of deep-learning methods to segment and parse forest point clouds (Windrim and Bryson 2020, Krisanski et al 2021), there is an increasing need to develop large databases of annotated trees in dense point clouds. To fill this knowledge gap and to further advance our ability to measure forests from UAV-LS data, we present a new benchmarking dataset.

2. Data

2.1 Input data

This benchmark is designed to provide the best quality aerial laser scanning data on the use of survey-grade UAV-LS data collected using RIEGL scanners of the VUX and mini-VUX series. Amongst the various UAV-LS sensors available today, the RIEGLones, when combined with high precision Inertial Measurement Units (IMUs), represent the state-of-the-art as they allow scanning at high frequency and the laser pulses are characterized by narrow beam divergence (i.e. small footprints) enabling the acquisition of very dense point clouds (1 – 10 k pts/m²) with larger canopy penetration rates and larger measurement accuracy compared to consumer-grade sensors (e.g. Velodyne VLP16).

To date, the available UAV-LS data for this benchmark covers different forest types across the world, including boreal coniferous forests, temperate deciduous and coniferous forests, savanna type of vegetation, and production forest plantations.

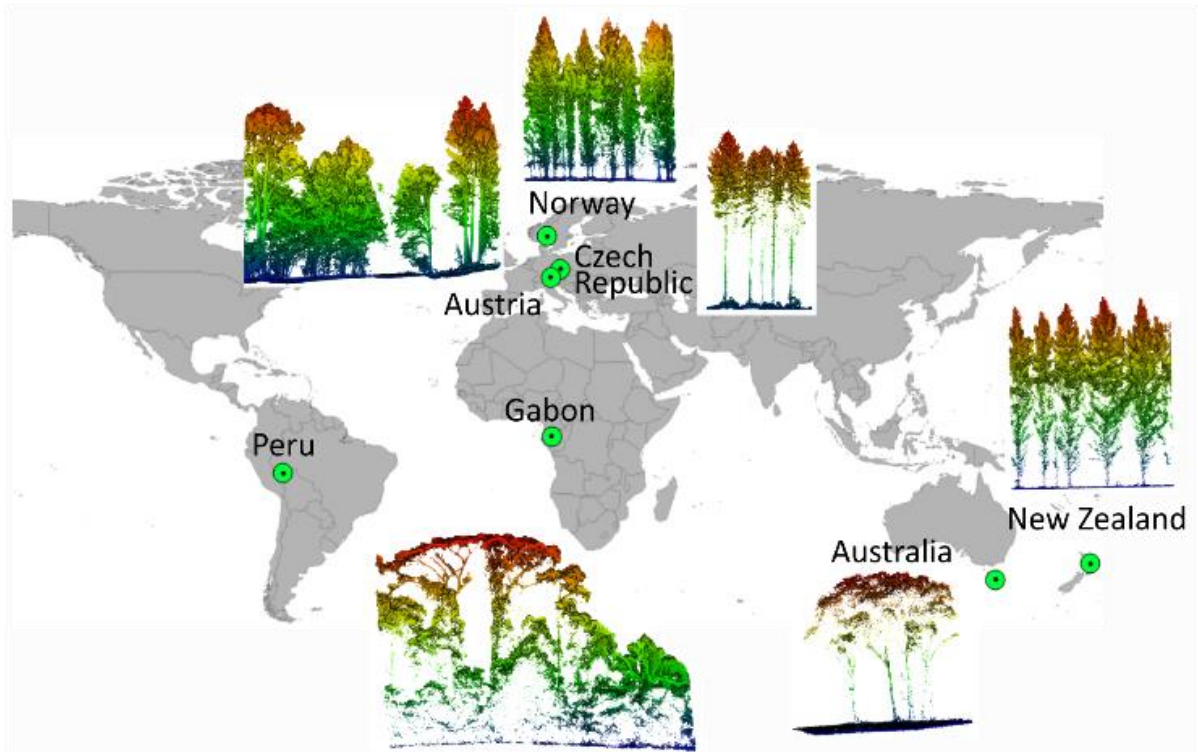


Figure 1. Geographical overview of the currently available drone laser scanning data

2.2. Manual annotation

A sample of the available point clouds were manually annotated into single-trees and in different components of the tree, namely stems, branches, and leaves/needles (see Figure 2). The point clouds were annotated with particular attention to segmenting all tree size classes including co-dominant and suppressed trees.

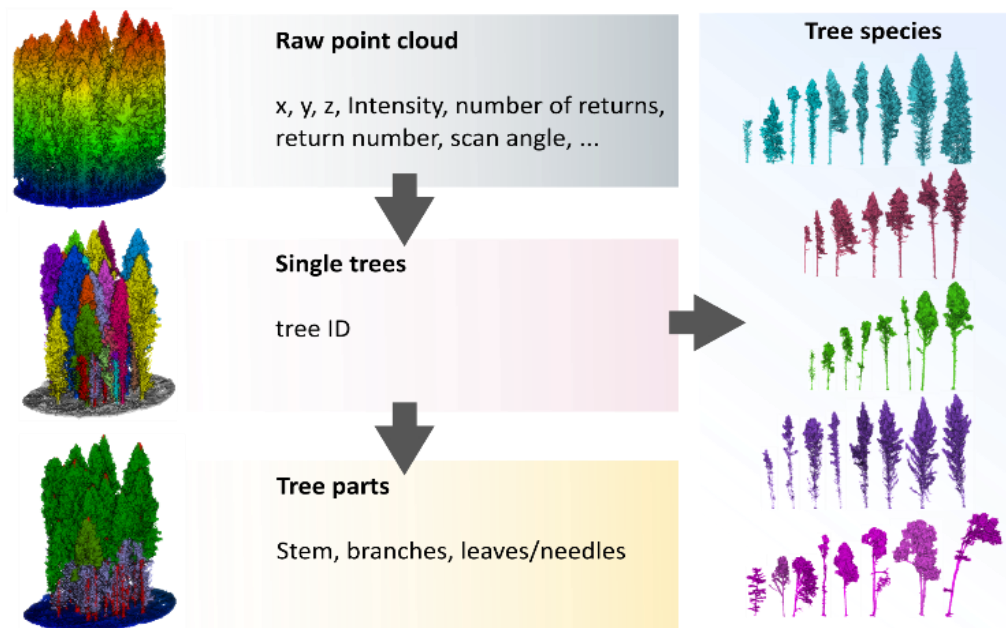


Figure 2. Structure of the annotation in the benchmark data with information regarding single trees, different tree parts, and tree species.

2.3 Field data

Field measurements were conducted in each of the sites included in the benchmark. The diameter at breast height (DBH) was measured for all the annotated trees. In addition, when available, other measurements such as tree species, height, and volume are included.

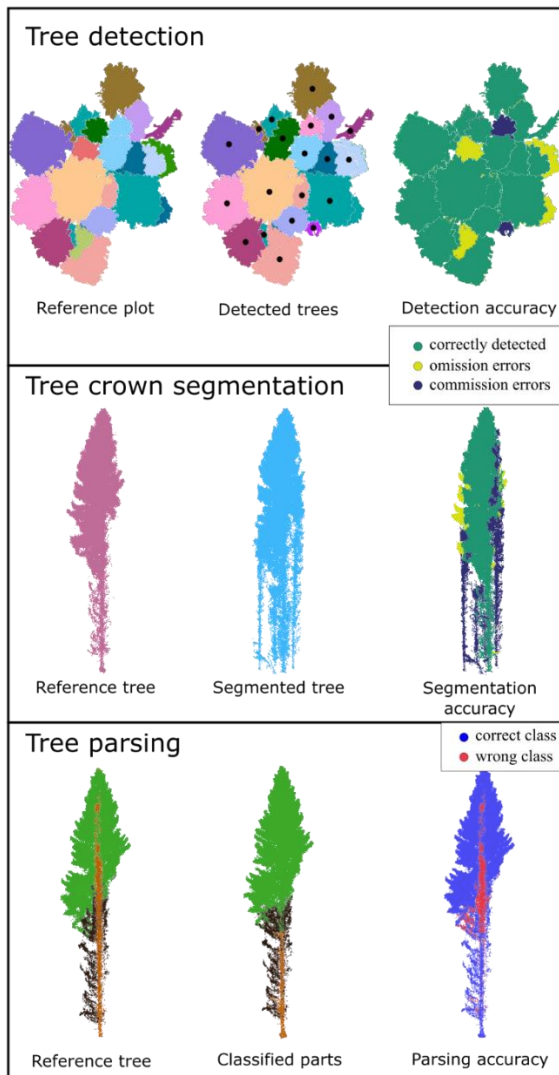


Figure 3. Workflow for benchmarking tree detection, segmentation and parsing algorithms.

3. Scope of the benchmark

The main aim of this benchmark is to provide a solid base for further advancing our ability to characterize forest structures and obtain in-situ measurements from very dense airborne laser scanning data. Future possibilities to utilize these data consist of:

- *Benchmarking* of algorithms for tree detection, segmentation, and parsing (Figure 3). By providing a consistent and independent validation data source this benchmark will allow ranking of different algorithms based on their performance across various forest types.
- *Development of deep-learning models* to automatically segment single trees and tree parts. The annotated data is particularly suitable for training deep learning models for semantic and instance segmentation of forest point clouds.
- *Development of methods for direct measurement of tree (DBH, volume, tree species) and forest biophysical properties (DBH distributions, volume, stem density).*

4. Open data

The UAV-LS data annotated as part of this benchmark will be publicly released for scientific purposes.

References

Brede, B.; Lau, A.; Bartholomeus, H.M.; Kooistra, L. Comparing riegli ricopter uav lidar derived canopy height and dbh with terrestrial lidar. *Sensors* **2017**, *17*, 16.

- Brede, B.; Calders, K.; Lau, A.; Raunonen, P.; Bartholomeus, H.M.; Herold, M.; Kooistra, L. Non-destructive tree volume estimation through quantitative structure modelling: Comparing uav laser scanning with terrestrial lidar. *Remote Sens. Environ.* **2019**, *233*, 14.
- Dalla Corte, A.P.; Rex, F.E.; de Almeida, D.R.A.; Sanquetta, C.R.; Silva, C.A.; Moura, M.M.; Wilkinson, B.; Zambrano, A.M.A.; Neto, E.M.D.; Veras, H.F.P., *et al.* Measuring individual tree diameter and height using gatereye high-density uav-lidar in an integrated crop-livestock-forest system. *Remote Sens.* **2020**, *12*, 15.
- Hartley, R.J.L.; Leonardo, E.M.; Massam, P.; Watt, M.S.; Estarija, H.J.; Wright, L.; Melia, N.; Pearse, G.D. An assessment of high-density uav point clouds for the measurement of young forestry trials. *Remote Sens.* **2020**, *12*, 4039.
- Jaakkola, A.; Hyypä, J.; Yu, X.W.; Kukko, A.; Kaartinen, H.; Liang, X.L.; Hyypä, H.; Wang, Y.S. Autonomous collection of forest field reference-the outlook and a first step with uav laser scanning. *Remote Sens.* **2017**, *9*, 12.
- Krisanski, S., Taskhiri, M.S., Gonzalez Aracil, S., Herries, D. and Turner, P., 2021 Sensor Agnostic Semantic Segmentation of Structurally Diverse and Complex Forest Point Clouds Using Deep Learning. *Remote Sensing*, *13*(8), p.1413.
- Liang, X.; Wang, Y.; Pyörälä, J.; Lehtomäki, M.; Yu, X.; Kaartinen, H.; Kukko, A.; Honkavaara, E.; Issaoui, A.E.I.; Nevalainen, O., *et al.* Forest in situ observations using unmanned aerial vehicle as an alternative of terrestrial measurements. *Forest Ecosystems* **2019**, *6*, 20.
- Pereira, H. M., Ferrier, S., Walters, M., Geller, G. N., Jongman, R. H. G., Scholes, R. J., *et al.* Essential biodiversity variables. *Science*, **2013**, *339*(6117), 277-278.
- Puliti, S.; Breidenbach, J.; Astrup, R. Estimation of forest growing stock volume with uav laser scanning data: Can it be done without field data? *Remote Sens.* **2020**, *12*, 19.
- Sankey, T.; Donager, J.; McVay, J.; Sankey, J.B. Uav lidar and hyperspectral fusion for forest monitoring in the southwestern USA. *Remote Sens. Environ.* **2017**, *195*, 30-43.
- Wallace, L.; Lucieer, A.; Watson, C.S. Evaluating tree detection and segmentation routines on very high resolution uav lidar data. *IEEE Trans. Geosci. Remote Sensing* **2014**, *52*, 7619-7628.
- Wallace, L.; Watson, C.; Lucieer, A. Detecting pruning of individual stems using airborne laser scanning data captured from an unmanned aerial vehicle. *International Journal of Applied Earth Observation and Geoinformation* **2014**, *30*, 76-85.
- Wang, Y.; Pyörälä, J.; Liang, X.; Lehtomäki, M.; Kukko, A.; Yu, X.; Kaartinen, H.; Hyypä, J. In situ biomass estimation at tree and plot levels: What did data record and what did algorithms derive from terrestrial and aerial point clouds in boreal forest. *Remote Sensing of Environment* **2019**, *232*, 111309.
- Wieser, M.; Mandlbürger, G.; Hollaus, M.; Otepka, J.; Glira, P.; Pfeifer, N. A case study of uas borne laser scanning for measurement of tree stem diameter. *Remote Sens.* **2017**, *9*, 11.
- Windrim, L. and Bryson, M. Detection, Segmentation, and Model Fitting of Individual Tree Stems from Airborne Laser Scanning of Forests Using Deep Learning. *Remote Sens.* **2020**, *12*, 1469.

Aboveground Biomass Assessment Using GEDI Data across Diverse Forest Ecosystems in India

I. Indirabai¹, R. Mukhopadhyay¹, L. I. Duncanson², J. D. Armston², M. Ekström^{1,3}, T. Gobakken⁴, E. Næsset⁴ and S. Saarela⁴

¹Department of Forest Resource Management, Swedish University of Agricultural Sciences, Umeå, Sweden
Email: {indu.indirabai; ritwika.mukhopadhyay; magnus.ekstrom}@slu.se

²Department of Geographical Sciences, University of Maryland, College Park, MD, USA
Email: {lduncans; armston}@umd.edu

³Department of Statistics, USBE, Umeå University, Sweden
Email: magnus.ekstrom@umu.se

⁴Faculty of Environmental Sciences and Natural Resource Management, Norwegian University of Life Sciences, Ås, Norway
Email: {terje.gobakken; erik.naesset; svetlana.saarela}@nmbu.no

Keywords: Aboveground Biomass, GEDI, Hierarchical Model-Based Inference, IPCC, Sentinel-2, Uncertainty Assessment.

1. Introduction

Aboveground biomass (AGB) and its quantification play an important role in understanding the global carbon cycle as well as carbon budget at the regional and national levels (Houghton et al., 2009; Narine et al., 2019; Quegan et al., 2019). The Kyoto Protocol is an international agreement linked to United Nations Framework Convention on Climate Change (UNFCCC). It promotes sustainable forest management and measures, enables the mitigation of climate change by conservation and enhancement of forests as sinks and reservoirs of greenhouse gases, and recognises the significance of forests in carbon sequestration (Kuh et al., 2018). Intergovernmental Panel on Climate Change (IPCC), - the international body to regular assessments of the scientific basis of climate change, its impacts, future risks and mitigation, - demands the member countries to generate national-level estimates of carbon stocks and exchanges (IPCC, 2007; IPCC, 2018). Indian forests can significantly contribute to climate change mitigation by carbon sequestration. Forest Survey of India (FSI) is an organisation under the Ministry of Environments and Forests, Government of India. It conducts surveys of forest resources, including national forest inventory (NFI), in the country and it has been regularly estimating growing stocks in Indian forests. The primary objective of NFI is to assess growing stock of trees, number of trees, bamboo, soil carbon, invasive species and other parameters depicting forest health and growth using a grid-based sampling. FSI estimates carbon stock in different pools at the national and state level using the NFI data following the methodology of Good Practices Guidance (GPG) developed by IPCC (FSI, 2019). Over 57% of the total forest cover constitute mainly very dense and moderately dense forests (FSI, 2019). There is a need for regional assessment of forest biomass and carbon stocks, due to the diverse forest ecosystems along with highly variable climatic and geographic features. (Salunkhe et al., 2018).

NASA's Global Ecosystem Dynamics Investigation (GEDI) launched on December 5, 2018, is the first spaceborne LiDAR designed for producing high resolution laser ranging observations of 3D structure for Earth's tropical and temperate forests. Quantifying the effects of vegetation disturbance and recovery on carbon storage, distribution of AGB, the potential of forests to sequester carbon and quantifying the spatio-temporal distribution of canopy structure and its influence on habitat and biodiversity are the main scientific objectives of GEDI (Dubayah et al., 2020). GEDI data products include footprint and gridded data, which are publicly available with lower-level products (L1 and L2) from NASA's Land Product Distributed Active Archive Centre (LPDAAC) and higher-level products (L3 and L4) from Oak Ridge National Laboratory Distributed Active Archive Center (ORNL DAAC). The L4A products are footprint-level predictions of aboveground biomass density (AGBD) obtained by parametric models that describe the relationship between L2A relative height metrics with field plot estimates of AGBD. Model calibration using simulated GEDI waveforms and a cross validation framework is developed to ensure geographic transferability (Hancock et al., 2019; Dubayah et al., 2020; Duncanson et al., in review).

European Space Agency's Sentinel-2 launched on June 23, 2015, is a wide-swath, high resolution, multispectral imaging mission (Drusch et al., 2012). Sentinel-2 data with high revisit frequency and systematic coverage have been tested to have potential applications in estimating forest biophysical

variables including tree cover (e.g., Godinho et al., 2017), AGB (e.g., Majasalmi and Rautiainen, 2016; Pandit et al., 2018; Puliti et al., 2019), growing stock volume (e.g., Chrysafis et al., 2017; Mura et al., 2018), and classifying highly diverse forest species in challenging mountainous environments (e.g., Grabska et al., 2019) and in riparian vegetation at regional scales (Daryaei et al., 2020). Mensah et al., (2020) studied the potential use of Sentinel-2 imagery in modelling tree growth and forest canopy dynamics by using heterogeneity indices.

Hierarchical model-based (HMB) inference is a novel inferential mode for environmental surveys using a combination of several sources of remotely sensed (RS) data including wall-to-wall multispectral optical data (e.g., Landsat, Sentinel) and LiDAR (e.g., airborne, spaceborne) data sets and field data. Typically, in HMB inference, the first source of information is RS data available wall-to-wall across the study region. The intermediate information source is sampled RS data, assumed to be more strongly correlated with the target variable than the wall-to-wall RS data. The third source of information is field data. Since two types of RS data are involved in the prediction of the target variable, two modelling steps are involved, one linking the target variable with sampled RS data and the other linking the expectation of the target variable with RS data available wall-to-wall. The method provides a theoretical approach for uncertainty assessment accounting for uncertainties due to the two modelling steps. The concept was first introduced by Saarela et al. (2016) for ordinary least squares (OLS) regression models, then it was elaborated for generalized least squares (GLS) regression models (Saarela et al., 2018) and nonlinear GLS (Saarela et al., 2020). In Saarela et al. (in review), the advantages and disadvantages, as well as under what conditions the novel inferential framework can outperform other estimation methods were outlined and discussed. The HMB inference can accommodate both the estimation of the target population parameters such as population mean or total and corresponding uncertainties over large areas, and the mapping of the variable of interest complementing with a map of uncertainties (e.g., Saarela et al. 2020).

The main objective of this study is to estimate the AGB and corresponding uncertainty and produce AGB maps over three large areas in India: Mudumalai (90 km²), Betul (50 km²) and Araku (120 km²), using a combination of sampled GEDI data and wall-to-wall Sentinel-2 data within the HMB inferential framework. The study explores the possibility to identify whether GEDI data can be used alone or in a combination with Sentinel-2 data, for the accurate AGB estimation in Indian forests.

2. Material and Method

The selected study area consists of the three protected forest ecosystems: Mudumalai forest in the which is a part of Western Ghats, Betul forest in the central part of India, and Araku forest, a part of Eastern Ghats (Figure 1). The Western Ghats includes a diversity of ecosystems ranging from tropical wet evergreen forests to montane grasslands containing numerous medicinal plants with unique shola ecosystem with evergreen forest patches. The Eastern Ghats geologically older than the Western Ghats supports a diverse array of tropical forests and has great conservation significance. The Eastern Ghats has tropical wet evergreen, semi evergreen, moist deciduous, dry deciduous, dry evergreen and thorn forests (Reddy et al., 2008; Reddy et al., 2014). Field data were collected by the sampling procedure from FSI and AGB were estimated using the volume and specific density of tree species present in each sampling plot (FSI, 1996).

Sentinel-2 data of December 2019 are used in the study. Using SNAP tools, Sentinel-2 imagery were subsetted for the corresponding study areas based on the bounding coordinates. Resampling and cloud masking were done as part of the preprocessing of Sentinel-2 imagery using the SNAP software (ESA, 2021; Zuhlke et al., 2015; Nuthammachot et al., 2018). Spectral bands Short Wave Infrared SWIR-1 (B11), Near Infrared (B8) and Blue (B2) of the imagery required for the study are selected, extracted and are resampled to 30m spatial resolution corresponding to the size of the sampling plot. The band combinations B11, B8 and B2 are suitable to monitor and highlight dense vegetation (Wang et al., 2019; Huete et al., 2002; Pandit et al., 2020). The variables in the L4A footprint data files are the AGB prediction, associated uncertainty metrics, quality flags identifying the most useful L2 data for

biomass predictions and simplifying the predictions selection, and the scaled and transformed GEDI L2A relative height metrics. The data are available to download from ORNL DAAC.

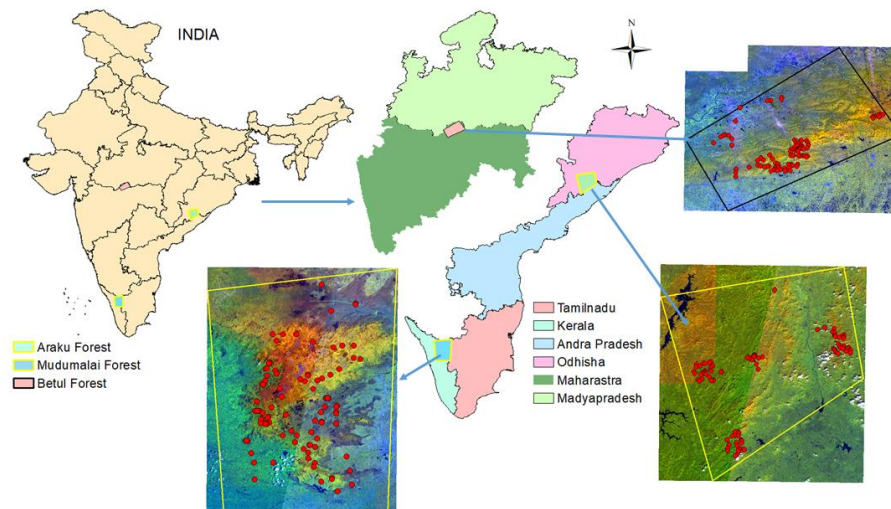


Figure 1: Study areas' locations (color composite of Bands B11, B8 and B2 of Sentinel-2 images were used for study area representation).

The estimation of the target population mean follows the HMB inference. We define two superpopulation models, the first model describes a relationship between AGB and GEDI data. The model information, such as estimated model coefficients and their estimated variance-covariance matrices, estimated R-squared and RMSE, are provided with the GEDI L4A product (Duncanson et al., in review). Then, we train a second model, linking L4A AGB with Sentinel-2 variables. The latter model is then used to predict AGB over our study areas using Sentinel-2 wall-to-wall data. It contains elements of uncertainty from each of two modelling steps, thus the variance-covariance matrix of estimated model parameters in the model is decomposed in two parts: one due to the conditional uncertainty related to the Sentinel-2 model fitting, and the second part is a propagated uncertainty due the GEDI L4A model fit.

For the mapping of AGB across our study areas, the Sentinel-based prediction model is applied at the Sentinel-2 pixel-level, and a complementary map of uncertainties is produced following the HMB theory (Saarela et al., 2020). The results will be compared with estimates obtained from a survey using a combination of field data and Sentinel-2 data within the model-based inferential framework (e.g., McRoberts, 2010).

3. Expected Results and Discussion

The methodology proposed in the study for the AGB estimation and the uncertainty measurements of AGB by utilizing GEDI L4A and Sentinel-2 can significantly contribute to quantifying the amount of carbon stored in the Indian forests thereby can help to calculate the carbon sequestration potential of forests under future climate and land-use scenarios. The resultant AGB uncertainty measurements and the AGB maps from the study can support intergovernmental policy initiatives such as REDD, UNFCCC and Kyoto Protocol in which India is involved in Clean Development mechanism (CDM) by giving information for climate adaptation and mitigation, sustainable land use and conservation of biodiversity. The combination of GEDI data with wall-to-wall Sentinel-2 data within the HMB inferential framework can predict the future response of forest carbon to climate change and land management decisions which is of high societal relevance and potential to simplify the reporting to IPCC. GEDI can reduce the uncertainty in the measurements of carbon loss and carbon gain by measuring the current biomass of forests globally thereby giving the net impact of forest disturbance and subsequent regrowth. Thus, information on the missing sink of carbon and carbon balance can be obtained which is the potential data needed for IPCC which can be used for the alternative conservation and development strategies.

Acknowledgement

Funding was provided by grants from the Swedish National Space Agency (SNSA-171/19), the Swedish Research Council for Sustainable Development (FORMAS: FR-2019/0007) and the Swedish Kempe Foundation (Kempestiftelserna: SMK-1847).

We acknowledge Professor Rama Rao Nidamanuri, Department of Earth and Space Sciences, Indian Institute of Space Science and Technology (IIST) Thiruvananthapuram, India for providing the field data which were taken as part of his funded projects Spectral Biochemical Analysis of Forest Species using Hyperspectral Remote Sensing and Development of a Standalone Atmospheric Correction Module for Hyperspectral Data, Department of Science and Technology (DST), Government of India.

References

- Chrysafis, I., Mallinis, G., Siachalou, S., & Patias, P. (2017). Assessing the relationships between growing stock volume and Sentinel-2 imagery in a Mediterranean forest ecosystem. *Remote Sensing Letters*, 8(6), 508-517.
- Daryaei, A., Sohrabi, H., Atzberger, C., & Immitzer, M. (2020). Fine-scale detection of vegetation in semi-arid mountainous areas with focus on riparian landscapes using Sentinel-2 and UAV data. *Computers and Electronics in Agriculture*, 177, 105686.
- Drusch, M., Del Bello, U., Carlier, S., Colin, O., Fernandez, V., Gascon, F., ... & Bargellini, P. (2012). Sentinel-2: ESA's optical high-resolution mission for GMES operational services. *Remote Sensing of Environment*, 120, 25-36.
- Dubayah, R., Blair, J. B., Goetz, S., Fatoyinbo, L., Hansen, M., Healey, S., & Silva, C. (2020). The Global Ecosystem Dynamics Investigation: High-resolution laser ranging of the Earth's forests and topography. *Science of Remote Sensing*, 1, 100002.
- Duncanson, L.I., Kellner, J.R., Armston, J.D., Dubayah, R.O., Hancock, S., Minor, D., Healey, S.P., Patterson, P.L., Saarela, S., Marselis, S., Silva, C.E., Bruening, J., Tang, H., Hofton, M., Blair, B., Scott, L., Goetz, S., Fatoyinbo, L., & data contributors (in review). Development of global LiDAR biomass density models for GEDI's L4A product. *Remote Sensing of Environment*.
- ESA. (2021) Science Toolbox Exploitation Platform (STEP). Sentinel Application Platform (SNAP). Available online: <https://step.esa.int/main/toolboxes/snap> (Assessed on March 15, 2021)
- Forest Survey of India. (2019). *India State of Forest Report-2019*. Forest Survey of India, Dehradun, Uttarakhand, 1(16), 3.
- FSI (1996). *Volume Equations for Forests of India, Nepal and Bhutan*. Forest Survey of India, Ministry of Environment and Forests, Govt. of India.
- Godinho, S., Guiomar, N., & Gil, A. (2018). Estimating tree canopy cover percentage in a mediterranean silvopastoral systems using Sentinel-2A imagery and the stochastic gradient boosting algorithm. *International Journal of Remote Sensing*, 39(14), 4640-4662.
- Grabska, E., Hostert, P., Pflugmacher, D., & Ostapowicz, K. (2019). Forest stand species mapping using the Sentinel-2 time series. *Remote Sensing*, 11(10), 1197.
- Hancock, S., Armston, J., Hofton, M., Sun, X., Tang, H., Duncanson, L. I., ... & Dubayah, R. (2019). The GEDI simulator: A large-footprint waveform lidar simulator for calibration and validation of spaceborne missions. *Earth and Space Science*, 6(2), 294-310.
- Houghton, R. A., Hall, F., & Goetz, S. J. (2009). Importance of biomass in the global carbon cycle. *Journal of Geophysical Research: Biogeosciences*, 114(G2).
- Huete, A., Didan, K., Miura, T., Rodriguez, E. P., Gao, X., & Ferreira, L. G. (2002). Overview of the radiometric and biophysical performance of the MODIS vegetation indices. *Remote sensing of environment*, 83(1-2), 195-213.
- IPCC (2007). *Climate change 2007: Impacts, Adaptation and Vulnerability*. Working Group II. Contribution to the fourth assessment report of the intergovernmental panel on climate change (IPCC). Cambridge
- IPCC, 2018: Global Warming of 1.5°C. An IPCC Special Report on the impacts of global warming of 1.5°C above pre-industrial levels and related global greenhouse gas emission pathways, in the context of strengthening the global response to the threat of climate change, sustainable development, and efforts to eradicate poverty [Masson-Delmotte, V., P. Zhai, H.-O. Pörtner, D. Roberts, J. Skea, P.R. Shukla, A. Pirani, W. Moufouma-Okia, C. Péan, R. Pidcock, S. Connors, J.B.R. Matthews, Y. Chen, X. Zhou, M.I. Gomis, E. Lonnoy, T. Maycock, M. Tignor, and T. Waterfield (eds.)]. World Meteorological Organization, Geneva, Switzerland, 32 pp.
- Kuh, K. F. (2018). The law of climate change mitigation: an overview. *Encyclopedia of the Anthropocene*, Elsevier, pp. 505-510
- Majasalmi, T., & Rautiainen, M. (2016). The potential of Sentinel-2 data for estimating biophysical variables in a boreal forest: a simulation study. *Remote Sensing Letters*, 7(5), 427-436.

- McRoberts, R.E. (2010). Probability-and model-based approaches to inference for proportion forest using satellite imagery as ancillary data. *Remote Sensing of Environment*, 114(5), 1017-1025.
- Mensah, A.A., Petersson, H., Saarela, S., Goude, M., & Holmström, E. (2020). Using heterogeneity indices to adjust basal area–Leaf area index relationship in managed coniferous stands. *Forest Ecology and Management*, 458, 117699.
- Mura, M., Botalico, F., Giannetti, F., Bertani, R., Giannini, R., Mancini, M., ... & Chirici, G. (2018). Exploiting the capabilities of the Sentinel-2 multi spectral instrument for predicting growing stock volume in forest ecosystems. *International Journal of Applied Earth Observation and Geoinformation*, 66, 126-134.
- Narine, L. L., Popescu, S., Neuenschwander, A., Zhou, T., Srinivasan, S., & Harbeck, K. (2019). Estimating aboveground biomass and forest canopy cover with simulated ICESat-2 data. *Remote Sensing of Environment*, 224, 1-11.
- Nuthammachot, N., Phairuang, W., Wicaksono, P., & Sayektiningsih, T. (2018). Estimating aboveground biomass on private forest using Sentinel-2 imagery. *Journal of Sensors*, 2018.
- Pandit, S., Tsuyuki, S., & Dube, T. (2020). Exploring the inclusion of Sentinel-2 MSI texture metrics in above-ground biomass estimation in the community forest of Nepal. *Geocarto International*, 35(16), 1832-1849.
- Puliti, S., Hauglin, M., Breidenbach, J., Montesano, P., Neigh, C. S. R., Rahlf, J., ... & Astrup, R. (2020). Modelling above-ground biomass stock over Norway using national forest inventory data with ArcticDEM and Sentinel-2 data. *Remote Sensing of Environment*, 236, 111501.
- Quegan, S., Le Toan, T., Chave, J., Dall, J., Exbrayat, J. F., Minh, D. H. T., & Williams, M. (2019). The European Space Agency BIOMASS mission: Measuring forest above-ground biomass from space. *Remote Sensing of Environment*, 227, 44-60.
- Reddy, C. S., Jha, C. S., & Dadhwal, V. K. (2014). Spatial dynamics of deforestation and forest fragmentation (1930-2013) in Eastern Ghats, India. *The International Archives of Photogrammetry, Remote Sensing and Spatial Information Sciences*, 40(8), 637.
- Reddy, C.S., Ugle, P., Murthy, M.S. R., & Sudhakar, S. (2008). Quantitative structure and composition of tropical forests of Mudumalai Wildlife Sanctuary, Western Ghats, India. *Taiwania*, 53(2), 150-156.
- Saarela, S., Holm, S., Grafström, A., Schnell, S., Næsset, E., Gregoire, T. G., ... & Ståhl, G. (2016). Hierarchical model-based inference for forest inventory utilizing three sources of information. *Annals of Forest Science*, 73(4), 895-910.
- Saarela, S., Holm, S., Healey, S. P., Andersen, H. E., Petersson, H., Prentius, W., ... & Ståhl, G. (2018). Generalized hierarchical model-based estimation for aboveground biomass assessment using GEDI and Landsat data. *Remote Sensing*, 10(11), 1832.
- Saarela, S., Holm, S., Healey, S.P., Patterson, P.L., Yang, Z., Andersen, H.E., Dubayah, R.O., Qi, W., Duncanson, L.I., Armston, J.D., Gobakken, T., Næsset, E., Ekström, M. & Ståhl, G. (in review). Comparing Methods for Forest Biomass Assessment in Connection with NASA's GEDI Mission. *Remote Sensing of Environment*.
- Saarela, S., Wästlund, A., Holmström, E., Mensah, A.A., Holm, S., Nilsson, M., Fridman, J. & Ståhl, G. (2020). Mapping aboveground biomass and its uncertainty using LiDAR and field data, accounting for tree-level allometric and LiDAR model errors. *Forest Ecosystems*, 7(43), 1-17.
- Salunkhe, O., Khare, P. K., Kumari, R., & Khan, M. L. (2018). A systematic review on the aboveground biomass and carbon stocks of Indian forest ecosystems. *Ecological Processes*, 7(1), 1-12.
- Wang, J., Xiao, X., Bajgain, R., Starks, P., Steiner, J., Doughty, R. B., & Chang, Q. ., (2019). Estimating leaf area index and aboveground biomass of grazing pastures using Sentinel-1, Sentinel-2 and Landsat images. *ISPRS Journal of Photogrammetry and Remote Sensing*, 154, 189-201.
- Zuhlke, M., Fomferra, N., Brockmann, C., Peters, M., Veci, L., Malik, J., & Regner, P. (2015, December). SNAP (sentinel application platform) and the ESA sentinel 3 toolbox. In *Sentinel-3 for Science Workshop* (Vol. 734, p. 21).

Deriving Forest Structural Biodiversity Traits with Terrestrial Laser Scanning

Atticus E.L. Stovall^{1,2}, Lola Fatoyinbo¹, John Armston², Lisa Patrick Bentley³, Kim Calders⁴, Mat Disney⁵

¹NASA Goddard Space Flight Center, 8800 Greenbelt Rd., Greenbelt, MD, United States
Email: atticus.stovall@nasa.gov; lola.fatoyinbo@nasa.gov

²Department of Geographical Sciences, University of Maryland, College Park, MD 20742, USA
Email: atticus@umd.edu; armston@umd.edu

³Department of Biology, Sonoma State University, 1801 E. Cotati Ave., Rohnert Park, CA 94928, USA
Email: lisa.bentley@sonoma.edu

⁴CAVElab - Computational & Applied Vegetation Ecology, Department of Environment, Ghent University, Belgium
Email: Kim.Calders@UGent.be

⁵UCL Department of Geography, Gower Street, London WC1E 6BT, UK
Email: mathias.disney@ucl.ac.uk

1. Introduction

Spatially representative maps of forest biodiversity are directly limited by a lack of suitable in-situ representations and drivers of ecosystem structure. Biota interact with ecosystems in three dimensions, yet structural indicators of biodiversity are typically only captured with one- (e.g. tree height) or two-dimensional (e.g. canopy cover) measures. More complex and objective measures of habitat structure or, what we call structural biodiversity traits (SBTs; e.g. volume, crown dimensions, tree-level leaf area, branching architecture) that are more compatible with remotely sensed measurements would refine floral and faunal biodiversity mapping efforts, but we currently lack a consistent, spatially representative global dataset of SBTs for testing scaling predictions.

Terrestrial Laser Scanning (TLS) is a ground-based LiDAR technology that directly addresses a lack of SBTs by enabling collection of unprecedented 3D measurements of tree- and plot-level structure, revolutionizing how we characterize forests (Calders et al., 2020; Disney, 2019). Now, we are able to capture detailed 3D tree measurements with TLS - from branching angle and crown architecture to tree volume and biomass - directly capturing the fundamental elements of structural biodiversity and habitat structure (Verbeeck et al., 2019). The measurements capable with TLS make it the single most promising technology for moving from traditional plot-based measures to next-generation 3D characterization of forests (Disney et al., 2019; Stovall & Shugart, 2018).

Here, we provide an overview of a recently funded project that will bring together thousands of TLS plot locations from the laser scanning community to develop a first of its kind global database of SBTs (Figure 1). With this database this project will enable hypothesis testing of unprecedented ecological questions.

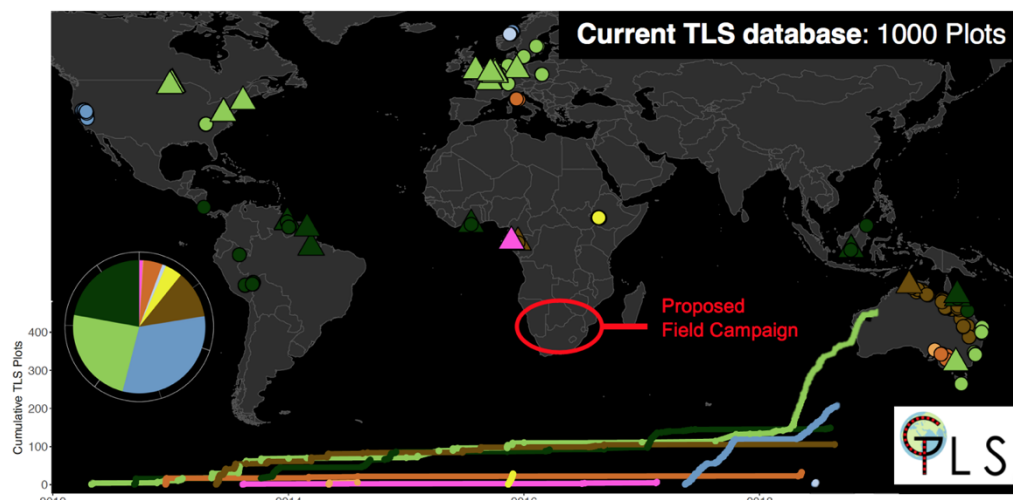


Figure 1: Current global TLS database of >1000 forest plots covering 10 biomes.

2. Methods

TLS is already collected at forest sites around the globe (Figure 1). Sites with processed tree-level data (triangles) span a large proportion of our database. Our preliminary assessment also highlights data gaps for future contributions and field campaigns planned in South Africa.

We will derive a standardized set of tree-level metrics from TLS data (See Table 1; Calders et al., 2015a; Krishna Moorthy et al., 2019; Raunonen et al., 2013; Verbeeck et al., 2019; Walter et al., 2021). In addition, we will derive plot-level estimates of cover, plant area index, plant area vegetation density, and leaf angle distribution (Calders et al., 2014; Stovall et al., 2021).

Table 1: 3D architecture structural biodiversity traits we will derive.

SBTs	Description
Top-heaviness	Ratio of total woody volume in the crown to the stem woody volume
Aspect ratio	Ratio of maximum crown width to crown height
Relative Crown Width	Ratio of maximum crown width to tree height
Crown Area	Maximum ground area covered by the crown viewed from above
Leaf Area	Total tree leaf area
Crown Density	Ratio of crown area to woody volume in the crown
Mass Taper Exponent	Exponent of a power law fit to the vertical profile of volume
Path Fraction	Ratio of mean to maximum base-to-twig path length
Crown Asymmetry	The ratio of maximum to mean of 8 angular crown segments
Branching Angle	The average angle between two cylinders at each branching point

3. Outlook and Impact

The key deliverable from this work will be a global database of 3D structural biodiversity traits (SBTs) that will refine our understanding of scaling relationships and can be leveraged for improved biodiversity mapping. Our work will provide a first-of-its-kind global analysis of the drivers of SBTs, directly improving predictions of aboveground structure in forests. Indeed, the results gleaned from this global-scale analysis of the controls on scaling relationships will inform functional ecosystem modeling efforts and remote sensing of biodiversity. A database of SBTs is a critical step towards informing a global remote sensing-based approach to mapping and monitoring the habitat structure and biodiversity, directly supporting conservation efforts.

Acknowledgments

We would like to thank all persons involved with the field work and TLS data collection used in this project. The project would not be possible without the contributions of TLS data from the following institutions/projects: University College London, NASA CMS 3D Change, University of Virginia, NASA Goddard Space Flight Center, University of Maryland, Sonoma State University, Wageningen University and Research, Ghent University, University of Yaoundé, Colorado State University, and TERN AusCover.

References

- Calders, K., Adams, J., Armston, J., Bartholomeus, H., Bauwens, S., Bentley, L. P., Chave, J., Danson, F. M., Demol, M., Disney, M., Gaulton, R., Krishna Moorthy, S. M., Levick, S. R., Saarinen, N., Schaaf, C., Stovall, A., Terry, L., Wilkes, P., & Verbeeck, H. (2020). Terrestrial laser scanning in forest ecology: Expanding the horizon. *Remote Sensing of Environment*, 251, 112102. <https://doi.org/10.1016/j.rse.2020.112102>
- Calders, K., Armston, J., Newnham, G., Herold, M., & Goodwin, N. (2014). Implications of sensor configuration and topography on vertical plant profiles derived from terrestrial LiDAR. *Agricultural and Forest Meteorology*, 194, 104–117. <https://doi.org/10.1016/j.agrformet.2014.03.022>
- Calders, K., Newnham, G., Burt, A., Murphy, S., Raunonen, P., Herold, M., Culvenor, D., Avitabile,

- V., Disney, M., Armston, J., & Kaasalainen, M. (2015). Nondestructive estimates of above-ground biomass using terrestrial laser scanning. *Methods in Ecology and Evolution*, 6(2), 198–208. <https://doi.org/10.1111/2041-210X.12301>
- Disney, M. (2019). Terrestrial LiDAR: a three-dimensional revolution in how we look at trees. *New Phytologist*, 222(4), 1736–1741. <https://doi.org/10.1111/nph.15517>
- Disney, M., Burt, A., Calders, K., Schaaf, C., & Stovall, A. (2019). Innovations in Ground and Airborne Technologies as Reference and for Training and Validation: Terrestrial Laser Scanning (TLS). *Surveys in Geophysics*. <https://doi.org/10.1007/s10712-019-09527-x>
- Krishna Moorthy, S. M., Calders, K., Vicari, M. B., & Verbeeck, H. (2019). Improved Supervised Learning-Based Approach for Leaf and Wood Classification From LiDAR Point Clouds of Forests. *IEEE Transactions on Geoscience and Remote Sensing*, 1–14. <https://doi.org/10.1109/TGRS.2019.2947198>
- Raumonen, P., Kaasalainen, M., Åkerblom, M., Kaasalainen, S., Kaartinen, H., Vastaranta, M., Holopainen, M., Disney, M., & Lewis, P. (2013). Fast Automatic Precision Tree Models from Terrestrial Laser Scanner Data. *Remote Sensing*, 5(2), 491–520. <https://doi.org/10.3390/rs5020491>
- Stovall, A. E. L., Masters, B., Fatoyinbo, L., & Yang, X. (2021). TLSLeAF: automatic leaf angle estimates from single-scan terrestrial laser scanning. *New Phytologist*, n/a(n/a). <https://doi.org/10.1111/nph.17548>
- Stovall, A. E. L., & Shugart, H. H. (2018). Improved Biomass Calibration and Validation With Terrestrial LiDAR: Implications for Future LiDAR and SAR Missions. *IEEE Journal of Selected Topics in Applied Earth Observations and Remote Sensing, Preprint(99)*, 1–11. <https://doi.org/10.1109/JSTARS.2018.2803110>
- Verbeeck, H., Bauters, M., Jackson, T., Shenkin, A., Disney, M., & Calders, K. (2019). Time for a Plant Structural Economics Spectrum. *Frontiers in Forests and Global Change*, 2. <https://doi.org/10.3389/ffgc.2019.00043>
- Walter, J. A., Stovall, A. E. L., & Atkins, J. W. (2021). Vegetation structural complexity and biodiversity in the Great Smoky Mountains. *Ecosphere*, 12(3). <https://doi.org/10.1002/ecs2.3390>

Performance test of tree segmentation algorithms for WLS point clouds

R. Bülbül¹, S. Reder¹, J.-P. Mund¹

¹University for Sustainable Development, Schicklerstr. 5 16225 Eberswalde (Germany)
Email: {ramazan.buelbuel; stefan.reder; jan-peter.mund}@hnee.de

1. Introduction

Individual tree detection and delineation of trees in dense laser point clouds provides significant information and tree parameters such as location of the stems, density and as species classification (Ke & Quackenbush, 2011). Wearable Laser Scanner (WLS) makes the point cloud acquisition viable and efficient with the help of the inertial measurement units (IMU). WLS results provide point cloud accuracy at a centimetre level. Further, it simplifies the preparation processes and decreases the processing time compared to stationary terrestrial laser scanner (Cabo C, 2018). Especially, the development of the simultaneous localization and mapping (SLAM) technology and the robotic operative system (ROS) allows to on-the-fly registration of point clouds and trajectories and the processing of 3D map without external positioning systems (Cabo C, 2018).

In this study, we compared three raster-based and two point-cloud-based algorithms, that were developed for the segmentation of LiDAR point clouds with the aim of individual trees detection and segmentation in data products captured with a WLS using SLAM technology.

2. Data and Methods

2.1 Equipment for Scanning

In this research, we've applied a GeoSLAM Zeb Horizon. This WLS scanner provides flexibility in field scans with its 100m range, lightweight, and user-friendly design (Solutions: ZEB Horizon, 2021).

2.2 Study Areas and data acquisition

We scanned 10 small scale plots (30m x 30m) in the arboretum near the forest campus of Eberswalde University which allowed collecting samples of different forest types and tree densities with different tree species and mixtures.

Table 1. Investigation Plots and Ground Truth Data

Plot	Tree Species	Latitude (N)	Longitude (E)	Trees per plot	Trees per ha
1 st Plot	<i>Pseudotsuga menziesii</i> , <i>Fagus sylvatica</i>	52.825672	13.812616	34	378
2 nd Plot	<i>Pinus sylvestris</i> , <i>Fagus sylvatica</i>	52.823815	13.812666	36	400
3 rd Plot	<i>Thuja plicata</i> , <i>Quercus petraea</i> , <i>Fagus sylvatica</i>	52.820535	13.810163	49	544
4 th Plot	<i>Picea abies</i>	52.819896	13.810939	45	500
5 th Plot	<i>Pinus sylvestris</i>	52.819757	13.808905	78	867
6 th Plot	<i>Betula pendula</i>	52.819337	13.809003	40	444
7 th Plot	<i>Larix decidua</i>	52.818644	13.808513	60	667
8 th Plot	<i>Pinus sylvestris</i> , mature stand	52.819285	13.806982	61	678
9 th Plot	<i>Pinus sylvestris</i> , <i>Pseudotsuga menziesii</i> , <i>Quercus petraea</i> , <i>Fagus sylvatica</i>	52.824366	13.802977	38	422
10 th Plot	<i>Pinus sylvestris</i> , pole stand	52.823008	13.799991	123	1367

2.3 Data pre-processing and preparation

Discrete Laser point data from the WLS scanner was processed to a point cloud using the GEOSlam HUB and afterwards clipped to the sample size of 30m x 30m. All point clouds of sample plots were classified into ground and off-ground points by applying the Progressive Morphological Filter (PMF) method (Zhang, et al., 2003). We generated a Digital Terrain Model (DTM) from ground points previously classified using the Inverse Distance Weighting (IDW) interpolation algorithm. Then, we normalized the DTM to generate the terrain normalization according (Liu, Skidmore, Heurich, & Wang, 2017). After terrain normalization, we separated only non-ground points for the further processing and individual tree segmentation.

2.4 Tree segmentation methods applied

After pre-processing and preparation of each point cloud data set mentioned above, we applied several algorithms for individual tree object segmentation algorithms and compared the number of detected trees. The different tree segmentation algorithms are briefly described in the following:

Watershed segmentation (WSS) (Canopy Maxima Model): First, the complement of the canopy maxima model is generated. This model is presumed to be immersed in the water basin. Dividing lines are established to prevent the water from going to both trees and to make the distinction for separating two neighbouring trees and used to identify each individual tree (Chen, 2006).

Particle swarming optimization (PSO) (Franceschi, 2018): Each particle of the swarm moves to a better position in the model towards its own previous local best, and towards the global best after iteration. A fitness function optimized the process. For all particles, a fitness value is calculated each time the extraction algorithm is running, and result will influence the direction of movement of particles through the rest of the in the following iteration (Franceschi, 2018).

Tree centric approach (TCA) (Dalponte 2016) is a raster-based segmentation using local maxima (treetops) to grow individual crowns within a rasterized canopy height model. Initially, to smooth the surface of rasterized CHM and decrease the amount of the local maxima points, a low-pass filter is applied. A local maximum is detected when a pixel has values greater than others in a circular moving window with a size of 5m. The extracted (identified and first return) four neighbouring pixels from CHM after identification and selection of the first return are added to this region if their vertical distance from the local maximum is within the limitation of user defined threshold. These iterations last for every pixel added and finally, a 2D convex hull is applied to the first returns. The ultimate polygons represent the individual segmented trees in the point cloud (Dalponte & Coomes, 2016).

In contrast to the algorithms introduced previously, the **region growth algorithm (RGA)** proposed by Li (2012) work on the point cloud base. The general rationale for this segmentation is that the horizontal gaps between trees are larger at the top than at the bottom. For this reason, segmentation starts by finding the global maximum as seed points for the region growth algorithm and processes discrete points bottom wards. Points are assigned to the nearest treetop, unless the distance is beyond a certain threshold (Li, Guo, Jakubowski, & Kelly, 2012).

The **Adaptive Mean Shift 3D Segmentation (AMS3D)** (Ferraz, 2016) has a similar scope and approach and generates 3D clusters of the individual tree crowns. It starts by calculating local maxima in density and height by using 3D kernels for each point that moves iteratively to denser regions until the kernels converge. Then, 3D clusters are computed by collecting the points that are converged to the same crown. This non-parametric approach is only depending on the size of the kernels, which are adapting to the size of the dense regions using allometric functions (Ferraz, 2016).

2.4 Evaluation

The numbers of trees detected with each segmentation algorithms were compared to the ground-truths data of each plot collected empirically using conventional forestry measures. Finally, we applied a regression analysis to compare the number of detected trees and determine whether the detection rate is changing according to the tree density and if so, to what extent.

3. Results & Discussion

In general, it can be observed that point cloud based approaches (ASM3D, RGA) outperform the raster-based algorithms (WSS, TCA, PSO) (Figure 1) and with a higher tree density, the share of not detected trees is rising (Figure 2).

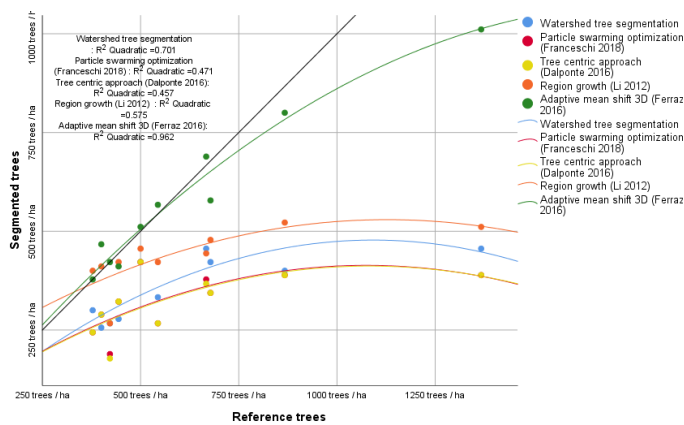


Figure 1 Number of segmented trees detected with different algorithms depending on the tree density of the stands.

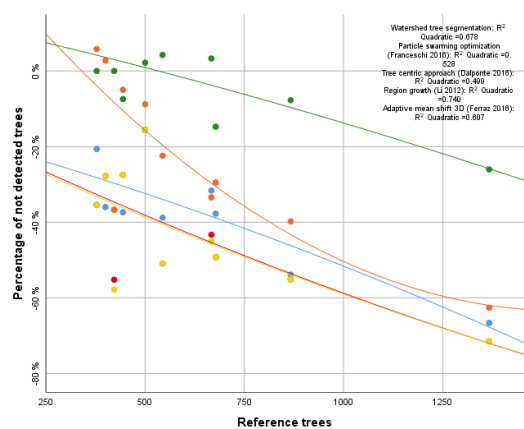


Figure 2 Relation between number of stems and the share of not detected trees.

The ASM3D performed best and, in contrast to other algorithms and more robust to higher tree densities of stands. Even in a pole stand with 1250 trees/ha, only 25% of the trees were not detected, while other approaches missed out more than 60% of the trees. For mature stands with less than 500 trees/ha, more than 90% of the trees were detected, but certain number of crowns were segmented in several parts, resulting in overestimation of the number of trees (Figure 2).

The RGA shows performance comparable to the AMS3D for stands with a density lower than 500 trees/ha. But with higher densities, the performance drops rapidly to detection rates similar of raster-based approaches (Figure 2). As RGA starts from treetops, it is also weak in detection understanding trees and instable processing separation of crowns that are intertwined with each other.

From the raster-based approaches, the WSA showed slightly better performance than the TCA and the PSO, which performed nearly identical. Even in mature stands with densities of less than 500 trees/ha, all raster-based approaches missed out more than 20% of the trees and the detection rates are linear declining with a rising density.

4. Conclusions

In our study, we could show the limits of raster-based segmentation approaches for WLS point clouds, especially in stands with high density. The same shortcomings were observed for the point-cloud-based region growth algorithm which is mainly depended on visible treetops. The ASM3D, developed for LiDAR point clouds, showed the best performance and was able to detect most trees (>85%) up to 850 trees/ha and is only falling off slightly afterwards (1250 trees/ha; 75% detection rate).

Acknowledgements

This proof-of-concept study was conducted as part of the WINMOL-Project (<https://winmol.thuenen.de/>) funded by the Fachagentur Nachwachsende Rohstoffe (FNR) and the Federal Ministry of Food and Agriculture, Germany (BMEL) (FNR funding number: **2220NR024A**)

References

Cabo C, D. P.-G.-A. (2018). Comparing Terrestrial Laser Scanning (TLS) and Wearable Laser Scanning (WLS) for Individual Tree Modeling at Plot Level. *Remote Sensing*, 10(4), 540. doi:doi.org/10.3390/rs10040540

- Chen, Q. B. (2006). Isolating Individual Trees in a Savanna Woodland Using Small Footprint Lidar Data . *Photogrammetric Engineering & Remote Sensing*, 72(8), 923–932. doi:10.14358/pers.72.8.923
- Dalponte, M., & Coomes, D. (2016). Tree-centric mapping of forest carbon density from airborne laser scanning and hyperspectral data. *Methods in Ecology and Evolution*, 7(10), 1236–1245. doi:10.1111/2041-210X.12575
- Ferraz, A. S. (2016). Lidar detection of individual tree size in tropical forests. *Remote Sensing of Environment*, 183, 318–333. doi:10.1016/j.rse.2016.05.028
- Franceschi, S. A. (2018). Identifying treetops from aerial laser scanning data with particle swarming optimization. *European Journal of Remote Sensing*, 51(1), 945–964. doi:10.1080/22797254
- Ke, Y., & Quackenbush, L. J. (2011). A review of methods for automatic individual tree-crown detection and delineation from passive remote sensing. *International Journal of Remote Sensing*, 32(17), 4725–4747. doi:10.1080/01431161.2010.494184
- Li, W., Guo, Q., Jakubowski, M., & Kelly, M. (2012). A New Method for Segmenting Individual Trees from the Lidar Point Cloud. *PHOTOGRAMMETRIC ENGINEERING & REMOTE SENSING*, 78(1), 75–84. doi:10.14358/PERS.78.1.75
- Liu, J., Skidmore, A., Heurich, M., & Wang, T. (2017). Significant effect of topographic normalization of airborne LiDAR data on the retrieval of plant area index profile in mountainous forests. *ISPRS Journal of Photogrammetry and Remote Sensing* *ISPRS Journal of Photogrammetry and Remote Sensing*, 132, 77–87. doi:10.1016/j.isprsjprs.2017.08.005
- Solutions: ZEB Horizon*. (15. February 2021). Von GeoSLAM: <https://geoslam.com/solutions/zeb-horizon/> abgerufen
- Zhang, K., Chen, S.-C., Whitman, D., Shyu, M.-L., Yan, J., & Zhang, C. (2003). A Progressive Morphological Filter for Removing Nonground Measurements From Airborne LIDAR Data. *IEEE TRANSACTIONS ON GEOSCIENCE AND REMOTE SENSING*, 41, 872 - 882. doi:10.1109/TGRS.2003.810682

The Forest Degradation Experiment (FODEX)

Iain McNicol¹, Chiara Aquino¹, Andrew Burt^{2,3}, Harry Carstairs¹, Mathias Disney^{2,3},
and Edward Mitchard¹

³ University of Edinburgh, School of GeoSciences, Crew Building, King's Buildings, Edinburgh, Scotland
Email: {i.mcnicol; edward.mitchard; chiara.aquino; harry.carstairs}@ed.ac.uk

² UCL Department of Geography, Gower Street, London WC1E 6BT, UK

³ NERC NCEO-UCL, Department of Geography, Gower Street, London WC1E 6BT, UK
Email: {a.burt; mathias.disney}@ucl.ac.uk

1. Introduction

The FODEX (Forest Degradation Experiment) is a 5-year project that aims to shed new light on the status of the world's tropical forests and how they are changing in response to human activities. Tropical forests and woodlands are estimated to contain 300 billion tonnes of carbon (Santoro et al. 2020), however we still don't know with any certainty whether these carbon stocks are increasing, or decreasing over time. This is in part because existing static maps of carbon stocks typically have wide uncertainties ($\pm 50\%$) (Mitchard et al. 2014), which precludes accurate and precise change detection. Maps of change are therefore rare (McNicol et al. 2018), and often not validated, and when they are, often no relationship is found between field- and remote sensing-estimated changes (Meyer et al. 2013). The project will address this uncertainty by developing new methods for mapping carbon stock change using satellite data, allowing us to accurately assess the balance of regrowth and anthropogenic disturbance across tropical forests and the status and resilience of the land surface carbon sink.

2. Methodology and data

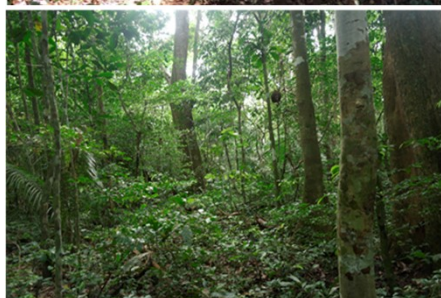


Figure 1 – The contrasting structure of the two sites is a central part of the project. Both images are taken inside our field plots
(top: Gabon, bottom: Peru)

1.1 Approach

This project is based on twin large scale field manipulation experiments located in Peru (Madre de Dios) and Gabon (Ivindo) where we are collecting Terrestrial Laser Scanning (TLS) data alongside traditional forest inventory data before and after controlled logging, meaning the change in aboveground tree volume and biomass (AGB) can be calculated with minimal error and used to train and test models of change. These data will be scaled using LiDAR data collected using a 3.3m wingspan UAV (Delair DT26X UAV) equipped with a Riegl miniVUX, and a 24 MP camera. The UAV has a nominal flight time of 50 - 70 minutes, and can cover 100 – 120 ha in a single flight, and so is capable generating high resolution data that is otherwise unobtainable using ground and/or satellite based platforms. From this, it is possible to derive large scale measurements of several tree biophysical properties such as height, crown dimensions, and vertical structure, while in some areas, the resolution and detail is such that individual trees can segmented (Puliti et al. abstract # 82). Using these data, we aim to generate thousands of hectares of biomass change data, which will then act as a basis for satellite-based methods to generate estimates across the tropics.

1.2 Data

The initial data collection (pre-logging) was conducted in 2019, and early 2020. At each site, four x 1- ha (100 x 100 m) plots were established and all trees >10 cm diameter measured, along with data on x,y position, tree condition, and species. Sites were selected to encompass a range of trees suitable for logging to allow a varying

intensity of logging between plots. The initial aim was to extract 10– 50% of the initial AGB, however in both areas, the number of trees required to achieve these values greatly exceeded the maximum number of trees permitted under FSC rules, meaning we targeted the extraction of 5 – 25% of the initial plot AGB, as estimated through the forest inventory data. The TLS data were collected concomitantly, with measurements taken at the intersections of a 10 x 10 m grid laid out across the plot. The UAV flights were also conducted during the same measurement campaign over a period of 7 days at each site, with missions performed in perpendicular lines and at a nominal altitude of 100 – 130 m above the ground surface with an average flight speed of 17 m/s (61 km/h). This results in a swath width of 100 – 120 m, with an average flight line spacing of 25 m (based on 70 – 80 % overlap), and a maximum laser beam footprint at ground level of 20 – 30 cm, reducing to 10 – 15 cm at the top of the canopy (40 – 50 m). The final post processed LiDAR point clouds have densities ranging from 250 – 1000 points m² in Peru, and 220 – 900 points m² in Gabon.

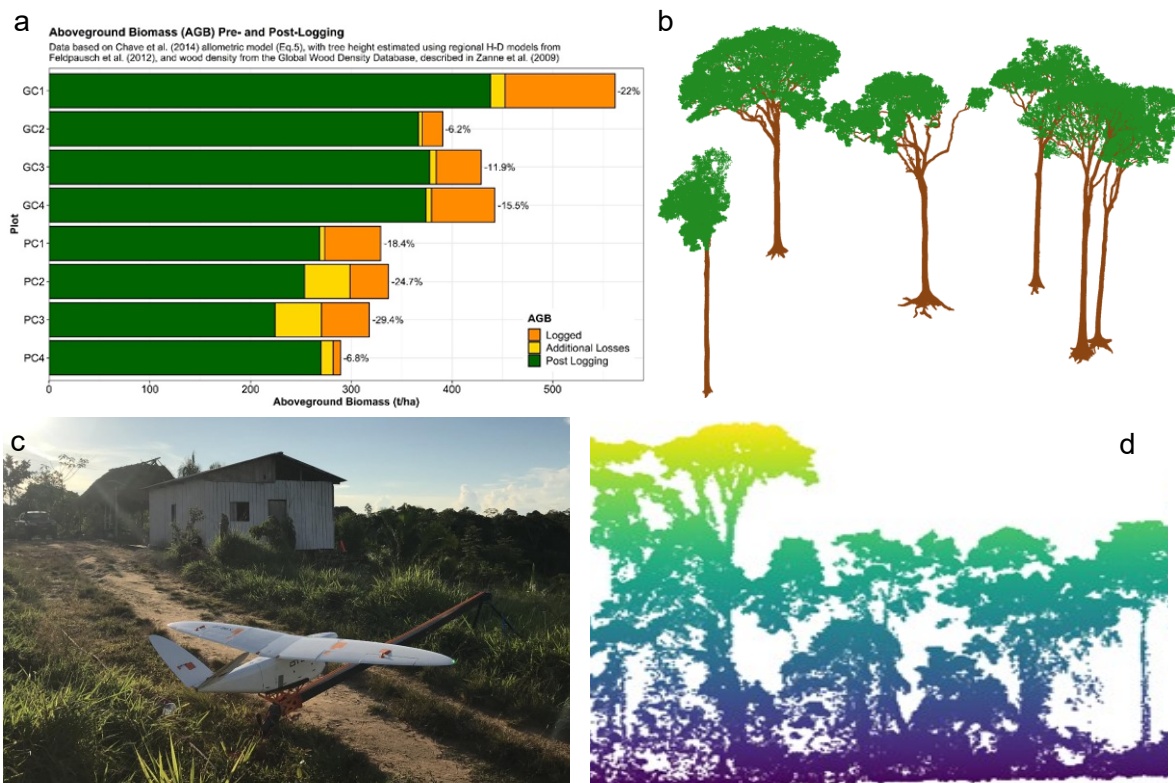
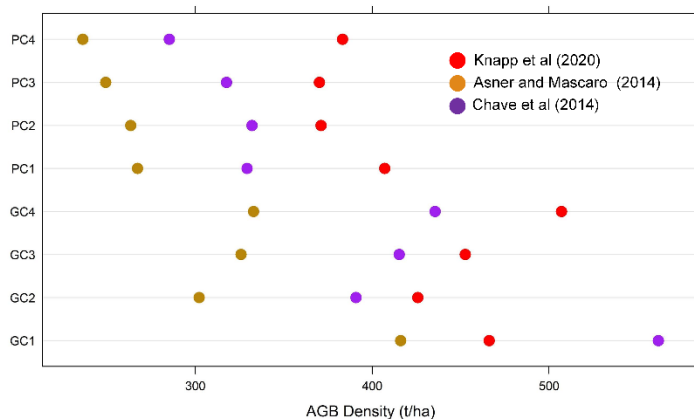


Figure 2 – Aboveground biomass stocks measured before and after logging using traditional inventory data (a). Terrestrial Laser Scanning will provide an improved basis for estimating the change in tree volume/ biomass (b), which will then be scaled using high resolution LiDAR data collected by our fixed wing UAV (c, d). The segmented trees in (b) were derived from TLS data collected in Gabon, and are 5 trees (of 8) that were logged in a single plot. The image in (c) was taken before take-off in Peru, and (d) shows a cross section of a forest patch in Gabon.

3. Results

Forest structure varies markedly across, and between our two study regions, with tree canopy heights in Gabon reaching 35 – 50 m in areas with a tree fractional cover > 50%, compared to 25 – 40 m in Peru, based on the UAV-LS data (Figures 1 and 2). Despite their comparatively low stature, the Peruvian forests are structurally more complex, with a clear sub-canopy layer 10 – 15 m in height whereas in Gabon, there is typically a single dominant tree layer varying little in height.

The inventory-based estimates of AGB were broadly consistent between field plots (Figure 2; Figure 3), with the %AGB extracted increasing (5 – 30 %) once collateral damage from tree felling and



removal was accounted for. Using a combination of the UAV-LS data, the forest inventory data, and a variety of published field and LiDAR based models (Asner and Mascaro et al. 2014; Knapp et al. 2020), we find wide range of biomass values for each plot (Figure 3). The TLS data will provide, in due course, accurate and precise estimates of AGB density and loss in each plot, against which changes will be compared, and new + existing methods validated.

Figure 3 - Applying different biomass estimation models yields very different results, which will be compared to the changes derived from the TLS data

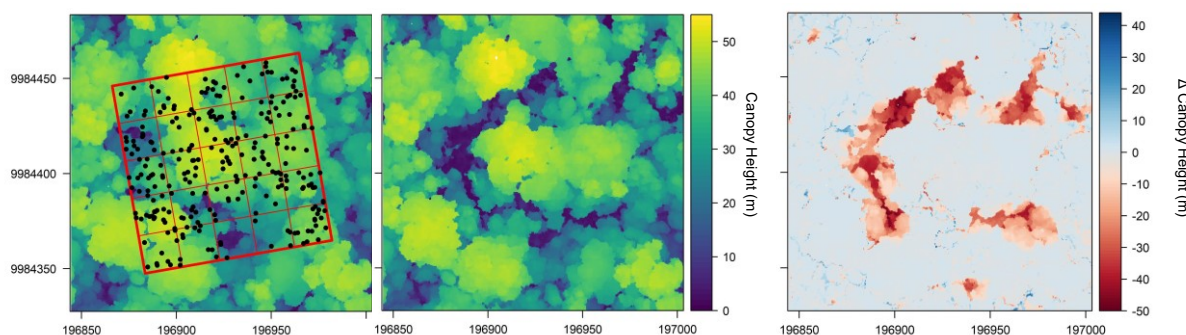


Figure 4 – (a) The change in tree canopy height after logging in and around one of the core 1-ha inventory plots in Gabon (GC4) where 16% of the initial AGB was removed.

4. References

- Asner, G.P. & Mascaro, J. (2014) Mapping tropical forest carbon: Calibrating plot estimates to a simple LiDAR metric. *Remote Sensing of Environment*, 140, 614–624.
- Chave, J., Réjou-Méchain, M., Búrquez, A., Chidumayo, E., Colgan, M.S., Delitti, W.B., Duque, A., Eid, T., Fearnside, P.M., Goodman, R.C., Henry, M., Martínez-Yrizar, A., Mugasha, W. a, Muller-Landau, H.C., Mencuccini, M., Nelson, B.W., Ngomanda, A., Nogueira, E.M., Ortiz-Malavassi, E., Péliissier, R., Ploton, P., Ryan, C.M., Saldarriaga, J.G. & Vieilledent, G. (2014) Improved allometric models to estimate the aboveground biomass of tropical trees. *Global Change Biology*, 1–14.
- Knapp, N., Fischer, R., Cazcarra-Bes, V. & Huth, A. (2020) Structure metrics to generalize biomass estimation from lidar across forest types from different continents. *Remote Sensing of Environment*, 237, 111597.
- Mitchard, E.T.; Saatchi, S.S.; Baccini, A.; Asner, G.P.; Goetz, S.J.; Harris, N.L.; Brown, S. Uncertainty in the spatial distribution of tropical forest biomass: a comparison of pan-tropical maps. *Carbon Balance Manag.* 2013, 8, 10, doi:10.1186/1750-0680-8-10.
- McNicol, I.M.; Ryan, C.M.; Mitchard, E.T.A. Carbon losses from deforestation and widespread degradation offset by extensive growth in African woodlands. *Nat. Commun.* 2018, 1–19, doi:10.1038/s41467-018-05386-z
- Meyer, V.; Saatchi, S.S.; Chave, J.; Dalling, J.W.; Bohlman, S.; Fricker, G.A.; Robinson, C.; Neumann, M.; Hubbell, S. Detecting tropical forest biomass dynamics from repeated airborne lidar measurements. *Biogeosciences* 2013, 10, 5421–5438, doi:10.5194/bg-10-5421-2013.
- Puliti, S., Pearse, G., Mitchard, E., McNicol, I., Bremner, M., Rutzinger, M., Surovy, P., Wallace, L., Hollaus, M., and Astrup, R. (2021) A New drone laser scanning benchmark dataset for characterisation of single-tree and forest biophysical properties. *SilviLaser Conference 2021*, Abstract 82.
- Santoro, M., Cartus, O., Carvalhais, N., Rozendaal, D., and 30 others (2020) The global forest above-ground biomass pool for 2010 estimated from high-resolution satellite observations. *Earth Syst. Sci. Data Discuss.*, 2020, 1–38.

Assessing the long-term effect of hurricanes on the Caribbean mangrove structure with GEDI L3 data

C. H. Amaral^{1,2}, B. Poulter², T. Fatoyinbo², D. Lagomasino³, P. Taillie⁴, G. Lizcano⁵,
R. M. Roman-Cuesta⁶

¹Universidade Federal de Viçosa, Department of Forest Engineering, Viçosa, MG 36570-900, Brazil
Email: chamaral@ufv.br

²NASA Goddard Space Flight Center, Biospheric Sciences Lab., Greenbelt, MD 20771, United States
Email: {benjamin.poulter; lola.fatoyinbo}@nasa.gov

³East Carolina University, Department of Coastal Studies, Greenville, NC 27858-4353, United States
Email: lagomasinod19@ecu.edu

⁴University of Florida, Department of Wildlife Ecology and Conservation, Gainesville, FL 32611, United States
Email: paultaillie@gmail.com

⁵Climate Scale, Rue Dieudonné Lefèvre, 17, 1020 Brussels, Belgium
Email: gil.lizcano@climatescale.com

⁶Wageningen University & Research, Laboratory of Geo-Information Science and Remote Sensing, 6708PB Wageningen - The Netherlands
Email: rosa.roman@wur.nl

1. Introduction

Mangrove forests are a key component of coastal ecosystems and play an essential role in protecting local communities from catastrophic storms, sheltering economic activities during hurricane exposure, and preventing permanent losses to economic activities (Hochard et al. 2019). Moreover, they are able to regulate the climate through carbon sequestration and storage and thus, their dynamics have a disproportionate impact on global carbon balance in comparison to other ecosystems (Friess et al. 2020). Therefore, increased frequencies and intensities of hurricanes are a major threat to the economic and ecologic stability of the Caribbean region (Collymore 2011; Camargo and Wing 2021). We herein aim to understand how the cumulative presence of hurricanes in the Caribbean and Gulf of Mexico regions (1979-2018) has affected the structure of the mangroves, particularly height, to navigate actions for regional coastal ecosystem conservation and restoration. To achieve this, we overlap the hotspots of hurricane wind affectation in that period, from the ERA5 reanalysis cumulative maximum winds at 31km resolution, and the Global Ecosystem Dynamics Investigation (GEDI) Level 3 (L3) gridded data at 1km resolution from 2019-2020 (Dubayah et al. 2021).

2. Data and Methods

2.1 Data

We used the 2019-2020 Global Ecosystem Dynamics Investigation (GEDI) Level 3 (L3) gridded mean canopy height, i.e., averages of the 30-m footprint RH100 metrics within each 1 sq. km cell (Dubayah et al. 2021). The Copernicus Climate Change Service (C3S) ERA5 reanalysis data (0.25° of spatial resolution and hourly temporal resolution) for maximum 3-second wind at 10 m height from 1979 to 2018 was used to estimate storm history (Hersbach et al. 2018). We also used 1996 and 2016 mangrove distribution data from the Global Mangrove Watch (GMW; Bunting et al. 2018) and data for the bio-regionalization of coastal and shelf areas (Spalding et al. 2007) for the entire Caribbean region, which comprises 25 countries from the southern United States down to Colombia and Venezuela (Figure 1).

2.2 Methods

We first generated grids for the annual maximum sustained wind speed from 1979 to 2018 from the ERA5 hourly wind data that summarizes the maximum 3-second wind at 10 m height at every 31 km. The annual maximum wind speed values for each grid-cell were calculated from the available hourly data and converted to kilometers per hour. From this 40-composite-bands file, we calculated the 40-year cumulative sustained wind speed (km/h), the number of times each cell present maximum sustained wind speed higher than 119 km/h, which classifies it as a hurricane according to the Saffir-Simpson Hurricane Scale, and the time since the last hurricane.

We then created a mangrove mask based on the intersection between the 1996 and 2016 GMW layers (i.e., the current and historical extent combined) and generated random sampling points with 1-km spacing within this region. For each point we extracted the GEDI canopy height (m) (i), the 40-years cumulative sustained wind speed (km/h) (ii), the history of hurricane impact from 1979 to 2018 (iii), and the time since the last hurricane (iv). Points with no missing values summed 1,806. We then calculated the non-parametric Spearman rank coefficient (r) between (i) and (ii) and (i) and (iv) and tested whether heights of mangrove groups (i), which were impacted by zero, one or two hurricanes from 1979 to 2018 (iii), originate from the same distribution by means of the Kruskal-Wallis test. We analyzed the data for the entire Caribbean region but also by ecoregion.

3. Results and Discussion

We found that the median canopy height of the Gulf of Mexico and Caribbean mangroves is 5.36m, ranging from 1.42 to 21.53m tall (Figure 1).

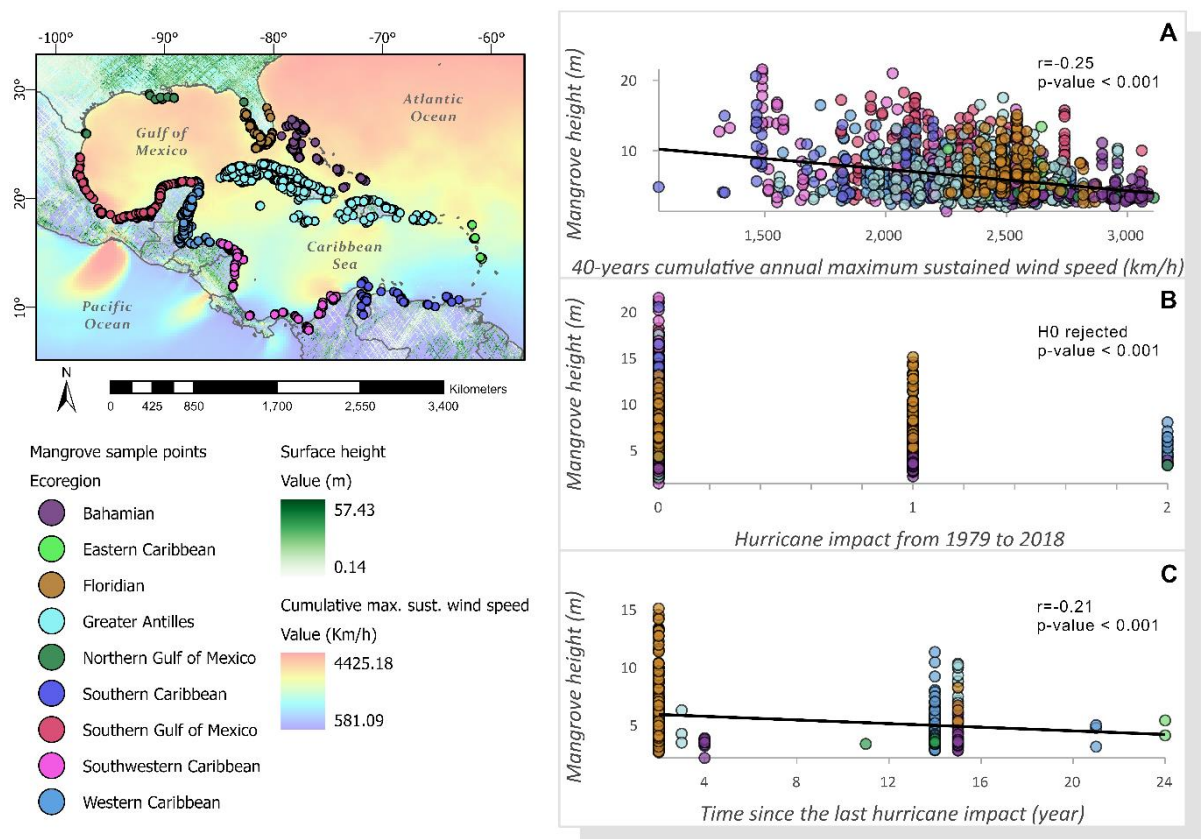


Figure 1: Location of sample points ($n = 1,806$) within the Gulf of Mexico and Caribbean regions where mangrove height was extracted using GEDI L3 data for 2019-2020, along a gradient of hurricane cumulative presence during the period 1979-2018.

Our results show a clear inverse relation between cumulative sustained wind speed from 1979 to 2018, and the height of Caribbean mangroves in 2019-2020 (Figure 1a). This relationship is corroborated by Simard et al. (2019) that correlated the global SRTM and ICESat-2/GLAS mangrove height estimates with the frequency of tropical cyclones. The tallest mangroves (of about 20 m) are in regions not affected

by the strongest wind gusts and that stand out for their lowest cumulative wind speeds, i.e., in the Southern and Southwestern Caribbean regions (Figure 1a and 1b). Conversely, mangroves are less structurally diverse and shorter than 10 m in regions affected twice by the strongest wind gusts and that also present the highest cumulative wind speeds over the studied time range, i.e., in the Bahamian, Northern Gulf of Mexico, and in some places of the Western Caribbean region (Figure 1a and 1b). All regions presented a tendency of height decrease with rising cumulative wind speeds and the degree of correlation between these two variables is moderate for the Southern ($r = -0.38$) and Southwestern Caribbean (-0.33) regions and strong for the Northern Gulf of Mexico (-0.58).

ERA5 reanalysis appears to underestimate the maximum sustained wind speed, even though it is considered consistent to capture wind speed ranges (e.g., Jourdi er 2020). Thus, the 119 km/h threshold captures higher category wind gusts with ERA5 data, like those observed in the 1995, 1998, 2004, 2005, 2008, 2015, 2016, and 2017 mega-hurricane seasons (Figure 1c). In general, we did not observe taller mangroves where the time since the last hurricane was longer, which suggests there was no regional pattern of structural resilience in mangroves hit by strong wind gusts. This expected pattern was seen in mangroves from the Greater Antilles ($r = 0.42$) and from the Northern Gulf of Mexico (0.41) moderately. The further exploration of GEDI L1 and L2 data will allow us to better understand the impact of hurricanes on the entire mangroves' vertical profiles.

4. Conclusions

GEDI L3 gridded data is a powerful dataset for understanding the long-term effect of extreme climate events on forest structure across large regions. Our results indicate that the cumulative impact of hurricanes seems to compromise the Caribbean mangrove structural diversity and that, in general, they appear not being structurally resilient upon hurricane impact.

Acknowledgements

This research was supported by BNP PARIBAS Foundation within the project "COastal biodiversity RESilience to increasing extreme events in Central AMerica (CORESCAM): implications for regional conservation and policy making".

References

- Bunting P, Rosenqvist A, Lucas RM, Rebelo LM, Hilarides L, Thomas, N, ... and Finlayson CM, 2018, The global mangrove watch—a new 2010 global baseline of mangrove extent. *Remote Sensing*, 10(10): 1669.
- Camargo SJ and Wing AA, 2021, Increased tropical cyclone risk to coasts. *Science*, 371(6528): 458-459.
- Collimore J, 2011, Disaster management in the Caribbean: Perspectives on institutional capacity reform and development. *Environmental Hazards*, 10(1): 6-22.
- Dubayah RO, Luthcke SB, Sabaka TJ, Nicholas JB, Preaux S and Hofton MA, 2021, *GEDI L3 Gridded Land Surface Metrics*, Version 1. ORNL DAAC, Oak Ridge, Tennessee, USA. <https://doi.org/10.3334/ORNLDAAC/1865>
- Friess DA, Krauss, KW, Taillardat P, Adame MF, Yando ES, Cameron C, ... and Sillanp a M, 2020, Mangrove Blue Carbon in the Face of Deforestation, Climate Change, and Restoration. *Annual Plant Reviews online*, 3(3): 427-456.
- Hersbach H, Bell B, Berrisford P, Biavati G, Hor anyi A, Mu oz Sabater J, Nicolas J, Peubey C, Radu R, Rozum I, Schepers D, Simmons A, Soci C, Dee D, Th epaut JN, 2018, *ERA5 hourly data on single levels from 1979 to present*. Copernicus Climate Change Service (C3S) Climate Data Store (CDS). Available at: <https://cds.climate.copernicus.eu/cdsapp>
- Hochard J P, Hamilton S and Barbier EB, 2019, Mangroves shelter coastal economic activity from cyclones. *Proceedings of the National Academy of Sciences*, 116(25): 12232-12237.
- Jourdi er B, 2020, Evaluation of ERA5, MERRA-2, COSMO-REA6, NEWA and AROME to simulate wind power production over France. *Advances in Science and Research*, 17: 63-77.
- Simard M, Fatoyinbo L, Smetanka C, Rivera-Monroy VH, Casta eda-Moya E, Thomas N and Van der Stocken T, 2019, Mangrove canopy height globally related to precipitation, temperature and cyclone frequency. *Nature Geoscience*, 12(1): 40-45.
- Spalding MD, Fox HE, Allen GR, Davidson N, Ferda a ZA, Finlayson MAX, ... and Robertson J, 2007, Marine ecoregions of the world: a bioregionalization of coastal and shelf areas. *BioScience*, 57(7): 573-583.

OPALS: A Flexible and Efficient Point Cloud Processing Software for Forest Application

J. Otepka¹, M. Hollaus¹, G. Mandlbürger¹, L. Gokl¹, W. Karel¹, B. Wöhrer¹, N. Pfeifer¹

¹Department of Geodesy and Geoinformation, TU Wien, Wiedner Hauptstraße 8, 1040 Vienna, Austria
Email: {johannes.otepka;markus.hollaus;gottfried.mandlbuerger;lukas.gokl;wilfried.karel;bruno.woehrer;norbert.pfeifer}@geo.tuwien.ac.at

1. Introduction

OPALS¹ (Orientation and Processing of Airborne Laser Scanning data) is a modular and efficient point cloud processing software (Pfeifer et al., 2015) developed at TU Wien, Department of Geodesy and Geoinformation. Although the development is mainly focussed on Airborne Laser Scanning (ALS) data, OPALS is well capable of handling huge point clouds from arbitrary sensors, like static and kinematic laser scanners, single photo LiDAR (SPL), range cameras, and photogrammetric point clouds computed by dense image matching (DIM), etc.

The strong scientific background of the software is emphasised by detailed documentation of the used algorithms and concepts, with many algorithms published additionally in scientific journals. Profound processing algorithms are, however, only one pillar of OPALS. Due to the rapid technological advances and miniaturisation, modern sensors achieve enormous measurement rates (> 1 Mhz) and point densities (>200 points/m²) resulting in huge data sets with billions of points. Hence, efficient processing strategies are an absolute necessity for a mature and operational point cloud processing software. For this reason, OPALS makes extensive use of today's multi-core processors. Based on its modular structure, it is further possible to distribute processing tasks from multiple independent computers up to large high-performance computing facilities.

OPALS consists of a range of small and well-defined modules for specific tasks. Each module can be accessed via command line, Python and C++ in a unified manner. Comprehensive workflows such as quality assessment are predefined in OPALS as Python scripts. Nevertheless, the modular and flexible structure also allows for establishing individual workflows in the preferred scripting/programming environment. Thereby, users can have full access to the individual point attributes as well as to a set of spatial queries based on generic neighbourhood definitions (Otepka et al., 2021).

From an application point of view, OPALS covers a wide range of typical processing tasks for vegetation mapping. In this contribution, we demonstrate the versatility of OPALS with three case studies covering different applications, sensors, and scales from single tree modelling using TLS to country-wide, ALS-based biomass estimation. Additionally, georeferencing and strip adjustment of UAV-borne laser scanning (ULS) data is demonstrated as first showcase since it is a prerequisite for most LiDAR processing tasks. Proper georeferencing and scan data alignment is of special importance whenever the application requires fusion of data from multiple flight strips (ALS/ULS) or scan stations (TLS) (e.g., stem diameter estimation) to unlock the full potential of the measured data.

2. Case studies

2.1. Strip Adjustment of ULS data

Depending on accuracy requirements and data quality, fine georeferencing for static LS and strip adjustment for kinematic LS can get necessary. This goes beyond the direct georeferencing provided by inertial and global satellite navigation sensors and/or the use of markers or other tie elements in TLS point clouds. It may include refining the calibration of the entire system. To decide where an improved georeferencing is necessary, typically a quality control based on differences on smooth areas between overlapping strips or TLS scan positions is performed. Statistical measures and visualisations of the differences allow assessing, if georeferencing improvements are necessary or not. In case improvement of sensor orientation is needed, opalsICP and opalsStripAdjust are the two modules for fine georeferencing of static and kinematic data sets. Special emphasis is also laid on precise orientation of

¹ <https://opals.geo.tuwien.ac.at>

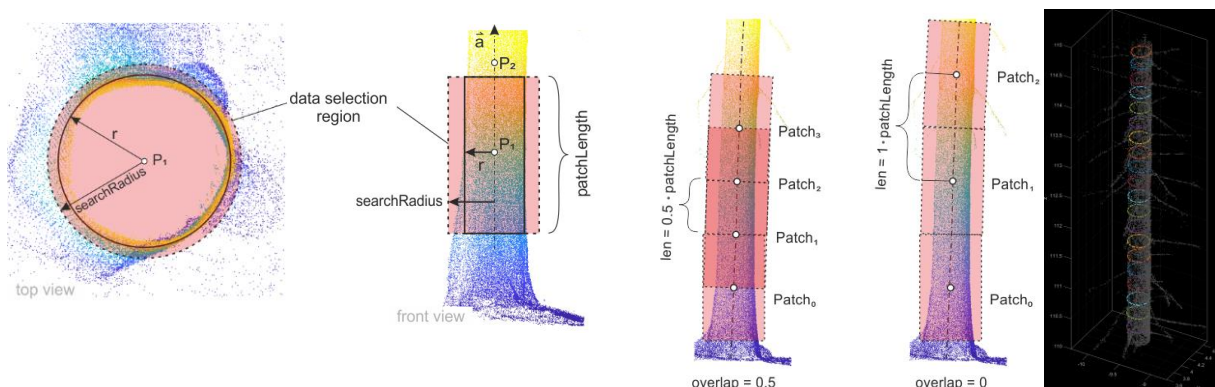
very high-resolution datasets from Unmanned Aerial Vehicles (UAV) as they play an important role in vegetation studies (Glira et al. 2017 and 2020). After strip adjustment, quality control is repeated to double check the remaining height residuals in overlapping areas or compared to external reference data. For the ULS dataset of an alluvial forest at the Pielach River in Lower Austria used by Wieser et al. (2018) for diameter at breast height (DBH) estimation, Glira et al. (2016) achieved a 25% reduction of the height discrepancies from originally 1.8 cm to 1.3 cm after strip adjustment. This can be considered the state of the art, and a further improvement of accuracy would require improvement of multiple components of ULS. However, “of the shelf” ULS missions often do not reach this accuracy.

2.2. Single Tree Modelling using TLS

In recent years, TLS has become the standard method for precise non-destructive three dimensional detection of trees. Commonly the data are acquired from multiple scan positions. Based on the co-registered point clouds different tree parameters can be derived. The most important tree parameters are tree height and DBH.

The opalsDBH module was developed for modelling individual tree stems. It features both estimation of DBH and modelling of full stems or branches by progressively robustly fitting cylinders or cones along the stem axis. Since the algorithm is fully 3D, opalsDBH can model vertical, slanted or even horizontal tree stems (deadwood, driftwood, etc.). Starting from a given approximate 3D location and axis direction, the module incrementally follows the tree stem in both directions if needed (Figure 1). The approximate 3D locations are derived by applying a voxel analysis. As output, the stem diameters for defined height intervals are derived as shown in Figure 2. Taper functions can be generated based on the stem diameters and the extracted tree heights. The data shown in Figure 1 is part of a coniferous dominated plot located in north-east Austria. The TLS acquisition was carried out in May 2017 using a Riegl VZ-2000 (RIEGL Laser Measurement Systems, Horn, Austria). Details on this data set can be found in Bruggisser et al. (2020). The entire processing chain starting with the co-registered point cloud and ending with the derived stem diameters along the stem can be carried out fully automatically.

Figure 3: Left: cross section of a stem point cloud overlaid with the search cylinder for selecting the



points considered for cylinder or cone modelling directly; Middle: trace models with different overlap settings; Right: stem diameters derived via cylinder fittings.

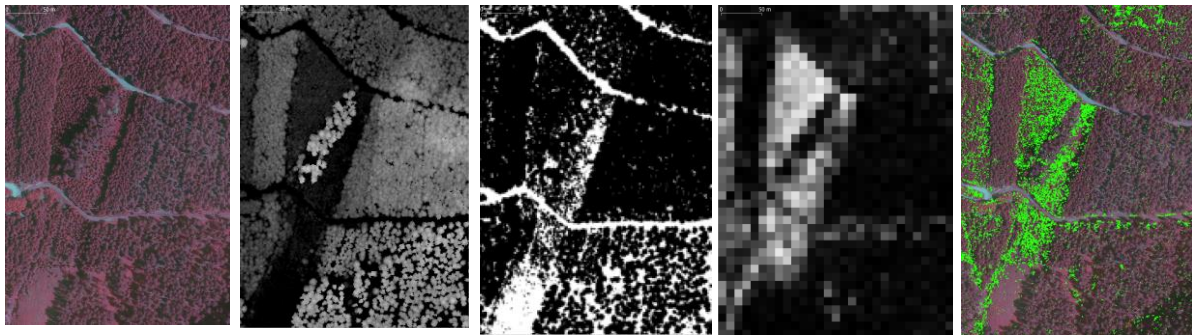
2.3. Country-wide processing of ALS data for deriving forest parameters

For country-wide applications it is beneficial to do tile based processing. Splitting input data into independent data tiles (with or without overlap) is a standard task within OPALS. Tiling limits the computational burden if re-computing becomes necessary, e.g., because of failure or crash due to network problems or other reasons. Even more importantly, processing can be distributed over multiple computers or nodes of a high-performance computing cluster if needed. In this showcase topographic models and forest structure parameters are derived for a ~17 000 km² study area in Austria. The ALS data was acquired within a district-wide ALS campaign carried out between 2008 and 2012 and consists of 6,219 individual ALS flight strips.

Starting from the georeferenced point clouds, the ALS data are split into 3,327 tiles with an extent of 2.2 x 2.2 km². The overlap between neighbouring tiles was set to 100 m. The digital surface model (DSM) was calculated with the opalsDSM module, which calculates the height of a DSM grid cell using the highest 3D point per raster cell for rough surface parts and moving least squares interpolation for smooth surfaces (Hollaus et al., 2010). The derived DSM delivers good results for canopy surfaces as well as for forest gaps. Furthermore, the normalized digital surface model (nDSM) was calculated by subtracting the digital terrain model (DTM) from the DSM. All these topographic models were processed with a spatial resolution of 1 x 1 m².

Based on the nDSM, forest gaps were derived by applying a height threshold and morphological image operations. Furthermore, the normalized point clouds were used to calculate the fractional cover by calculating the ratio between terrain and all points. Finally, parameters describing the vertical forest structure were derived from the point cloud by applying a voxel approach. The derived structural layers contain information about the availability and density of understorey but also about the vertical distribution of the canopy layers. Figure 2 shows exemplary subsets of the derived products.

Figure 2: from left to right: CIR orthophotos, nDSM (black = 0 m, white >50 m); gap map (white = gaps,



black = no gap); fractional cover (black=0%, white = 100%); vertical layer between 1 and 2 m (green = voxel with vegetation filled) overlaid to the NIR orthophoto.

3. Summary and Outlook

OPALS is a modular and efficient software package for processing 3D point clouds from arbitrary sensors. As demonstrated by the three showcases, it contains a variety of tools for forest applications at different scales. A detailed list of vegetation related scripts and modules can be found on the opals homepage². Furthermore, OPALS provides advanced tools for fine georeferencing and system calibrations at the highest possible accuracy level.

The modular structure allows distributed processing for optimal processing speed in case of huge projects, as e.g. the country-wide ALS showcase was computed on multiple high-end workstations. Furthermore, the Linux version of OPALS has successfully been used, to process large projects on the Vienna Scientific Cluster 3 (Otepka et al., 2019).

OPALS is currently developed to reach version 3, which will bring two major improvements: The flexibility of spatial neighborhood definitions in point clouds has been largely improved and multi-band raster files are now supported to the full extent and in a uniform way. OPALS version 3 will be released in summer 2021.

Acknowledgements

The ALS data was provided by the province of Styria, Austria. This research was partly conducted within the CONFIRM project (project No. 873674) funded by the Austrian Research Promotion Agency (FFG) under the 15th Austrian Space Applications Program (ASAP).

² https://opals.geo.tuwien.ac.at/html/nightly/pkg_opalsForest.html

References

- Bruggisser M, Hollaus M, Otepka J, Pfeifer N, 2020, Influence of ULS acquisition characteristics on tree stem parameter estimation. *ISPRS Journal of Photogrammetry and Remote Sensing*, 168, 2020, 28-40.
- Glira P, Pfeifer N, Mandlbürger G, 2016, Rigorous Strip adjustment of UAV-based laserscanning data including time-dependent correction of trajectory errors. *PE & RS*, 82 (12), 945-954.
- Glira P, Pfeifer N, Mandlbürger G, 2019, Hybrid Orientation of Airborne LiDAR Point Clouds and Aerial Images, *ISPRS Ann. Photogramm. Remote Sens. Spatial Inf. Sci.*, IV-2/W5, 567-574.
- Hollaus M, Mandlbürger G, Pfeifer N, Mücke W, 2010, Land cover dependent derivation of digital surface models from airborne laser scanning data. *IAPRS Volume XXXVIII Part 3A*, 221-226.
- Otepka J., Pöchtrager M., Hollaus M., Loghin A., Piermattei L., Briese C., Pfeifer N., 2019, Landesweite Punktwolkenprozessierung mit OPALS am Supercomputer VSC3, 20. Internationale Geodätische Woche Obergurgl 2019, Hanke K., Weinold T. (ed.); Wichmann, (2019)
- Otepka J., Mandlbürger G., Karel W., Wöhrer B., Ressler C., Pfeifer N., 2021, A Framework for Generic Spatial Search in 3D Point Clouds, *ISPRS Ann. Photogramm. Remote Sens. Spatial Inf. Sci.*, V-2-2021.
- Pfeifer N, Mandlbürger G, Otepka J, Karel W, 2014, OPALS - A framework for Airborne Laser Scanning data analysis, *Computers, Environment and Urban Systems*, 45, 125 - 136.
- Wieser M, Mandlbürger G, Hollaus M, Otepka, J, Glira P and Pfeifer N, 2018, A Case Study of UAS Borne Laser Scanning for Measurement of Tree Stem Diameter. *Remote Sensing*, 9(11), 1154.

Challenges to Collaboration in International Research: Lessons from Terrestrial Laser Scanning

K. A. Slavik¹

¹Science-Based Business, Faculty of Science, Leiden University, Einsteinweg 55
2300 RA, Leiden

Email: k.a.slavik@sbb.leidenuniv.nl

1. Introduction

Terrestrial laser scanning is a method of remote sensing with applications to ecological research. A relatively young research method, the first literature demonstrating the application of ground-based laser scanning technologies to ecology and forestry was published in the early 2000s (Lovell et al. 2003). Over the past 20 years, advances in instrument technology and data processing have enabled the development of novel measurement approaches and expanded the application of terrestrial laser scanning beyond traditional structural metrics. The data generated through terrestrial laser scanning is now used, amongst others, to estimate aboveground biomass, model branch architecture, conduct habitat assessments, generate vertical profiles of vegetation structure and quantify fuel loads (Beland et al. 2019, Calders et al. 2020, Disney 2019). Terrestrial laser scanning also has potential applications to other forms of remote sensing measurement systems (Beland et al. 2019) and 3D modelling (Disney 2019). Such developments are fostered by working and sharing with colleagues (Laudel 2001).

International collaborations play an important role in terrestrial laser scanning. The diverse range of disciplines and countries that collaborations in terrestrial laser scanning bring together builds not only connections between researchers but also encourages the standardisation and sharing of algorithms, data and best practices for field work (Beland et al. 2019). However, terrestrial laser scanning research has also struggled to attract expertise from across many disciplines, such as remote sensing, physics, engineering and computer science, and has instead focused on training forest ecologists to perform these functions (Calders et al. 2020). Terrestrial laser scanning is therefore an interesting and unique context in which to study international collaborations.

Terrestrial laser scanning, like all of science, is an increasingly international and collaborative endeavor. International collaborations across science are driving research (Adams 2013), with high-impact research papers increasingly authored by international teams (Adams 2012). Collaborating in international research is facilitated by advances in communications technology, which increase the interconnectedness of researchers (Wagner and Leydesdorff 2005). International research collaborations are however complex and diverse in terms of structure, coordination and purpose (Katz and Martin, 1997). Researchers who collaborate internationally must overcome political, logistical and cultural barriers and negotiate a range of challenges, including lack of funding for international research, restrictions on material and data sharing and differences in academic standards (Matthews et al. 2020). These challenges to collaborative international research are also potentially applicable to terrestrial laser scanning.

This research paper seeks to improve our understanding of the collaborative dynamics in terrestrial laser scanning by exploring how researchers experience collaborations involving terrestrial laser scanning. In doing so, this research project aims to address the following research questions: How do the challenges and barriers identified by Matthews et al. (2020) manifest in terrestrial laser scanning and what strategies do researchers employ to overcome them? How does the structure and coordination of international collaborations reinforce or mitigate the challenges and barriers? What are the consequences of the challenges, barriers and strategies for the scientific output? Ultimately, the results of this research will hopefully support terrestrial laser scanning researchers and inform more effective organisation and coordination of international research collaborations.

2. Data and Methods

This study draws on data collected from 17 (at present) semi-structured interviews with researchers whose current or previous research activities are associated with terrestrial laser scanning. The

interviewees were initially drawn from participants in an international network focused on terrestrial laser scanning and expanded through a snowball sampling technique. The interviewees were based in 11 different countries across Europe, North America and Australia. The interviewees were asked a series of questions designed to create data about their own background as well as to provoke stories about their experiences in international research collaborations involving terrestrial laser scanning. Particular attention was paid to any challenges the interviewees experienced and how these challenges were addressed.

After transcribing the interviews, the language and stories shared by the interviewees were analysed and thematically coded according to the research questions using the qualitative analysis software Atlas.ti. The initial coding framework was based on the barriers and challenges introduced by Matthews et al. (2020) and elaborated on throughout the coding process following an inductive, grounded theory approach (Charmaz 2014). The coding framework was judged as complete when no new themes emerged from the data. In addition to the interviews, documents from an international network associated with terrestrial laser scanning were also coded. The resulting thematic codes were then compared and analysed to identify any patterns or trends within the data.

3. Results and Discussion

Researchers who participate in international collaborations in terrestrial laser scanning tend to fall into one of four categories (see Table 1). The categories are not exclusive; it is possible for an individual to exist within multiple. Each category of expert offers different skills and has different demands from collaborations. The four categories differ in their understanding of the goals and the state of development of terrestrial laser scanning. When two or more different categories participate together in a collaboration, they must negotiate these sometimes-conflicting perspectives, even when the collaboration has a clear, shared goal.

Table 1: Typology of experts in terrestrial laser scanning.

	Tool Developers	Data Gatherers	Data Analysers	Data Users
Role:	Build the equipment	Operate the equipment in the field to collect data	Make sense of the data collected in the field	Use the generated data for their own applications
Disciplines:	Engineers; physicists	Remote sensing specialists	Modellers; mathematicians	Ecologists; Forest managers
See TLS as a(n):	Engineering problem	Research field	Research field	Tool
Development status:	Advanced	Advanced	Intermediate	Early days

Amongst the many reported challenges to international collaborations in terrestrial laser scanning, the most common was funding, which echoes the findings of Matthews et al. (2020). Many interviewees reference the constraints that available funding has on their ability to engage with international collaborations. In general, experts join international research collaborations in terrestrial laser scanning for the following seven reasons: data sharing, instrument sharing, networking, learning, obtaining funding, conducting fieldwork and bridging expertise. The further goals of this research is to understand how these motivations differ across the four expert categories.

The structure and coordination of the international collaborations can be reduced to four ideal collaboration types (Figure 1), based on the degree of formality and number of countries involved. The collaboration types differ in terms of funding, pre-existing relationships between members and shared research interests. These differences give each type their own set of coordination, organisational and management challenges. The preliminary findings suggest that some of the collaboration types are more suited for certain goals than others. Moving forward, this research hopes to shed light on how the emerging challenges and reasons to collaborate differ across the types of collaborations.

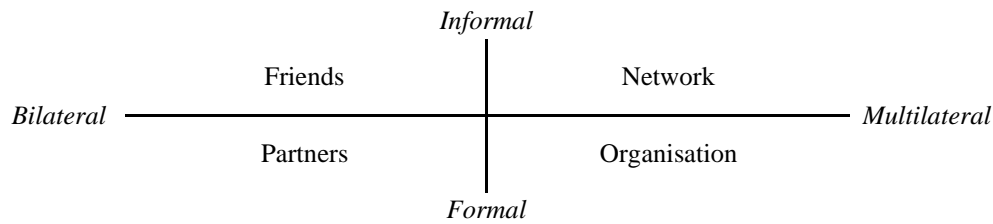


Figure 1: Typology of international research collaborations.

4. Conclusions

Terrestrial laser scanning is a unique case study for investigating the collaborative dynamics of international research. International research collaborations in terrestrial laser scanning connect diverse researchers and facilitate the standardisation and sharing of algorithms, data and best practices for field work. Researchers involved in international collaborations in terrestrial laser scanning can be grouped into four categories of experts, which differ in terms of their role, discipline and view of terrestrial laser scanning. Researchers participate in these international collaborations for a variety of reasons. Participants in international collaborations in terrestrial laser scanning also face a range of challenges, the most common being funding. The differences between four categories of terrestrial laser scanning experts can cause tensions, which the participants must negotiate. The structure of international collaborations can be divided into four basic types, distinguished by formality and number of involved countries. Each type has their own advantages and disadvantages. As this research project moves forward, it will explore how the reasons for participating, the challenges the participants face and the categories of experts differ with the four types of collaborations. Understanding how the different types of collaborations constrain or support researchers in their everyday work is essential to building more effective international collaborations in the future. This research is still ongoing and feedback on the direction and preliminary findings is extremely helpful.

Acknowledgements

This research is conducted as part of a project that has received funding from the European Research Council (ERC) under the European Union's Horizon 2020 research and innovation programme (Grant agreement No. 819533).

References

- Adams, J., 2013. The fourth age of research. *Nature* 497, 557–560. <https://doi.org/10.1038/497557a>
- Adams, J., 2012. The rise of research networks. *Nature* 490, 335–336. <https://doi.org/10.1038/490335a>
- Beland, M., Parker, G., Sparrow, B., Harding, D., Chasmer, L., Phinn, S., Antonarakis, A., Strahler, A., 2019. On promoting the use of lidar systems in forest ecosystem research. *For. Ecol. Manag.* 450, 117484. <https://doi.org/10.1016/j.foreco.2019.117484>
- Calders, K., Adams, J., Armston, J., Bartholomeus, H., Bauwens, S., Bentley, L.P., Chave, J., Danson, F.M., Demol, M., Disney, M., Gaulton, R., Krishna Moorthy, S.M., Levick, S.R., Saarinen, N., Schaaf, C., Stovall, A., Terry, L., Wilkes, P., Verbeeck, H., 2020. Terrestrial laser scanning in forest ecology: Expanding the horizon. *Remote Sens. Environ.* 251, 112102. <https://doi.org/10.1016/j.rse.2020.112102>
- Charmaz, K., 2014. *Constructing Grounded Theory*. SAGE.
- Disney, M., 2019. Terrestrial LiDAR: a three-dimensional revolution in how we look at trees. *New Phytol.* 222, 1736–1741. <https://doi.org/10.1111/nph.15517>
- Katz, J.S., Martin, B.R., 1997. What is research collaboration? *Res. Policy* 26, 1–18. [https://doi.org/10.1016/S0048-7333\(96\)00917-1](https://doi.org/10.1016/S0048-7333(96)00917-1)
- Laudel, G., 2001. Collaboration, creativity and rewards: why and how scientists collaborate. *Int. J. Technol. Manag.*
- Lovell, J.L., Jupp, D.L.B., Culvenor, D.S., Coops, N.C., 2003. Using airborne and ground-based ranging lidar to measure canopy structure in Australian forests. *Can. J. Remote Sens.* 29, 607–622. <https://doi.org/10.5589/m03-026>
- Matthews, K.R.W., Yang, E., Lewis, S.W., Vaidyanathan, B.R., Gorman, M., 2020. International scientific collaborative activities and barriers to them in eight societies. *Account. Res.* 27, 477–495. <https://doi.org/10.1080/08989621.2020.1774373>
- Wagner, C.S., Leydesdorff, L., 2005. Network structure, self-organization, and the growth of international collaboration in science. *Res. Policy* 34, 1608–1618. <https://doi.org/10.1016/j.respol.2005.08.002>

The Effect of Tree Species and Seasonality on Forest Height Measurements Using an Aerial Laser Scanner – A Case Study in Latvia

J. Ivanovs¹, A. Lazdins¹, M. Lang^{2,3}

¹Latvian State Forest Research Institute Silava, Rigas street 111, LV-2121, Latvia
Email: {janis.ivanovs, andis.lazdins}@silava.lv

²Tartu Observatory, University of Tartu, Tõravere, Tartumaa 61602, Estonia
Email: lang@to.ee

³Institute of Forestry and Rural Engineering, Estonian University of Life Sciences, Kreutzwaldi 5, Tartu 51014, Estonia

1. Introduction

Forest resource inventory can be done in different ways and scales. In Europe and elsewhere in the world, national scale information is obtained through the National Forest Inventory (NFI), while surveys of specific stands are carried out to get information in local scale. Typically, forest stand surveying is done manually, but this process is time consuming. Time consumption can be reduced by using remote sensing technologies such as aerial laser scanning (ALS). Scientific publications indicate that there is a high correlation between ALS measurements and actual tree height (McRoberts, Andersen, & Næsset, 2014).

Using ALS data, various forest inventory-related parameters are modeled, such as tree height, biomass volume, tree species distribution, and other parameters, but various authors point out that statistical models based on single-scanner data cannot be used for areas scanned with different ALS scanner settings, because that may introduce systematic errors (Næsset, 2014). The same applies to data collected during different growing seasons (Villikka, Packalén, & Maltamo, 2012). This study uses ALS data collected nationally for the period 2013-2019 in both leaf-off and leaf-on periods to develop statistical models to determine tree height across the country. NFI plots were used as field data in the development of the models, while a database of forest parcels was used for validation.

1. Data and Methods

Latvia is located in the hemiboreal zone, where both conifers and deciduous trees are found. The most popular tree species are *Betula pendula*, *Pinus sylvestris* L. and *Picea abies*. The acquisition of ALS data in the territory of Latvia has been organized by the Latvian Geospatial Information Agency in the period from 2013 to 2019 and the work has been performed by various companies. Measurements were performed using Leica ALS70, Riegl LMS-Q680i and Riegl LMS-Q780i scanners as shown in Figure 1. The flights are performed in both leaf and leafless periods and the minimum point density is 4 points per square meter. This study uses ALS data obtained in the period from 2013-2018.

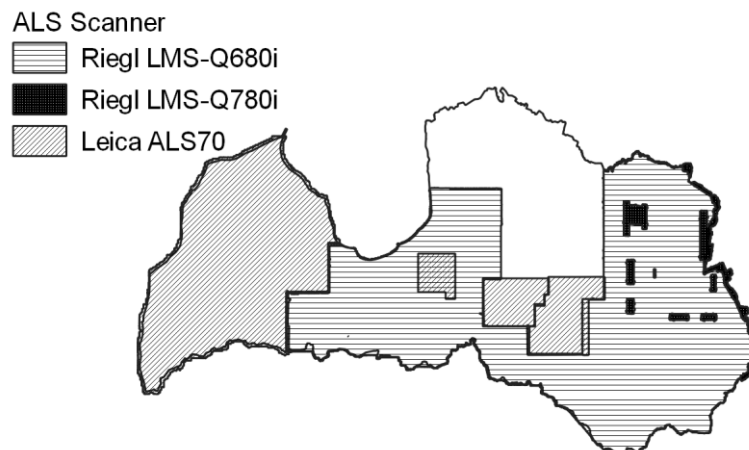


Figure 1: ALS coverage in Latvia 2013-2018

NFI data are obtained over a 5-year cycle and in total more than 16,000 permanent plots are surveyed on both forest and non-forest land. More information about Latvian NFIs is available at Tomppo, Gschwantner, Lawrence, & McRoberts, 2010.

During this research, tree height models were developed, taking into account the information on the composition of tree species and the season. Only a part of the NFI plot centers have coordinates determined with a high-resolution GPS sensor, so the models are developed stratified, in one case using all plots, while in the other only plots with well-defined coordinates. The accuracy of the coordinates of the centers of the NFI plots before the precise measurement was with an average deviation of 2 m from the center. Fusion software is used to cut out NFI plot areas from the ALS point clouds and to calculate the vertical distribution of points.

ALS statistical information was compared with NFI measurements with a + - 2 year lag and the 75th, 80th, 90th, 95th and 99th ALS height percentiles were compared with NFI tree heights. The models are stratified by conifers and deciduous trees, different tree species and different seasons. R squared and RSE values were compared between different height percentiles and the most accurate height prediction models were selected. Tree height models have been developed only for those tree species in which at least 30 observations have been recorded.

1. Results and Discussion

During the research, models were developed to predict the height of trees in the distribution of conifers and deciduous trees, as well as different tree species and also seasonally. Isolated tree species include species such as *Pinus sylvestris L.*, *Picea abies*, *Betula pendula*, *Alnus glutinosa*, *Populus tremula* and *Alnus incana*. R squared values range from 0.730 to 0.964 and RSE values range from 1,508 to 2,812. The lowest values are observed for deciduous tree species leaf-on and in the intermediate state between leaf-on and leaf-off. The highest R squared values are for *Pinus sylvestris L.*, regardless of the season.

The Riegl LMS-Q780i scanner showed the highest accuracy among ALS scanners, however, the number of observations for the development of individual models for different tree species was too small. Riegl LMS-Q680i and Leica ALS70 scanners have been used in large areas of the country and tree height models have been developed for all the above-mentioned tree species. The Leica ALS70 scanner shows on average slightly higher accuracy than the Riegl LMS-Q680i, with R squared values averaging 0.904 and 0.873, respectively.

Acknowledgements

This study was funded through the FACCE ERA-GAS project INVENT (NO: NRC 276398, SE: FORMAS FR-2017/0006, DK: DIF 7108-00003b, LV: ES RTD/2017/32)

References

- McRoberts, R. E., Andersen, H.-E., & Næsset, E. (2014). Using Airborne Laser Scanning Data to Support Forest Sample Surveys (pp. 269–292). https://doi.org/10.1007/978-94-017-8663-8_14
- Næsset, E. (2014). Area-Based Inventory in Norway – From Innovation to an Operational Reality (pp. 215–240). https://doi.org/10.1007/978-94-017-8663-8_11
- Tomppo, E., Gschwantner, T., Lawrence, M., & McRoberts, R. E. (2010). *National Forest Inventories : pathways for common reporting*. Springer.
- Villikka, M., Packalén, P., & Maltamo, M. (2012). The Suitability of Leaf-off Airborne Laser Scanning Data in an Area-based Forest Inventory of Coniferous and Deciduous Trees. *Silva Fennica*. Retrieved from <http://www.metla.fi/silvafennica/full/sf46/sf461099.pdf>

Branch detection based on TLS data

M. Hollaus¹, J. Otepka¹, J. Galle², G. Bronner³

¹ TU Wien, Department of Geodesy and Geoinformation, Wiedner Hauptstraße 8-10, 1040 Vienna, Austria
Email: (markus.hollaus, johannes.otepka)@geo.tuwien.ac.at

² TU Wien, Department of Geodesy and Geoinformation, Wiedner Hauptstraße 8-10, 1040 Vienna, Austria
Email: e11714934@student.tuwien.ac.at

³ Umweltdata GmbH, Knabstraße 7/4, 3013 Tullnerbach, Austria
Email: g.bronner@umweltdata.at

1. Introduction

Terrestrial Laserscanning (TLS) has been established as the standard method for detailed 3D scanning and reconstruction of trees with millimetre accuracy. The data acquisition is commonly done with multi-scan acquisitions to minimize occlusions on the stems. Assuming that the co-registration of the individual TLS scans have a high accuracy i.e. less than few millimetres, the 3D stem can be reconstructed e.g. with quantitative structure models (QSM) or cylinder fittings. Until now, the branch detection was not of great importance because for economical purposes mainly the stem volume is of interest.

In this contribution, an operational approach for branch detection and assessment of the branch diameter classes based on multi scan TLS data is presented. The investigations were carried out for a test area in Carinthia, southern Austria.

2. Study area and data

2.1 Study area and data

The study area is located in the southern part of Austria, in the federal state of Carinthia. For the spruce dominated forest stand a TLS campaign with a Riegl VZ400i was carried out on 5th of November 2020. In total 18 scan positions were needed to cover approx. 1.700 m².

The forest stand is even-aged with tree heights >30m and about 120 years old. The stand obviously has grown up with large tree spacing and no pruning: in most cases the dead branches go down the whole stem, the living branches start already in 7-10m height. The density in comparison to yield-table expectations (“Fichte Hochgebirge”) is about 80%.

The scan positions were chosen unplanned intuitively between the trees. The distance between consecutive scan positions was about 10 steps (5-8 meters). With a scan resolution of 20 x 20 millidegrees one single record takes only 3 minutes, so accurate planning of scan-positions was considered to be not necessary. The Riegl software RiSCAN PRO is able to co-reference scan-positions without artificial tie-points. The whole scanning fieldwork took less than 2 hours.

3. Methods

TLS pre-processing

The acquired TLS scans were co-registered with RiSCAN MultiStationAdjustment (MSA2), which works without artificial tie-points. The co-registered point cloud was exported as las-file.

Stem modelling

Based on the co-registered point cloud a digital terrain model (DTM) was derived using a hierarchic robust method implemented in the OPALS software (Pfeifer et al., 2014). In addition to the DTM a digital surface model (DSM) was calculated using the landcover-dependent approach described in Hollaus et al. (2010). Finally, the normalized digital surface model (nDSM) was computed by

subtracting the DTM from the DSM. All of these topographic models have a raster resolution of 0.2 x 0.2 m². The DTM was further used to normalize the heights of the point cloud, and the nDSM was used to assess the tree height.

To model the stems with cylinders approximate position of the individual stems are needed. Based on a voxel approach the stem positions are detected by analysing the point densities in successive layers. Finally, the stem is modelled by robust least-square fittings of cylinders to neighbouring points of the detected stem positions.

Branch detection

The branch detection and branch diameter estimation is done on equirectangular projections (Eysn et al., 2013) of branch points. Based on the modelled stem cylinders the branch points are selected within a cylindrical shell around the stem (internal radius is cylinder radius plus 5 cm, external radius is cylinder radius plus 10 cm). The equirectangular projection is done for each tree separately and uses the cylinder angle as x-axis and the height as y-axis. The point density and the distribution of the distances are used for detecting the branch positions. The branch diameters are estimated by quantiles based on the 3D branch point extends. For this branch diameter estimation only the horizontal range of the classified branch points is considered because no points on the upper side of the branches are available due to the scanning geometry.

The branch processing of the TLS data was done with the OPALS software (Pfeifer et al., 2014) and Python.

4. Results and discussion

The automatic detection of individual tree positions has a high degree of completeness. For trees with a diameter at breast height (DBH) >0.15 m the completeness is >95%. Also the stem modelling with a series of cylinders lead to high completeness and correctness. In average stems could be modelled up to two third of the tree height (Figure 1). For the upper parts of the scanned spruce trees occlusions of the stems increase dramatically due to the increase of branches, which is why, a reliable direct modelling of the stem is no longer possible.

The applied branch detection approach leads to high degree of completeness and works fully automatic. As can be seen in Figure 1e also the diameter classes can be estimated based on the TLS data.

5. Conclusion and Outlook

The presented workflow shows a robust way of extracting stem and branch information from TLS data. The derived 3D stem model can be used for e.g. estimating stem biomass, deriving taper functions, or for timber assortment. The branch information can also be used for timber assortment but also as a kind of “finger printing” of the individual trees. In future work the potential of using such “branch finger printing” in addition to the stem properties (i.e. taper function, deviation from the circular cross section, etc.) for certification of stem origin will be investigated.

Acknowledgements

This research was partly funded by the Austrian Research Promotion Agency (FFG).

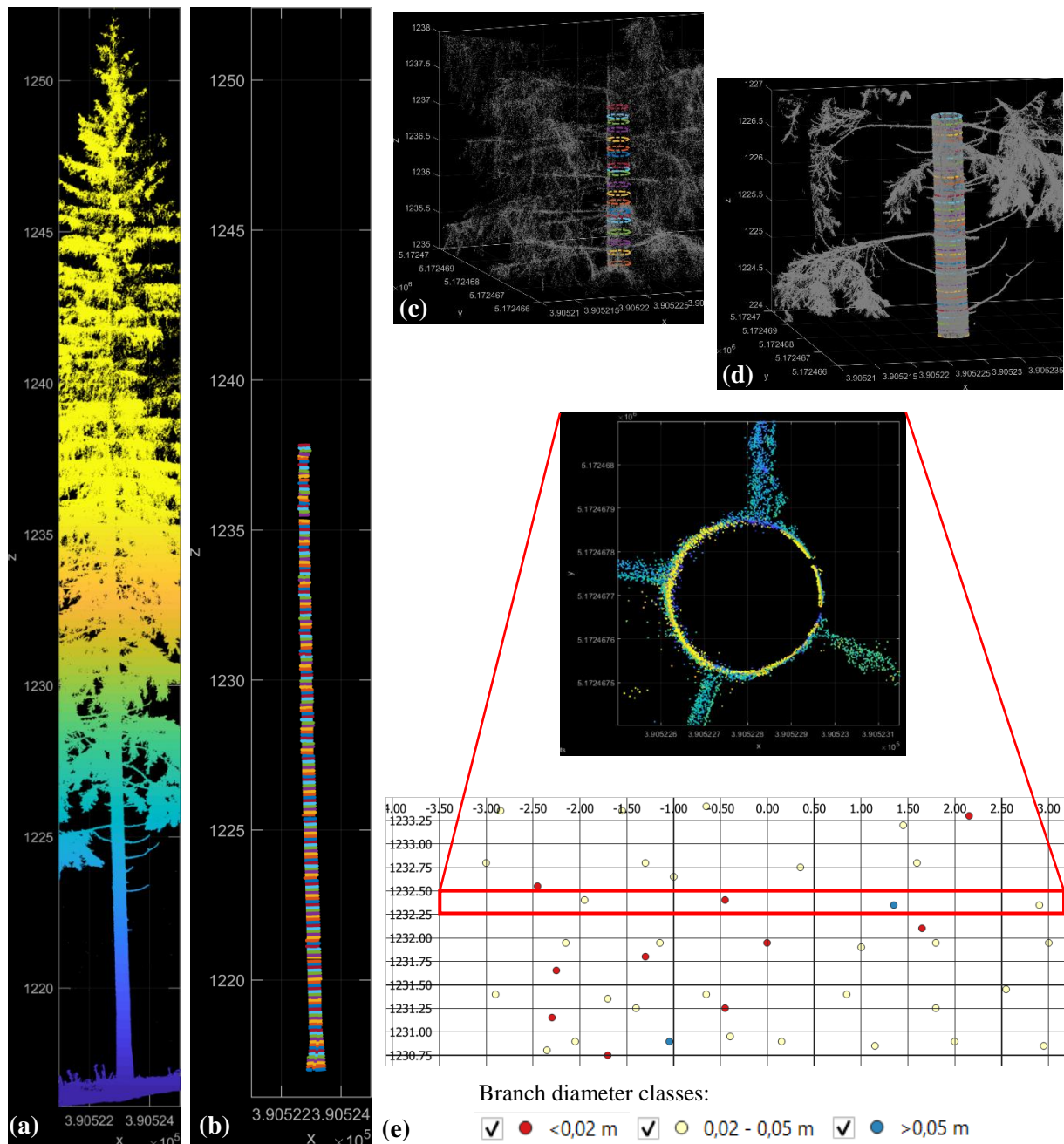


Figure 1: (a) TLS point cloud of an extracted tree, (b) modelled tree stem, (c, d) point clouds for different height slices overlaid with the fitted stem models, (e) subset of the equirectangular map with the detected branch positions. The x-axis correspond to the cylinder angle and the y-axis to the height. The colors represent the different diameter classes.

References

- Eysn, L., Pfeifer, N., Ressler, C., Hollaus, M., Graf, A. and Morsdorf, F., 2013: A Practical Approach for Extracting Tree Models in forest Environments Based on Equirectangular Projections of Terrestrial Laser Scans. *Remote Sensing* 5, 5424-5448. <https://doi.org/10.3390/rs5115424>
- Hollaus, M., Mandlburger, G., Pfeifer, N. and Mücke, W., 2010. Land cover dependent derivation of digital surface models from airborne laser scanning data, *ISPRS Commission III Symposium PCV 2010 -- Photogrammetric Computer Vision and Image Analysis*, Paris, pp. 221-226.
- Pfeifer, N., Mandlburger, G., Otepka, J. and Karel, W., 2014: OPALS - A framework for Airborne Laser Scanning data analysis. *Computers, Environment and Urban Systems* 45, 125-136. <https://doi.org/10.1016/j.compenvurbsys.2013.11.002>

Low altitude LiDAR and TLS point clouds for improved tree detection

M. Hirschmugl^{1,2}, H. Fellner³, R. Wack⁴, G. Bronner³, M. Schardt¹

¹Joanneum Research, Steyrergasse 17, 8010 Graz
Email: {manuela.hirschmugl, mathias.schardt}@joanneum.at

²University of Graz, Heinrichstrasse 36, 8010 Graz
Email: manuela.hirschmugl@uni-graz.at

³Umweltdata, Knabstraße 7/4, 3013 Tullnerbach
Email: {h.fellner; g.bronner}@umweltdata.at

⁴Aeromap, Niederöblarn 83, 8960 Niederöblarn
Email: r.wack@aeromap.at

1. Introduction

The background of the contribution is the proposed 3-stage forest inventory (Bronner et al., 2018), which involves a third data level between the well-known wall-to-wall airborne laserscanning (ALS) data and the similarly well-known terrestrial laser scanning (TLS) data. We call this intermediate data layer “low altitude laser scanning” (LALS), as it is acquired from an ultralight airplane at low flying altitude and with a tilted sensor to allow a slightly oblique viewing angle. This constellation resulted in a point density of 400 points/m². Previous work on similarly high resolution data has reported high accuracies (Dersch et al., 2021) in managed forests, while we apply this system in a forest, which is currently in transition to a continuous cover forestry (CCF) management system. CCF is a nature-based solution (NBS) system, which relies on single tree harvesting and near-natural species and age mixtures to pertain a resilient and still productive forest (Burschel und Huss 1997, Schütz 2001, O’Hara and Gersonde 2004, Pretzsch 2006).

The research questions tackled in this study are

- 1) How well do existing approaches perform in areas of CCF?
- 2) How well can different approaches be combined to achieve better accuracies?
- 3) How can the different information sources be merged to generate added value?

2. Data and Methods

2.1 Data

The LALS data was acquired at a flying altitude of about 150 m above ground level. The sensor, a Riegl VUX240, was tilted backwards at an angle of 20°. Each strip was flown in both directions with 1.8 MHz at an average speed of 125 km/h. This led to a point density of approximately 200 pts/m² per overpass resulting in a total point density of approximately 400 pts/m². An example of the acquired point cloud is shown in Figure 1. The data shows a lot of detail and at the forest edge (Fig. 1) or in open stands, also the individual stems are visible.

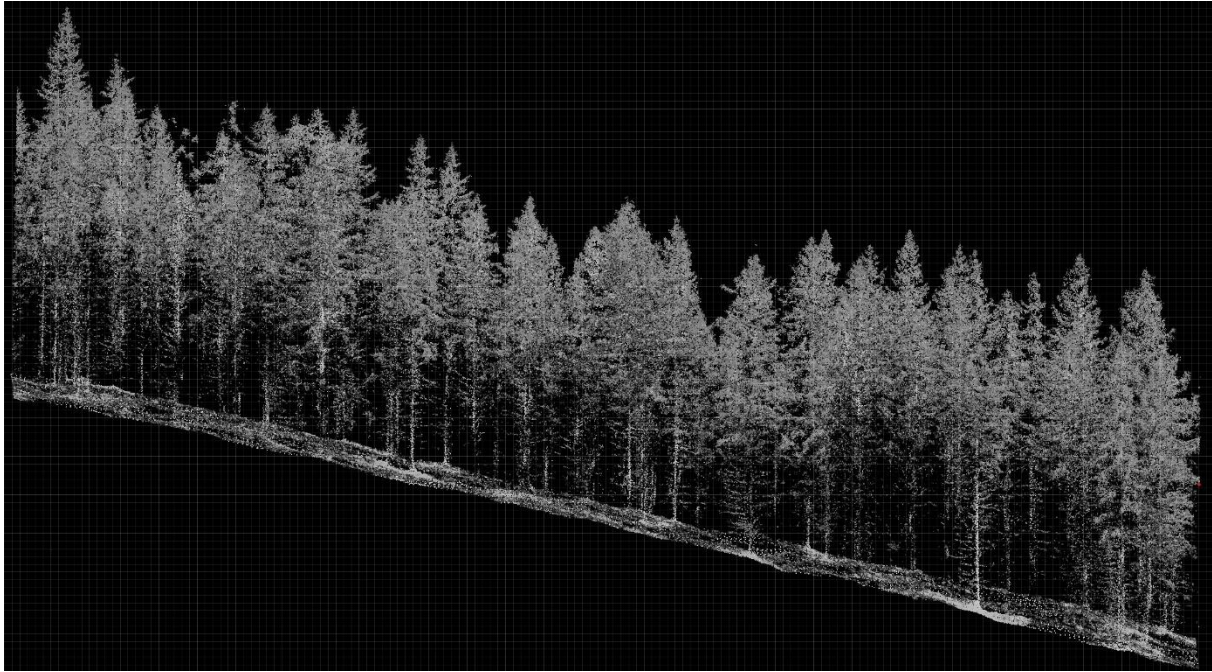


Figure 1: Point cloud of LALS data.

TLS data was acquired using a Riegl VZ-400i during the vegetation periods in summer 2020 and 2021. In 2020, only one scan position per plot was used, in 2021, per sample plot, 10 to 15 scan positions were recorded without artificial tie-points. The co-referencing of scan-positions was calculated by RiScan Multi-Station-Adjustment. The resolution during scan acquisition was 40x40 mdeg, which produces several million points per 360° scan. The point clouds were filtered with regard to the deviation, reflectance, range and isolated points. The TLS tree detections of 2020 were done using OPALS (<https://opals.geo.tuwien.ac.at/>). The TLS tree detections for TLS data of 2021 were done by Forest Design (www.forestdesign.ro). For reference purposes, 151 trees were measured in the field. The measuring was done in 18 plots by measuring the centre point of each plot with GPS and using distance and azimuth to calculate the individual tree positions. This procedure resulted in a rather low tree location accuracy, which has to be taken into account when evaluating the results. The low number of reference trees is a result of the angle count sampling with a k-factor of four, which means that every sample tree represents four square metres per hectare. This means, that smaller trees were only measured, if they were located very close to the plot centre. Table 1 summarizes the TLS and field measured tree locations.

Table 1. Tree counts used for comparison.

Source	Software	No. of plots	No. of trees	Available infos
TLS 2020	OPALS	6	683	Position (TLS), DBH
TLS 2021	Forest Design	1	1884	Position (TLS), DBH, estimated height, volume and species
Field work	-	18	151	Position (GPS center coordinate & distance & azimuth)

2.2 Methods

The methods used in this work consist of both, existing and well-established methods like tree top detection from nDSM data (Hirschmugl et al., 2007) as well as of further developments of most recent advancements, like the Bird's Eye View (BEV) method (Windrim and Bryson, 2020) and their combination. For eliminations of double-detections, Python-based scripting was used. The overall workflow is depicted in Figure 2.

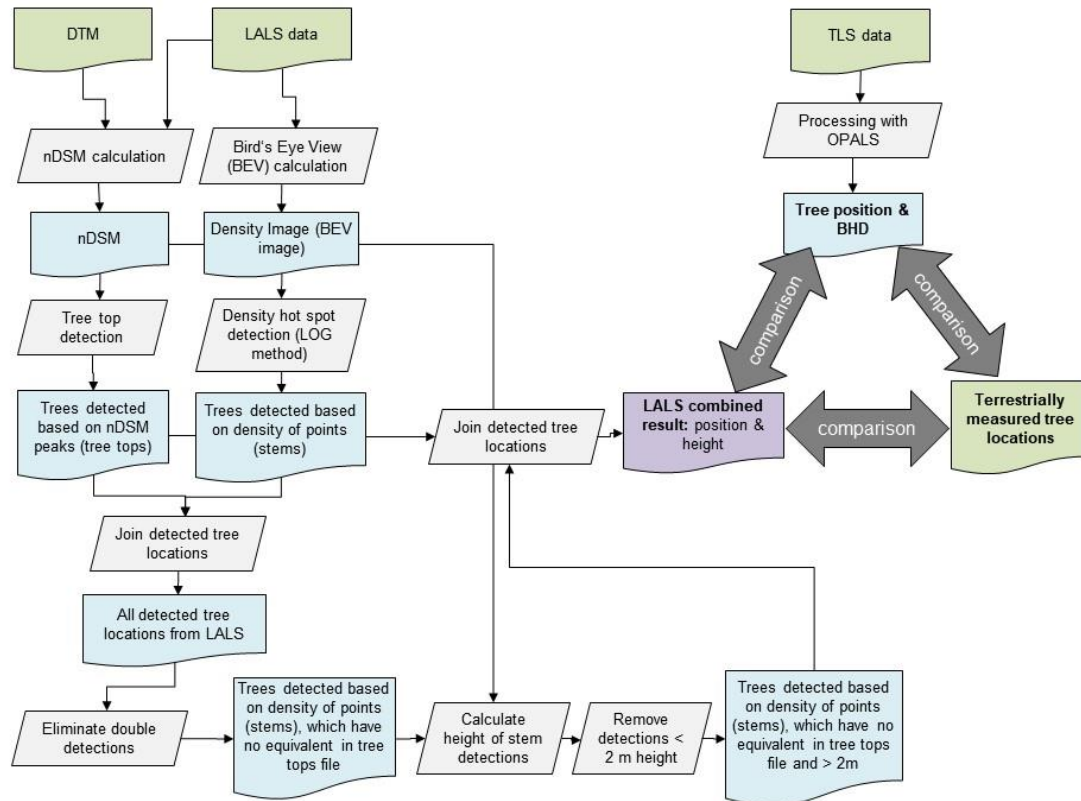


Figure 2: Workflow.

In the first step, an nDSM is calculated from the LALS data and an existing DTM. This nDSM at a resolution of 0.5 m is used to detect tree tops. In parallel, the LALS data alone is used to calculate the so-called Bird's Eye View (BEV), which is basically the density of LiDAR returns per spatial entity. A regular grid of 10 by 10 cm was used to calculate this density. In previous works, this BEV image showed the stems as bright blobs (Windrim and Bryson, 2020), circles or semi-circles due to the high density of returns at the stem (Dalla Corte et al., 2020). In the BEV image of our CCF, the stems are not well depicted and unfortunately, the BEV image does not show any circle-like objects potentially useable for stem detection (compare Figure 3 and Figure 7). However, the BEV image does show the crown and main branches as areas of higher density (Figure 3). This higher density can be interpreted in the same way as higher nDSM values and can thus be treated with the same approaches. The LOG method (Hirschmugl, 2008) was used for this purpose.

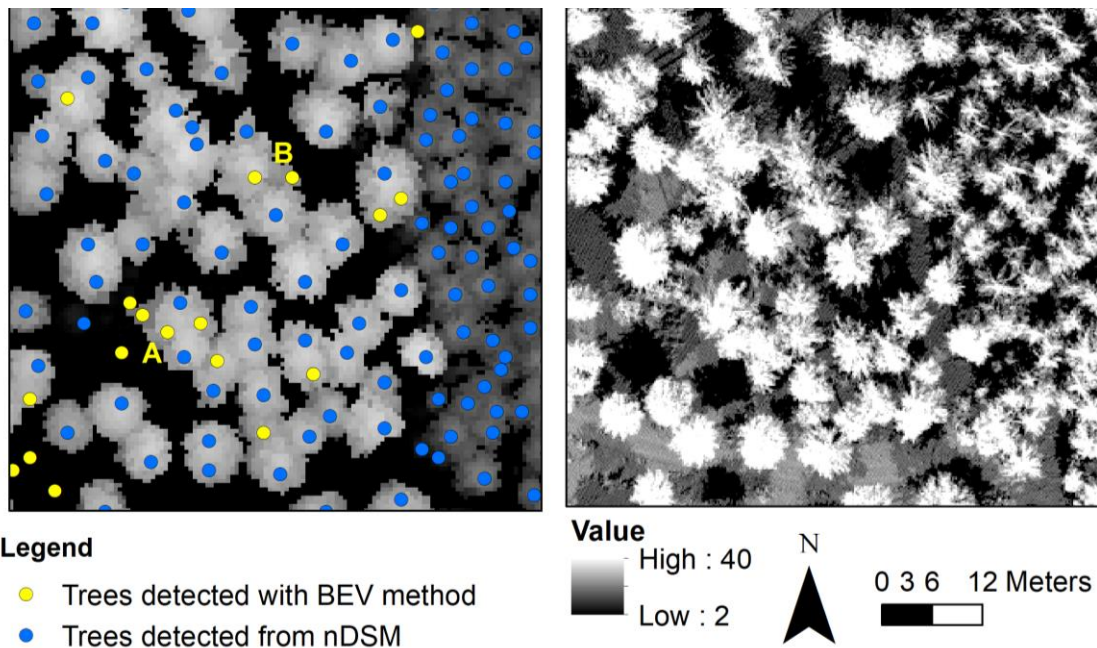


Figure 3: Comparison of nDSM-based results (blue) and additional BEV-based results (yellow). The gray values in the background images (2 – 40) represent height above ground in m (left) and number of LiDAR returns per pixel (right)

In order to avoid multiple detections of the same tree, we decided to retain only those BEV detections, which lack an nDSM equivalent. These additional detections and the advantages are shown in Figure 3. The BEV method allows detecting individual trees in a patch of deciduous trees, which were considered as one tree in the nDSM method due to missing distinct maxima in height (Figure 3A). Further, small trees between or under larger trees can be detected by the BEV method (Figure 3 B).

3. Results and Discussions

The comparison of the results with the field measurements (Figure 4) shows, that the inclusion of the BEV data allows detecting trees, previously not found with the nDSM approach alone, such as small, understory trees (Figure 4 A) or individual deciduous trees (Figure 4 B). In addition, small trees neither captured by the nDSM approach, nor covered in the field measurement (due to the high k-factor), but visible in the data, could be detected with the BEV approach (Figure 4 C). All 151 field measured trees were detected with the combined nDSM/BEV approach. The assessment of omission and commission error is not possible with this ground truth data, as the field measurements are not a full assessment, but only a count sampling with k-factor 4.

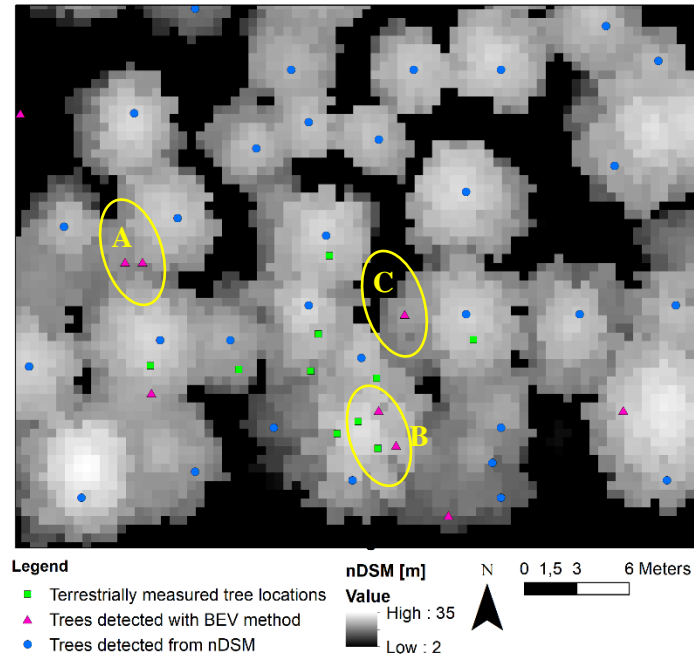


Figure 4: Results of the LALS tree detection approaches (BEV, nDSM) compared to field measurements.

Due to the limitations of the available field measurements, we compared the combined results also to TLS measured tree locations. The TLS tree locations were manually adjusted to match the nDSM due to the originally inaccurate GPS-based geolocation. The two data sets show a very good agreement for all the main trees (see **Fehler! Verweisquelle konnte nicht gefunden werden.** and Figure 6: stars = TLS-based tree locations, points = combined LALS tree locations). There are also LALS detections, which have no equivalent in the TLS measurements (**Fehler! Verweisquelle konnte nicht gefunden werden.** A&B). The trees in **Fehler! Verweisquelle konnte nicht gefunden werden.** (A) may be very small trees, which were either not covered with the TLS or could also be commission errors in the LALS data. Tree detections marked in **Fehler! Verweisquelle konnte nicht gefunden werden.** with (B) are probably missing in the TLS detections due to occlusion by other trees. This theory is supported by the location of to the only scan position. However, there are also some omission errors compared to the TLS measurements; see **Fehler! Verweisquelle konnte nicht gefunden werden.** (C).

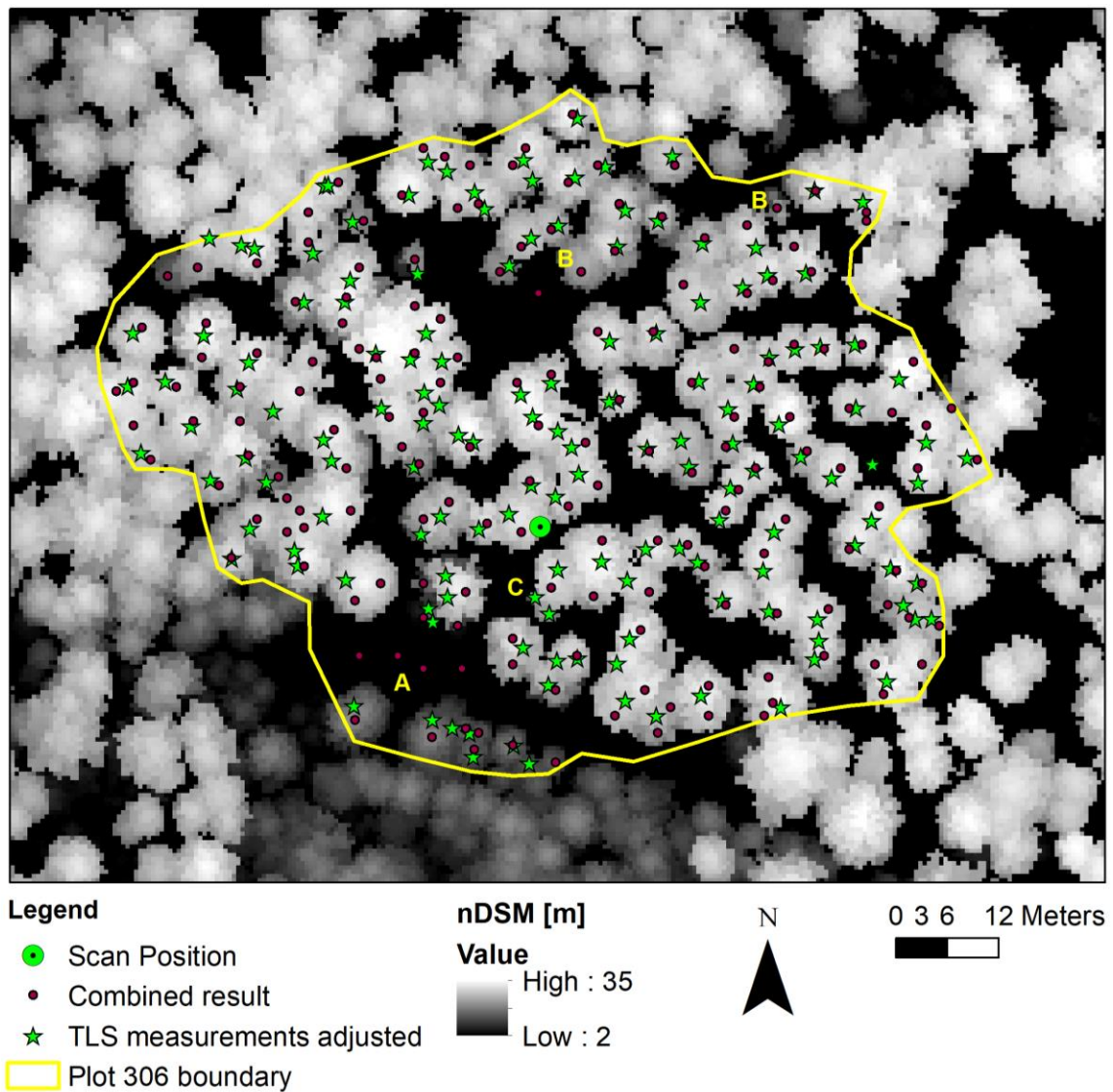


Figure 5: Results of the LALS tree detection compared to TLS measurements 2020 using OPALS.

Another comparison was done using results from the second TLS scan campaign done 2021 with multiple scan positions and the processing chain from Forest Design (FD, for more details see www.forestdesign.ro). This approach detects much more trees, but we could not verify the results in the field so far. Figure 6 compares the results of TLS FD with the combined LALS results. There is a general good agreement of both data sets in rather open stands (A). In areas marked with (B), there are many more stems detected from the TLS data than from the LALS data, which could be correct, especially in young forest areas. However, more field work or visual interpretation of the point cloud is needed to verify this assumption.

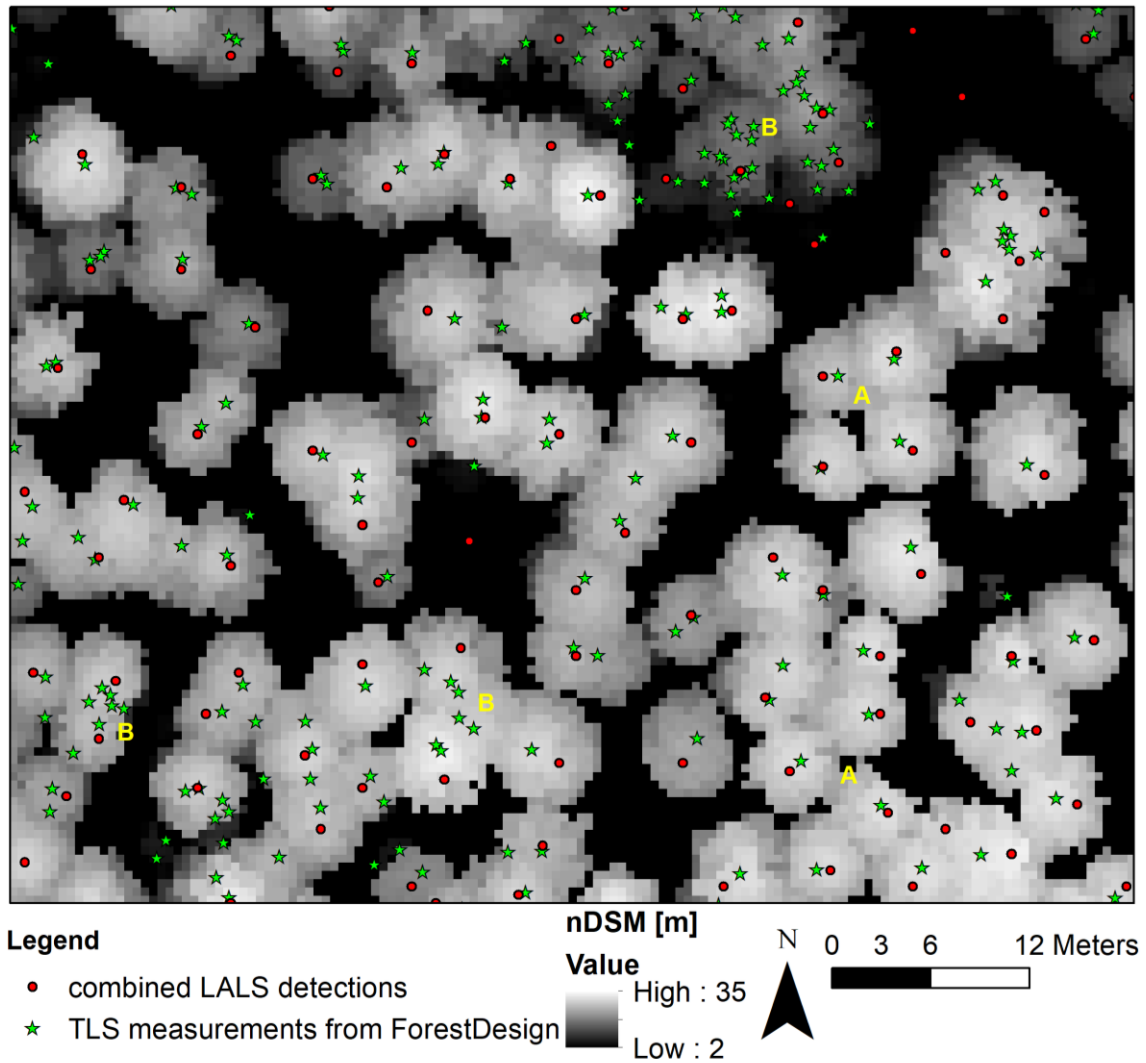


Figure 6: Results of the LALS tree detection compared to TLS measurements using FD.

The next logical step is the combination of TLS and LALS results. This will be further studied, once a proper automated geolocation of the TLS data is achieved. The combination will allow combining the height information from the nDSM with the DBH measured by the TLS and the derivation of the stem axes of the individual trees.

Aside from the TLS and LALS combination, future work is threefold. The first part covers a better use of the BEV images. A segmentation of the BEV image into 2m height intervals, as shown in Figure 7, is expected to allow crown base estimation and will be tested in a deep learning approach to further improve tree detection. A new field campaign including a full assessment will allow to calculate both the commission and omission errors. In the frame of this exercise, we will also look specifically at deciduous trees. The third part is to compare and combine the LALS data with standard ALS data to work out the mutual benefits and ideal combination possibilities.

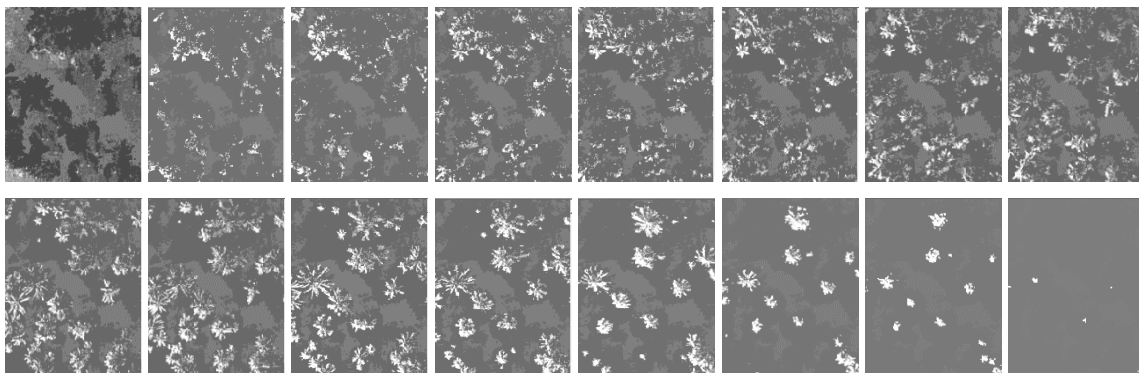


Figure 7: Vertical distribution of LALS points in 2 m interval from ground level up to 32 m

5. Conclusions & Outlook

This study shows that LALS data is suitable to detect most major trees confidently. Combining different tree detection approaches resulted in the better detection of small, partly understory trees and individual stems in deciduous forests. However, most recent results from TLS data analysis suggest, that still small trees are omitted. This needs to be verified in the field. Once, proper geolocation accuracy of the TLS measurement is achieved, the automated combination of LALS tree position and TLS data will further add to the amount of detected trees and to the number of available forest parameters by providing for example the diameter at breast height (DBH) or even species. The next steps include the assessment of the crown base from LALS data, the comparison with standard ALS data and the combination of all levels (TLS, LALS and ALS) into a complete system.

Acknowledgements

This study received funding from the Austrian Research Promotion Agency (FFG) in the frame of the COIN network “DeepDigitalForest”.

References

- Burschel P. und Huss J., 1997. Grundriss des Waldbaus, Kapitel 6.1.3 S. 108 ff, 2. Neubearbeitete und erweiterte Auflage Parey Bucherverlag Berlin ISBN, 3-8263-3045-5
- Dalla Corte, A.P., Rex, F.E., Almeida, D.R.A. de, Sanquetta, C.R., Silva, C.A., Moura, M.M., Wilkinson, B., Zambrano, A.M.A., Cunha Neto, E.M. da, Veras, H.F.P., Moraes, A. de, Klauberg, C., Mohan, M., Cardil, A., Broadbent, E.N., 2020. Measuring Individual Tree Diameter and Height Using GatorEye High-Density UAV-Lidar in an Integrated Crop-Livestock-Forest System. *Remote Sensing* 12, 863. <https://doi.org/10.3390/rs12050863>
- Dersch, S., Heurich, M., Krueger, N., Krzystek, P., 2021. Combining graph-cut clustering with object-based stem detection for tree segmentation in highly dense airborne lidar point clouds. *ISPRS Journal of Photogrammetry and Remote Sensing* 172, 207–222. <https://doi.org/10.1016/j.isprsjprs.2020.11.016>
- G. Bronner and M. Hirschmugl and R. Wack and B. Jawecki, 2018. Three Phase Forest Inventory Design with 1) wall-to-wall ALS, 2) very dense ALS on sample stripes and 3) fieldwork sample plots. Presented at the FORESTSAT 2018, Maryland.
- Hirschmugl, M., 2008. Derivation of Forest Parameters from UltracamD Data (phdthesis). Graz University of Technology.
- Hirschmugl, M., Ofner, M., Raggam, H., Schardt, M., 2007. Single tree detection in very high resolution remote sensing data. *Remote Sensing of Environment* 110, 533–544.
- Windrim, L., Bryson, M., 2020. Detection, Segmentation, and Model Fitting of Individual Tree Stems from Airborne Laser Scanning of Forests Using Deep Learning. *Remote Sensing* 12, 1469. <https://doi.org/10.3390/rs12091469>

Effects of segment length on burned forest classification with ICESat-2 Data

Meng Liu¹, Sorin Popescu¹, Lonesome Malambo¹

¹Department of Ecology & Conservation Biology, Texas A&M University, College Station, TX 77843
Email: meng.liu@tamu.edu; s-popescu@tamu.edu; mmoonga@tamu.edu.

1. Introduction

Forests store a huge amount of carbon and play a critical role in controlling global carbon balancing and cycling. However, increased frequency and extent of fires are a growing concern (Cattau et al., 2020; Liu and Yang, 2020) and threaten forest health as well as the sustainability of terrestrial ecosystems. Fires have become more severe and destructive in response to a warming climate with many examples such as the 2018 California wildfire, the 2019 Amazon forest fire, and the 2020 Australia wildfire. These extreme fire events emphasize the necessity of fire occurrence monitoring and forecasting over space and time. Accurately classifying burned forest is critical for the analysis of fire patterns and carbon emissions as well as understanding the effects of climate change on ecosystems.

NASA's Ice Cloud and land Elevation Satellite-2 (ICESat-2) mission provides global photon counting LiDAR data with a 14 m footprint and the along track sampling distance of 0.7 m, which come with three pairs and offer new opportunities for burned forest classification. Each pair contains a strong beam and a weak beam distinguished by a designed energy ratio of 4:1. The ICESat-2 mission provides datasets like the geolocated photon data (ATL03), which comprises precise latitude, longitude and elevation of each photon point where a photon interacts with land surface. By kicking out noises and classifying photons, Neuenschwander and Pitts (2019) produced the Land and Vegetation height product (ATL08), which comprises estimated terrain and canopy height measurements at 100 m segments along tracks. The ATL08 product, with a nominal spatial resolution of 100 m by 14 m, provides various canopy and terrain related metrics in each segment such as mean canopy height and max canopy height. Liu et al. (2020) leveraged ATL08 data to classify burned forest along ICESat-2 tracks with an overall accuracy of up to 83%. However, few studies investigate the effects of segment length on burned forest classification when using ICESat-2 data.

Previous studies were focused on a specific spatial resolution when using LiDAR data in fire analysis. It must be noticed that spatial resolution has significant impacts on land cover classification (Roth et al., 2015) and canopy structure characterization. However, few studies have fully investigated the effects of spatial resolution when classifying burned forest with LiDAR data. In this study, we sought to analyse the effects of spatial resolution on burned forest classification based on ICESat-2 photon counting data.

2. Data and methods

2.1 Study area and data

The Carr fire complex, containing the Carr fire and the Delta fire (Figure 1d), in the temperate forest in northern California was employed. In this study, the ATL03 data whose ground track go through the burned areas were downloaded from the National Snow & Ice Data Center (NSIDC). To avoid interference of regrowth in burned regions, only data collected after fire events and in the same year of the fires were selected. Due to cloud obstructions, only one ground track was available (Figure 1d). ATL08 data corresponding to the selected ATL03 products were also downloaded to provide classification labels (terrain, canopy, and noise). Pre-fire and post-fire Sentinel-2 data (Figure 1a and b) were also downloaded as ancillary data. The forest map (Figure 1c) was obtained from ISODATA classification using pre-fire Sentinel-2 image, with an overall accuracy of 87% and the kappa of 0.74. The fire perimeters were downloaded from the CalFire (<https://www.fire.ca.gov/>) and rasterized to 10m to produce the burn map (Figure 1d).

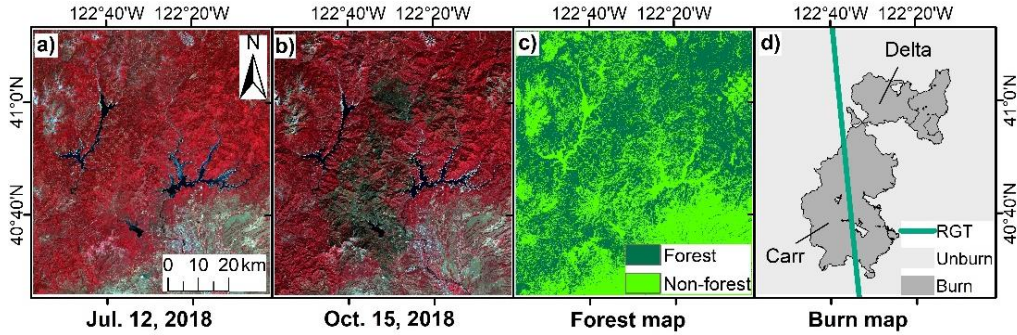


Figure 1. Sentinel-2 data: (a) pre-fire image, (b) post-fire image, (c) forest map and (d) burn map.

2.2 Segments classification

ATL03 photon points were summarized at different segment lengths, i.e. 10m, 30m, 60m, 100m, 200m, and 250m, producing 26 LiDAR metrics (Figure 2). If over 90% of Sentinel-2 pixels within a segment were forest type, this segment would be defined as a forest segment. In the same way, the forest segments were overlaid with the corresponding burn map. If over 90% of pixels within a forest segment were burned, this forest segment would be defined as a burned forest segment. Conversely, if over 90% of pixels were unburned, this forest segment would be labelled as an unburned forest segment. The Random Forest classification method was further employed to classify burned segments of ICESat-2 data from unburned ones. We chose the Random Forest method because it has no assumptions on data distributions (non-parametric) and can process high-dimensional data.

3. Results and Discussion

In Figure 2, average values of canopy metrics are changing along with spatial resolutions in both burned and unburned samples (Figure 2), which means spatial resolutions can influence canopy structures we detected. For instance, the maximum canopy height (max) are increasing when spatial resolutions get coarser, which is due to biomass consumption and sparser canopy after the fire. The average number of canopy photon points (num_cpy) in both burned and unburned samples are also increasing along with spatial resolutions. Furthermore, burned samples have lower numbers of canopy photons than the unburned ones.

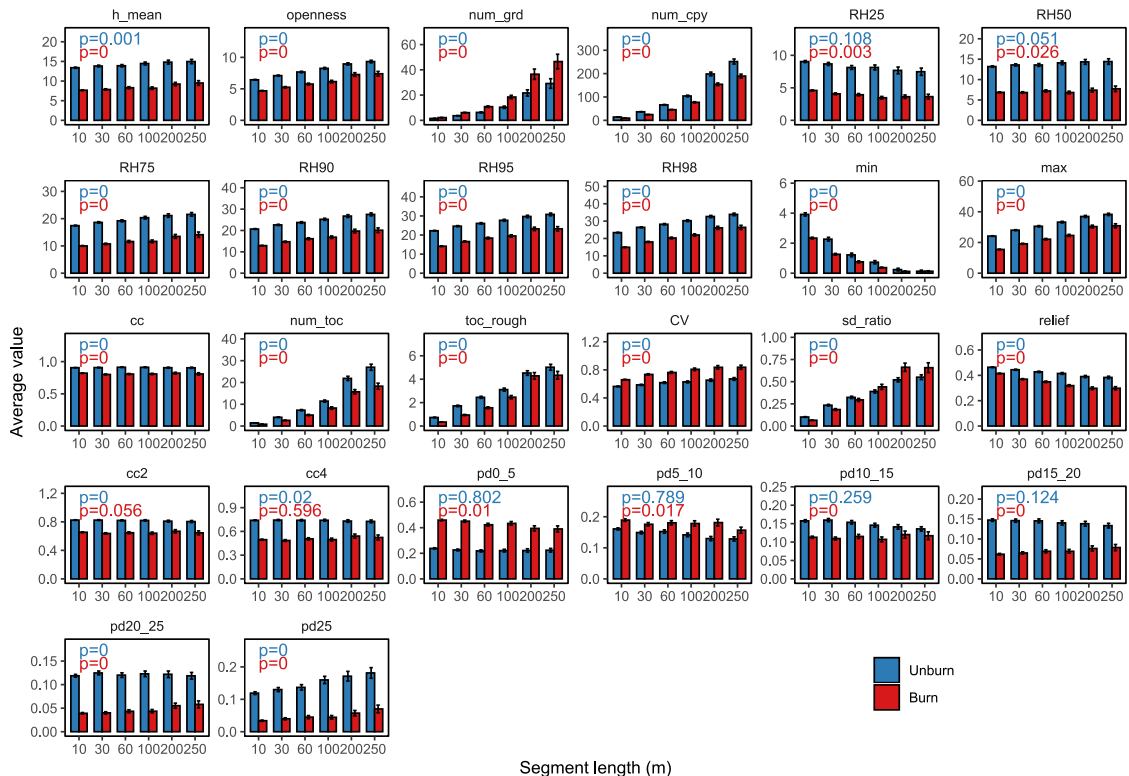


Figure 2. The average value of each canopy related metric in the temperate forest in California using strong beams, where the error bars are standard errors.

The classification accuracies of segments from both strong beams and weak beams are increasing along with spatial resolutions (Figure 3a) and saturate at 100 m segment length. It is worth noting that, samples of weak beams always have lower accuracies than those of strong beams. This is due to lower point density since energy in weak beams is only $\frac{1}{4}$ of that in strong beams. With lower point density, it is more difficult to distinguish real ground points, canopy points, and noises, causing more errors in metrics calculation and burned forest classification. Figure 3b shows the distribution of burned and unburned forest segments at 100m using strong beams, whose classification accuracy is 81.57%. The distribution of segments are comparable with the reference burn map.

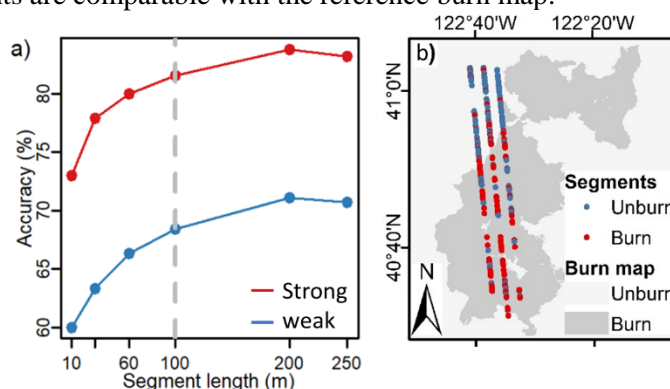


Figure 3. Burned forest classification: (a) classification accuracy at different segment lengths and (b) distribution of classified segments at 100m length using strong beams.

4. Conclusions

This study analyses the effects of segment length (spatial resolution) on burned forest classification using spaceborne LiDAR data. ICESat-2/ATLAS photon counting data were summarized at different segment length, e.g. 10 m, 30 m, 60 m, 100 m, 200 m, and 250 m, to match commonly used spatial resolutions. Results show that canopy structure characterization is significantly influenced by segment length. The classification accuracies of burned forest are increasing along with coarser spatial resolutions and saturate at 100 m segment length. Moreover, accuracies of burned forest classification based on strong beams are higher than those of weak beams. These findings demonstrate that spatial resolution will influence canopy characterization and fire monitoring. As more spaceborne LiDAR data are available and accumulating, e.g. ICESat-2 data and GEDI data, further research can explore more applications of LiDAR data in fire management and extend the use of LiDAR data to applications in ecological recovery and carbon dynamics.

Acknowledgements

This research was funded by NASA's ICESat-2 SDT (Grant # NNH19ZDA001N).

References

- Cattau, M. E., Wessman, C., Mahood, A., and Balch, J. K. (2020). Anthropogenic and lightning-started fires are becoming larger and more frequent over a longer season length in the U.S.A. *Global Ecology and Biogeography* 29, 668–681. doi:10.1111/geb.13058.
- Liu, M., Popescu, S., and Malambo, L. (2020). Feasibility of Burned Area Mapping Based on ICESAT-2 Photon Counting Data. *Remote Sensing* 12, 24. doi:10.3390/rs12010024.
- Liu, M., and Yang, L. (2020). Human-caused fires release more carbon than lightning-caused fires in the conterminous United States. *Environ. Res. Lett.* 16, 014013. doi:10.1088/1748-9326/abcbbc.
- Neuenschwander, A., and Pitts, K. (2019). The ATL08 land and vegetation product for the ICESat-2 Mission. *Remote Sensing of Environment* 221, 247–259. doi:10.1016/j.rse.2018.11.005.
- Roth, K. L., Roberts, D. A., Dennison, P. E., Peterson, S. H., and Alonzo, M. (2015). The impact of spatial resolution on the classification of plant species and functional types within imaging spectrometer data. *Remote Sensing of Environment* 171, 45–57. doi:10.1016/j.rse.2015.10.004.

Instance segmentation for single tree delineation using drone-based multispectral imagery and lidar data

S. Dersch^{1,5}, A. Schoettl^{4,5}, P. Krzystek^{1,5}, M. Heurich^{2,3}

¹Dept. of Geoinformatics, Munich University of Applied Sciences, 80333 Munich, Germany
Email: {sebastian.dersch;peter.krzystek}@hm.edu

²Faculty of Environment and Natural Resources, University of Freiburg, Germany
Email: marco.heurich@wildlife.uni-freiburg.de

³Bavarian Forest National Park, Dept. of Visitor Management and National Park Monitoring, 94481 Grafenau, Germany
Email: marco.heurich@npv-bw.bayern.de

⁴Dept. of Electrical Engineering and Information Technology, Munich University of Applied Sciences, 80333 Munich, Germany
Email: alfred.schoettl@hm.edu

⁵Institute for Applications of Machine Learning and Intelligent Systems, Munich University of Applied Sciences, 80333 Munich, Germany

Abstract

Forests are an essential part of our environment. They produce oxygen, act as carbon sinks and dust filters, thereby improving air quality. Climate change, high demand for wood as raw material, and land-use change will adversely affect forests, requiring more frequent forest inventories to enable strategic forest management in the years to come. Remote sensing methods are feasible to acquire this information in large areas at a much lower cost.

Recently, deep learning-based approaches in remote sensing forestry has gained much attention because of the prospect of better accuracy. For instance, methods for tree species classification using multispectral imagery and lidar have been reported to perform better than 90% in terms of overall accuracy. Contrary, single tree segmentation via deep learning is more challenging. So far, only a few approaches apply instance segmentation that imbed two-stage object detectors to delineate single trees with multispectral imagery. Apparently, these methods show under- and over segmentation in highly dense forest areas. In this work, we aim to overcome these effects by using lidar data as well in the instance segmentation approach Mask R-CNN.

Our experiments were conducted near the Kranzberg Roof Project (KROOF) research site, which is located at 11°39'42" E, 48°25'12" N, approximately 35 km northeast to Munich. Most of the mixed forest is characterized by large groups of beeches surrounded by spruces. Tree heights vary between 20 m and 36 m. Data was captured in three flight missions at the end of July 2020 using a DJI 460 copter equipped with a Riegl miniVUX-1UAV LiDAR scanner and a Micasense RedEdge-MX Dual multispectral camera. Flight missions were conducted at an altitude of 90 m above ground with a flight speed of 5 m/s. Because of the high overlap (50%), a mean point density of 500-600 pts/m² was achieved. A true orthophoto was generated using the digital surface model (DSM) of the lidar point cloud. Moreover, the lidar intensity was calibrated in a data driven approach using the lidar distance. Finally, a multilayer data structure was created containing ten multispectral channels, the lidar DSM, and several lidar metrics representing the penetration in the forest area. For training, we labelled 230 trees by visual interpretation and subdivided the dataset into training (80%) and validation (20%). Next, we randomly placed the labelled tree segments into new artificial images of size 512x512 pixel. The segments, which were randomly rotated and re-scaled by 10%, covered 80% of the image size.

In the experiments, we trained the Mask R-CNN using the augmented dataset containing 1200 images in total. The backbone Resnet50 was frozen at the second stage using the pre-trained weights as initial weights. The comparison between training loss and validation loss revealed no overfitting of the Mask R-CNN model. Future experiments will focus on tests (1) using the RGB channels, (2) using multispectral channels (e.g. NIR, NDVI, NDRE), (3) using lidar-based metrics (e.g. DSM, lidar intensity, penetration rate), and combinations of (1), (2), and (3).

Model-Assisted Estimation of Timber Volume by Means of Harvester and ALS Data

J. Rätty^{1*}, R. Astrup¹, J. Breidenbach^{1*}

¹Norwegian Institute of Bioeconomy Research (NIBIO), Høgskoleveien 8, 1433 Ås
Email: {janne.raty; rasmus.astrup; johannes.breidenbach}@nibio.no

*Corresponding author

1. Introduction

Cut-to-length harvesters can provide ground-truth data for predicting forest attributes using airborne laser scanning (ALS) data (Söderberg et al. 2021). Harvester datasets are, however, not a representative sample, which may cause limitations regarding the applicability of the harvester datasets in forest inventories. Harvests are typically carried out in actively managed and harvest-ready forests, which means that the use of harvester-collected ground-truth data as reference data may lead to systematic errors in maps and estimates of forest attributes. It is not fully understood if systematic errors can be of relevance in the estimation of forest attributes when training models with harvester data.

Our objective was to study the applicability of harvester data in the model-assisted (MA) estimation (e.g. Rätty et al. 2021) of timber volume in a 250,000 ha study area in Norway. We predicted timber volume for National Forest Inventory (NFI) plots using harvester and ALS data and evaluated systematic errors using correction factors associated with the MA estimates. We also compared the efficiencies of the direct (field data-based) and MA estimators.

2. Data and Methods

2.1 Study area and data

The 250,000 ha study area is located in the Innlandet county in Norway and comprises seven municipalities: Etnedal, Gausdal, Nordre Land, Nordre-Aurdal, Vang, Vestre Slidre, and Øystre-Slidre. In the study area, forests cover 215,000 ha of which 65% are dominated by Norway spruce (*Picea abies* [L.] Karst.).

The NFI data utilized here were collected between 2014 and 2018. We used plots in the lowland stratum (Breidenbach et al. 2020) where sample plots are located on a 3×3 km systematic grid. The field plots are circular plots (250 m²) and each tree with a DBH ≥ 5 cm was measured. There were 157 spruce-dominated field plots (248 field plots in forest, 277 field plots in total) within our study area.

The harvester data used for the fitting of a volume model were collected from spruce-dominated clear-cut areas using a Komatsu 931XC harvester in 2020 and 2021. DBH was registered for each harvested tree and the tree heights were predicted using taper curves. Treetop volumes missing from harvester data were predicted using tree-level volume functions. The harvester registered the XY position of the harvester head for each harvested tree with a positioning accuracy of approximately 5–10 m. The trees were linked to the stand-like segments of Norwegian Forest Resource Map SR16 (Astrup et al. 2019). The SR16 segments were further cropped using alpha-shapes (α -shapes) around the XY positions of the harvested trees. The resulting segments are called harvested segments.

The harvested trees were also linked to the SR16 grid cells (256 m²). We omitted grid cells with obvious discrepancies between the mean height of harvested trees and the 95% ALS height percentile. We also omitted grid cells with less than 66% of cell area in the harvested segments. In total, 166 harvested segments (minimum 0.1 ha, mean 0.7 ha) and 2,953 grid cells comprising 80,099 harvested trees were used for modelling. The mean timber volume associated with the harvested segments and grid cells were 220 and 225 m³·ha⁻¹.

Low-density (< 5 pulses per m²) ALS data were collected from the study area between 2011 and 2017. Standard ALS data processing steps of the area-based approach were carried out, and a set of ALS predictor variables (features) like mean height, height percentiles and density metrics were calculated

for the harvested segments, harvested SR16 grid cells, and NFI plots. The set of ALS features comprised 28 features computed from the ALS point cloud.

2.2 Prediction of volume

We fitted k nearest neighbour (NN) models ($k = 5$) using both the harvested SR16 grid cells and the harvested segments. Three predictor variables were selected by means of an optimization algorithm.

2.3 Estimation methodology

We estimated the mean volume for spruce-dominated forests in the study area from the NFI data (direct estimation). The variances were estimated for both direct and MA estimates. In the MA estimation, the NN models were applied to the NFI plots, and the prediction residuals associated with the NFI plots were utilized in the variance estimation.

The performances of the MA and direct estimators were compared using the relative efficiency (RE, ratio of variances), and the half width of 95 % confidence intervals (CI). Our main interest was on the estimates of correction factors ($\hat{\mu}_{cor}$) that indicate the magnitude of systematic errors in the synthetic (“pixel counting”) estimate. The CIs and correction factors are presented as a percentage value in terms of direct estimates (Räty et al. 2021).

3. Results and Discussion

Despite the good performance of the NN models (Figure 1), the non-zero correction factors of MA estimates showed that the synthetic (“pixel-counting”) estimate of timber volume resulted in systematic errors (Table 1). The NN model fitted using the harvested segments produced a negative correction factor (overestimation). This indicates that the NN model was not capable of extrapolating outside the training data which was mainly collected from mature forests. The NFI data also comprised plots from younger forests for which volume was often overestimated. The NN model fitted using the SR16 grid cells as modeling units resulted in a positive correction factor (underestimation). The positioning errors of trees were non-negligible and may have negatively affected the predictive performance of the NN model fitted using the harvested SR16 grid cells (Figure 1). It is also worth noting that the time lag between the ALS data acquisition and NFI data differs from the time lag between the ALS data acquisition and harvester data, which can also be a minor source of systematic errors.

The use of the harvester-based models resulted in a considerable efficiency gain compared with the direct estimation regardless of the modeling unit (Table 1). The largest RE of 6.17 was achieved using the NN model fitted using harvested segments. The additional use of harvester and ALS data more than halved the CI of the estimate.

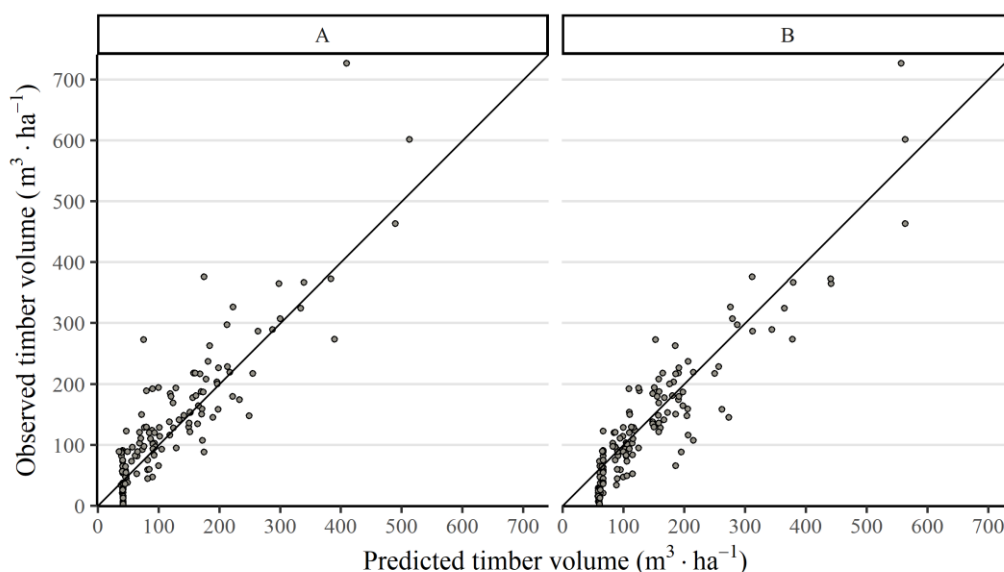


Figure 1. Predicted versus observed timber volumes of spruce-dominated National Forest Inventory field plots. A: model fit using harvested SR16 grid cells and B: model fit using harvested segments.

Table 1. Characteristics associated with the estimation of timber volume for spruce-dominated forests of the study area. RE – relative efficiency, MA – model-assisted.

Modeling unit	Direct estimate $\hat{\mu}$ ($\text{m}^3 \cdot \text{ha}^{-1}$)	Half 95% CI $\hat{\mu}$, (%)	Half 95% CI $\hat{\mu}_{MA}$, (%)	Correction factor $\hat{\mu}_{cor}$, (%)	RE
Grid cell	121.17	14.42	6.65	8.18	4.71
Segment			5.81	-11.39	6.17

4. Conclusions

We draw the following conclusions: (1) The use of a model fitted using cut-to-length harvester and ALS data results in considerable efficiency gains in the model-assisted estimation of timber volume. (2) Harvester data can be valuable for model fitting despite of non-negligible uncertainties in harvester-recorded stem positions. (3) Synthetic (“pixel-counting”) estimates of harvester-based forest attribute maps can result in systematic errors that need to be corrected for to avoid wrong conclusions.

Acknowledgements

This study was supported by NIBIO (Norwegian Institute of Bioeconomy Research) and the PRECISION project (NFR# 11067). We acknowledge Simon Berg for technical support with the harvester data.

References

- Astrup R, Rahlf J, Bjørkelo K, Debella-Gilo M, Gjertsen A-K, Breidenbach J, 2019. Forest information at multiple scales: development, evaluation and application of the Norwegian forest resources map SR16. *Scandinavian Journal of Forest Research*, 34: 484-496.
- Breidenbach J, Granhus A, Hysten G, Eriksen R, Astrup R, 2020. A century of National Forest Inventory in Norway – informing past, present, and future decisions. *Forest Ecosystems*, 7:46.
- Räty J, Astrup R, Breidenbach J, 2021. Prediction and model-assisted estimation of diameter distributions using Norwegian national forest inventory and airborne laser scanning data. *Canadian Journal of Forest Research*.
- Söderberg J, Wallerman J, Almäng A, Möller JJ, Willén E, 2021. Operational prediction of forest attributes using standardised harvester data and airborne laser scanning data in Sweden. *Scandinavian Journal of Forest Research*, 36: 306-314.

Mobile laser scanning with iPad Pro LiDAR

Martin Mokroš^{1,2*}, Arunima Singh¹, Julián Tomašík³, Juliana Chudá³, Piotr Wężyk⁴, Xinlian Liang⁵

¹Faculty of Forestry and Wood Sciences, Czech University of Life Sciences Prague, Kamycká 129, 16500 Prague, Czech Republic

²Department of Forest Harvesting, Logistics and Ameliorations, Faculty of Forestry, Technical University in Zvolen, T. G. Masaryka 24, 960 01 Zvolen, Slovakia

³Department of Forest Resources Planning and Informatics, Faculty of Forestry, Technical University in Zvolen, T. G. Masaryka 24, 960 01 Zvolen, Slovakia

⁴Department of Forest Resource Management, Faculty of Forestry, University of Agriculture in Krakow, 31-425 Krakow, Poland

⁵The State Key Laboratory of Information Engineering in Surveying, Mapping and Remote Sensing, Wuhan University, 430070, Wuhan, China

Abstract

The possibilities to capture three-dimensional point clouds of forest ecosystems from the ground keep expanding. During the last 20 years, terrestrial laser scanning (TLS) has been the most investigated remote sensing approach for acquiring information of forests and individual trees. The results of such research showed a high estimation accuracy for tree positions, volume, diameter at breast height (DBH), height and other biometric parameters. An alternative approach is mobile laser scanning (MLS) which can be placed on a car/train or carried/hold by an operator, with the advantage of being fast and convenient data acquisition.

Currently, an additional approach to conduct mobile laser scanning implements smartphones or tablets with embedded LiDAR sensor. The recent iPad Pro and iPhone 12 Pro are equipped with both high-resolution RGB cameras and LiDAR sensor. In this study, we compared the performance of such a mobile device on eight research plots with 25 m by 25 m dimensions. Altogether, 268 trees were included in the analyses (DBH > 7.0 cm). As reference point clouds we have used TLS (FARO). All tree positions on research sites were measured traditionally using total station and DBH was measured by measuring tape.

Tree detection rate ranged from 100% to 90.6% for TLS and from 87.5% to 64.5% for iPad Pro. DBH estimation root mean square error (RMSE) of TLS and iPad ranged from 1.0 cm to 2.0 cm and from 2.6 cm to 3.4 cm, respectively. And relative RMSE ranged from 3.7% to 6.4% and from 8.6% to 12.9%. The correlation between reference and estimated DBH was $r^2 = 0.996$ for TLS and $r^2 = 0.973$ for iPad Pro.

Results showed high potential of iPad Pro equipped in LiDAR sensor for further usage within the forest inventory. Currently, the data acquisition was done without using the Simultaneous Localization and Mapping (SLAM) algorithm. We believe that the results are going to be even more accurate and reliable with implementation of robust SLAM algorithms.

Assessing the potential of adaptive individual tree detection to improve accuracy of area-based stand density modelling in ALS-assisted forest inventory

Martín-Alcón, S.^{1*}, Duque-Lazo, J.¹, Tomé Morán, J.L.¹

¹Agresta S. Coop

*Email: smalcon@agresta.org

1. Introduction

Airborne Laser Scanning data enables the accurate three-dimensional characterization of vertical forest structure, and have proven to be an information-rich asset for forest managers, enabling the generation of highly detailed digital elevation models and the estimation of a range of forest inventory attributes with high accuracy (Coops et al., 2021; White et al., 2016). The most common LiDAR-derived forest attributes in the bibliography are height, volume, above ground biomass, canopy cover and basal area. Despite being a variable of great importance for forest management, tree density is not a variable frequently estimated from ALS data using area-based approaches. Several studies (Goerndt et al., 2011, 2010; Hall et al., 2005; Næsset and Bjercknes, 2001) have shown that estimation of tree density using area-level LiDAR metrics was difficult because of the lack of correlation between density and canopy height characteristics.

ALS data have also been successfully used to identify individual trees across forest stands, thanks to easily accessible and applicable algorithms. The local maxima CHM-based methods are the most frequently found in literature to identify the treetops, due to its simplicity and ease of use compared to other methods based on full point cloud analysis (Latella et al., 2021; Wu et al., 2016; Zhao et al., 2014). The CHM-based approaches have proven to be quite effective in very regular vegetation pattern, especially when only one layer of the tree canopy is present, and in coniferous stands. Nevertheless, this approach may provide lower-accuracy results when applied under more complex structures (Ene et al., 2012; Richardson and Moskal, 2011). The accuracy of the CHM-based methods used to identify individual trees is known to be highly influenced by the parameter setting. It has been described the extreme sensitivity to the size of the cell window that is used to inspect the CHM and detect the height maxima. The window size, indeed, represents the main and most critical parameter to achieve satisfactory accuracy. A large window smooths the variations of canopy height and drastically reduces the detected peaks, whereas a small one can dramatically increase the number of peaks. Although it is known that the optimum value of this parameter depends on stand characteristics such as the species composition, its height, degree of irregularity, or degree of competition, the literature does not provide robust criteria for the window size setting and, therefore, the CHM-methods require site-specific measurements and calibration (Latella et al., 2021; Popescu and Wynne, 2004).

In this paper we analyze the potential for using individual tree detection (ITD) to improve the accuracy of tree density estimation in ALS area-based forest inventories. To do that, we use a CHM-based algorithm for tree detection based on a local maximum filter, with adaptive parametrization of the window size based on stand structural attributes. The experiment uses inventory data from even-aged *Pinus radiata* plantation forests, and compares the result of stand density estimation when: (1) modelled using only point cloud-derived metrics, (2) modelled using point cloud-derived metrics together with the number of trees detected by ITD, (3) calculated from basal area (G) and quadratic mean diameter (Dg), both modelled with point cloud-derived metrics, and (4) calculated directly through ITD.

2. Data and Methods

2.1 Field data

Field data was acquired from the Spanish National Forest Inventory (northern Atlantic region). We used 82 plots measured from November 2017 to March 2018 in the provinces of Gipuzkoa and Bizkaia, dominated by *Pinus radiata* (more than 90% of basal area of this species). Only plots where trees were accurately geolocated (manually checked with the help of orthophotos and LiDAR-derived CHM) were

included in this sample. Each NFI plot is made up of 4 subplots with a radius of 5, 10, 15 and 25 meters. In these four subplots, the trees were measured with DBH greater than 7.5, 12.5, 22.5 and 42.5 cm respectively. Consequently, within the 10-meter subplot, all trees with diameter greater than 12.5 were measured. We used this subplot for subsequent analysis.

2.2 ALS data

ALS data were acquired by Hazi foundation within the LIFE Healthy Forest project (LIFE14 ENV/ES/000179), cofounded by the Basque government, between March and October 2017, using a LEICA ALS70-HP system with a mean density of 2.2 pulse/m² and RMSEZ < 0.15 meter. Pre-processed data is available in 500×500 m tiles, with points already classified as ground, low and high vegetation, buildings, outliers and unknown. All point cloud data analyses in this work have been performed with the functions of the lidR package for R (Roussel et al., 2020).

2.3 Data analysis

We first run tree detection on the area covered by the field plots using the algorithm *lmf*, implemented in the *find_trees* function of the lidR package for R. We did it iteratively with the parameter window size (*ws*) taking values from 2 to 8 each 0.2 m. The *hmin* parameter was set to 6 meter to be coherent with the minimum diameter of 12.5 cm measured in the 10-meter IFN plots, and the *shape* parameter was set as “circular”, since the natural crown of *Pinus radiata* tends to this shape. For each value of *ws* and in each plot, we compared the result of tree detection with the trees measured in the field. We assessed the quality of the results by calculating the ratio *trees detected (CHM) / trees measured (field)*, named as “*ratio_det_ifn*”.

We then selected as the optimal *ws* value for each plot that with the lower error in that ratio, computing the error as: $abs(1 - ratio_det_ifn)$. Once we had the optimal *ws* value for each plot, we analysed its relationship with the ALS point-cloud metrics at the plot level, and fitted an Extreme Gradient Boosting (XGB) model using the *xgboost* package for R (Chen and Guestrin, 2016), to predict the optimal *ws* parameter depending on them.

On the other hand, we fitted predictive models for stem density, basal area and the quadratic mean diameter as usual in area-based approach, using ALS point-cloud derived metrics as predictors. To process ALS metrics, the point cloud was clipped to the corresponding NFI 10-meter subplot. Models were fitted using XGB as well.

Finally, we used the predicted value for the optimal *ws* parameter to run ITD within each plot, and modelled again stand density adding the resulting number of trees detected by ITD as an additional variable to point-cloud derived metrics. In order to compare all possible ways to estimate stem density within this workflow, we also compute the stem density from predicted basal area (*G*) and quadratic mean diameter (*Dg*).

3. Results and discussion

Our results showed that the optimal value for the *ws* parameter has a significant relationship with certain ALS point-cloud derived metrics. Concretely, the best model to predict *ws* used standard deviation, entropy and interquartile range of height distribution, together with the mean height, as predictors, and reported a relative RMSE of 26.837%. Overall, predicted values of *ws* varied depending on mean tree size and tree size inequality, as reflected by the point-cloud metrics selected in the best model.

When we used the predicted *ws* parameter to detect the number of trees within the plots, and related the resulting number of trees with the stand density measured in the NFI field plots, we found that the number of detected trees using this methodology is not a good standalone predictor for stand density (RMSE: 39.757%). However, its performance improves when used in combination with a selection of ALS point-cloud derived metrics, concretely, the 95th percentile of height returns, and the Canopy Relief Ratio (i.e., a quantitative descriptor of the relative shape of the canopy from altimetry observation). This combination of variables allowed us to reach 19.061% relative RMSE in the estimation of stand density, compared to 24.376% obtained when using the best combination of ALS point-cloud derived metrics alone. The alternative of calculating the density from the predicted *G* and *Dg* reported 23.947% relative RMSE.

The result of this study shows the potential of this workflow for improving the accuracy in stand density estimation based on ALS point-cloud metrics, but is just a promising first step that deserves further development with the use of variable radius search windows, as well as the use of alternative tree detection methods.

Acknowledgements

This research was primarily supported by the European Commission through funding via SME Instrument, to the project FORESTMAP (REF. 858664, Quick and cost-effective integrated web platform for forest inventories), within its task 2.4. (Development of algorithms based on airborne LIDAR). Joaquin Duque-Lazo contribution was also supported by the postdoctoral grant PTQ2018-010230, awarded by the National Programme for the Promotion of Talent and Its Employability of the Ministry of Economy, Industry, and Competitiveness (Torres-Quevedo program), which is partially funded by the European Social Fund (ESF) from the European Commission. Authors are also grateful to the Basque Government and Hazi foundation as providers of LiDAR data, and the Spanish Government as the provider of National Forest Inventory data.

References

- Chen, T., Guestrin, C., 2016. XGBoost: A Scalable Tree Boosting System, in: Proceedings of the 22nd ACM SIGKDD International Conference on Knowledge Discovery and Data Mining, KDD '16. Association for Computing Machinery, New York, NY, USA, pp. 785–794. doi:10.1145/2939672.2939785
- Coops, N.C., Tompalski, P., Goodbody, T.R.H., Queinnec, M., Luther, J.E., Bolton, D.K., White, J.C., Wulder, M.A., van Lier, O.R., Hermosilla, T., 2021. Modelling lidar-derived estimates of forest attributes over space and time: A review of approaches and future trends. *Remote Sens. Environ.* 260, 112477. doi:10.1016/j.rse.2021.112477
- Ene, L., Næsset, E., Gobakken, T., 2012. Single tree detection in heterogeneous boreal forests using airborne laser scanning and area-based stem number estimates. *Int. J. Remote Sens.* 33, 5171–5193. doi:10.1080/01431161.2012.657363
- Goerndt, M.E., Monleon, V.J., Temesgen, H., 2011. A comparison of small-area estimation techniques to estimate selected stand attributes using LiDAR-derived auxiliary variables. *Can. J. For. Res.* 41, 1189–1201. doi:10.1139/x11-033
- Goerndt, M.E., Monleon, V.J., Temesgen, H., 2010. Relating forest attributes with area-And tree-based light detection and ranging metrics for western Oregon. *West. J. Appl. For.* 25, 105–111. doi:10.1093/wjaf/25.3.105
- Hall, S.A., Burke, I.C., Box, D.O., Kaufmann, M.R., Stoker, J.M., 2005. Estimating stand structure using discrete-return lidar: An example from low density, fire prone ponderosa pine forests. *For. Ecol. Manage.* 208, 189–209. doi:10.1016/j.foreco.2004.12.001
- Latella, M., Sola, F., Camporeale, C., 2021. A density-based algorithm for the detection of individual trees from lidar data. *Remote Sens.* 13, 1–22. doi:10.3390/rs13020322
- Næsset, E., Bjercknes, K.O., 2001. Estimating tree heights and number of stems in young forest stands using airborne laser scanner data. *Remote Sens. Environ.* 78, 328–340. doi:10.1016/S0034-4257(01)00228-0
- Popescu, S., Wynne, R., 2004. Seeing the Trees in the Forest: Using Lidar and Multispectral Data Fusion with Local Filtering and Variable Window Size for Estimating Tree Height. *Photogramm. Eng. Remote Sensing* 70, 589–604. doi:citeulike-article-id:12239493
- Richardson, J.J., Moskal, L.M., 2011. Strengths and limitations of assessing forest density and spatial configuration with aerial LiDAR. *Remote Sens. Environ.* 115, 2640–2651. doi:10.1016/j.rse.2011.05.020
- Roussel, J.R., Auty, D., Coops, N.C., Tompalski, P., Goodbody, T.R.H., Meador, A.S., Bourdon, J.F., de Boissieu, F., Achim, A., 2020. lidR: An R package for analysis of Airborne Laser Scanning (ALS) data. *Remote Sens. Environ.* 251, 112061. doi:10.1016/j.rse.2020.112061
- White, J.C., Coops, N.C., Wulder, M.A., Vastaranta, M., Hilker, T., Tompalski, P., 2016. Remote Sensing Technologies for Enhancing Forest Inventories: A Review. *Can. J. Remote Sens.* 42, 619–641. doi:10.1080/07038992.2016.1207484
- Wu, B., Yu, B., Wu, Q., Huang, Y., Chen, Z., Wu, J., 2016. Individual tree crown delineation using localized contour tree method and airborne LiDAR data in coniferous forests. *Int. J. Appl. Earth Obs. Geoinf.* 52, 82–94. doi:10.1016/j.jag.2016.06.003
- Zhao, D., Pang, Y., Li, Z., Liu, L., 2014. Isolating individual trees in a closed coniferous forest using small footprint lidar data. *Int. J. Remote Sens.* 35, 7199–7218. doi:10.1080/01431161.2014.967886

Mapping riparian forest species for biodiversity analysis by fusion of Airborne LiDAR and multispectral satellite imagery

Housseem Njimi¹, Nesrine Chehata², Frédéric Revers³

¹UR17DN01 Aviation school of Borj El Amri, Tunisia
Email:housseemnjimi@gmail.com

² EA Géoresources & Environnement, Université Michel Montaigne/Bordeaux INP
Email:nesrine.chehata@ensegid.fr

³ UMR BIOGECO, INRAE
Email:frederic.revers@inrae.fr

1. Introduction

In order to ensure sustainable management of forest resources, the study of the functioning and dynamics of forest resources is essential. Multispectral and 3D LiDAR remote sensing data sources are valuable tools for understanding the relationship between forest structure, biodiversity and microclimate. Remote sensing metrics can be derived either on 3D vegetation structures, biophysical variables or on forest species mapping.

This study focuses on mapping riparian forest species in the canopy strata using a fusion of Airborne LiDAR data and multispectral multi-sources satellite imagery; Sentinel-2 and Pleiades at tree level. The idea is to assess the contribution of each data source in the tree species classification at the considered level and to have first interpretations on relationships with biodiversity taxons (herbaceous, terrestrial invertebrates et vertebrates) which were sampled on each site. Indeed, tree specie composition and mapping are known to modify biodiversity responses.

The fusion was processed at feature-level and decision level. At feature level, LiDAR 2D attributes were derived and combined with vegetation indices. At decision level, LiDAR data was used for 3D tree crown delimitation providing a unique tree or a group of trees that are used as a support for the species classification. Data augmentation techniques were used to increase training samples.

Best results were obtained by the fusion of Sentinel-2 time series and LiDAR data with a Kappa of 0.656 thanks to red-edge based indices that better discriminate vegetation species and the temporal resolution of Sentinel-2 images that allows monitoring the phenological stages helping discriminate the species.

2. Data and methods

2.1 Study Area

The study site is located in south western France. Ciron watershed and its riparian forest is an affluent of the Garonne known for a climatic refuge for beech, on the warm margin of its European range. This riparian forest is made up of an assemblage of species such as Oak, Beech, Locust, Pine, etc. Twenty-eight sites forming a three-dimensional structure gradient are defined. They are located over thirty kilometers along the Ciron and 5 km along an affluent in which the riparian forest is bordered by pine forests (maritime pine) in order to homogenize the potential impact of the surrounding landscape on the biodiversity of flora and fauna in the riverine forest.

2.2 Data

Joint airborne acquisition and in-field observations were conducted in autumnal season with tree foliage on 3rd and 4th October 2019. Trees were measured on canopy and shrub strata leading to more than 31 unbalanced classes. In this study we only focus on canopy classes that are limited to 5 classes. Train and Test data were selected using individual tree crowns generated after the segmentation process. They consist of 165 and 73 samples, respectively.

Complementary data were used exploiting spectral and temporal information (Sentinel-2), very high resolution (VHR) imagery (Pleiades) and geometric information from LIDAR data. 11 Sentinel-2 images were used from January to December 2019, one VHR Pleiades image on the 3rd September 2019 and 632 tiles of 3D point clouds with 50pts/m² density covering the whole site.

2.3 Methodology

LiDAR and multispectral data were first co-registered manually exploiting the high accuracy of Lidar data. Each data source was processed separately and then fused at feature and decision levels [1]. First, DSM and DTM were processed at a resolution of 0.25 m. A DHM was then derived leading to a map of canopy height as well as 2D attributes such as Intensity, point density, number of echoes and height range.

3D Lidar point clouds were segmented using PyCrown [2] method. It provides a 3D segmentation of individual trees besides a raster segmentation. It is based on local maximum search (i.e. tree tops) and region growing with regard to user-defined parameters (distance of a crown point from its top and point height w.r.t crown average heights).

11 Sentinel-2 images were used in TOA reflectance. 10 spectral bands of 10-20 m were used and resampled to 0.25 m. Besides 7 vegetation indices [3] were derived for each date based on near infrared and red edge channels: NDVI, GRVI1, Clre, NDVIre3, NDre2, SAVI, MSAVI2. Soil adjusted indices such as SAVI and MSAVI2 were used to better handle non dense tree species. Totally, 10 initial bands and 7 vegetation indices were used per date leading to 187 spectral bands.

Fusion was first processed at feature level by concatenating spectral and geometric LiDAR attributes. Different feature combinations were used to assess the importance of spectral, temporal or spatial information. At decision-level, segmented LiDAR regions were used to derive spectral attributes at an object-level using attributes' mean and standard deviation over each segmented region. Due to few training data, data augmentation techniques were used using Gaussian Noise filtering increasing the samples per twice. Finally, the classification was processed using a Random Forest classifier. Results are evaluated using Overall accuracy, kappa and per class precision and recall.

3. Results and Discussions

Table 1 resumes the obtained classification accuracies with different fusion configurations and measuring data augmentation impact. Table 2 presents the precision and recall values per specie.

Table 1. Comparison of classification accuracies using different fusion configurations with and without data augmentation

	Classification	Kappa	OA
Without data augmentation	Sentinel-2 (single date) + LIDAR	0.481	0.594
	Pleiades + LIDAR	0.434	0.548
	Sentinel-2 (multi dates) + LIDAR	0.508	0.607
	Sentinel-2 (single date) + Pléiades + LIDAR	0.493	0.595
With data augmentation	Sentinel-2 (mono-date) + LIDAR	0.527	0.620
	Pleiades + LIDAR	0.495	0.598
	Sentinel-2 (multi-dates) + LIDAR	0.656	0.694
	Sentinel-2 (mono-date) + Pléiades + LIDAR	0.582	0.665

Table 2. Comparison of precision and recall per specie using data augmentation

	Pedonculate Oak	Tauzin Oak	Black Alder	Maritime Pine	Other
Precision	0.47	0.91	0.54	0.73	0.85
Recall	0.56	0.71	0.89	0.8	0.48

The best results are given with the combination of multi dates Sentinel-2 images and LiDAR data showing the importance of temporal and spectral resolution of Sentinel-2 which contributed the most in the classification of forest species.

We actually obtained 0.656 as Kappa and 0.694 as Overall Accuracy. Otherwise, the very high spatial resolution of Pleiades (2m) caused a decrease in the evaluation metrics. This is probably due to detected shadows.

The data augmentation improved the obtained results as it allowed more training samples. The best configuration has also shown that *Tauzin Oak*, *Maritime Pine* and the class *Other* have precision values superior to 0.727 which means that at least 72.7% of these species were correctly labeled. Otherwise, less than 54.2% of *Pedonculate Oak* and *Black Alder* were correctly labeled.

Results have also shown that the classifier under-estimates the *Pedonculate oak* and the class *Other* (low recall values compared to other classes) while it over estimates the *black alder* (high recall value 0.88 and low precision value 0.54)

Figure 1 shows the 2D segmentation result and the corresponding forest species classification using the best fusion configuration on Site 21.

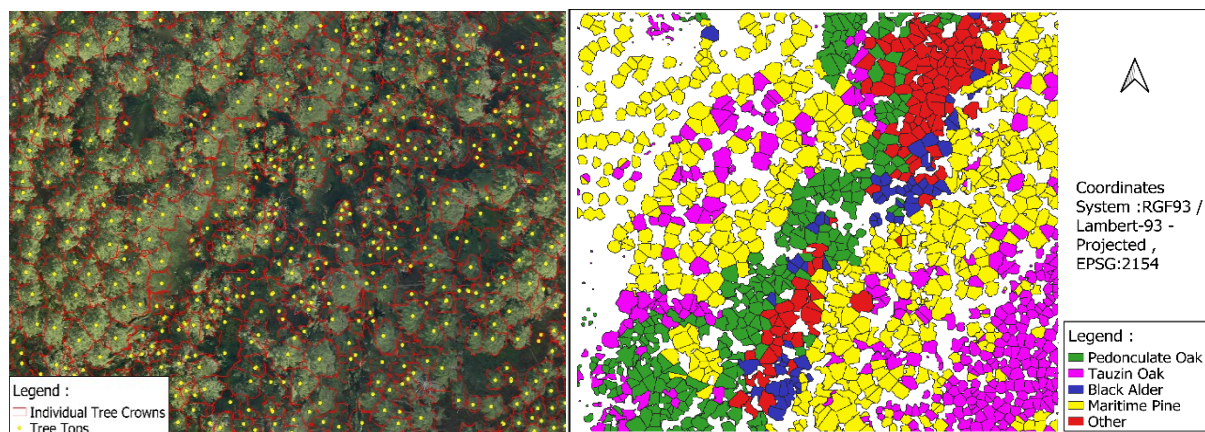


Figure 1: Results on Site 21 : From left to right : Individual Tree Crowns Delineation , Forest Species Classification

4. Conclusions

This study allowed the evaluation of Airborne LiDAR data and multispectral satellite imagery fusion in order to classify riparian forest species. The results revealed the importance of data augmentation, temporal and spectral resolution of Sentinel-2 satellite in the process of classification added to the importance of LiDAR data in the individual tree crown delineation. The best fusion configuration gave respectively 0.656 and 0.694 as kappa and OA values respectively.

Further work will focus on providing spatial metrics from species patterns and measuring their relationships with biodiversity taxons.

Acknowledgements

Authors want to thank the French National Space Agency for their support through the TOSCA FRISBEE project.

References

- [1] E. Tusa, A. Laybros, J.-M. Monnet, M. Dalla Mura, J.-B. Barré, G. Vincent, *et al.*, "Fusion of hyperspectral imaging and LiDAR for forest monitoring," *Data Handling in Science and Technology*, vol. 32, pp. 281-303, 2020.
- [2] M. Dalponte and D. A. Coomes, "Tree-centric mapping of forest carbon density from airborne laser scanning and hyperspectral data," *Methods in ecology and evolution*, vol. 7, pp. 1236-1245, 2016.
- [3] N. Touihri, N. Chehata, H. Chakroun, and T. S. Chahed, "Contribution of Sentinel 2 images spectral bands for mapping forest land cover: Application to Tbeynia site, Jendouba, Tunisia."

VirtSilv A.I. 3D platform for sustainable forest management

M.D. Nita¹, B. Candrea¹, C. Cucu-Dumitrescu¹, B. Grama¹, I. Iuga¹

¹Forest Design SRL, Nicovalei 33, Brasov, Romania
Email: mihai@forestdesign.ro

1. Introduction

Climate-Smart Forestry is a sustainable forest management approach for increasing these positive climate impacts on society (Verkerk et al. 2020). In response to climate change, the approach intends to reduce greenhouse gas emissions, adapt forest management to create resilient forests, and focus on active forest management with the goal of sustainability by increasing productivity while simultaneously offering all forest benefits (Nabuurs et al. 2017; Bowditch et al. 2020).

Nowadays, the availability and affordability of equipment and techniques are continuously increasing. LIDAR devices have become more portable, at ever-increasingly affordable prices, along with techniques for generating 3D scenes from measurements (Tang et al. 2015). This has enabled the building of virtual worlds that reflect the natural landscapes using precision measurements. Particularly, terrestrial lidar systems collect large amounts of data varying from tens of thousands to billions of 3D points to determine the 3D space surrounding a given point in 3D (Paris et al. 2017)

Virtual tree measurements are achieved today by using software applications and allometric approaches (Yu et al. 2013; Kankare et al. 2015; Liang et al. 2014; Astrup et al. 2014; Newnham et al. 2015; Tomşa, Curtu, and Niţă 2021). However, the quality of results and maturity of these algorithms are still low (Tansey et al. 2009; Li et al. 2012). Furthermore, there is no technological group on the market that would be able to provide a complete set of solutions to the problem, from the measurements in the forest to creating digital twins of each tree (Raumonen et al. 2013). As a platform that responds to the realities of the forest, VirtSilv provides industry-specific services in all segments (Forest Design 2020). VirtSilv is an online platform that uses AI customizable algorithms to produce unique shapes of trees as digital support for a fully automated traceability IT circuit between forest management, transport, and the wood industry.

The article aimed to validate the automatic workflow of processing 3D pointclouds to produce digital twins for every tree in a specific forest using GeoSLAM mobile LiDAR scanner and VirtSilv AI platform.

2. Materials and Methods

2.1 Study area and data

Several measurement campaigns were carried out, using mobile LIDAR device and traditional forest inventory tools (tape for DBH and vertex logger IV for height), focusing on 3 plots of 1 ha size in Carpathian Mountains, Ciucas Massif.

The plots were scanned using ZEB Horizon, a scanner based on LiDAR technology, and included in the category of Terrestrial Laser Scanners (TLS). This is a 3D scanner of high-speed used for measurements that require recording of details. ZEB Horizon Scanner uses laser technology, weighing 1.3 kg it is designed for outdoor applications that require scanning up to 100 m and at an accuracy of 1-3 cm. The scanner uses a rotating mirror to beam around the area that is scanned. The measurement characteristics consist of up to 300,000 repetitions per second. Data acquired using GEOSLAM Horizon technology is a point cloud in the form of three-dimensional data compiled using SLAM (simultaneous localization and mapping). The scanning time suitable to produce dense pointclouds was on an average of approximately 20 minutes/hectare for each plot.

2.2 VirtSilv software

The raw data generated during the scanning process enables the visual identification of individual tree structures, but they are not yet quantitatively differentiated. To create individual raw material for digital twin, VirtSilv first separates the ground from the trees, and then it reconstructs each tree separately. For segmentation the algorithm takes 3 steps to estimate each tree's footprint simultaneously. The algorithm begins at a large nucleus of points with high density and then grows by accretion until it meets neighbouring trees. The novelty of VirtSilv is that parallelize the computation so the average processing time of segmentation for 1 hectare of scanned forest is 30 minutes.

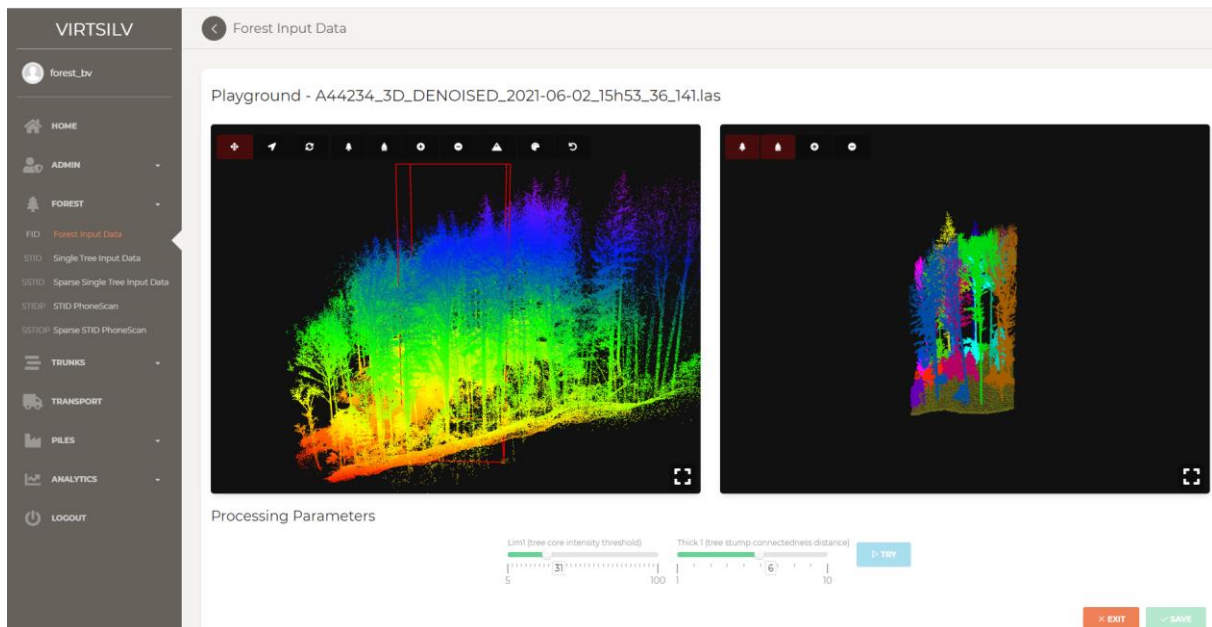


Figure 1: Raw data processing dashboard.

When all the individual tree segments are identified, the remaining task is to recognize tree trunks and model their numerical dimensions on a simple and flexible basis, thereby giving the potential for the digital twinning process. To overcome the limitations of current techniques, VirtSilv algorithms are designed around the following principles (figure 2):

- The trunk shape of segments of sufficiently small height can be approximated very well by inclined cone trunks.
- The vertical projection of the data obtained from segments of sufficiently small height can be approximated by a ring of points with relatively high density.
- Generally, the successive segments in the vertical array are very well aligned, in the sense that the angle and bending of each segment, concerning that vertical changes are low.

Thus, the VirtSilv algorithm is focused on extracting chains of cone trunks as a numerical model for trunks. The average time of producing the 3D model of a tree digital twin is less than one minute.

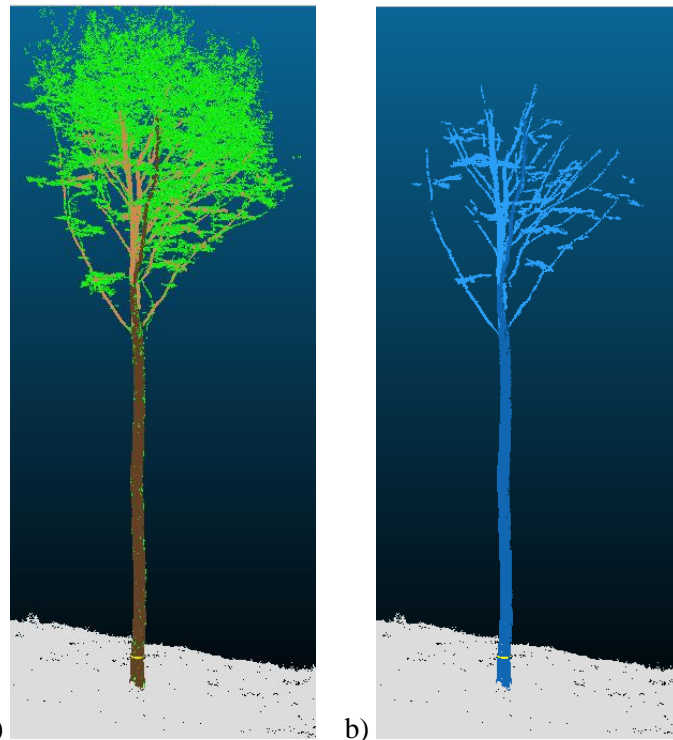


Figure 2: Single tree point classification in a) trunk, branches and leaves+ small branches and b) model generated for woody part

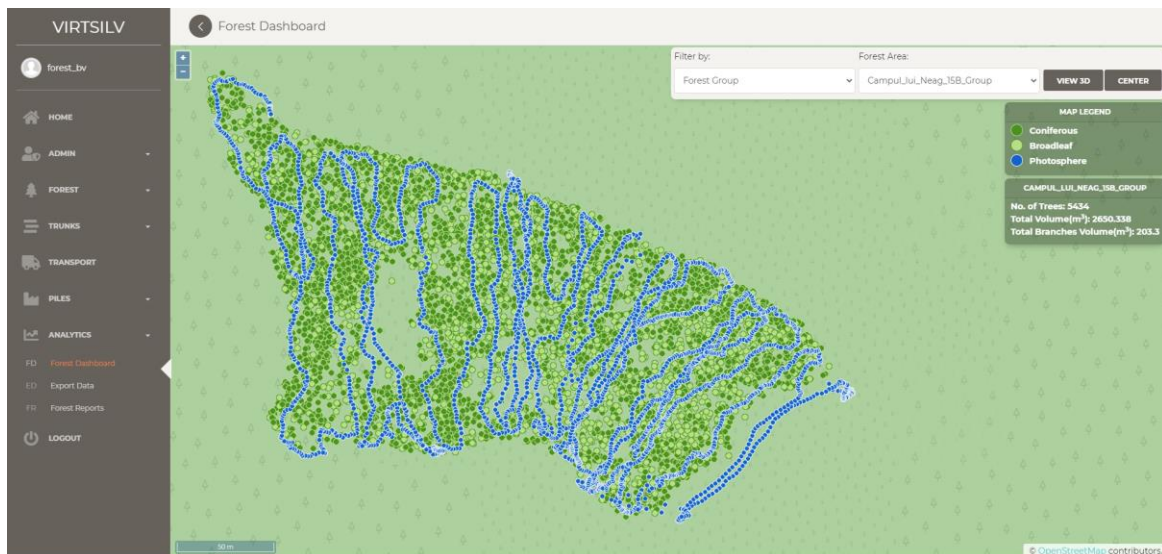


Figure 3: The final product dashboard.

3. Conclusion

A number of 1399 trees were scanned with LiDAR to create digital twins and for validation were measured with traditional tools such as tape and vertex. The segmentation algorithm developed in the platform to extract individual 3D trees an accuracy varying between 95-98% was recorded. This result was higher in accuracy than reported by other solutions. When compared to traditional measurements the bias for diameter at breast height (DBH) and height was not significant. Digital twinning offers a blockchain solution for digitalization and AI platforms are able to provide technological advantage in preserving and restoring biodiversity with sustainable forest management.

References

- Astrup, Rasmus, Mark J. Ducey, Aksel Granhus, Tim Ritter, and Nikolas von Lüpke. 2014. "Approaches for Estimating Stand-Level Volume Using Terrestrial Laser Scanning in a Single-Scan Mode." *Canadian Journal of Forest Research* 44 (6): 666–76. <https://doi.org/10.1139/cjfr-2013-0535>.
- Bowditch, Euan, Giovanni Santopuoli, Franz Binder, Miren del Río, Nicola La Porta, Tatiana Kluvankova, Jerzy Lesinski, et al. 2020. "What Is Climate-Smart Forestry? A Definition from a Multinational Collaborative Process Focused on Mountain Regions of Europe." *Ecosystem Services* 43 (June): 101113. <https://doi.org/10.1016/j.ecoser.2020.101113>.
- Forest Design. 2020. "VirtSilv: <https://Virtsilv.Com/>." <https://virtsilv.com/>.
- Kankare, Ville, Xinlian Liang, Mikko Vastaranta, Xiaowei Yu, Markus Holopainen, and Juha Hyypä. 2015. "Diameter Distribution Estimation with Laser Scanning Based Multisource Single Tree Inventory." *ISPRS Journal of Photogrammetry and Remote Sensing* 108 (October): 161–71. <https://doi.org/10.1016/j.isprsjprs.2015.07.007>.
- Li, Wenkai, Qinghua Guo, Marek K. Jakubowski, and Maggi Kelly. 2012. "A New Method for Segmenting Individual Trees from the Lidar Point Cloud." *Photogrammetric Engineering and Remote Sensing* 78 (1): 75–84. <https://doi.org/10.14358/PERS.78.1.75>.
- Liang, Xinlian, Ville Kankare, Xiaowei Yu, Juha Hyypä, and Markus Holopainen. 2014. "Automated Stem Curve Measurement Using Terrestrial Laser Scanning." *IEEE Transactions on Geoscience and Remote Sensing* 52 (3): 1739–48. <https://doi.org/10.1109/TGRS.2013.2253783>.
- Nabuurs, Gert-Jan, Philippe Delacote, David Ellison, Marc Hanewinkel, Lauri Hetemäki, and Marcus Lindner. 2017. "By 2050 the Mitigation Effects of EU Forests Could Nearly Double through Climate Smart Forestry." *Forests* 8 (12). <https://doi.org/10.3390/f8120484>.
- Newnham, Glenn J., John D. Armston, Kim Calders, Mathias I. Disney, Jenny L. Lovell, Crystal B. Schaaf, Alan H. Strahler, and F. Mark Danson. 2015. "Terrestrial Laser Scanning for Plot-Scale Forest Measurement." *Current Forestry Reports* 1 (4): 239–51. <https://doi.org/10.1007/s40725-015-0025-5>.
- Paris, Claudia, David Kelbe, Jan van Aardt, and Lorenzo Bruzzone. 2017. "A Novel Automatic Method for the Fusion of ALS and TLS LiDAR Data for Robust Assessment of Tree Crown Structure." *IEEE Transactions on Geoscience and Remote Sensing* 55 (7): 3679–93. <https://doi.org/10.1109/TGRS.2017.2675963>.
- Raunonen, Pasi, Mikko Kaasalainen, Markku Åkerblom, Sanna Kaasalainen, Harri Kaartinen, Mikko Vastaranta, Markus Holopainen, Mathias Disney, and Philip Lewis. 2013. "Fast Automatic Precision Tree Models from Terrestrial Laser Scanner Data." *Remote Sensing* 5 (2): 491–520. <https://doi.org/10.3390/rs5020491>.
- Tang, Jian, Yuwei Chen, Antero Kukko, Harri Kaartinen, Anttoni Jaakkola, Ehsan Khoramshahi, Teemu Hakala, Juha Hyypä, Markus Holopainen, and Hannu Hyypä. 2015. "SLAM-Aided Stem Mapping for Forest Inventory with Small-Footprint Mobile LiDAR." *Forests* 6 (12): 4588–4606. <https://doi.org/10.3390/f6124390>.
- Tansey, K., N. Selmes, A. Anstee, N. J. Tate, and A. Denniss. 2009. "Estimating Tree and Stand Variables in a Corsican Pine Woodland from Terrestrial Laser Scanner Data." *International Journal of Remote Sensing* 30 (19): 5195–5209. <https://doi.org/10.1080/01431160902882587>.
- Tomşa, Vlăduţ Remus, Alexandru Lucian Curtu, and Mihai Daniel Niţă. 2021. "Tree Shape Variability in a Mixed Oak Forest Using Terrestrial Laser Technology: Implications for Mating System Analysis." *Forests* 12 (2). <https://doi.org/10.3390/f12020253>.
- Verkerk, P. J., R. Costanza, L. Hetemäki, I. Kubiszewski, P. Leskinen, G. J. Nabuurs, J. Potočník, and M. Palahí. 2020. "Climate-Smart Forestry: The Missing Link." *Forest Policy and Economics*. Elsevier B.V. <https://doi.org/10.1016/j.forpol.2020.102164>.
- Yu, Xiaowei, Xinlian Liang, Juha Hyypä, Ville Kankare, Mikko Vastaranta, and Markus Holopainen. 2013. "Stem Biomass Estimation Based on Stem Reconstruction from Terrestrial Laser Scanning Point Clouds." *Remote Sensing Letters* 4 (4): 344–53. <https://doi.org/10.1080/2150704X.2012.734931>.

Evaluation of the Positional Accuracy of Trees Derived Using SLAM

J. Chudá¹, M. Mokroš^{2,3}, M. Sivák¹, R. Kadlečík¹

¹Department of Forest Resource Planning and Informatics, Faculty of Forestry, Technical University in Zvolen, T. G. Masaryka 24, 960 01 Zvolen, Slovakia; xchudaj@is.tuzvo.sk, xsivakm@is.tuzvo.sk, xkadlecikr@is.tuzvo.sk

²Department of Forest Harvesting, Logistics and Amelioration, Faculty of Forestry, Technical University in Zvolen, T. G. Masaryka 24, 960 01 Zvolen, Slovakia; xmokros@is.tuzvo.sk

³Excellent research EVA4.0, Faculty of Forestry and Wood Sciences, Czech University of Life Sciences Prague, Kamýcká 129, 165 00 Prague, Czech Republic; mokros@fld.czu.cz

1. Introduction

It is a known fact that forest stands as sets of objects geomorphologically highly structured in connection with variable terrain conditions amplify the influence of specific described factors on positioning accuracy and thus reduce it by moving the value of the resulting positioning error far beyond the permissible deviation.

Traditional methods of positioning, Global Navigation Satellite Systems (GNSS) technology in cooperation with total stations, provides more than a few advantages, but several pitfalls in more complex conditions, too (Keefe et al., 2019).

The trend in collecting information about the forest is currently focused on the application of contactless devices, new technologies and ideally their combinations. The positional accuracy derived from the outputs of carried device will be evaluated in this topic. We assume that it is possible to refine the estimation of determining the position of objects by thoughtful data collection under the forest canopy. The handheld mobile laser scanner ZEB HORIZON which uses simultaneous localization and mapping technology will be used for data collection.

2. Data and Methods

This study was conducted in a managed forest located in Central Slovakia. The forest stand is managed by the Forest Enterprise of the Technical University in Zvolen. Two main research plots were developed in the areas with slightly different conditions. The age of research area 1 (RA1) is 85 years, with a density of 133 trees per hectare, and the age of research area 2 (RA2) is 60 years with a density of 344 trees per hectare. The dominant tree species at both research areas is beech (*Fagus sylvatica* L.) (45% - RA1, 95% - RA2), at the RA 1 followed by spruce (*Picea abies* (L.) Karst.) (30%), oak (*Quercus petraea*) (20%), and fir (*Abies alba* Mill.) (5%) without the understory, and at the RA 2 followed by fir (*Abies alba* Mill.) (2%), spruce (*Larix decidua* Mill.) (2%), oak (*Quercus petraea*) (1%) with the understory made up by beech (*Fagus sylvatica* L.) with DBH \leq 8 centimeters (100%). Every research area was divided into two square plots with dimensions 25 x 25 m.

The positions of 235 trees were measured by the total station on the trunks at the height of 1.3 m above the terrain, and the tree axes determination was done by shifting every point about one-half of its measured DBH during the office work. The DBH were manually measured at the height of 1.3 m using standard steel diameter tape. For each measurement, the 1.3 m height was determined individually by measuring tape. Except for tree position, the four reference spheres were placed on all plot's corners and their polar coordinates were measured.

The experimental data was collected by lightweight handheld mobile scanner ZEB Horizon developed by GeoSLAM Ltd. (UK), consist of a laser scanner, a low-cost Inertial Measurement Unit (IMU), a camera, a data logger, and accessories (S. Chen et al., 2019; Ryding et al., 2015) works on the principles of SLAM. The device was carried by a uniform rectilinear movement over the research area according to predefined marked schemes – dense, medium, and thin research area coverage. The recording of the plots took approximately from 7 to 18 min. The estimation of tree position was connected with the estimation of tree diameter. For this purpose, the DendroCloud software was used (Koreň et al., 2017). Detailed information about the workflow used within the software can be found in Koreň (2019).

3. Results and Discussion

The use of mapping systems based on simultaneous positioning and mapping as a more favorable alternative to traditional methods of static mapping in a complicated environment has been described in Chen et al. (2018) The work of James & Quinton (2014), Bienert et al. (2006) or Ryding et al. (2015) examine the applications of mobile laser scanners and SLAM technology to various industries, not exclude forestry.

The main goal of the presented work was to evaluate the positional accuracy of objects recorded by alternative approaches in the field of obtaining positional data in the forest environment and to assess the suitability of using technologies in relation to positioning accuracy standards, in relation to a possible increase in the efficiency of mapping work in the forest environment, which will be ensured by accelerating the whole process of collecting information about the environment with the expected achievement of very accurate results. The following is an evaluation of the accuracy of the derived position of trees extracted from a SLAM device (Table 1).

Table 1. Efficiency of field work comparison

Research area	plot	Line type	Data acquisition duration [min]	Trees		Positional RMSE				
				reference	derived	X	Y	Z	Horizontal	Overall
1	A	dense	13	98	96	0.113	0.068	0.501	0.053	0.399
		medium	8		62	0.101	0.051	0.336	0.073	0.337
		thin	7		34	0.042	0.055	0.223	0.093	0.232
	B	dense	14	58	48	0.058	0.058	0.311	0.067	0.324
		medium	11		40	0.070	0.090	0.248	0.089	0.262
		thin	12		48	0.064	0.069	0.252	0.086	0.269
2	F	dense	15	24	25	0.043	0.032	0.149	0.126	0.157
		medium	11		25	0.063	0.038	0.150	0.119	0.166
		thin	9		19	0.042	0.084	0.151	0.068	0.177
	G	dense	16	55	55	0.024	0.064	0.121	0.082	0.137
		medium	18		48	0.060	0.061	0.117	0.108	0.149
		thin	8		47	0.035	0.079	0.113	0.094	0.141
Average:			11.8			0.060	0.062	0.223	0.088	0.229

Considering the positioning error in the direction of the X axes, we were in all cases able to reach values lower than 0.12 m, in the direction of the and Y axes lower than 0.09 m and in the direction of Z axes 0.13 m. The average horizontal RMSE acquires value 0.088 m, and after taking into account the height 0.229 m.

Many authors explore the possibilities of using SLAM in relation to the forest environment and various ecosystems. Nevalainen et al. (2020) in forest work and navigation of logging and transport technologies, Hyyppä et al. (2020) compares SLAM with other mobile laser scanning technologies in boreal forest conditions, and Ali et al. (2020) examines it in relation to mobile robotics, autonomous management research and forestry.

The time of data acquisition is directly related to the cost of data acquisition. Since the authors use different methods for the collection of HMLS equipment, it is appropriate to point out its effectiveness by calculating the time for which 1 ha of area can be recorded by the equipment. On the first hand, some works performed relatively long time data acquisition e.g. Chen et al. (2019) 333 min/ha per operator or Ryding et al. (2015) 200 min/ha per operator, on the other hand, some authors decreased data acquisition duration to lower and more effective time period e.g. James & Quinton (2014) 81 min/ha per operator or Cabo et al. (2018) 36 min/ha per operator. Our research achieved very effective acquisition time at the amount of 19 min/ha per operator.

4. Conclusions

In this study, a handheld mobile laser scanning (HMLS) device ZEB HORIZON has been used for mapping and inventory of forest. The goal of this study was to evaluate the positional accuracy of objects

in research areas. Reference data were obtained by the total station. The validation of the positional accuracy of the HMLS data was performed by comparing this data with reference data.

Acknowledging the positioning error in the direction of the X-axis, we can achieve values lower than 12 cm, in the Y-axis direction lower than 9 cm and in the Z-axis direction lower than 13 cm. The average horizontal RMSE reaches a value of 8.8 cm, while taking into account the height of the objects, RMSE reaches 22.9 cm. In this study, we achieved a very efficient data collection, and it would be possible to scan 1 ha with this method in less than 19 minutes.

Many authors demonstrated possibilities of the HMLS e. g. Ryding et al. (2015), James & Quinton (2014) or Chen et al. (2019). The study results show that the used HMLS technology appears to be economical and technical solution for planning some forestry activities that do not require millimeter accuracy of measurement. Spatial division of forest stands and objects can help in planning fire-fighting measures, creating digital models, planning logging, etc.

5. References

- Ali, I., Durmush, A., Suominen, O., Yli-Hietanen, J., Peltonen, S., Collin, J., & Gotchev, A. (2020). FinnForest dataset: A forest landscape for visual SLAM. *Robotics and Autonomous Systems*, 132, 103610. <https://doi.org/10.1016/j.robot.2020.103610>
- Bienert, A., Maas, H.-G., & Scheller, S. (2006). Analysis of the information content of terrestrial laserscanner point clouds for the automatic determination of forest inventory parameters. *Workshop on 3D Remote Sensing in Forestry*, 14 th-15 th.
- Cabo, C., Del Pozo, S., Rodríguez-González, P., Ordóñez, C., & González-Aguilera, D. (2018). Comparing terrestrial laser scanning (TLS) and wearable laser scanning (WLS) for individual tree modeling at plot level. *Remote Sensing*, 10(4). <https://doi.org/10.3390/rs10040540>
- Chen, S., Liu, H., Feng, Z., Shen, C., & Chen, P. (2019). Applicability of personal laser scanning in forestry inventory. *PLoS ONE*, 14(2), e0211392. <https://doi.org/10.1371/journal.pone.0211392>
- Chen, Y., Tang, J., Jiang, C., Zhu, L., Lehtomäki, M., Kaartinen, H., Kajaluoto, R., Wang, Y., Hyypä, J., Hyypä, H., Zhou, H., Pei, L., & Chen, R. (2018). The accuracy comparison of three simultaneous localization and mapping (SLAM)-based indoor mapping technologies. *Sensors (Switzerland)*, 18(10). <https://doi.org/10.3390/s18103228>
- Hyypä, E., Yu, X., Kaartinen, H., Hakala, T., Kukko, A., Vastaranta, M., & Hyypä, J. (2020). Comparison of backpack, handheld, under-canopy UAV, and above-canopy UAV laser scanning for field reference data collection in boreal forests. *Remote Sensing*, 12(20), 1–31. <https://doi.org/10.3390/rs12203327>
- James, M. R., & Quinton, J. N. (2014). Ultra-rapid topographic surveying for complex environments: The handheld mobile laser scanner (HMLS). *Earth Surface Processes and Landforms*, 39(1), 138–142. <https://doi.org/10.1002/esp.3489>
- Keefe, R. F., Wempe, A. M., Becker, R. M., Zimelman, E. G., Nagler, E. S., Gilbert, S. L., & Caudill, C. C. (2019). Positioning methods and the use of location and activity data in forests. V *Forests* (Roč. 10, Číslo 5, s. 458). MDPI AG. <https://doi.org/10.3390/f10050458>
- Koreň, M. (2019). *DendroCloud User Guide: Version 1.49*. gis.tuzvo.sk/dendrocloud/download/dendrocloud_1_49.pdf
- Koreň, M., Mokroš, M., & Bucha, T. (2017). Accuracy of tree diameter estimation from terrestrial laser scanning by circle-fitting methods. *International Journal of Applied Earth Observation and Geoinformation*, 63(December), 122–128. <https://doi.org/10.1016/j.jag.2017.07.015>
- Nevalainen, P., Li, Q., Melkas, T., Riekk, K., Westerlund, T., & Heikkonen, J. (2020). Navigation and mapping in forest environment using sparse point clouds. *Remote Sensing*, 12(24), 1–19. <https://doi.org/10.3390/rs12244088>
- Ryding, J., Williams, E., Smith, M. J., & Eichhorn, M. P. (2015). Assessing handheld mobile laser scanners for forest surveys. *Remote Sensing*, 7(1), 1095–1111. <https://doi.org/10.3390/rs70101095>

Effect of airborne laser scanning pulse density on accuracy in quantifying forest structure using an unmanned aerial vehicle.

Matthew J. Sumnall¹, Timothy J. Albaugh¹, David R. Carter¹, Rachel L. Cook², Cully Hession³, Otávio C. Campoe⁴, Rafael A. Rubilar⁵, Randolph H. Wynne¹ and Valerie A. Thomas¹.

¹ Virginia Polytechnic Institute and State University, Department of Forest Resources and Environmental Conservation, 228 Cheatham Hall, Blacksburg, VA 24061, USA.

Email: msumnall@vt.edu; talbaugh@vt.edu; davidcarter@vt.edu; wynne@vt.edu; thomasv@vt.edu.

² North Carolina State University, Department of Forestry and Environmental Resources, 2800 Faucette (Campus Box 8008 Dr, Raleigh, NC 27695.

Email: rlcook@ncsu.edu

³ Virginia Polytechnic Institute and State University, Biological Systems Engineering Department, 204 Seitz Hall, Blacksburg, VA 24061, USA.

Email: chession@vt.edu

⁴ Universidade Federal de Lavras, Lavras, MG, BR.

Email: otavio.campoe@ufla.br

⁵ Cooperativa de Productividad Forestal. Departamento de Silvicultura, Facultad de Ciencias Forestales, Universidad de Concepción. Victoria 631, Casilla 160-C, Concepción, Chile.

Email: rafaelrubilar@udec.cl

1. Introduction

Accurate quantification of forest structure is required for a number of practical applications including management, environmental protection, fire behavior analysis, and carbon accounting. Stand structure is typically estimated through manual field measurement. This approach is often constrained by site accessibility, the availability of effective measurement techniques, management requirements and the cost of labor. The development and application of remote sensing technologies have opened new frontiers in terms of the scale of data acquisitions and the features that can be measured. In particular, airborne laser scanning (ALS) remote sensing for forestry operations has broadened forest mensuration capabilities. These tools are being integrated into the mensuration practices of forest industry but questions remain regarding the deployment and accuracy of ALS.

Recent improvements in technology have permitted the use of unmanned aerial vehicles (UAVs) as a viable remote sensing platform offering a combination of multi-temporal high-resolution data captured at a significantly lower survey cost (Rothmund et al., 2017), but often only at small scales. There is uncertainty that high pulse densities will yield better accuracy in the estimation of forest features. Jakubowski et al. (2013) state that metrics related to coverage (e.g. canopy cover) were more sensitive to low pulse densities (<20 pulses m⁻²) as opposed to metrics such as tree height, diameter at breast height, shrub height and total basal area which were relatively unaffected until pulse density reduced to below 1 pulse m⁻². Features of interest which are smaller than the plot-level, in particular individual trees, are subject to more uncertainty regarding a minimum required pulse density for the specific detection of that feature (e.g. Kamoske et al. 2019).

Various light penetration indices have been developed in order to estimate leaf area index (LAI) at the field plot level, generally defined as total one-sided leaf surface area per ground surface area (Chen and Black, 1992). By their nature, these approaches are highly dependent on the density and structure of vegetation in situ and a pulse density high enough to return data from the lower vertical strata of a forest plot is required to ensure accuracy. Additional uncertainty comes from transferring these approaches to different sites and ALS acquisitions.

There is a growing volume of research literature concerning the development of increasingly complex methods for the delineation of individual tree crowns (ITC). More recently, methods have been developed to delineate ITCs directly from ALS point cloud returns that could potentially improve delineations, as stated in Kaartinen et al. (2012) and Ferraz et al. (2016). Improving the accuracy of ITC delineations may be

possible with new methodologies that include higher pulse densities. Depending on which structural feature is being estimated, there are varying degrees of accuracy in their measurement.

The overall goal of this study was to evaluate the effects of a range of ALS pulse densities, from high (>300 pulses m⁻²) to low (0.25 pulses m⁻²), have on our ability to delineate individual trees and on the accuracy of individual tree estimates of top height and crown width, and plot-level LAI.

2. Data and Methods

Our study location was an 8-year-old experimental site with varying of individual tree and stand structures of loblolly pine (*Pinus taeda* L.) plantation forest in the North Carolina, USA (34°49'49.63"N, 78°35'18.52"W). The site contains different three planting densities (low, medium and high densities - 618, 1236 and 1854 trees per hectare, respectively), six genetics and two levels of silviculture. A total of 108 field experimental units were established with 63 trees in each (7 rows of 9 trees) (more details can be found in Yáñez et al. 2017). Field measurements for individual trees consisted of: (i) GPS locations; (ii) tree top height (measured via hypsometer); (iii) crown horizontal extent; and (iv) survival (in year 9). LAI measurements using a LI-COR LAI 2200 plant canopy analyzer (LI-COR, 2012).

Discrete return UAV ALS data was acquired in August 2017 to coincide with peak-leaf area conditions. A laser pulse density of >300 pulses m⁻² was acquired with up to two returns per laser pulse. Eight pulse densities were randomly subsampled for testing purposes, these were: 300, 100, 50, 10, 5, 1, 0.5 and 0.25 pulses m⁻².

Initial ITCs were delineated by implementing the method outlined in Li et al. (2012). This approach functions directly to the point-cloud. A number of modifications to this approach are proposed, which exploit 3D clustering and distance between clusters to refine the ITC classification. ITCs were then paired with the closest field tree via GPS coordinates, unless the distance was over 1 m. LAI was estimated using the above/below ratio index (ABRI) as described in Sumnall et al. (2021). In addition to a comparison of estimated versus field values, a (generalized) linear mixed-effects model approach was implemented in order to state if the difference between the estimates created is significant.

3. Results and Discussion

The success of the ITC method used in the current research is mainly dependent on stem density, in addition to ALS pulse density. Delineation accuracy, when stratifying for the three stem densities tested, was relatively consistent in terms of RMSE ($\pm 6\%$) for pulse densities above 5 pulses m⁻². The largest proportion of delineated ITCs that corresponded to field GPS coordinates were observed within plots that had the lowest stem density. Correct ITC delineations accounted for a mean of 85% for low-density, 70% for medium-density and 55% for high-density plots, as illustrated in Figure 1. No commission error was observed within the current research. From this, we conclude that some ITC objects represent a cluster of tree crowns.

For estimates of tree top height higher pulse densities (≥ 50 pulses m⁻²) are more accurate. Stratification of results by planting stem density showed differences in terms of root mean square error (RMSE), where high-density plots were the poorest. RMSE values ranged from of 0.48 to 1.25 m (300 pulses m⁻²) to 1.74 to 1.85 m (0.25 pulses m⁻²).

The accuracy of crown diameter estimates decreases relative to decreases in ALS pulse density. RMSE values ranged from of 0.98 to 1.78 m (300 pulses m⁻²) to 2.11 to 3.29 m (0.25 pulses m⁻²). For pulse density greater than or equal to 50 pulses m⁻², RMSE for all stem densities tested was relatively consistent (± 0.2 m) when stratifying by the three stem densities.

The correspondence between ALS estimates and field measured LAI was relatively similar across all pulse densities above 1 pulses m⁻². RMSE varied from 0.78 to 1.11. These RMSE values were higher to those reported in Sumnall et al. (2021). We must assume this increase in uncertainty was related to the method of acquisition. The indirect nature of the field measurement represents an additional source of uncertainty.

When considering the comparison of pulse density results, only comparisons between higher pulse densities (between 300 and 50 pulses m⁻²) resulted in statistical difference ($p > 0.05$) for all metrics estimated. The implication of which is that features may or may not be present at different pulse densities.

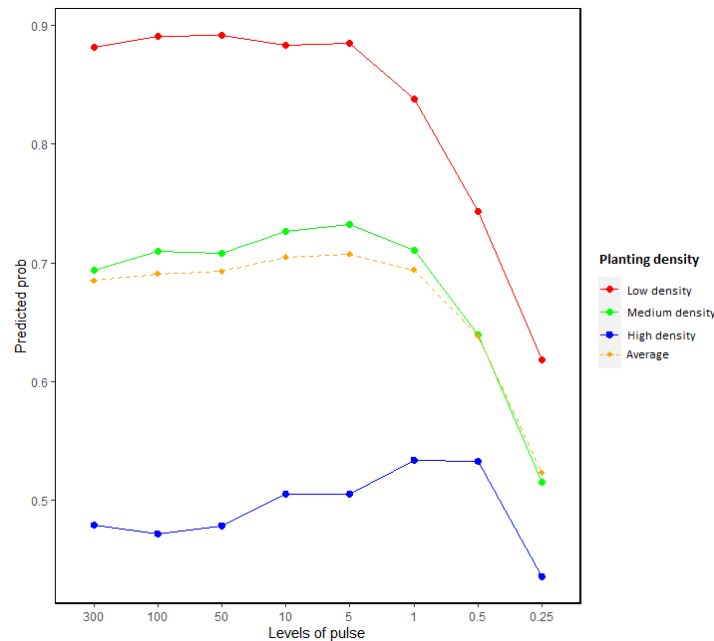


Figure 1: The detection probability of individual tree crowns relative to pulse density, stratified by stem density (low = 618 trees per hectare (TPH), medium = 1236 TPH, high =1854 TPH).

4. Conclusions

The tradeoff of data quality and coverage against cost when planning new ALS acquisitions is a critical one for forest managers. For the plot scale estimates of LAI, estimate accuracy was relatively consistent, and only decreased at low pulse densities (≤ 5 pulses m⁻²) as observed in other research (e.g. Kamoske et al., 2019 and Shao et al., 2019). When considering the ITC-scale, however, estimates appeared to be more sensitive to pulse density. Where higher pulse densities produced the highest accuracy (i.e. lowest RMSE). This implies that the size of the object being studied is an important consideration when designing an ALS acquisition with regards to pulse density. One of the main limitations of the method outlined in the current research is the success of the ITC delineation. In all cases, 100% of the stems in a plot were not located correctly in the current study, implying that some of the ITC delineations were clusters of crowns.

6. Acknowledgements

This work was funded by the Forest Productivity Cooperative.

References

Ferraz, A., Saatchi, S., Mallet, C. and Meyer, V., 2016. Lidar detection of individual tree size in tropical forests. *Remote Sensing of Environment*, Vol. 183, p.318-333.

Jakubowski, M.K., Guo, Q. and Kelly, M., 2013a. Tradeoffs between lidar pulse density and forest measurement accuracy. *Remote Sensing of Environment*, Vol. 130, p.245-253.

Kaartinen, H., Hyypä, J., Yu, X. W., Vastaranta, M., Hyypä, H., Kukko, A., Holopainen, M., Heipke, C., Hirschmugl, M., Morsdorf, F., Naesset, E., Pitkanen, J., Popescu, S., Solberg, S., Wolf, B. M., and Wu, J. C., 2012. An international comparison of individual tree detection and extraction using airborne laser scanning. *Remote Sensing*, Vol. 4 (4), p. 950-974.

- Kamoske, A.G., Dahlin, K.M., Stark, S.C. and Serbin, S.P., 2019. Leaf area density from airborne lidar: Comparing sensors and resolutions in a temperate broadleaf forest ecosystem. *Forest Ecology and Management*, Vol. 433, p. 364–375.
- Shao, G., Stark, S.C., de Almeida, D.R. and Smith, M.N., 2019. Towards high throughput assessment of canopy dynamics: The estimation of leaf area structure in Amazonian forests with multitemporal multi-sensor airborne lidar. *Remote Sensing of Environment*, Vol. 221, p. 1–13.
- Sumnall, M.J., Trlica, A., Carter, D.R., Cook, R.L., Schulte, M.L., Campoe, O.C., Rubilar, R.A., Wynne, R.H. and Thomas, V.A., 2021. Estimating the overstory and understory vertical extents and their leaf area index in intensively managed loblolly pine (*Pinus taeda* L.) plantations using airborne laser scanning. *Remote Sensing of Environment*, Vol. 254, p.112250.

Occupation of Canopy Space in European Temperate Old-Growth Forest observed by TLS

K. Král¹, A. Missarov^{1,2}, M. Krůček¹, M. Petrov^{1,2}

¹The Silva Tarouca Research Institute, Department of Forest Ecology, Lidická 25/27, 602 00 Brno, Czech Republic
Email: kamil.kral@vukoz.cz, krucek.martin@gmail.com

²Mendel University in Brno, Faculty of Forestry and Wood Technology, Zemědělská 3, 613 00 Brno, Czech Republic
Email: azim.misarov@gmail.com, petrovichal@gmail.com

1. Introduction

Forests are intrinsically three-dimensional systems with complex vertical structure, much stronger than in any non-forest terrestrial ecosystem. Canopy disturbances, tree regeneration, tree growth and competition (especially aboveground competition for light) all take place in real 3D space. These processes cannot be explicitly represented and understood by two-dimensional forest census/stem-mapping, as different tree species can have different requirements and growth strategies (species traits) including significantly different crown sizes, shapes and plasticity (Krůček et al. 2019). Different species also often occupy the canopy space in different height-levels thus forming a species-specific and site-specific vertical canopy stratification.

While traditional tree census (Condit 1998) is still indispensable field-research approach, terrestrial laser scanning (TLS) can effectively provide its valuable superstructure and complement the tree base coordinates by real three-dimensional description of individual trees (Calders et al. 2018). Such data can be easily used for description and quantification of canopy space occupation and vertical canopy stratification (Hess et al. 2018), which is due to the historical lack of data for many natural forest types still unavailable or based on sparse and imprecise measurement techniques (Apostol et al. 2018).

Here we introduce computationally straightforward approach for description of canopy space occupancy and its vertical stratification at the stand level using TLS data. It has a potential to bring a new level of knowledge about occupation of the canopy space by different tree species and tree-individuals and to answer fundamental questions such as:

- i) What is actual canopy space occupation and its vertical distribution in various forest types?
- ii) What is the vertical hierarchy of species and how it varies with site conditions?
- iii) What is a frequency and magnitude of inter-specific and intra-specific crown-to-crown interactions and how it varies with changing observation scale?

2. Data and Methods

2.1 Study Sites and Data

On each of the three research plots several hectares of the stand have been scanned by terrestrial laser scanner Leica ScanStation P20. At each plot data from 1ha have been post-processed up-to tree segmentation using the 3DForest software (Trochta et al. 2017). The individual tree clouds have been linked to tree census data to get the record of tree status (live/dead, complete/fragmented), field-measured reference DBH and species. The three sites cover the altitudinal gradient from lowland floodplain forest (alluvial hardwood) of Ranšpurk (mean altitude of 153m) through sub-montane beech dominated Žofín forest (alt. 780m) to montane spruce-beech forest of Boubín (alt. 1095m). All research plots represent natural forests left to spontaneous development, the latter two are original forests with no or negligible historical direct human impact (Vrška and Adam 2009).

2.2 Methods

In the segmented point cloud the crowns of all individual trees of DBH \geq 10cm were automatically delineated in the 3DForest software. The canopy/crown point cloud was normalized into heights above the ground and voxelized in gradually increasing resolutions: 0.25m, 0.5m, 1m. Every voxel was

labelled as occupied if included at least one crown point. Along with that a unique tree ID was recorded for each occupied voxel. According to the tree ID the data from the tree census database were linked to individual occupied voxels, so we could analyse co-occupation of voxels by different trees, species, etc. All voxels occupied by individual trees were summed to provide canopy occupancy statistics (Table 1). For calculation of total percentage of occupied space the 2% of the highest filled voxels were omitted.

3. Results and Discussion

Volume (and share) of occupied canopy space naturally changes with the voxel size used. In alluvial floodplain forest it ranges from 4.7 m³ per m² for 0.25m voxel size to 14.6 m³ per m² for 1m voxel size (Table 1, Figure 1a). More enlightening thus might be relative comparison between different sites observed in the same resolution (Figure 1b,c,d). Somewhat surprisingly, total mean canopy volume in the Raňšpurk floodplain forest is quite the same as in the Žofín beech dominated forest - almost 9 m³ per m² for 0.5m voxel size (Table 1). However, as the aboveground canopy space in Žofín forest is occupied up to higher levels (up to 45m), relative mean occupation of canopy space there is lower than in Raňšpurk (Table 1, Figure 1). In other words, in the floodplain forest where tree heights can only exceptionally exceed 36m, similar total canopy volume is packed into a smaller space than in monodominant beech forest.

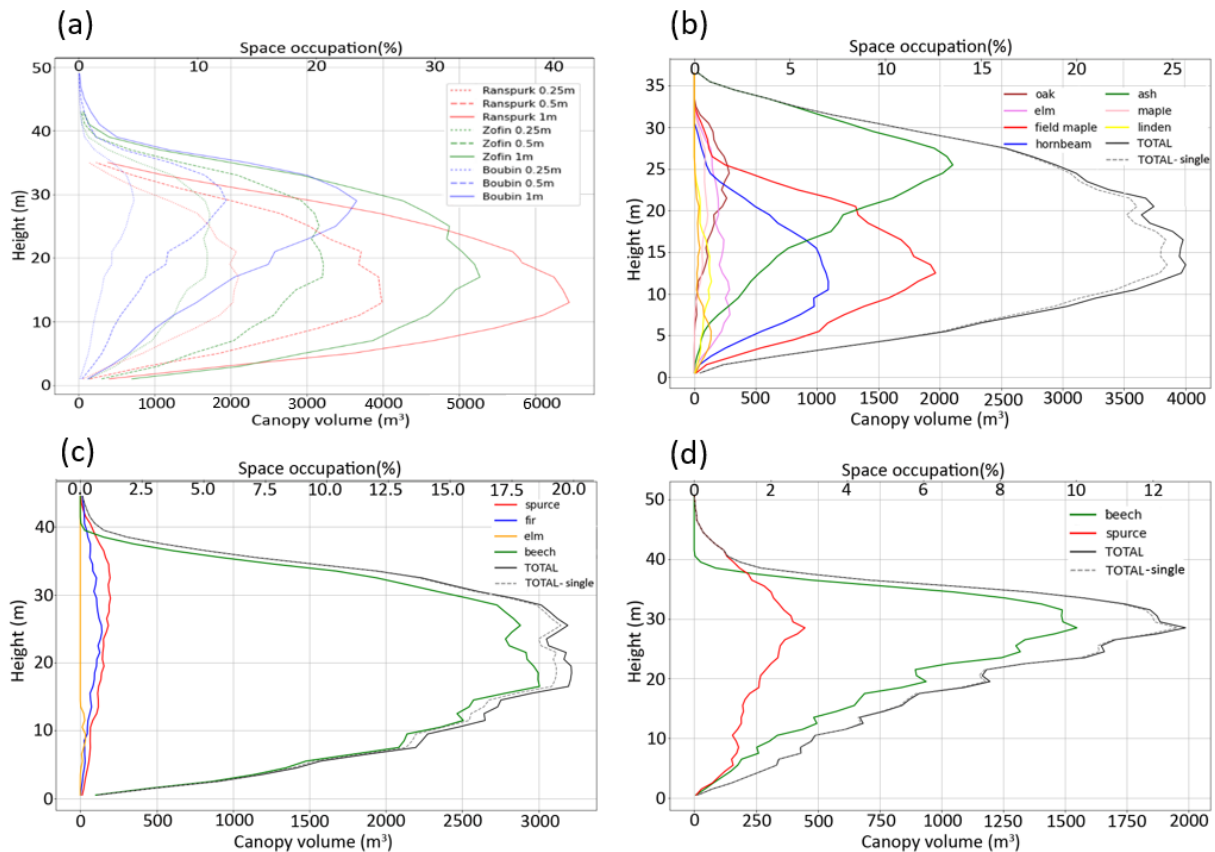


Figure 1: Comparison of vertical distribution of occupied canopy space in all three sites using different voxels sizes (a); and canopy space occupation by different tree species observed through 0.5m voxels in alluvial hardwood forest of Raňšpurk (b), beech dominated sub-montane Žofín forest (c) and montane spruce-beech Boubín forest (d).

Contrasting tree species richness of the two sites very likely plays an important role in this thanks to niche complementarity effect, leading to higher space occupation efficiency (Hess et al. 2018). While in Žofín about 90% of occupied forest canopy is formed by European beech, Raňšpurk forest canopy is composed of narrow-leaved ash (35%), field maple (34%), and hornbeam, accompanied by other four less common tree species (Figure 1b,c). Ash forms the upper canopy layer peaking in about 26m above ground, while field maple and hornbeam dominate in the lower canopy layer with the peak between 10

and 15m above the ground. All species together however form unimodal vertical canopy space occupation, not dissimilar to that of beech dominated Žofín forest.

Table 1. Canopy volume density and relative canopy space occupation observed at different scales (voxel sizes) in the three study sites.

Study Site	Canopy volume density (m ³ /m ²)			Space occupancy (%)		
	vox. 0.25m	vox. 0.5m	vox. 1m	vox. 0.25m	vox. 0.5m	vox. 1m
Ranšpurk	4.7	8.9	14.6	9.2	17.6	28.7
Žofín	4.6	8.8	14.5	7.7	14.8	24.4
Boubín	1.4	3.8	7.8	2.4	6.3	12.9

Effect of higher space occupation efficiency may be observed also at the fine scale of individual voxels. Canopy voxels of 0.25m size are in species rich floodplain forest co-occupied by more than one tree crown in 1.2% of cases, while in beech-dominated Žofín forest it's about 0.7% of cases.

Somewhat different picture may be observed in the spruce-beech montane forest of Boubín, where the canopy volume is formed of three-quarters of beech and one quarter of spruce, both peaking around 30m above the ground (Figure 1d). Spruce having long crowns spanning from few meters above the ground up to 51m. Although beech is about 10m shorter, it also fills mostly the upper half of the canopy space. Overall, the canopy volume is less than half of the two other sites (Table 1), due to several reasons as higher abundance of spruce, predominance of big trees with less understory, harsher climate and thinning effect of 2008 Emma wind disturbance.

4. Conclusions

Presented method provides direct quantitative and qualitative description of forest canopy occupancy and may be used as a standard approach for comparison of forest canopy in different forest types, species mixtures, management approaches and/or before/after silviculture measures or natural disturbances. Recent advances in processing drone lidar data (Krůček et al. 2020) promise possible up-scaling of the approach beyond the level. On the contrary, when focused on individual trees, the approach may be used for unprecedented quantification of local “canopy niche” of particular trees/species and their canopy interactions.

Acknowledgements

The work was supported by the Inter-Action grant LTAUSA18200 of the Ministry of Education Youth and Sports of the Czech Republic.

References

- Apostol B, Chivulescu S, Ciceu A, Petrila M, Pascu I, Apostol E, Leca S, Lorent A, Tanase M, Badea O, 2018, Data collection methods for forest inventory: a comparison between an integrated conventional equipment and terrestrial laser scanning. *Annals of Forest Research* DOI:10.15287/afr.2018.1189
- Calders K, Origo N, Burt A, Disney M, Nightingale J, Raunonen P, Åkerblom M, Malhi Y, Lewis P, 2018, Realistic Forest Stand Reconstruction from Terrestrial LiDAR for Radiative Transfer Modelling. *Remote Sensing*, 10(6): 933; <https://doi.org/10.3390/rs10060933>.
- Condit RS, 1998, *Tropical Forest Census Plots*. Springer Berlin Heidelberg, D.
- Hess C, Härdtle W, Kunz M, Fichtner A, von Oheimb G, 2018, A high-resolution approach for the spatiotemporal analysis of forest canopy space using terrestrial laser scanning data. *Ecology and Evolution*, 8, 6800-6811.
- Krůček M, Trochta J, Cibulka M, Král K, 2019, Beyond the cones: How crown shape plasticity alters aboveground competition for space and light-Evidence from terrestrial laser scanning. *Agricultural and Forest Meteorology*, 264, 188-199.
- Krůček M, Král K, Cushman K, Missarov A, Kellner JR, 2020, Supervised Segmentation of Ultra-High-Density Drone Lidar for Large-Area Mapping of Individual Trees. *Remote Sensing*, 12, 3260.
- Trochta J, Krůček M, Vrška T, Král K, 2017, 3D Forest: An application for descriptions of three-dimensional forest structures using terrestrial LiDAR. *PLoS one*, 12 (5): e0176871.
- Vrška T and Adam D, 2009, Important localities of natural forests. In: Hrnčiarová T and Mackovčín P, (eds), *Atlas of the Landscape of the Czech Republic*, Czech Ministry of Environment and The Silva Tarouca Research Institute, Praha–Průhonice, p 352. ISBN 978-80-85116-59-5.

Global Ecosystem Dynamics Investigation data enable structural patterns assessment in Amazon rainforest

A. S. S. Ribeiro¹, B. A. F. de Mendonça², C. H. Amaral¹

¹Universidade Federal de Viçosa, Departamento de Engenharia Florestal, 36570-900 MG, Brazil
Email: acaua.ribeiro@ufv.br; chamaral@ufv.br

²Universidade Federal Rural do Rio de Janeiro, Departamento de Silvicultura, 23890-000 RJ, Brazil
Email: brunoafmendonca@gmail.com

1. Introduction

The Amazon rainforest is the most extensive tropical forest in the world and also the most biodiverse (Ter Steege et al. 2013). However, maintaining this biodiversity has been a challenge due to the rising deforestation, predatory exploitation and forest fires, which lead to the loss of ecosystems (Silva Júnior et al. 2020). Thus, efforts have been made by researchers in the search for new forms of sustainable use and monitoring of forest resources (e.g., Paiva et al. 2020).

The Global Ecosystem Dynamics Investigation (GEDI) mission aims to providing high-quality measurements of the vertical structure of tropical and temperate forests around the globe through a huge variety of products, including canopy height, canopy coverage and vertical profile, leaf area index (LAI), topography and biomass (Dubayah et al., 2020). These freely-available data might aid activities on sustainable forest management, such as land cover and use dynamics, distinction of vegetation types and definition of permanent preservation areas. Even though there are other Lidar missions (e.g., ICESat Geoscience Laser Altimeter System), GEDI is the first orbital system primarily designed for structural characterization of forests, with technical features for accurately measuring those with dense and continuous upper canopies, like the Amazon rainforest. Thus, we here aim to explore GEDI data to assess forest structural patterns at National Forest of Purus (NFP), southwestern Amazon, in order to test whether GEDI metrics are a powerful dataset to support actions of sustainable use and conservation.

2. Data and Methods

2.1. Study Area

Our study has been carried out in the National Forest of Purus (NFP), a conservation national park for sustainable use, which stands out for its 256,000 ha of highly conserved tropical forest in the southwestern Amazon (Figure 1).

2.2. Geo-environments mapping

We used as an initial basis the NFP geo-environments units that were manually mapped and characterized by Brandão et al. (2010). First, we map them and other land use and cover features with aid of machine learning algorithm by using the following covariates: nine surface reflectance images from the Sentinel 2A Multi Spectral Instrument visible to shortwave infrared bands (with 20 m spatial-resolution) from 08/15/2019, the calculated Normalized Difference Vegetation Index (NDVI; 20 m), and a surface elevation grid from the Shuttle Radar Topography Mission (SRTM; 30 m). Samples for model training and validation were manually collected for each class, totaling 549 polygons and 9,225 pixels. The following geo-environmental units were identified in the study site: i) Dissected Plateaus with Terra-firme Forest over Latosols and Argisols (DP); ii) Slopes and Ramps with Forests over Argisols (SR); iii) Alluvial Plains with Fluvial Neossols and Gleysols (AP); iv) Anthropized areas with traditional land use; v) River beaches; and vi) Water bodies. The Random Forest algorithm was used to perform the geo-environments mapping using 70% of the samples for training and the remaining (30%) for model validation following Fernandes Filho (2019).

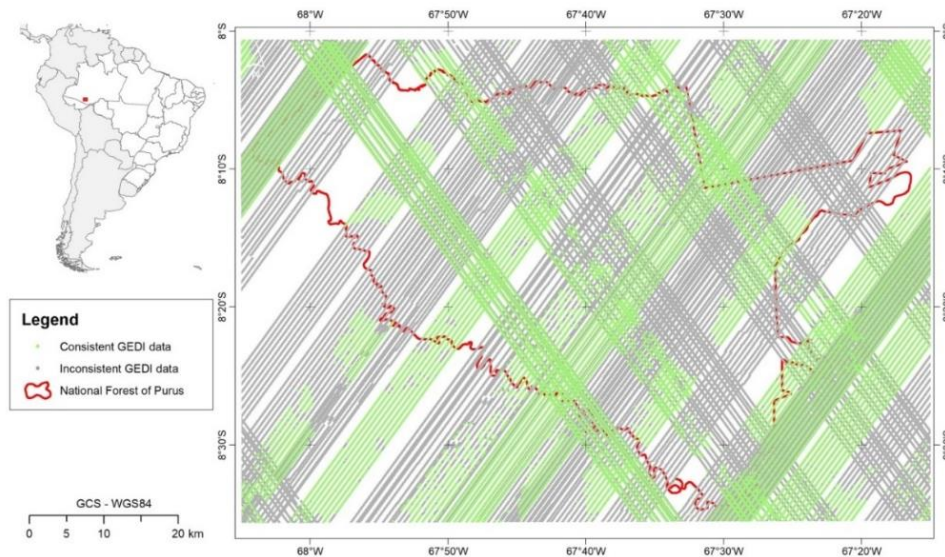


Figure 1: Location of the National Forest of Purus (NFP) in southwestern Amazon and coverage of GEDI data in the NFP and surroundings. In green is the used high-quality GEDI dataset.

2.3. GEDI data acquisition and processing

We obtained the GEDI data from the NASA Earth Data collection and processed the level 2B products through the rGEDI package (Silva et al. 2019). Firstly, a selection of the consistent data was carried out by using the data quality indicator (i.e., $quality_flag = 1$). They totalled 141,560 points at the end of processing, which corresponds to 27% of the total data covering the study area up to 08/31/2020 (Figure 1). The GEDI metrics obtained and evaluated in this study were the Canopy height – $rh98$ (meters) and the Plant Area Index – PAI (unitless). Those metrics were extracted from each footprint (point) for each mapped geo-environment (DP: 67,248 points; SR: 49,939 points; AP: 24,373 points). To test the hypothesis that the GEDI metrics are effective for distinguishing the forest structure, they were analyzed for the entire database and by geo-environment. In this sense, the Skewness normality test was conducted to verify the distribution of the data and the identity of the different population's distribution function was tested through the Kruskal-Wallis test ($\alpha = 0.05$) and the Dunn's post-hoc test.

3. Results and Discussion

DP showed the highest PAI median value (i.e., $PAI = 3.19$), followed by SR (3.01) and AP (2.23), with significant differences between the three geo-environments (Figure 2). This result reveals the potential of GEDI-based PAI data to distinguish Amazonian “Terra Firme” (on DP, and SR) from lowland (AP) forests structurally. Canopy height is also a good parameter to discriminate those forests, while AP forests presented a median height of 22.37 m, SR and DP forests stood out for heights of 23.78 and 24.02 m respectively.

Our results indicate an important application of GEDI data for mapping forest structure and diversity across the landscape, as they corroborate previous studies in the Amazon region. Some of them demonstrate variations in the structure and biomass of upland and lowland forests in the Amazon (e.g., Aldana et al., 2017; Bredin et al., 2020). Significant differences in the field-based height of these two forest types was found by Bredin et al. (2020) in the region of the Juruá river. They found taller forests on the upland than on the floodplain. The same was found by Hill et al. (2011) in the Peruvian Amazon from airborne lidar-based estimation. On the other hand, Aldana et al., (2017) found a greater amount of biomass in the floodplain areas in relation to the Terra Firme forests, this difference being related to the greater fertility of the soils in the floodplains. Further studies exploring the GEDI waveforms and other metrics, in addition to soil data, will allow us to better find and understand structural patterns across the studied Amazonian forest, supporting actions for sustainable use and conservation.

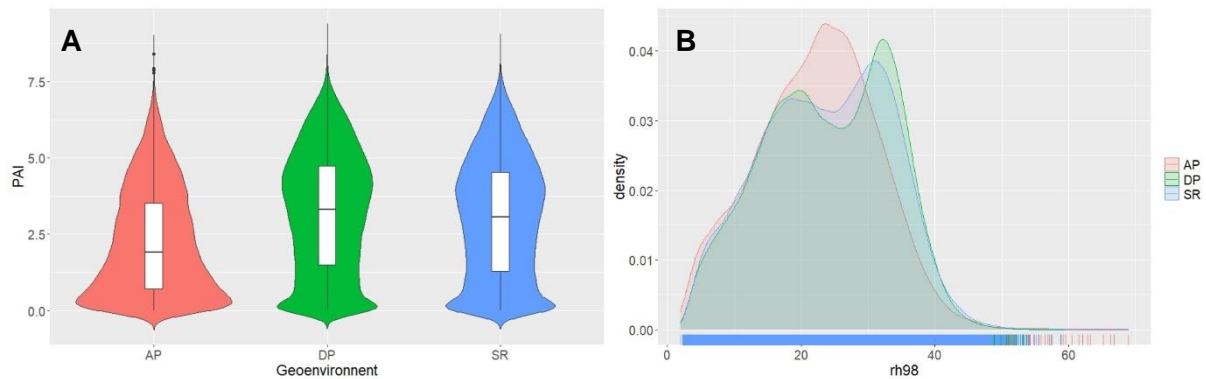


Figure 2: Violin plot of the Plant Area Index - PAI (A) and density plot of the height estimates - rh98 (B) from the forests on Alluvial Plains (AP), Dissected Plateaus (DP), and on Slopes and Ramps (SR).

4. Conclusions

The GEDI data applied to the mapped geo-environmental units showed significant differences between forests that occur in different portions of the terrain by structurally segregating upland from lowland forests mainly. GEDI proved to be a useful tool for assessing the structure of different Amazonian forests and supporting their sustainable use and conservation.

References

- Aldana AM, Villanueva B, Cano Á, Correa DF, Umaña MN, Casas LF, ... and Stevenson PR, 2017, Drivers of biomass stocks in Northwestern South American forests: Contributing new information on the Neotropics. *Forest Ecology and Management*, 389: 86–95.
- Brandão PC, Soares VP, Simas FNB, Schaefer CEGR, Souza AL, Mendonça BAF, 2010, Caracterização de geoambientes da floresta nacional do Purus, Amazônia Ocidental: uma contribuição ao plano de manejo. *Revista Árvore*, 34(1): 115-126.
- Bredin YK, Hawes JE, Peres CA and Hugaasen T, 2020, Structure and Composition of Terra Firme and Seasonally Flooded Várzea Forests in the Western Brazilian Amazon. *Forests*, 11(12): 1361.
- Dubayah R, Blair JB, Goetz S, Fatoyinbo L, Hansen M, Healey S, ... and Silva C, 2020, The Global Ecosystem Dynamics Investigation: High-resolution laser ranging of the Earth's forests and topography. *Science of Remote Sensing*, 100002.
- Fernandes Filho EI, 2019, *labgeo*: Collection of Functions to Fit Models with Emphasis in Land Use and Soil Mapping. R Package Version 0.3.9.3. Available at: <https://github.com/elpidiofilho/labgeo> (accessed on 11 Jan 2021).
- Paiva PFPR, de Lourdes Pinheiro Ruivo M, da Silva Júnior OM, de Nazaré Martins Maciel M, Braga TGM, de Andrade MMN, ... and Ferreira BM, 2020, Deforestation in protect areas in the Amazon: a threat to biodiversity. *Biodiversity and Conservation*, 29: 19-38.
- Silva CA, Hamamura C, Valbuena R, Hancock S, Cardil A, Broadbent EN, Almeida DRA, Silva Junior CHL, Klauberg C, 2019, *rGEDI*: NASA's Global Ecosystem Dynamics Investigation (GEDI) Data Visualization and Processing. version 0.1.9. Available at: <https://CRAN.R-project.org/package=rGEDI> (accessed on 5 Jan 2021).
- Silva Junior CHS, Aragão LE, Anderson LO, Fonseca MG, Shimabukuro YE, Vancutsem C, Achard F, Beuchle R, Numata I, Silva CA, Maeda EE, Longo M, Saatchi SS, 2020, Persistent collapse of biomass in Amazonian forest edges following deforestation leads to unaccounted carbon losses. *Science advances*, 6(40): eaaz8360.
- Ter Steege H, Pitman NCA, Sabatier D, Baraloto C, Salomão RP, Guevara JE, Phillips OL, Castilho CV, Magnusson WE, Molino JF, ... and Silman MR, 2013, Hyperdominance in the Amazonian Tree Flora. *Science*, 342(6152): 1243092.
- Hill RA, Boyd DS and Hopkinson C, 2011, Relationship between canopy height and Landsat ETM+ response in lowland Amazonian rainforest. *Remote Sensing Letters*, 2(3): 203-212.

Estimating total fuel load in tropical savanna using NASA's GEDI spaceborne lidar and machine learning

Rodrigo Vieira Leite¹, Carlos Alberto Silva², Eben North Broadbent³, Cibele Hummel do Amaral¹, Veraldo Liesenberg⁴, Danilo Roberti Alves de Almeida⁵, Midhun Mohan⁶, Sérgio Godinho^{7,8}, Adrian Cardil^{9,10,11}, Caio Hamamura¹², Bruno Lopes de Faria¹³, Pedro H. S. Brancalion⁵, André Hirsch¹⁴, Gustavo Eduardo Marcatti¹⁴, Ana Paula Dalla Corte¹⁵, Angelica Maria Almeyda Zambrano¹⁶, Máira Beatriz Teixeira da Costa¹⁷, Eraldo Aparecido Trondoli Matricardi¹⁷, Anne Laura da Silva¹⁴, Lucas Ruggeri Ré Y Goya¹⁴, Ruben Valbuena¹⁸, Bruno Araujo Furtado de Mendonça¹⁹, Celso H. L. Silva Junior^{20,21}, Luiz E. O. C. Aragão^{20,22}, Mariano García²³, Jingjing Liang²⁴, Trina Merrick^{25,26}, Andrew T. Hudak²⁷, Jingfeng Xiao²⁸, Steven Hancock²⁹, Sassan Saatchi³⁰, Carine Klauberg¹⁵

¹Department of Forest Engineering, Federal University of Viçosa (UFV), Av. Peter Henry Rolfs, 36570-900, Viçosa, MG, Brazil; {rodrigo.leite; chamara} @ufv.br

²School of Forest, Fisheries, and Geomatics Sciences, University of Florida, University of Florida, PO Box 110410 Gainesville, FL 32611; c.silva@ufl.edu

³Spatial Ecology and Conservation (SPEC) Lab, School of Forest, Fisheries, and Geomatics Sciences, University of Florida, Gainesville, FL 32611 USA; eben@ufl.edu

⁴Department of Forest Engineering, College of Agriculture and Veterinary, Santa Catarina State University (UDESC), Lages, SC, Brazil; veraldo.liesenberg@udesc.br

⁵Department of Forest Sciences, "Luiz de Queiroz" College of Agriculture, University of São Paulo (USP/ESALQ), Piracicaba, SP, Brazil; {danieloraa; pedrob} @usp.br

⁶Department of Geography, University of California—Berkeley, Berkeley, CA 94709, USA; mid_mohan@berkeley.edu

⁷EaRSLab—Earth Remote Sensing Laboratory, University of Évora, 7000-671 Évora, Portugal

⁸Institute of Earth Sciences (ICT), Universidade de Évora, Rua Romão Ramalho, 59, 7002-554, Évora, Portugal; sgodinho@uevora.pt

⁹Technosylva Inc, La Jolla, CA, USA, adriancardil@gmail.com

¹⁰Department of Crop and Forest Sciences, University of Lleida, Lleida, Spain

¹¹Joint Research Unit CTFC - AGROTECNIO, Solsona, Spain

¹²Federal Institute of Education, Science and Technology of São Paulo, SP, 11533-160, Brazil; hamamura.caio@ifsp.edu.br

¹³Department of Forest Science, Federal University of Vales do Jequitinhonha e Mucuri, (UFVJM) Campus JK, Diamantina, MG, Brazil, blfaria@gmail.com

¹⁴Federal University of São João Del Rei – UFSJ, Sete Lagoas, MG, Brazil, 35701-970; {gustavomarcatti, hirsch_andre} @ufsj.edu.br; {annelsilva11, lucasgoya42.lr} @gmail.com; carine_klauberg@hotmail.com

¹⁵Department of Forest Engineering, Federal University of Paraná (UFPR), Curitiba, PR, Brazil, 80.210-130; anacorte@ufpr.br

¹⁶Spatial Ecology and Conservation (SPEC) Lab, Center for Latin American Studies, University of Florida, Gainesville, FL 32611 USA; aalmeyda@ufl.edu

¹⁷Department of Forestry, University of Brasília, Campus Darcy Ribeiro, Brasília, DF, Brazil - 70.910-900; mairabeatrizteixeira@hotmail.com; ematricardi@gmail.com

¹⁸School of Natural Sciences, Bangor University, Bangor LL57 2W, UK. r.valbuena@bangor.ac.uk

¹⁹Silviculture Department, Universidade Federal Rural do Rio de Janeiro, Rua da Floresta, Seropédica, RJ, 23897-005, Brazil; brunomendonca@ufrj.br

²⁰National Institute for Space Research, Earth Observation and Geoinformatics Division, Av. dos Astronautas, 1758, São José dos Campos SP 12227-010, Brazil, celsohlsj@gmail.com, luiz.aragao@inpe.br

²¹Universidade Estadual do Maranhão (UEMA), Departamento de Engenharia Agrícola, São Luís, MA, 65055-310, Brazil

²²College of Life and Environmental Sciences, University of Exeter, Exeter, UK

²³Environmental Remote Sensing Research Group, Department of Geology, Geography and the Environment, Universidad de Alcalá, Calle Colegios 2, Alcalá de Henares, 28801, Spain. mariano.garcia@uah.es

²⁴Department of Forestry and Natural Resources, Purdue University, West Lafayette, IN, USA, alpenbering@gmail.com

²⁵Department of Earth and Environmental Science, Vanderbilt University, Nashville, TN 37240, USA

²⁶Department of Geography, Florida State University, Tallahassee, FL, USA. tmerrick@fsu.edu

²⁷US Department of Agriculture, Forest Service, Rocky Mountain Research Station, 1221 South Main Street, Moscow, ID 83843, USA, andrew.hudak@usda.gov

²⁸Earth Systems Research Center, Institute for the Study of Earth, Oceans, and Space, University of New Hampshire, Durham, NH 03820, USA. j.xiao@unh.edu

²⁹School of GeoSciences, University of Edinburgh, United Kingdom of Great Britain and Northern Ireland. steven.hancock@ed.ac.uk

³⁰NASA-Jet Propulsion Laboratory, California Institute of Technology, Pasadena, CA 91109, USA sasan.s.saatchi@jpl.nasa.gov

1. Introduction

The understanding of wildfire dynamics is important to mitigate climate change and guide conservation practices in several ecosystems in the world. Savannas are generally fire-adapted but human activities have affected fire regimes and the landscape characteristics (Bowman et al. 2013). Presently, the most flora-rich savanna in the world, the Brazilian Cerrado, has also experienced those effects (Schmidt et al., 2018).

One of the main factors affecting fire is the amount of biomass available for burning, defined as fuel load. Remote sensing technologies are used for local scale fuel load mapping mainly using airborne lidar data (Gajardo et al. 2014). However, for large scale fuel load mapping spaceborne data is required. The recently launched spaceborne lidar sensor GEDI (Global Ecosystem Dynamics Investigation, Dubayah et al. 2020) holds potential to meet this demand. GEDI was developed to penetrate forests with about 95-98% (daytime and night-time measurements, respectively) of canopy cover to efficiently retrieve the vegetation vertical structure. Nonetheless, GEDI potential for fuel load estimation has not been broadly investigated yet.

In this study, we developed a methodological approach using GEDI and field data to train a Random Forest (RF) algorithm to estimate fuel load in the Cerrado biome. Our approach allowed us to quantify the fuel load of several types of vegetation in the study area.

2. Data and Methods

We established 50 sample plots of 900 m² in four Cerrado conservation sites. In the field, we collected fuel loads of different vegetation layers including surface, herbaceous, shrubs, and woody layers. The study sites were surveyed with the GatorEye Gen 1 UAV system (Broadbent et al. 2021) with a dual-return lidar to obtain the high-density point clouds. The UAV-lidar 3D point cloud was used to build GEDI-like waveforms using the GEDI simulator (Hancock et al. 2019, Silva et al. 2020) that is able to reproduce the on-orbit GEDI data characteristics. We calculated waveform metrics of relative height at the 98th percentile (m), canopy cover fraction (%), plant area index and foliage height diversity using the rGEDI package (Silva et al. 2020). The metrics were used to train a RF algorithm with the total field-measured fuel load (*TFL*) as the response variable. The model's performance was assessed in a 5-fold cross-validation using the coefficient of determination (R^2), absolute (Mg ha⁻¹) and relative (%) root square mean error (RMSE) and mean difference (MD). Finally, we applied the model to the on-orbit GEDI footprints over the Cerrado biome and aggregated the estimations into 1-km grid cells.

3. Results and Discussion

The RF had a relatively good performance to estimate *TFL* with $R^2 = 0.71$, RMSE = 23.01 Mg ha⁻¹, RMSE (%) = 40.78, MD = 0.22 Mg ha⁻¹ and MD (%) = 2.09. This performance is related to the GEDI's potential of better obtaining vegetation structure over previous spaceborne lidar missions. Part of the uncertainty may be due to the inclusion of near-surface vegetation layers, such as herbaceous and ground fuels, that are commonly not considered but represent an important fuel component. The GEDI footprint density varied for different Cerrado regions for which the models were applied to map the total fuel load (Figure 1). Most of the data gaps are expected to be filled with upcoming data releases. Alternatively, data fusion with other spaceborne sensors can be used to derive wall-to-wall maps and or improve spatial resolution of the fuel load map. The presented framework represents a key point for advancing the understanding of fuel load accumulation over large areas and its effects on ecosystem functioning and carbon emissions. This is especially important in Cerrado where integrated fire management solutions that depend on large-scale fuel load characterization are taking place to preserve fire history and biodiversity (Schmidt et al., 2018).

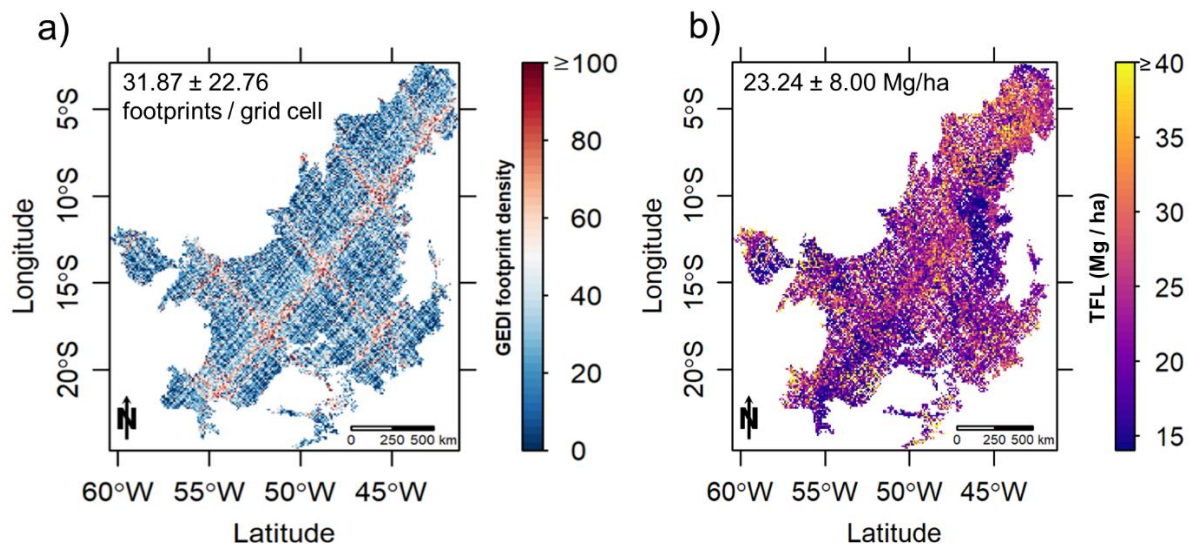


Figure 1. GEDI footprint density (a) and total fuel load (*TFL*) estimates (b) at 1km grid cells for the entire Cerrado biome. Values within plots represent mean \pm standard-deviation of *TFL* estimates and GEDI footprints in (a) and (b), respectively.

4. Conclusion

We evaluated the potential of using GEDI data to estimate total fuel load in the Cerrado biome. Our methodological approach based on GEDI footprints showed relatively high accuracy to estimate total fuel load in the study area. Our modeling approach is an advance for large-scale fuel load mapping in the Cerrado biome and it shows potential to be applied to other fire-prone ecosystems worldwide.

Acknowledgements

This project was supported by the Brazilian National Council for Scientific and Technological Development (CNPq, grant 442640/2018-8, CNPq/Prevfogo-Ibama N° 33/2018). R.V.L. was supported by CAPES (#88887.463733/2019-00).

References

- Bowman, D. M., O'Brien, J. A., & Goldammer, J. G. (2013). Pyrogeography and the global quest for sustainable fire management. *Annual Review of Environment and Resources*, 38, 57-80. <https://doi.org/10.1146/annurev-environ-082212-134049>
- Broadbent, E. N., Zambrano, AM. A., Omans, G., Adler, A., Alonso, P., Naylor, D., Chenevert, G., Murtha, T., Vogel, J., Almeida, D. R. A., Dalla Corte, A. P., Silva, C. A., Prata, G. A., Merrick, T., D'Oliveira, M. V. N., Detto, M., Ferreira, MP., Wilkinson, B. E., Ferreira, M.E., Muller-Landau, H. C. (2021). In prep. The GatorEye Unmanned Flying Laboratory: sensor fusion for 4D ecological analysis through custom hardware and algorithm integration, accessed May 23 2021. Retrieved from <http://www.gatoreye.org>
- Hancock, S., Armston, J., Hofton, M., Sun, X., Tang, H., Duncanson, L. I., Dubayah, R. (2019). The GEDI simulator: A large-footprint waveform lidar simulator for calibration and validation of spaceborne missions. *Earth and Space Science*, 6(2), 294-310. <https://doi.org/10.1029/2018EA000506>
- Silva, C. A., Hamamura, C., Valbuena, R., Hancock, S., Cardil, A., Broadbent, E. N., Almeida, D. R. A., Silva Junior, C. H. L., Klauber, C. (2020). rGEDI: NASA's Global Ecosystem Dynamics Investigation (GEDI) Data Visualization and Processing. version 0.1.8, accessed on May 23 2021, available at: <https://CRAN.R-project.org/package=rGEDI>
- Schmidt, I. B., Moura, L. C., Ferreira, M. C., Eloy, L., Sampaio, A. B., Dias, P. A., & Berlinck, C. N. (2018). Fire management in the Brazilian savanna: First steps and the way forward. *Journal of applied ecology*, 55(5), 2094-2101. <https://doi.org/10.1111/1365-2664.13118>
- Dubayah, R., Blair, J. B., Goetz, S., Fatoyinbo, L., Hansen, M., Healey, S., Hofton, M., Hurtt, G., Kellner, J., Luthcke, S., Armston, J., Tang, H., Duncanson, L., Hancock, S., Jantz, P., Marselis, S., Patterson, P. L., Qi, W., Silva, C. (2020a). The Global Ecosystem Dynamics Investigation: High-resolution laser ranging of the Earth's forests and topography. *Science of Remote Sensing*, 1, 100002. <https://doi.org/10.1016/j.srs.2020.100002>

Drone LiDAR for mistletoe recognition and monitoring

A. Missarov^{1,2}, Y. Krasylenko³, M. Krůček¹, M. Slavik⁴, B. Nutfullin⁵, K. Král¹

¹Department of Forest Ecology, The Silva Tarouca Research Institute, Lidická 25/27, 602 00 Brno, Czech Republic
Emails: kamil.kral@vukoz.cz, krucek.martin@gmail.com

²Faculty of Forestry and Wood Technology, Mendel University in Brno, Zemědělská 3, 613 00 Brno, Czech Republic
Email: azim.misarov@gmail.com, petrovnichal@gmail.com

³Department of Cell Biology, Centre of the Region Haná for Biotechnological and Agricultural Research, Faculty of Science, Palacký University Olomouc, Šlechtitelů, 27, 78371, Olomouc, Czech Republic
E-mail: j_krasylenko@ukr.net

⁴Department of Forest Management, Czech University of Life Sciences Prague, Kamýčká 129, 165 00 Praha - Suchbátka, Czech Republic
E-mail: mslavik@fd.czu.cz

⁵Faculty of Computational Mathematics and Cybernetics, Lomonosov Moscow State University, Leninskiye Gory, 119991 Moscow, Russian Federation
E-mail: bulat15g@gmail.com

1. Introduction

Within the last decade the rapidly developing technologies such as laser scanning, so called Light Detection and Ranging (LiDAR), remote sensing, and machine learning have tremendously changed the face of forest ecology. Laser scanning provides the spatial overview and the precise three-dimensional object description (Wehr et al., 1999), while remote sensing collects large volumes of environmental data, including those from the inaccessible habitats (Pajares et al., 2015). Finally, machine learning allows the data to be processed at a deeper level (Jordan et al., 2015).

The recognition and monitoring of small- and medium-size tree-related microhabitats (TrMs) inhabited by fungi, mosses, ivies, mistletoes, etc. (Frey et al., 2020) are important, since they are well-recognized indicators of tree and whole-forest health. Moreover, TrMs supports the diversity of insects, birds, animals and plants, including mistletoes, in forest ecosystems. Mistletoes are taxonomically diverse group of aerial hemiparasitic plants from the Loranthaceae, Viscaceae, Santalaceae, Amphorogynaceae, and Misodendraceae families (order Santalales), attaching to their hosts by root-like structure called the haustorium and being largely dependent on water and nutrient supply from the hosts (Nickrent et al., 2010). There are two main mistletoe species in the Czech Republic – deciduous yellow-berried mistletoe (*Loranthus europaeus* Jacq.; Loranthaceae) parasitizing mostly European oak (*Quercus robur* L.) hosts and rarely other trees (Danilhelka et al., 2012; Krasylenko et al., 2019), and the ever-green European mistletoe (*Viscum album* L.; Santalaceae) with three subspecies – *V. album* sbsp. *album* with the broad host preferences, *V. album* sbsp. *austriacum* specialized on *Pinus*, and *V. album* sbsp. *abietis* parasitizing *Abies* (Wild et al., 2019).

The early forest remote studies were based on the terrestrial lidar scanning (TLS)-produced data, which are presented as dense and precise point clouds with the mm accuracy (Rehush et al., 2018). On the other hand, TLS requires a labor-intensive data acquisition and could be used only on the relatively small areas. The accuracy and density of TLS data decrease from bottom to the top (Dassot et al., 2011). Other approach, an unmanned laser scanning (ULS), as compared to TLS, is significantly more sparse and less accurate, but the maximum density and accuracy ULS achieves at the canopy level. The biggest advantage, however, is that ULS can provide the data sufficient for the detailed observations from the larger territory (Kellner et al., 2019; Krůček et al., 2020). In our studies we focus on mistletoe recognition. The population structure and spatial distribution of mistletoes on the host trees make them suitable objects for ULS. Furthermore, these parasitic plants are perennial, slowly growing and long-living (some *Viscum* specimens can exist for more than 30 years), being clearly visible by the naked eye in all seasons, and especially well-resolved in fall, winter and early spring.

2. Materials and Methods

2.1 Data collection and study sites

The data was collected using RiCOPTER, a remotely piloted airborne laser scanning system equipped with Riegel VUX1 UAV scanner (RIEGL, USA) at the altitude about 60 m above the ground. In March 2019 two flights with criss-cross flight directions were performed. The remote scanning covered the area of circa 20 ha located in the floodplain of the Morava and the Dyje Rivers. In its subsoil are the sediments of the Vienna Basin; above them are deposited fluvial gravels, on which sandy flood clays lie. The bottomland hardwood forest covers the largest area of the protected area. Dominant species are narrow-leaved ash (*Fraxinus angustifolia* Vahl.), field maple (*Acer campestre* L.), hornbeam (*Carpinus betulus* L), small-leaved linden (*Tilia cordata* Mill.), and European oak (*Q. robur*) (Janik et al., 2008).

More than twenty *Viscum* and *Loranthus*-colonized trees of different species were recorded during a field survey on the well-studied and documented part of Ranšpurk National Nature Reserve in South Moravian Region characterized by the predominance of *T.cordata* with a few *Q. robur* and *C. betulus* individuals. The precise GPS coordinates of each tree in the forest plots parasitized by mistletoes were juxtaposed with the point cloud.

2.2 Data processing

In the machine learning terms, the mistletoe detection belongs to the object classification issue. The whole plot space were divided by the big voxels (2 m*2 m*2 m) using the CloudCompare software (<https://www.danielgm.net/cc/>). Each voxel was classified as “with mistletoe” or “without mistletoe”. A key limitation for the machine learning methods efficiency is the training dataset range, since a larger dataset obviously means the higher accuracy of the prediction. To make is large enough, the data augmentation technique was used by adding the slightly modified copies of already existing data or newly created synthetic data based on the primary sample (Bohak et al., 2020). Point cloud segments with the mistletoes were cut into numerous voxels of the required sizes at various angles allowing them to intercept. The mistletoe-containing areas were cut in the way that the different training voxels had different spatial distribution of mistletoe inside different voxels. Moreover, noise, artificial branches and twigs were added to increase the training sample range to several hundreds items.

A few machine and deep learning models will be tested and compared basing on the mistletoe as the key organism in these studies. The conventional machine and deep learning approaches require different algorithms of the data pre-processing. The deep learning effectively uses the raw data, though Random Forest (RF) and Support Vector Machine (SVM) methods need more compact feature vectors (Breiman 2001). The large voxels will be divided into 125 smaller voxels, and for each of the sub-voxels the point density will be computed. Altogether, 125 values will form the feature vector. As part of the deep learning approach, two extra approaches will be tested: 2D- and 3D-trained convolutional neural networks (CNNs). For the volumetric pre-trained networks, the whole point cloud inscribed in the big voxel (Maturana et al., 2015) will be used, while for the flat pre-trained networks the rasterized multiview orthographic projections (MVOPs) (Carlbom et al., 1978) are suitable.

3. Results and Discussion

Based on general information, we expect that the deep learning approach will be more efficient. All methods have hypothetical pros and cons, but the experiment will show the most effective solution for a recent case. It is reasonable to assume that the deep learning approach will be the most beneficial for the recognition of mistletoes in our experimental plot. However, it is significantly more computationally intense (Le Cun et al., 2015). In case the results of classical machine learning models will show relatively similar accuracy of prediction, it is worth preferring it for further practical applications. The obvious advantage of three-dimensional meshes is that we are exploring 3D objects. However, the development of 3D networks lags far behind the development of two-dimensional ones. This means that the pre-trained 2D networks were trained on significantly larger sample, which makes them more accurate “on average“ (Le Cun et al., 2015).

4. Conclusions

The proposed method can be employed both in the forest management by arborists and dendrologists as well and in the forest ecology research. For example, the accurate spatial distribution maps of mistletoes are very helpful for the evaluation of the degree of the mistletoe infection rate as well as for the host tree health and performance. Also, this methodology can be extended to the task of the detection of other types of TrMs, such as hollows or bird nests.

Acknowledgements

The work was supported by the Inter-Action grant LTAUSA18200 of the Ministry of Education Youth and Sports of the Czech Republic.

References

- Bohak C, Slemenik M, Kordež J, Marolt M, 2020. Aerial LiDAR data augmentation for direct point-cloud visualisation. *Sensors*, 20: 2089.
- Breiman L, 2001. Random forests. *Machine Learning*, 45(1): 5–32.
- Carlhom I, Paciorek J, 1978. Planar geometric projections and viewing transformations. *Computing Surveys*, 10:465–502.
- Danihelka J, Chrtek JJr, Kaplan Z, 2012. Checklist of vascular plants of the Czech Republic. *Preslia* 84: 647–811
- Dassot M, Constant T, Fournier M. 2011. The use of terrestrial LiDAR technology in forest science: application fields, benefits, and challenges. *Annals of Forest Science*, 68:959–74.
- Janik D, Adam D, Vrska T, Unar P, Kral K, 2011. Field maple and hornbeam populations along a 4-m elevation gradient in an alluvial forest. *European Journal of Forest Research* 130(2): 197–208.
- Jordan MI, Mitchell TM, 2015. Machine learning: Trends, perspectives, and prospects. *Science* 349, 255–260.
- Frey J, Asbeck T, Bauhus J, 2020. Predicting tree-related microhabitats by multisensor close-range remote sensing structural parameters for the selection of retention elements. *Remote Sensing* 12, 867.
- Kellner JR, Armston J, Birrer M, Cushman KC, Duncanson L, Eck C, Falleger C, Imbach B, Král K, Krůček M, Trochta J, Vrška T, Zraggen C, 2019. New opportunities for forest remote sensing through ultra-high-density drone lidar. *Surveys in Geophysics*. 40:959–977.
- Krasylenko YA, Gleb RY, Volutsa OD, 2019. *Loranthus europaeus* (Loranthaceae) in Ukraine: an overview of distribution patterns and hosts. *Ukrainian Botanical Journal*, 76(5): 406–417.
- Krůček M, Král K, Cushman K, Missarov A, Kellner JR, 2020. Supervised segmentation of ultra-high-density drone LiDAR for large-area mapping of individual trees. *Remote Sensing*, 12, 3260.
- LeCun Y, Bengio Y, Hinton G, 2015. Deep learning. *Nature*, 521(7553):436–444.
- Maturana D, Scherer S, 2015. Voxnet: A 3D convolutional neural network for real-time object recognition. *International Conference on Intelligent Robots and Systems*.
- Nickrent DL, Malécot V, Vidal-Russell R, Der JP, 2010. A revised classification of Santalales. *Taxon*, 59(2): 538–558.
- Pajares G, 2015. Overview and current status of remote sensing applications based on unmanned aerial vehicles (UAVs). *Photogrammetric Engineering and Remote Sensing* 81: 281–329.
- Rehush N, Abgeg M, Waser L, Brandli U, 2018. Identifying tree-related microhabitats in TLS point clouds using machine learning. *Remote Sensing* 10, 11.
- Wehr A, Lohr U, 1999. Airborne laser scanning—an introduction and overview. *ISPRS Journal of Photogrammetry and Remote Sensing* 54: 68–82.
- Wild J, Kaplan Z, Danihelka J, Petřík P, Chytrý M, Novotný P, Rohn M, Šulc V, Brůna J, Chobot K, Ekrt L, Holubová D, Knollová I, Kocián P, Štech M, Štěpánek J, Zouhar V, 2019. Plant distribution data for the Czech Republic integrated in the Pladias database. – *Preslia* 91: 1–24.

ALS based forest information for forest fire danger modelling

M. Hollaus¹, S. Schlaffer¹, M. Müller², H. Vacik², N. Pfeifer¹, W. Dorigo¹

¹TU Wien, Department of Geodesy and Geoinformation, Wiedner Hauptstraße 8-10, 1040 Vienna, Austria

Email: (markus.hollaus, stefan.schlaffer, norbert.pfeifer, wouter.dorigo)@geo.tuwien.ac.at

²BOKU Wien, Institute of Silviculture, Peter-Jordan-Straße 82/II, 1190 Vienna, Austria

Email: (mortimer.mueller, harald.vacik)@boku.ac.at

1. Introduction

The worldwide increase in large-scale and intensive wildfires as a result of climate change and human activities represents a major challenge for the future (Conedera et al., 2018; Dowdy et al., 2019). The central and northern parts of Europe, including the Alpine region, are currently exposed to a comparatively low risk. However, a future increase in the number, extent and intensity of forest fires is expected here as well. Even though Austria is not commonly regarded as a hotspot of forest fires, dozens to hundreds of fires occur each year (Müller et al., 2015). For modelling the risk of forest fires, information about forest fuel structure is essential as forest structure influences fire behaviour itself but also exerts an impact on fuel moisture, e.g. by shading. However, these components have only been inadequately characterized in forest fire danger assessment systems so far (Müller et al., 2020). In recent years, several studies have demonstrated the assessment of forest structure information based on airborne laser scanning (ALS) data (Hollaus et al., 2012; Leiterer et al., 2013; Lim et al., 2003). Due to the country-wide availability of ALS data, the potential of ALS derived forest structure information was investigated within the CONFIRM project, which aims at developing a pre-operational integrated forest fire danger assessment system at a high spatial resolution of 100 m (Zotta et al., 2020). In this contribution, several forest structure variables are derived from ALS data to serve as input for future forest fire risk assessments.

2. Study area and data

The study area comprises the state of Styria, located in southern Austria. Styria is a mountainous, forest-rich state and comprises a total area of 16,401 km². Forest covers 61.5% of the total area and consists of 82.5% coniferous trees and 17.5% deciduous trees. The dominant coniferous tree species is spruce (*Picea abies*) with 57.8%, the dominant deciduous tree species is European beech (*Fagus sylvatica*) with 7.7% (BFW, 2021). ALS data organised in flight strips were provided by the state administration of Styria. Additionally, meta-data, such as month and year of data acquisition, were available. A digital terrain model (DTM) with a spatial resolution of 1x1 m, derived from ALS data, was available for the entire study area.

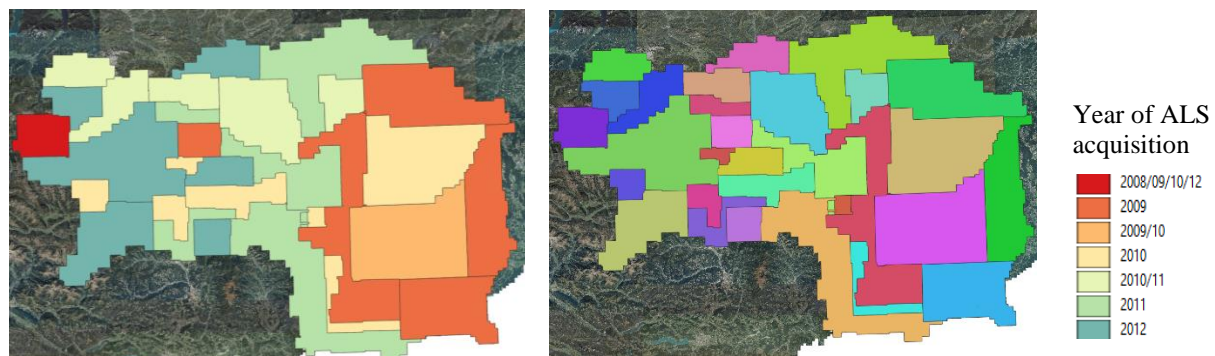


Figure 1: Left: ALS acquisition blocks for Styria. Right: Year of ALS data acquisition for the test site Styria.

3. Methods

Based on the ALS strips, a digital surface model (DSM) with a spatial resolution of 1x1 m was calculated based on the approach described in Hollaus et al. (2010). This approach uses the benefits of different algorithms and delivers optimal results for canopy surfaces as well as for forest gaps. In addition to the DSM, a normalized digital surface model (nDSM) was calculated by subtracting the DTM from the DSM. The nDSM represents the tree heights. From the DTM, slope and exposition maps were calculated. The ALS data are available in the UTM projection (zone 33, EPSG:32633).

Based on the nDSM, **forest gaps** were derived by applying a height threshold to the nDSM. Every nDSM pixel within the forest area with heights < 1 m was classified as forest gap pixel. The forest area map was provided by the Austrian Research Centre for Forests (BFW)¹ and has a spatial resolution of 1x1 m. The classified forest gap pixels were used as input for calculating the forest gap fraction at a spatial resolution of 10x10 m and 100x100 m. The latter is the target resolution of the pre-operational integrated forest fire danger assessment system. The final forest gap maps represent the percentage of forest gaps within each 100x100 m pixel.

Information on **solar radiation** is important for characterizing the variability of fuel moisture patterns over the whole vegetation period. Based on the DSM, the potential incoming solar radiation was calculated for every month using SAGA-GIS². To minimize processing time, the original resolution of the DSM of 1x1 m² was aggregated to 2x2 m² via bilinear interpolation. The temporal resolution was set to two hours, whereas for each month different start and end times for the modelling were selected. The derived total incoming solar radiation serves as an indicator of the drying out of forest gaps.

Vertical forest structure, e.g. the presence of understory vegetation, is of importance for fire propagation and fire intensity as fire ladders can lead to the conversion of surface fires to crown fires. To characterize the vertical forest structure, the ALS data were analysed using a voxel approach. It is assumed that within the forest area every ALS point (echo) represents a vegetation element. Thus, every voxel (1 x 1 x 1 m³) is checked for the occurrence of ALS points. If ALS points are present, the respective voxel is classified as a filled vegetation voxel. The derived three-dimensional data layers allow a detailed study of the vertical and horizontal forest structure to detect e.g. understory or lower parts of the canopy. The ALS data were processed using the OPALS software package (Pfeifer et al., 2014).

4. Results and discussion

All the described products were derived for the entire area of Styria. As shown in Figure 2, forest gaps are clearly visible in the ALS derived products. The modelled potential incoming solar radiation allows to identify forest gaps that receive a high incoming solar radiation. The seasonal influence on solar radiation is shown in Figure 2 and will be considered in the forest fire risk assessment model. The derived nDSM clearly shows forest gaps as well as stands characterised by different tree heights (Figure 3). The profile through the 3D ALS point cloud, shown in Figure 3, allows identifying differences in the vertical forest structure.

5. Conclusion and Outlook

The study shows that country-scale derivation of forest structure information by ALS data can be achieved in an operational way. For the operational use of the model, three maps for the characterization of the vegetation on 100 x 100 m should be available:

- The characterization of the vegetation with respect to the ignition risk considers potential incoming solar radiation and tree species.
- The characterization of vegetation with respect to fire spread considers data on forest gaps and tree species. The risk of spread is assigned to fire behaviour.
- The characterization of the vegetation with respect to fire intensity considers the forest gaps, fire ladders, and the map of tree species. The fire intensity is also assigned to fire behaviour.

The derived products are an essential input for forest fire risk assessment. Within the CONFIRM project, the novel forest structure information will be combined with meteorological data, remote sensing-derived estimates of tree species and fuel moisture, and socio-economic indicators (e.g. population

¹ <https://www.bfw.gv.at/hochgenaue-waldkarte-waldinventur/>

² http://www.saga-gis.org/saga_tool_doc/2.2.2/ta_lighting_2.html

density, land use, infrastructure, tourism indicators) to estimate forest fire danger at a high spatial and temporal resolution. The suitability of risk modelling approaches based on expert knowledge as well as on machine learning is currently being assessed.

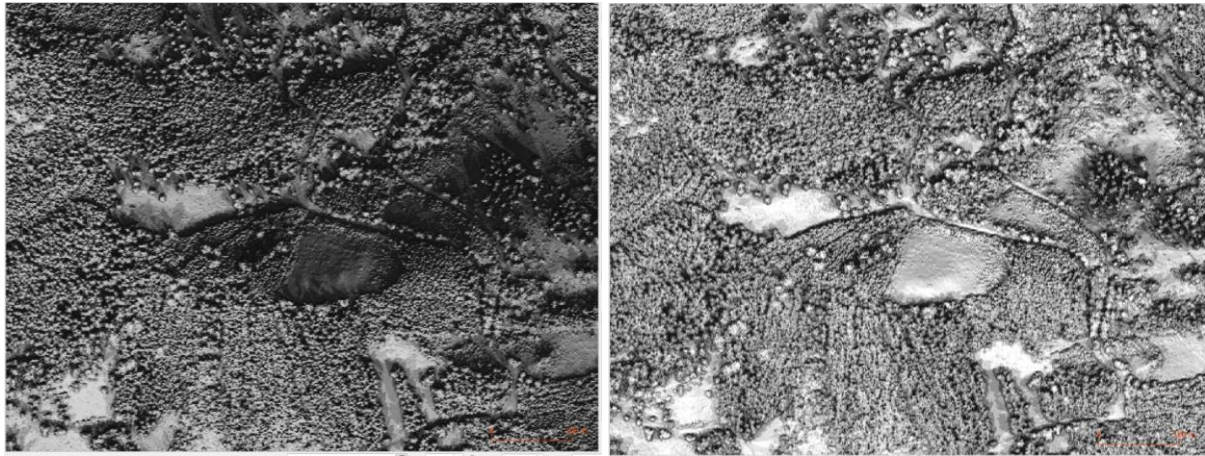


Figure 2: Examples of total incoming solar radiation based on ALS derived DSM, March (left), June (right). Dark pixel values indicate low solar radiation and bright pixel values high solar radiation.

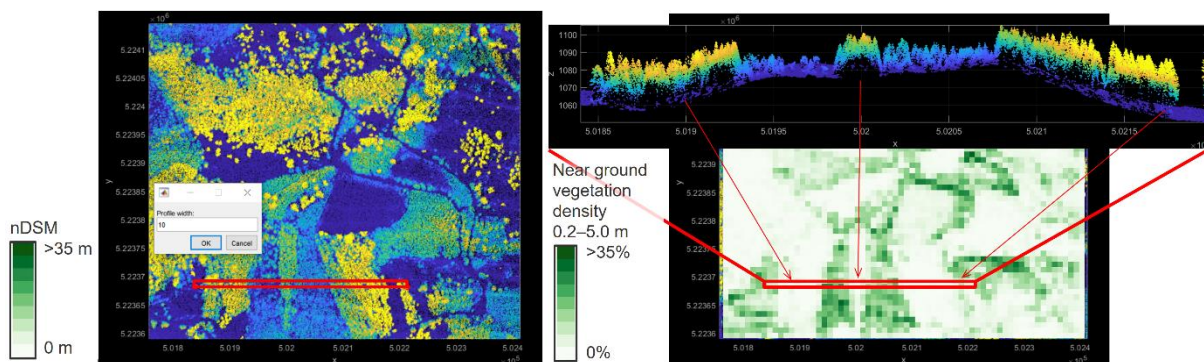


Figure 3: nDSM derived from ALS data (left), near ground vegetation density derived using a voxel approach (right).

Acknowledgements

This research was conducted within the CONFIRM project (project No. 873674) funded by the Austrian Research Promotion Agency (FFG) under the 15th Austrian Space Applications Program (ASAP).

References

- BFW, 2021. ÖWI - interim results Styria. https://bfw.ac.at/cms_stamm/500/images/OEWI/Steiermark_OEWI_16_18.pdf. Last accessed May 2021.
- Conedera, M., Krebs, P., Valese, E., Cocca, G., Schun, C., Menzel, A. and Pezzatti, G.B., 2018: Characterizing Alpine pyrogeography from fire statistics. *Applied Geography* 98, 87-99. <https://doi.org/10.1016/j.apgeog.2018.07.011>
- Dowdy, A.J., Ye, H., Pepler, A., Thatcher, M., Osbrough, S.L., Evans, J.P., Di Virgilio, G. and McCarthy, N., 2019: Future changes in extreme weather and pyroconvection risk factors for Australian wildfires. *Scientific Reports* 9 (1), 10073. <https://doi.org/10.1038/s41598-019-46362-x>
- Hollaus, M., Mandlbürger, G., Pfeifer, N. and Mücke, W., 2010: Land cover dependent derivation of digital surface models from airborne laser scanning data. In: (Eds.): *International Archives of the Photogrammetry, Remote Sensing and Spatial Information Sciences - ISPRS Archives*, 38, 221-226.
- Hollaus, M., Mücke, W. and Eysn, L., 2012: Forest structure and stem volume assessment based on airborne laser scanning. *Ambiência* 8, 471-482.

Leiterer, R., Mücke, W., Morsdorf, F., Hollaus, M., Pfeifer, N. and Schaepman, M., 2013: Operational forest structure monitoring using airborne laserscanning. *Photogrammetrie, Fernerkundung, Geoinformation* 3, 173-184.

Lim, K., Treitz, P., Wulder, M., St-Onge, B. and Flood, M., 2003: LIDAR remote sensing of forest structure. *Progress in Physical Geography* 27 (1), 88-106.

Müller, M.M., Vacik, H. and Valsecchi, E., 2015: Anomalies of the Austrian Forest Fire Regime in Comparison with Other Alpine Countries: A Research Note. *Forests* 6 (4), 903-913. <https://doi.org/https://doi.org/10.3390/f6040903>

Müller, M.M., Vilà-Vilardell, L. and Vacik, H., 2020: Towards an integrated forest fire danger assessment system for the European Alps. *Ecological Informatics* 60 60, 101151. <https://doi.org/https://doi.org/10.1016/j.ecoinf.2020.101151>

Pfeifer, N., Mandlbauer, G., Otepka, J. and Karel, W., 2014: OPALS - A framework for Airborne Laser Scanning data analysis. *Computers, Environment and Urban Systems* 45, 125-136. <https://doi.org/10.1016/j.compenvurbsys.2013.11.002>

Zotta, R.-M., Atzberger, C., Degenhart, J., Hollaus, M., Immitzer, M., Krajinz, H., Lick, H., Müller, M.M., Oblasser, H., Schaffhauser, A., Schlaffer, S., Vacik, H. and Dorigo, W., 2020. CONFIRM – Copernicus Data for Novel High-Resolution Wildfire Danger Services in Mountain Regions, EGU General Assembly 2020, Online, pp. 1. <https://doi.org/https://doi.org/10.5194/egusphere-egu2020-19288>

Toward a Definitive Assessment of the Impact of Leaf Angle Distributions on LiDAR Structural Metrics

R. Wible¹, K. Patki¹, K. Krause², and J. van Aardt¹

¹Rochester Institute of Technology, Chester F. Carlson Center for Imaging Science, 54 Lomb Memorial Drive, Rochester, NY, 14623, USA
Email: vanaardt@cis.rit.edu

²Battelle, 1685 38th St. Suite 100, Boulder, CO, 80301, USA
Email: kkrause@battelleecology.org

1. Introduction

Ecological research relies on measurement and mapping of the changing patterns in biochemical and structural traits of vegetation regions over time, which enables ecologists to quantify and understand carbon cycling processes and its impact on global warming (Zhao et al., 2009). Such measurements are obtained using remote sensing, where established relationships between imaging spectroscopy and light detection and ranging (LiDAR) signals and plant functional traits like nutrient levels, leaf area index (LAI), leaf area angles, etc. already exist. However, little work exists on a definitive assessment of especially the linkages between spectral-structural variation.

Variation in radiometric and LiDAR signals can be attributed to many factors, such as leaf and wood optical properties, canopy attributes (LAI, leaf and stem orientation, and foliage clumping), background soil reflectance, illumination conditions, and viewing geometry, among others (Asner, 1998; Ollinger, 2011). Such properties can be directly or indirectly related to both the underlying biochemistry and the leaf structural properties (Ollinger, 2011; Baldocchi et al., 2020). For example, some of this variation can be mitigated by properly selecting temporal specifics for data collection, and via a better understanding of the impacts of structural variation and its impact on spectral response.

The overarching objective of this project therefore is to better understand the connection between plant (forest) structure and traits and thereby improve interpretation of remote sensing data in order to better map and monitor ecosystems assess. The specific objective is to assess the impact of forest leaf angle distribution (LAD) on both spectral and structural approaches to forest trait assessment. This was achieved by constructing a detailed, physics- and biophysics-based virtual scene.

2. Data and Methods

2.1 Research Site

The study area is a 500x700m tract located at the Prospect Hill tract within Harvard Forest, a National Ecological Observatory Network (NEON) NEON research site, located in Petersham, Massachusetts, USA (42°32'19.79"N, 72°10'31.81"W). The area consists of a mix of coniferous and deciduous trees, shrubs, and bushes, with prominent species Eastern Hemlock (*Tsuga canadensis*), Red Maple (*Acer rubrum*), Winter Berry (*Ilex verticillata*), Yellow Birch (*Betula alleghaniensis*), Northern Red Oak (*Quercus rubra*) and Mountain laurel (*Kalmia latifolia*).

2.2 Simulation Development

In order to understand the impact of changing leaf angle distribution, we built a virtual 3D model of a complex forest, with which we can experiment with leaf angles for each tree. We gathered field data from the online Harvard Forest Data Archive (harvardforest1.fas.harvard.edu), which contains information about geographic locations, height, and diameter at breast height (DBH) values of all plants.

3D models of vegetation were obtained from OnyxTREE BROADLEAF (V. 7.0) and OnyxTREE CONIFER (V. 7.0), a software suite used for procedural modeling of vegetation (www.onyxtree.com) The software requires a number of tree parameters as inputs and outputs faceted triangular meshes of the trees (Romanczyk et al., 2013). Multiple model variants for common species were created using OnyxTREE and instantiated in the scene at provided positions, so that the species at least matched the larger genus. Optical properties (reflectance and transmittance) for each species were obtained from real

measurements taken from the online ecological spectral database ECOSIS (ecosis.org). Spectral variation was created via PROSPECT (pypi.org/project/prosail), by randomly adjusting leaf parameters.

We used DIRSIG, a physics-based rendering and simulation tool designed and developed at RIT, for virtual image and LiDAR data generation. DIRSIG uses Monte Carlo ray tracing and is capable of capturing radiometrically accurate images of virtual scenes with passive illumination (sunlight, skylight, moonlight, starlight, and in-scene lights) in the Visible-NIR-SWIR wavelength ranges (Romanczyk et al., 2013). We obtained the images for this study using DIRSIG version 5 (2021.19). The spectral specifications used for the imager in DIRSIG were: i) wavelengths ranging from 400-1100nm (to spectral index derivation), ii) wavelength band centers separated by 5nm, iii) a FWHM bandwidth of 5nm, and iv) a Gaussian band shape; these parameters were based on the NEON Airborne Observation Platform (AOP) near-infrared imaging spectrometer specifications. Spatial specifications used were: i) pixel array of 1100 x 800 (virtual hyperspectral 2D spatial array to simplify data collection), ii) a pixel size of 22x22um, and iii) an imager placed at the center of the virtual scene at a height of 3km to capture the entire plot. The scenes were collected at 10h00 Eastern Standard Time (EST). The LiDAR simulation specifications were based on a Gemini ALTM LiDAR system (Table 1). Platform motion was modeled based on GPS/IMS data from the 2019 NEON platform and directly input into the DIRSIG platform motion file. Simulated data were compared to the 2019 NEON sensor data as three main categories: i) visual inspection, ii) spectral signatures/indices, and iii) LiDAR data, in terms of a limited statistical analysis of height and structure.

Table 1. LiDAR simulation specifications, as per the Gemini ALTM LiDAR system.

Wavelength	1064nm
Accuracies	5-30cm elevation; 1/ 5,500 x Altitude (m AGL) horizontal
Effective laser repetition rate	Programmable; 33-167kHz
Scan width (FOV)	Programmable; 0-50°
Scan frequency	Programmable; 0-70Hz
Beam divergence	Dual divergence: 0.25mrad (1/e) and 0.8 mrad (1/e)
Range/intensity capture	Up to four range/intensity measurements, including 1 st , 2 nd , 3 rd , and last returns

3. Results and Discussion

Simulated images from the RGB, imaging spectroscopy (HSI), and LiDAR sensors were successfully simulated (Figures 1a-c), for i) a 1024x512 RGB image (3,000 meters above sea level), ii) a 246 band HSI image (380-2500nm), and iii) a 40x30m LiDAR discrete point cloud. We observed that the variation in canopy color, tree species, and density are clearly visible, thus providing a realistic feel to the scene (Figure 1a). Visually the real image looks denser with a high percentage of trees overlapping, even though the simulation is geographically accurate. This discrepancy was attributed to OnyxTREE models not incorporating crown competition.

Spectrally the images were expected to be similar since the simulation used signatures from the real NEON HSI image. Figure 1b shows this to be mostly true, except for two classes in the simulated plot that exhibited almost twice as large values as the other vegetative signatures; this was attributed to the outer 100m buffer that surrounds the 3D model.

Structurally the 3D model heights and DBH values were based on field and sensor data, so the expectation was that the simulated values will mirror reality. The only simulated data initially available for analysis was a 40x30m discrete LiDAR point cloud (Figure 1c). Next steps will include incorporation of planophile and erectophile leaf distributions, and assessing their impact on especially discrete return LiDAR metrics (Figure 2 shows an initial spectral comparison).

4. Conclusions

The validation and extended LAD impact analysis of the 3D DIRSIG model is not complete. We presented an initial functionality, where we have developed a spectrally and structurally robust virtual scene of an actual forest site from Harvard Forest, USA. We have shown the capability to simulate both HSI and LiDAR sensors, as well as vary LAD. Next steps include a more extensive vetting of the actual scene, followed by an assessment of how field-observed LAD values, and the variation thereof, impact

both spectral and LiDAR metrics associated with forest trait assessment. Additional results for the structural analysis will be presented at the conference.

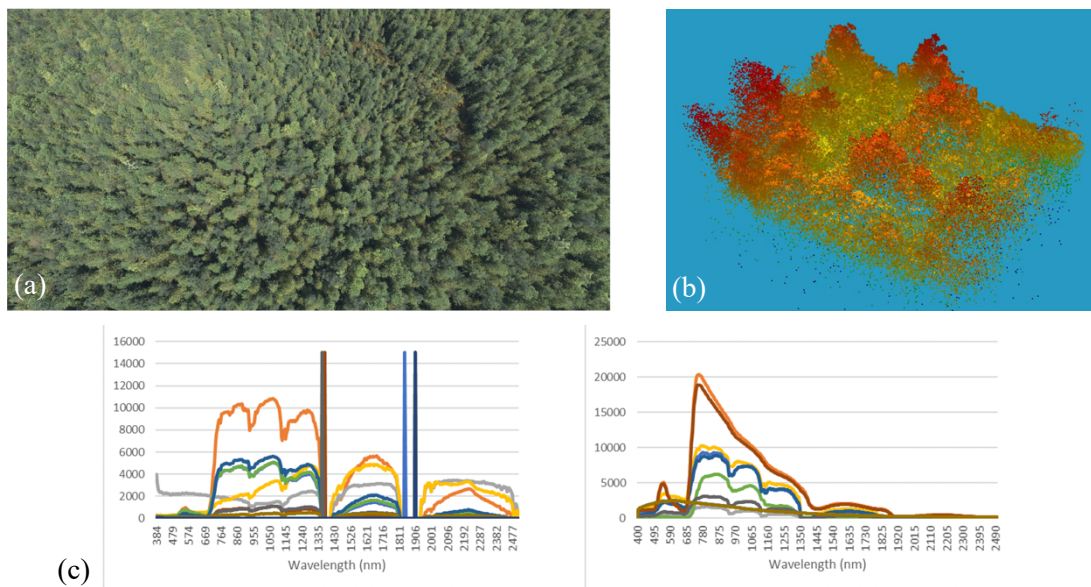


Figure 1: a) RGB rendering of the Harvard Forest Scene (1024x512 pixels); b) a comparison of spectral profiles (random species); and c) the simulated 40x30m discrete return LiDAR point cloud.

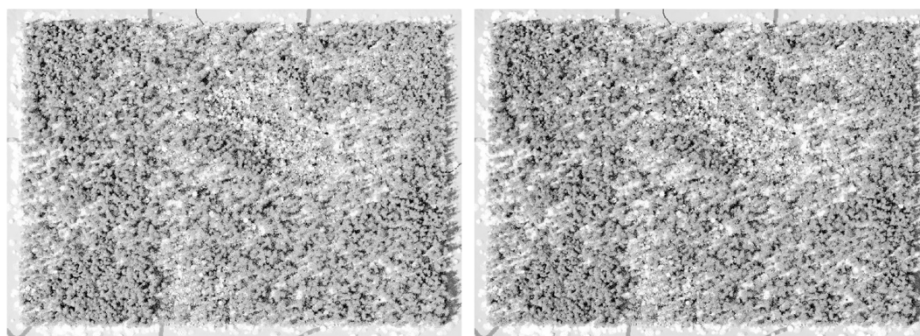


Figure 2: An initial, qualitative spectral comparison (500x700m) of planophile (left) vs. erectophile (right) LAD, as expressed via simplistic normalized difference vegetation index (NDVI) images (dark = low, bright = higher). Next steps will involve more explicit LAD definitions and an assessment of their impacts on both spectral and structural forest traits.

Acknowledgements

We gratefully acknowledge funding from the National Geospatial Intelligence Agency (award #HMO476010008) and NASA (award # 80NSSC20K1730/PO806052). Any findings and opinions expressed here are those of the authors alone.

References

- Asner GP, 1998, Biophysical and Biochemical Sources of Variability in Canopy Reflectance, *Remote Sensing of Environment* 64(3): 234-253.
- Baldocchi D, Y Ryu, B Dechant, E Eichelmann, K Hemes, S Ma, CR Sanchez, R Shortt, D Szutu, A Valach, J Verfaillie, G Badgley, Y Zeng, and JA Berry, 2020, Outgoing Near-Infrared Radiation From Vegetation Scales With Canopy Photosynthesis Across a Spectrum of Function, Structure, Physiological Capacity, and Weather, *Journal of Geophysical Research: Biogeosciences* 10.1029/2019JG005534 (17p).
- Ollinger S, 2011, Sources of variability in canopy reflectance and the convergent properties of plants, *New Phytologist* 189: 375-394.
- Romanczyk P, , 2013, Assessing the impact of broadleaf tree structure on airborne full-waveform small-footprint LiDAR signals through simulation, *Canadian Journal of Remote Sensing* 39(1): S60-S72.
- Zhao K, S Popescu, and R Nelson, 2009, Lidar remote sensing of forest biomass: A scale-invariant estimation approach using airborne lasers, *Remote Sensing of Environment* 113(1): 182-196.

Three attempts to detect changes in tropical forests using repeat LiDAR scans

T. D. Jackson¹, S. Hickman¹, J. Ball¹, T. Swinfield¹, M. Nunes², G. Vincent³, M. Aubry-Kientz⁴, D. A. Coomes¹

¹ Department of Plant Sciences, University of Cambridge, Downing Street, Cambridge, CB2 3EA
Email: {tj312; shm4; jgcb3; tws36; dac18}@cam.ac.uk

² Department of Geosciences and Geography, University of Helsinki, Helsinki, Finland
Email: matheus.nunes@helsinki.fi

³ AMAP, University of Montpellier, France
Email: gregoire.vincent@ird.fr

⁴ UMR EcoFoG, AgroParisTech, Kourou, French Guiana
Email: melaine.aubry.kientz@gmail.com

1. Introduction

Networks of permanent field plots have detected an increase in the carbon stored in tropical forests over recent decades¹. This increase is thought to be driven in part by CO₂ fertilization. However, uncertainty remains about the scale and frequency of disturbance events, and whether they too are increasing with climate change. Recent work has shown that small-scale disturbance events (<0.1 ha) account for the majority of biomass turnover in tropical forests². Airborne Laser Scanning (ALS) provides data at the appropriate scale and spatial resolution to study these processes. We use repeat ALS data to measure these changes in three ways:

1. By tracking large trees over time to determine whether their mortality rate is it balanced by recruitment.
2. Studying changes in the number and size distribution of canopy gaps, which are markers of disturbance.
3. By measuring the overall change in canopy height and comparing this with repeat field inventory data.

2. Data and Methods

2.1 Airborne Laser Scanning data and processing

ALS data was collected for two sites in Malaysia (Sepilok and Danum) and two sites in French Guiana (Paracou and Nouragues), covering a total area of 84 km² (or 8400 ha). ALS data was processed with LASTools³ to create a Digital Surface Model (DSM), Digital Terrain Model (DTM) and Canopy Height Model (CHM) at 1 m spatial resolution. We cropped the short Kerangas forest in Sepilok out of these analyses since it has a distinct forest structure and may bias comparisons between sites.

Table 1. Overview of study sites, ALS data and canopy gap dynamics.

Site	Country	Years scanned	Area (km ²)	Canopy gaps (# km ⁻²)		
				Initial	Recovered (yr ⁻¹)	New (yr ⁻¹)
Danum	Malaysia	2014	23	966	80	47
Sepilok		2020	25	710	44	48
Paracou	French	2016	10	280	65	53
Nouragues	Guiana	2019	26	565	96	62

2.2 Individual tree growth and mortality rates

We manually delineated tree crowns using the CHM and RGB images, which were captured alongside the ALS data. This manual data set prioritizes large trees (those easily visible from above) which account

for the majority of aboveground biomass⁴. Using this data set we then optimized a watershed-type segmentation algorithm (<https://github.com/swinersha/UAVforestR>) using Bayesian optimisation to segment large trees from the CHM. Independently, we trained a convolutional neural network, based on a Mask RCNN architecture, to segment trees in the RGB images. We then combined results from these two independent segmentation methods to give a dataset of accurately delineated large trees across Sepilok Reserve. Finally, we extracted the canopy height for each tree in both years from the ALS data. This allowed us to count how many large trees had died between scans and estimate their mortality rate.

2.4 Canopy gap dynamics

We defined canopy gaps as contiguous areas in the CHM < 10 m above ground level between 10 m² and 10,000 m² using ForestGapR⁵. For each site, we matched gaps which overlap in both years to determine how many new gaps occurred during the interval between scans, and how many gaps recovered.

2.3 Canopy height change

We calculated the change in canopy height (ΔH) in two ways: (a) as the difference between the first and second CHM and (b) the difference between DSMs. (a) is robust to any vertical misalignment between the scans while (b) is robust to any bias in ground detection. We found that low pulse densities caused underestimation of canopy height and so confined our analysis to areas with pulse densities greater than 10 pulses per square metre. In order to reduce noise (from geolocation errors, wind etc) we aggregated the ΔH rasters to 20 m spatial resolution. We calculated slope, aspect and topographic position index (TPI) for each site and tested whether spatial patterns in ΔH were related to topography using multiple linear regression.

3. Results and discussion

3.1 Individual tree analysis

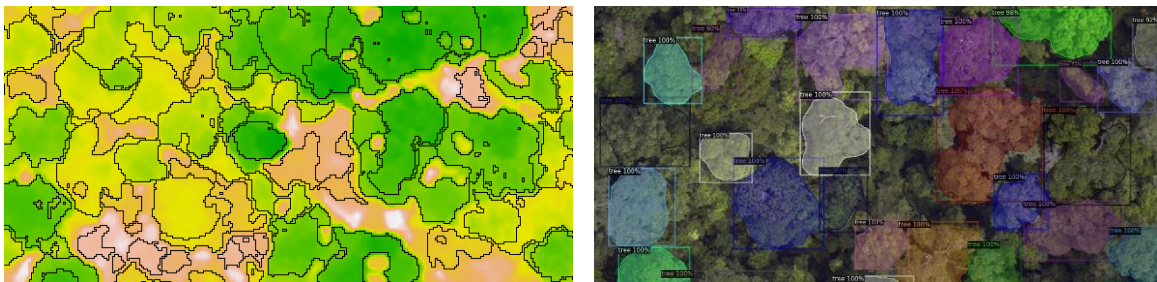


Figure 1: Watershed tree crown delineation from the canopy height model using UAVforestR (left), and instance segmentation of tree crowns from RGB imagery using Mask RCNN (right).

Large trees were often found growing close together with interlocking crowns. ALS segmentation methods rely on structural assumptions (such as crown radius allometry) to segment these difficult cases, but allometry data is severely limited for these large trees. We found that differences in colour helped distinguish trees, but the exact boundary of the crown was difficult to accurately delineate either manually or automatically. Therefore, we have a high level of confidence that each polygon represents a single tree, but uncertainty over the exact boundary. This limits our ability to detect lateral growth of the tree crowns, which is an important component of tree growth, particularly for large trees.

From the 861 manually segmented trees in Danum and Sepilok we found that just under 10% (76 trees) had died (reduction in height by >5 m) between 2014 and 2020. We found no trend with tree height. Ongoing work will dramatically increase this sample size using automatically segmented trees crown.

3.2 Decrease in the number and size of canopy gaps

The number of canopy gaps decreased in three out of the four sites (Table 1). In Sepilok there was a slight increase in the number of canopy gaps, but a decrease in the total area of gaps. This suggests that,

over the interval between scans, recovery outpaced new disturbances in these forests. Further analysis will determine whether new gaps were spatially clustered, e.g. near existing gaps or on hilltops.

3.3 Increase in canopy height

All sites showed a net increase in canopy height over time. This suggests an increase in carbon storage, although field data are needed to confirm this (analysis ongoing). This increase in canopy height was robust to variations in pulse density and ground detection accuracy, since a similar increase was observed in both the CHMs and DSMs at high pulse densities. Further work is needed to test whether this increase is sensitive to other differences in ALS scanning parameters between years. Also, we found that these height changes were sensitive to the scale of spatial aggregation, with much lower growth rates at 1 m resolution. After accounting for initial canopy height, topographic metrics explained less than 10% of the variation in ΔH .

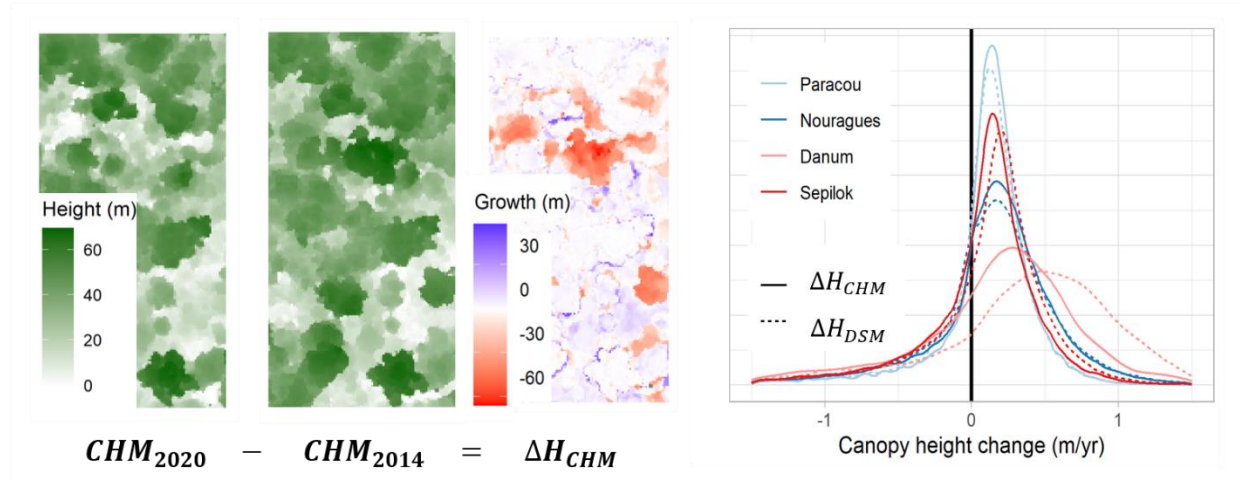


Figure 2: Left – example canopy height models and height change raster for Sepilok. Right - change in canopy height across four tropical forest sites (20 m resolution, > 10 pulses m^{-2})

4. Conclusions

Repeat airborne laser scanning data were used to study changes in tropical forests canopy structure over time. We found an overall increase in canopy height (although further analysis is needed to confirm this) and a decrease in the number of canopy gaps. Ongoing work will determine whether these findings align with field data, and whether large trees are growing or dying.

Acknowledgements

TDJ and DAC were funded through NERC grant NE/S010750/1. SH is funded by the EPSRC grant EP/S022961/1. We would like to acknowledge our project partners; the Sabah Biodiversity Center, Sabah Forestry Department, the Danum Valley Management Committee, Forest Research Center (Sabah) and the South East Asia Rainforest Research Partnership (SEARRP). This is a publication of Laboratoire d'Excellence CEBA (ANR-10-LABX-25).

References

1. Hubau W, Lewis SL, Phillips OL, et al. Asynchronous carbon sink saturation in African and Amazonian tropical forests. *Nature*. 2020;579(7797). doi:10.1038/s41586-020-2035-0
2. Espírito-Santo FDB, Gloor M, Keller M, et al. Size and frequency of natural forest disturbances and the Amazon forest carbon balance. *Nat Commun*. 2014;5. doi:10.1038/ncomms4434
3. Isenberg M. LASTools “Efficient LiDAR Processing Software.” 2021. <http://rapidlasso.com/LAStools>
4. Bastin JF, Barbier N, Réjou-Méchain M, et al. Seeing Central African forests through their largest trees. *Sci Rep*. 2015;5. doi:10.1038/srep13156
5. Silva CA, Valbuena R, Pinagé ER, et al. ForestGapR: An r Package for forest gap analysis from canopy height models. *Methods Ecol Evol*. 2019;10(8):1347-1356. doi:10.1111/2041-210X.13211

Boreal-wide biomass estimation with ICESat-2

L. Duncanson¹, A. Neuenschwander², P. Montesano³, N. Thomas⁴, A. Mandel, D⁵. Minor, E. Guenther², S. Hancock⁶, C. Silva⁷, J. Armston¹, T. Feng¹, R. Dubayah¹, V. Leitold¹, J. White⁸, M. Wulder⁸.

¹2181 Lefrak Hall, University of Maryland, College Park, MD 20742

Email: lduncans@umd.edu

Email: minord@umd.edu

Email: armston@umd.edu

Email: tuofeng@terpmail.umd.edu

Email: dubayah@umd.edu

Email: vleitold@umd.edu

²University of Texas, Austin

Email: amyn@arlut.utexas.edu

Email: eguenther@arlut.utexas.edu

³NASA Goddard / SSAI

Email: paul.m.montesano@nasa.gov

⁴NASA Goddard / ESSIC

Email: thomas.neumann@nasa.gov

⁵Developmentseed

Email: alex@developmentseed.org

⁶University of Edinburgh

Email: steven.hancock@ed.ac.uk

⁷University of Florida

Email: carlos_engflorestal@outlook.com

⁸Canadian Forest Service, Natural Resources Canada

Email: joanne.white@canada.ca

Email: mike.wulder@canada.ca

1. Introduction

Aboveground biomass is a critical element of the global carbon cycle, both in terms of the large magnitudes of carbon stored in aboveground woody material, and the ecological carbon-climate feedbacks related to disturbances from pests and fire which are particularly important for carbon cycling in the boreal system. To date, high resolution biomass maps have been largely unavailable across the boreal system due to a dearth of active remote sensing data sensitive to forest structure at the spatial scales of boreal forest processes (~30m – 1 ha). ICESat-2 has produced forest height products at a 100-m segment resolution through the ATL08 product (Fig 1, Neuenschwander & Pitts, 2019), but the mission does not have an official biomass requirement or product. This research presents early results from two recently funded NASA projects (one through NASA's ABoVE program, and one through the ICESat-2 Science Team). These projects focus on using height data from ICESat-2 to estimate and map woody aboveground biomass for the boreal domain.

We explore the transference of models developed for NASA's Global Ecosystem Dynamics Investigation (GEDI) mission (Dubayah et al., 2020, Duncanson et al., 2020) that translate height measurements into estimates of biomass based on a global field and airborne lidar campaign, and compare these with models using simulated ICESat-2 over field plots. ATL08 has been reprocessed to the 30-m segment length and Relative Height (RH) metrics have been recomputed including ground photons to be more comparable to GEDI's RH metrics. We fit exhaustive suites of OLS models with different height predictors, and apply the best performing model per PFT to 30-m ATL08 for the globe north of 50 degrees latitude,

producing estimates of AGBD and associated standard error for each 30-m ATL08 segment for the growing season. We then link AGBD from ATL08 to a wall-to-wall covariate stack at a 30 m resolution from Landsat and the Copernicus DEM. We fit a random forest model to predict AGBD from the covariate stack for each 40 km tile across the study domain. We propagate uncertainties from the field to ATL08 models through to the ATL08 to Landsat model through bootstrapping both sets of models fits to produce pixel-level estimates of uncertainty. The resulting 30-m AGBD and uncertainty products are representative of growing season conditions between 2019-2020.

2. Figures and Tables

2.2 Figures

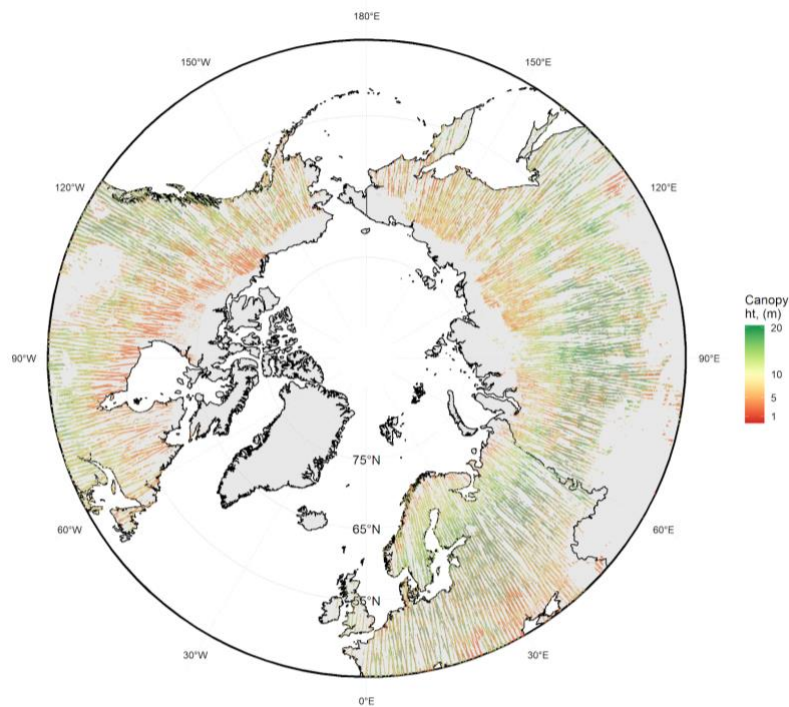


Fig 1. Relative Height (RH98) from ICESat-2's ATL08 product between 45 and 75 N captures height gradients by latitude.

2.3 Tables

Table 1 The top model for each MODIS Plant Functional Type and region stratum in the scenario where RH98 was forced into models and no RH metric lower than RH50 was considered. R squared (Rsq), %RMSE, mean residual error (MRE) and Slope were all calculated from geographic cross validation. MRE was the absolute mean binned residual error, expressed in Mg/ha.

Strata	R ²	%Rmse	MRE	Transform	Predictors
DBT North America	0.77	38.47	7.6	sqrt-sqrt	RH60, RH98
ENT North America	0.77	69.27	13.89	sqrt-sqrt	RH60, RH98
ENT Europe	0.69	52.55	2.04	sqrt-sqrt	RH98
Deciduous Broadleaf Trees	0.73	40.3	9.88	sqrt-sqrt	RH60, RH98
Evergreen Needleleaf Trees	0.69	63.35	5.73	sqrt-sqrt	RH98
Europe	0.67	53.33	4.1	sqrt-sqrt	RH98
North America	0.77	62.47	9.79	sqrt-sqrt	RH70, RH98

Acknowledgements

We gratefully acknowledge data collection and provision of field and airborne lidar from the National Ecological Observatory Network (NEON), a program sponsored by the National Science Foundation and operated under cooperative agreement by Battelle, as well as from NASA's Land Vegetation and Ice Sensor (LVIS).

References

- Dubayah, R., Blair, J. B., Goetz, S., Fatoyinbo, L., Hansen, M., Healey, S., ... & Silva, C. (2020). The Global Ecosystem Dynamics Investigation: High-resolution laser ranging of the Earth's forests and topography. *Science of remote sensing*, 1, 100002.
- Duncanson, L., Neuenschwander, A., Hancock, S., Thomas, N., Fatoyinbo, T., Simard, M., ... & Dubayah, R. (2020). Biomass estimation from simulated GEDI, ICESat-2 and NISAR across environmental gradients in Sonoma County, California. *Remote Sensing of Environment*, 242, 111779.
- Neuenschwander, A., & Pitts, K. (2019). The ATL08 land and vegetation product for the ICESat-2 Mission. *Remote sensing of environment*, 221, 247-259.

Moving on from Foliage Height Diversity: determining maximum entropy in 3-dimensional variables

R. Valbuena¹, S. Adnan², M. Maltamo², L. Mehtätalo³, R.N.L. Ammaturo⁴, T. Lovejoy⁵

¹ Bangor University, School of Natural Sciences, UK
Email: r.valbuena@bangor.ac.uk

² University of Eastern Finland, School of Forest Sciences, Finland
Email: adnan@uef.fi; matti.maltamo@uef.fi

³ University of Eastern Finland, School of Computing, Finland
Email: lauri.mehtatalo@uef.fi

⁴ University of Strathclyde, Mathematics and Statistics, UK
Email: nla32@cam.ac.uk

⁵ UN Foundation and George Mason University, Virginia, USA
Email: tlovejoy@unfoundation.org

1. Introduction

McArthur and McArthur's (1961) foliage height diversity (FHD) is widely used for determining structural complexity, from LiDAR vertical height (H) profiles (Lefsky et al. 2002, Vierling et al. 2008, Simonson et al. 2014). FHD has however largely failed to disentangle the relationships between the ecosystem structural diversity and biodiversity, with early reports such as those from Thomas Lovejoy (1972) in the Amazon not finding evidences in the light of FHD. It remains unclear whether FHD is the most suitable means to determine the structural complexity of ecosystems.

The calculation of FHD involves layering the vertical profile, which is essentially unnatural to describe a continuous variable (X) such as height, and involve subjective steps such as the determination of the size of these layers, from which the value of FHD obtained is ultimately dependent upon. This is because FHD is based on Shannon's (1948) entropy index, which was not originally designed to describe continuous variables, but meant for abundance data for categorical variables. In Adnan et al. (2021) we provided a mathematical framework for determining maximum entropy in 3D remote sensing datasets based on Lorenz curves and Gini (1921) coefficients (GC) determined from theoretical continuous distributions, intended to replace FHD as entropy measure in vertical profiles of LiDAR heights. This framework was developed for 1-dimensional variables (1D; X) such as tree heights, and 2-dimensional variables (2D; $Z \propto X^2$) such as basal areas, and hereby we extend it to 3-dimensional variables (3D, $Z \propto X^3$) such as volumes.

Structural complexity is an essential morphological trait of forest ecosystems, complementary to others like vegetation height or cover (Schneider et al. 2017, Fahey et al. 2019, Valbuena et al. 2020). But the means to measure the structural complexity of forests lacks consensus (Neumann and Starlinger 2001, Lexerød and Eid 2006, Valbuena et al. 2012). Two types of approaches, those measuring entropy (McArthur and McArthur 1961) versus those measuring variability (Weiner 1990), have effectively been merged in the framework presented in Adnan et al. (2021), by showing how maximum entropy can be flagged up from values of a variability measure such as the Gini coefficient. Formal deductive proofs for maximum entropy at $GC = 0.33$ for 1-dimensional variables (Adnan et al. 2021), and $GC = 0.50$ for 2-dimensional variables (Valbuena et al. 2012, 2107), have been presented, which hereby are extended toward the value of $GC = 0.60$ for 3-dimensional variables.

2. Methods

Let $E[X]$ be the expectation a random variable X with probability density function (p.d.f.) $f_X(x)$, cumulative distribution function (c.d.f.) $F_X(x)$, quantile function (inverse of the c.d.f.) $F_X^{-1}(p)$. The Lorenz curve $L_X(p)$ specifies the accumulated proportion of the total of X that is attributed to a given accumulated share of the population ordered by increasing X :

$$L_X(p) = \frac{\int_0^p F_X^{-1}(t) dt}{E[X]}, \text{ for } 0 \leq p \leq 1 \quad (1)$$

The Gini coefficient is the twice area between the Lorenz curve and the diagonal line $L_X(p) = p$, which is thus assessed with the integral:

$$GC_X = 1 - 2 \int_0^1 L_X(p) dp \quad (2)$$

When considering the distribution LiDAR heights $X = H$, the Lorenz curve $L_H(p)$ specifies the proportion of total accumulated ranked heights (usually in decreasing order, but it can be either). If considering 2-dimensional variables, such as basal area $X = BA = D^2$, then it gives the proportion of basal area for ranked trees (best in increasing order, to express competitive dominance, following Valbuena et al. 2013). We can also be interested in 3-dimensional variables, such as volume $X = V = HD^2$. The methods consist in mathematical proofs demonstrating values of Lorenz curves (1) Gini Coefficient (2) that can be used to characterize maximum entropy from theoretical distributions of 3-dimensional variables, which can be employed to substitute the use of FHD and avoid its unnatural partitioning of continuous variables into layers.

3. Results

3.1 Maximum Entropy in 3-dimensional variables: volume

Tree volumes are also calculated from a transformation of other dimensions $V = aHD^2$. Again, given the scale-invariability property of Lorenz curves, and thus we can consider the Lorenz curve and Gini coefficient of transformation $Z = X^3$ when $X \sim U(0, \theta)$.

The c.d.f. and p.d.f of the transformed variable are:

$$F_{X^3}(z; \theta) = \begin{cases} 0, & \text{for } z \leq 0 \\ \sqrt[3]{z}/\theta, & \text{for } 0 \leq z \leq \theta^3 \\ 1, & \text{for } z \geq \theta^3 \end{cases} \quad (3)$$

$$f_{X^3}(z; \theta) = \begin{cases} \frac{1}{3\theta^3\sqrt{z}}, & \text{for } 0 \leq z \leq \theta^3 \\ 0, & \text{otherwise} \end{cases} \quad (4)$$

Thus, the quantile function and expected value of Z are:

$$F_{X^3}^{-1}(p) = \theta^3 p^3 \quad (5)$$

$$E[X^3] = \frac{\theta^3}{4} \quad (6)$$

Substituting these in Equation (1), the Lorenz curve becomes (Figure 1):

$$L_{X^2}(p) = \frac{\int_0^p \theta^3 t^3 dt}{\theta^3/4} = \frac{\theta^3 p^4/4}{\theta^3/4} = p^4 \quad (7)$$

And thus, substituting in Equation (2), the Gini coefficient of a uniform distribution becomes:

$$GC = 1 - 2 \int_0^1 p^4 dp = 1 - \frac{2}{5} = \frac{3}{5} \quad (8)$$

Hence, for any variable $Z \propto X^3$ that is proportional to the third power of X , such as of V , the $GC_{X^3} = 0.60$ corresponds to the maximum entropy of X .

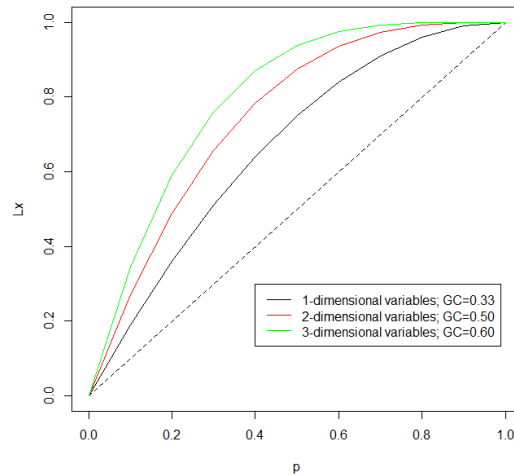


Figure 1: Lorenz curves for 1, 2 and 3-dimensional variables.

4. Discussion

In previous contributions we have showed a threshold of interest which flags up maximum entropy in forest ecosystems at the Gini Coefficient value of $GC_{X^2} = 0.50$ (Valbuena et al. 2012, 2017). In Adnan et al. (2021) we further deduced that the value $GC_H = 0.33$ can be used when interested in the study of LiDAR height profiles. In this contribution we show how higher order extensions can be further deduced, and show the formal proof for the maximum entropy value of $GC_{X^3} = 0.60$ applicable to 3-dimensional variables. In order to achieve these generalized conclusions, we use theoretical distribution functions and show how their parameters propagate into Lorenz curves and values of the Gini Coefficient directly dependent on those parameters. Further extensions can be similarly deduced based on ecological assumptions on ecosystem distributions.

These threshold allows to compare the entropy of the ecosystem using a statistic of dispersion, arguing that for continuous variables it is more correct to use the Gini Coefficient because it avoids the factitious binning step required when computing FHD (McArthur and McArthur, 1961). Gini coefficient is less computationally demanding than FHD, but in Valbuena et al. (2012) we also showed that it is conceptually better.

References

- Adnan S, Maltamo M, Packalen P, Mehtätalo L, Ammaturo R.N.L., and Valbuena R, 2021, Determining maximum entropy in 3D remote sensing height distributions and using it to improve aboveground biomass modelling via stratification. *Remote Sensing of Environment*, 260: 112464.
- Fahey RT, Atkins JW, Gough CM, Hardiman BS, Nave LE, Tallant JM, Nadehoffer KJ, Vogel C, Scheuermann CM, Stuart-Haëntjens E, and Haber LT, 2019, Defining a spectrum of integrative trait-based vegetation canopy structural types. *Ecology letters*, 22 (12): 2049–2059.
- Lefsky MA, Cohen WB, Parker GG, and Harding DJ, 2002, Lidar remote sensing for ecosystem studies. *BioScience*, 52 (1): 19–30.
- Lexerød NL, and Eid T, 2006, An evaluation of different diameter diversity indices based on criteria related to forest management planning. *Forest Ecology and Management*, 222: 17–28.
- Lovejoy TE, 1972, Bird species diversity and composition in Amazonian rain forests. *American Zoologist*, 12: 711-2.
- McArthur RH, and McArthur JW, 1961, On bird species diversity. *Ecology*, 42: 594–598.
- Neumann M, and Starlinger F, 2001, The significance of different indices for stand structure and diversity in forests. *Forest ecology and Management*, 145(1-2): 91–106.
- Schneider FD, Morsdorf F, Schmid B, Petchey OL, Hueni A, Schimel DS, and Schaepman ME, 2017, Mapping functional diversity from remotely sensed morphological and physiological forest traits. *Nature communications*, 8 (1): 1–12.
- Shannon CE, 1948, A mathematical theory of communication. *The Bell System Technical Journal*, 27: 379–423 and 623–656.
- Simonson WD, Allen HD, and Coomes DA, 2014, Applications of airborne lidar for the assessment of animal species diversity. *Methods in Ecology and Evolution*, 5 (8): 719–729.
- Sung PY, and Bera AK, 2009, Maximum entropy autoregressive conditional heteroskedasticity model. *Journal of Econometrics*. 150 (2): 219–230.
- Valbuena R, Packalén P, Martín S, and Maltamo M, 2012, Diversity and equitability ordering profiles applied to study forest structure. *Forest Ecology and Management*, 276:185–195.
- Valbuena R, Packalen P, Mehtätalo L, García-Abril A, and Maltamo M, 2013, Characterizing forest structural types and shelterwood dynamics from Lorenz-based indicators predicted by airborne laser scanning. *Canadian journal of forest research*, 43 (11): 1063–1074.
- Valbuena R, Maltamo M, Mehtätalo L, and Packalen P, 2017, Key structural features of boreal forests may be detected directly using L-moments from airborne lidar data. *Remote Sensing of Environment*, 194: 437–446.
- Valbuena R, O'Connor B, Zellweger F, Simonson W, Vihervaara P, Maltamo M, Silva CA, Almeida DRA, Danks F, Morsdorf F, and Chirici G, 2020, Standardizing Ecosystem Morphological Traits from 3D Information Sources. *Trends in Ecology & Evolution* 35 (8): 656–667.
- Vierling KT, Vierling LA, Gould WA, Martinuzzi S, and Clawges RM, 2008, Lidar: shedding new light on habitat characterization and modeling. *Frontiers in Ecology and the Environment*, 6 (2): 90–98.
- Weiner J, 1990, Asymmetric competition in plant populations. *Trends in Ecology & Evolution*, 5 (11): 360–364,

Characterizing precision benchmarks for stand height and cover estimates derived from existing, conventional, stand-level, photo-based forest inventories

Piotr Tompalski^{1,2}, Joanne C. White², Nicholas C. Coops¹, Michael A. Wulder², Antoine Leboeuf³, Ian Sinclair⁴, Chris Butson⁵, Marc-Olivier Lemonde³

¹*Faculty of Forestry, University of British Columbia, 2424 Main Mall, Vancouver, BC, V6T 1Z4, Canada.*

²*Canadian Forest Service, (Pacific Forestry Centre), Natural Resources Canada, 506 West Burnside Road, Victoria, BC, V8Z 1M5, Canada*

³*Direction des Inventaires Forestiers, Ministère des Forêts, de la Faune et des Parcs du Québec, Quebec City, QC G1H 6R1, Canada*

⁴*Natural Resources Information Section, Science and Research Branch, Ontario Ministry of Natural Resources and Forestry, Ontario Forest Research Institute, 1235 Queen Street, Sault Ste Marie, Ontario, P6A 2E5, Canada*

⁵*Forest Analysis and Inventory Branch, Forest Stewardship Division, Ministry of Forests, Lands, Natural Resource Operations and Rural Development, PO Box 9512, Station Provincial Government, Victoria, BC, V8W 9C2, Canada*

Accurate information on forest resources is fundamental for sustainable forest management. Manual aerial photointerpretation is used as a cost-effective source of data for forest inventories; however, the process of photointerpretation is inherently subjective and is often undertaken by multiple photointerpreters for a given forest management area. In contrast, airborne laser scanning (ALS) data enable characterization of forest structure in a systematic fashion with quantifiable levels of accuracy and precision that often exceed required targets and standards. However, the gains associated with the use of new technologies for forest inventory are difficult to measure because the quality of existing photointerpreted inventories have rarely been quantified.

In this study we characterized the uncertainty of the photo-based measures of stand height and canopy cover, using airborne laser scanning (ALS) data as reference. By incorporating three study sites located in three Canadian jurisdictions we explored the existing photointerpretation standards and then used the ALS data to mimic the specific guidelines for determining canopy height and cover.

The results showed that the agreement between the ALS-based reference values and the photointerpreted attributes was not consistent across the jurisdictions. Results indicated that precision was greater for photointerpreted estimates of height, with a relative standard deviation ranging from 22–29% among our three sites, compared to estimates for canopy cover, with precision ranging from 28%–59%. In addition, the relationship between the estimates of height was linear, and non-linear for canopy cover. Several factors influenced the precision, including dominant species, stand structure, age, and canopy complexity. Most importantly results were not consistent among our three study sites indicating that site-specific forest conditions and photointerpretation procedures influence the precision of photointerpreted estimates.

CASALS: an Adaptive Lidar and Spectrometry SmallSat for a NASA Explorer Mission

David Harding, Guangning Yang, Jeffrey Chen, Mark Stephen, Xiaoli Sun, David Durachka, Hui Li, Wei Lu, James Mackinnon, Travis Wise, Jon Ranson and Philip Dabney

All at: NASA Goddard Space Flight Center, 8800 Greenbelt Rd, Greenbelt, MD 20771, USA
Email: david.j.harding@nasa.gov

1. Introduction

Continuation of laser altimeter observations of the Earth's land and ice sheet topography, sea ice thickness and vegetation structure, begun by NASA's ICESat, ICESat-2 and GEDI missions, is crucial for monitoring and predicting the response of the Earth's surface to climate and land cover change over decadal scales. We are developing an observing system, consisting of a highly efficient, adaptive lidar and a spectrometer, intended for a SmallSat mission later in this decade. The system could serve as the foundation for long-term monitoring of the vertical dimension, composition, and function of the Earth's surface in a series of moderate-cost satellites. The approach addresses three of the Explorer Observables recommended in the 2017 Earth Science Decadal Survey (Committee on the Decadal Survey 2017): ice elevation, snow depth and snow water equivalent, and ecosystem structure. It can also serve as a pathfinder for global mapping of Surface Topography and Vegetation (STV) and the Planetary Boundary Layer (PBL), the two recommended longer-term Incubation Observables.

1.1 Concurrent Artificially-intelligent Spectrometry and Adaptive Lidar System

The observing system, the Concurrent Artificially-intelligent Spectrometry and Adaptive Lidar System (CASALS), includes a lidar which can rapidly adapt the laser footprint locations across a 7km wide swath and a VNIR-SWIR spectrometer with a ≥ 30 km wide swath and 30m pixels. CASALS combines lidar and spectral imaging to merge height data with information about composition and function, thereby enabling new capabilities for characterizing the physical state of the Earth's surface and processes acting upon it. Real-time data analysis, utilizing deep learning models based on techniques such as Long-term Short-term and temporal convolutional networks, will enable autonomous lidar targeting. Use of deep learning enhanced tensor completion will enable software-defined compressive sensing to optimize the adaptive sampling patterns. We are using very large Goddard Lidar Hyperspectral Thermal (G-LiHT) airborne data sets for training and model development. On-board processing will also enable reduction of downlink data volume by intelligent data selection, product generation and compression optimized for land cover specific science and application objectives.

2. CASALS Sensors

2.1 Adaptive Lidar

The block diagram in Figure 1 depicts the high-level functions of the CASALS laser transmitter, receiver, and electronics assemblies. All functionality is based on highly efficient, compact, space-qualifiable components to minimize size, weight, and power to enable a SmallSat implementation. The laser transmitter is based on a state-of-the-art, high-efficiency, 1 micron, solid-state, pulsed laser operating at up to 120KHz, with a compact, photonic integrated circuit (PIC) seed laser and a Yb fiber power amplifier. The laser beam is scanned across a 7km wide swath using a novel passive approach, with no need for a mechanism. This is accomplished by wavelength tuning the seed laser at high-speed, over the range 1.020 and 1.045 microns, and transmitting the beam through a wavelength-to-angle dispersive grating (Figure 1). The receiver telescope will employ free-form optics to reduce its size and weight. In a standard ESPA SmallSat bus, the aperture diameter would be 0.4m. In an ESPA Grande SmallSat the aperture could be as large as 0.9m. Because there is no beam splitting, individual laser pulses are received sequentially. Filtering before the lidar detector is done to reduce solar background noise, rejecting sunlight outside the laser tuning range. Linear-mode, photon-sensitive detection will be done using a 2x64 pixel version of a 2x8 state-of-the-art, HgCdTe detector array developed by DRS,

Inc. in collaboration with NASA GSFC (Sun et al. 2019). Although the laser operates at rates up to 120KHz in our concept, each element of the array will only detect pulses at a maximum rate of 8KHz, thereby preventing cloud folding and enabling profiling of the entire atmospheric column. Using multiple digitizers, the detector's analog output will be recorded at high speed for surface altimetry waveforms and at lower speed for atmospheric cloud and aerosol distributions.

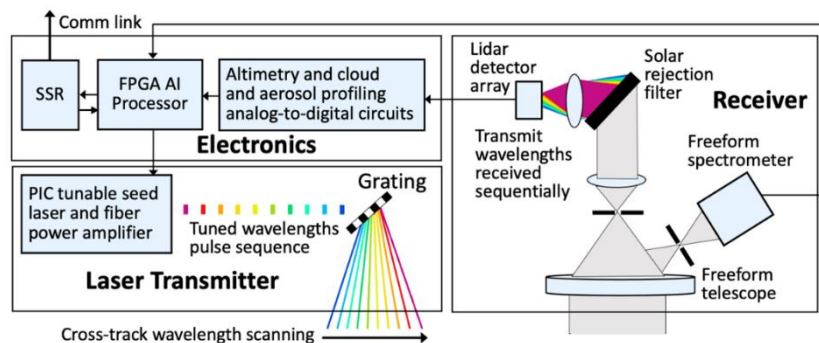


Figure 1: Block diagram of CASALS subsystems, major components and scanning method.

An accompanying, look-ahead thermal microbolometer (not shown) at 1km resolution will image a wide-swath to identify cloud-free areas day and night over land and ice sheets. Autonomous lidar targeting decisions in clear areas will be based on an on-board global land-cover map, spectral image analysis, prioritization of science and application objectives, and tasking uploads for critical dynamic events such as outlet glacier surges, active volcanoes, or ecosystem-damaging insect infestations. Targeting decisions and compressive sensing will be used to configure the adaptive beam scanning to best serve the objectives for a land cover type or event. Figure 2 depicts various configuration options.

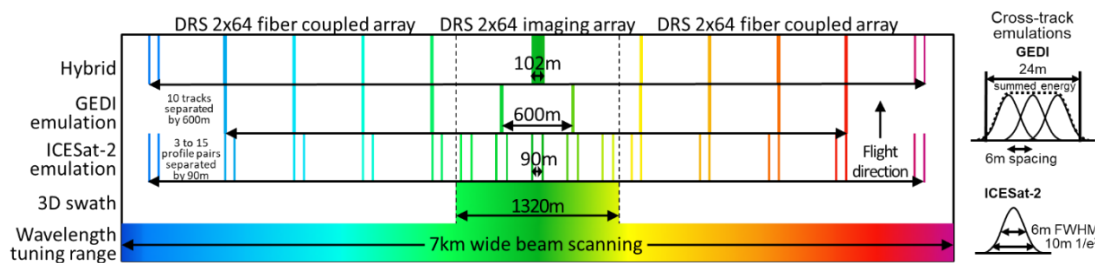


Figure 2: Example configurations of CASALS wavelength-tuned, cross-track beam locations, depicting 3D swath mapping, ICESat-2 and GEDI profile emulations, and a hybrid configuration.

Rapidly tuning the wavelength points 10m diameter ($1/e^2$) footprints to any location separated by 6m across a 7km wide field-of-view (FOV). The DRS 2x64 pixel detector array will not be able to image the entire swath. Our concept is to image a central swath, up to 1,320m wide onto one array, achieving 3-D lidar swath mapping from space for the first time. A second array would be fiber coupled to specific locations across the receiver FOV, enabling continuity with the profile patterns of ICESat-2, with as many as 15 pairs of profiles separated by 90, and GEDI, with as many as 10 profiles separated by 600m. ICESat-2 emulation would use single footprint profiles to match that mission's ~10m footprints, whereas GEDI-emulation would use 3 profiles with 6m cross-track spacing to match that mission's 24m diameter footprints (Figure 2). Along-track footprint spacing can be rapidly changed, from overlapping to widely spaced by changing pulse-rate, to optimize footprint density depending on target height complexity.

The expected lidar performance has been predicted using a comprehensive modelling capability that extends models done for previous missions at Goddard (Sun et al 2013). The model includes more complete treatments of ranging error due to laser speckle, detector timing jitter, finite digitizer sampling and solar background noise. It also estimates the relative random error (RRE) of the surface reflectance measurement. Baseline modelling is for a laser transmitting 30 wavelengths at a total rate of 53KHz with 11W average optical power and a 0.4m receiver telescope, using six design cases developed for the ICESat-2 mission (1a: ice sheet interior, 4: outlet glacier, 7a: tropical flat with moderate and very dense

canopy covers, 9b: boreal hilly with sparse and dense canopy covers). Key performance factors are the number of detected photons and the RMS ranging error for single laser pulses and for 24 overlapping pulses, as well as the solar noise photon rate. The 24 pulses define either a 12m x 72m profile segment emulating the ICESat-2 data product or a 24m x 24m area emulating a GEDI footprint. For cases 1a and 4 profile segments, the predicted ranging errors are similar to those predicted pre-launch by the ICESat-2 project for that mission's photon-counting strong beam (0.01 and 0.13m, respectively). The very low noise DRS detector array, low solar background and the 500 to 600 predicted signal photons for GEDI-emulation vegetation waveforms (cases 7a and 7b), yields SNR levels typical of those acquired by high-pulse energy, full-waveform, large-footprint lidars of the type used by GEDI (Sun et al 2013). For ground topography in the vegetation design cases, the predicted single-footprint RMS ranging errors fall between the 0.5m threshold and 0.1m aspirational vertical accuracy goals identified in a study of the Decadal Survey STV Observable conducted for NASA (STV Study Team 2021), other than the very challenging 7a case with 99% canopy closure.

2.2 Imaging Spectrometer

Several design factors are being evaluated for the spectrometer. Those include swath width, wavelength range, band width, band sampling (continuous hyperspectral or discrete multispectral), optical design (traditional or free-form) and configuration with the lidar (sharing a telescope, separate telescopes on one satellite or separate satellites flying close in time on the same orbit path). The baseline is a traditional optical design developed for a GSFC forest-ecosystem SmallSat mission concept with a 30km swath and 21 narrow VNIR and SWIR bands optimized for vegetation function indices and atmospheric correction. Several additional bands would be added for characterization of snow and ice properties, including grain size, contaminant levels and water concentration. A more advanced spectrometer in development at GSFC is also being considered, with a 90km swath and full VNIR and SWIR spectrum, using free-form optics to dramatically reduce size and weight compared to traditional spectrometers.

3. Development Status

The CASALS lidar technologies are being developed and demonstrated in two steps. We are demonstrating the transmitter and receiver functions at 1.5 micron using high-maturity, in-hand components, and will range horizontally to calibration and natural targets over distances of about 1km. The electronics will use commercial National Instruments PIXe cards. Demonstration of this prototype is expected in late 2021, done in combination with commercial VNIR hyperspectral and SWIR multispectral cameras. Meanwhile, with industry and university partners, we are migrating the laser transmitter components to 1 micron, which is necessary to achieve the efficiencies needed for spaceflight use. That lidar and spectrometry system will be capable of operating at high altitudes, up to 20km. We are also migrating the data system to an FPGA processor which emulates the GSFC SpaceCube spaceflight processor architecture. Demonstration of this prototype is expected in late 2022.

Acknowledgements

This work is being supported by the GSFC Radical Innovation Initiative, the NASA Earth Science Technology Office IIP and ACT programs and the NASA Small Business Innovation Research program.

References

- Committee on the Decadal Survey for Earth Science and Applications from Space Space Studies Board, 2017, *Thriving on Our Changing Planet: A Decadal Strategy for Earth Observation from Space*, The National Academies Press, Washington, D.C.
- STV Study Team, 2021, *Observing Earth's Changing Surface Topography and Vegetation Structure: A Framework for the Decade*, NASA Surface Topography and Vegetation Incubation Study. National Aeronautics and Space Administration.
- Sun X, Abshire JB, McGarry JF, Neumann GA, Smith JC, Cavanaugh JF, Harding DJ, Zwally HJ, Smith DE and Zuber MT, 2013, Space Lidar Developed at the NASA Goddard Space Flight Center - The First 20 Years, *IEEE Journal of Selected Topics in Applied Earth Observations and Remote Sensing*, 6(3): 1660-1675.
- Sun X, Abshire JA, Krainak MA, Lu W, Beck JD, Sullivan III WW, Mitra P, Rawlings DM, Fields RA, Hinkley DA and Hirasuna BS, 2019, HgCdTe avalanche photodiode array detectors with single photon sensitivity and integrated detector cooler assemblies for space lidar applications, *Optical Engineering*, 58(6): Paper 067103.

Using advanced airborne remote sensing as a sampling tool to support forest inventory in interior Alaska, USA

H-E. Andersen¹, J. Strunk², B. Cook³, D. Morton³, M. Alonzo⁴, A. Finley⁵, C. Babcock⁶, and S. Cahoon⁷

¹USDA Forest Service Pacific Northwest Research Station, University of Washington, Box 352100, Seattle, WA 98195 USA
Email: hans.andersen@usda.gov

²USDA Forest Service Pacific Northwest Research Station, Olympia Forestry Science Laboratory, Olympia, WA 98512 USA
Email: jacob.strunk@usda.gov

³NASA Goddard Space Flight Center, Biospheric Sciences Laboratory Code 618, Greenbelt, MD 20771 USA
Email: bruce.cook@nasa.gov, douglas.morton@nasa.gov

⁴American University, Department of Environmental Science, Washington DC 20016 USA
Email: alonzo@american.edu

⁵Michigan State University, Department of Forestry and Geography, East Lansing, MI 48824 USA
Email: finleya@msu.edu

⁶University of Minnesota, Department of Forest Resources, St. Paul, MN 55108 USA
Email: cbabcock@umn.edu

⁷USDA Forest Service Pacific Northwest Research Station, Anchorage Forestry Sciences Laboratory, Anchorage, AK 99501 USA
Email: sean.cahoon@usda.gov

1. Introduction

The USDA Forest Service Forest Inventory and Analysis (FIA) program is mandated by US Congress to implement a forest inventory and monitoring system in the boreal forests of interior Alaska, and extending the FIA inventory into this region has been identified as a strategic priority for the national program. Given the extreme logistical challenges and high costs associated with implementing a field inventory in this remote region – where there is virtually no transportation infrastructure and almost every plot requires a helicopter to access – there is a strong interest in leveraging state-of-the-art remote sensing technology to support the FIA inventory in interior Alaska. For this reason, FIA has partnered with NASA-Goddard to implement an innovative, multi-level sampling design in this region, where a sparse grid of field plots is supplemented with high-resolution airborne remote sensing data collected with the multi-sensor G-LiHT (Goddard Lidar-Hyperspectral-Thermal) system. Initial results from the first inventory unit (Tanana Valley) indicate that use of model-assisted estimation in a 2-stage design can increase the precision of estimates for key inventory attributes (biomass, carbon).

2. Data

2.1 Forest inventory data

The FIA program established 690 field inventory plots on forested conditions in the Tanana inventory unit during the period 2014-2018. Field plots were established on a regular hexagonal grid, with a spacing between plots of approximately 11 km, resulting in a field sampling intensity of 1 plot per 12000 ha. The standard FIA plot design was used, where each plot consists of a cluster of four 1/60th ha fixed-A large number of forest attributes were measured at each plot, including measurements of tree size, species and condition (live/dead), downed woody materials, lichens/moss, and soil properties (bulk density, carbon, etc.) (Cahoon et al., *in prep*), as well as condition-level attributes such as forest type, stand size, etc. In addition, high-precision GNSS receivers were used to obtain high-quality spatial coordinates for each FIA subplot (Andersen et al., *in prep*). Total aboveground biomass for individual trees (live and dead) was calculated using published biomass equations (Cahoon et al., *in prep*) and total biomass, by forest type, was calculated for each plot.

2.1 G-LiHT airborne remote sensing data

High-resolution airborne remote sensing data was collected with the Goddard Lidar-Hyperspectral-Thermal (G-LiHT) system in a strip sampling mode over the entire Tanana unit in 2014 and 2018 (fig. 1). This multi-sensor instrument provides 1) detailed forest structure and terrain morphology using lidar scanning, 2) forest composition and health measurements using imaging spectrometry, and 3) surface temperature measurements using thermal scanning (Cook et al., 2013). G-LiHT data were acquired in nominal 350 meter side swaths along flight lines (spaced approx. 9,200 meters apart, oriented in a NE-SW direction) that were planned to cover every potentially-forested FIA field plot. In the end, G-LiHT measurements were acquired over 906 out of 1,091 total FIA plots in the Tanana Unit (most of the plots missed by G-LiHT were in clearly unvegetated rock/ice areas of the Alaska Mountain Range, etc.).

3. Methods

3.1 Post-stratified, 2-stage model-assisted estimation framework

The standard estimation approach in the FIA program uses post-stratification (Bechtold and Patterson, 2005), where the stratification is usually based on a combination of spatial layers including satellite-derived land cover classification (e.g. National Land Cover Dataset (NLCD), Dewitz, 2019), and other environmental gradients such as precipitation, elevation, etc. In order to incorporate the additional information provided by the G-LiHT strip sample in interior Alaska, we utilize a post-stratified ratio estimator under a two-stage design, where the FIA plots and G-LiHT acquisition can be seen as a two-stage (cluster) sampling design, with the G-LiHT swaths (strips) treated as clusters (1st stage) and the FIA plots represent a subsample within the clusters (2nd stage). The efficiency of the estimation from this two-stage design can be further improved through post-stratification and by accounting for the length of the strips (via ratio estimation). The resulting estimator is a post-stratified, ratio estimator for model-assisted estimation in a two-stage design (Andersen et al., 2011; Ringvall et al., 2016; Strunk et al., 2014). Following Ringvall et al. (2016), the response variable is a forest inventory attribute (possibly for a specific domain, such as forest type) summarized at the FIA plot-level, and the predictor variables are G-LiHT derived metrics extracted from the footprint of the FIA plot (average lidar-derived canopy height, hyperspectral-based forest type classification), and a linear regression model is developed relating the inventory attribute to lidar metrics.

FIA plots are distributed about 9 km apart along each G-LiHT strip (1,091 total FIA plots), and remote sensing (RS) plots (with the same spatial configuration and size as a FIA plot) were distributed at 200 meter intervals along the center of each G-LiHT strip (fig 3; 73,509 total RS plots). At each of these RS plots, the regression model is used to predict the inventory parameter. In addition, if the population is post-stratified, where the number of remote sensing plots within each stratum is assumed to be known without error, the model-assisted regression estimate for the specified inventory attribute in a given strip and stratum can be calculated. In cases where a RS plot is missing (mountainous areas, low clouds, etc.), the value for the RS plot measurement (lidar and/or forest type classification) was imputed as the mean lidar height or most commonly occurring forest type class within the stratum. A ratio-to-size estimator at the stratum level and the post-stratified ratio estimator can be calculated. The variance estimator of the post-stratified ratio estimator takes into account 1) the variance of the model-assisted estimator within strips, 2) variance between strips, and 3) the dependency between stratum-level estimates within strips. A variance estimator can be applied in cases where only a small portion of the strips may cover individual strata (Ringvall et al., 2016). However, with very small strip- and stratum-level plot sample sizes the variance estimator is likely highly variable or even impossible to calculate. Therefore the variance estimator is modified to replace stratum- and strip-level residual variance with the stratum-level residual variance calculated across all strips, which we assume will be more stable and, if anything, will be a conservative estimate because residuals within strips are likely to be spatially-autocorrelated). It should be noted that this variance estimator assumes that the G-LiHT strips, RS, and FIA plot subsamples are collected as a simple random sample in both stages. In reality, both the FIA data (regular hexagonal grid) and the G-LiHT strips (evenly-spaced strip sample) represent a systematic sample, not a simple random sample. This likely leads to an overestimation of variance,

although it should be noted that small samples at the strip level can also lead to unreliable variance estimators (Ringvall et al., 2016). Further research on optimal field sampling intensity, stratification, and use of hyperspectral-based forest type classification within this 2-stage design and model-assisted inferential framework is needed and ongoing.

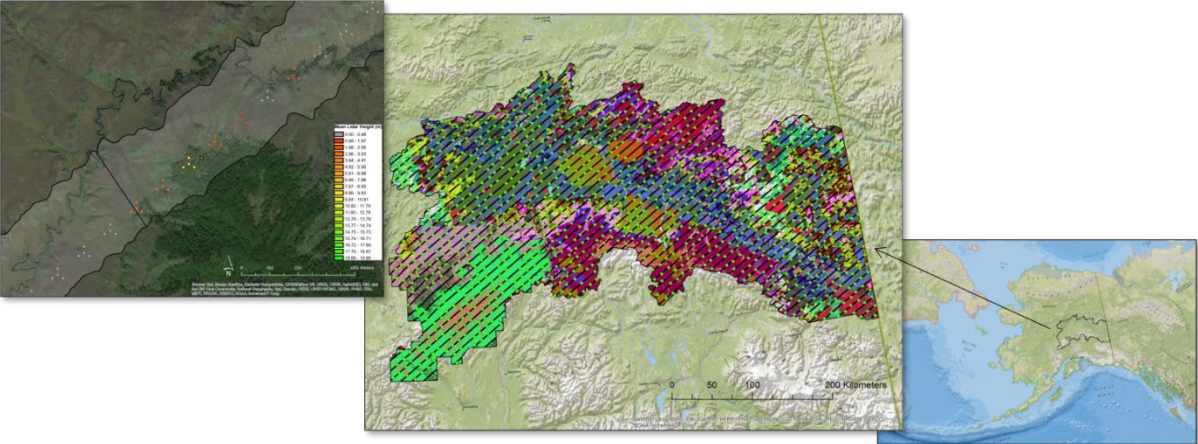


Figure 1: Alaska, USA (right), Tanana inventory unit (center) with FIA plots (green dots), G-LiHT flight lines (black) and post-strata (various colors). Left inset image shows G-liHT swath covering RS plots and FIA plot (dark outline), colored by lidar canopy height.

4. Results

A comparison of the tabular estimates for aboveground tree biomass, by forest type, provided by the standard post-stratified and post-stratified ratio estimator is shown in Table 1. These results indicate that incorporating the G-LiHT lidar height measurements in the estimator through a ratio estimator can significantly improve the precision of the inventory estimates. The standard errors (SE) of the post-stratified ratio estimators are generally lower than the post-stratified estimator, with the most significant reduction in the more aggregated estimators (i.e. total biomass, all softwood, all hardwood) and less improvement in the precision of biomass estimates for specific domains (i.e. forest types).

Table 1 - Comparison of standard FIA post-stratified and post-stratified ratio estimates under a two-stage design of aboveground biomass by forest type, Tanana Unit, Alaska, 2018

Forest type	Post-stratified		Post-stratified Ratio	
	Total	SE	Total	SE
Softwoods		<i>thousand tons</i>		
White Spruce	71,113	9,151	68,807	7,767
Black Spruce	101,820	6,368	99,948	5,761
Tamarack	527	309	522	399
Total Softwoods	173,460	9,811	169,277	7,654
Hardwoods				
Paper Birch	74,553	8,370	70,140	5,667
Aspen	22,114	4,631	20,375	4,711
Balsam Poplar	5,118	2,323	4,850	1,503
Total Hardwoods	101,786	9,244	95,390	6,769
Nonstocked				
< 10% live trees	25	16	25	360

Total	275,271	12,008	264,667	7,407
-------	---------	--------	---------	-------

5. Discussion and conclusions

The results of this study indicate that incorporating airborne lidar sampling in the FIA sampling design in interior Alaska – through model-assisted estimation – can improve the precision of key inventory estimates, such as aboveground biomass and carbon. The gains in precision are most pronounced for aggregate estimates, such as total biomass or total biomass for hardwoods/softwoods. The gains in precision for more specific domains (forest type) are much less pronounced, indicating that more informative predictor variables, or perhaps more sophisticated modelling approach, should be used to leverage the information provided by G-LiHT measurements to improve domain-level estimation. Going forward, FIA and NASA are proceeding with data collection in other regions of interior Alaska and it is expected that FIA will continue to leverage the detailed information provided by this airborne data to increase the reliability and value of the scientific products from this inventory and monitoring program.

Acknowledgements

Funding support for this study was provided by the NASA Carbon Monitoring System and USDA Forest Service Forest Inventory and Analysis program.

References

- Andersen, H.-E.; Strunk, J.; R. McGaughey. *Improving the Quality of FIA Plot Coordinates in the Pacific States using High-Precision GNSS Technology*. In prep.
- Andersen, H.-E.; Strunk, J.; Temesgen, H. 2011. Using airborne light detection and ranging as a sampling tool for estimating forest biomass resources in the upper Tanana Valley of Interior Alaska. *West. J. of Applied Forestry* 26:157-164..
- Bechtold, W.A.; Patterson, P.L. 2005. The enhanced Forest Inventory and Analysis program—national sampling design and estimation procedures. Gen. Tech. Rep. SRS 80. Asheville, NC: U.S. Department of Agriculture, Forest Service, Southern Research Station. 85 p.
- Cahoon, S.; Baer, K. eds. *Forest Resources of the Tanana Unit: 2018*. In prep.
- Cook, B. D.; Corp, L.; Nelson, R.; Middleton, E.; Morton, D.; McCorkel, J.; Masek, J.; Ranson, K.J.; Ly, V. Montesano, P. 2013. NASA Goddard's Lidar, Hyperspectral and Thermal (G-LiHT) airborne imager. *Remote Sensing* 5:4045-4066, doi:10.3390/rs5084045.
- Dewitz, J. 2019. National Land Cover Database (NLCD) 2016 Products: U.S. Geological Survey data release, <https://doi.org/10.5066/P96HHBIE>.
- Ringvall, A.; Ståhl G., Ene, L.; Næsset, E.; Gobakken, T.; Gregoire, T. 2016. A poststratified ratio estimator for model-assisted biomass estimation in sample-based airborne laser scanning surveys. *Canadian Journal of Forest Research* 46:1386-1395.
- Strunk, J.; Temesgen, H.; Andersen, H.-E.; Packalen, P. 2014. Prediction of forest attributes with field plots, Landsat, and a sample of lidar strips. *Photogrammetric Engineering & Remote Sensing*. 80(2): 143-150.

Machine Learning for Tree Species Identification from LiDAR & Imagery

Trevor Hooper¹, Mike Parlow², Hazel Jeong³
D'Laine Robertson-Hooper⁴, Geoff Lawless⁵

¹Forsite Consultants Ltd, PO BOX 2079, Salmon Arm, BC, V1E 4R1
Email: thooper@forsite.ca

²Forsite Consultants Ltd, PO BOX 2079, Salmon Arm, BC, V1E 4R1
Email: mparlow@forsite.ca

³Forsite Consultants Ltd, PO BOX 2079, Salmon Arm, BC, V1E 4R1
Email: hjeong@forsite.ca

⁴Forsite Consultants Ltd, PO BOX 2079, Salmon Arm, BC, V1E 4R1
Email: drobotson-hooper@forsite.ca

⁵Forsite Consultants Ltd, PO BOX 2079, Salmon Arm, BC, V1E 4R1
Email: glawless@forsite.ca

1. Introduction

The investigators sought to explore and examine the impact of varied remote sensing inputs for species identification using machine learning. The foundation of the research was a multi-class support vector machine (SVM) learning adaptation originally developed in 2012. The latter used LiDAR as the exclusive input for species identification and leveraged spatial density, trunk & branch geometry, and the intensity attribute. In the new effort, the team attempted to adapt and incorporate spectral as well as land form information to the SVM descriptor list. 251 new descriptors were created and ranked alongside the existing 847 descriptors. The research team sought to determine the optimal combination of descriptors for species identification accuracy. The result was an increase in stem accuracy in a cross-fold validation test of between 8% and 13% for a mix of 13 conifer and deciduous species.

1.1 Background

The Tree Species Identifier (TSI) system uses a bottom-up approach where metrics are measured and predicted first at the individual tree level. The individual tree process captures height, canopy characteristics, and species from the LiDAR. From those inputs, the system can calculate estimates of the diameter at breast height (DBH) as well as volume. Once the analysis has been completed at the single tree level, the outputs can be rolled up to larger reporting units. The results individual tree inventory can also be used for statistical adjustments across the land base using an area-based enhanced forest inventory approach.

First developed in 2012, the process has successfully analysed over 2 billion trees and produced operational inventories derived from hundreds of terabytes of LiDAR across millions of forested hectares.

1.2 Tree Species Identifier Process

First the LAS is reviewed, cleaned, and prepared for analysis. Analysts review an array of factors including the consistency of point density, the intensity calibration, and any gaps in the coverage. Then TSI segments the individual trees from the point cloud and produces an area shapefile for each tree. The

system calculates a number of attributes including height, slope, crown area, aspect, local density, and live crown percentage. Each tree also receives a unique ID at this point in the process.

The segmentation parameters used are selected based on a variety of stand characteristics using a blend of classic watershed techniques and point finding routines. Individual tree inventories from LIDAR tend to underestimate the number of stems as the software can only include what the sensor sees. Missed stems are typically smaller ones hiding under larger ones or those in tight clumps with a common height. Conversely, leaning trees can sometimes be segmented into multiple trees. As LiDAR point densities increase, say above 16-20 pts/m², the segmentation algorithm is able to adapt resulting in higher overall tree segmentation accuracy as well as understory segmentation.

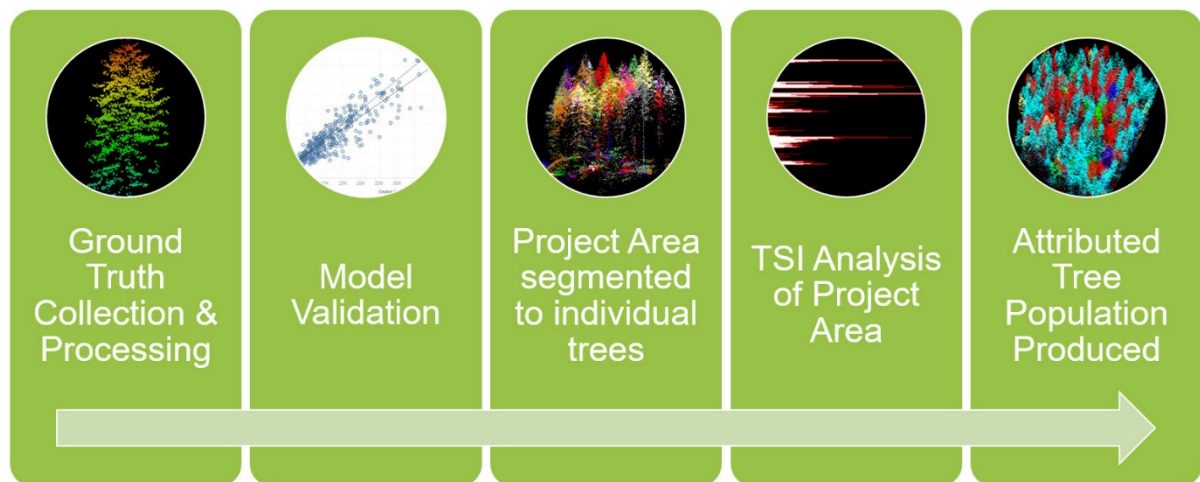


Figure 1: Tree Species Identifier Process

The next step in the species identification process is the collection of ground truth trees to be used in the TSI species prediction model. Trees are collected based on species, height, and location within the project area of interest by field crews and/or photo-interpretation. The goal is to acquire 100 to 300 samples of each species in the project area. The required number of samples per species varies project to project based on the complexity of the species mix and the size of the area under consideration. Using methods refined over 9 years, a trained 2-person field crew can collect 800 trees over 5 days.

Once the trees are captured, analysts attempt to match up the field or photo-interpretation collects with the correct tree in the LiDAR point cloud. The quality control success rates vary depending primarily on canopy density and GPS signal strength. Next the tree samples that have passed quality control are translated into machine-learning numeric “descriptors” in TSI. The software translates the information in each tree’s point cloud into numeric descriptors based on geometry, density, and reflectivity. This step is at the heart of the TSI capability and the focus of the research. The model validation proceeds with the derived descriptors and the resulting model is used to perform a discrete analysis of each segmented tree.

Diameter at breast height (DBH) is derived from the tree height and species using established biometric models. The DBH is then used to calculate gross and merchantable volume for each tree.

2.0 Descriptor Research

The research team collected remote sensing inputs over forest areas in the Canadian province of British Columbia. The imagery data included 30 cm resolution 4-band RGB-NIR ortho-photo as well as 10 m resolution satellite Sentinel-2 multispectral. Terrain data included 2m resolution wetness and sunlight maps derived from the LiDAR. The Provincial Forestry Ministry also provides ecosite information and predictive ecosystem mapping, land base metrics that provide broad soil and moisture information, both of which were incorporated. The LiDAR was flown with a 10-12 pts/m² point density.

6 descriptor test combinations were tested:

1. Baseline: 10-12 ppm LiDAR only
2. Baseline plus LiDAR-derived intensity images from two channels
3. Baseline plus 4-band RGB-NIR
4. Baseline plus terrain characteristics
5. Baseline plus 4-band RGB-NIR & terrain characteristics
6. Baseline plus 4-band RGB-NIR & terrain characteristics & LiDAR-derived intensity images

The descriptors were run against a ground truth set of 4,395 trees including 13 species.

FD	Douglas Fir	CW	Western Red Cedar
LW	Western Larch	AC	Black Cottonwood
BL	Balsam Fir	AT	Trembling Aspen
PY	Ponderosa Pine	EP	Paper Birch
PL	Lodgepole Pine	DP	Lodgepole Pine (Dead)
SX	Spruce (hybrid)	SN	Snag
RP	Lodgepole Pine (Red - Dying)		

Table 1: Species included in the test

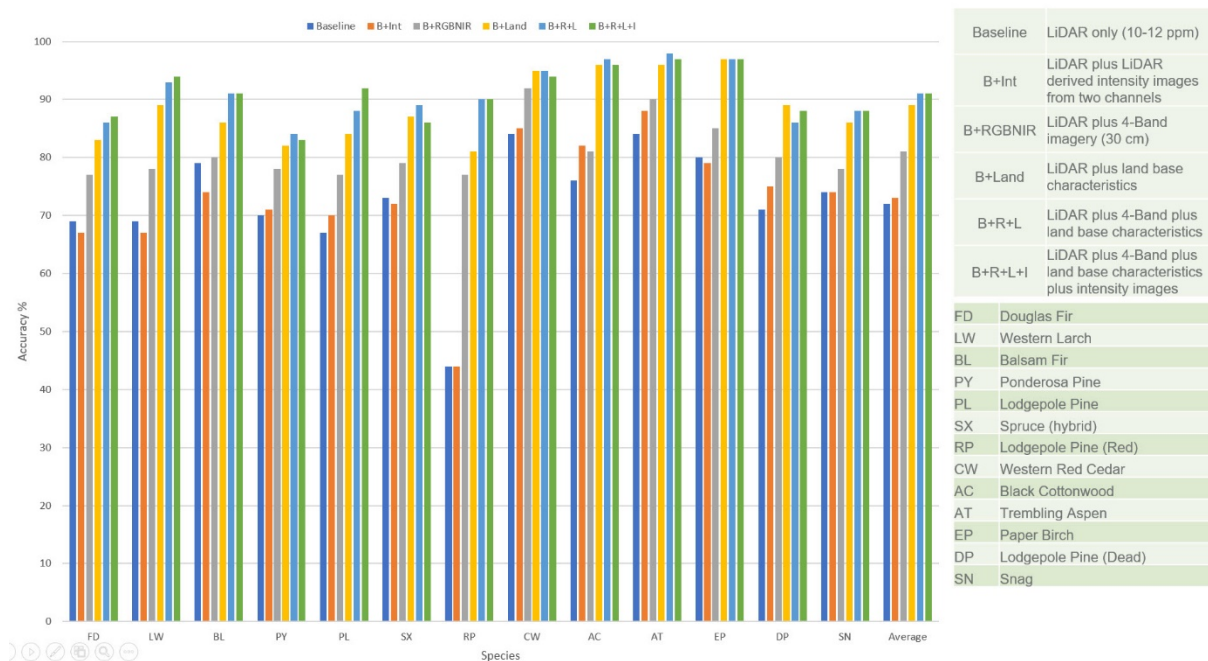


Figure 2: Species Results by descriptor set

The general trend evidenced by the trials was that as the descriptor sets added additional remote sensing and terrain input information, species accuracy improved. This trend held for conifer and deciduous classes broadly as well as dead or stressed trees. The largest improvement was seen for dying lodgepole pine (red) while the highest accuracies were recorded for the deciduous species.

True label	FD	LW	BL	PY	PL	SX	SR	CW	AC	AT	EP	DP	SN
FD	445	3	2	47	2	16	24	3	7	0	6	0	2
LW	15	51	0	3	1	3	3	6	1	0	0	0	0
BL	1	0	295	0	20	35	3	0	0	0	0	3	3
PY	42	8	0	265	0	1	10	4	1	3	3	0	5
PL	6	2	4	0	327	14	4	1	4	7	6	8	3
SX	20	1	35	1	38	265	3	3	2	0	3	2	2
SR	62	2	33	20	46	5	82	4	6	4	5	10	23
CW	10	3	4	4	0	8	2	168	9	0	2	0	3
AC	12	0	0	3	7	6	10	5	233	29	12	1	6
AT	1	1	0	0	14	2	2	0	32	403	11	3	4
EP	6	2	2	7	26	0	9	3	4	25	170	0	7
DP	3	0	0	0	8	3	0	0	0	3	0	258	48
SN	6	0	4	3	2	4	12	1	4	3	0	68	289

	precision	recall	f1-score	support
FD	0.71	0.80	0.75	557
LW	0.70	0.61	0.65	83
BL	0.78	0.82	0.80	360
PY	0.75	0.77	0.76	342
PL	0.67	0.85	0.75	386
SX	0.73	0.71	0.72	375
SR	0.50	0.27	0.35	302
CW	0.85	0.79	0.82	213
AC	0.77	0.72	0.74	324
AT	0.84	0.85	0.85	473
EP	0.78	0.65	0.71	261
DP	0.73	0.80	0.76	323
SN	0.73	0.73	0.73	396
accuracy			0.74	4395
macro avg	0.73	0.72	0.72	4395
weighted avg	0.74	0.74	0.73	4395

Table 2: Baseline Species Accuracy Confusion Matrix

True label	FD	LW	BL	PY	PL	SX	SR	CW	AC	AT	EP	DP	SN
FD	511	1	0	38	1	1	2	1	0	0	0	1	1
LW	8	70	0	0	0	0	3	2	0	0	0	0	0
BL	1	0	317	0	10	25	1	0	0	0	0	3	3
PY	35	0	0	300	0	0	3	2	0	0	0	1	1
PL	0	0	1	0	368	9	2	0	0	1	0	4	1
SX	5	0	18	0	10	338	0	0	0	0	0	1	3
SR	12	3	10	7	11	2	237	0	2	0	1	2	15
CW	4	0	0	0	0	1	0	204	2	1	0	0	1
AC	0	0	1	1	0	1	1	3	310	3	2	1	1
AT	0	0	0	1	1	1	1	0	3	461	4	0	1
EP	0	0	0	1	3	1	0	0	2	7	247	0	0
DP	4	0	1	0	4	0	0	0	0	0	0	201	23
SN	3	0	3	3	1	0	12	0	1	0	0	36	337

	precision	recall	f1-score	support
FD	0.88	0.92	0.90	557
LW	0.95	0.84	0.89	83
BL	0.90	0.88	0.89	360
PY	0.85	0.88	0.87	342
PL	0.90	0.95	0.93	386
SX	0.89	0.90	0.90	375
SR	0.90	0.78	0.84	302
CW	0.96	0.96	0.96	213
AC	0.97	0.96	0.96	324
AT	0.97	0.97	0.97	473
EP	0.97	0.95	0.96	261
DP	0.86	0.90	0.88	323
SN	0.87	0.85	0.86	396
accuracy			0.91	4395
macro avg	0.91	0.90	0.91	4395
weighted avg	0.91	0.91	0.91	4395

Table 3: Final Species Accuracy Confusion matrix

The most significant improvement was in dying lodgepole pine (SR). A working hypothesis was that SR would improve as a result of the addition of spectral descriptors. While true, SR accuracy also improved with the addition of terrain characteristics in the absence of spectral data. Douglas fir and ponderosa pine confusion was reduced from 89 direct errors to 73 direct errors. The latter improvement fell short of expectations as the two species have distinct spectral signatures. Those distinct signatures enable rigorous accuracies in photo-interpretation and so more improvement was expected. One possible explanation is that the geometry and density descriptors derived from the point cloud may have some embedded biases that need to be addressed in future research. Another possible explanation is the introduction of noise by the imagery due to parallax offsets that degraded the predictive power of the descriptor.

Structure-Mediated Differences in Foliar Illumination and Their Effects on Diurnal Changes in a Pine Plantation Photochemical Reflectance Index

P. T. Williams¹, D. J. Harding², V. A. Thomas¹, R. H. Wynne¹, K. F. Huemmrich², K. J. Ranson², E. M. Middleton², P. K. Campbell²

¹Department of Forest Resources and Environmental Conservation, Virginia Tech, Blacksburg, VA
Email: {paigetw; thomasv; wynne}@vt.edu

²Biospheric Sciences Laboratory, NASA Goddard Space Flight Center, Greenbelt, MD
Email: {david.j.harding; karl.f.huemmrich; kenneth.j.ranson; elizabeth.m.middleton; petya.k.campbell}@nasa.gov

1. Introduction

Rapid changes in atmospheric trace gases, the resulting changes to climate, and numerous other anthropogenic effects are changing the function of forests globally. These anthropogenic changes to forest function affect gross primary productivity (GPP) and thus the potentially mitigative effect of forest growth on the rate of atmospheric carbon dioxide increase. GPP can be modelled as the product of light use efficiency (LUE), photosynthetically active radiation (PAR), and the fraction of PAR absorbed by foliage (fPAR). While robust satellite-derived PAR and fPAR estimates have been routine for decades, LUE has been more difficult to quantify over space and time. This is in part because foliar LUE is dependent on the amount of incident light, typically being lower for sunlit foliage receiving light exceeding that which can be used in photosynthesis. Very high spatial resolution optical images can be used to determine whether a pixel is receiving direct (sunlit) or diffuse (shaded) light, or a mixture of both. However, given that canopy structure mediates the light environment, lidar data, the gold standard for quantifying canopy structure, is needed to enable articulation of the within-canopy light environment.

The photochemical reflectance index (PRI), derived using image spectroscopy, has been used successfully to estimate LUE (Zhou et al., 2017). This study incorporates high-resolution airborne imaging spectroscopy and lidar data to investigate the vertical distribution of light and PRI. This research enhances our understanding of forest light utilization, which we expect will lead to improved model estimation of GPP.

2. Study Area

The study area in the coastal plain of North Carolina, USA is a 420 m x 420 m plot centred on the Ameriflux US-NC2 flux tower in a loblolly pine stand planted in 1993 with NNW-SSE rows. (Figure 1). During establishment of the stand, drainage channels were constructed every 5th row and broad-leaf, deciduous vegetation was planted to stabilize the banks. In 2009, every fifth pine row was removed, and regrowth dominated by broad-leaf vegetation has subsequently filled those rows.

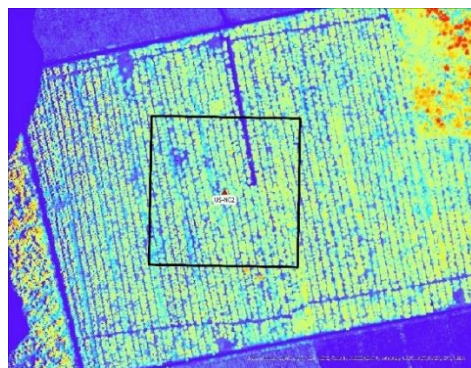


Figure 1: Study area 420 m x 420 m plot centered on US-NC2 overlain on G-LiHT's 2 m lidar canopy height model. North is to the top and blue to red correspond to increasing canopy height.

3. Airborne Remote Sensing Data Fusion

Goddard Lidar, Hyperspectral and Thermal (G-LiHT) (Cook et al., 2013) airborne data were collected in October 2013 at Parker Tract in eastern North Carolina during the FLEX-US Airborne Campaign (Middleton et al., 2017). Ten flights spanned the time range from 10:00 am to 4:30 pm on October 26th and 27th. Deciduous broad-leaf foliage was present on these dates. G-LiHT's products, gridded at 2 m resolution, include digital terrain models (DTM) and canopy height models (CHM) derived from lidar point clouds. We added those models to produce a canopy surface model (CSM). G-LiHT's 114 hyperspectral bands, with 5 nm band widths, have been calibrated to a surface reflectance product and co-registered with the height models.

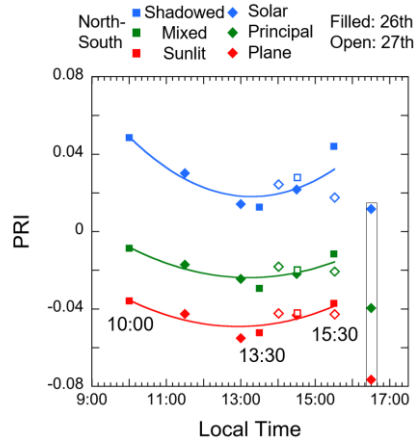


Figure 2: Time series of PRI stand means for the three light environment classes for flights oriented North-South and in the solar principal plane, and 2nd order polynomial fits excluding the last flight.

For each flight, we computed PRI using the normalized difference of two narrow-band, green wavelengths at 531 nm and 570 nm (Gamon, 1997). Before PRI was calculated, a Normalized Difference Vegetation Index (NDVI) threshold of 0.5 and below was implemented to eliminate non-vegetated pixels that are not photosynthetically active. Sunlit, mixed illumination and shadowed parts of the canopy were classified based on the reflectance distributions of 2 m pixel panchromatic images produced by averaging G-LiHT wavelength bands from 525 nm to 600 nm. The panchromatic band pixels were classified based on the mean and standard deviation of the reflectance distribution (sunlit > mean + 1 sigma, mixed between ± 1 sigma, and shadow < mean - 1 sigma). Stand mean PRI was computed for each flight and illumination class (Figure 2).

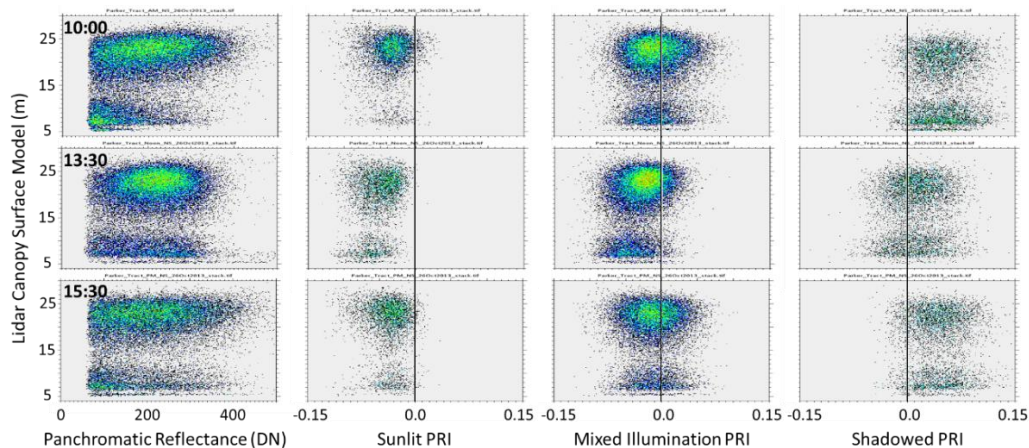


Figure 3: Height distributions of panchromatic reflectance and PRI for 2m pixels, with colors indicating the density of plotted points (increasing from black to red).

To assess the diurnal vertical distribution of reflectance and PRI for the different illumination classes, the CSM height of each hyperspectral pixel was determined for three times of day (10:00, 13:30, and 15:30) for North-South flights on the 26th (Figure 3). The 13:30 CSM was used for each distribution, under the assumption that the structure was invariant through the day.

4. Results and Discussion

Mean PRI is negative for the sunlit class and positive for the shadow class, indicative of low and high LUE, respectively (Figure 2). The mixed illumination class falls between these. PRI is higher at the beginning and end of the day and decreases during the midday, likely due to the availability of light exceeding the capacity of photosynthetic activity when the solar zenith angle is small. The latest flight observed the plot close to the “hot-spot” solar backscatter orientation which can cause anomalous PRI results (Cheng et al., 2012) and is potentially the cause of the departure from the diurnal trend.

The height distributions (Figure 3) show a clear delineation between the 20-year-old upper canopy, the lower regrowth understory, and the flat ground. The panchromatic reflectance depicts the depth to which light is penetrating the canopy. For the 10:00 and 15:30 flights, the upper canopy exhibits decreasing reflectance as height decreases, indicative of less direct light illumination of the foliage and a greater amount of shadow (assuming the reflectivity of the foliage does not change with height). The understory is primarily in shadow, indicated by its mostly low reflectance and the associated predominance of shadowed pixels in the PRI distributions as compared to sunlit. At 13:30, the upper canopy reflectance is more uniform, and the understory reflectance includes higher values and is more equally distributed between illumination classes. Presumably, this is because the higher mid-day direct sunlight oriented more in-line with the rows creates fewer shadows and reaches deeper into the canopy.

For all illumination classes, the reduction in mid-day PRI, as compared to the earlier and later flights, occurs at all heights (Figure 3). At 10:00 and 15:30 the PRI of the upper canopy and understory are equivalent, but at 13:30 the understory exhibits lower PRI than the upper canopy for the sunlit and mixed illumination classes. This suggests that the reduced mid-day efficiency of the broadleaf foliage dominating the understory is more sensitive to excessive illumination than the loblolly pine. The return of the PRI values in the afternoon to the morning levels implies that stresses lowering mid-day photosynthetic efficiency, due to excessive illumination and possibly increased temperature or reduced water availability, do not continue into the later afternoon.

This novel fusion of canopy reflectance, the PRI hyperspectral functional index, and a lidar representation of structure introduces a new method to gain a better understanding of the light environment of forests and the diurnal variation in LUE. It is a step forward in modelling structure-mediated forest productivity and carbon sequestration.

Acknowledgements

This work was funded by the U.S. Department of Agriculture McIntire-Stennis Formula Grant program (Project number 1007054 (VA-136633), “Detecting and Forecasting the Consequences of Subtle and Gross Disturbance on Forest Carbon Cycling”), NASA Goddard Space Flight Center, and the Virginia Tech Department of Forest Resources and Environmental Conservation.

References

- Cheng YB, Middleton EM, Zhang Q, Corp LA, Dandois J, Kustas WP, 2012, The photochemical reflectance index from directional cornfield reflectances: Observations and simulations. *Remote Sensing of Environment*, 124, 444–453.
- Cook BD, Corp LA, Nelson RF, Middleton EM, Morton DM, McCorkel JT, Masek JG, Ranson KR, Ly V and Montesano PM, 2013, NASA Goddard’s LiDAR, Hyperspectral and Thermal (G-LiHT) Airborne Imager, *Remote Sensing*, 5: 4045-4066.
- Gamon JA, Serrano L, Surfus JS, 1997, The photochemical reflectance index: an optical indicator of photosynthetic radiation use efficiency across species, functional types, and nutrient levels. *Oecologia*, 112(4), 492–501.
- Middleton E, Rascher U, Corp L, Huemmrich K, Cook B, Noormets A, Schickling A, Pinto F, Alonso L, Damm A, Guanter L, Colombo R, Campbell P, Landis D, Zhang Q, Rossini M, Schuettemeyer D, Bianchi, 2017, The 2013 FLEX—US airborne campaign at the Parker Tract loblolly pine plantation in North Carolina, USA. *Remote Sensing*, 9(6), 612.
- Zhou Y, Hilker T, Ju W, Coops NC, Black TA, Chen JM, Wu X, 2017, Modeling gross primary production for sunlit and shaded canopies across an evergreen and a deciduous site in Canada. *IEEE Transactions on Geoscience and Remote Sensing*, 55(4), 1859–1873.

NASA's Global Ecosystem Dynamics Investigation (GEDI): Progress towards global mapping of aboveground biomass

J. Armston¹, R. Dubayah¹, S. Healey², J.R. Kellner³, L. Duncanson¹
M. Hofton^{1,4}, J.B. Blair⁴, J. Bruening¹, H. Tang¹, S. Luthcke⁴

¹Department of Geographical Sciences, 2181 Lefrak Hall, University of Maryland, College Park, MD, USA, 20742
Email: armston@umd.edu; dubayah@umd.edu; lduncans@umd.edu; jamis@umd.edu; htang@umd.edu

²USDA Forest Service, Rocky Mountain Research Station, 507 25th St, Ogden, UT, USA
Email: sean.healey@usda.gov

³Institute at Brown for Environment and Society & Department of Ecology, Evolution and Organismal Biology
Brown University, Providence RI, USA
Email: kellner@brown.edu

⁴NASA Goddard Space Flight Center, Greenbelt, MD, USA
Email: michelle.a.hofton@nasa.gov; james.b.blair@nasa.gov; scott.b.luthcke@nasa.gov

1. Introduction

The Global Ecosystem Dynamics Investigation (GEDI) was proposed and selected as part of NASA's Earth System Science Pathfinder (ESSP) Earth Ventures 2 (EV-2) competition. The GEDI mission represents the culmination of almost 30 years of effort on the part of the terrestrial ecology community to provide critical data on the structure of the Earth's forests towards key science questions regarding the aboveground carbon balance of the Earth's land surface, the role of the land surface with regards to atmospheric CO₂ concentrations, and the impact of ecosystem structure on habitat quality and biodiversity.

The GEDI instrument was successfully launched in December of 2018 and subsequently installed on the Japanese Experiment Module-Exposed Facility (JEM-EF) on board the International Space Station (ISS). GEDI became fully operational in April 2019, when it began its two-year prime science mission and as of June 2021 has publicly released more than 18 months of on-orbit data over the Earth's tropical and temperate forests. The key driving factor that has determined mission operations during its prime mission is the GEDI Level 1 science requirements. All measurement requirements trace back towards achieving these. In terms of aboveground biomass density (AGBD), the GEDI mission is designed to acquire lidar canopy vertical profile data required to estimate AGBD for the Earth's global tropical and temperate forests at ≤ 1 km resolution. At the end of a two-year mission, AGBD of at least 80% of the 1 km cells is expected to be estimated with a precision (standard error of the mean) of the larger of ± 20 Mg / ha or 20% of the estimate, whichever is greater.

Here we present the status of GEDI's progress towards global mapping of AGBD and will discuss the major successes and challenges in achieving the measurement performance required for input to this mapping, as well as the outlook for an extended mission through to 2023.

2. Key results

In collaboration with the forest remote sensing and terrestrial ecology communities, GEDI has developed the Forest Structure and Biomass Database (FSBD), which is comprised of 31,414 simulated waveforms that are collocated with footprint level estimates of aboveground biomass. These have provided the means to train models representative of the entire GEDI observation domain (Hancock et al., 2019; Dubayah et al., 2020). Selected Level 4A models used to predict footprint AGBD from Level 2A canopy height metrics have % RMSE that range

from 28.66% (evergreen broadleaf trees in Australia) to 66.89% (evergreen broadleaf trees in Africa), with a mean %RMSE of 51.34% across all selected models.

Between April 2019 and September 2020, over 5.7 billion science quality land surface shots were acquired, which has quantified spatial variation in canopy height, cover and vertical profile metrics at unprecedented spatial resolution. Evaluation of Level 2A estimates of canopy height collocated with the GEDI FSBD over evergreen broadleaf forests has shown an overall RMSE of 2.09 m to date, which is approaching the mission design precision of 2 m. Similarly, evaluation of on-orbit Level 2B canopy cover estimates using NASA Land, Vegetation and Ice Sensor (LVIS) data has shown an overall RMSE of 13%, which is within the mission design accuracy of minimum 10-20% (Bergen et al., 2009).

GEDI uses hybrid model-based statistical estimators to infer the mean AGBD and its uncertainty within each grid cell from the Level 4A models and predictions of AGBD (Patterson et al. 2019). GEDI ground tracks are treated as cluster samples under the hybrid inference paradigm, and at least two clusters are required to create a valid estimate. The output of this process is the Level 4B product, for which preliminary 1 km maps of AGBD and uncertainty estimated from quality waveforms acquired under leaf-on conditions between April 2019 and September 2020 are shown in Figure 1. Estimates are aggregated over larger areas for comparison with independent estimates from national forest inventory data (e.g., Menlov & Healey, 2020), accounting for dependencies between grid cells due to the same Level 4A models being applied and the same GEDI tracks intersecting multiple grid cells.

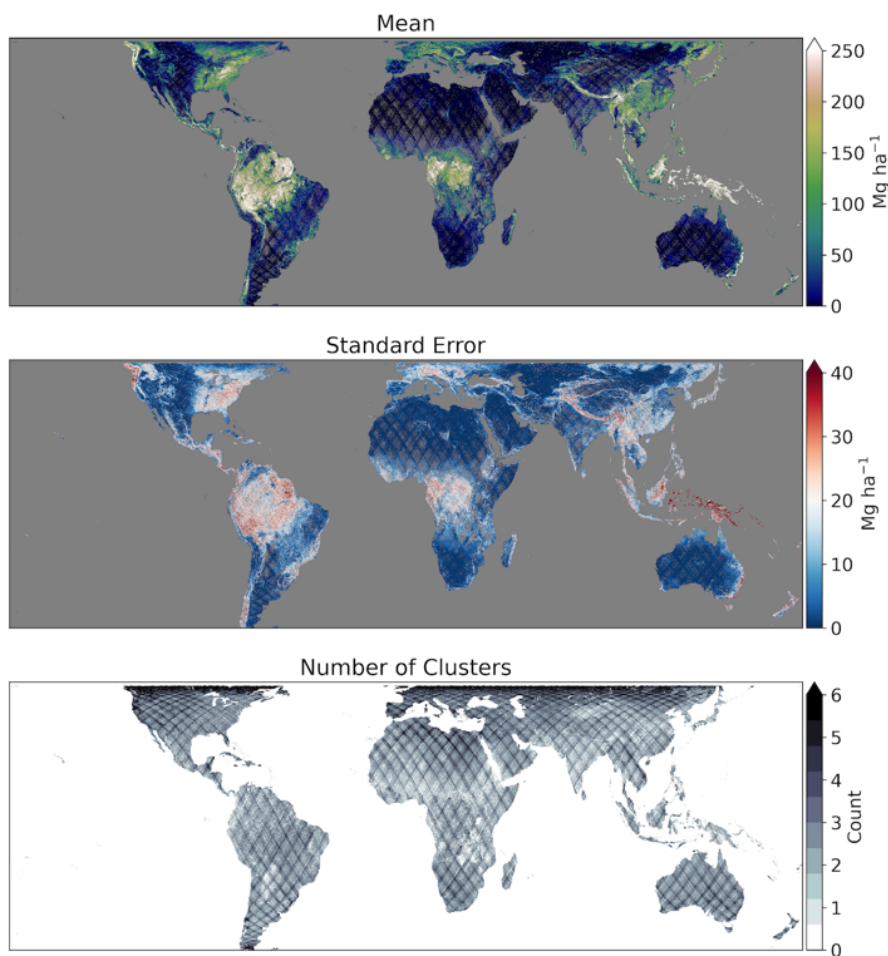


Figure 1. Preliminary Level 4B maps of 1 km estimates of the mean aboveground biomass density (top), standard error of the mean (middle), and the number of clusters (tracks) with quality waveforms acquired under leaf-on conditions used for estimation (bottom). These maps are based on 18 months of on-orbit data acquired between April 2019 and September 2020.

3. Status and outlook

GEDI has met or exceeded expectations with regards to the quality and quantity of its observations, derived canopy height, cover and vertical profile metrics, and how these are applied to advance GEDI science questions. GEDI is the first mission to design and implement a formal inference framework for the estimation of AGBD, enabling comparison with independent estimation of AGBD at multiple scales and unprecedented insights into the global quantity and distribution of carbon stocks. GEDI's prime mission was two-years, ending on-orbit acquisitions on 30 March 2021. New challenges introduced by unplanned change in the ISS altitude has recently limited GEDI's ability to uniformly sample the Earth's surface. Therefore, a longer time on orbit is now required to fully meet mission science requirements, with estimates ranging from 2-4 years depending on whether the ISS changes its orbital altitude.

Acknowledgements

GEDI funding is from NASA contract #NNL 15AA03C to the University of Maryland for the development and execution of the GEDI mission (Ralph Dubayah, Principal Investigator).

References

- Bergen, K. M., Goetz, S. J., Dubayah, R. O., Henebry, G. M., Hunsaker, C. T., Imhoff, M. L., Nelson, R. F., Parker, G. G., & Radeloff, V. C., 2009, Remote sensing of vegetation 3-D structure for biodiversity and habitat: Review and implications for lidar and radar spaceborne missions, *Journal of Geophysical Research*, 114, G00E06. <https://doi.org/10.1029/2008JG000883>.
- Dubayah, R., Blair, J. B., Goetz, S., Fatoyinbo, L., Hansen, M., Healey, S., ... & Silva, C., 2020, The Global Ecosystem Dynamics Investigation: High-resolution laser ranging of the Earth's forests and topography. *Science of Remote Sensing*, 1, 100002.
- Hancock, S., Armston, J., Hofton, M., Sun, X., Tang, H., Duncanson, L., et al., 2019, The GEDI simulator: A large-footprint waveform lidar simulator for calibration and validation of spaceborne missions. *Earth and Space Science*, 6, 294–310. <https://doi.org/10.1029/2018EA000506>
- Menlove, J. & Healey, S.P., 2020, A Comprehensive Forest Biomass Dataset for the USA Allows Customized Validation of Remotely Sensed Biomass Estimates. *Remote Sensing*. 12(24): 4141. <https://doi.org/10.3390/rs12244141>
- Patterson, P.L., Healey, S.P., Ståhl, G., Saarela, S., Holm, S., Andersen, H.-E., Dubayah, R., Duncanson, L.I., Hancock, S., Armston, J., Kellner, J.R., Cohen, W.B. & Yang, Z., 2019, Statistical Properties of Hybrid Estimators Proposed for GEDI – NASA's Global Ecosystem Dynamics Investigation. *Environmental Research Letters*, 14(6), 065007. <https://doi.org/10.1088/1748-9326/ab18df>

Influence of variations in remotely quantified functional traits and diversity on gross primary productivity

V. A. Thomas¹, R. H. Wynne¹, P. K. Campbell², D. J. Harding², K. F. Huemmrich², E. M. Middleton², K. J. Ranson², and P. T. Williams¹

¹Department of Forest Resources and Environmental Conservation, Virginia Tech, Blacksburg, VA, USA
Email: {paigetw; thomasv; wynne}@vt.edu

²Biospheric Sciences Laboratory, NASA Goddard Space Flight Center, Greenbelt, MD, USA
Email: {david.j.harding; karl.f.huemmrich; kenneth.j.ranson; elizabeth.m.middleton; petya.k.campbell}@nasa.gov

1. Introduction

Traits associated with structural (morphological) diversity are an important subset of plant functional traits, the morphological or physiological characteristics that are functionally relevant for growth, reproduction and survival (Ma et al. 2019) and are at the crossroads between responses to the environment and ecosystem properties (Díaz et al. 2013). Functional traits influence forest ecosystem carbon dynamics. Metrics that quantify canopy structural diversity are much more strongly associated with forest productivity than traditional biodiversity measures like species richness and phylogenetic diversity (Aponte et al. 2020).

Theories that have emerged to explain the influence of functional traits on productivity include niche complementarity (Tilman et al. 1997) and the mass ratio hypothesis (Grime 1998). Niche complementarity is the idea that co-existing species within the forest will use different resources, and that high species diversity will increase the variability of functional traits and increase ecosystem function and productivity. The mass ratio hypothesis (Grime 1998) states that "immediate controls are in proportion to inputs to primary production" and "are determined to an overwhelming extent by the traits and functional diversity of the dominant plants and are relatively insensitive to the richness of subordinates and transients." Mass ratio has been shown to be more related to forest productivity than niche complementarity in numerous within- and across-biome forest ecosystem studies (e.g., Watt et al. 2020), particularly outside the humid tropics (Madrigal-González et al. 2020).

Both the mean and dispersion of functional traits at a given scale are typically quantified. The mean is most often weighted by the abundance of constituent species or other taxonomic groupings, the *community weighted mean*. Descriptors of dispersion of functional traits represent the *functional diversity* (Wang and Gamon, 2019) within a community, landscape, or coarser spatial scales (Ma et al. 2019). Forest productivity has been shown to be associated with community-weighted means (Ammer 2019). Being able to quantify status and changes in functional diversity is increasingly important as both pressures on, and the needs for, forests continue to increase. Plant functional traits vary both across and within species (Schneider et al. 2017) and can be mapped using remote sensing (Schneider et al. 2020).

Both physiological and morphological traits are needed for full characterization of functional diversity using remote sensing (Schneider et al. 2017, Ma et al. 2019), necessitating the use of sensors enabling quantification of canopy structure (Aponte et al. 2020) as well as function. Further, high-spatial resolution (or other comparable) data enabling quantification of canopy structure is needed to address multiple scattering and contrasting illumination and to control for varying amounts of vegetation percentage cover in fine spectral resolution measurements (Wang and Gamon 2019). Considering the natural circadian dynamics in photosynthetic function, observation of daily rhythms must be accelerated.

Improved articulation of carbon exchange between forest ecosystems and the atmosphere thus requires diurnal and seasonal observations combining the mean and dispersion of *functional traits*, morphological and physiological characteristics relevant for growth.

2. Objective

Our overall objective is to determine how gross primary productivity is influenced by variations in remotely quantified functional traits and their diversity across space and time.

3. Methods

3.1 Study Sites

The study sites are two AmeriFlux tower sites in Virginia, USA, Sweet Briar Land-Atmosphere Research Station (AmeriFlux site US-SB1) and National Ecological Observatory Network (NEON) Mountain Lake Biological Station (AmeriFlux Site US-xML). Sweet Briar is an evergreen needleleaf forest (managed loblolly pine), and Mountain Lake a deciduous broadleaf forest, the two principal forest types in the southeastern United States.

3.2 Eddy Covariance Data and Site Characterization

Since the two sites are in the AmeriFlux network, standardized sets of measurements are collected to describe ecological processes, including continuous (every 30 minutes) eddy covariance measurements of canopy photosynthetic uptake. Photosynthetic function responds to environmental stresses, such as low or high temperatures or water availability, along with seasonal growth patterns. In addition to CO₂ fluxes, flux towers collect meteorological measurements including air temperature, humidity, incident photosynthetically active radiation (PAR), precipitation, and net radiation that provide information on environmental conditions.

3.3 Airborne Data

Data from both small unmanned aerial systems (sUAS) and manned aircraft (from the hyperspectral and lidar NEON Airborne Observation Platform acquisition in 2021 at the Mountain Lake site) are being used. Optical sUAS data are collected using Cubert FirefLEYE snapshot hyperspectral imaging system (HIS) camera mounted on a SkyFish M6 with a total wavelength range of 450 to 998 nm with spectral band widths (FWHM) ranging from 4 nm at 450 nm to 29 nm at 988 nm. A second focal plane provides high resolution panchromatic observations. The integrated pan camera has a ground resolution of 0.03 m and shares the same front-end optics with the HIS camera. These data are used to produce canopy surface reflectance hyperspectral cube (HIS), sunlit and shaded canopy fractions, and canopy surface models using structure from motion. A YellowScan lidar system mounted on a Vapor 35 helicopter is used to collect ultra-high-density airborne laser scanning (ALS) data over each site once per growing season. The NEON Level 3 Ecosystem Structure product (1 m x 1 m canopy height model) is being used from the 2021 NEON Airborne Observatory acquisition over the Mountain Lake site.

COVID restrictions on field work restricted us to only one sUAS acquisition in the summer of 2020. All these restrictions have now been lifted in Virginia, so the full suite of acquisitions is taking place in 2021, including two sets of diurnal measurements in both sunlit and shaded conditions for both study sites using the FirefLEYE and one ultra-high-density ALS acquisition for each site.

3.4 Functional Diversity Metrics

We are using two relatively simple metrics based on the relative contributions of species at the sites: Community weighted means (CWM) of each functional trait (as well as standard deviations, minimums, and maximums) and the functional divergence index (FDi), which describes the variation in functional traits, proportioned by species (1):

$$FDi = \frac{2}{\pi} \arctan(5V), V = \sum p_i (\ln x_i - \overline{\ln x})^2, p_i = \frac{a_i}{\sum a_i} \quad (1)$$

where V is the weighted variance of functional trait x , a_i is the relative cover of each community type at the site. FDi ranges from 0-1 with no units.

Space precludes listing each site-level trait and its corresponding citation. Physiological traits include indices associated with live green vegetation, vigor, the xanthophyll cycle, light use efficiency, leaf water, and chlorophyll content. Structural traits include LAI quantiles, canopy height and canopy height quantiles, and shadowed and sunlit fractions. Figure 1 shows a partial example of the metric derivation workflow using a limited set of functional traits derived from our 2020 sUAS data and airborne lidar.

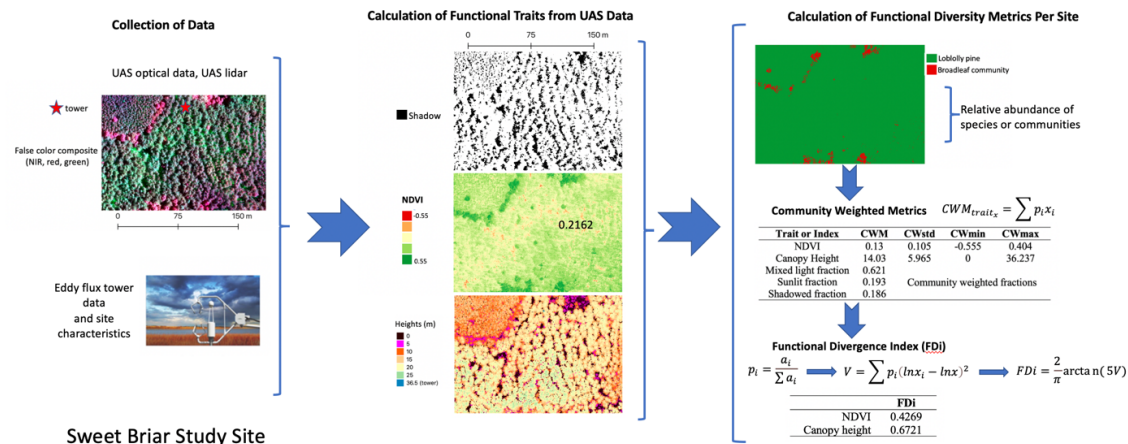


Figure 1: Workflow describing the calculation of functional traits, community-weighted functional diversity metrics, and functional divergence indices.

3.5 Statistical analysis to explore functional diversity and productivity across sites

The community-weighted metrics and functional divergence indices are being used to (1) compare the functional diversity throughout the course of a day in for a sunny and cloudy day at each site during the peak of the growing season, and (2) examine the effects of the functional traits on gross primary production.

4. Impact

The recently released IPBES-IPCC workshop report on biodiversity and climate change (Pörtner et al. 2021) makes it clear that limiting global warming and protecting biodiversity are necessary and mutually supporting goals. Developing means by which the combined structure and function of forested ecosystems can be monitored, from canopy to global scales, is becoming vital to human well-being.

3. References

- Ammer, C, 2019, Diversity and forest productivity in a changing climate. *The New Phytologist*, 221(1):50–66.
- Aponte, C, Kasel, S, and others, 2020, Structural diversity underpins carbon storage in Australian temperate forests. *Global Ecology and Biogeography*, 29(5):789–802.
- Díaz, S, Lavorel, S, de Bello, F, Quétier, F, Grigulis, K., and Robson, TM, 2007, Incorporating plant functional diversity effects in ecosystem service assessments. *Proceedings of the National Academy of Sciences of the United States of America*, 104(52):20684–20689.
- Grime, JP, 1998, Benefits of plant diversity to ecosystems: immediate, filter and founder effects. *The Journal of Ecology*, 86:902–910.
- Ma, X, Mahecha, MD, and others, 2019, Inferring plant functional diversity from space: the potential of Sentinel-2. *Remote Sensing of Environment*, 233:111368.
- Madrigal-González, J, Calatayud, J, and others, 2020, Climate reverses directionality in the richness-abundance relationship across the world's main forest biomes. *Nature Communications*, 11(1):5635.
- Pörtner, HO, Scholes, RJ, and others, 2021, IPBES-IPCC co-sponsored workshop report on biodiversity and climate change; IPBES and IPCC.
- Schneider, FD, Ferraz, A, Hancock, S, Duncanson, LI, Dubayah, RO, Pavlick, RP, and Schimel, DS, 2020. Towards mapping the diversity of canopy structure from space with GEDI. *Environmental Research Letters*, 15:115006.
- Schneider, FD, Morsdorf, F, Schmid, B, Petchey, OL, Hueni, A, Schimel, DS, and Schaepman, ME, 2017. Mapping functional diversity from remotely sensed morphological and physiological forest traits. *Nature Communications*, 8(1):1441.
- Tilman, D, Knops, J, Wedin, D, Reich, P, Ritchie, M, and Siemann, E, 1997, The influence of functional diversity and composition on ecosystem processes, *Science*, 277(5330):1300–1302.
- Wang, R, and Gamon, JA, 2019, Remote sensing of terrestrial plant biodiversity. *Remote Sensing of Environment*, 231:111218.
- Watt, MS, Buddenbaum, H, and others, 2020, Monitoring biochemical limitations to photosynthesis in N and P-limited radiata pine using plant functional traits quantified from hyperspectral imagery. *Remote Sensing of Environment*, 248:112003.

Deep learning with 3D laser data to identify tree species

A. Kato¹ and N. Tsutsumida²

¹ Course of Landscape, Graduate School of Horticulture, Chiba University, 648 Matsudo Matsudo Chiba, 271092, Japan
Email: akiran@faculty.chiba-u.jp

² Department of Information and Computer Sciences, Graduate School of Science & Engineering, Saitama University
255 Shimo-Okubo, Sakura ward, Saitama city, Saitama, 338-0825, Japan
Email: narut@mail.saitama-u.ac.jp

1. Introduction

The 3D laser technology is commonly available for automatic driving system to detect collision on the road. The rapid 3D sensor development enables us to monitor trees along the road if the sensor can identify trees. To identify trees, a fast laser processing technique is required. In image processing, a semantic segmentation has been developed to classify rough sketch of objects (cars, buildings, and vegetation) on 2D landscape images. However, the vegetation has not been classified more by species name. The species identification by laser can play an important role for urban tree recognition. The mobile mapping systems only cover a portion of canopy or one side of stems. The technique to identify species from the limited view of a tree is needed to develop an accurate species identification system.

Deep learning (DL) is one of the most powerful machine learning techniques automatically identify unique features of objects based on training samples. DL has been extensively used for classification in remote sensing. The native species was identified in Spanish savanna to get more than 90% accuracy compared to 70% accuracy of conventional object-based classification (Guirado *et al.*, 2017). Individual palm trees in Malaysia were identified and segmented over densely populated stands from Quickbird (Digital Globe Inc.) high resolution images to reach 90% accuracy (Li *et al.*, 2017). However, high accuracy needs a large number of training samples. To reduce collecting samples, the transfer learning has been proposed to borrow the network built from different training samples (Carranza-Rojas *et al.*, 2017). But it is still challenging to collect samples efficiently and the DL accuracy relies on the number of training data. This study proposes a way to generate 2D images of different view angles from a 3D tree virtually as an efficient way to provide 2D training samples for DL processing.

2. Methodology

2.1 Study site and field data

The study site was located at Shinjuku Gyoen National Park in downtown Tokyo, Japan. The park has 58.3 ha area and trees has been preserved since 1591. The five tree species were selected and used for this study (Figure. 1), Italian stone pine (*Pinus Pinea*), Himalayan cedar (*Cedrus deodara*), black pine (*Pinus thunbergii*), London planetree (*Platanus x acerifolia*), cherry blossom (*Prunus spp.*). The 10 trees were sampled from each species and the total 50 trees were scanned by terrestrial laser scanner. The reason to choose these species was to have unique shapes and the bigger size among trees in the park. We conducted fieldwork between August to November in 2020. The terrestrial laser scanner used for this study was LMS511 (SICK Inc.). A tree was scanned from two vantage points to cover the front and the back of a tree to get an entire shape. LMS511 laser scanner has 905mm wavelength, 4.7 mrad, 40 m max. distance, and -60° to 90° vertical angle range. The field data was tree height, diameter at breadth height (DBH), crown width, the lowest height of branch and stem. We only used tree height and DBH for the validation of the laser scanner coverage.

2.2 Methodology

The software named cloud compare was used to merge 3D data taken from the two scanning locations (the front and the back of a tree). During the process, the objects such as a fence and shrub were removed only to extract a tree. To create input images for DL processing, the 2D images were generated from

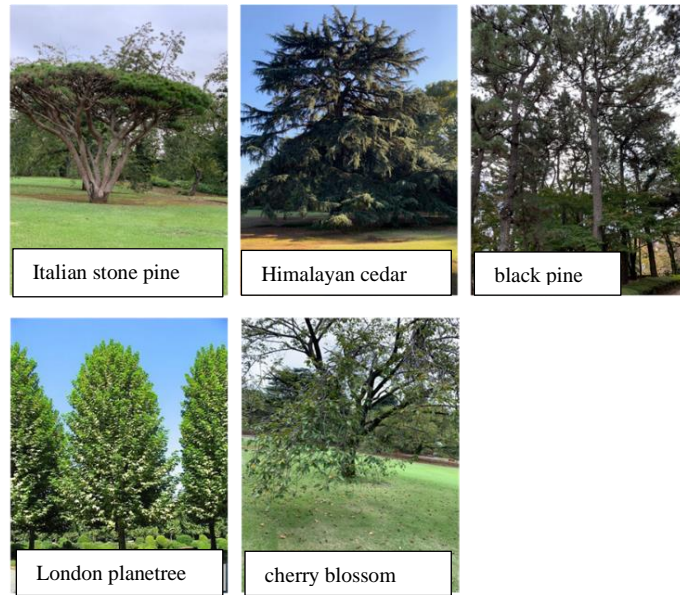


Figure 1: Tree species used for this study.

various viewpoints of a 3D tree virtually. The 3D data was coloured by height and was viewed from different vertical and horizontal angles to create 2D images. For this study, we set the vertical angles for 0° , 30° , 60° , and 90° and horizontal angles for 0° , 90° , 180° , and 270° . The total 16 images were generated from one tree (Figure. 2). DL processing used for this study was Visual Recognition of IBM Watson Studio (IBM Inc.) to identify tree species. The 70% of entire samples was used as training dataset and the rest 30% was used as validation dataset. The total images generated by this method were 5 (species) x 10 (trees) x 16 (images) = 800 (images).

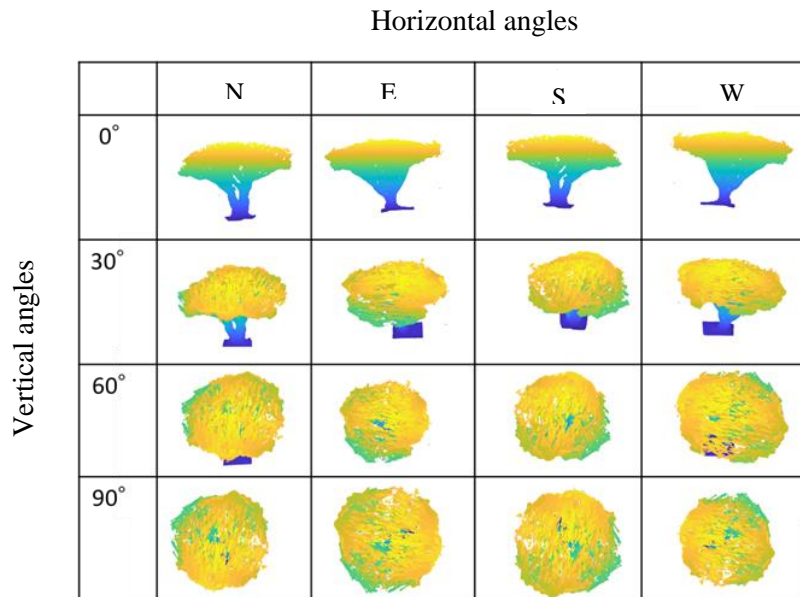


Figure 2: Generating different view angle 2D images from a 3D tree for DL processing.

3. Results and Discussion

Tree height and DBH had good relation between field and laser measurement. Tree height had 0.94 of R^2 value ($p < 005$) and DBH measurement had 0.7 of R^2 value ($p < 005$). The sensor used for this study has enough capability to cover the upper height vertically and reach enough depth inside canopy horizontally. And tree height and DBH were the most trustable parameters from field data to validate this sensor capability.

DL result showed the listed species with ratio. The highest number of the ratio was used as the species identified from DL. Furthermore, the training and validation data was separated by vertical angle to obtain each accuracy by angle (Table 1). The overall accuracy was derived by all data (Table 2). From Table 1, London planetree had similar shapes within the same species samples and Italian pine was the most unique shape different from the other species. They were identified accurately. Cherry blossom, black pine, and Himalayan cedar had more irregular and diverse shapes from various looking angles. It was difficult to find the common feature during DL process among training dataset. Therefore, the within-species variance was more than the among-species variance. Black pine and Himalayan pine were misclassified each other by 40%. From Table 1 and 2, overall accuracy had the lower accuracy than each angle accuracy. From Table 1, 60° view angle had the best accuracy to identify species through this method.

To improve the accuracy for irregular shape trees, stem, leaves, and branching structure can be separately trained (Joly et al., 2014). Then the weighted score among separated components can be used to find the best identification result from DL. This 2D image generation approach helps simplify classifying (or labelling) objects from massive 3D data (Xie et al., 2020). The terrestrial laser has been used for DL in the past study for tree species identification (Lin and Herold, 2016). Our approach took a different way to use 2D images generated from 3D data instead of measuring tree parameters from 3D from their approach. Our approach is more efficient way to reduce the cost and time to prepare training samples and a flexible way to provide input images for DL processing.

Table 1. Accuracy assessment separated by angle

	Italian pine	Himalayan cedar	black pine	London planetree	cherry blossom
0	75%	8%	42%	100%	42%
30	92%	25%	8%	100%	0%
60	100%	42%	42%	100%	0%
90	83.30%	16.70%	33.30%	100%	8%

Table 2. Overall accuracy

	Italian pine	Himalayan cedar	black pine	London planetree	cherry blossom
all angles	68.80%	20.80%	12.50%	95.80%	18.80%

References

- Carranza-Rojas, J., Goeau, H., Bonnet, P., Mata-Montero, E., and Joly A. (2017) Going deeper in the automated identification of Herbarium specimens, *BMC Evolutionary Biology* 17, 181
- Guirado, E. Tabik, S., Alcaraz-Segura, D., Cabello, J., and Herrera F., (2017) Deep-learning versus OBIA for scattered shrub detection with google earth imagery: ziziphus lotus as case study, *Remote Sensing* 9:1220
- IBM Watson Studio, <https://www.ibm.com/jp-ja/cloud/watson-studio> (access date: 2021.6.1)
- Joly, A. Goëau, H., Bonnet, P., Bakić, V., Barbe, J., Selmi, S., Yahiaoui, I., Carré, J., Mouysset, E., Molino, J-F., Boujemaa, N., Barthélémy, D. (2014) Interactive plant identification based on social image data, *Ecological Informatics* 23: 22-34
- Li, W., Fu, H., Yu, L., and Cracknell, A. (2017) Deep learning based oil palm tree detection and counting for high-resolution remote sensing images, *Remote Sensing* 9: 22
- Lin, Y. and Herold, M. (2016) Tree species classification based on explicit tree structure feature parameters derived from static terrestrial laser scanning data, *Agricultural and Forest Meteorology*, 216: 105-114
- Xie, Y., Tian, J., and Zhu, X.X. (2020) Linking points with labels in 3D, *IEEE Geoscience and Remote Sensing Magazine* December 2020: 38-59.

Identifying Secondary Forests in the Brazilian Amazon using Spaceborne Lidar

R. H. Wynne¹, V. A. Thomas¹, Benjamin D. Miller¹, Luis Marcelo Tavares de Carvalho², Stella Zucchetti Schons do Valle¹

¹Virginia Tech Department of Forest Resources and Environmental Conservation, Blacksburg, VA, USA
Email: {wynne; thomasv; benmiller; szschons}@vt.edu

²Federal University of Lavras, P.O. Box 3037, 37200-900, Lavras-MG, Brazil
Email: passarinho@ufla.br

1. Introduction

Lidar data have been shown to be helpful in discriminating secondary from primary forest, both alone and in combination with other sensors. Drake et al. (2002) used the Laser Vegetation Imaging Sensor (LVIS) to examine primary forests and secondary forests at 14, 22, and 31 years at La Selva Biological Station. Four waveform-derived metrics (lidar canopy height, height of median energy, height/median ratio, and ground return ratio) were evaluated. Secondary growth sites were virtually indistinguishable from older (22 and 31 years old) secondary forests with respect to the height/median and ground return ratios, but the height of median energy and height/median ratio enabled separation of secondary from primary forest regardless of the age of the former. Castillo et al. (2012) also used LVIS data to characterize secondary forests in Guanacaste, Costa Rica (a tropical dry forest site). Using only three return levels (heights at which the normalized cumulative return energy reached 50, 75, and 100% of the total energy reflected by the target) they were able to separate successional stages of secondary forest. A preceding study by almost the same team (Castillo-Núñez et al., 2011) found maximum canopy heights to be estimated reasonably accurately (RMSE = 1.3 m) by waveform lidar (using only the LVIS canopy elevations maximum canopy height) in the same tropical dry forest environment. Caughlin et al. (2016) estimated canopy cover and height associated with forest regrowth in Los Santos Province, Panama using a canopy height model derived from Carnegie Airborne Observatory-2 waveform data and the mean photosynthetic fraction derived from four Landsat Thematic Mapper images acquired near the same time as the lidar data.

A study of forest transition in the Amazon requires separation of primary from secondary forest. With optical data this is only feasible for a short period after the initiation of regrowth unless the area of prior clearing is known. In either case small clearings and subsequent secondary regrowth can be missed. Secondary growth mapping using maps of primary forest loss is, of course, limited to the accuracy and minimum mapping unit of those maps. Lidar data appear able to discriminate secondary from primary forest for decades after regrowth began, but their suitability for land cover and land use change studies has heretofore been limited by their necessarily limited coverage. That has now changed in the area of NASA spaceborne lidars.

2. Objective

Our overall objectives are to (1) use the Rural Environmental Registry (Cadastro Ambiental Rural - CAR), current MapBiomass classifications, stand maps from industrial partners, and our collaborator's expertise to identify classes of land use histories of interest, with a focus on disturbed areas that appear have recovered to secondary forests, and (2) use NASA spaceborne lidars (GEDI02B and ATL08 products) to develop a structurally-mediated identification and characterization of secondary forests in portions of the legal Amazon.

3. Methods

3.1 Study Area

We are initially focusing only on (1) areas of the Amazon that MapBiomass has classified as forests that were previously recorded as having been cleared in the CAR, and (2) known forest plantations.

3.2 CAR

The CAR is an online, electronic land registry and is required for all private land properties in Brazil. In the CAR, the landowner (with assistance from a qualified technical professional or the government) reports to the state and federal governments the extent of each of these areas and where they are located within the property in question. As of May 2019, the number of registered properties was 5,983,649, which summed up to a total area of approximately 24 times the size of Germany, with 205 million hectares of original vegetation cover.

3.3 MapBiomias

The Brazilian Annual Land Use and Land Cover Mapping Project (MapBiomias) is a multi-institutional collaboration that has generated a Landsat-derived land use and land cover time series for Brazil, computed in Google Earth Engine. The products include 30 m land use and land cover maps, 28-layer image mosaics including spectral bands and indices, derived maps and statistics organized by biome from 1985.

3.4 Lidar Data

Metrics from GEDI (02B) and ICESat-2 (ATL08) are being used. 19 variables in GEDI02B (elev_lowest mode, toplec, botloc, Pgap (z, theta), cover, cover_z, pai, pai_z, pavd_z, Rh100, rhog, rhov, Rg, Rv, local_beam_elevation, Omega, Ross-G, LC, and Sensitivity) are in the modeling framework. There are 34 canopy variables in the ATL08 product, but we are only using relative height metrics, reducing that by 12. As such, the metrics used are canopy_h_metrics (25, 50, 60, 70, 75, 80, 85, 90, 95), h_canopy, h_mean_canopy, h_dif_canopy, h_min_canopy, h_max_canopy, canopy_openness, toc_roughness, h_canopy_quad, n_ca_photons, n_toc_photons, centroid_height, canopy_flag, Landsat_flag. The 91-day repeat of ICESat-2 is substantially reducing data availability in some persistently cloudy forests.

3.5 Finding Secondary Growth using MapBiomias and CAR data

The CAR data by themselves do not have secondary growth as a class. We are identifying secondary growth as CAR-identified forest loss that is forest on the 2019 MapBiomias classification. Neither the CAR nor MapBiomias is completely correct (otherwise we would not need to assess secondary forest growth with spaceborne lidar data), but with field verification by trained interpreters at the Universidade Federal de Lavras we are able to create a high-quality random but balanced sample of secondary forest growth, along with areas that have not been disturbed and those that have been disturbed but on which (secondary) forests have not been re-established.

3.5 Analysis

Classification is being conducted using random forests. We recently pioneered an iterative modeling framework approach in which each random forests model is run with an iterative bootstrapping approach to include all available in-bag training data while also using an out-of-bag sample for model evaluation. The result of this process is that each individual footprint or segment has 500 labels, enabling a *de facto* estimate of uncertainty at the segment or footprint level, as the strength of the assignment can be determined from the distribution of assigned classes. Classification accuracy is being assessed using standard methods.

4. Early Results

While the analyses are not yet complete, visualizations indicate some likelihood of success (Figure 1 and Figure 2). In Figure 1, the upper left shows actual ground hits for the “3L” beam of ICESat-2 ground reference track 1268 on June 20, 2019 (left track) and on December 20, 2018 (right track) for a small area in the western Amazon where secondary forest patches have been identified in the CAR. The lower left shows an enlarged CAR polygon with 3 highlighted ICESat-2 ATL08 samples. Samples A and B are outside the CAR polygon, with no known history of disturbance. Sample C is secondary forest. The right-hand side of the figure shows cumulative relative heights extracted from ATL08 data for the three samples.

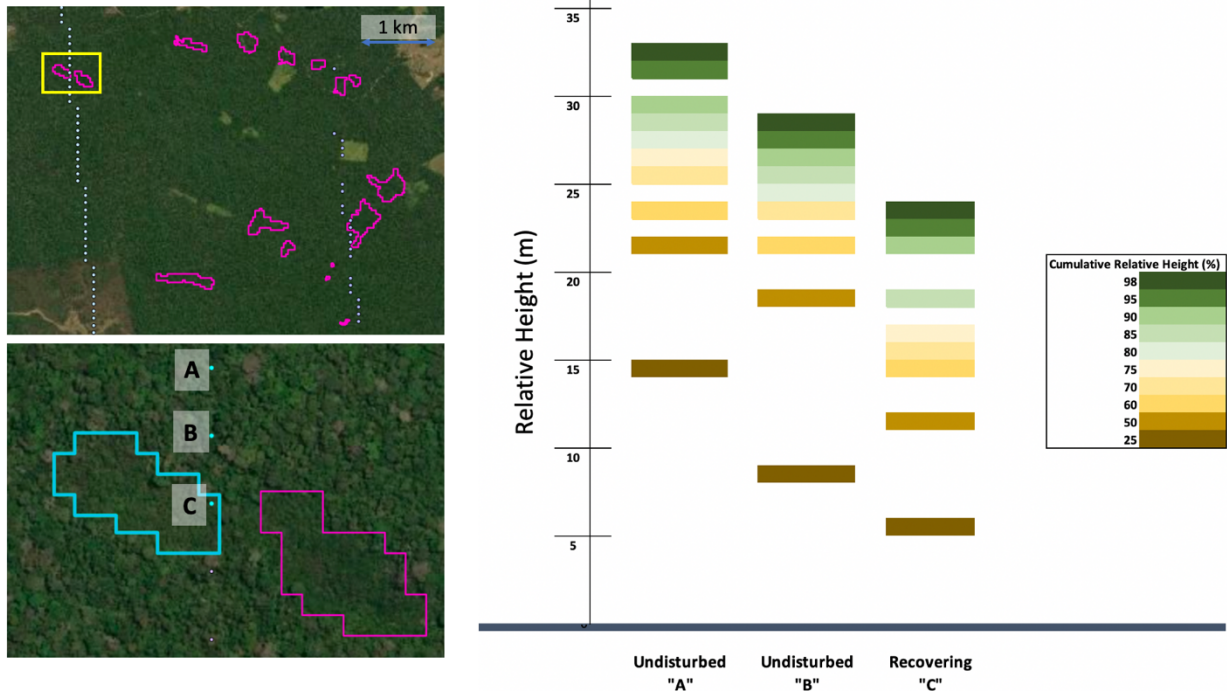


Figure 1. Examples of interactions between ICESat-2 and the CAR.

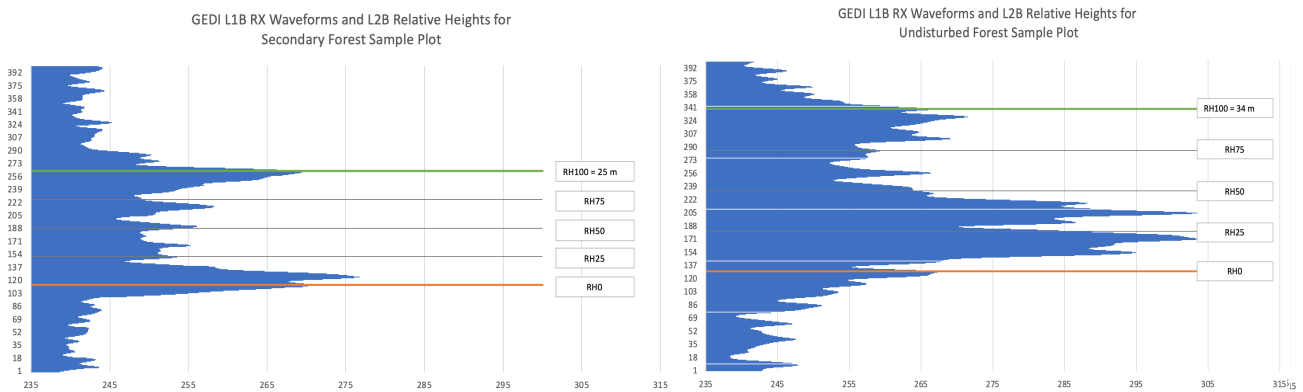


Figure 2. Examples of interactions between GEDI and the CAR.

Figure 2 shows specified shots chosen from ground hits for beam 0010 of GEDI ground reference track 3218 on July 8, 2019 in the western Amazon where secondary forest polygons from the CAR were supplemented with examples in surrounding undisturbed forest. Shown in this figure are extracted RX waveforms from the GEDI 1B product along with estimated relative heights from GEDI 2B.

References

- Castillo, M, Rivard, B, Sanchez-Azofeifa, GA, Calvo-Alvarado, J, and Dubayah, R, 2012, Lidar remote sensing for secondary tropical dry forest identification. *Remote Sensing of Environment*, 121:132–143.
- Castillo-Núñez, M, Sanchez-Azofeifa, and others, 2011, Delineation of secondary succession mechanisms for tropical dry forests using LiDAR. *Remote Sensing of Environment*, 115:2217–2231.
- Caughlin, TT, Rifai, SW, Graves, SJ, Asner, GP, and Bohlman, SA, 2016, Integrating lidar-derived tree height and Landsat satellite reflectance to estimate forest regrowth in a tropical agricultural landscape. *Remote Sensing in Ecology and Conservation*, 2(4):190–203.
- Drake, JB, Dubayah, RO, and others, 2002, Estimation of tropical forest structural characteristics using large footprint lidar. *Remote Sensing of Environment*, 79(2):305–319.

ICESat-2 for Forestry Applications

Amy Neuenschwander¹

¹University of Texas at Austin, Austin, TX 78701

Email: amy@csr.utexas.edu

1. Introduction

On September 15, 2018 NASA launched the ICESat-2 (Ice, Cloud, and land Elevation Satellite-2) laser altimeter from Vandenberg Air Force Base. Although the primary mission goal of ICESat-2 is to monitor changes in the cryosphere, ICESat-2 also collects elevation data over the Earth's land surfaces providing geodetic measurements to support a wide range of terrestrial applications. In the temperate and tropical regions, ranging measurements from ICESat-2 are used to produce estimates of terrain and canopy heights of the world's forests. The density and vertical distribution of the returned photons from within the canopy can be utilized to infer information regarding forest biomass, canopy volume, habitat mapping, biodiversity, and parameterization of land-climate models. The ICESat-2 satellite is in a polar orbit (92 degrees) and is the only space based laser altimeter capable of collecting ranging measurements over all land surfaces.

The instrument onboard ICESat-2 is the Advanced Topographic Laser Altimeter System (ATLAS) and ATLAS is sensitive to detect single photons reflected from the surface. ATLAS uses a 532 nm laser that fires at a rate of 10 kHz (or every 70 cm on the Earth's surface) which facilitates high spatial resolution in the along-track direction. A diffractive optical element splits the ATLAS laser into 6 beams; 3 beam pairs approximately 3 km apart. Each beam pair is comprised of a strong beam and weak beam. Because ATLAS is sensitive at the photon level, solar background noise can present a challenge in the analysis or photon counting data. ICESat-2 is a profiling lidar and a result of the beam configuration is high resolution in the along-track direction; however gaps exist between beams. In the mid-latitudes, ICESat-2 operates in vegetation mode which consists of off-nadir pointing the satellite to a different ground track each 91-day repeat cycle. Thus, rather than repeating an orbit every 91 days, ICESat-2 will point to a different location on the Earth to improve the spatial sampling. Over a period of two years, this series of off-pointing maneuvers has reduced the distance between tracks at the equator from 29 km to approximately 2 km. As the mission continues through time with more off-pointing maneuvers, the distance between ground tracks will continue to decrease.

1.1 Land and Vegetation Data Product (ATL08)

Because ATLAS is a photon counting system operating at a much lower energy than typical waveform or discrete return lidar systems, only a handful of photons (~1 – 2) are returned from each outgoing laser pulse. The actual number of returned photons is a function of the surface reflectance and varies over different forest types. As such, determination of the surface (both ground and top of canopy) requires the accumulation of photons across a larger distance. Because the detectors on ATLAS are sensitive at the photon level, they will also detect solar background photons both above and below the reflected signal photons. The algorithm utilized to create the Land and Vegetation Data Product (ATL08) uses a series of cluster/density filters to eliminate background noise and iterative filters to identify the ground and top of canopy surfaces. The ATL08 algorithm then labels each photon as ground, canopy, top of canopy, or noise and subsequently reports statistics for both the ground and canopy for a 100 m step size along the orbit direction.

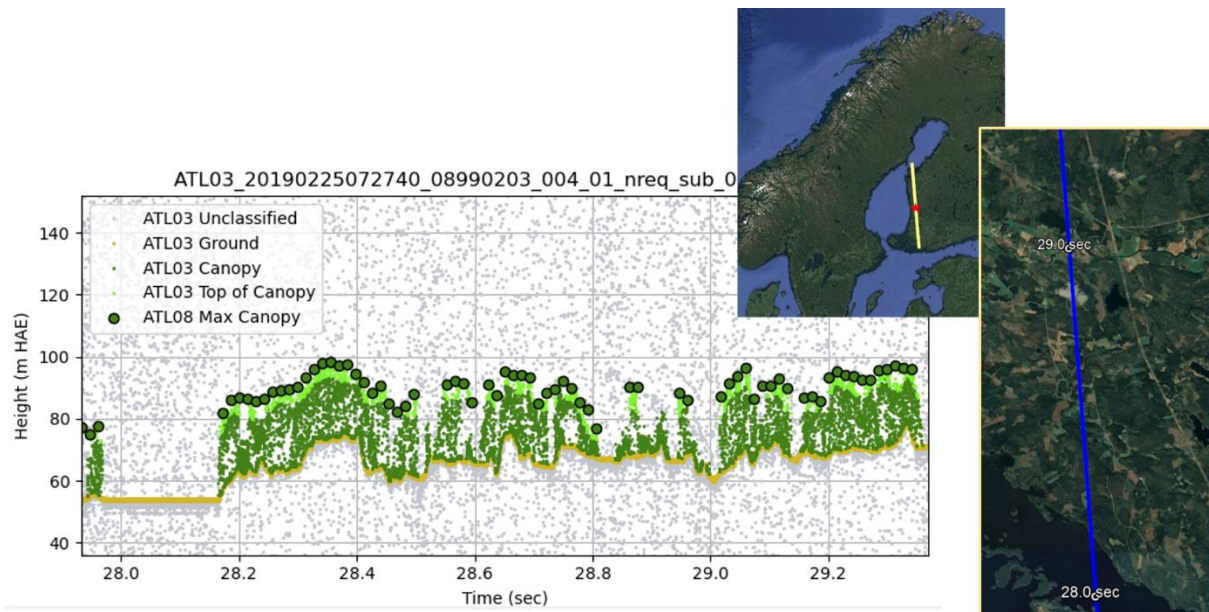


Figure 1: Transect of ICESat-2 data over Western Finland. The individual photons available on the ATL03 data product are color coded with the assigned label (ground, canopy, top of canopy, or noise) from the ATL08 algorithm. The large green dots correspond to the ATL08 canopy height value reported every 100 m in the along-track direction.

2 Results of Canopy Height Estimates

Figure 2 illustrates the ATL08 canopy height errors plotted against canopy cover for managed forests in Southern Finland (Neuenschwander et al. 2020). The mean absolute errors for each stratification scenario show that the ATL08 canopy height errors improved as canopy cover increased from 10–40%. The MAE plateau from 40–80% and then gradually increase above 80%. These results, combined with the results from the terrain residuals indicate that at low canopy cover (<40%) where the terrain estimates are more accurate, ICESat-2 likely does not capture enough canopy reflections to obtain an accurate estimate of a canopy height. Canopy heights are most accurate in the 40-80% range of canopy cover, with dense cover (>80%) associated with increasing errors when there are likely less ground photons being reflected and detected.

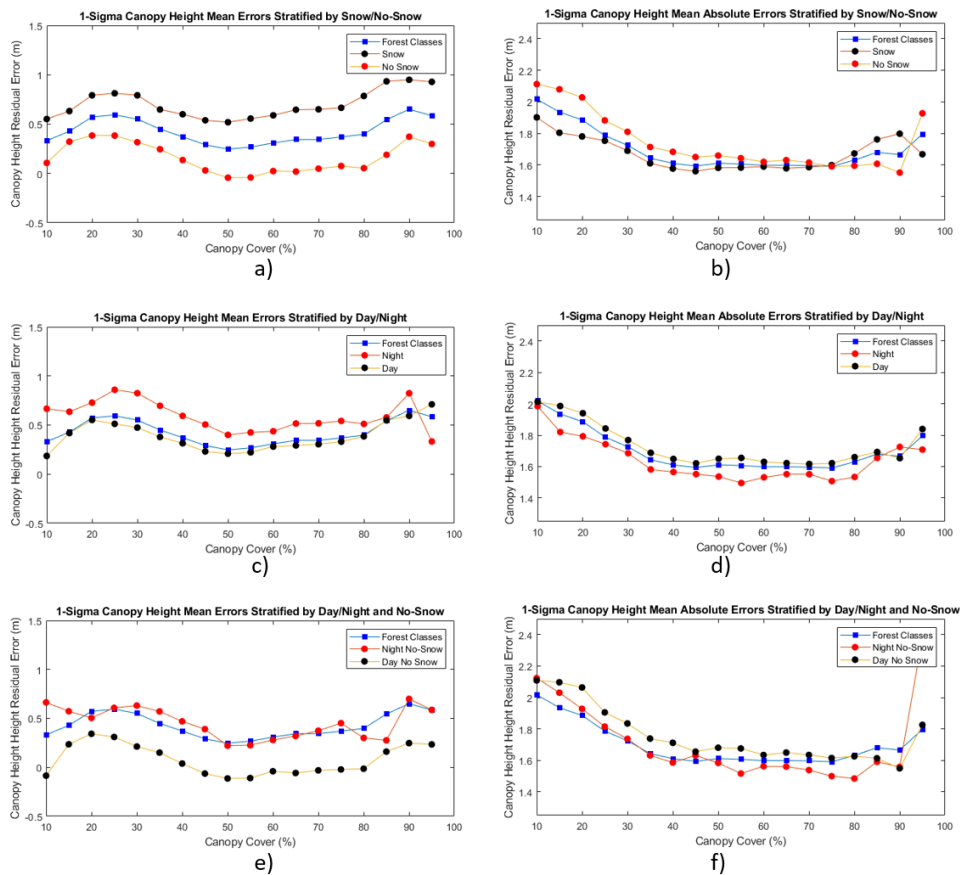


Figure 2. Canopy height residuals of ATL08 strong beam 1-sigma plotted against canopy cover a) mean errors stratified by snow/no-snow b) mean absolute errors stratified by snow/no-snow c) mean errors stratified by day/night d) mean absolute errors stratified by day/night conditions e) mean errors stratified by day/night for no-snow conditions and f) mean absolute errors stratified by day/night for no-snow conditions. (From Neuenschwander et al. 2020)

Results from this study indicate that the strong beam consistently provided better canopy height estimates than the weak beam. For forested classes, canopy height retrievals during the summer months at night yielded the lowest errors with a mean bias of 0.56 m and a RMSE% of 13.75% which is in line with canopy height retrievals from lidar estimates of forest canopies (Næsset, 1997; Magnussen and Boudewyn 1998, Næsset and Økland 2002, Næsset 2007). Much of the success of the canopy height retrievals in the Neuenschwander (2020) Finland study are based on the ability to accurately determine the underlying terrain. In other regions where atmospheric conditions or vegetation cover limits the detection of the ground surface, canopy height estimates will certainly be less accurate. We found that ATLAS data acquired during the summer months (May–August) had the lowest canopy height errors (mean ~0.5 m, RMSE ~2.5 m, %RMSE ~14.5%). In snow conditions, the canopy height errors are larger (mean ~1.1 m, RMSE ~2.7 m, %RMSE ~16.3%), however, these larger errors are likely the result of seasonal differences between ICESat-2 and the airborne lidar data used as reference, as well as snow-covered terrain biasing the relative canopy heights.

Although ICESat-2 was not specifically designed for canopy height retrievals, it has shown to provide useful canopy height estimates for global observations, particularly at latitudes where GEDI does not collect data.

Acknowledgements

This work is funded through the NASA Cryospheric Office for the ICESat-2 Science Team grant (NNH19ZDA001N-ICESAT2) and NASA's Terrestrial Ecology program Arctic Vulnerability Experiment (ABoVE) grant (NNH18ZDA001N-TE).

References

- Næsset, E. 1997. "Determination of mean tree height of forest stands using airborne laser scanner data." *ISPRS Journal of Photogrammetry & Remote Sensing*, Vol. 52: pp. 49–56.
- Næsset, E., and Økland, T. 2002. "Estimating tree height and tree crown properties using airborne scanning laser in a boreal nature reserve." *Remote Sensing of Environment*, Vol. 79: pp. 105–115.
- Næsset, E. 2007. "Airborne laser scanning as a method in operational forest inventory: status of accuracy assessments accomplished in Scandinavia." *Scandinavian Journal of Forest Research*, Vol. 22: pp. 433–442.
- Neuenschwander, A. and Pitts, K., 2019. The ATL08 land and vegetation product for the ICESat-2 Mission. *Remote Sensing of Environment*, 221: 247-259. [doi: 10.1016/j.rse.2018.11.005]
- Neuenschwander, A., Guenther, E., White, J., Duncanson, L., and Montesano, P. 2020 Validation of ICESat-2 terrain and canopy heights in boreal forests. *Remote Sensing of Environment*, 251. <https://doi.org/10.1016/j.rse.2020.112110>

Repeatability of TLS-based tree diameters on permanent sample plots

Günther Bronner, Helga Fellner, Kathrin Birnbauer

Umweltdata GmbH, Knabstraße 7/4, 3013 Tullnerbach, Austria
Email: g.bronner@geo.tuwien.ac.at

1. Introduction

Time series of traditional tree diameter measurements on permanent forest inventory sample plots may comprehend several decades, especially in NFI time series. Under such circumstances, the exact position on the stem, where a calliper is positioned to measure diameters (e.g. DBH) is critical. Stems cross sections are not perfectly circular, more often elliptic or irregular, especially regarding deciduous tree species. A slightly dislocated calliper can produce a significant failure which sometimes exceeds the annual increments between the measurements. For this reason, in a NFI-compliant TLS solution the scan accuracy and the scanner placement is critical for single stem related repeatability.

A second issue is the method of diameter extraction. Most often, stem related point clouds are fitted to cylinders. In this case, noise influences from sensor, multi-station-adjustment, bark and wind influences can hardly be separated. The method of arc-detection within single scan-lines (Eric Hyyppä et al 2020) allows more accurate and robust diameter extraction. However, arc-detection in scan-lines requires roughly horizontal scan lines and therefore a tilt mount for TLS devices.

This study investigates the influence of scan patterns, scan resolution and scan-line direction on repeatability of diameter results from point-clouds recorded with a Riegl VZ400i using a tilt mount.

2. Study area and data

The test site is an old-grown beach-dominated mixed stand near Vienna. In total, 6 circular sample plots with 20m radius were defined and the center points were permanently marked to follow up with future measurements. The trees are scanned from 12 scan positions using different patterns of scan positions, different scan resolutions and different direction of scan lines (vertical vs. horizontal). To estimate repeatability, the 12 scan positions are split into two sub-sets of 6 scan positions per sample plot per method (uneven and even numbers of scan positions). The results of the corresponding sub-sets are compared and evaluated regarding repeatability of tree diameters.

The data (point clouds as LAZ) will be made available for open access.

3. Methods

The scanner recordings and diameter extraction are currently in progress.

The method of diameter extraction is chosen to best fit to the scan method.

Three variants are investigated:

- a) Vertical scan lines in 40x40 mdeg resolution, scan-positions in radius 20m round centre point; tree diameter by cylinder fitting

- b) Horizontal scan lines in 10x100 mdeg resolution, scan-positions in radius 20m round centre point; tree diameter by arc detection
- c) Horizontal scan lines in 5x100 mdeg resolution, scan-positions in radius 2m round centre point; tree diameter by arc detection

We expect an enhanced diameter-related repeatability with horizontal scan lines and arc detection methods for diameter extraction. The results will be evaluated until the conference.

Outlook

Horizontal super-dense scan-lines from TLS scanning in forest environment in combination with arc-analysis for stem detection has a high potential for enhanced repeatability, especially regarding an accurate derivation of annual increments by time series of point clouds.

Acknowledgements

This research is partly funded by the Austrian Research Promotion Agency (FFG).

References

Eric Hyypä, Antero Kukkoa, Risto Kajaluoto, Joanne C. White, Michael A. Wulder, Jiri Pyörälä, Xinlian Liang, Xiaowei Yu, Yunsheng Wang, Harri Kaartinena, Juho-Pekka Virtanena, Juha Hyypää 2020
Accurate derivation of stem curve and volume using backpack mobile laser scanning
ISPRS Journal of Photogrammetry and Remote Sensing 161 (2020) 246-262

Forest stand structure assessment using airborne laser scanning and forest inventory data – working towards a nationwide wall to wall coverage

L. Ender¹, D. Kükenbrink¹, C. Ginzler¹

¹Swiss Federal Institute for Forest, Snow and Landscape Research, Zürcherstrasse 111, CH-8903 Birmensdorf
Email: {linus.ender; daniel.kuekenbrink; christian.ginzler}@wsl.ch

Keywords: ALS, National Forest Inventory, forest structure, canopy layering

To ensure sustainable forest management, understanding and monitoring of forest stand metrics is crucial. The Swiss National Forest Inventory (NFI) continuously assesses the status and development of the Swiss forests on more than 6000 plots distributed on a regular grid all over the country. Vertical stand structure is one important parameter acquired by the NFI. While fundamental in forest planning it is also known to be a good proxy for e.g. habitat diversity, light availability or recreational potential. However, the assessment of vertical forest stand structure is difficult and is therefore currently assessed by experts in the field, which may be subject to observer bias. A possible way to reduce such uncertainties due to human error could be given by remote sensing. The Swiss Federal Office of Topography swisstopo is currently about to produce a nationwide airborne laser scanning (ALS) dataset of classified point clouds with an average point density of 15 – 20 pts/m². In this contribution, we present a method to assess vertical stand structure from ALS and NFI data. Our approach focuses on the analysis of return height distribution within the canopy in conjunction with machine learning. We stay close to the definition for stand structure specified by the Swiss NFI, which allows us to use their stand structure assessment as training data. We aim to apply the fitted model to the Swiss forests to produce a nationwide wall-to-wall stand structure assessment.

Application-oriented approach to monitoring the dynamics of avalanche tracks using conventional forest inventory parameters and Lidar-based change detection.

V. Berger^{1,2}, H. Kirchmeir¹, M. Hirschmugl^{3,4}

¹E.C.O. Institute of Ecology, Lakeside B07b, 9020 Klagenfurt, Austria
Email: {berger; kirchmeir} @e-c-o.at

²Carinthia University of Applied Sciences, Europastraße 4, 9524 Villach, Austria

³Joanneum Research, Steyrergasse 17, 8010 Graz, Austria
Email: manuela.hirschmugl@joanneum.at

⁴University of Graz, Heinrichstr. 36, 8010 Graz

1. Introduction

Sites affected by avalanches are considered as highly dynamic sites and are therefore of high ecological value. A wide spectrum of environmental conditions occurs in a narrow space. Due to the uneven mechanical impact of avalanches within the avalanche path, important niches and microhabitats are generated. Often adjacent forest stands cause a braking effect due to deadwood, uprooted trees and breaking trees (Bartelt and Stöckli, 2001). Depending on the size of the avalanche, damage to tree cover can be limited to the loss of a few trees, but can also clear several hectares of mature forest stands (CCA, 1995). All these processes lead to a heterogeneous habitat mosaic, which has a positive effect on species diversity (Rixen and Brugger, 2004). Aside from the effect on biodiversity, the protective function of forest stands also plays an important role in alpine regions. To capture the impact on and of forests, topographic Lidar can be used to simulate runoff scenario based on vegetation height models (Brožová et al., 2020). Forest and vegetation structure, on the one hand, influence the flow of avalanches and are, on the other hand, formed by the impact of avalanches. Therefore, monitoring the vegetation structure is an essential prerequisite to understand the dynamic processes within the avalanche tracks.

In order to capture the dynamics of avalanche tracks, multi-temporal area-based topographic Lidar data are of high benefit in addition to conventional forest inventory. A comparison of laser scanning data at two different points in time was used here to capture the dynamic of the avalanche path.

2. Data and Methods

2.1 Study Area, Data Acquisition and Processing

The study area is located to the southeast of Tamischbach Mountain in the Gesäuse National Park, Austria. Inventory plots are located at two avalanches paths in this area. The avalanche path Brett in the east covers an area of four hectares and is characterized by grass- and shrubland. The second avalanche path in the west is called the Hochkar, which can be divided into areas with frequent avalanche influence and areas which are only influenced during extreme events. The last extreme event happened in 2005.

Table 1. Technical specifications of ALS data used.

Year	Sensor	Point density	Frequency
2010	Riegl LMS-Q560	Min. 4 pts/m ² below 2000 m a.s.l.; min. 2 pts/m ² above 2000 m a.s.l.	200 KHz
2020	Riegl VUX240	200 pts/m ² /overpass; 2 overpasses = 400 pts/m ²	1.8 MHz

In 2010 a terrestrial baseline survey at 32 monitoring points was realised (Carli and Zimmermann, 2011). In 2021 the survey was re-conducted according to the methodological guideline for forest inventory of the Gesäuse National Park (Carli and Kreiner, 2009; Berger et al., 2020). In addition, high-resolution aerial imagery and airborne laser scanning data (ALS) were recorded in the study area. The aerial survey took place on 6/5/2020. During the evaluation, the current laser scanning data was compared with an existing laser scanning dataset from 2010 (source: GIS-Steiermark). The technical details of both ALS campaigns are shown in Table 1. Clearly, the two datasets are not fully comparable due to better sensor and lower flight altitude in 2020 compared to 2010.

2.2 Methods

The comparison of the height provides an insight into the change in vegetation height, which records the development of the vegetation since the last aerial survey. Image processing followed standard Lidar data handling. From the 2010 data, a digital terrain model (DTM) was generated using the point classification and a set of interpolation. This DTM was used to calculate vegetation height in both time periods for two reasons. First, there are not major changes in the terrain to be expected and second, we wanted to avoid potential differences coming from the data properties and processing to jeopardize comparability. For both time periods, digital surface models (DSMs) at a spatial resolution of 0.5 m were extracted using only points classified as vegetation. Clearly, the 2020 data would allow to extract a much higher resolutions DSM based on the given point density, but again, for comparability, we decided to process both data set to the same spatial resolution. As the maximum value per pixel is extracted from the laser scanning data, no overall bias caused by the different point density is to be

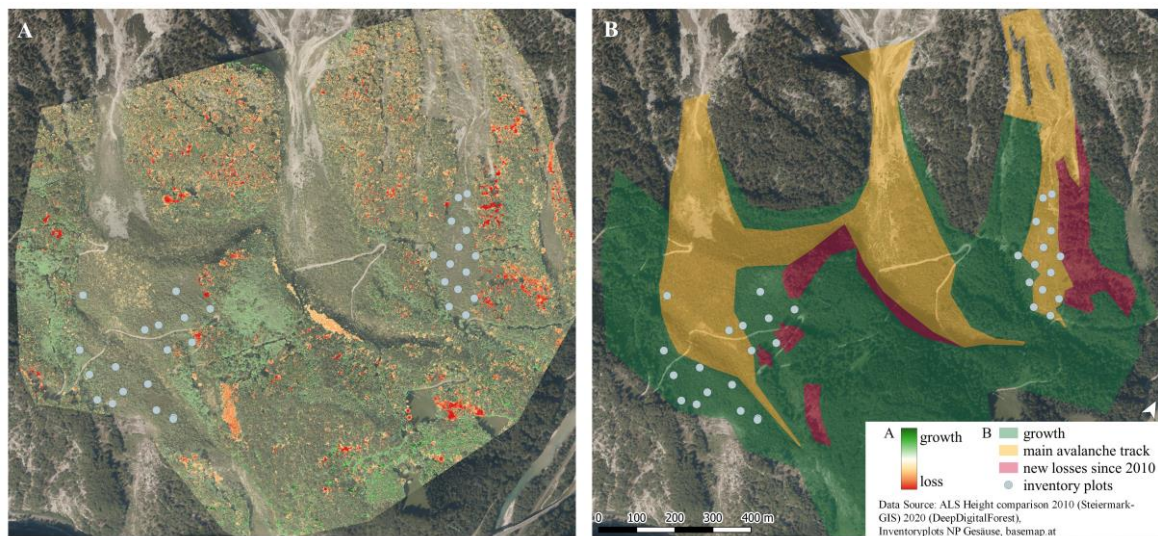


Figure 1: A) The difference in vegetation height between the years 2010 (source: GIS-Steiermark, 2010) and 2020 (DeepDigitalForest) shows the loss of trees (orange to red) and the growth of trees (green) B) The green area reflects an increase in vegetation height since 2010, the main avalanche track is displayed in orange and the loss of forest stands since 2010 in red.

expected. These DSMs were combined with the DTM to generate the two vegetation height models. They were clipped to a maximum of 60 m to remove outliers, mainly stemming from birds in the high resolution 2020 data. This clipping further reduces differences caused by the different acquisition settings rather than vegetation changes. Finally, both nDSMs were smoothed by a 3x3 median filter. The two vegetation height models were then subtracted to visualize the patterns of vegetation change. The colours represent the changes in vegetation height: while greenish colours indicate vegetation growth, yellow-orange colours indicate areas where the trees have been pushed down by avalanches. The small red patches are missing individual trees that had fallen between surveys (Figure 1).

3. Results and Discussion

From the orthophoto, it can be seen that some trees have fallen due to an avalanche event, as the orientation of the dead wood coincides with the flow direction of the avalanche track. The red patches in the map indicate significant loss of vegetation height where individual trees have fallen. The yellow-orange areas indicate areas where trees have been downed by avalanches, but most have not been destroyed. Open areas without significant regeneration since 2010 show no increase in stand height. A general growth of trees can be observed in areas of closed forest stands that have not suffered impact of avalanches during the period considered. On the map, some gaps caused by natural mortality of individual trees are visible. Thus, growth can be used to infer the impact of avalanche events on the tree population. When analysing the entire avalanche path, it is clear that only small-scale tree stands have been destroyed by avalanches since 2010.

Based on the 116-hectare survey area, 41 hectares have been affected by avalanches on a more or less yearly basis since 2010. These areas are characterized by grassland and lying or hanging living young trees with an average diameter at breast height (DBH) of 30 mm. Since 2010, about 7 hectares of previously mature forest was changed into grassland due to an avalanche event. There are also 68 hectares within proximity to the affected area which show an increase of height compared to 2010. The results of the ALS height comparison reflect the forest stand parameters that were assessed within the conventional forest inventory. The basic structure of the vegetation distribution can also be read from the laser scanning data. While the Hochkar avalanche path has average vegetation heights of 2.06 m, the Brett avalanche track has significantly lower vegetation with heights of only 1.32 m on average. The standard deviation is on a similar level with 2.35 m and 2.15 m, respectively.

4. Conclusions

The recording of forest structure in the context of long-term monitoring with conventional survey methods is particularly difficult. A description of the forest structure with lying trees is often impossible with existing inventory keys. Above all, the threshold values are not designed for the representation of lying or hanging trees. The application of a clipping threshold, whereby only trees above a certain diameter are surveyed, results in hardly any trees being recorded, although the biomass on the plots is relatively high due to the dense stand despite the low DBH. Furthermore, the recording of single trees from a height of 5 m leads to the fact that living trees that are lying or bent are not recorded, because their absolute height above ground is below this threshold. An extension of the existing inventory keys is therefore inevitable, especially for ecological questions that exceed the forestry usability.

By combining methodological conventional in-situ approaches with topographic Lidar technologies, a higher comparability of parameters, such as structural elements, can be achieved since they no longer depend solely on the estimation of the operator. The two-dimensional recording of the forest structure by means of aerial laser scanning images makes it possible to record the forest structure and the individual trees along the entire avalanche path.

The main advantages of the topographic Lidar approach in the practical assessment compared to field measurements are:

- the wall-to-wall information without any interpolation needed
- the information on otherwise inaccessible areas
- the area-based change detection on vegetation dynamics

Acknowledgements

The input data and results are results emerged from the research project “DeepDigitalForest” (consortium: Umweltdata, Joanneum Research, AeroMap, Sovereign Order of the Knights of Malta Grand Priory for Austria, Sebastian Pauli Geoinformatics, and E.C.O. Institute of Ecology). The authors thank the Austrian Research Promotion Agency (FFG) for funding and the Gesäuse National Park for the possibility and support of data collection within the protected area.

References

- Bartelt P and Stöckli V, 2001, The influence of tree and branch fracture, overturning and debris entrainment on snow avalanche flow. *Annals of Glaciology* 32, 209–216.
- Berger V, Köstl T, Steinbauer K, Kirchmeir H, 2020, Walddynamik 2019- 2020. Wiederholungsaufnahme von Vegetation und Verjüngung über großflächigen lawinar entstandenen Waldlichtungsfluren (Tamischbachturm, Gesäuse). *Bericht im Auftrag von: Nationalpark Gesäuse GmbH, Klagenfurt*
- Brožová N, Fischer J-T, Bühler Y, Bartelt P, Bebi P, 2020, Determining forest parameters for avalanche simulation using remote sensing data. *Cold Regions Science and Technology* 172(2020).
- Carli A and Kreiner D, 2009, Waldinventur Nationalpark Gesäuse 2006-2009.
- Carli A and Zimmermann T, 2011, Entwicklung von Vegetation und Verjüngung über großflächigen lawinar entstandenen Waldlichtungsfluren (Tamischbachturm, Gesäuse). *Bericht im Auftrag von: Nationalpark Gesäuse GmbH*
- CCA, 1995, Observation Guidelines and Recording Standards for Weather, Snowpack and Avalanches. Canadian Avalanche Association.
- Rixen C, Brugger S, 2004, Naturgefahren – ein Motor der Biodiversität. *Forum für Wissen*. 67 - 71

A stepwise approach for deriving timber assortments of trees from Terrestrial Laser Scanning data

Alvites C.¹, Santopuoli G.², Hollaus, M.³, Pfeifer, N.³, Mauro M.⁴, Moresi F.V.⁴, Marchetti, M.¹, Lasserre, B.¹

¹ Dipartimento di Bioscienze e Territorio, Università degli Studi del Molise, Cda Fonte Lappone snc, 86090 Pesche (IS), Italy. Email: {cesar.alvites, marchettimarco, lasserre}@unimol.it.

² Dipartimento di Agricoltura, Ambiente e Alimenti, Università degli Studi del Molise, Via De Sanctis snc, 86100 Campobasso, Italy. Email: giovanni.santopuoli@unimol.it.

³ Department of Geodesy and Geoinformation, TU Wien, Vienna 1040, Austria. Email: {markus.hollaus, norbert.pfeifer}@geo.tuwien.ac.at.

⁴ Department of Innovation in Biological, Agro-food and Forest Systems, DIBAF, University of Tuscia, 01100 Viterbo, Italy. Email: {f.v.moresi, m.maesano}@unitus.it

1. Introduction

Forests provide many goods and services to humans; one of the main goods provided by forests is roundwood.

The roundwood offers socio-economic and environmental benefits to forest owners and stakeholders, mainly because it plays a crucial role in the forestry production chain (SoEF 2020). The roundwood products can be classified into many timber assortments e.g., pulpwood, saw-log, fuelwood, and other industrial roundwood.

Nowadays, quantitative and qualitative information on timber assortments became crucial for implementing sustainable forest activities. Innovative tools and methods are necessary to facilitate the assessment of timber assortments with high accuracy. Despite the enormous efforts made over the years to improve the accuracy of the estimates, several challenges are still evident, particularly for mixed and multi-layered forests.

For these reasons, this study introduces a stepwise approach for catching timber assortment information of standing trees using Terrestrial Laser Scanning (TLS) data in mixed-species and multi-layered Mediterranean forests (Central Italy).

2. Data and Methods

2.1 Study area and ground truth field data

The study area was located in Bosco Pennataro (41°42' N, 14° 12' E), in Molise region (Central of Italy) (Figure 1). Bosco Pennataro is characterized by a high tree species richness and heterogeneity of forest structure, forming a multi-layered and mixed forest.

Field data were collected in 2016 within five squared field plots (hereafter ADS) of 529 m² (23m * 23m). All trees with a diameter at breast height (DBH) ≥ 0.025m were measured through the Field-Map tool (<https://www.fieldmap.cz/>). Many forest-related characteristics surveyed from standing trees were: DBH, tree height (TH), the height of the first attached branch or branch union (TH₁).

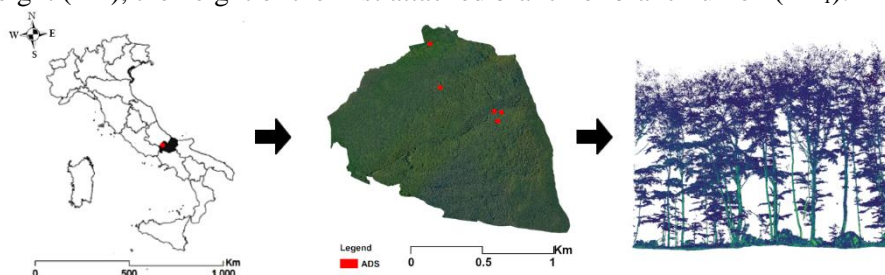


Figure 1 Study area. From left to right: the location of the study area concerning Italy; the distribution of the five squared field plots (ADS) within Mediterranean forests; a vertical slice of Terrestrial Laser Scanning (TLS) data for one ADS.

2.2 Terrestrial Laser Scanning data

The collection of TLS point cloud was carried out in July 2018. The TLS point cloud was acquired using a device named Leica ScanStation P30/40 (hereafter LSS) (<https://leica-geosystems.com/it-it/>). The horizontal and vertical field-of-view of this device was 360° and 290°, respectively.

A total of 178 single trees, divided into five ADS, were scanned using the Leica ScanStation P30/40 namely LSS device (about 9 scans for each ADS). To optimize the huge quantity of collected TLS point cloud, we clip each TLS point cloud based on a box dimension of 27m * 27m using many OPALS (Orientation and Processing of Airborne Laser Scanning data) modules, such as opalsImport, opalsAlgebra, and opalsExport (<https://opals.geo.tuwien.ac.at/html/stable/index.html>). The five TLS scans including the geographic coordinates (i.e. x, y, z) and intensity feature were used as input data for the subsequent steps.

2.3 Ground truth TLS point cloud

Based on the TLS point cloud, some tree variables, as maximum-end diameter, (e.g., trunk base THbase); minimum-end diameter, (e.g. at the end of the trunk assortment – TH₁); trunk length, were manually measured using point picking tool through CloudCompare software. The useful trunk section from TLS point cloud was ranged between THbase and TH₁ (Liang et al. 2018).

To extract the timber assortment information of trees, we selected all trees having a DBH > 0.20m. To improve the characterization accuracy of each trunk section, we divided and classified the logs into merchantable logs ($2.5\text{m} \leq \text{length of log} \leq 3\text{m}$) and non-merchantable logs ($2.5\text{m} < \text{length of log}$).

Qualitative and quantitative information for both types of logs was gathered through vary log measurements e.g., straightness (STR; cm m^{-1} ; equation 1), tapering (TAP; cm m^{-1} ; equation 2), minimum-end and maximum-end diameter of logs (Dmax and Dmin; m); length of log (L; m) (Nosenzo 2007).

2.4 TLS analysis

Four steps were implemented for computing the TLS point cloud: a) timber-leave discrimination; b) tree detection and DBH estimation; c) stem reconstruction and d) timber assortment assessment.

The timber-leave discrimination was performed using geometric-based features from TLS point clouds through Random Forests algorithm. The tree detection allows us to find the tree position and to estimate the DBH of detected trees. The stem reconstruction, corresponding to the trunk section of detected trees, was based on a cylinder-fitting approach implemented in opalsDBH OPALS module. The timber assortment assessment provides both qualitative and quantitative information of trunk sections from standing trees (Figure 2).

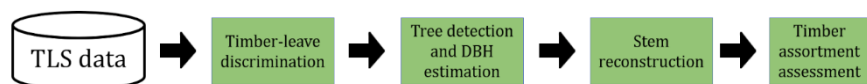


Figure 2 Workflow of Terrestrial Laser Scanning (TLS) processing. The green rectangles represent the steps. DBH is the diameter at breast height.

3. Results and Discussion

3.1 Timber-leave point clouds discrimination

Results revealed that Random Forests algorithm has accurately discriminated the timber from the leaves points in a mixed-species and multi-layered forest, and it was supported by a similar great accuracy (0.98), sensitivity (0.98), and specificity (0.98) values obtained for all five squared field plots, namely ADS. Despite the optimal performance showed by Random Forests, we observed an occlusion effect from large to small trees. It was more evident in the understory layer. However, these occlusion factors were worsened in trees having lianas (Vicari et al. 2019).

3.2 Tree detection and DBH estimation

We detected 151 out of 178 observed trees, reaching an average detection rate accuracy equal to 84.4%, with a high uniformity/similarity among the ADS, based on the standard deviation values ($SD = \pm 4.7\%$).

All trees with a DBH > 0.30m were detected. The comparison between predicted and observed DBH measurements from correctly detected trees has outlined that the linear model excluding outlier values was more accurate (R-squared = 0.84; RMSE = 0.02m) than that including outlier values (R-squared = 0.67; RMSE = 0.08m). The problem to identify the trees with a DBH lower than 0.30m might be supported by the shadow effects from large to small trees and/or from branches to trunk, TLS point cloud quality, error in the assembly, the verticality of stems, the non-circular shape of the trunk and the tree species composition (Liang et al. 2018).

3.3 Stem reconstruction

We reconstructed 47 out of 70 observed trees using TLS point cloud through a cylinder-fitting approach, reaching an average stem reconstruction accuracy equal to 67.2%, with a low similarity/uniformity among the ADS (SD = $\pm 14.86\%$). Results indicated that more than three-quarters of the trunk section was described by cylinders. The factor conditioned the reconstruction of trees was straightness of trees, the difference of cylinder diameter, TLS point cloud quality, and the forest structure.

3.4 Timber assortment estimation

Results about timber assortment quantification demonstrated that nearby 75% of logs provided by reconstructed trees were quantified, particularly, 134 out of 179 merchantable logs and 34 out of 40 non-merchantable logs were quantified.

As regards Timber assortment classification, results demonstrated that 8 out of 11 assortment types were more accurate, based on the small difference between predicted and observed quantity of merchantable logs (± 2 units). We observed that a part of the logs was “missing” in both log types. We assumed that the occurrence of this problem might be associated with the irregular stem form (i.e. stem straightness) and the irregularities on the bark (i.e. geometry defects: knots, bulges, microhabitats).

4. Conclusion

This study introduces a stepwise approach for extracting the timber assortment information of standing trees using TLS point cloud in a mixed species and multi-layered Mediterranean forest. This is very important to assess and implement sustainable forest management.

Moreover, four conclusions may be drawn from the stepwise approach used for analysing the TLS point cloud. First, accurate timber-leaves discrimination favoured the reconstruction of dominant trees species; second, this stepwise approach proved to be more efficient for large trees (> 0.20m of DBH) and it is advantages for timber assortment assessment; third, the cylinder-fitting approach was powerful, despite the straightness of trees; fourth, the forest structure, bark surface, and microhabitats can influence the success of the reconstruction of trees. Our approach better works in veteran trees, this is a significant outcome, because this approach is focused on trees with a greater timber volume.

Reference

- Liang X, Hyyppä J, Kaartinen H, Lehtomäki M, Pyörälä J, Pfeifer N, Holopainen M, Brolly G, Francesco P, Hackenberg J, Huang H, Jo H-W, Katoh M, Liu L, Mokros M, Morel J, Olofsson K, Poveda-Lopez J, Trocha J, Wang D, Wang J, Xi Z, Yang B, Zheng G, Kankare V, Luoma V, Yu X, Chen L, Vastaranta M, Saarinen N, Wang Y, 2018, International benchmarking of terrestrial laser scanning approaches for forest inventories, ISPRS journal of photogrammetry and remote sensing. 144: 137-179. <https://doi.org/10.1016/j.isprsjprs.2018.11.008>.
- Nosenzo A, 2007, Determinazione degli assortimenti ritraibili dai boschi cedui di castagno: l'esempio della bassa Valle di Susa (Torino). *Forest@-Journal of Silviculture and Forest Ecology*, 4(1), 118, Retrieved from <http://www.sisef.it/>
- SoEF,2020, Summary for Policy Markers State of Europe's Forest 2020, (Vol. 4, pp. 64–75).
- Vicari MB, Disney M, Wilkes P, Burt A, Calders K and Woodgate W, 2019, Leaf and wood classification framework for terrestrial LiDAR point clouds. *Methods in Ecology and Evolution*, 10(5), 680-694. DOI: 10.1111/2041-210X.13144.

Multispectral Images SPOT for Urban Forest Monitoring

S. Bonilla-Bedoya¹, D. Mejía Coronel², R. Zalakeviciute³

¹ Research Center for the Territory and Sustainable Habitat, Universidad Tecnológica Indoamérica, Machala y Sabanilla, 170301 Quito, Ecuador

Email: santiagobonillab@hotmail.es

² Centro de Estudios Ambientales, Universidad de Cuenca, Ecuador

Email: danilo.mejia@ucuenca.edu.ec

³ Intelligent & Interactive Systems Lab (SI2 Lab) and Biodiversidad, Medio Ambiente y Salud (BIOMAS), Facultad de Ingeniería y Ciencias Agropecuarias (FICA),

Email: rasazalake@gmail.com

1. Introduction

When studying land use and land cover changes in urban and hyper-urban areas, finer scales of information are required to accurately identify fragments of other coverages, such as forest, trees, green areas, soils, etc. In that sense, optical images such as SPOT have proven to be a solution for better understanding urban phenomena (Weber & Hirsch, 1992; Sertel et al., 2015; Li et al., 2019). Moreover, they now have a historical record that allows them to overcome the challenges of time scale to quantify changes.

In this context, this study aimed to identify and estimate land cover changes in an urban space. This information provides tools to address the challenges of urban sustainability and green infrastructure design. To achieve this goal, we set out to quantify over a five-year period (2013–2017) the changes in land cover with an emphasis on impervious cover, forest fragments, urban trees, and urban green areas.

2. Data and Methods

To determine the temporal changes in urban forest cover and climate variability in recent years, we first quantified changes in forest cover and urban green areas over a five-year period (2013–2017) using high-resolution imagery in a mountain city: Quito at 2,815 m.a.s.l. (Figure 1).

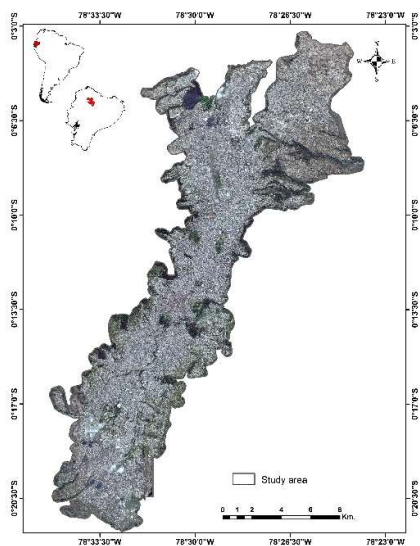


Figure 1. Study Area: Quito hyper urban gradient

We classified two images: SPOT 6 sensors (PMS 1503537, ORT 2956463201, June 23, 2013) and SPOT 7 (PMS 1512376, ORT 2956433101, December 16, 2017). The resolution of this type of image (*cell: 1.5*1.5*) provides a suitable scale for the identification of green areas and urban forests (Andersson et al., 2009; du Toit et al., 2011). The two images were divided into five segments to facilitate classification. From these images, a land use classification process was initiated, which included three phases: atmospheric correction with the ATCOR tool - Ground Reflectance Workflow (Geomatica, 2019); mosaic generation with the OrthoEngine tool (Geomatica, 2018a); and finally, a classification process based on objects through the Object Analyst tool (Geomatica, 2018b).

This last tool was applied on high resolution images and performed an object-based image analysis. First, it segments an image for classification, then an analysis phase determines the classification process and, it is characterized by the extraction of statistical and geometric features from the object/polygon layer. Statistical features are a function of image pixels within an object and SPOT bands. Whereas the geometric features: circular, elongated compact and rectangular are calculated by analyzing the boundaries of the polygons created in the segmentation process (Geomatica, 2018b; Bonilla-Bedoya et al., 2020).

Then, we generated a grid over the SPOT. This was useful to distribute the land cover classification training polygons. The classes considered were forest component, grassland, impervious, agriculture, shrubs and herbs, soil, and water. For the evaluation, a new class sample was generated that considered approximately 25% of the total area of each land cover. These data were used to cross-check a confusion matrix and errors of omission and commission to derive a validation kappa index.

The land cover classification for 2013–2017 and a cross-tabulation matrix allowed the total change of the coverage categories to be quantified. This process considered both the net change and the swap in addition to the gross gains and losses (Pontious, 2004; Alo & Gilmore, 2008; Bonilla-Bedoya et al., 2014). In addition, this enabled the visualization of differences between the systematic or random transitions among the different categories that make up the urban landscape (Pontious et al., 2004; Alo & Gilmore, 2008).

3. Results

Classification of the SPOT images (2013, 2017) yielded a mean kappa index calculated from the five sections into which each image was divided (Table 1). The categories of impervious cover, forest, green areas, and shrub-herb dominate the urban landscape of this city. The most important processes of loss, gain, and exchange in the landscape occur in these categories (Table 2). In addition, our results demonstrate an increase in the impervious category and the loss of urban vegetation, represented by the sum of the categories: forest, green areas, and shrub-herb (Figure 2). However, in parallel with this change, we observed an increase in forests and urban woodland that compensated for losses in the shrub-herb and green areas categories (Table 3)

Table 1. Mean and standard deviation of the Kappa Index considering the five classification sections 2013-2017.

Land cover	Kappa index	
	2013 <i>mean±sd</i>	2017 <i>mean±sd</i>
Agriculture	0,95±0,07	0,810.08
Forest	0.89±0.11	0,92±0.06
Green areas	0.87±0.16	0,72±0.18
Impervious	0.90±0.20	0,94±0.04
Shurb and herbaceous	0.75±0.17	0,65±0.39
Soil	0.87±0.10	0,72±0.14
Water	0.80±0.45	0,69±0.47

Table 2. Gain, Loss, Total Change, Interchange, Absolute value of net change of Quito City (2013-2017)

Land cover	Gain (%)	Loss (%)	Total change (%)	Interchange (%)	Absolute value of net change
Agriculture	1.00	2.41	3.41	2.00	-1.41
Forest	8.49	4.54	13.03	9.09	3.94
Green areas	4.39	6.20	10.59	8.79	-1.80
Impervious	9.54	5.26	14.80	10.51	4.28
Shrub and herb	4.60	9.01	13.61	9.21	-4.41
Soil	1.29	1.89	3.17	2.58	-0.60
Water	0.04	0.05	0.08	0.07	-0.01

Table 3. Systematic transitions in the gain and loss function.

Year 2013	Year 2017	Gain (Observed minus expected)		Loss (Difference divided by expected)	
Forest	Agriculture	0	0	0.04	0.51
Forest	Green areas	0.09	0.16	0.26	0.62
Forest	Impervious	-1.19	-0.43	-1.8	-0.53
Forest	Shrub and herb	1.38	2.06	1.42	2.25
Forest	Soil	-0.06	-0.36	0.01	0.08

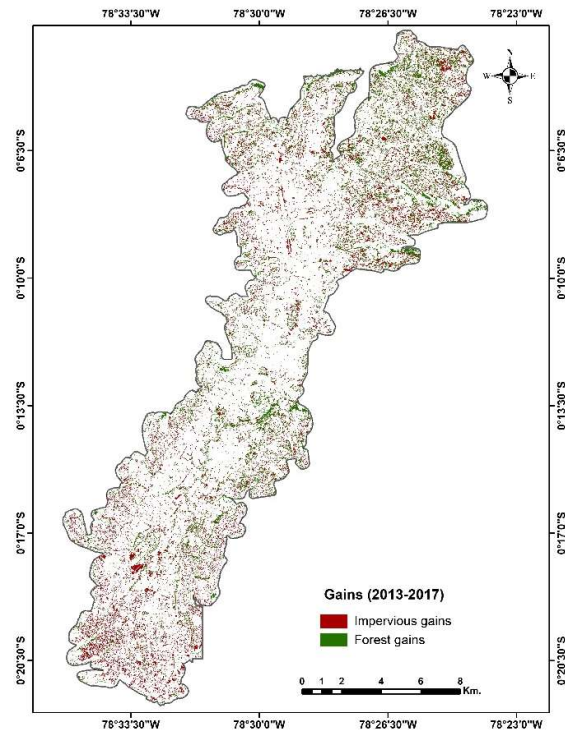


Figure 2. Gains: Forest and impervious cover categories

4. Discussion

We estimate land cover changes (2013-2017) of a mountain city (Bonilla-Bedoya et al., 2020). Remote sensing methods applied to SPOT images allowed, compared to other sensors, to present information at a fine and precise scale for urban research (Liang et al., 2012). It allows to identify, in relatively recent periods, variations in land cover and land use in urban landscapes.

The loss of urban vegetation, represented by the sum of forest, green areas, and shrub-grass categories is complemented by an increase, over time, in tree cover and urban fragments at the expense of shrub and green area categories. These dynamics in urban cover change indicate the pressure exerted by hyper-urban infrastructure on the few spaces that could be allocated to hyper-urban greenery

However, this methodology for understanding the dynamics of green infrastructure in the city could be enhanced by assessing forest stand conditions and forest components in urban and peri-urban areas by integrating new approaches, such as those involving airborne laser scanning (LiDAR) data (Alonso et al., 2016).

5. Conclusions

Remote sensing and geographic information systems applied to the study of land use, land cover, and forest change along urban-rural-natural gradients are essential tools for planning initiatives. The conversion of urban land use and land cover affects the environmental conditions of a city and the wellbeing of its citizens.

Understanding the spatio-temporal variations of urban forests more accurately and at an appropriate scale are challenges that aim to accurately quantify urban forest ecosystem services. This information for the design of planning policies in the framework of environmental justice could make a difference in the value of contemporary urban land.

Therefore, including methods that incorporate appropriate technologies, such as LiDAR, to improve the scale first; and the accuracy of forest allometric models derived from the metrics taken by these technologies would complement the advances in the multispectral domain and reduce uncertainty.

Acknowledgements

The authors would like to thank to Corporación Ecuatoriana para el Desarrollo de la Investigación y Academia - CEDIA for the financial support given to the present research, development, and innovation work through its CEPRA program, especially for the “Resiliencia ambiental en sistemas socio-ecológicos urbanos de ciudades neotropicales, casos Quito y Guayaquil” fund.

References

- Alonzo, M., McFadden, J. P., Nowak, D. J., & Roberts, D. A. (2016). Mapping urban forest structure and function using hyperspectral imagery and lidar data. *Urban Forestry and Urban Greening*, *17*, 135–147. <https://doi.org/10.1016/j.ufug.2016.04.003>
- Alo, C., & Gilmore, R. (2008). Identifying systematic land-cover transitions using remote sensing and GIS : the fate of forests inside and outside protected areas of Southwestern Ghana. *Environment and Planning B: Planning and Design*, *35*, 280–296. <http://doi.org/10.1068/b32091>
- Andersson, E., Ahrné, K., Pyykönen, M., & Elmqvist, T. (2009). Patterns and scale relations among urbanization measures in Stockholm, Sweden. *Landscape Ecology*, *24*, 1331–1339. <http://doi.org/10.1007/s10980-009-9385-1>

- Bonilla-Bedoya, S., Molina, J.R., Herrera-Machuca, M.A., 2014. Fragmentation patterns and systematic transitions of the forested landscape in the upper Amazon region, Ecuador 1990–2008. *J. For. Res.* 25 (2):301–309. <https://doi.org/10.1007/s11676-013-0419-9>.
- Bonilla-Bedoya, S., Mora, A., Vaca, A., Estrella, A., Ángel, M., 2018. Modelling the relationship between urban expansion processes and urban forest characteristics: an application to the Metropolitan District of Quito. *Comput. Environ. Urban Syst.* (September), 101420. <https://doi.org/10.1016/j.compenvurbsys.2019.101420>.
- Du Toit, M., & Cilliers, S. (2011). Aspects influencing the selection of representative urbanization measures to quantify urban – rural gradients. *Landscape Ecology*, 26, 169–181. <http://doi.org/10.1007/s10980-010-9560-4>
- Geomatica. (2018a). Atmospheric correction (with ATCOR). Ontario.
- Geomatica. (2018b). Geomatica OrthoEngine. Ontario.
- Geomatics. (2017). PCI geomatica enterprises. Ontario: PCI Geomatics Enterprises.
- Li, X., Chen, W.Y., Sanesi, G., 2019. Remote sensing in urban forestry : recent applications and future directions. *Remote Sens.* 11 (1144), 1–20.
- Pontius, R. G., Shusas, E., & Mceachern, M. (2004). Detecting important categorical land changes while accounting for persistence. *Agriculture, Ecosystems and Environment*, 101, 251–268. <http://doi.org/10.1016/j.agee.2003.09.008>
- Sertel, E., & Akay, S. S. (2015). High resolution mapping of urban areas using SPOT-5 images and ancillary data. *International Journal of Environment and Geoinformatics*, 2(2), 63–76.
- Weber, C., & Hirsch, J. (1992). International Journal of Remote Sensing Some urban measurements from SPOT data: urban life quality indices. *International Journal of Remote Sensing*, (17), 3251–3261. <http://doi.org/10.1080/01431169208904116>

Precision Thinning - a comparison of stand-level and pixel-level thinning in Norway spruce and Scots pine stands

Magnus Persson¹, Renats Trubins², Ljusk-Ola Eriksson¹, Johan Bergh¹,
Johan Sonesson³, Emma Holmström²

¹Linnaeus University, Sweden
Email: {magnus.j.persson, ola.eriksson, johan.bergh} @lnu.se

²Swedish University of Agricultural sciences, Sweden
Email: {renats.trubins, emma.holmstrom} @slu.se

³Skogforsk, Sweden
Email: johan.sonesson@skogforsk.se

Abstract

Precision forestry allow decision making on tree level or pixel-level, as compared to stand-level data. However, little is known about its long-term effects on within-stand variation, stand economy and growth. In this study, silviculture was optimized in 20 conifer-dominated forest stands located in the boreo-nemoral region of southern Sweden. Two thinning scenarios were tested; optimization using a stand-based approach; Stand level thinning (SLT) and precision thinning approach; Precision thinning (PT).

Mean annual increment of living stem volume (MAInet) was significantly higher for PT than SLT for the full rotation ($p = .002$) but not regarding Net Present Value (NPV, $p = .10$). The within-stand variation in basal area ($m^2/ha-1$) was significantly lower at the end of the rotation compared to the start of the simulation for both SLT ($p < .001$), and PT ($p < .001$). At the end of the rotation, SLT had significantly higher variation in basal area compared to PT ($p < .001$). The results indicate the there is no clear long-term benefit or drawback in basing silvicultural decision on pixel-level information as compared to stand level data when optimizing stand economy. However, PT was the upper hand since within-stand variation can be accounted for and targeted during harvest planning.